Technology Collaboration Programme on
Heat Pumping Technologies (HPT TCP)

Annex 41

Cold Climate Heat Pumps

Improving low ambient temperature performance of air-source heat pumps

Final Report

Operating Agent: The United States

2017

Report no. HPT-AN41-1

Published by

Heat Pump Centre
c/o RISE – Research Institutes of Sweden
Box 857, SE-501 15 Borås
Sweden
Phone: +46 10 16 55 12
Fax: +46 33 13 19 79

Production

Heat Pump Centre, Borås, Sweden

ISBN 978-91-88349-89-7
Report No. HPT-AN41-1

Preface
This project was carried out within the Technology Collaboration Programme on Heat Pumping Technologies (HPT TCP) which is an Implementing agreement within the International Energy Agency, IEA.

The IEA
The IEA was established in 1974 within the framework of the Organization for Economic Cooperation and Development (OECD) to implement an International Energy Programme. A basic aim of the IEA is to foster cooperation among the IEA participating countries to increase energy security through energy conservation, development of alternative energy sources, new energy technology and research and development (R&D). This is achieved, in part, through a programme of energy technology and R&D collaboration, currently within the framework of over 40 Implementing Agreements.

The Technology Collaboration Programme on Heat Pumping Technologies (HPT TCP)
The Technology Collaboration Programme on Heat Pumping Technologies (HPT TCP) forms the legal basis for the Heat Pumping Technologies Programme. Signatories of the TCP are either governments or organizations designated by their respective governments to conduct programmes in the field of energy conservation.

Under the TCP collaborative tasks or "Annexes" in the field of heat pumps are undertaken. These tasks are conducted on a cost-sharing and/or task-sharing basis by the participating countries. An Annex is in general coordinated by one country which acts as the Operating Agent (manager). Annexes have specific topics and work plans and operate for a specified period, usually several years. The objectives vary from information exchange to the development and implementation of technology. This report presents the results of one Annex. The Programme is governed by an Executive Committee, which monitors existing projects and identifies new areas where collaborative effort may be beneficial.

The Heat Pump Centre
A central role within the HPT TCP is played by the Heat Pump Centre (HPC). Consistent with the overall objective of the HPT TCP the HPC seeks to advance and disseminate knowledge about heat pumps, and promote their use wherever appropriate. Activities of the HPC include the production of a quarterly newsletter and the webpage, the organization of workshops, an inquiry service and a promotion programme. The HPC also publishes selected results from other Annexes, and this publication is one result of this activity.

For further information about the Technology Collaboration Programme on Heat Pumping Technologies (HPT TCP) and for inquiries on heat pump issues in general contact the Heat Pump Centre at the following address:
IEA Heat Pump Centre
c/o RISE - Research Institutes of Sweden
Box 857, SE-501 15 BORÅS, Sweden
Phone: +46 10 16 55 12

Final Report: IEA HPT TCP Annex 41
Cold Climate Heat Pumps

Participating Countries
Austria
Canada
Japan
United States

Compiled by
Van D. Baxter, P.E.
Oak Ridge National Laboratory

Prof. Eckhard Groll, PhD.
Reilly Professor of Mechanical Engineering
Purdue University

Karen Sikes
CSRA Inc.

August 2017

This page intentionally left blank.

ANNEX 41 PARTICIPANTS AND CONTRIBUTORS

Country	*Primary Contact*	*Backup Contact/Support*
Austria	***Thomas Fleckl*** ***Christoph Reichl***	
	AIT Austrian Institute of Technology *Center for Energy* *A-1210 Vienna, Giefinggasse 2* *E-mail: Thomas.fleckl@ait.ac.at* *Office Tel: 43 50 550 6616 Fax: 43 50 550 6679* *E-mail: christoph.reichl@ait.ac.at* *Office Tel: 43 50 550 6605*	
	René Rieberer	
	Graz University of Technology *Institute of Thermal Engineering* *A-8010 Graz, Inffeldgasse 25/B* *E-mail: rene.rieberer@tugraz.at* *Office Tel: 43 316 873 7302 Fax: 43 316 873 7305*	
Canada	***Daniel Giguére***	
	Canmet Energie/Canmet Energy *Resources Naturelles Canada* *Naturelles Resources Canada* *1615 Bvd Lionel-Boulet* *Varennes, Québec* *J3X 1S6 Canada* *E-mail: Daniel.Giguere@rncan-nrcan.gc.ca*	
	Brice Le Lostec	
	Laboratoire des Technologies de l'Energie *Institut de Recherche* *Hydro-Québec* *600 de la Montagne* *Shawinigan, Québec* *G9N 7N5 Canada* *Phone: (819) 539-1400 poste 1434* *Fax: (819) 539-1409* *E-mail: lelostec.brice@lte.ireq.ca*	
Japan	***Masafumi Katsuta, team leader***	
	Professor in Graduate School of Environment and Energy Engineering, and President JSRAE *Waseda University* *3-4-1, Ohkubo, Shinjuku-ku* *Tokyo 169-8555, JAPAN* *Phone: +81-3-5286-3251* *Fax: +81-495-24-6190* *E-mail: katsuta@waseda.jp*	
	Takeshi Hikawa, team secretary	
	Director, Technical Research Department *Heat Pump & Thermal Storage Center of Japan* *Hulic Kakigaracho Bldg.* *1-28-5 Nihonbashi Kakigaracho Chuo-ku* *Tokyo 103-0014, JAPAN* *Phone: +81-3-5643-2404* *Fax: +81-3-5641-4501* *E-mail: hikawa.takeshi@hptcj.or.jp*	
United States	***Eckhard Groll***	
	Reilly Professor of Mechanical Engineering, Purdue University	

(Annex Operating Agent)	***Ray W. Herrick Laboratories*** ***140 S. Martin Jischke. Dr.*** ***West Lafayette, IN 47907 USA*** ***Phone: 765-496-2201*** ***E-mail: groll@purdue.edu***	
	Omar Abdelaziz ***Van Baxter*** ***Bo Shen***	
	Building Technologies Research & Integration Center ***Oak Ridge National Laboratory*** ***PO Box 2008, Bldg 3147, MS-6070*** ***Oak Ridge, TN 37831-6070*** ***Phone: 865-547-2098 (Abdelaziz)*** ***E-mail: abdelazizoa@orln.gov*** ***Phone: 865-547-2104 (Van Baxter)*** ***E-mail: baxtervd@ornl.gov*** ***Phone: 865-574-5745 (Bo Shen)*** ***E-mail: shenb@ornl.gov*** ***Fax: 865-574-9338***	

Acknowledgement: The Annex Co-Operating Agents gratefully acknowledge the research contributions and support of the above noted participants and contributors.

ABSTRACT

Heat pump technology provides a significant potential for CO_2 emissions reduction. Annex 41 revisits research and development work in different countries to examine technology improvements leading to successful heat pump experience in cold regions. The primary focus is on electrically driven air-to-air or air-to-water air-source heat pumps (ASHP), with air or hydronic heating systems, since these products suffer severe loss of heating capacity and efficiency at lower outdoor temperatures. Other heat pump technologies were also investigated, including ground-source heat pumps and solar-assisted heat pumps. The main technical objective is to identify solutions leading to ASHPs with heating SPF > 2.63 W/W, recognized as a renewable technology. The main outcome of this Annex is information-sharing on viable means to improve ASHP performance in cold climate locations – loosely defined for purposes of the Annex as locales with a significant number of hours having ambient temperatures < -7°C. Austria, Canada, Japan, and the US (OA) participated in the Annex, which officially began in July 2012.

This page intentionally left blank.

TABLE OF CONTENTS

This page intentionally left blank.

PART 1: EXECUTIVE SUMMARY

1 INTRODUCTION TO ANNEX 41

In 2012 the International Energy Agency (IEA) Heat Pump Programme (HPP; now HPT, Heat Pumping Technologies Programme) established Annex 41 to investigate technology solutions to improve performance of heat pumps for cold climates. Four IEA HPP member countries are participating in the Annex – Austria, Canada, Japan, and the United States (U.S.). The principal focus of Annex 41 is on electrically driven air-source heat pumps (ASHP) since that system type has the lowest installation cost of all heat pump alternatives. They also have the most significant performance challenges given their inherent efficiency and capacity issues at cold outdoor temperatures. Availability of ASHPs with improved low ambient performance would help bring about a much stronger heat pump market presence in cold areas, which today rely predominantly on fossil fuel furnace heating systems.

During the mid-1970s, following the first oil embargo, interest in use of heat pumps to provide space heating began to increase in much of the developed world (OECD countries). Many northern U.S. electric power companies began experiencing increasing peak kilowatt (kW) demands during the heating season as shortages of natural gas and oil led to increased usage of direct electric heating. In response they began investigating the use of ASHPs as a means of mitigating the increased peak demands. ASHPs are almost universally applicable to buildings in all parts of the world and, given that they were the primary type available, were of main interest as an alternative electrical heating system at that time. However, as noted above, they suffer both heating capacity (output) and efficiency (coefficient of performance or COP) degradation as the outdoor ambient temperature drops while at the same time the building heat demand is increasing. As such, ASHPs require a supplemental heating source – usually direct electric resistance heating elements – to bridge the gap between the building heat demand and the ASHP heating output. This feature causes lower seasonal performance and limits peak electric demand reduction potential leading to limited acceptance of ASHPs in areas that experience large numbers of hours at cold temperatures (loosely defined as ≤ -7°C for purposes of Annex 41). In addition, typical heat pump compressors fail to work at extremely low ambient temperatures due to the significantly high pressure ratios and discharge temperatures. A primary criterion for ASHPs to achieve good seasonal performance in cold areas is, therefore, achieving high heating output (capacity) at low ambient temperatures so as to minimize reliance on supplemental heat sources and maximize the overall system heating seasonal performance factor (HSPF in Btu/Wh or the dimensionless equivalent SCOP).

For the reasons noted above, ASHPs have been the primary heat pump type of interest for Annex 41. However, ground source and solar-assisted heat pumps (GSHP and SAHP) have also been addressed by some of the participants. A primary technical objective of the Annex is to define pathways to enable ASHPs to achieve an "in field" $SPF_h \geq 2.63$ W/W (HSPF ≥9.0 Btu/Wh), the minimum level necessary in order to gain recognition as a renewable technology in the European Union.

As stated in the 27 February 2013 legal text for the Annex the work was divided into four main tasks:

- Task 1: Critical literature survey – Participants undertook a literature review and review of results from prior related research to identify candidate ASHP system design possibilities for further evaluation and study.
- Task 2: System design and application studies - modeling and/or laboratory-controlled measurements - The focus was on detailed analyses of promising component/system concepts including outdoor heat exchanger frosting/defrosting issues considering the system performance and cost implications as well as design

and control issues. Laboratory prototype and field prototype testing may be included in this task as well.

- Task 3: Simulations of energy savings impacts of prototype advanced ASHP design - This task involved seasonal/annual performance simulations based on the Task 2 studies to estimate energy and emissions savings potential.
- Task 4: Report and information dissemination - Each participant has provided a final country report addressing their respective results from the tasks above. These have been assembled into this final Annex report by the Operating Agent. A number of possible further areas for study are included.

Annex members have focused on two primary areas to address the cold climate performance problems noted above. First, advanced Cold Climate Heat Pumps (CCHPs) with low-temperature capacity-enhancement approaches have been developed. Secondly, detailed analytical and experimental investigations on outdoor heat exchanger (OHX) frosting have been conducted, primarily by the Japanese and Austrian teams.

1.1 Objectives

This project is primarily focused on electrically-driven ASHPs with air or hydronic heating systems (e.g., air-to-air or air-to-water heat pumps) since these products have the greatest challenge in providing sufficient heat output and maintaining high efficiency levels at lower outdoor temperatures. Electric ASHPs generally have the lowest installation cost of all heat pump alternatives, but also the greatest performance challenges at cold outdoor temperatures. One of these is loss of heating capacity. Traditional ASHPs lose 80% of their heating capacity at outdoor temperatures of -25°C compared to the rated performance at 8.3°C. This means that traditional ASHPs must use low-efficiency backup heat at lower temperatures, as noted in Figure ES-1. The other major issue is the loss of capacity due to frosting and defrosting of the outdoor heat exchanger (OHX) at moderate outdoor temperatures between about -5°C to 5°C (noted in Figure ES-1).

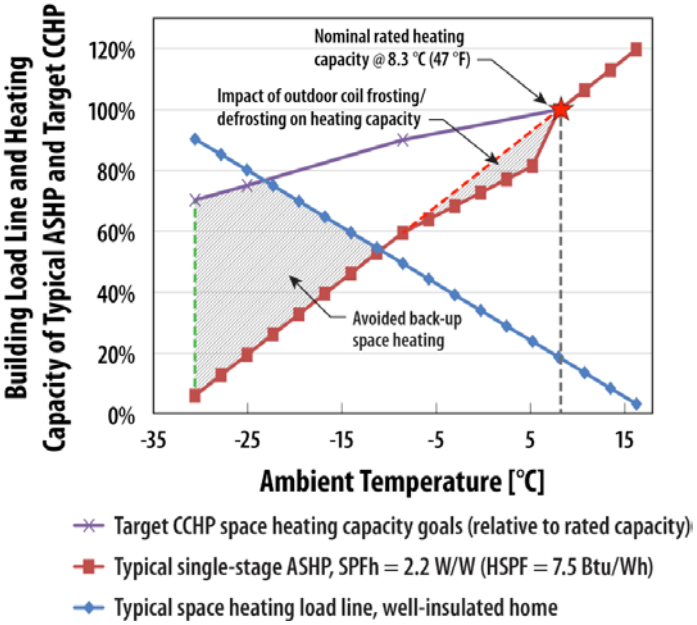

Figure ES-1: Space heating capacity for target CCHP (per Table ES-1 below) vs. typical single-stage ASHP

Technical performance goals for CCHPs as established by the U.S. Department of Energy's Building Technology Office (DOE/BTO) are listed in Table ES-1.

Table ES-1: U.S. CCHP performance targets

Outdoor Temperature	Heating Capacity
8.3°C (47°F)	9-21 kW (2.5-6 tons), nominal rating
-25°C (-13°F)	≥75% of nominal rating

A major technical objective as stated in the Annex legal text is to identify solutions that can lead to improved ASHPs for cold climate application with a heating SPF ≥ 2.63 W/W, the minimum level necessary in order to gain recognition as a renewable technology in the EU.

These objectives have parallel interest under the IEA Framework of Implementing Agreements (now Technology Collaboration Partnerships, TCP) as the intent is to identify, quantify, and deliver information to key industry stakeholders and policy makers and to provide pertinent resources to building owners and operators. The objectives will be achieved by independent studies and investigations performed by the country-specific participants. The main output of this Annex is information sharing on viable means to improve ASHP heating performance under cold ambient temperature conditions so that better cross-country understanding is achieved to reduce energy consumption (and the related CO_2-emissions) while satisfying the needs of building owners and operators.

1.2 Target Audience and Benefits

The sectors targeted for this Annex include:

- HVAC practitioners responsible for designing, selecting, and sizing heat pump systems in varied applications with a focus on cold ambient locations.
- Building owner/operators in cold regions interested in achieving improved comfort conditioning and efficiency performance from their HVACR equipment.
- Entities charged with minimizing energy utilization (i.e., utilities, utility commissions, energy agencies, legislative bodies, etc.) in varied heat pump applications and geographic conditions.

1.3 Annex Activities and Time Schedule

Table ES-2 breaks down Annex 41 tasks and time schedule.

Table ES-2: Annex 41 tasks and time schedule (actual)

Start Date	End Date	Annex 41 Activities
July 2012	March 2013	Task 1 – Critical literature survey
Dec 2012	June 2015	Task 2 – System design and application studies - modeling and/or laboratory-controlled measurements
June 2014	March 2017	Task 3 – Simulations of energy savings impacts of prototype advanced ASHP design
Jan 2013	July 2017	Task 4 – Report and information dissemination

1.4 Summary of Principal Outcomes

Table ES-3 summarizes the principal outcomes resulting from the activities of each Annex participant.

Table ES-3: Principal outcomes of performance improvement techniques investigated by Annex participants

Annex Participants	CCHP Investigated Techniques	Resulting Performance Improvements	Reference
Austria (AIT)	Coil frost measurements and analyses	• Wind tunnel tests of outdoor heat exchangers (OHX) show multiport extrusion (MPE) compact heat exchangers experience less air flow reduction due to frost growth than conventional tube-and-fin (CTF) heat exchangers at both 10°C and -25°C air temperature (80% RH in both cases); therefore, they can maintain better air flow.	Reichl, et al., 2015; Strehlow, et al., 2015; Popovac, et al., 2015a; Popovac, et al., 2015b
Austria (Technical University, Graz)	Evaluation of compressor liquid injection (LI) for cold climate performance improvement	• Lab tests show LI capability to extend compressor performance envelope for air-water heat pumps down to -20°C or lower with high water supply temperatures • System analyses for several cold climate locations show seasonal COP improvements of up to 12%	Hengel et al., 2013; Zoier,2014; Moisi, et al., 2015
Canada (CanmetENERGY)	Novel SAHP (solar-assisted HP) using ice-based thermal storage	• Lab tests/simulations estimate >60% space and water heating energy savings potential • Potential cost-effective alternative to GSHPs in Canadian climates especially for retrofit applications	Tamasauskas, et al., 2012
	Zeotropic refrigerant mixtures	• Evaluations of potential for zeotropic mixture of R32 and CO2 to improve system efficiency and low temperature capacity • Results show possibility of ~30% seasonal COP improvement with variable mixture composition control components included in heat pump system • Plans to build & test lab prototype	Hakkaki-Fard, et al., 2014; Hakkaki-Fard, et al., 2016
Canada (Hydro Quebec LTE)	Revisions to seasonal efficiency rating standard to better represent heat pump performance in cold climates	• Field testing of ASHP systems pointed out inadequacies in seasonal efficiency rating metrics per Canadian Heat Pump rating standard CAN/CSA-C656-05 for cold climate applications • Office of Energy Efficiency issued bulletin requiring changes in ASHP heating performance ratings and reporting; specifically required adding capacity and COP ratings for -17.8 °C outdoor temperatures by 2014.	NRCan 2010, Office of Energy Efficiency Bulletin 7177, Reporting Cold Climate Performance,
Japan	Coil surface frosting R&D (Waseda University)	• Innovative frost growth measurement & visualization technique (resolution to 0.02 mm) • Frost growth model developed; comparison with measurements for	Yasui, et al 2017 (Conference paper O.1.6.2); Yamashita, 2009; Tao, et al., 1994; Le Gall, et al., 1997

Annex Participants	CCHP Investigated Techniques	Resulting Performance Improvements	Reference
		different surface geometries • Applied frost model to heat pump system model; coil frost growth measured vs. simulated	
	Novel frost-free air source heat pump water heater (ASHPWH) system (Central Research Institute of the Electric Power Industry, CRIEPI)	• System retards frosting by dehumidifying air using a desiccant-coated heat exchanger • Potential for 20-30% boost in COP at a temperature of -7°C and relative humidity of 60-80%.	Zhang, et al., 2017 (Conference paper O.1.6.3)
United States	Two (parallel, equal-sized) compressor field test CCHP prototype (ORNL, Emerson)	• Achieved measured $SCOP_h$ ~3.0 over two winters (2015 and 2016) • 40% energy savings in coldest month; possible to eliminate backup electric heat • Heating COP at -25°C was >2.0; ~3.8 at 8.3°C (including cycling losses)	Shen, et al., 2017 (Conference paper P.1.5.6); Shen et al., 2014
	Novel oil-flooded HP cycle development and evaluation (Purdue University Herrick Labs)	• Approaches isothermal vapor compression process • High oil circulation rates remove heat of compression & significantly reduce discharge temperature, which expanded compressor operation envelope to much lower ambient temperatures • Improvements in heating capacity range up to 19% at the lowest ambient temperature tested (-17.8°C)	Bell, et al., 2011; Yang, et al., 2014; Ramaraj, et al., 2016
Complementary market promotion activities* [*These efforts were conducted independently of the Annex but took place during the Annex working	U.S. Northeast Energy Efficiency Partnership	• Established voluntary CCHP specification; latest version (2017) posted on NEEP web site (see next column) • For variable speed (VS) ASHPs only; requires rated SCOPh ≥2.93 per ANSI/AHRI Standard 210/240 • Web site contains list of nearly 300 ASHPs that meet the requirements; 80% are ductless minisplit or multisplit (VRF) types	Northeast Energy Efficiency Partnerships, 2017
	U.S. Electric Power Research Institute (EPRI), Next Generation (NextGen) Heat	• ASHPs only but VS compressor not required; other capacity control approaches acceptable • Two levels of NextGen specification requirements • Tier 1 requires same rated SCOPh as NEEP CCHP spec above; rated	Domitrovic, 2017

Annex Participants	**CCHP Investigated Techniques**	**Resulting Performance Improvements**	**Reference**
period and will continue for foreseeable future]	Pump specifications	heating capacity at -8.3°C to be ≥80% of rated capacity at 8.3°C; requires control scheme to limit backup heat use; must have demand response capability • Tier 2 requires rated SCOPh ≥3.81; rated heating capacity at -15°C to be ≥80% of rated capacity at 8.3°C; requires control scheme to limit backup heat use; must have demand response capability; only ~7% of ASHPs listed on NEEP site currently meet Tier 2 requirements	

2 COUNTRY SPECIFIC SIGNIFICANT RESULTS AND FINDINGS

2.1 Austria

Two primary research teams comprise the Austrian Annex 41 team. One is the team at the Center for Energy, Austrian Institute of Technology (AIT) in Vienna, led by Dr. Thomas Fleckl and Dr. Christoph Reichl. The other is the Institute of Thermal Engineering (IWT, Institut für Wärmetechnik) of the Graz University of Technology (TU Graz), led by Dr. René Rieberer.

2.1.1 TU Graz contributions

Simulation work has been carried out at IWT in order to investigate the potential of nine different heat pump cycles for cold climate applications, shown in Table ES-4. Simplified simulation models of promising heat pump layouts have been carried out using the Engineering Equation solver (EES) program in order to increase the range of application and efficiency. The investigated refrigerant was R410A.

Table ES-4: Investigated cycle layouts and parameters (according to Zoier, 2014)

Model No.	Description	Stages	Additional parameters
01	Conventional cycle	1	-
02	Cycle with internal heat exchanger (IHX)	1	Efficiency of IHX
03	Cycle with flooded evaporator, low pressure (LP) accumulator (separator)	1	Pump efficiency, Pressure drop in LP cycle
04	Two stage cycle with intercooler	2	Temperature difference to saturation curve, intermediate pressure level (IP)
05	Liquid injection cycle	1	Intermediate pressure level, injection mass flow
06	Vapor injection with internal heat exchanger (IHX or Economizer_IHX)	2	Efficiency of IHX , intermediate pressure level
07	Vapor injection with receiver (Economizer_receiver)	2	intermediate pressure level
08	Cascade system	2	Temperature difference between low and high temperature (HT) cycle, refrigerant
09	Ejector cycle	1	Ejector efficiency

The cascade cycle has shown COP improvements up to 5% compared to the conventional cycle. Vapor injection (VI) with flash tank or with an internal heat exchanger (IHX) shows a COP increase in the range of 4% and 10%, respectively, at -30°C evaporation temperature. The work of Hengel et al. (2013) also showed slight COP improvements for the economizer with internal heat exchanger, especially at higher heating supply temperatures. Intercoolers show a rather high decrease of COP and heating capacity if the heat removed from the intercooler is not used. The IHX cycle resulted in similar values as the conventional cycle and showed no improvement in any category. The liquid injection (LI) cycle caused minor COP losses in a range of 2% but identical heating capacity compared to the conventional cycle. The resulting compressor outlet temperatures could have been decreased within all models except the IHX cycle. The most promising layouts in this regard are cascade, intercooling, and LI, with a drop in compressor outlet temperatures of 19 K, 21 K and 32 K respectively compared to the conventional cycle at an evaporation temperature of -30 C.

An investigation of the LI cycle by Lammert (2013) noted the possibility to enable a significantly larger compressor operation envelope by lowering the compressor discharge temperature, which is of special interest in case of high condensation temperatures (see Figure ES-2). Overall the LI concept does not offer as great an improvement to ASHP efficiency and capacity as does for instance the vapor injection (VI) approach, but it does offer a rather simpler means to allow ASHPs to operate at very low ambient temperatures. This may result in ~10% energy savings compared to a standard heat pump combined with a furnace heating backup (Lammert, 2013).

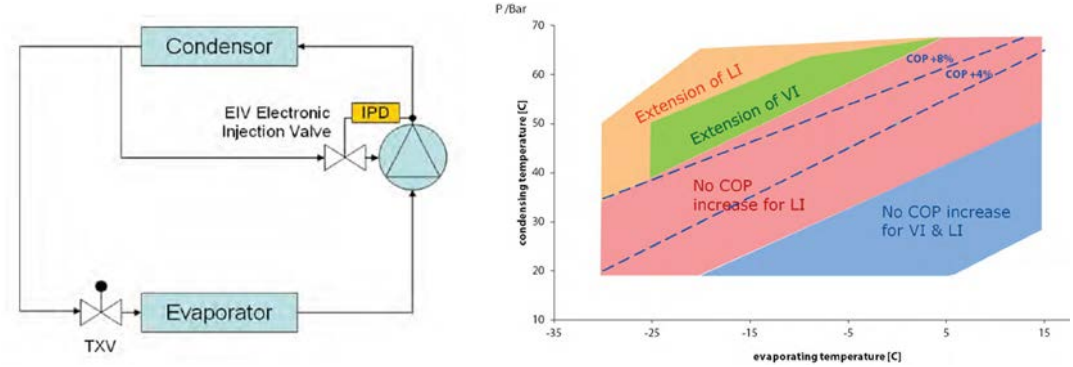

Figure ES-2: Liquid injection: basic layout (left); compressor envelope (right) (Lammert, 2013)

Based on the simplified calculations, a more detailed model of the LI cycle was set up. For the calculation of the heat transfer, the evaporator and condenser are divided into different sections considering phase transformation (gaseous, two phase and liquid). Estimated supplier provided U-values have been applied for each individual section. Moreover, area fractions of the heat exchangers for each section depending on the pressure level and temperatures are calculated to estimate the two-phase flow along the heat exchanger. Initial temperatures derived from ambient temperature and water outlet temperature are applied to start the pressure iteration process. The refrigerant mass flow as well as isentropic efficiencies for the high and low pressure stage can be calculated according to polynomial functions given by manufacturer data in dependence of p_{evap} and p_{cond}. The air volume flow is also given by manufacturer data and remained constant. The state of ambient air has been defined by temperature, pressure and relative humidity. The injection is controlled by means to a temperature threshold. If the discharge temperature of the high stage compressor is below this threshold, injection is inactive. The injection mass flow can then be calculated iteratively by comparison of the current discharge temperature (T_{cond_in}) with the set maximum compressor outlet temperature (T_{VI}).

The LI cycle was been chosen for more detailed study for two primary reasons. First, it has a less complex layout compared to the cascade and economizer systems. Secondly, it has the ability to increase the range of heat pump application for cold climates in terms of compressor outlet temperature. Furthermore, a LI prototype air-to-water heat pump (AWHP) was available to carry out experimental analysis. The detailed model considers heat transfers on the heat sink and heat source heat exchanger and calculates the resulting evaporation/condensation pressure level iteratively. Furthermore polynomial functions provided by manufacturer data are used to describe the volumetric efficiency of the compressor and the isentropic efficiencies based on evaporation and condensation temperature.

Lab test results with the LI prototype (Zoier, 2014) are shown in Figure ES-3. The effect of the refrigerant injection on compressor discharge temperature is clear especially for the highest water outlet temperatures (W55 and W60). The injection allows an extension of compressor operation for low ambient temperatures, especially at high water temperatures

and thus pressure ratios as suggested by the analyses. The discharge temperatures under the lower water outlet temperature conditions (W35 and W45) were below the defined threshold (125°C) for LI activation at all times hence the refrigerant injection was not active. However, the discharge temperature at -19°C and W45 was 126°C without injection activation which might be caused by a measurement error.

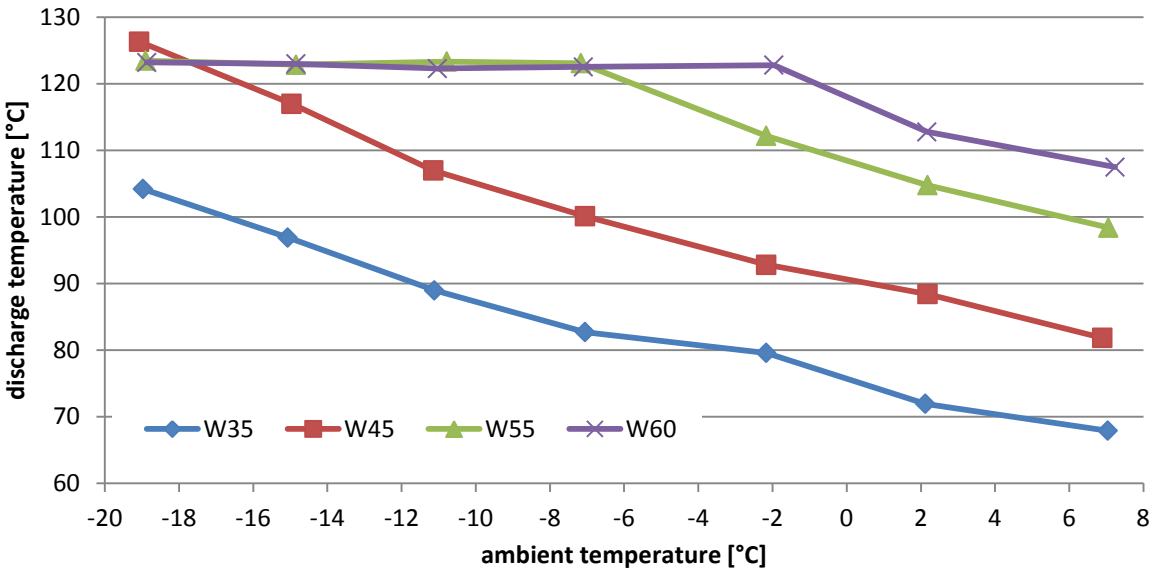

Figure ES-3: Discharge temperature in dependence of water outlet and ambient temperature according to Zoier (2014)

An assessment of an LI cycle AWHP system was conducted to calculate energy savings compared to a conventional AWHP without LI in five cities (Anchorage, Graz, Helsinki, Minneapolis, and Moscow). It must be noted that while the results are overestimated quantitatively compared to the experimental data (Moisi et al., 2015), they do illustrate a qualitative trend. With a water supply temperature of 35°C, no injection is needed at all and no difference was seen between the SPF results for the conventional and LI AWHP systems. A difference between the conventional and the LI systems is observed at a water supply temperature of 45°C (Figure ES-4). With increasing operation time of the LI System at lower ambient temperatures (approx. below -20°C), the SPF improvement compared to the conventional system increases since no backup heater is necessary. In the case of Minneapolis for example, an SPF improvement of 12% can be achieved compared to the conventional system. On the other hand, Graz shows no effect at all since the minimum ambient temperature is too high for the activation of liquid injection (approx. -12°C). However, the threshold ambient temperature for the injection activation is dependent on the control strategy. Another fact is clear, that with an increasing heat supply temperature this threshold rises to higher ambient temperatures. Therefore, a liquid injection system can be interesting for more moderate climates and high temperature heating systems in the course of refurbishments in order to realize a monovalent heating system as well as for hot water production.

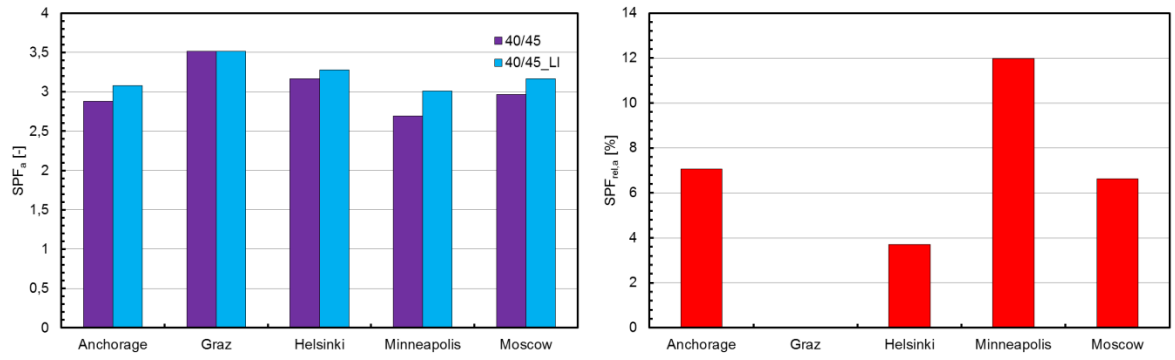

Figure ES-4: Comparison of SPF (left) and relative SPF improvement (right) for LI and conventional AWHPs with a 45°C water supply

A LI system can increase the range of application to lower ambient temperatures. Compared to a conventional air source heat pump system with a direct electrical backup heater, annual efficiencies can be improved depending on the time the heat pump operates at lower ambient temperatures.

2.1.2 AIT contributions

The AIT team technical contributions to Annex 41 focus on improving AWHP evaporator performance. This is a part of the EU Green Heat Pump Project (EU-FP7 research project) coordinated by AIT with contributions from several European industrial partners as well as research institutes (Zottl, 2016). Figure ES-5 illustrates the overall EU-FP7 project approach.

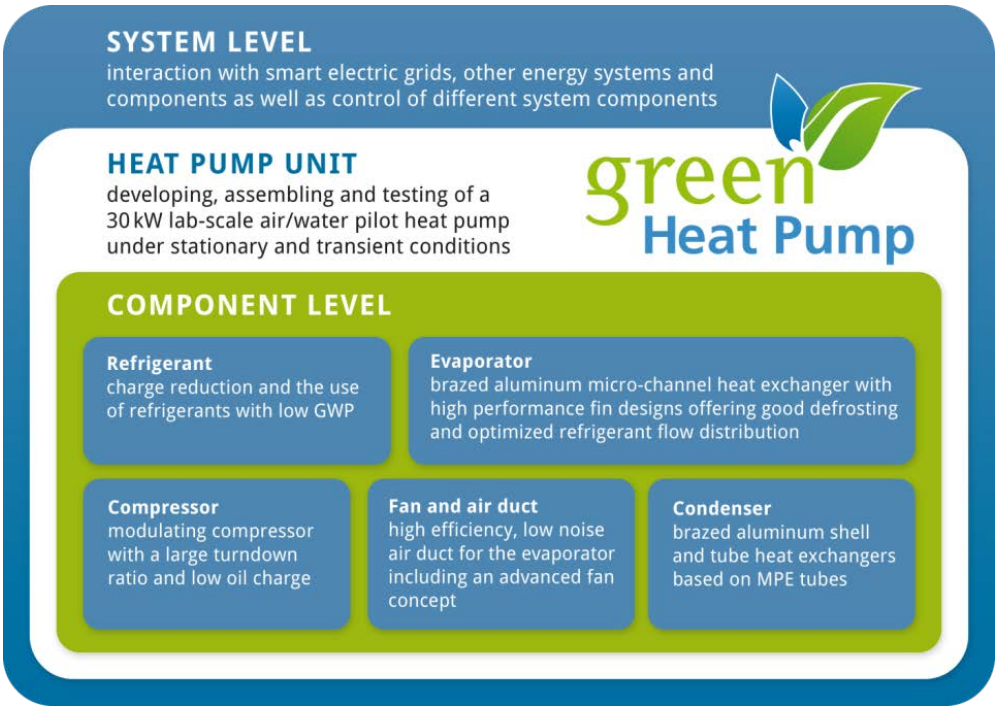

Figure ES-5: EU-FP7 Green Heat Pump project objectives (Zottl, 2016)

AIT's research activities were focused on the investigation of evaporator frosting in cold climates, in search of an evaporator design with good frosting/defrosting performance and optimized refrigerant distribution. A small-scale wind tunnel test apparatus was constructed at AIT for experimental evaluation of the frosting performance of candidate fin designs for the system multiport extrusion (MPE) compact heat exchanger evaporator design. Figures

ES-6 and ES-7 show a photograph and schematic of the wind tunnel. Seven different fin designs were mounted on an MPE tube and tested in the wind tunnel. Figure ES-8 and Table ES-5 illustrate a sample MPE compact heat exchanger with the tested fin characteristics and dimensions. Results for icing time (t_{ICE}; the longer, the better) and average heat transfer duty (the greater, the better) are shown in Table ES-6. Both wavy fin designs showed reasonable balance between long icing times and high mean heat transfer, and are recommended for the system evaporator designs.

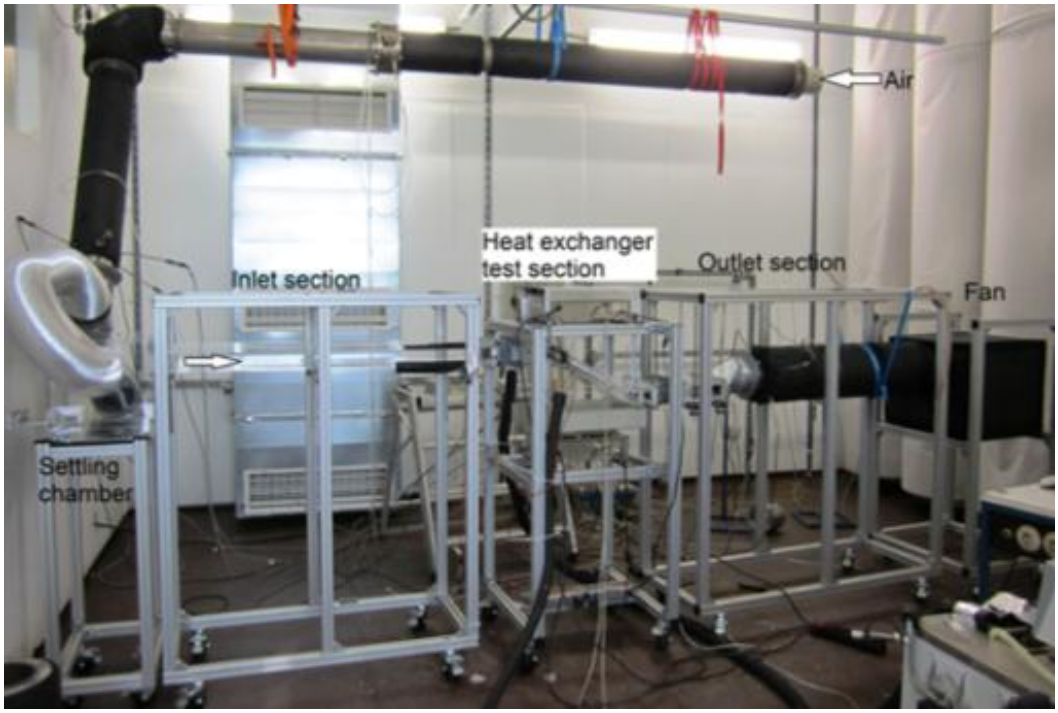

Figure ES-6: Small-scale wind tunnel at AIT (Zottl, 2016)

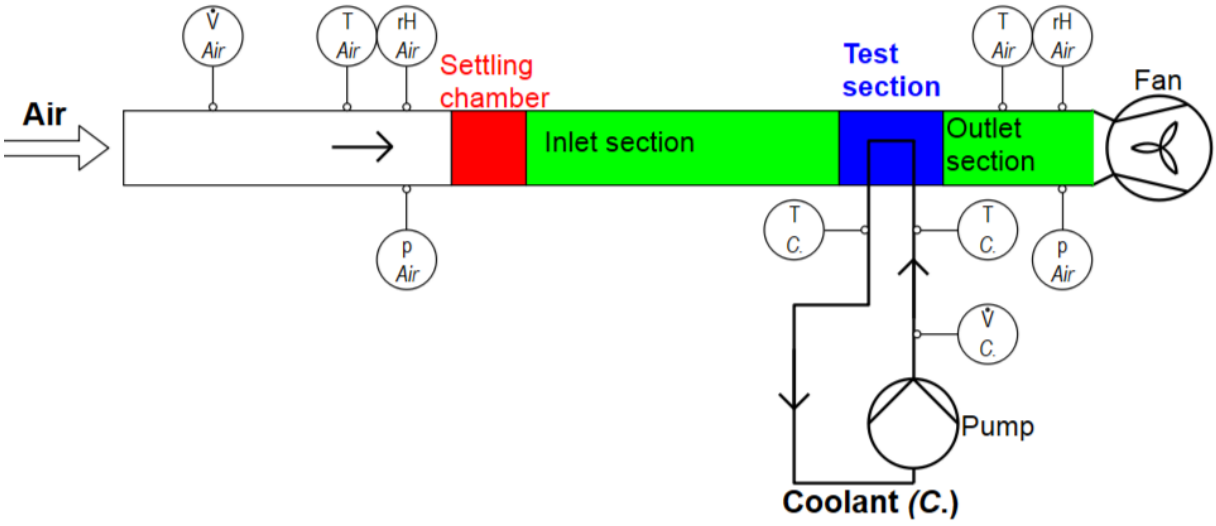

Figure ES-7: Wind tunnel diagram showing instrumentation scheme (Zottl, 2016)

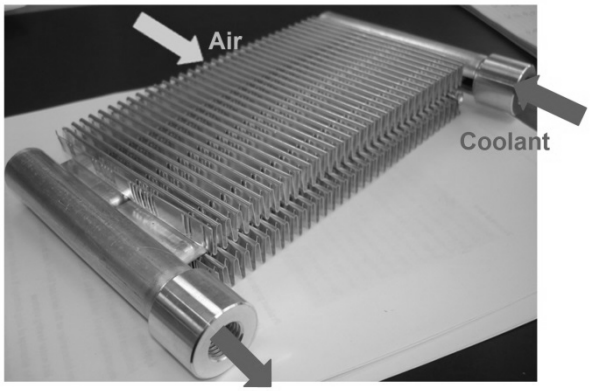

Figure ES-8: Typical fin sample with wavy fins mounted on a MPE tube

Fin / Name of the sample	Height	Pitch
Plain fin #1	10,4 mm	5,0 mm
Plain fin #2	10,4 mm	10,0 mm
Wavy fin #1	10,4 mm	5,0 mm
Wavy fin #2	10,4 mm	8,0 mm
Lanced fin #1	10,0 mm	4,8 mm
Louvered fin #1	10,4 mm	5,3 mm
Plain/louvered fin #1	10,4 mm	--

Table ES-5: Summary of fin samples tested

	Mean values	
Fin / Name of the sample	t_{ICE}	$\dot{Q}_{mean}$
Plain fin #1	3059 s	156 W
Plain fin #2	4688 s	104 W
Wavy fin #1	2380 s	166 W
Wavy fin #2	3767 s	135 W
Lanced fin #1	1300 s	163 W
Louvered fin #1	1766 s	167 W
Plain/louvered fin #1	883 s	117 W

Table ES-6: Fin frosting performance test results (Zottl, 2016)

Wind tunnel tests determined that the MPE heat exchangers have better frosting characteristics than conventional tube-and-fin (CTF) heat exchangers. This can be seen in Figure ES-9, which depicts evaporator frost accumulation rate vs. time, and shows that the resulting reduction of air flow through the evaporator (relative to the maximum flow rate) is less for the MPE and the CTF case. The MPE evaporator has been included in research toward developing an innovative AWHP system prototype. Shown in Figure ES-10 is a comparison of measured frost distribution (left side) to simulated frost distribution (right side) resulting from the refrigerant temperature variation inside the evaporator. The view is looking from above onto the horizontally mounted heat-exchanger with refrigerant entering from the bottom of the figure. The blue bars indicate horizontal sums and vertical sums for each condensate weighing station. Horizontal bars to the left of the left-side graph show that frost builds up predominantly at the refrigerant entrance while the vertical bars indicate the extent of refrigerant fluid maldistribution. Simulation results on the right-hand side of Figure ES-10 are similar to the measured results on the left-hand side.

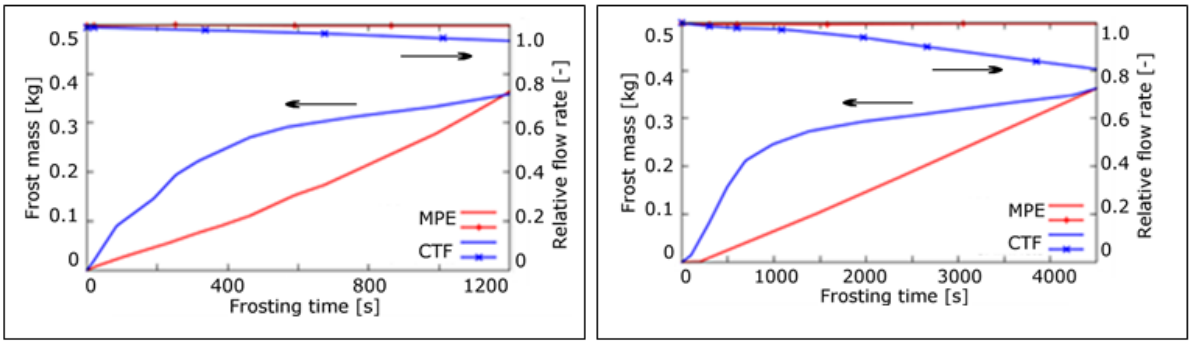

Figure ES-9: Frost mass growth and relative flow rate for advanced (MPE) and standard (CTF) heat exchanger configurations, at ambient temperatures 10°C (left) and -25°C (right)

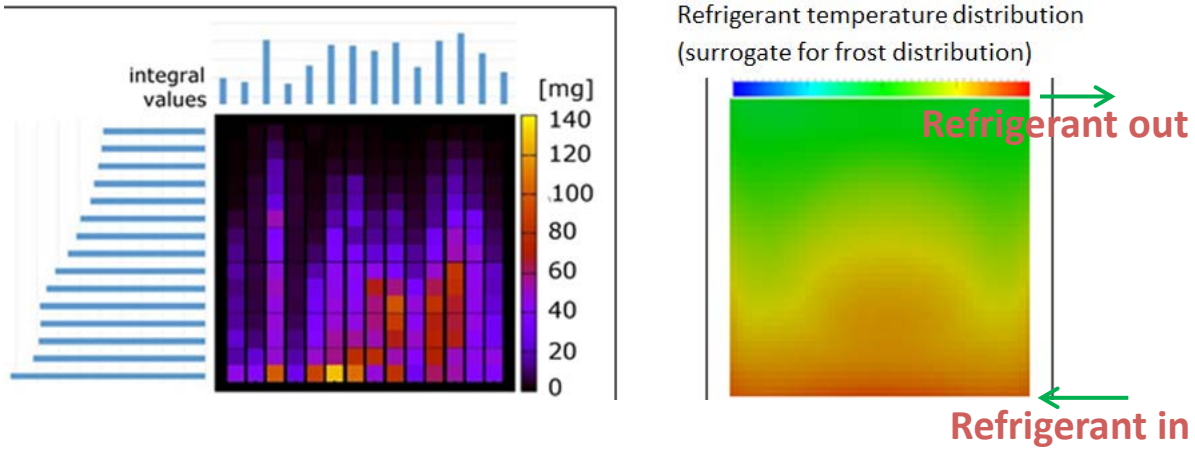

Figure ES-10: Measured (left) vs. simulated (right) frost distribution on MPE evaporator from AWHP system tests

2.2 Canada

Canada has two research institutes comprising its Annex 41 team. One is at CanmetÉnergie of National Resources Canada led by Dr. Daniel Giguère. The other is at the Laboratoire des Technologies de l'Energie (LTE) of Hydro-Québec led by Dr. Brice Le Lostec.

In Canada space heating is responsible for 64% and 50% of the energy use for residential and commercial buildings, respectively. Water heating is second with 17% and 8%, respectively. Heat pumps have potential to significantly reduce buildings energy use but current ASHP technology has poor performance in most Canadian locations, typically in cold or very cold climate regions. GSHPs can provide significant energy savings but are still too expensive to penetrate much of the Canadian market.

2.2.1 CanmetENERGIE Contributions

CanmetÉnergie's R&D activities related to CCHP technologies aim to improve the efficiency and cost effectiveness of several heat pump system types for the Canadian market. Their R&D for Annex 41 focused on four main areas (Giguère, 2014):

1. Advanced vapor compression (VC) cycles, with a focus on the ejector-compressor hybrid cycle
2. GSHP technology using carbon dioxide (CO_2) as the ground loop fluid and as the heat pump refrigerant

3. Solar-assisted heat pump (SAHP) system using an ice slurry fluid
4. Use of refrigerant mixtures with moderate to high temperature glides in ASHP systems

Ejector-Compressor Hybrid Cycle

While the hybrid ejector/compressor system is relatively simple in concept (Figure ES-11), the main development challenge lies in understanding well the two-phase-flow that takes place inside the ejector component. Current ejector research findings are not well described in the literature.

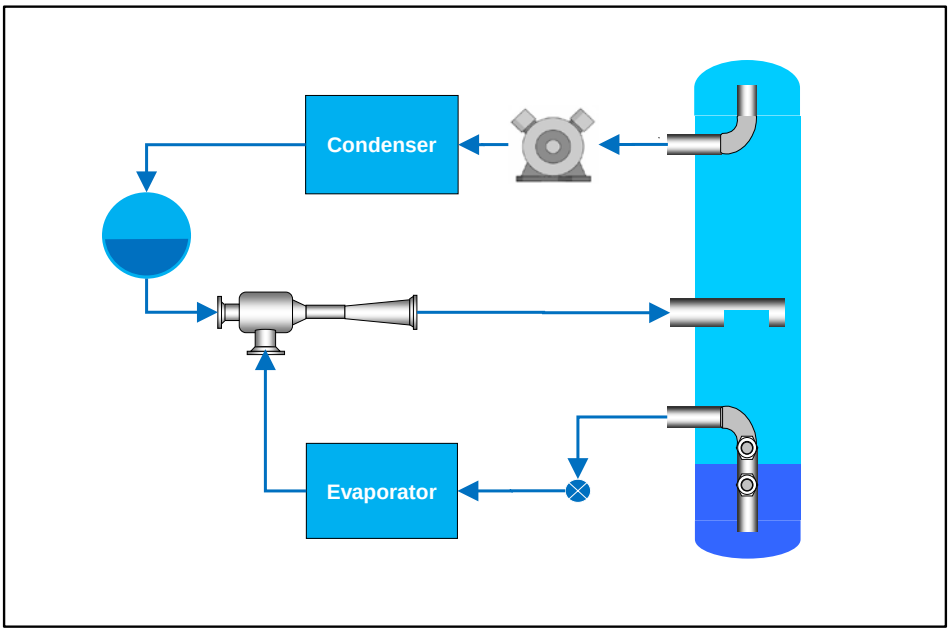

Figure ES-11: An example of a hybrid ejector/compression air-source HPs

To gain a better understanding of the two phase flow ejector and integration into a heat pump, a hybrid ejector/compressor test bench for heating applications was constructed and some tests performed under a previous research project. The test bench uses a variable speed compressor combined with an electronic expansion valve for maximum flexibility of operation. Its nominal heating capacity is 10 kW, which corresponds to the typical capacity of residential and light commercial applications. This test bench has been upgraded for this project with the refrigerant recently replaced from R410A to R134a due to partial fractionation occurring in the separator. Preliminary results have shown appropriate compression ratios; however, entrainment ratios would need to be improved. Our efforts are now directed towards the development of a better ejector for R134a (current ejector in test bench was designed for R410a) that will lead to higher entrainment ratios.

Coupled with the hybrid ejector/compressor test bench, a second test bench, dedicated solely to the study of the two phase ejector component was also constructed for this project. Capable of inducing a wide range of operating conditions, the two phase ejector test bench will generate in- depth knowledge and experimental results used to validate numerical models.

These experimental activities, coupled with the modeling work and validation of results, will significantly improve our knowledge on the design of two-phase-flow ejector components and heat pump systems.

Solar-Assisted Heat Pump System

SAHP systems, which rely on solar energy to supply or supplement heat pump operations, offer an attractive alternative to ASHPs and GSHPs more commonly found in the Canadian market. Solar based systems are often challenging to design and implement because they (i) require significant thermal storage capacity to bridge the temporal discrepancy between solar availability and thermal demand, and (ii) experience reduced collector efficiencies in the winter months when thermal demand in cold climates is highest. To address these issues, Canmet has worked extensively on the development of a new SAHP concept using ice-based latent storage.

Figure ES-12 is a schematic of the SAHP system (for both space heating and water heating) that was investigated by the team. The thermal storage tank in the schematic contains an ice slurry mixture that is circulated between the solar collectors and the evaporator of the heat pump when in SAHP operation mode.

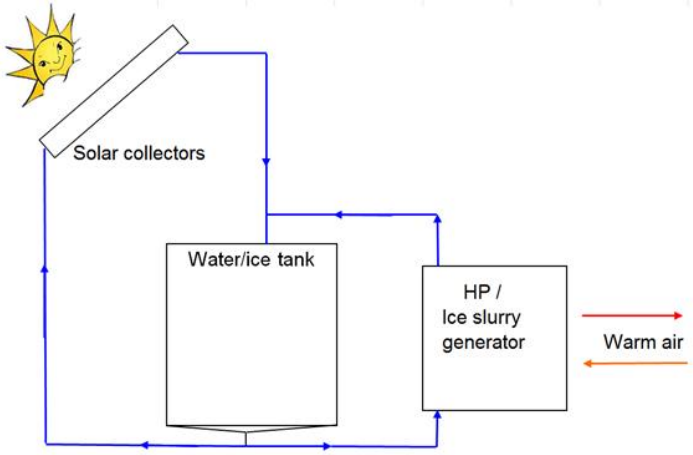

Figure ES-12: Solar-assisted heat pump system

Using validated energy models, it is estimated that such a system can reduce the energy use for space and domestic water heating in high performance homes between 61% and 66%, depending on the location of the building. Table ES-7 summarizes projected system sizing for typical existing homes in Eastern Canada. Provided that the ice generation/storage technology can be sourced at a reasonable cost, the proposed SAHP offers a cost-effective alternative to the current generation of GSHPs and is particularly interesting for retrofit applications where it may be difficult to add ground heat exchangers.

Table ES-7: Suggested SAHP design parameters for typical Canadian housing

Parameter	Suggested Value/Range
Solar Collector Area	30 m^2 to 40 m^2
Ice Storage Tank Volume	Approx. 5 m^3
Heat Pump/Ice Generator Capacity	10 kW (3 tons)

CO_2 in GSHPs

GSHPs are one of the most efficient commercially available space heating systems in Canada – typically yielding a high annual COP (~3) and reducing the space heating energy consumption by up to 65%. Typically high first costs remain a barrier to widespread market adoption and thus the main objective of the project is to find ways to reduce the initial

investment cost or further increase the efficiency of the system to make it a more attractive solution. Furthermore, with the phase-out of HCFC refrigerants now in effect for new equipment and the next step phasing down HFC refrigerants, several projects are evaluating the feasibility of using CO_2 as the working fluid. CO_2 has a low global warming potential and the thermo-physical properties provide several advantages.

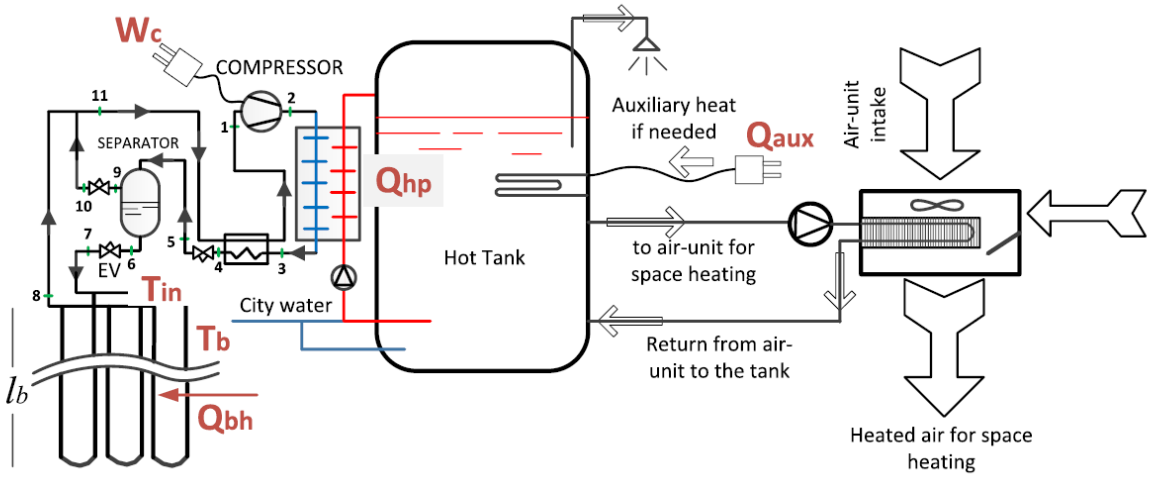

Figure ES-13: CO_2 GSHP-DX system

The objective of this work is to contribute to the advancement of underground heat extraction technologies using CO_2 as a phase change fluid carrier and to provide a cost effective and environmentally friendly alternative to GSHP systems commercially available today. One proposed configuration is as shown in Figure ES-13. The work consists of conducting experimental work on a new test bench at Canmet facility and developing simulation models to support the optimization of CO_2 ground loop configuration and operation.

CO_2 is much less sensitive to pressure drop than synthetic refrigerants, which enables the downsizing of the borehole U tube diameter. The underground heat exchanger performance is 13.6 m/kW, which compares favorably to the conventional secondary fluid borehole that shows 17 to 26 m/kW with 20 mm to 50 mm pipe diameters. The seasonal COP of the heat pump increases by 21% for a 150% increase in borehole length. For the same scenario, the heating capacity of the heat pump increases by 15%. This demonstrates the importance of the borehole sizing on the efficiency of the heat pump.

This work shows the importance of the proper sizing of the heat pump capacity for a specific application. GSHPs show the lowest energy consumption, but ASHPs remain the most attractive heat pumping option for residential users. Future work on GSHPs should continue to address overcoming the high cost or achieving improved seasonal efficiency by meeting DHW loads in addition to space heating loads.

Refrigerant Mixtures

The use of refrigerant mixtures is becoming more and more common in air conditioning and refrigeration. In 1965, the ASHRAE Guide and Databook Fundamentals and equipment published three azeotropic refrigerant mixtures: R500, R501 and R502. In 2013, the 'ASHRAE Handbook Fundamentals' listed 65 zeotropic mixtures and 14 azeotropic mixtures. This number is growing each year. These new blends meet the need of the market which must deal with the phase-out and phase-down of CFCs, HCFCs and HFCs. To replicate the

performance and characteristics of these refrigerants for specific applications it was necessary to create this diversity of mixtures.

One of the features of zeotropic blends is the temperature glide (Figure ES-14). At constant pressure, the mixture boiling temperature (bubble point) is lower than the condensing temperature (dew point). By matching the temperature glide of the refrigerant with the temperature glide of the fluid to cool in an air conditioning or chiller system, a 10 to 15% COP improvement can be achieved with a temperature glide of 5.5°C. If the application allows a temperature glide of 10°C, the COP of the heat pump could be improved by up to 30% theoretically.

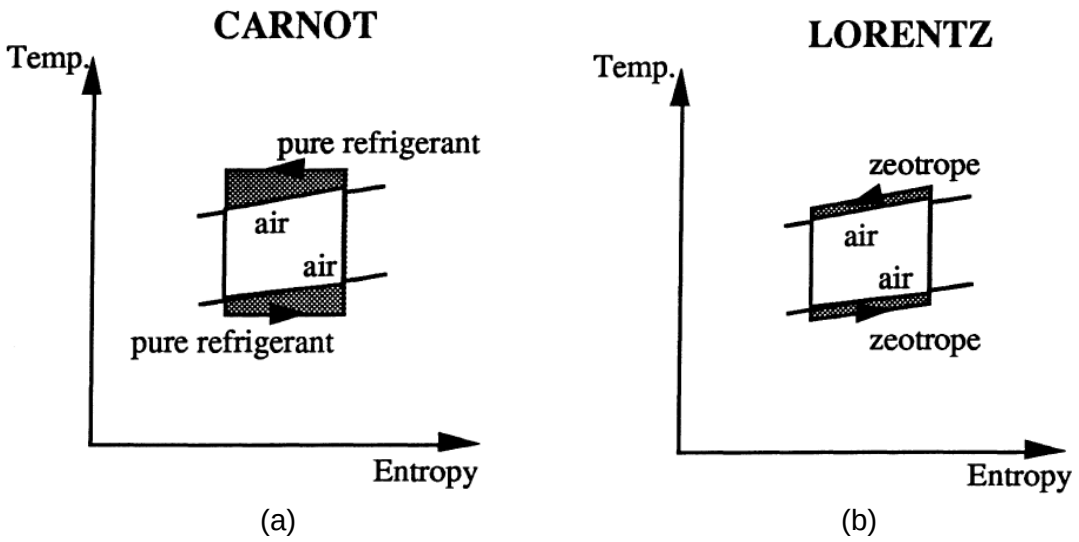

Figure ES-14: (a) Typical Carnot refrigeration cycle (b) Lorentz cycle demonstrating temperature glide

A heat pump simulation model was developed to assess the benefits of different refrigerant blends without modifying the main heat pump system components: compressor, evaporator and condenser. Among all the mixtures studied, R32/CO_2 (80/20) mixture presents better performance potential for this study. The mixture is non-toxic with a GWP of approximately 540, which is 75% lower than the GWP of R410A. Moreover, it is a zeotropic mixture with approximate temperature glides of 6°C and 8.5°C in the evaporator and condenser respectively.

To assess the performance of various refrigerant mixtures, residential building energy models were used. Five refrigerant cases were simulated using the same heat pump components:

- Case 1 (reference case): Standard R410A air source heat pump, with a nominal heating capacity of 7.7 kW at 8°C outdoor temperature. This unit meets 75% of the total space heating load, so 25% of the load was provided by the auxiliary heating system.
- Case 2: Same as reference case with a variable speed compressor
- Case 3: Fixed mixture of 80% R32 and 20% CO_2
- Case 4: Variable composition (VC) mixture R32 - CO_2 with a reservoir located at the compressor suction to manage the concentration of CO_2
- Case 5: Fixed 80% R32 and 20% CO_2 with a variable speed compressor

The results of the simulation are summarized in Table ES-8 with the heat pump (HP) contribution indicating the percentage of the annual heating capacity met by the heat pump and the seasonal COP of the system.

Table ES-8: Simulation results for five refrigerant mixture cases

Refrigerant Case	Capacity	HP contribution	COP seasonal
	kW	kWh/kWh	kWh/kWh
R-410A	7.7	75%	2.16
R-410A VSD	7.7	91%	2.73
R32-CO2 80/20	8.1	84%	2.46
R32-CO2 VC	9.0	93%	2.81
R32-CO2 80/20 VSD	8.1	97%	2.98

These simulations show a potential COP improvement of ~14% (2.46 vs. 2.16) just by swapping the refrigerant in a heat pump. But, the COP could be improved by ~30% (2.81 vs. 2.16) if the basic mechanical design of the heat pump was modified to include VC control. In other words, to get the total benefit of the refrigerant mixture glide, the air flow rates and the air coils' circuiting should be revised or redesigned. The design of refrigerant mixtures is a promising approach for heat pumps COP improvement. The next steps in this project will be to confirm experimentally the performances predicted by the model and to design a heat pump unit adapted to refrigerant mixtures with a strategic temperature glide.

2.2.2 Laboratoire des Technologies de l'Energie (LTE) Contributions

Previous to its involvement in the Annex 41 program, Hydro-Québec's LTE had conducted laboratory and field testing of air-to-air and air-to-water heat pump systems (Dumont & Le Lostec, 2014). The lab testing involved a cold climate system design, and tests have been conducted for outdoor temperatures down to -25°C (-13°F). Field-tested systems included the cold climate design, conventional ASHPs, and ductless ASHPs.

LTE's R&D under Annex 41 focused on:

1. Quantifying efficiency improvements of traditional air-source heat pumps, ASHPs, utilizing cycle enhancements – two-stage and variable-speed compressors and vapor-injection
2. Analysis of the C656 standard (CSA (2006, 2014)), Canadian heat pump efficiency test standard, to understand its limits and identify areas for improvement

<u>Enhanced Air-Source Heat Pumps</u>

In order to foster the emergence of cold climate heat pumps on the market, efforts are being made at Hydro-Québec's energy technology laboratory (LTE) to characterize the equipment and propose solutions to promote the deployment of numerous air-source heat pump technologies.

The field test results of this study, shown in Figure ES-15, demonstrate that ASHPs installed according to current practices allow them to generate significant annual energy savings of between 25% and 30% in the case of conventional heat pumps and between 45% and 50% in the case of variable speed heat pumps as compared to resistive heating equipment. Variable speed heat pumps therefore generate greater energy savings than conventional heat pumps; however this remains difficult to precisely quantify due to the small number of samples. It is important to mention that the quality of the installation of heat pumps has an impact on the performance of the overall heating system. The airflow, refrigerant load and heating equipment controls (or the interaction between the various devices) are factors that should not be overlooked when they can have a significant impact on the generation of energy savings, and this applies for the entire life cycle of the equipment. Furthermore,

unless a major problem occurs (a refrigerant leak for example), it is difficult for an individual to identify when a heat pump's operation is less than optimal because of poor installation practices.

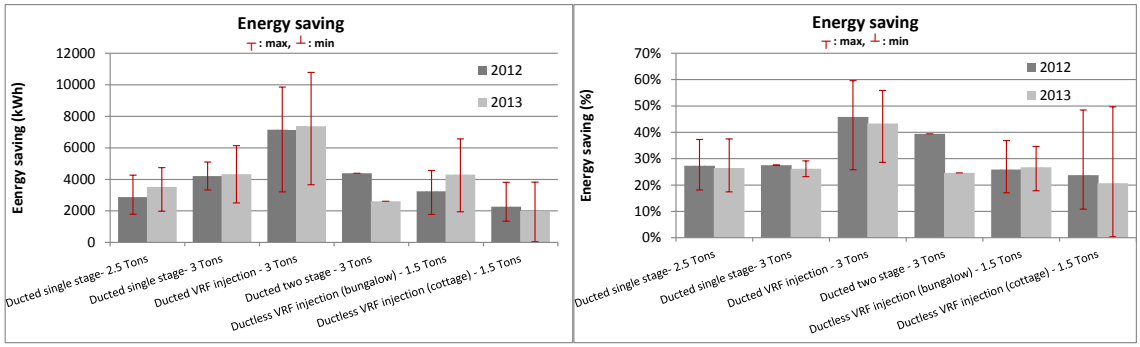

Figure ES-15: Energy savings by heat pump category

Our measurement campaign also demonstrated that rated HSPFs as defined by CAN/CSA-C656-05 (similar procedure as AHRI 210/240) is not a criterion adapted to represent energy savings although there is a link between the average coefficient of performance of the systems we studied and the HSPF. It should be noted that the Office of Energy Efficiency (OEE) issued a publication in 2010, *Bulletin on Reporting Cold Climate Performance* (http://www.nrcan.gc.ca/energy/regulations-codes-standards/bulletins/7177), recommending modifications to CAN/CSA-C656-05 so that the performance of heat pumps used in cold climates is better represented in the standard. One requirement from this modification was additional standard testing to report heating capacity and COP at -17.8°C (0°F) be put in place by January 1, 2014. This would require that standardization labs be in a position to meet the criteria of the tests proposed by the OEE.

CAN / CSA C656 Standard

If the HSPF is a selection criterion for a potential Program on heat pumps, it is important to know the limitations and work to close the gaps, either by modifying the calculation of HSPF and/or establishing criteria to meet the needs. HSPF, which is a standardized performance criterion, does not result in energy savings predictions that are representative of what is observed in the field. Moreover, with the advent of new technologies such as variable speed compressors with or without refrigerant injection (vapor or liquid), the current HSPF calculation procedure does not give a realistic energy saving difference between the different technologies (Figure ES-16). This is explained partly by the calculation assumptions which aim to idealize the operation of heat pumps below the balance point. For some heat pumps with variable speed, including wall units, low temperature standard capabilities (-8.3°C) are not always based on the maximum speed of the compressor. Therefore, it is difficult to rely on this criterion to identify the most efficient equipment.

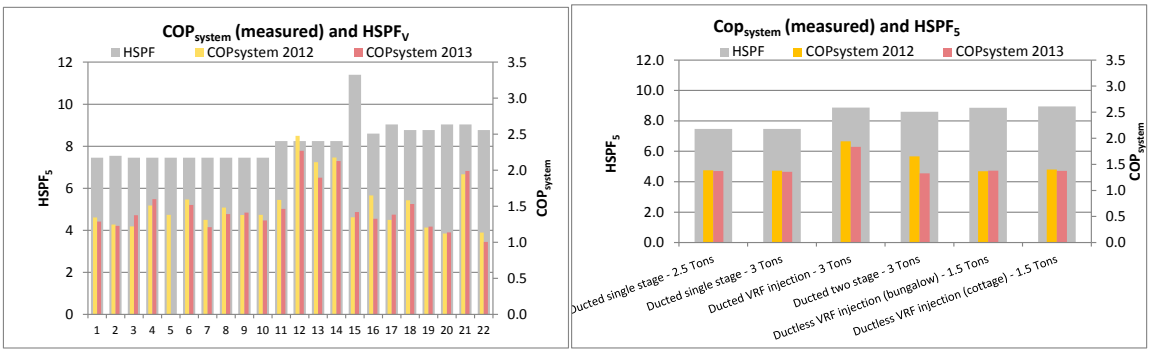

Figure ES-16: HSPF of heat pumps

In general, the modification of a standard is relatively tedious. Different actors have different interests that must be taken into account. For example, when revising the Energy Star label, manufacturers were concerned about the workload that could represent the addition of low temperature standardized tests and take into consideration regional weather conditions rather than national. Therefore, if an amendment to the C656 standard should be carried out, it would be appropriate that these changes are also made to the American AHRI 210/240 in order not to create obstacles to the development of the Canadian market. One way not to be overlooked is the job of Annex 39 of the IEA, which aims to standardize internationally the heat pump performance criteria.

2.3 Japan

Japan has a large Annex 41 team (Table ES-9) consisting of experts from national organizations for professional heat pump technology research.

Table ES-9: Japan Annex 41 team organization

Leader	
Prof. Katsuta, Waseda University	
Secretary	
Takeshi Hikawa (**HPTCJ)	
Board Members	
Prof. Koyama, Kyushu University	Prof. Ohkubo, Tamagawa University
Prof. Shikazono, the University of Tokyo	Prof. Saito, Waseda University
Prof. Fukuta, Shizuoka University	Associate Prof. Asano, Kobe University
Prof. Kagawa, National Defense Academy of Japan	Dr. Hashimoto, Central Research Institute of Electric Power Industy (CRIEPI)
Plus researchers from industries (Mitsubishi Electric, Mitsubishi Heavy Industries, Daikin, Toshiba Carrier, Hitachi Appliance), and electric power companies (Hokkaido Electric and Tokyo Electric)	
NEDO*: Official Contracting Party, Delegate to IEA Heat Pumping Technologies Program	

*NEDO: New Energy and Industrial Technology Development Organization
**HPTCJ: Heat Pump & Thermal Storage Technology Center of Japan

The annual energy consumption per household in the cold climate area of Japan (e.g., Hokkaido) is about 1.7 times as high as compared to that in the mild temperature area (e.g., Kanto or Tokyo). Space heating and water heating account for about 80% of the total energy usage (Figure ES-17) presenting a significant opportunity for energy and cost savings. Due to the energy conservation needs, several ASHP systems for cold climate areas were developed relatively early and already marketed in Japan. Japan's R&D contributions to Annex 41 have been primarily focused on better understanding of OHX frosting/defrosting performance to facilitate development of a heat pump system model with an improved OHX

frost model. The new model is expected to help developed improved cold climate ASHP systems in the future. A number of early stage advanced system developments have also been described along with advances in properties research for R32 (a leading refrigerant candidate for future heat pumps, alone or in blends).

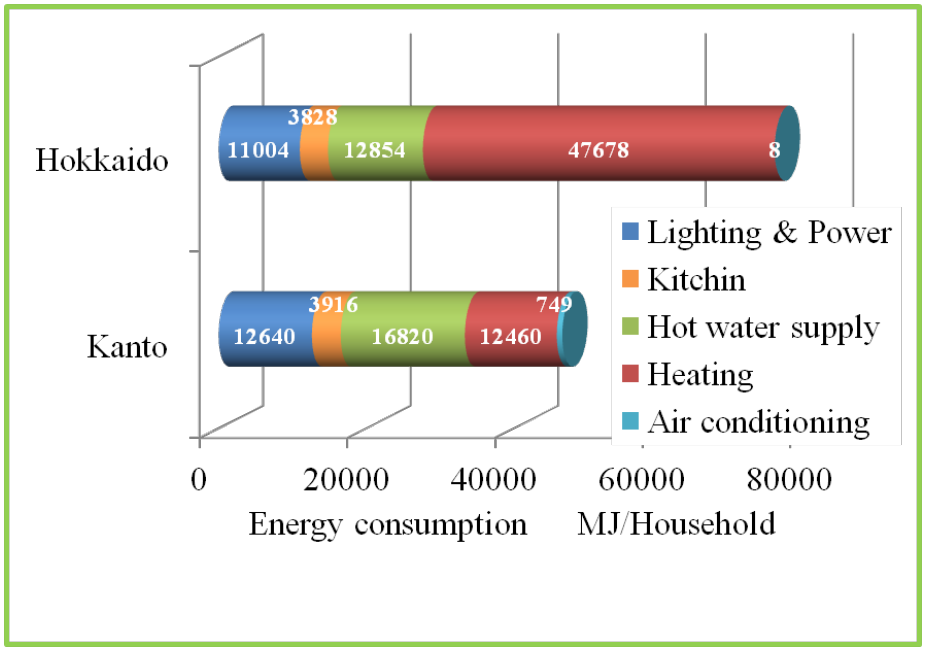

Figure ES-17: Annual energy consumption per household in the cold climate area

2.3.1 Task 1 literature & technology review

A comprehensive review was performed in primarily two areas: cold-climate heat pumps and fundamental research on frost formation in heat exchangers. Recent developments in R32 thermophysical property measurements and models were also reported.

The cold-climate heat pump review encompassed several publications that focused on the functionality and improvement of heat pumps and air conditioners working in cold climates (-25°C). Emphasis was given to novel architecture and packaging as well as heat exchanger modifications to improve performance. A number of ASHP products (mostly single-zone and multi-zone ductless types) with improved cold climate performance have been introduced to the market by Japanese manufacturers (Mitsubishi, Toshiba, Hitachi, Daikin, others). They employ a number of heat pump cycle innovations including variable speed compressor technology, vapor injected compressors, liquid injected compressors, etc. Rated performance characteristics show capability to maintain heating capacity at 70% to 90% of rated capacity down to -20°C to -25°C outdoor temperatures. Most meet the requirements of recently released cold climate heat pump specifications by the U.S. Northeast Energy Efficiency Partnership (NEEP). These developments demonstrate the technical feasibility to develop ASHPs with significantly improved cold climate heating performance compared to conventional products.

The second component of the literature review focused on fundamental frost formation simulations and calculations as well as experimental results for validation and discussion of various setup regimes that affect heat exchanger performance. The literature went on to detail models for frost formation and heat flux at different frosted conditions. Conclusions were drawn that wettability of the cooling surface significantly affected the physical force required for removal. In Tasks 2 and 3 the frost model was developed further and

incorporated into an ASHP system model for use in analysis and design of future heat pump systems.

Finally, in order to use any refrigerant, especially a relatively new one like R32, reliable and accurate thermophysical property information is required. Accurate isobaric heat capacity (c_p) data is one of pieces of information needed to design application systems. Hozumi et al. (1994) reported speed of sound of gaseous R32 at temperatures from 273 K to 343 K and at pressures from 0.02 MPa to 0.25 MPa. Kubota et al. (1995) reported 18 R32 c_p measurements in the gas phase obtained from 303 K to 343 K and from 0.12 MPa to 0.5 MPa by using a flow calorimeter. Kagawa et al. (2012a) reported 32 c_p measurements similarly obtained from 274 K to 353 K and from 0.65 MPa to 2.4 MPa. More recently Kagawa et al. (2012b) reported on additional R32 c_p data obtained at temperatures from 282 K to 319 K and at pressures from 1.0 MPa to 2.4 MPa. These data sets have been used to evaluate several equations of state (EOS). In addition curves of the isobaric ideal-gas heat capacity ($c_{p,0}$) and the vapour saturation heat capacity (c_p") of R 32 were determined using the data (Kagawa et al, 2012b). The data along with the derived curves of $c_{p,0}$, and c_p" and the EOS evaluated are shown in Figure ES-18. These data will be very useful for improving available models so as to represent reliable thermodynamic properties of R-32 and refrigerant mixtures with R-32 that are used for cold climate A/C and heat pump systems.

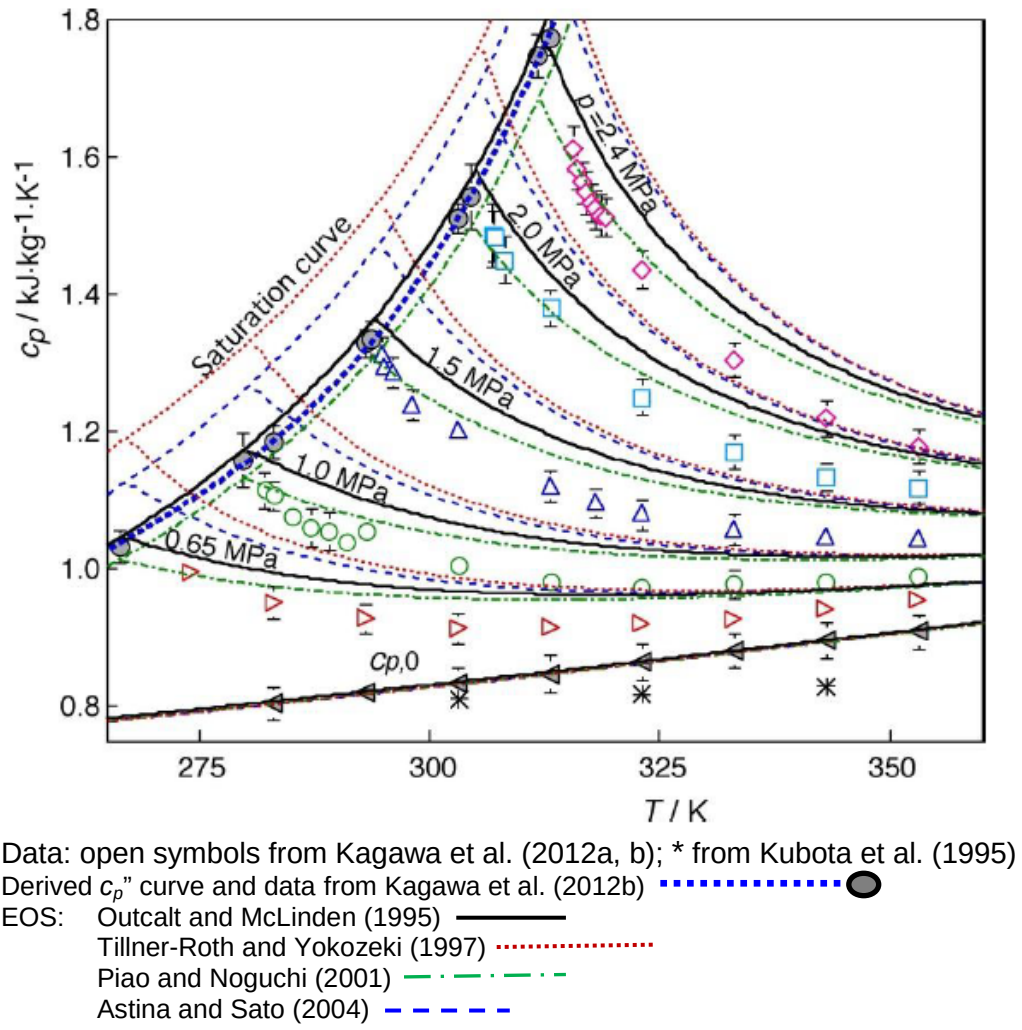

Data: open symbols from Kagawa et al. (2012a, b); * from Kubota et al. (1995)
Derived c_p" curve and data from Kagawa et al. (2012b)
EOS: Outcalt and McLinden (1995)
Tillner-Roth and Yokozeki (1997)
Piao and Noguchi (2001)
Astina and Sato (2004)

Figure ES-18: Isobaric heat capacity measurements for R-32 – experimental data (symbols) vs. several equations of state, EOS (lines)

2.3.2 Task 2 and 3 highlights

To further investigate potential improvements of refrigeration cycles in cold-climate operations, three principal areas of research were explored: frost formation simulation and validation, usage of thermosiphons to collect heat from ground layers, and frost free heat pump for water heating.

Frost Formation Simulation and Experimentation

A detailed analysis of frost formation in heat pump heat exchangers was performed in order to generate and validate a numerical model. Experimentation utilizing controlled inlet air temperature, inlet absolute humidity, cooling surface temperature, and initial flow rate was performed to analyze the frost formation and density across various geometries. In analyzing various parameters and their effect on frost formation, a numerical model was built to predict frost formation given different operating schemes.

In parallel to the modeling efforts, an experimental setup was created to validate the numerical model and also to perform optimization and apply improvements (Figure ES-19). The test equipment consists of a temperature-controlled air supply unit, blower, volume flow meter, test section, and ducts that connect these main units. In the temperature-controlled air supply unit, air temperature and humidity are adjusted to certain levels. The air is fed by the blower to the cooled test section, where frost forms between two flat plates. The air that has passed the test section returns to the temperature-controlled air supply unit for recirculation. The condition of air before and after the test section and the heat flux into the test section are measured. At the same time, frost layer heights are measured by means of image processing. A finless heat exchanger that has the shape as shown in Figure ES-20 was designed. This study used an aluminum test section that duplicates the air-side flow paths in an outdoor heat exchanger (OHX). Table ES-10 represents the test conditions while Table ES-11 and Figure ES-21 provide the design parameters and details of the test section, respectively.

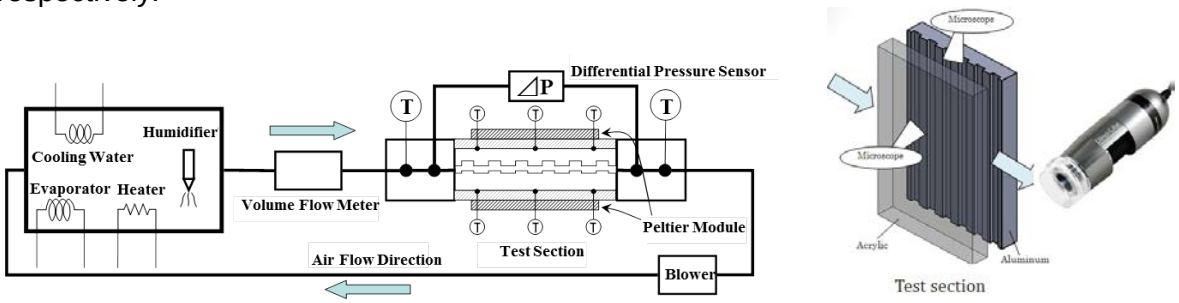

Figure ES-19: Schematic view of test equipment (left) and new visualization technique (right)

Table ES-10: Test conditions

Inlet air temperature T_a	ºC	7.0
Inlet absolute humidity X_a	kg/kg'	0.0053
Cooling surface temperature T_w	ºC	–10.0
Initial flow rate	m³/h	5.0

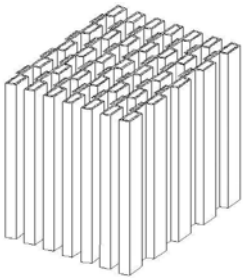

Figure ES-20: Overall view of heat exchanger

Table ES-11: Design parameters

		No.1	No.2	No.3
(1) Height of convex a_l	mm	2.0	1.2	2.8
(2) Depth of concave a_u	mm	2.8		
(3) Width of concave/convex l	mm	8.0		
(4) Pitch of convex/concave L	mm	16.0		
(5) Angle of convex/concave α	deg.	10		
(6) Number of convex/concave N		6		

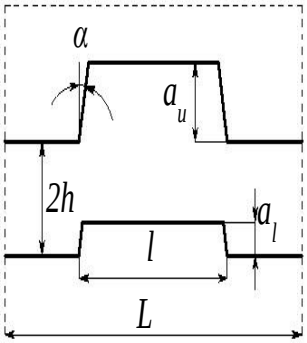

Figure ES-21: Concave- and convex-patterned test section details

From digital microscope images, the diameters and intervals of frost pillars are measured (see Figure ES-22 for example for test section No. 2), and the frost transition time is also specified. The visualization technique used provided a maximum resolution of 0.02 mm. The taller the convex height became, the higher the initial air velocity (the Reynolds number) became at the point where the flow path was narrow. As a result, initial frost pillar diameters and frost pillar intervals became smaller, indicating that the difference in initial air velocity (the Reynolds number) had an influence on the mode of frost pillar formation.

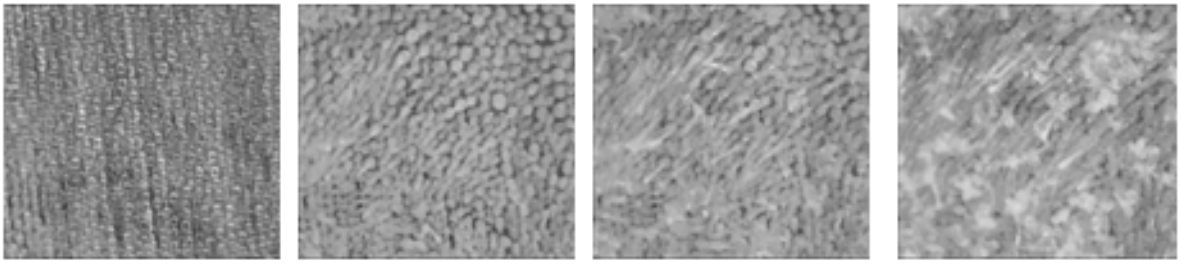

(a) 2min (b) 4min (c) 5min (d) 7min

Figure ES-22: Process of frost layer growth (No. 2)

Analysis of frost layer growth was conducted based on the calculation model suited for each frost layer growth process. Frost layer growth process is classified into three stages: "crystal growth stage," "frost layer growth stage," and "frost layer full growth stage." Because this test was not designed to analyze frost pillars melting on the frost layer surface, the analysis of the frost layer growth process was conducted based on the crystal growth stage and the frost layer growth stage.

Between the concave- and convex-patterned flat plates, the transition from water vapor to frost pillars occurs first in the upstream area and gradually moves toward the downstream area. Based on frost growth observation results, a transition period is practically defined as the time between the point when the mean frost layer height becomes about 0.10 mm and 80% of the time when the flow path becomes completely blocked. The point of the transition is calculated to shift linearly from the start to the end of the transition period. Figure ES-23 shows the comparison results of calculated and measured mean frost layer densities. Likewise, Figure ES-24 shows the comparison results of calculated and measured mean frost layer heights.

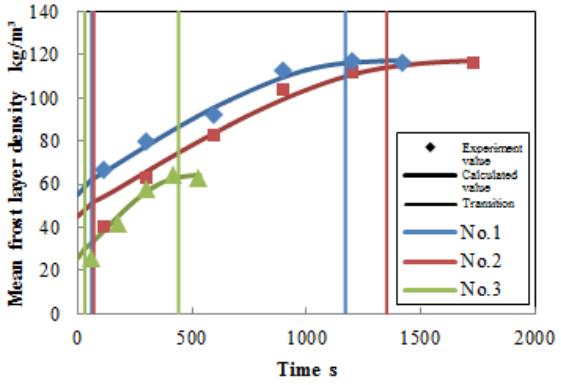

Figure ES-23: Comparison of mean frost layer density

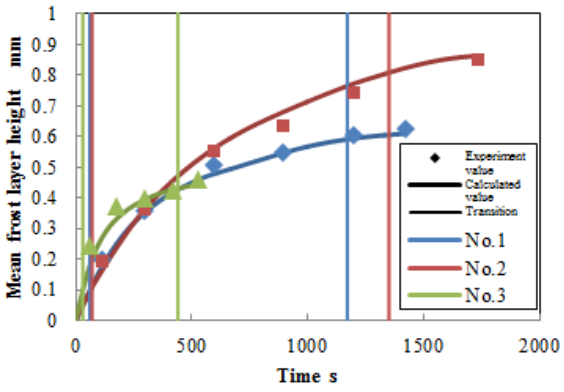

Figure ES-24: Comparison of mean frost layer height

In Task 3, the Japanese team extended the frost R&D work to apply the frost growth model in an ASHP system model and validate it with system test data. This study created a system model with the frost model embedded in heat exchanger routines. Figure ES-25 shows the results of frost weight changes, indicating that frost weight almost linearly increases with time. As shown in Figure ES-26, the numerical calculation of power consumption agreed with its experiment result relatively well.

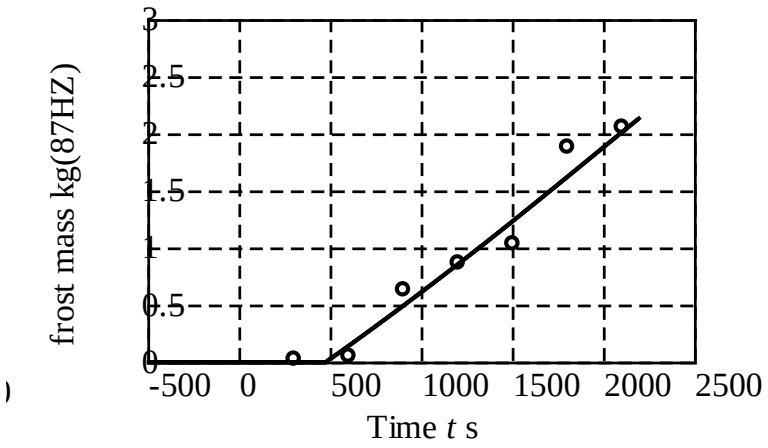

Figure ES-25: Frost mass

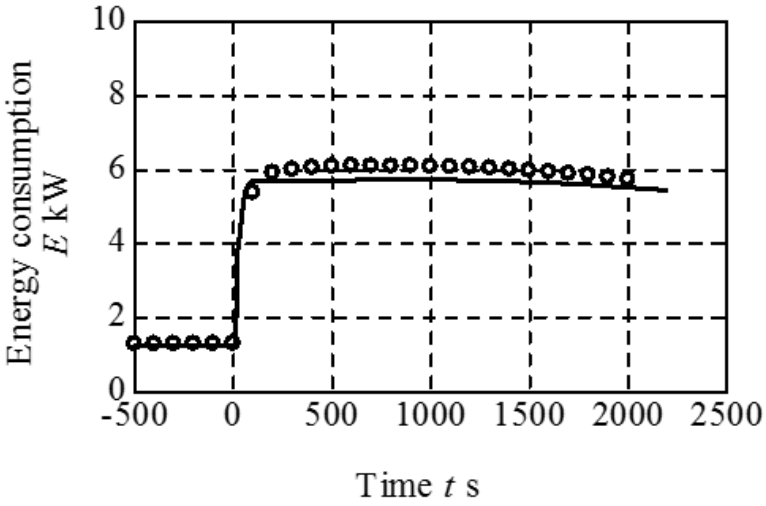

Figure ES-26: Energy consumption

Use of Thermosiphons to Collect Heat from Ground Layers

Thermosiphons with a new shape were designed and evaluated for their ability to collect ground heat for a GSHP system using CO_2 as the working fluid. Figure ES-27 illustrates the experimental apparatus and characteristics of the thermosiphon designs tested. An internal "showering" tube was used to promote wetting of the thermosiphon wall with liquid CO_2.

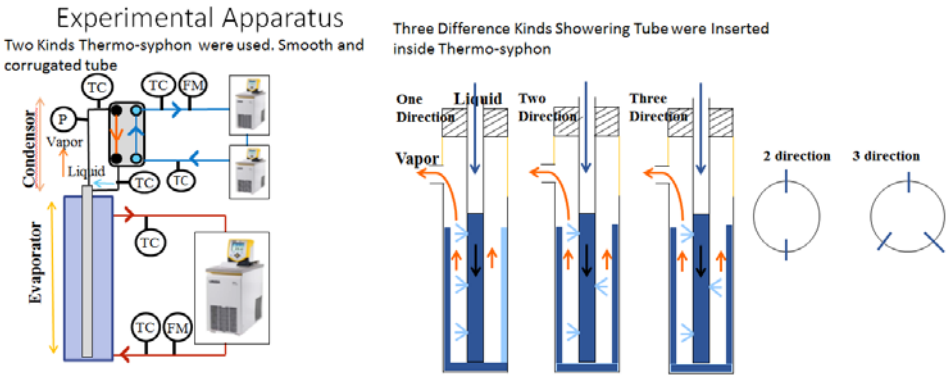

Figure ES-27: Thermosiphon tube test appratus schematic, left; and test evaporator characteristics, right

It was found that using smooth wall construction demonstrated better heat transfer than corrugated due to lower thermal barrier. Additionally, the length and number of thermosiphons was analyzed showing their improved effectiveness in different setups. Empirical relations were also used to explain the performance of the thermosiphon. The novel technology provided ample increase in COP in heat pump simulations. In the case where no showering tube is used, the number of thermosiphons required to achieve the targeted COP 2.8 is 14 for the tube length of 10 m, and 9 for 15 m (Figure ES-28). Similarly, in the case where a three-direction showering tube is used, the number of thermosiphons required is 13 for the tube length of 10m, and 9 for 15 m (Figure ES-29). Based on these results, in the case where 10-m-long thermosiphons are used, the use of a three-direction showering tube successfully reduced the number of thermosiphons required (in this connection, note that COP was calculated as annual performance factor (APF) here).

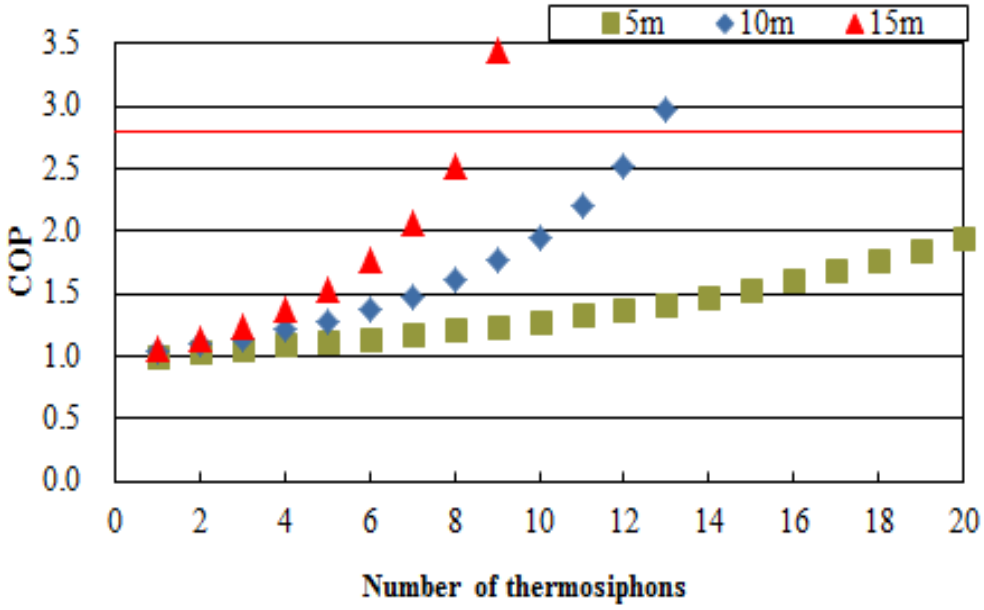

Figure ES-28: Results of heat pump simulations (smooth tubes without showering tube)

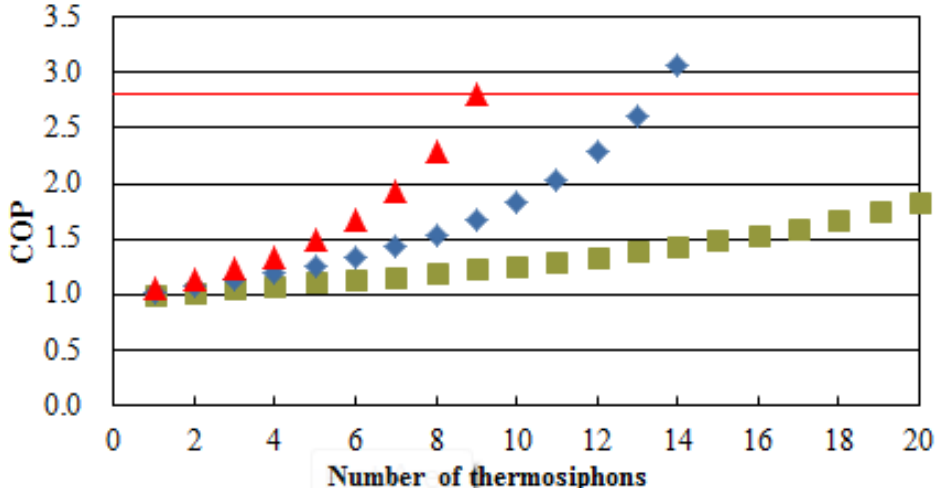

Figure ES-29: Results of heat pump simulations (smooth tubes with three-direction showering tube)

Frost Free Heat Pump for Water Heating

Air source heat pump water heaters (ASHPWHs) are widely applied as an economic form of heating. One of the largest problems in ASHPWHs is evaporator frosting, and the subsequent need for defrosting at a low ambient temperature and high relative humidity. We proposed a frost-free air- source heat pump water heater system with integrated solid desiccant, in which frost formation can be significantly mitigated by dehumidifying air before it enters the ASHPWH evaporator.

This system consists of a desiccant-coated refrigerant/air heat exchanger (1), an uncoated refrigerant/air heat exchanger (2), a compressor (3), a refrigerant/water heat exchanger (4), a water storage tank (5), a pump (6), two expansion valves (7, 8), a fan (9) and three air valves or dampers (10, 11, 12), as shown in Figure ES-30 (left side). With respect to the moisture moving in the desiccant, the operation process of the ASHPWH system can be

classified into two modes: adsorption mode (AD mode) and desorption mode (DE mode). In AD mode, both (1) and (2) are evaporators with the air valve 10 closed and valves 11 and 12 open. Outdoor air is drawn across both evaporators and dehumidified by the desiccant coating on (1).

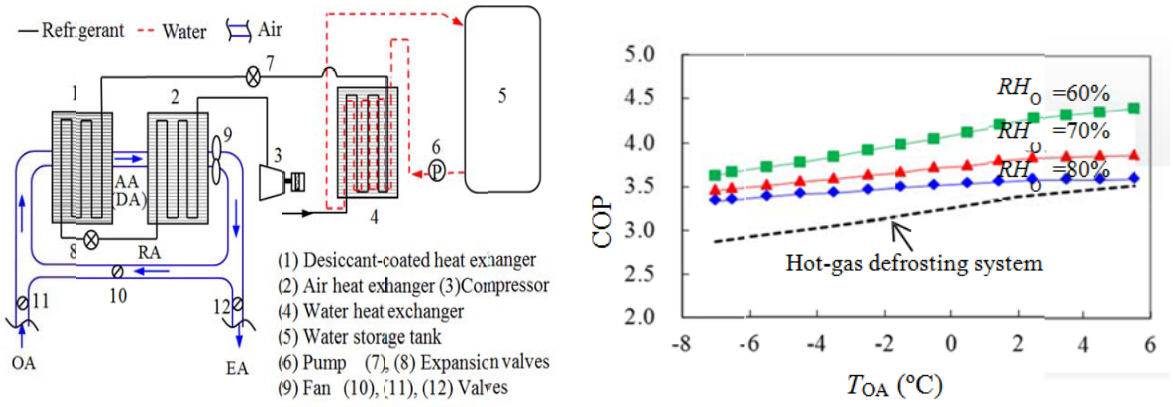

Figure ES-30: Schematic diagram of the frost-free AS HPWH system (left) and performance simulation results (right)

During DE mode, the expansion valve (7) is opened and another expansion valve (8) throttled. Therefore (1) becomes a condenser, and (2) remains an evaporator. Simultaneously, air valve (10) is opened and valves (11, 12) closed to form a closed air cycle between (1) and (2). The refrigerant exiting from compressor (3) initially transfers part of its heat into the water at (4), and then dissipates the remainder at (1), regenerating the desiccant coating and heating and moisturizing the return air (RA) to state DA. The hot and humid air (DA) is then passed through (2), in which the refrigerant is vaporized by obtaining heat from DA, and finally, leaves at state RA. Therefore, the total heat load added to DA in (1), including sensible and latent heat, could be completely recycled in (2). As a result, zero heat loss at the air side and continuous heat output to water are realized. Because the released moisture is exhausted at (2), the evaporation temperature of the refrigerant in (2) must exceed 0°C while in DE mode. A single period is ended when this moisture adsorbed by the desiccant in AD mode is completely discharged in DE mode.

The effectiveness of this system has been analyzed experimentally and numerically. Figure ES-30 (right side) illustrates the results that about a 20%-30% boost in COP could be achieved at a temperature of -7°C and relative humidity of 60-80%. This technology is also applicable to other air source heat pumps for heating, etc.

2.4 United States

U.S. CCHP R&D efforts described in the Task 1 and Task 2/3 reports focused on analyses and experimental (lab and field) investigation of several advanced VC cycles for ASHPs. Vapor injection (VI) cycle concepts, two-capacity compressors, variable speed (VS) compressors, parallel compressors, two-stage cycles with economizers, an oil-flooded compressor cycle concept, and several other advanced cycle approaches have been investigated. Based on early stage analyses, three CCHP cycle concepts were identified as among the most promising for meeting the goals – two-stage economizer cycle, oil-flooded compressor cycle, and a single-stage cycle using parallel compressors.

A brief summary of current promotional efforts for advanced ASHP systems, including CCHP applications, is given at the end of this section.

2.4.1 Two-stage economizer system

A field test of an advanced two-stage ASHP designed for cold climate operation has been completed at Camp Atterbury, a U.S. Army base outside Edinburgh in Indiana (Caskey et al., 2013). The heat pump is a two-compressor (two-stage) system with an economizer VI loop, similar to the concept analyzed by Bertsch et al. (2008). It featured a large tandem scroll compressor (two parallel compressors) for capacity boosting during low ambient temperature heating operation and a variable speed scroll compressor for cooling operation and moderate ambient temperature heating. The test was conducted under the DOD's Energy Security Technology Certification Program (ESTCP). Two identical military barracks from available buildings located at Camp Atterbury were selected for the field demonstration. The originally installed HVAC system was a natural gas furnace with a split system A/C. A side-by-side performance comparison between the originally installed HVAC systems and the two pre-commercial heat pump units developed at Purdue University was conducted during the 2012-2013 heating season. The heat pump units had a design heating capacity of 18.34 kW (62,580 BTU/h) at an ambient temperature of -20^{o}C (4^{o}F).

The heat pump performance was compared to the existing HVAC system. For the monitored period at the Army site the ASHP system achieved approximately 19% source energy savings vs. the baseline gas furnace system but utility costs were higher due to the low price the Army pays for natural gas at the site. Using average Indiana residential electricity and gas prices, the utility costs for the ASHP and baseline furnace would have been comparable. This operation cost equivalence despite the energy savings of the ASHP is because the price for natural gas in Indiana is about one-third that of electricity per unit of energy delivered, which is true of most locations in the United States. The ASHP used no electric backup heating during the test period. Using ASHRAE Standard 55 (ASHRAE, 2010) to evaluate the thermal comfort indicated that the heat pump was able to maintain comfort levels throughout the heating season. Furthermore, while the first cost of the two-stage ASHP will be higher than that of a conventional single-stage ASHP, the installation and maintenance costs are estimated to be comparable.

2.4.2 Two-port vapor injected compression with regeneration

Additional research at Purdue University's Herrick Labs focused on the experimental investigation of a commercially available 17.5 kW (5-ton) heat pump that was retrofitted with a two-port vapor injected scroll compressor. The injection ports within the two compression pathways were located in the fixed scroll with different distances from the suction chamber. The vapor at the two injection pressure levels was generated using two flash tank separators in a cascade configuration. This configuration made it necessary to not only control the superheat but also the liquid levels in the separators and subcooling of the refrigerant leaving the condenser.

Baseline performance data of the heat pump without vapor injection was obtained and compared with test data obtained for the two-port vapor injection system. For the baseline, the injection lines to the compression pockets were plugged within the fixed scroll to reduce dead volume and re-expansion losses. Also, the vapor-separator section was shut off and bypassed. In the second step, the plugs were removed and a staged expansion process was performed using the separator section. The generated vapor from each separator was injected into the respective compressor port causing an intercooling effect on the compression process.

With identical compressor speed, a 28% improvement in capacity was achieved at the 8.33°C design point, when compared to the baseline without vapor injection. When the baseline and vapor injected system capacity were matched by adjusting compressor speed, the COP increased by up to 6% at -8.33°C. Results of a bin-type analysis of the

experimental results predict an improvement in the heating seasonal performance factor (HSPF) of 6% for Minneapolis and nearly 7% for ANSI/AHRI 210/240 cold climate region V.

2.4.3 Oil-flooded compressor system

Further research at Purdue University's Herrick Labs focused on the experimental investigation conducted with a commercially available 17.5 kW (5-ton) heat pump that was retrofitted with oil-flooded compression and regeneration. The indoor coil face area was kept unchanged while an additional heat exchanger was added as the oil cooler in the air flow path. In addition, a counter-flow plate heat exchanger with low pressure drops was used as the regenerator. Figure ES-31 provides a schematic and p-h cycle diagram for the schematic.

The results show that high oil circulation rates remove heat of compression and significantly reduce discharge temperature. By injecting oil in the compression process and using internal regeneration, the improvements in COP and heating capacity range from 4% to 15% and from 1% to 19%, respectively, depending on the oil mass fraction and operating temperatures compared with a conventional heat pump (without regenerator and without oil injection). As shown in Figure ES-32, oil circulation had little impact on heating capacity at the nominal rating operation condition (8.3°C), and the highest capacity improvement was observed at lowest ambient temperature (-17.8°C).

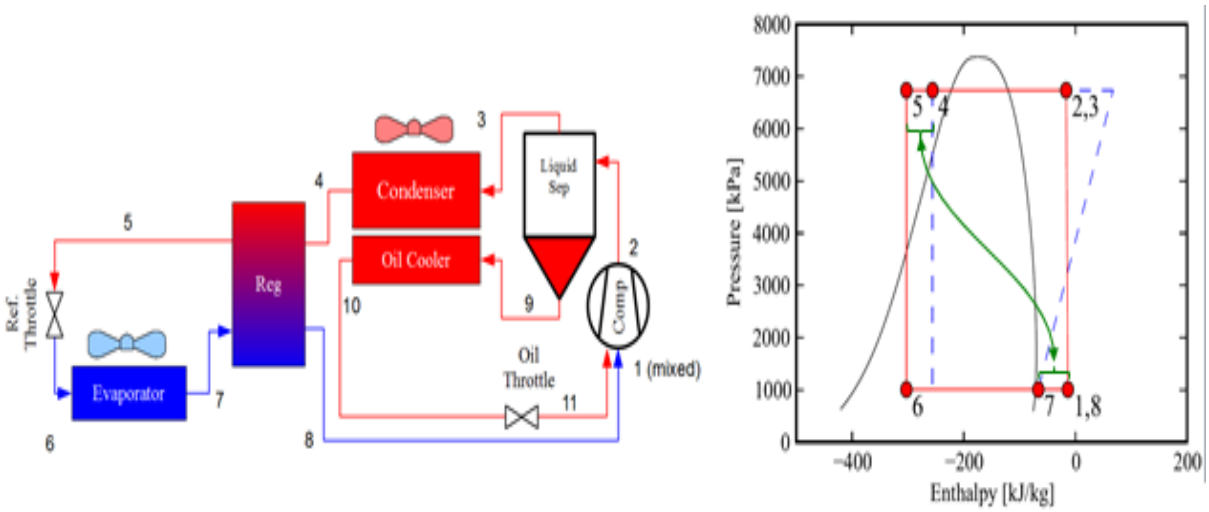

Figure ES-31: Schematic (left) and p-h cycle diagram (right) of flooded compressor cycle concept -from Bell et al. (2011)

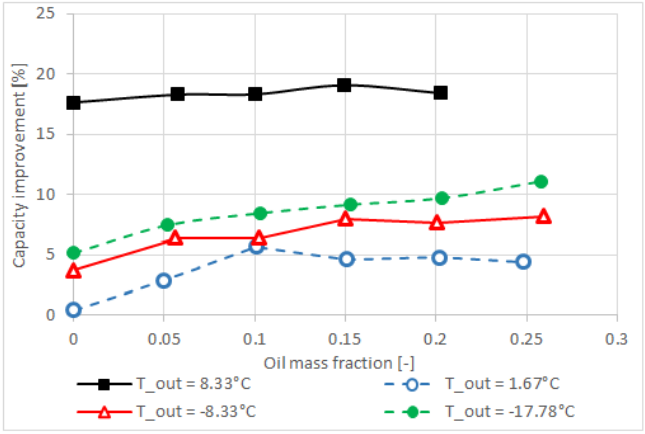

Figure ES-32: Capacity improvement between oil-flooded system with regeneration and baseline system

2.4.4 Single-stage ASHP with two parallel compressors

Analyses and lab evaluations led to development of a prototype ASHP featuring a pair of equal size, single-speed scroll compressors (one for cooling and mild ambient heating; both for cold ambient heating), see schematic in Figure ES-33. A laboratory prototype test system was built by modifying a 17.5 kW (~60,000 Btu/h or 5-ton) rated cooling capacity, single-speed, conventional ASHP and replacing its original compressor with a pair of equal size, single-speed compressors providing 10.6 kW (~36,000 Btu/h or 3 tons) of rated cooling capacity by operating only one compressor in cooling mode. Lab-measured performance indices indicated that the designs under investigation maintained their seasonal performance well over the full range of house performance levels. By comparison, the single-speed baseline loses 23% in seasonal performance in Region IV between the DHRmin (rated) and DHRmax heating load lines.

Based on the promising lab results, a prototype CCHP using parallel heating-optimized scroll compressors was constructed and installed in an occupied, single-story ranch home in central Ohio in January 2015 for field testing. The prototype (outdoor section pictured in Figure ES-34) replaced the original home HVAC system – a conventional single-speed ASHP with rated cooling capacity of ~10.0 kW (34000 Btu/h) at 35°C (95°F) and heating capacity of ~10.3 kW (35000 Btu/h) at 8.3°C (47°F), equipped with a 19.5 kW supplemental resistance heater for second stage and full back-up heating.

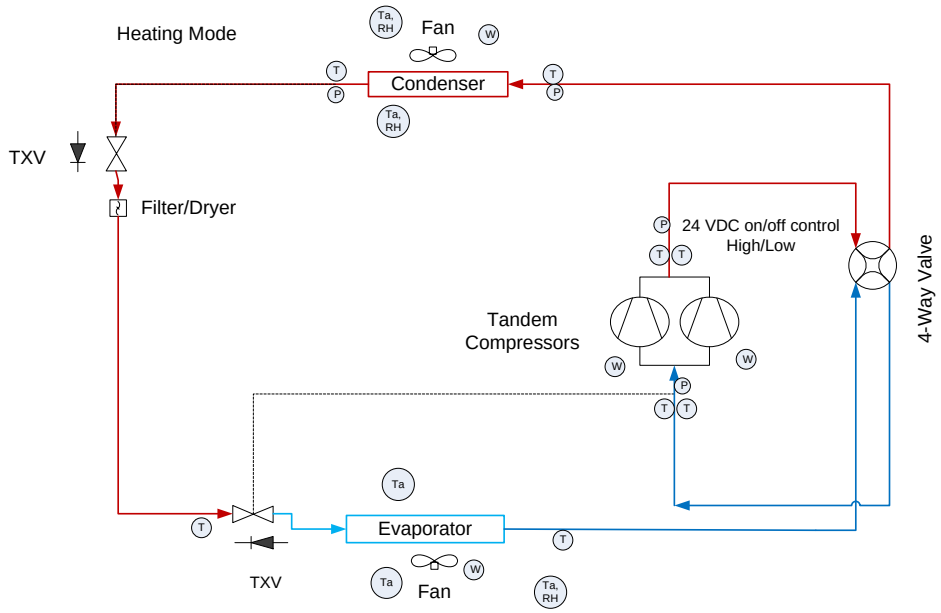

Figure ES-33: Field test prototype CCHP refrigerant schematic

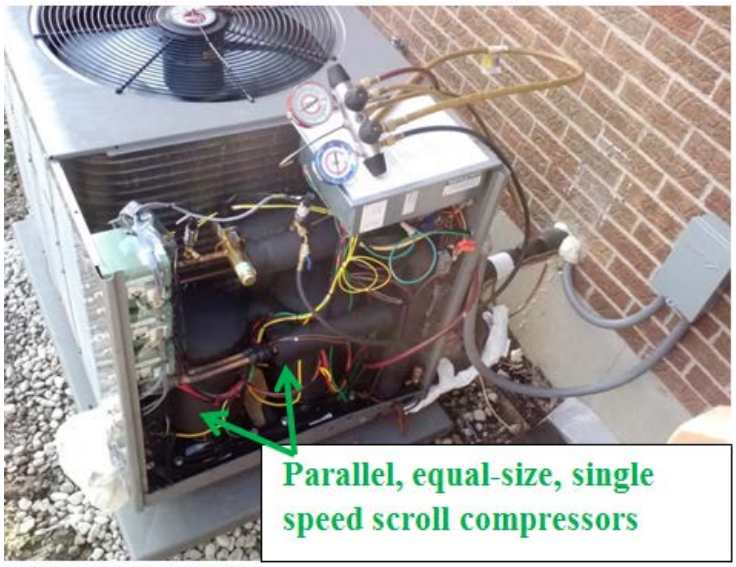

Figure ES-34: Prototype (using two compressors) being installed for field testing in a US residence

Field tests of the prototype in 2015 and 2016 demonstrated an average measured seasonal heating COP of about 3.0 and realized energy savings of more than 40% in comparison to a conventional ASHP during the coldest month (average temperature ~-7°C; minimum temperature -25°C). Results showed that at -25°C the unit had enough heating capacity that no backup heat was required (see Figure ES-35) at the test house. It is encouraging to see that, at -25°C, the field-measured COP was 2.2, i.e. 120% more efficient than resistance heating.

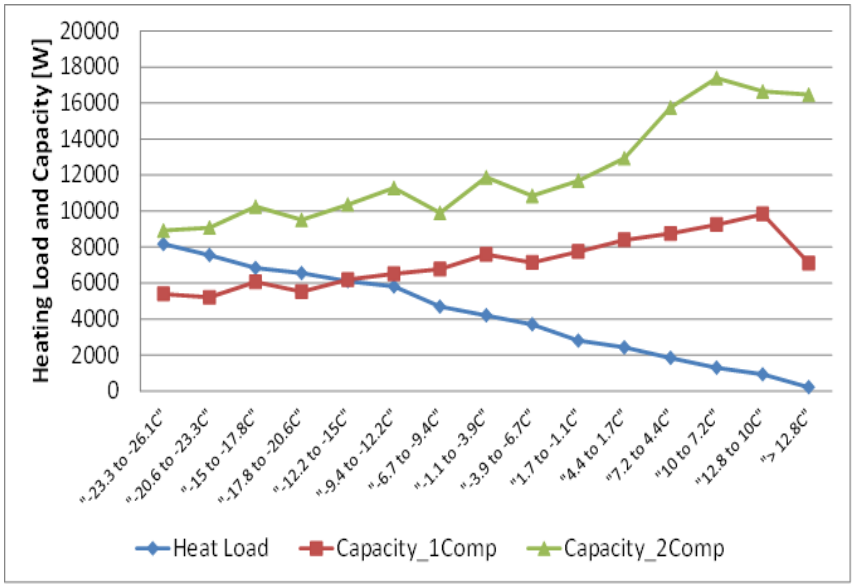

Figure ES-35: Two compressor CCHP prototype: measured average heating capacity (for 1 and 2 compressors) and building heat load vs. outdoor temperature

2.4.5 Complementary CCHP Market Promotion Activities

The US Northeast Energy Efficiency Partnership (NEEP) established a voluntary specification for cold climate ASHPs to help promote wider use of heat pumps in the northern parts of the US and the Northeast area. The specification was initially established in late 2014 with the most recent update effective January 1, 2017, and can be downloaded from the NEEP web site http://www.neep.org/initiatives/high-efficiency-products/emerging-technologies/ashp/cold-climate-air-source-heat-pump. It covers only air-to-air type variable-speed ASHPs (AWHPs and GSHPs are excluded). In order to be listed as complying with the NEEP specification, manufacturers' products must have a rated SCOPh ≥2.93 (US HSPF ≥10) for US climate region IV (moderate heating requirements) per AHRI Standard 210/240. In addition they must report space heating capacity and COP (from laboratory test data or engineering data) for at least 8.3°C, -8.3°C, and -15°C (47°F, 17°F, and 5°F) and at lower temperatures if available.

As of March 24, 2017, nearly 300 individual variable-speed ducted and ductless heat pump models were listed as complying with the latest NEEP CCHP specification V2.0. The list can be downloaded from the link above. Over 80% of the products listed are ductless types, either single-zone (2.6 to 9.4 kW nominal heating capacity) or multi-zone (2.9 to 14.1 kW nominal capacity). The remainder are centrally ducted (US type central air distribution systems) of about 6.5 to 16.5 kW nominal heating capacity.

The Electric Power Research Institute (EPRI) has also developed a specification for advanced ASHPs or Next Generation Heat Pumps (NextGen) (Domitrovic, 2017). This specification has two different levels or tiers. Under Tier 1 ASHP products must meet the same SCOPh requirement as for the NEEP specification above (≥2.93) but must also have space heating capacity at -8.3°C ≥80% of the rated capacity at 8.3°C. Under Tier 2, products must have a rated SCOPh ≥3.81 (US HSPF ≥13) for US climate region IV and a space heating capacity at -15°C ≥80% of the rated capacity at 8.3°C. Only about 7% of the products listed on the NEEP website currently meet the more stringent Tier 2 requirements.

3 ANNEX 41 FUTURE RESEARCH NEEDS

Numerous suggestions for future exploration have been identified by the participants as a result of Annex 41 efforts. Several of these are listed in brief below.

- Austria
  - Further experimental testing of other promising heat pump cycles
  - Detailed evaluation of an ejector cycle due to the promising results of the simplified modelling.
  - Improved compressor model for the LI cycle in order to improve the accuracy of the simulation results.
  - The measurement of the frost performance of the heat exchanger within the entire evaporator heat pump unit, including the quantification of the spatial frosting distribution. This will be linked to the change of acoustic emissions due to subsequently icing of the heat exchanger. This topic will be covered in the newly established Annex 51 (Acoustic Signatures of Heat Pumps), which started in April 2017.
- Canada
  - Semi-Virtual Test Bench for Measuring Heat Pump Performance
    - Will allow better understanding of interaction between heat pumps, the buildings where they are located, and the conventional resistive heating devices that are also present in the buildings
    - Also enables analysis of the control algorithms implemented in the thermostats.
  - Heat Pump Sizing Effort
    - Assess the sizing of heat pumps in Quebec (C656, F280, C273.5, rule of thumb, land characterization, market analysis ...) so that the sizing proposed by the C656 Standard is representative of Quebec situations and Canada.
  - Hybrid Ejector – Compressor Heat Pump
    - Based on the appropriate integration of compressor and ejector technologies using air as a heat source
    - Effort is now directed towards the development of a better ejector for R-134a (current ejector in test bench was designed for R410a) that will lead to higher entrainment ratios.
  - Solar-assisted Heat Pump
    - Investigate alternative ice generation approaches to lower equipment costs and increase maximum possible ice fractions
    - Evaluate system for larger buildings (multi-unit residential, office buildings) to examine different ratios of collector and storage area to building thermal loads
    - Evaluate potential of combining ice storage with liquid-based Building Integrated Photovoltaic/Thermal (BIPVT) system.
  - CO_2 Ground Source Heat Pump
    - Address overcoming the high cost of achieving improved seasonal efficiency by meeting DHW loads in addition to space heating loads
  - Refrigerant Mixtures
    - Confirm experimentally the performance predicted by the simulations with a prototype heat pump lab unit adapted to refrigerant mixtures with a strategic temperature glide.
- Japan
  - Build on frost modeling and testing work by conducting numerical simulations on repeated frost/defrost cycles to facilitate development of more efficient

heat pump operational methods and future ASHP systems with improved heating performance.
    - Propose feasibility research on the commercial practical use of thermosiphon evaporator GSHP in Hokkaido to embed heat pipes and try heat recovery using foundation piles. Both new construction and rennovation applications will be a target for this research
    - Design and build a prototype of the frost-free heat pump system, and test its performance
- United States
    - Parallel Compressor Prototype CCHP
        - Evaluate concept for other heat pump types (e.g. air-water ASHP, Brine/water-to-water, etc.)
    - Vapor-injected Compression with Economizing System
        - In the tested configuration, the injection ports did not include check valves. This is most likely the cause for the smaller performance improvement than predicted by the simulations.
    - Evaporator R&D
        - A larger fin pitch and tube diameter should be used for cold climate heat pumps to reduce the effects of frostbuild-up and refrigerant side pressure drop.
    - Oil-flooded Heat Pump Concept
        - Determine optimal circulating oil mass fraction as a function of outdoor temperature and superheat
        - Control superheat at inlet of compressor to allow the refrigerant to leave the evaporator as two-phase flow and to be superheated in the regenerator

4 REFERENCES

Astina, I.M., Sato, H., 2004, “A Rational Helmholtz Fundamental Equation of State for Difluoromethane with an Intermolecular Potential Background,” Int. J. Thermophys., Vol. 24, pp. 963-990.

Bell I. H., E. A. Groll, and J. E. Braun. 2011. “Performance of Vapor Compression Systems with Compressor Oil Flooding and Regeneration,” *International Journal of Refrigeration*, Vol. 34, No. 1, pp. 225-233.

Domitrovic, R., Personal communication to Van Baxter, April 2017.

Hakkaki-Fard, A., Z. Aidoun, P. Eslami-Nejad, (2016). Evaluation of refrigerant mixtures in three different cold climates residential air-source heat pumps, ASHRAE Transactions, Vol 122, Part 2, June 2016.

Hakkaki-Fard, A., Z. Aidoun, and M. Ouzzane, Applying refrigerant mixtures with thermal glide in cold climate air-source heat pumps, Appl. Therm. Eng., 62, 2014, pp. 714-722.

Hengel, F., R. Rieberer, A. Heinz, 2013. Theoretische Analyse zur Effizienzsteigerung durch Drehzahlregelung und Economizer-Schaltung bei einer Luft/Wasser Waermepumpe, DKV-Tagung, Hannover, AA IV.10.

Hozumi, T., Sato, H., Watanabe, K., 1994, “Speed of Sound in Gaseous Difluoromethane, J. Chem. Eng. Data,” 39, pp. 493-495.

Kagawa, N., Matsuguchi, A., Watanabe, K., 2012a, “Measurements of Isobaric Heat Capacity of R32”, Int. J. Refrig., Vol. 35, pp. 1014–1020.

Kagawa N, Matsuguchi A, Yamaya K, Watanabe K. Behavior of isobaric heat capacity of r 32 in the gas phase, 2012b, Proc. the 6th Asian Conference on Refrigeration and Air Conditioning Paper No.2954 (Xi’an, 8/27/2012).

Kubota, H., Sotani T., Kunimoto Y., 1995, “Isobaric Specific Heat Capacity of Difluoromethane at Pressure up to 0.5MPa”, Fluid Phase Equilibria, Vol. 104, 413-419.

Le Gall, R., J.M. Grillot and C. Jallut, “Modelling of Frost Growth and Densification”, Int. J. of Heat Mass Transfer. 28,(7) (1997), 3177-3187.

Moisi H., Rieberer R.; Fleckl T., Popovac M., Reichl Ch., 2015: IEA HPP-Annex41, Task 2-Simulation Models and Prototype Experiments, Task-2 Report, Graz, Vienna.

Northeast Energy Efficiency Partnerships, 2017. “Cold Climate Air Source Heat Pump.” Accessed June 2017. http://www.neep.org/initiatives/high-efficiency-products/emerging-technologies/ashp/cold-climate-air-source-heat-pump.

Natural Resources Canada (NRCan), 2010. “Bulletin on Reporting Cold Climate Performance.” Office of Energy Efficiency Bulletin 7177.

Outcalt, S.L., McLinden, M.O., 1995, “Equations of State for the Thermodynamic Properties of R32 (Difluoromethane) and R125 (Pentafluoroethane),” Int. J. Thermophys., Vol. 16, 79-89.

Piao, C.-C., Noguchi, M., 2001. “Thermodynamic Properties of HFC-32 (Difluoromethane),” Int. J. Refrig., Vol. 24, pp. 519-530.

Popovac, M., S. Seichter, C. Reichl, P. Benovsky, 2015a. Implementation and application of the frost growth and densification model for numerical analysis of heat pump frosting performance Ammonia and CO_2 Refrigeration Technologies, April 16-18, 2015, Ohrid, Republic of Macedonia.

Popovac, M., S. Seichter, P. Benovsky, T. Fleckl. Ch. Reichl, 2015b. Numerical Analysis of the Frosting Performance of the air-side of a heat-pump, 24th IIR international congress of refrigeration, August 16-22, 2015, ICR2015, Yokohama, Japan.

Ramaraj, S., Braun, J.E., Groll, E.A, and Horton, W.T. (2016). “Performance analysis of liquid flooded compression with regeneration for cold climate heat pumps,” Int’l J. Refrigeration, Vol. 68, August 2016, Pages 50–58.

Reichl, Ch., A. Strehlow, T. Oltersdorf, S. Braungardt, M. Pröhl, P. Benovsky, M. Popovac, T. Fleckl, GreenHP: Next Generation Heat Pump for Retrofitting Buildings – new evaporator component for large capacity air-to-water heat pumps, Advanced HVAC & Natural Gas Technology Conference, May 6-9, 2015, Radisson BLU Hotel Latvija Conference Center, Riga, Latvia; DOI: 10.7250/rehvaconf.2015.015; page 100-109.

Shen B. et al. Field Investigation of an Air-Source Cold Climate Heat Pump. Paper no. P.1.5.6 in the Proceedings of the 12th IEA Heat Pump Conference 2017, May 15-18 2017, Rotterdam, Netherlands.

Shen, B., O. A. Abdelaziz, and C. K. Rice. 2014. "Compressor Selection and Equipment Sizing for Cold Climate Heat Pumps," paper no. P.6.11 in the Proceedings of the 11th IEA Heat Pump Conference 2014, May 12-16 2014, Montréal (Québec) Canada.

Strehlow A., C. Martín-Callizo, T. Oltersdorf, M. Popovac, Ch. Reichl. GreenHP: Heat Exchangers for Next Generation Heat Pump, 4th International Congress and Exhibition on Aluminium Heat Exchanger Technologies for HVAC&R, 10-11 June, 2015, Hotel Radisson Blu Scandinavia, Düsseldorf, Germany.

Tamasauskas, J., Poirier, M., Zmeureanu, R., and Sunye, R., Modeling and Optimization of a Solar Assisted Heat Pump Using Ice Slurry as a Latent Storage Material Solar Energy, Solar Energy, 86(11), pp. 3316-3325, (2012).

Tao, Y. X., Mao, Y., and Besant, R. W., 1994, "Frost Growth Characteristics on Heat Exchanger Surfaces: Measurement and Simulation Studies," Proceedings of the 1994 ASME International Mechanical Engineering Congress and Exposition, Chicago, IL, Nov. 1994, HTD-Vol 286 , pp. 29–38.

Tillner-Roth, R., Yokozoki, M., 1997, "An International Standard Equation of State for Difluoromethane (R-32) for Temperatures from the Triple Point at 136.34 K to 435 K and Pressures up to 70 MPa," J. Phys. Chem. Ref. Data, Vol. 25, pp. 1273-1328.

Yamashita, K. "Frost phenomena under the Low Temperature Environment" Ph.D. Thesis, Tamagawa University, (2009) (in Japanese).

Yang, B., Blatchley, T., Bach, C.K., Braun, J.E., Horton, W.T., and Groll, E.A., "Application of Oil Flooded Compression with Regeneration to a Packaged Heat Pump System," Proc. of the 15th Int'l Refrig. and Air Cond. Conf. at Purdue, Paper 2631, Purdue University, West Lafayette, IN, July 14-17, 2014, 10 pages.

Yasui K., et al. Study on the Frosting Phenomena between Concavity and Convexity Plate under Forced Convection – Detailed Observation and Analysis of Frost Layer Growth. Paper no. O.1.6.2 in the Proceedings of the 12th IEA Heat Pump Conference 2017, May 15-18 2017, Rotterdam, Netherlands.

Zhang L. et al. A new method for preventing air-source heat pumps and refrigerators from frosting. Paper no. O.1.6.3 in the Proceedings of the 12th IEA Heat Pump Conference 2017, May 15-18 2017, Rotterdam, Netherlands.

Zoier, H., 2014: Betriebsverhalten von Aussenluft-Waermepumpen bei tiefen Aussenlufttemperaturen, Masterthesis, Institute for Thermal Engineering, TU-Graz.

Zottl, A., GreenHP Project Final Report, 01/12/2012 to 30/08/2016. AIT Austrian Institute of Technology. http://cordis.europa.eu/docs/results/308/308816/final1-fp7-308816-greenhp-publishable-final-report.pdf.

PART 2: COUNTRY REPORTS

This final Annex 41 report is a compilation of individual efforts undertaken by the four participating countries, each with individual reports, noted below, that are incorporated into this volume.

Austrian Team Final Country Report

IEA HPT TCP Annex 41
"Cold Climate Heat Pumps"

Submitted by:

Franz Hengel
Johannes Riedler
René Rieberer (contact: rene.rieberer@tugraz.at)
Andreas Heinz
Heinz Moisi

Graz University of Technology
Institute of Thermal Engineering
Inffeldgasse 25/B, 8010 Graz, Austria

Thomas Fleckl (contact: thomas.fleckl@ait.ac.at)
Christoph Reichl
Mirza Popovac

AIT – Austrian Institute of Technology
Energy Department
Giefinggasse 2, 1210 Wien, Austria

June 6, 2014

TABLE OF CONTENTS

EXECUTIVE SUMMARY

COLD CLIMATE HEAT PUMPS: SIMULATION MODELS AND PROTOTYPE EXPERIMENTS; ENERGY SAVINGS ASSESSMENT OF AN ASHP WITH LIQUID INJECTION FOR COLD CLIMATE APPLICATIONS

Tasks 2 and 3 cover the simulation and experimental modeling of multiple topics relating to cold climate heat pumps including:

- Evaluation of simplified air source heat pump models at low ambient temperatures
- Detailed model and experimentation of a liquid injection (LI) cycle
- Simulation of an air/water heat pump using a variable speed compressor and economizer
- Frosting performance of heat exchangers
- Energy savings of a LI cycle for cold climate applications.

Task 2: Simulation Models and Prototype Experiments

Simulation work has been carried out at the Institute of Thermal Engineering (IWT, Institut für Wärmetechnik) in order to investigate the potential of nine different heat pump cycles for cold climate applications. Simplified simulation models of promising heat pump layouts have been carried out using the Engineering Equation solver (EES) program in order to increase the range of application and efficiency. The investigated refrigerant has been R410A. The heat pump cycle with ejector to utilize the expansion work showed by far the best performance. However, because the model is highly theoretical and simplified, this cycle should be investigated in more detail to verify its advantages. The cascade cycle has shown COP improvements up to 5% compared to the conventional cycle. Heating capacity could have been increased up to 44%, although the same refrigerant has been used in both stages. Further investigation has to be carried out in order to find an appropriate refrigerant couple. Vapor injection with flash tank or with an internal heat exchanger (IHX) shows a COP increase in the range of 4% and 10%, respectively, at -30°C evaporation temperature. The work of Hengel et al. (2013) also showed slight COP improvements for the economizer with internal heat exchanger, especially at higher heating supply temperatures. Intercoolers show a rather high decrease of COP and heating capacity if the heat removed from the intercooler is not used. The IHX cycle resulted in similar values as the conventional cycle and showed no improvement in any category. The LI cycle caused minor COP losses in a range of 2% but identical heating capacity compared to the conventional cycle. The resulting compressor outlet temperatures could have been decreased within all models except the IHX cycle. The most promising layouts in this regard are cascade, intercooling, and LI, with a drop in compressor outlet temperatures of 19 K, 21 K and 32 K respectively compared to the conventional cycle at an evaporation temperature of -30 C.

Based on the simplified calculations, a more detailed model of the LI cycle has been set up. The LI cycle was been chosen for more detailed study for two primary reasons. First, it has a less complex layout compared to the cascade and economizer systems. Secondly, it has the ability to increase the range of heat pump application for cold climates in terms of compressor outlet temperature. Furthermore, a LI prototype was available to carry out experimental analysis. The detailed model considers heat transfers on the heat sink and heat source heat exchanger and calculates the resulting evaporation/condensation pressure level iteratively. Furthermore polynomial functions provided by manufacturer data are used to describe mass flow, electric power consumption and isentropic efficiencies based on evaporation and condensation temperature.

A LI prototype heat pump system with a scroll compressor has been investigated at the IWT. In order to simulate ambient conditions, a climatic chamber has been used. The heat sink

has been provided by a thermal storage with re-cooling system. The measurement procedure has been carried out according to EN-14511 for an ambient temperature range of -19°C to 7°C and different heating supply temperatures (35°C, 45°C, 55°C, 60°C). The analyzed data confirmed the results from the simplified model analyses that the liquid injection has a minor influence on COP and heat capacity, but the range of application can be extended to lower ambient temperatures for high heating supply temperatures. Furthermore it is interesting to see that the ambient temperature has almost no influence on the electrical consumption of the compressor.

The comparison with simulation results showed a major disagreement with the experimental data. Specifically, the electrical consumption of the compressor showed a high deviation, which is interesting since manufacturer data has been utilized. For example, results for the measured refrigerant mass flow are 15% to 20% lower than predicted with the compressor maps. Furthermore, the neglected pressure drops in heat exchangers and piping contribute to the disagreement. The simplified modelling of the LI process also has effects on the model accuracy and the assumption of equal pressure ratios and equal isentropic efficiencies for each stage.

The frosting characterization of different fin geometries and surface structures (coatings) is possible by using a wind tunnel setup placed inside a climate chamber. With the distributor test-bench, new and existing flow distributing technologies can be characterized. Both experimental and numerical techniques are feasible for the pre-selection of fin types. Several techniques are readily developed to support any evaporator design. Some of the methods (PIV, Shadowgraphy, Video analysis) could also be used for investigations in the climate chambers and test-benches on full scale HEXs in heat pumps. Furthermore, with a careful implementation of the frost growth and densification model (which captures well the main physical phenomena of the frosting process) into the OpenFOAM fluid flow solver suite, 3D unsteady numerical simulations of the frosting performance over heat exchanger fins have enabled a deeper look at the spatial and temporal distribution of the flow characteristics that are relevant for the frosting process.

The experimental investigation of the heat exchanger frosting behavior revealed the interdependence between the icing time of a given fin geometry and the resulting mean heat transfer. Given that the fin geometry has an influence on the icing properties and the overall mean heat transfer, the wavy fins seem to be a good compromise between a good heat transfer and a proper icing time. Blocking takes place at the most exposed fin surfaces at the inlet area, which has been observed both by experiments and numerical simulations. When comparing advanced heat exchanger types with commonly available standard ones, it has been experimentally observed that the fin geometry design of multi-port extrusion (MPE) fin heat exchanger has a positive impact on the frost creation in the initial frosting phase. As the frost creation progresses over the entire fin surface, however, the process is further dominated by the main geometrical characteristics (fin spacing): here the advanced heat exchanger type characteristics have lower impact, as compared to a standard conventional tube fin (CTF) heat exchanger type. The observed effect is more pronounced at the ambient conditions with more absolute humidity.

Task 3: Energy Savings Assessment of an ASHP with Liquid Injection for Cold Climate Applications

As outlined in Task 2, an air-to-water heat pump using LI can increase operational hours in cold climate regions by reducing compressor outlet temperatures. Thus, lubricant related problems can be avoided. The increased time of operation can also have positive effects on seasonal performance factors (SPF) depending on the kind of auxiliary heat preparation (direct electrical, oil, gas etc.). In order to quantify the effects of an LI-System compared to a conventional heat pump system, a simple methodology has been developed to estimate the

seasonal performance in dependence of different locations and heat sink temperature levels. However, only space heating has been considered (domestic hot water preparation has been neglected).

Based on the prototype testing and simulation of a Liquid-Injection air-to-water heat pump system in Task 2 (Moisi et al., 2015), characteristics for heating capacity, electrical consumption and compressor outlet temperature have been derived in order to carry out an annual performance estimation. A simple methodology has been developed to estimate the annual thermal energy and electrical consumption of a heat pump system with and without liquid injection. The heating system has been considered as monovalent with an electrical backup heater. A reference building based on IEA SHC Task 32 has been utilized to derive heat load characteristics for five different locations. Combining the climate data of the five locations with the heat pump and building characteristics, a seasonal performance factor has been estimated for two different heating system supply temperatures and a comparison of the LI-System to a conventional system has been carried out.

The results showed that, with a supply temperature of 35°C, no injection is needed at all. Therefore, no difference between the SPF results for the conventional and LI system occurred. The resulting SPF values are in a range of 3.8 (Anchorage) and 4.3 (Graz). The main influence on SPF has been the ambient temperature. The results are surely overestimated quantitatively according to the experimental data (Moisi et al., 2015), but can point out a qualitative trend. A difference between the conventional and the LI system in terms of performance can be observed at a supply temperature of 45°C. With increasing operation time of the LI System at lower ambient temperatures (approx. below -20°C), the SPF improvement compared to the conventional system increases since no backup heater is necessary. In the case of Minneapolis for example, an SPF improvement of 12% can be achieved compared to the conventional system. On the other hand, Graz shows no effect at all since the minimum ambient temperature is too high for the activation of liquid injection (approx. -12°C). However, the threshold ambient temperature for the injection activation is dependent on the control strategy. Another fact is clear, that with an increasing heat supply temperature this threshold rises to higher ambient temperatures. Therefore, a liquid injection system can be interesting for more moderate climates and high temperature heating systems in the course of refurbishments in order to realize a monovalent heating system as well as for hot water production.

A LI system can increase the range of application to lower ambient temperatures. Compared to a conventional air source heat pump system with a direct electrical backup heater, annual efficiencies can be improved depending on the time the heat pump operates at lower ambient temperatures.

Austrian Team Report

IEA HPT TCP Annex 41
"Cold Climate Heat Pumps"

Task 1 - Literature and Technology Review

Submitted by:

Franz Hengel
Johannes Riedler
René Rieberer (contact: rene.rieberer@tugraz.at)
Andreas Heinz

Graz University of Technology
Institute of Thermal Engineering
Inffeldgasse 25/B, 8010 Graz, Austria

Thomas Fleckl (contact: thomas.fleckl@ait.ac.at)
Christoph Reichl

AIT – Austrian Institute of Technology
Energy Department
Giefinggasse 2, 1210 Wien, Austria

June 6, 2014

TABLE OF CONTENTS

LIST OF TABLES

LIST OF FIGURES

1 INTRODUCTION

In Austria and Europe (and other countries in the world) there is a trend to install air-source heat pumps (ASHP) mainly due to their low installation cost, but the market for ASHP's in cold regions is limited. Therefore, the challenge is to improve the heating capacity and Coefficient of Performance (COP) of such system. To increase the heating capacity and the COP for ASHP's in cold climate regions compared to a standard heat pump cycle a possibility is a modification of the heat pump cycle. Hence this Annex Report deals with a literature review concerning studies on ASHP's, especially in cold climate regions, which has already been carried out and refers to the following issues:

- Heat pump capacity characteristics,
- heat pump layouts and its modifications,
- control strategies of heat pumps,
- system integration of heat pumps, and
- heat pump components.

Here follows a short characterization of the Austrian heat pump market as well as a look on the European market.

1.1 Austrian Market Development

The development of the Austrian heat pump market (Figure 1) can be characterized by an early phase of technology diffusion in the 1980's (mainly heat pumps for water heating) followed by a significant market decrease and a second increase starting from the year 2001 (now mainly heat pumps for space heating). The second diffusion period came together with the introduction of energy efficient buildings which offered good conditions for an energy efficient operation of heat pumps because of low temperature needs in the heating system and low energy consumption for space heating.

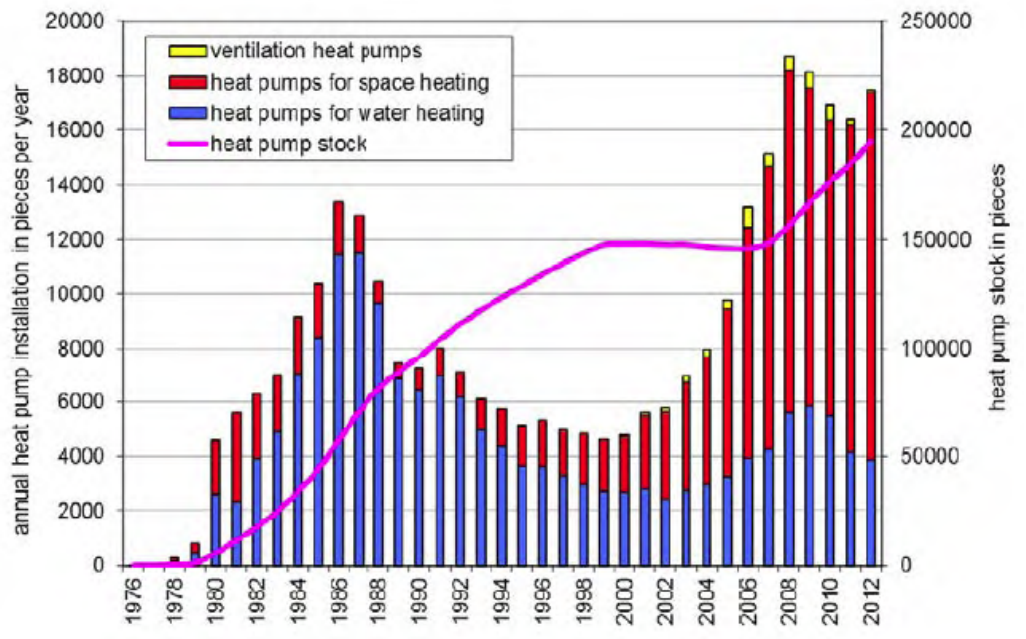

Figure 1: Heat pump market development in Austria until 2012 (Biermayr et al., 2013)

According to Biermayr et al. (2013) the total sales of heat pumps (national market and export market) increased from 2011 to 2012 by 9.8%, from 25.271 to 27.754 systems. In particular in the sector of heat pumps up to 20 kW there was a clear increase of the sales figures of 14.0%. In this sector the national market (+12.7%) as well as the export market (+16.6%)

increased. A decrease could be observed with heat pumps in the high power segment (>80 kW) and with ventilation heat pumps. On the national market hot water heat pumps decreased slightly.

The percentage of the export market was 37% in quantity of the total sales in 2012. This is a slight increase compared to 2011. In 2012 the Austrian heat pump sector (production, trade and installation) had an amount of total sales of 212.3 million Euro and 1,127 full time jobs. Figure 2 depicts the market share of the different heat pump types (Brine-to-water, water-to-water, air-to-water, air-to-air and direct evaporation ground source heat pumps) in Austria from 1990 to 2012. Air-to-water heat pumps show an increasing trend for the last ten years caused by the low installation costs and due to the lower complexity of air as the heat source. Brine-to-water heat pumps show a decreasing market share since 2007 as well as direct evaporation ground source heat pumps since 1998. Water-to-water and air-to-air heat pumps play a minor role on the Austrian market.

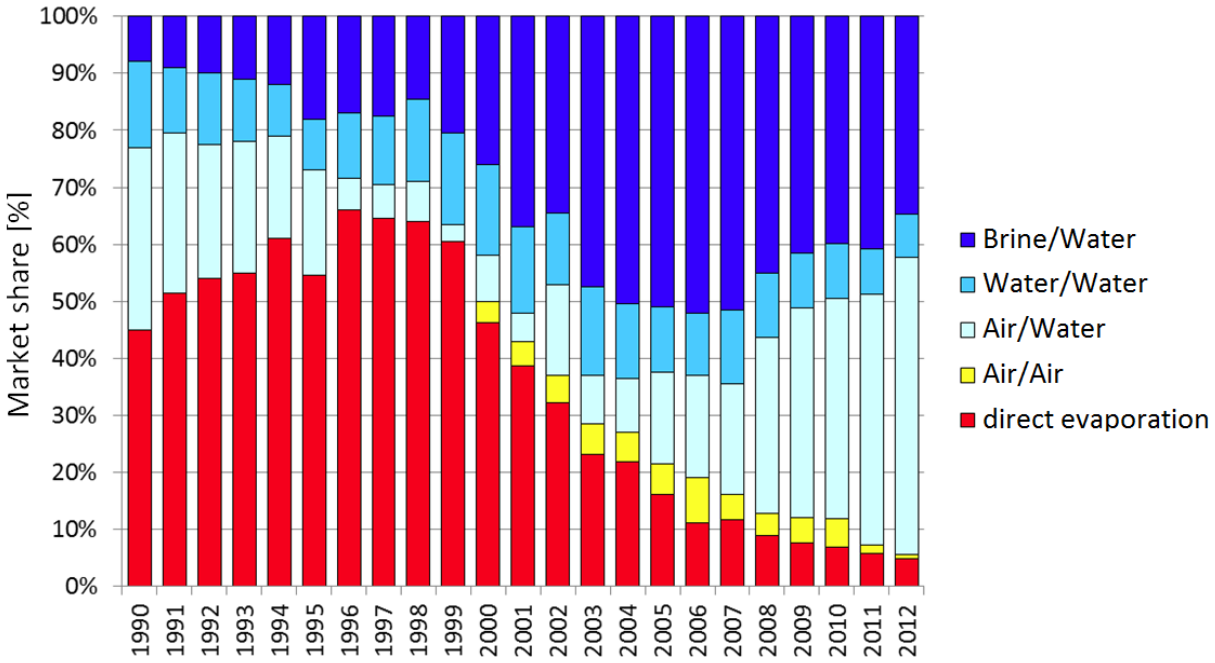

Figure 2: Market share for heat pump heat sources in Austria until 2012 (Biermayr et al., 2013)

At present research and development of heat pump systems focus on installations combined with other technologies: e.g. solar thermal systems or photovoltaic systems, new energy-services as air-conditioning, cooling of rooms or renovating buildings in regard to humidity problems.

The range of innovations is completed with steady improvements of the system efficiency, the use of new driving energy as natural gas and the use of the heat pump technology in smart grids.

1.2 Market Development Europe (EHPA)

Taking a look on the European heat pump market, one can see that air-to-water heat pumps play an important role. Figure 3 shows that this heat pump type ("H-air/water") has a larger share than ground-couples systems. However, reversible air-to-air heat pumps represent the largest share. For further information on the European market, here it is referred to the European Heat Pump Association (EHPA, http://www.ehpa.org/) which comprises 107 members from 22 European countries.

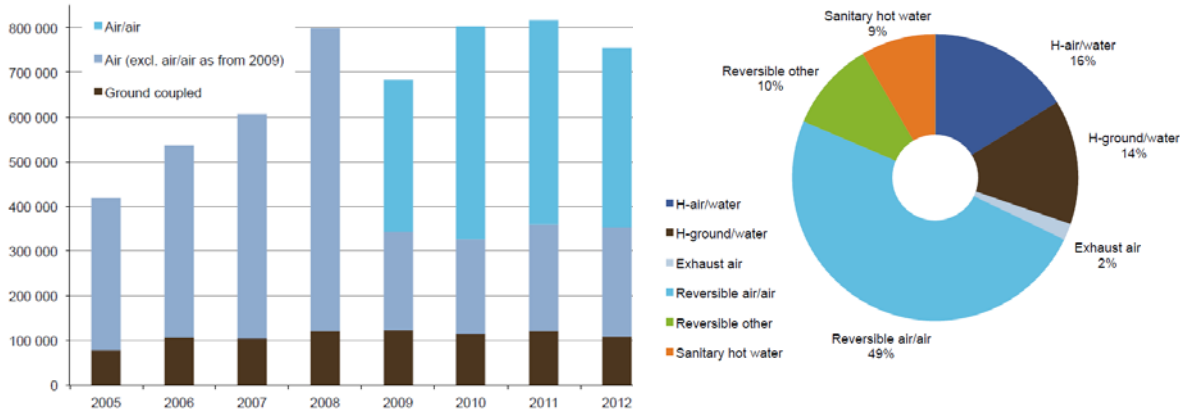

Figure 3: European Heat Pump Market – left: heat pump sales by energy source in the period 2005 – 2012; right: split of heat pump sales 2012 (Nowak, 2013)

2 CAPACITY CHARACTERISTICS OF A HEAT PUMP

This chapter shows the different operating modes of heat pumps as well as alternatives to the compression heat pumps.

2.1 Operating Modes of Electrically Driven Heat Pumps

Heat pump systems can be basically operated in two different kinds of operating modes for supplying the overall heat demand to the building:

- Monovalent (Figure 4, left)
- Bivalent (Figure 4, right)
  - bivalent-alternative
  - bivalent-parallel

With the first operating mode – monovalent – the heat pump unit covers the heat load of the building without any additional heating system. Concerning air source heat pumps (ASHP) without speed controlled compressor the heating capacity decreases significantly with dropping ambient temperature because of a decreasing suction gas density and the pressure ratios could be very high. For ground source heat pumps (GSHP) and water source heat pumps (WSHP) the variation of the source temperature is relatively low compared to the ASHP, so that both systems are preferable applied for this operating mode. However, ASHP's are also applied using this operating mode and therefore – especially in cold climates – it is necessary to improve both heating capacity and efficiency (Coefficient of Performance).

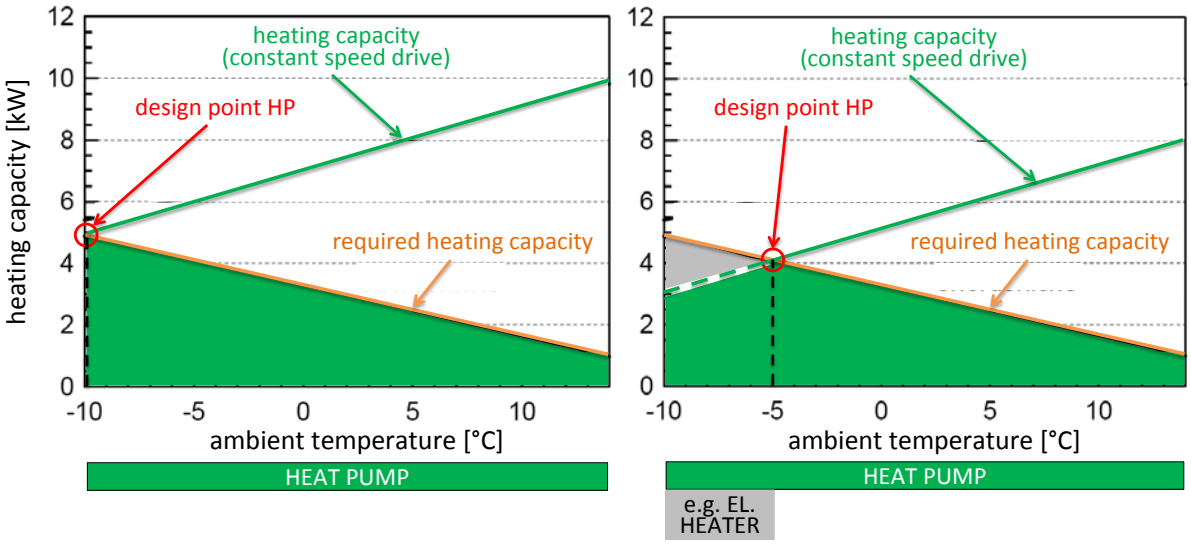

Figure 4: Schematical illustration for monovalent mode (left) and bivalent (right)

By using a bivalent operating mode an additional heating system – generally driven with fossil fuels – is applied to support the heat pump system at low ambient temperatures. If a bivalent-alternative (Figure 5) operating mode is used either the heat pump or the second heating system is on. If the ambient temperature drops below a certain set point the heat pump is switched off and the secondary heating system is switched on.

Another operating mode in the class of bivalent is bivalent-parallel (Figure 6). In this case the heat pump runs all the time if heating demand occurs, but if the ambient temperature drops below the defined set point a secondary heating system is switched on to support the heat pump system.

Concerning the operating mode “mono energetic”, which is basically a bivalent-parallel mode, the second heating system is an electric heating system, which is cheap in its investment. But the payback period depends mainly on the electricity price.

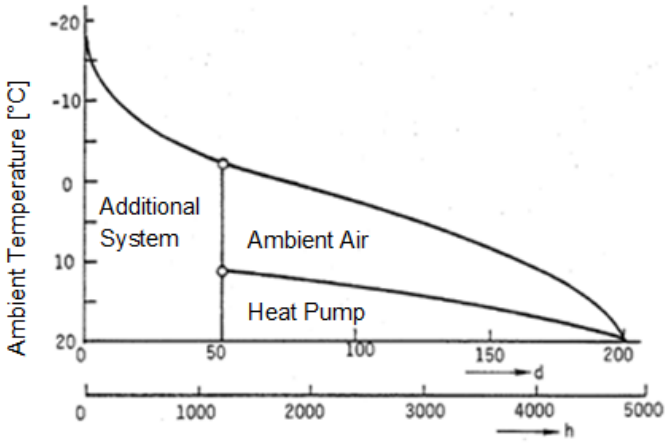

Figure 5: Bivalent alternative operating mode (Halozan, 1980)

Halozan (1980) has done some investigations concerning ASHP in bivalent systems. The author stated that heat pumps should primarily run with the operating mode bivalent-parallel if the same energy source is used for both the heat pump and the conventional heating system due to higher efficiencies of the heat pump. Whereas by using a heating system with

fossil fuel, the operating mode bivalent-alternative should be primarily used in cold conditions.

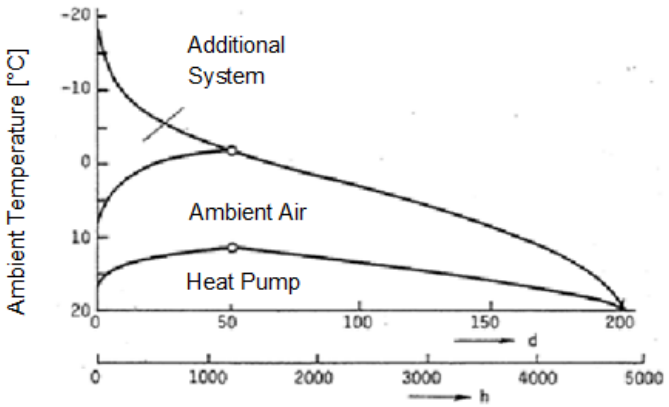

Figure 6: Bivalent parallel operating mode (Halozan, 1980)

2.2 Absorption Heat Pumps

Another type of heat pump is an absorption heat pump (Figure 7). This is worth to be mentioned in case of bivalent operating mode. “Typically” an absorption heat pump is designed in such a way, that it can cover the heating demand at moderate ambient temperatures. At lower ambient temperatures the boiler supplies the rest of the required capacity. However, the use of such heat pumps in domestic buildings is rather seldom up to now. Possibly this technology may play a more important role in future.

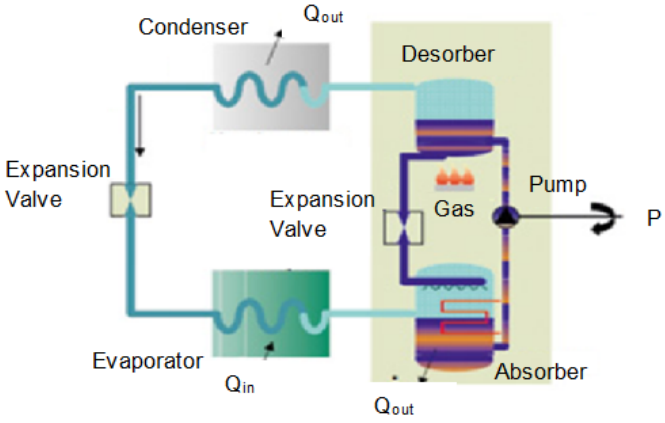

Figure 7: Absorption heat pump system (IKZ Fachplaner, 2014)

2.3 Gas-Engine Driven Heat Pump

An alternative to an electrically driven compression heat pump is to drive the compressor with a gas motor. For instance, Sanaye and Asgari (2013) established a simulation model to investigate such a system and validated the model with experimental results.

This gas-engine driven air-to-water heat pump (Figure 8) is composed of two major thermodynamic cycles (including the vapor compression refrigeration cycle and the internal combustion gas engine cycle) as well as a refrigerant-water plate heat exchanger.

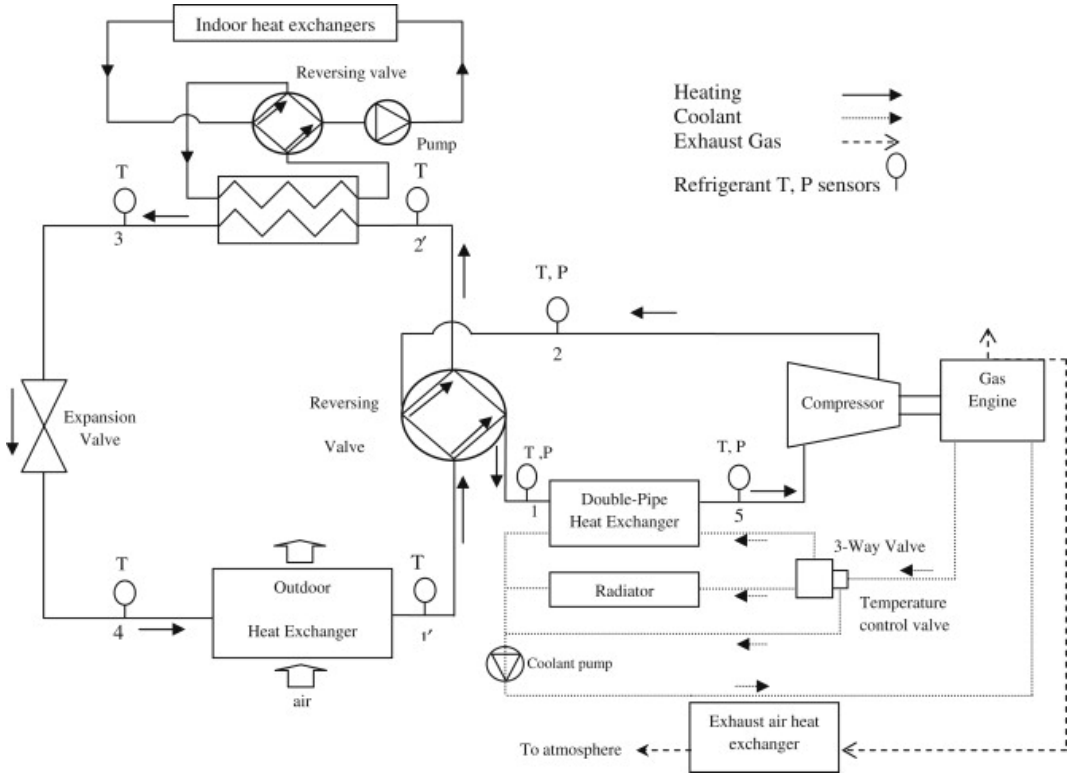

Figure 8: Schematic diagram of a gas engine driven air-to-water heat pump cycle (Sanaye and Asgari, 2013)

The thermal modeling of gas engine driven air-to-water heat pump system with engine heat recovery heat exchangers was performed here for the heating mode of operation (in which it was required to model engine heat recovery heat exchanger). The modeling was performed using typical thermodynamic characteristics of system components, Artificial Neural Network and the multi-objective genetic algorithm optimization method. The comparison of modeling results with experimental ones showed an acceptable agreement for operating pressure, gas engine fuel consumption, outlet water temperature, engine rotational speed, and system primary energy ratio.

3 HEAT PUMP LAYOUTS

ASHP systems are widely used in residential heating and cooling systems due to their low installation costs and their effectiveness (Heo et al., 2011). At low ambient air temperatures and especially with heating systems that require high flow temperatures these systems are operated at high pressure ratios and therefore achieve relatively poor Seasonal Performance Factors (SPF) in cold climates. Other problems are that the heating capacity of ASHP decreases and that the compressor discharge temperature increases to very high values at low ambient temperatures. In order to improve ASHP systems for the application in colder climates vapor injection systems are one possibility.

Figure 9 depicts a comparison of a standard heat pump cycle (left side) with a heat pump using an economizer cycle with heat exchanger (right side) in a temperature-enthalpy diagram. It can be seen that the compressor discharge temperature is lowered. Furthermore, the condenser capacity as well as the coefficient of performance can be increased by using an economizer cycle compared to the standard heat pump cycle at high pressure ratios. Due to the lower discharge temperature the economizer-cycle is well suited for cold climate regions. But this heat pump layout is one of several “advanced heat pump layouts” (e.g.

cascade cycle, economizer with different layouts, etc.) which are discussed within this chapter to increase the heating capacity and the performance especially in cold regions.

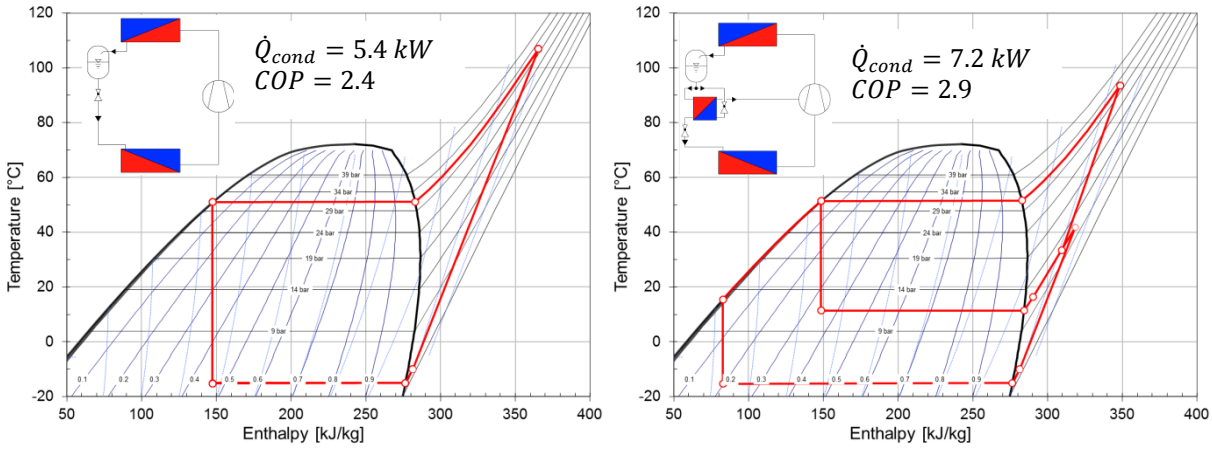

Figure 9: Standard heat pump cycle (left) and economizer cycle (right) in a temperature-enthalpy diagram of R410A (Hengel et al., 2014)

Lastly this chapter considers a heat pump cycle layout with an ejector. Although there are only few public literature available, this system seems to be promising for increasing both the heating capacity and the efficiency.

3.1 Vapor Injection Cycle

By means of a vapor injection into the compressor at an intermediate pressure the compressor discharge temperature can be reduced and both the heating capacity and the COP of the heat pump can usually be increased at low evaporation temperatures. Scroll compressors with midstage injection ports are available from several manufacturers, e.g. Copeland, Mitsubishi, Danfoss, etc. Some publications dealing with vapor injection has been found:

Liegeois & Winandy (2008) have tested three different R407C-compressors an A/C compressor (“ZR”), a modified heat pump compressor (the same like the A/C compressor but with an enlarged operation map and performance at high condensing temperatures – “ZH”), and a heat pump compressor with injection port (“ZH-KVE”). The chosen compressors family satisfy heating requirements between 5 kW and 40 kW at t_{evap} = -6.7°C /t_{cond} = 50°C. Figure 10 shows the vapor injection heat pump cycle as economizer cycle with internal heat exchanger (“HX”) and “ZH-KVE” scroll compressor.

The compressors were tested under “hard” conditions, for example at an ambient temperature of -15°C and a supply water temperature of +55°C. The compressor with injection port allows the heat pump to use an economizer cycle. Due to the injection port the operating map is larger compared to the other two compressors (“ZR” and “ZH”) (Figure 11).

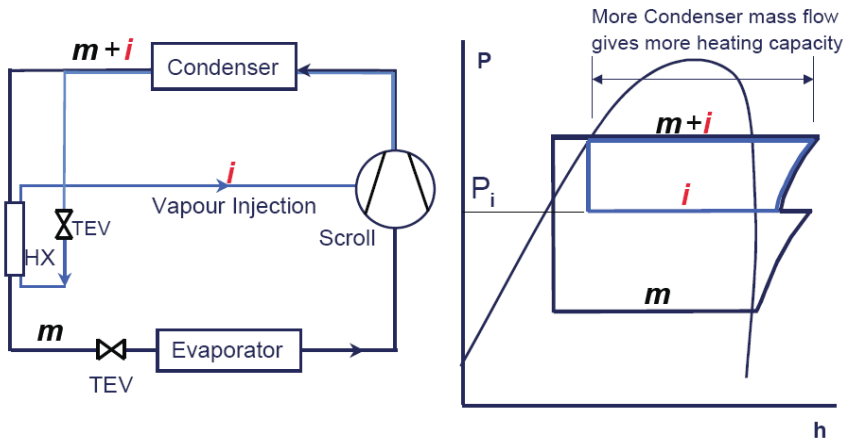

Figure 10: Vapor-injected scroll compressor with enhanced vapor compressor cycle (Liegeois & Winandy, 2008)

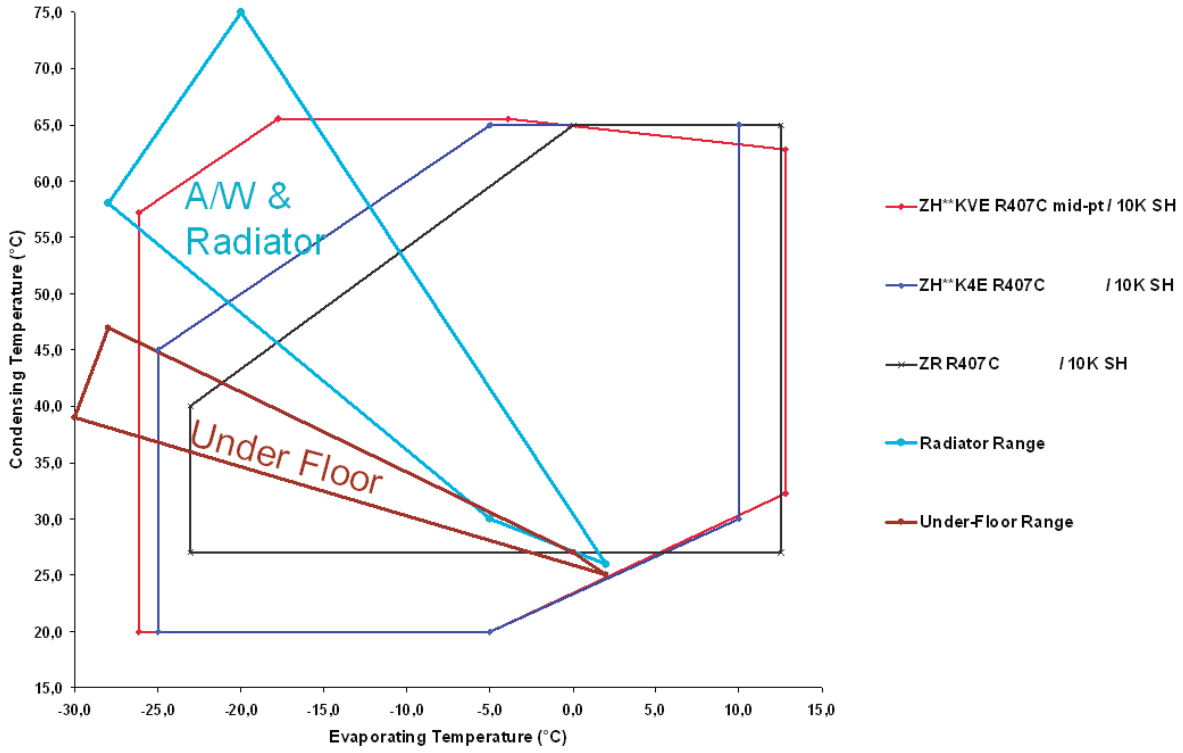

Figure 11: Operating map of compressors for ASHP applications (Liegeois & Winandy, 2008)

The results from this study show that the higher the temperature difference between evaporator and condenser is, the higher is the energy saving compared to the other two compressors (compare to Figure 12).

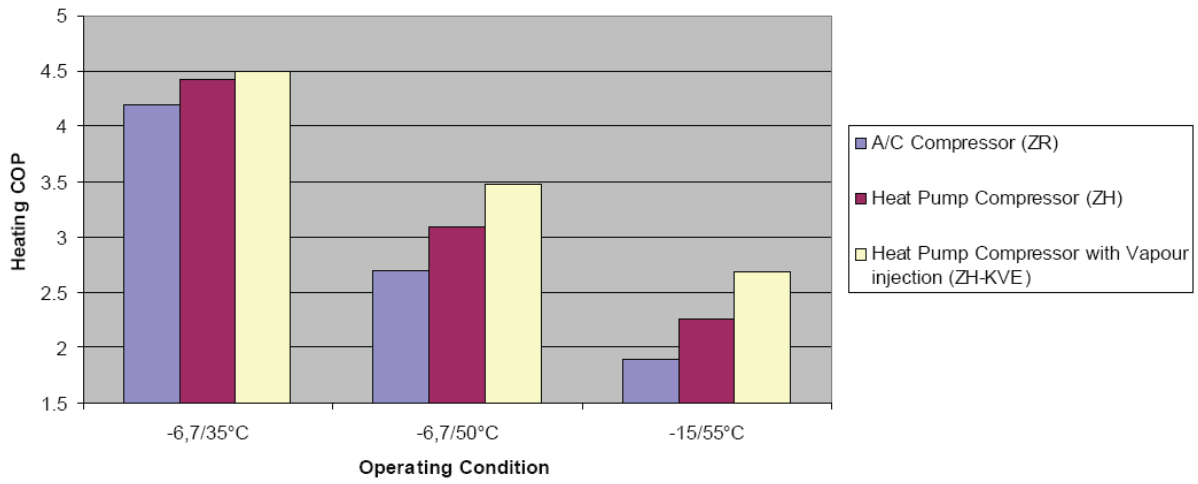

Figure 12: Performance Comparison (Liegeois & Winandy, 2008)

Zehnder et al. (2000) have also evaluated a heat pump system with scroll compressor and vapor injection. The injected refrigerant is evaporated partially by an internal heat exchanger (Figure 13). A glycol-water heat pump with 12 kW heat capacity at B-5/W50 was built and tested in the laboratory at several conditions (B: -5°C, 0°C and 5°C at W: 35°C and 50°C and B: -10°C at W: 60°C). “B” is the brine inlet temperature to the evaporator, and “W” denotes the water outlet temperature of the condenser. The refrigerant was R407C.

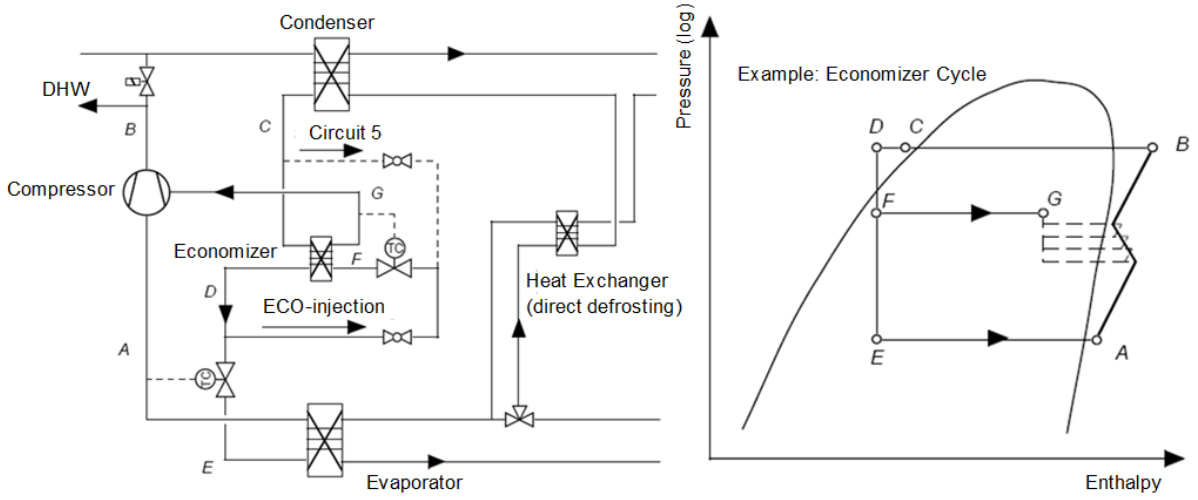

Figure 13: Heat pump cycle layout and the according logp-h-diagram (Zehnder et al., 2000)

Figure 14 shows on the left side the heating capacity depending on the evaporator inlet temperature “Glycol Inlet Temperature” and the condenser outlet temperature (W35 for 35°C and W50 for 50°C) for two refrigerant cycles with vapor injection at mid stage (“ECO” and “S5”, according to the cycle layout shown in Figure 13). The right picture illustrates the influence of the injection mass flow rate for the “ECO”-refrigerant cycle at different glycol inlet temperature of the evaporator (-5°C and -10°C) and different condenser outlet temperatures (50°C and 60°C) compared to the system without mid-stage injection (“KE”).

Measurements at stationary test conditions show with injection at mid stage an increase of the heat capacity by 15% compared to the values without injection (Figure 14, left). The heat output is not affected by the position of the manually controlled injection valve (Figure 14, right), but the compressor outlet temperature can be controlled by the amount of injected

refrigerant (Figure 15). The application range for this heat pump is enlarged and at the point B-10/W60 the maximum system temperature has been reduced from 110°C to 75°C.

Figure 16 shows the COP compared to the glycol inlet temperature at the evaporator for all three heat pump layouts and two different outlet temperatures at the condenser (35°C and 50°C). It can be seen that the COPs for both refrigerant cycle layouts using vapor injection are comparable but higher compared to the refrigerant cycle layout with non-injection at mid stage.

Figure 17 depicts the COP against the injection mass flow rate for two operating conditions, evaporator inlet temperature of -5°C at condenser outlet temperature of 50°C (B-5/W50) and evaporator inlet temperature of -10°C at condenser outlet temperature of 60°C (B-10/W60). The results show the highest COP at an injection mass flow rate of about 6 g/s for both operating conditions. By increasing the injection mass flow rate the COP is decreasing linearly and a reduction up to 15% occurs at B-10/W60.

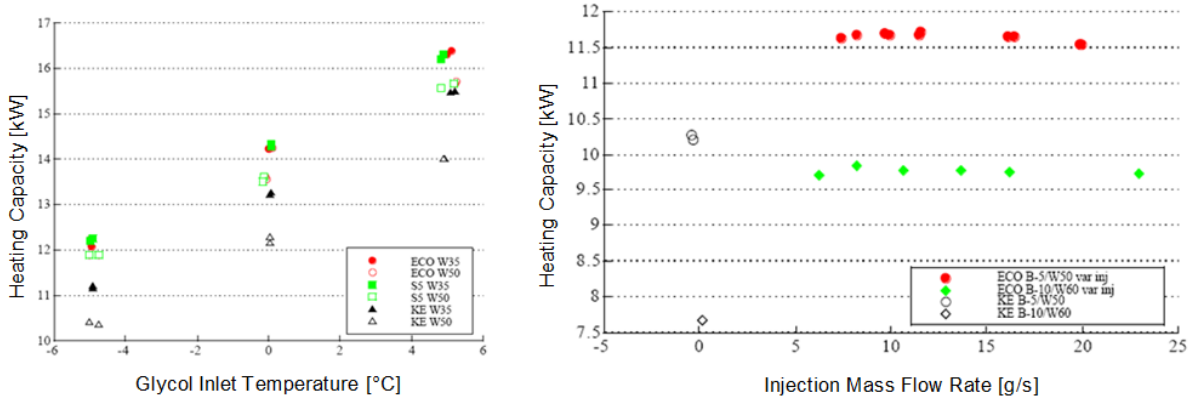

Figure 14: Heating capacity against glycol inlet temperature on the evaporator side (left) and heating capacity against injection mass flow rate at B-5/W50 and B-10/W60 (right) (Zehnder et al., 2000)

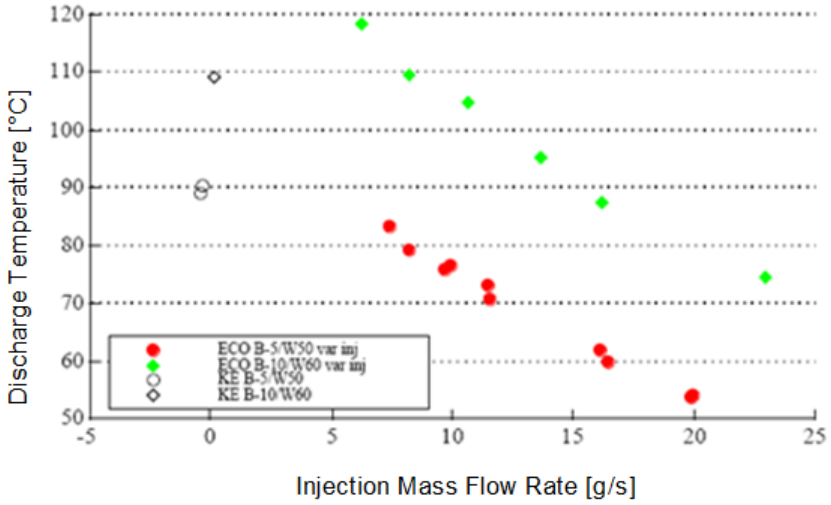

Figure 15: Discharge temperature against the injection mass flow rate at B-5/W50 and B-10/W60 (Zehnder et al., 2000)

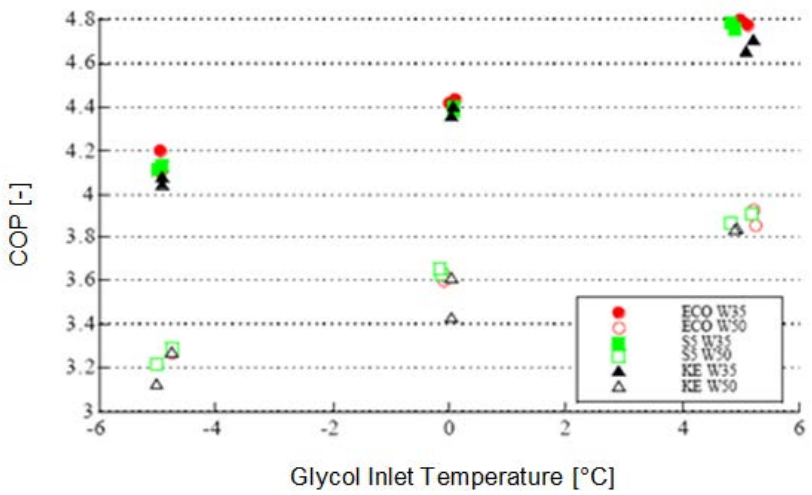

Figure 16: Coefficient of performance against glycol inlet temperature at condenser outlet temperature of 35°C (W35) and 50°C (W50); injection mass flow rate controlled by the thermostatic expansion valve (Zehnder et al., 2000)

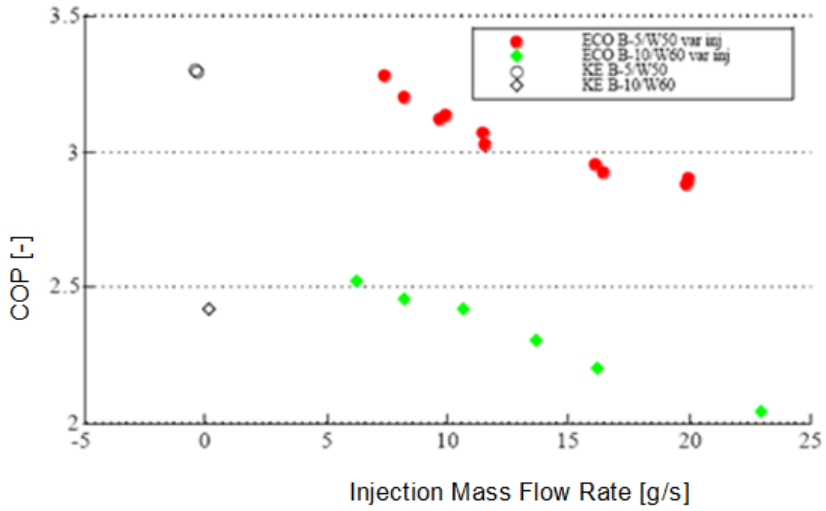

Figure 17: Coefficient of performance against the injection mass flow rate at B-5/W50 and B-10/W60 (Zehnder et al., 2000)

Another experimental investigation concerning air source heat pumps (ASHP) with scroll compressors in cold regions have been done by Guoyan et al. (2003). The authors compared two types of heat pump layouts where one is an economizer cycle with an internal heat exchanger and the other one is a conventional “standard” heat pump cycle. A scheme of the heat pump principle is shown in Figure 18 on the left side and the corresponding lgp-h diagram on the right side where the points 1-2-2’-3 describes the two-stage compression process of the economizer cycle. The point 3’ is only used for the compression process in case of a single-stage compression.

The results of the experimental tests show similar results compared to Liegeois & Winandy (2008) and Zehnder et al. (2000), see above. Guoyan et al. (2003) show measuring results for the economizer cycle concerning the heating capacity for two different condensing temperatures (t_c = 45°C and t_c = 48°C) against different evaporating temperatures t_e (Figure 19, left) as well as the power input depending on the evaporating temperature (Figure 19, right).

The heating capacity decreases linearly with decreasing of the evaporation temperature for both condensing temperatures, where the heating capacity at t_c = 45°C shows slightly higher values (about 5.1 kW vs. 5.2 kW at t_e = -25°C). This is mainly due to the compressor efficiency which is lower at higher pressure ratios.

The power input decreases with decreasing evaporating temperatures for both condensation temperatures, which leads to the results for the COP (here called: "Energy Efficiency Ratio" EER = heating capacity / Power input)) in Figure 20 on the left side. The right side of Figure 20 represents the discharge temperature against the evaporating temperature. Due to the vapor injection the discharge temperature does not reach 130°C at an evaporation temperature of -25°C for both condensation temperatures, this prevents the compressor for possible deteriorations.

Lastly the authors compared the economizer cycle with the conventional heat pump cycle. The results show for the heating capacity, power input and energy efficiency of the economizer cycle at t_e = -15°C / t_c = 45°C an improvement of 8.6%, 2.5% and 6%, respectively, and at t_e = -12°C / t_c = 45°C 5.5%, 1.6%, 3.7%, respectively.

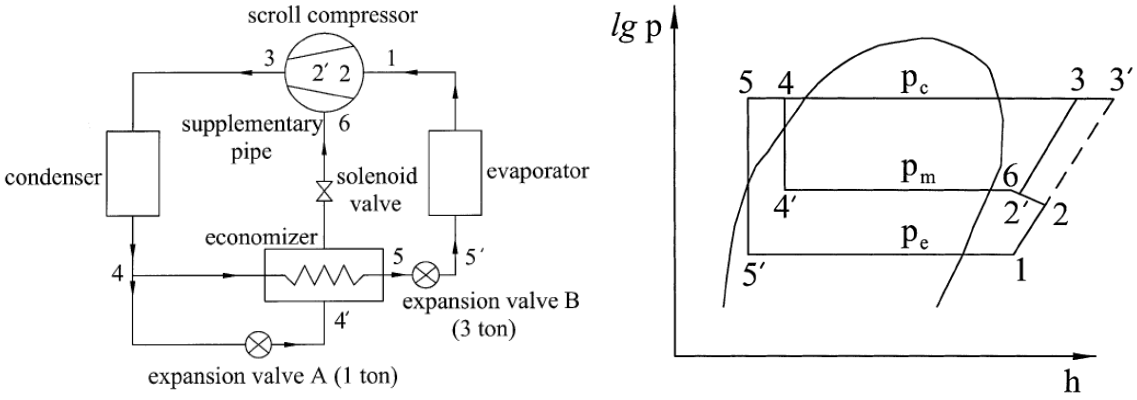

Figure 18: Scheme of the ASHP cycle (left) and regarding lgp-h diagram (right) (Guoyan et al., 2003)

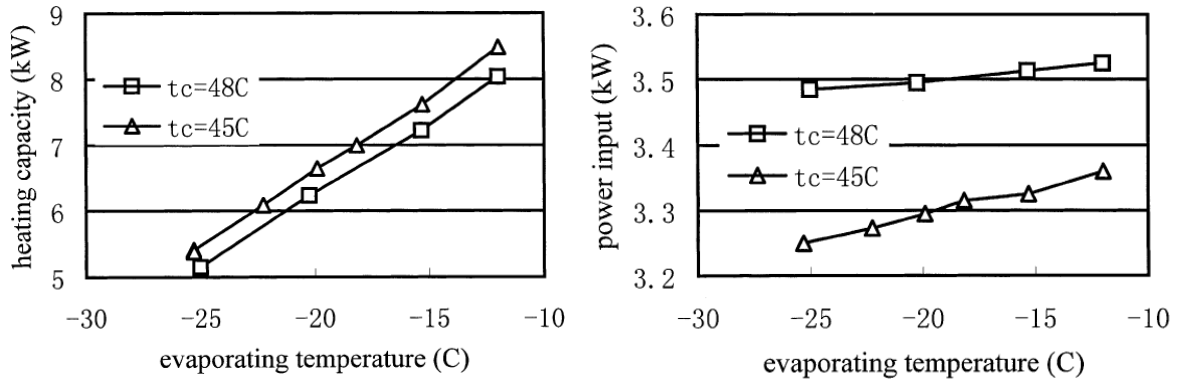

Figure 19: Heating capacity (left) and power input (right) against evaporating temperatures for two condensing temperatures (Guoyan et al., 2003)

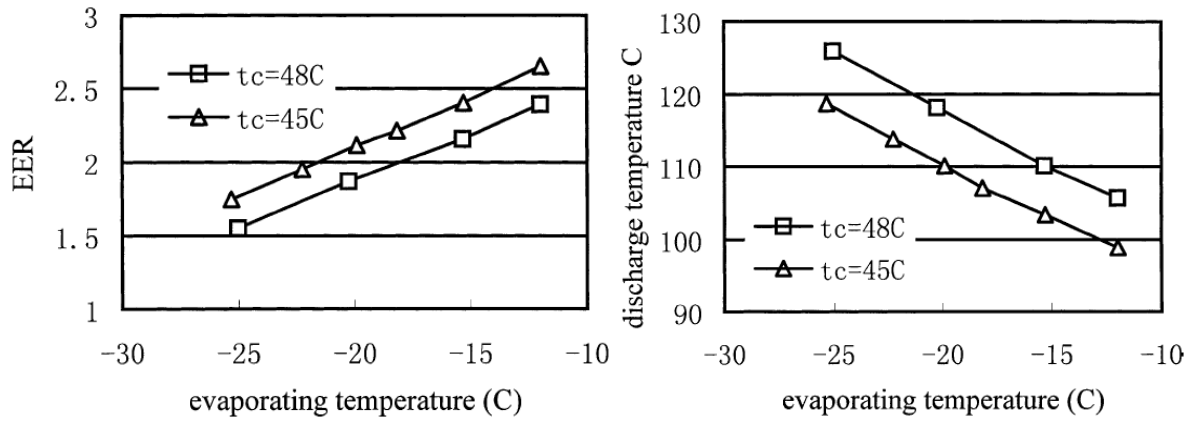

Figure 20: Efficiency energy rate (EER) (left) and discharge temperature (right) against the evaporating temperatures for two condensing temperatures (Guoyan et al., 2003)

Shuxue et al. (2014) investigated a two stage compression heat pump system with dual cylinder rolling piston compressors by means of simulations. A schematically diagram is shown in Figure 21.

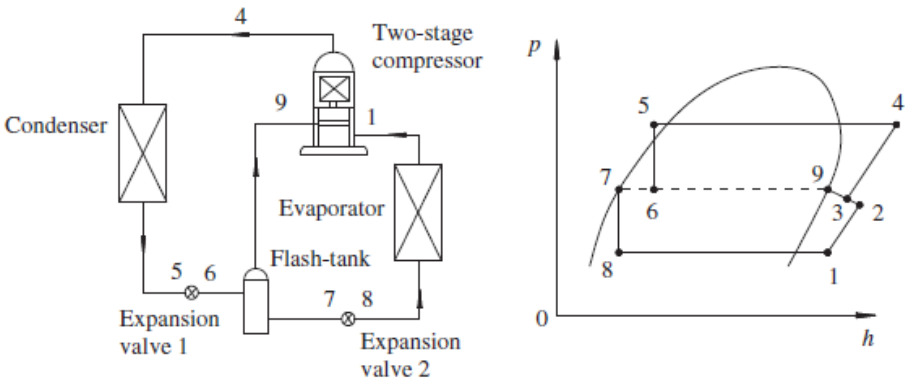

Figure 21: Two-stage compression refrigeration/heat pump system (Shuxue et al., 2014)

The two stage compressor consists of three parts, according to the operating pressure. The low pressure part consists of the low pressure cylinder with the suction line coming from the evaporator. The intermediate part is including the mixing chamber between the high pressure cylinder and the low pressure cylinder and the vapor injection, coming from the flash-tank. Finally there is the high pressure part with the high pressure cylinder, whose pressure line is connected to the condenser. COPs were simulated at three different evaporating temperatures and different volume ratios ε, regarding the volumes of the two compressors.

$$\varepsilon = \frac{v_1}{v_3 \cdot (1+\delta)} \quad (1)$$

With:

ε …. volume ratio high pressure cylinder to low pressure

v_1….specific volume in state point 1 (Figure 21)

v_2….specific volume in state point 3 (Figure 21)

δ…..relative vapor injection mass ($\delta = \dot{m}_9/\dot{m}_1$, Figure 21)

Figure 22 shows the results of the heating COP against the different volume ratios.

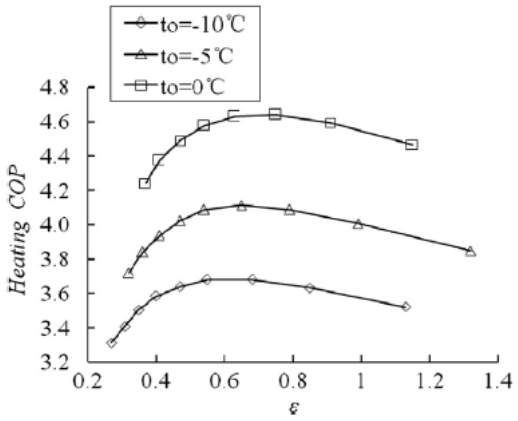

Figure 22: The variation of heating COP with ε (Shuxue et al., 2014)

At a certain value of ε, the heating COP reaches a maximum. As a result of this, the used ε for designing such systems should be between 0.65 and 0.78.

Afterwards the heating performance at very low temperatures (between -28°C and -24°C) was investigated experimentally. The results of the power input ("P"), the heating capacity ("Q_k") and the COP_H, relative to the values reached at 7°C evaporation temperature, are shown in Figure 23. At an evaporation temperature of -24°C, the heating capacity reached 55% and the COP reached about 60%. This figure shows also the advantage of the two stage compression system in comparison to the single stage system with respect to the decrease in heating capacity and COP_H at dropping evaporation temperatures.

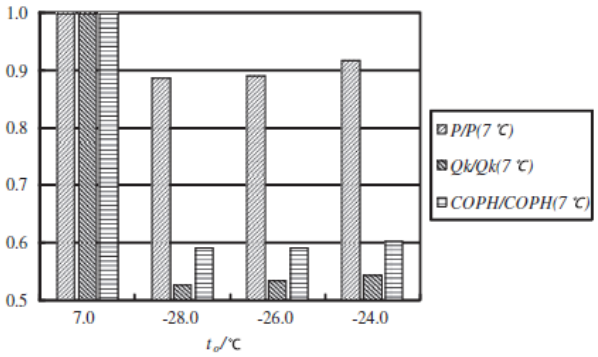

Figure 23: Variation of heating performance ratio at low evaporation temperatures (Shuxue et al., 2014)

Another investigation on two stage compression heat pump systems with rolling piston compressors was done by Xu et al. (2012). The high pressure compressor was used as a rolling piston compressor. The two low pressure compressors were used as twin rolling pistons with inverter technology. The aim was to investigate the behavior of the resulting COP and the available heating capacity of the system in dependence of the intermediate pressure, which occurred due to the injection process that took place between the two compressor stages. These tests have been performed especially for very cold temperatures,

reaching -30°C. Figure 24 shows a schematic diagram of the two stage compression cycle. The used experimental setup of the whole system can be seen on Figure 25.

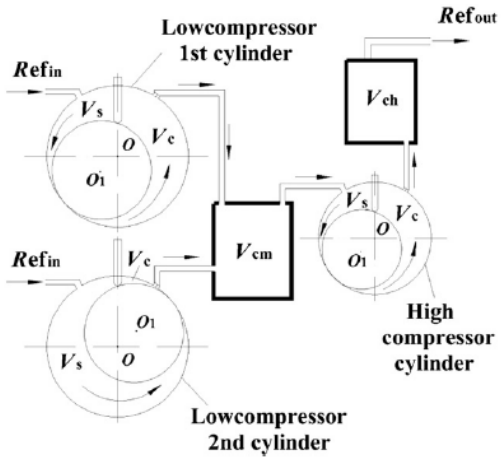

Figure 24: Schematic diagram of dynamic coupling model in two-stage compression cycle (Jin et al., 2012)

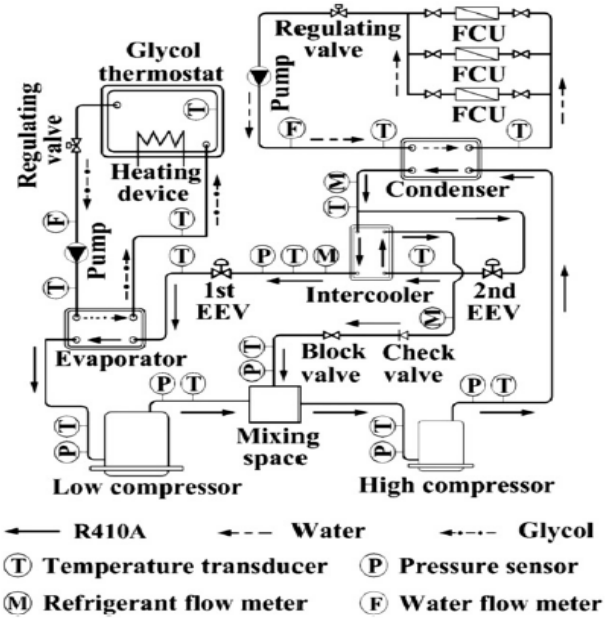

Figure 25: Schematic diagram of experimental device (Jin et al., 2012)

Results of the heating capacity and the COP in dependence of the used intermediate pressure p_m at different evaporation temperatures are shown in Figure 26. The system performance results under different conditions show that the heating capacity almost increases linearly with the increase of the intermediate pressure and the COP has a trend of first increasing and then decreasing with the increase of the intermediate pressure. However the COP is nearly independent of the intermediate pressure.

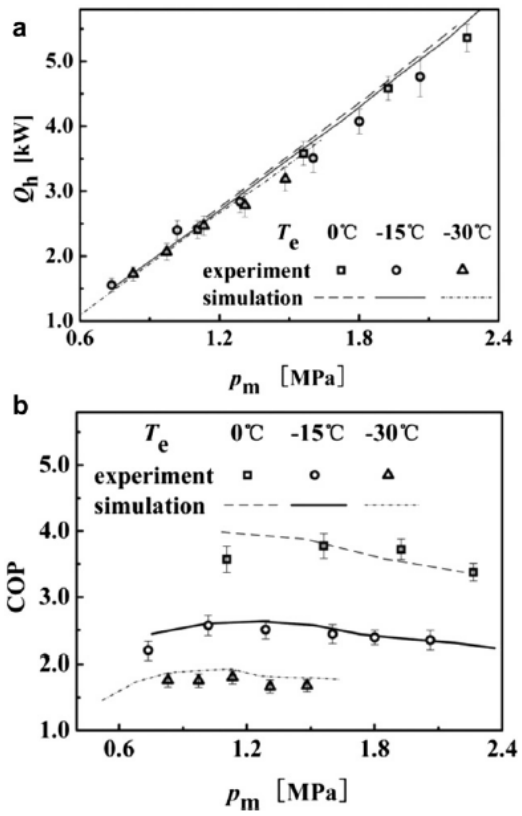

Figure 26: Variation on heating performance with p_m; (a) Variation of the heating capacity; (b) Variation of the COP (Jin et al. 2012)

3.2 Liquid Injection

A possible improvement of ASHPs for cold climates is liquid injection to the (scroll) compressor. According to Lammert (2013) this measure enlarges significantly the compressor envelope by lowering the compressor discharge temperature, which is of special interest in case of high condensation temperatures (see Figure 27). However, liquid injection ("LI") does not offer the advantageous of an economizer flow chart (vapour injection, "VI") with respect to efficiency and capacity, but it is a rather simple measure allowing air-source heat pumps to be operated at very low ambient and condensation temperatures. This may result in ca. 10% energy savings compared to a standard heat pump combined with a furnace heating backup (Lammert, 2013).

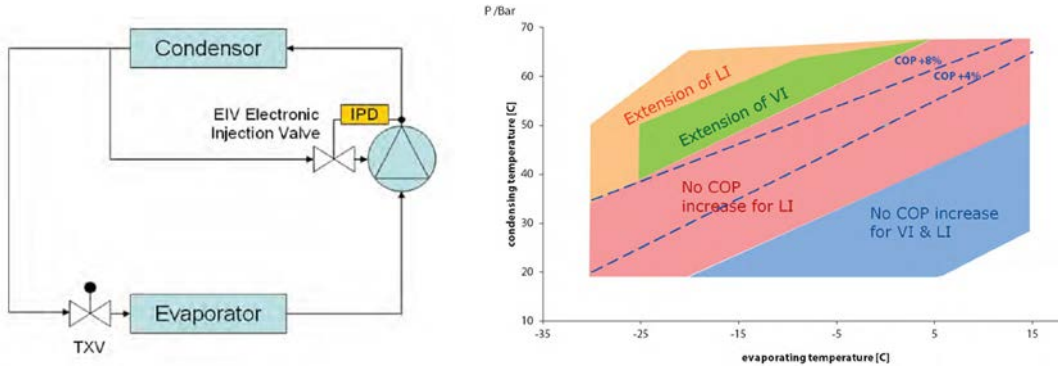

Figure 27: Liquid Injection – left: basic layout, right: compressor envelope (Lammert, 2013)

3.3 Ejector Cycle

Another option which seems promising with respect to energy efficiency is the use of an ejector system. Yari and Sirousazar (2007) have theoretically analyzed an ejector-vapor compression refrigeration cycle with internal HeX (heat exchanger) and intercooler. This system is compared to a conventional ejector-vapor compression refrigeration cycle in detail (Figure 28), and in addition both systems are compared to two vapor-compression refrigerant cycles by using R125 as refrigerant. Figure 29 depicts the corresponding diagrams for the advanced ejector cycle, lgp-h on the left hand side and T-s on the right hand side.

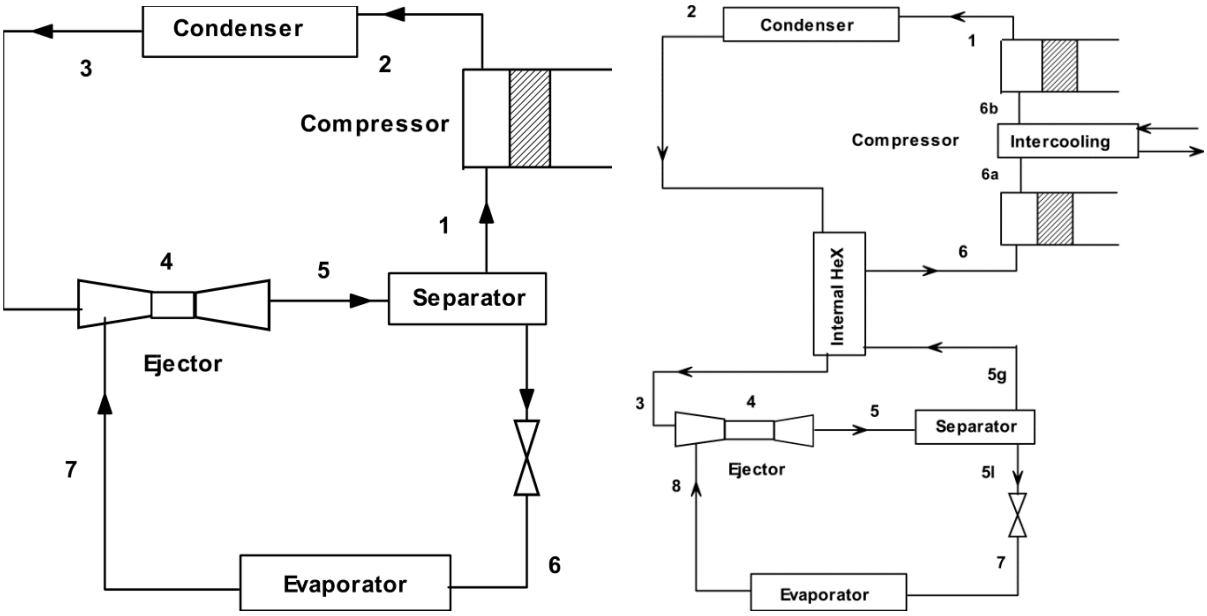

Figure 28: Scheme of conventional ejector-vapor cycle (left) and advanced ejector-vapor cycle (right) (Yari and Sirousazar, 2007)

For the vapor-compression cycle one is equipped with an internal heat exchanger and an intercooler and the other one is a conventional heat pump cycle.

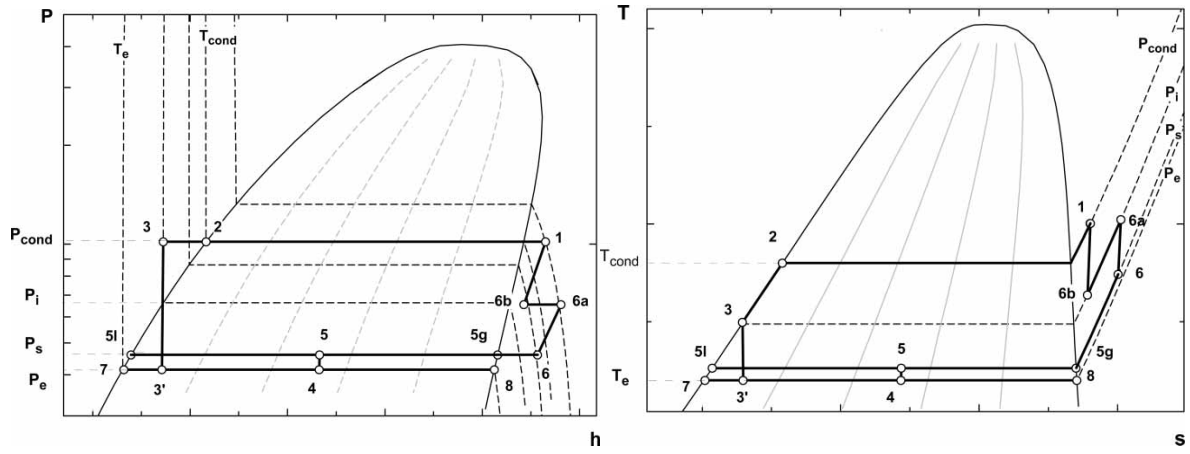

Figure 29: Lgp-h diagram (left) and T-s diagram (right) of the advanced ejector cycle (Yari and Sirousazar, 2007)

Figure 30 shows the variation of the COP of the two ejector-vapor compression refrigeration cycles against the evaporation temperature at a given condensation temperature of

T_c = 313 K (40°C). "Present cycle" in Figure 30 indicates the advanced ejector cycle and "Ejector-compression cycle" presents the standard ejector cycle. The COP of the advanced ejector cycle is in average about 8.6% higher than the conventional cycle. The reason for the higher COP of the advanced ejector cycle is that the COP is mainly depending on the ejector entrainment ratio, which is in average 27% higher for the advanced ejector system due to the cycle layout.

Yari and Sirousazar (2007) have also analyzed both ejector cycles with different refrigerants. The results are shown in Figure 31 for constant operating conditions, T_e = 278 K (5°C) and T_c = 313 K (40°C). From this figure, it can be seen that the best performance is obtained with R141b, with a COP of approximately 6.3.

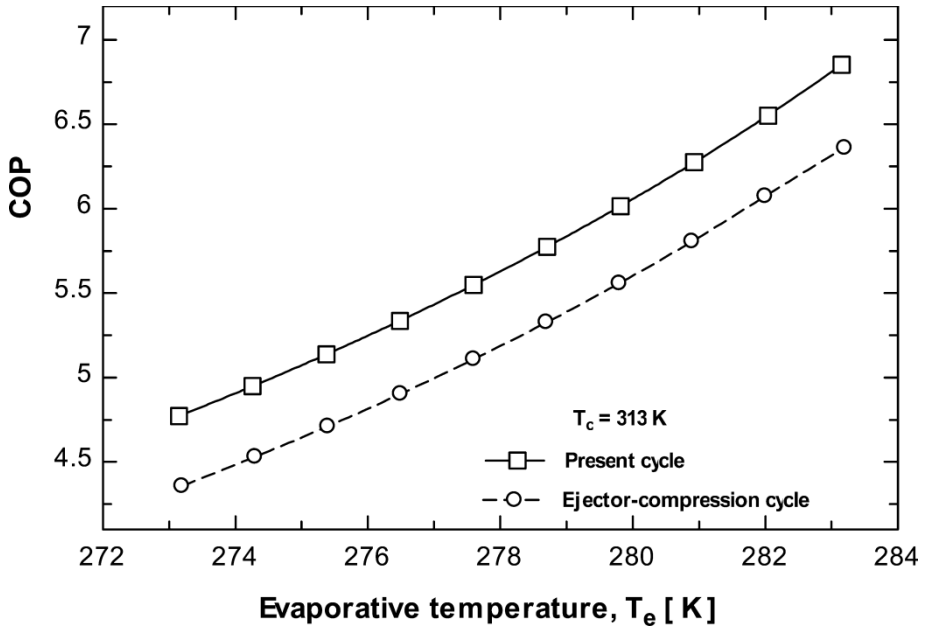

Figure 30: COP versus evaporative temperature for R125 (Yari and Sirousazar, 2007)

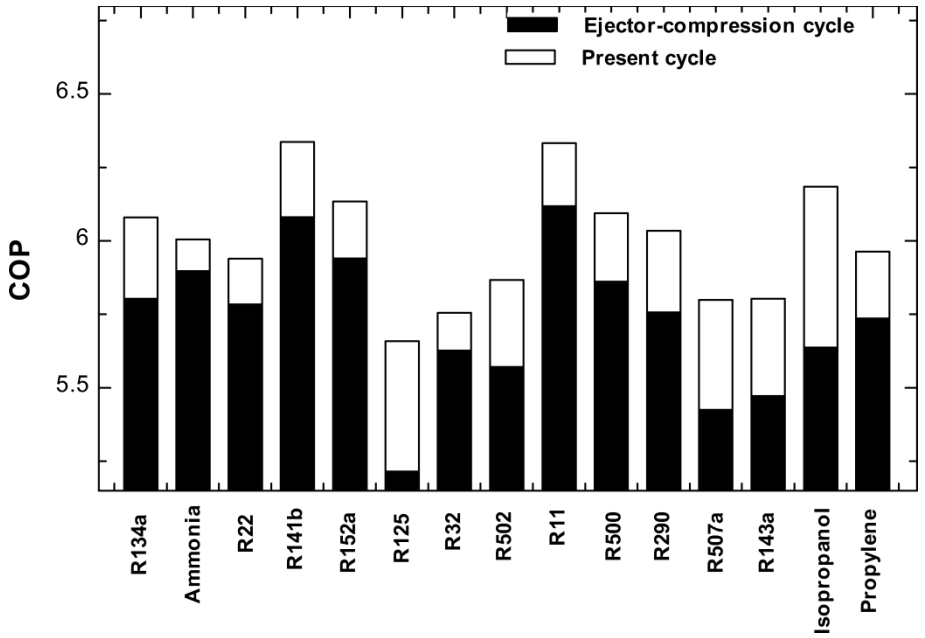

Figure 31: COP of conventional and advanced ejector-compression cycles for various fluids (Yari and Sirousazar, 2007)

As mentioned above the authors also compared both ejector systems with two “standard” vapor compression systems. Figure 32 shows the results for the COP and the second law efficiency for the refrigerant R125 at $T_e = 278$ K and $T_c = 313$ K. The highest COP is achieved by the advanced ejector-vapor compression cycle (about 5.66), followed by the advanced vapor compression cycle with internal heat exchanger and intercooler (COP of about 5.44).

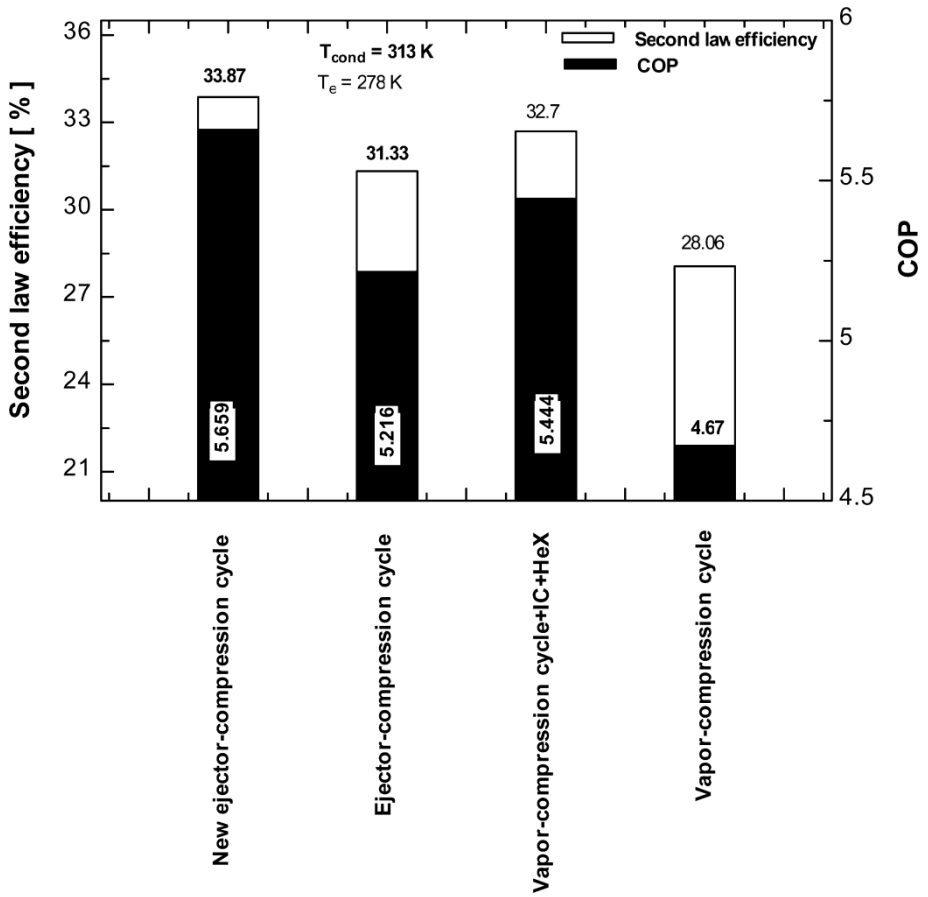

Figure 32: COP and second law efficiency values comparison of the vapour compression cycles for R125 (Yari and Sirousazar, 2007)

Although there is no consideration of evaporation temperature below -7°C, which is relevant for cold climates, the ejector-vapor compression refrigerant cycle seems to be promising with respect to energy efficiency. Due to lack of information further investigations on this topic should be carried out.

3.4 Cascade Systems

There is only a small amount of information about cascade systems in the public literature available, which deals with such system in cold regions. One is Bertsch and Groll (2008), who investigated three systems (Figure 33) by means of system simulations.

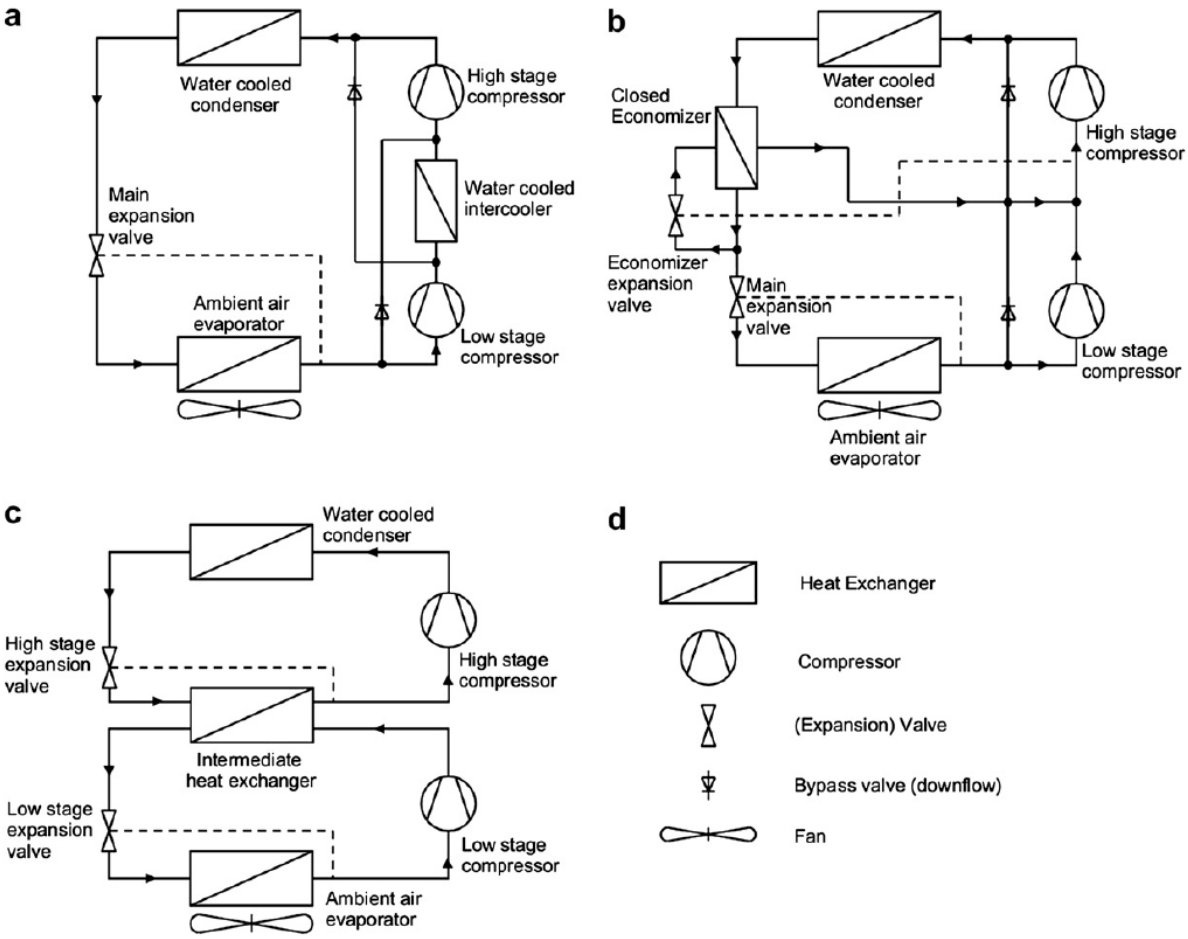

Figure 33: Simplified schematics of (a) two-stage cycle with intercooler, (b) two-stage cycle with closed economizer, (c) cascade cycle, and (d) list of symbols (Bertsch and Groll, 2008)

The results show COPs of above 2 for all systems at the lowest outdoor temperature of -20°C and a water supply temperature of 50°C, and all three cycles are predicted to be able to satisfy the heating load. The authors stated that the only noticeable difference between a cascade system and other cycles is at warmer ambient temperatures (Figure 34 and Figure 35). Here the COP of the cascade cycle is considerably lower than that of the economizer and intercooler cycles maybe due to the sizing of the high stage cycle of the cascade system.

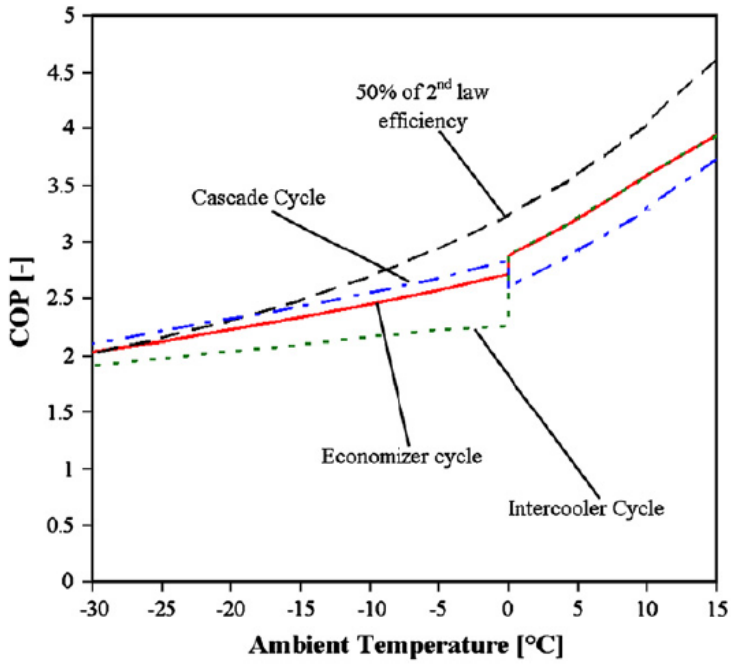

Figure 34: Simulation results of the Coefficient of Performance (COP) for two-stage cycle with intercooler or economizer and for cascade cycle at 50°C supply temperature (Bertsch and Groll, 2008)

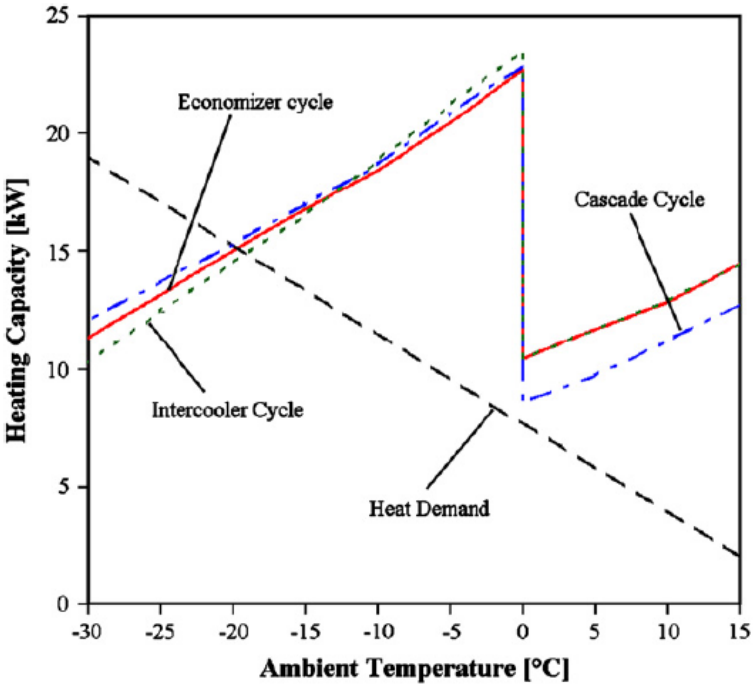

Figure 35: Simulation results of the heating capacity for two-stage cycle with intercooler or economizer and for cascade cycle at 50°C supply temperature (Bertsch and Groll, 2008)

All in all the authors concluded that the economizer cycle would be the best choice for an ASHP in colder climates. For further information see US report on Task 1 of Annex 41.

3.5 Conclusion

The literature study concerning heat pump layouts show promising results for the economizer cycle, the cascade system and the ejector system. The first two layouts are suitable for low evaporation temperatures and their performance and heating capacity are satisfying for cold climates. The investigations show an improvement in efficiency and heating capacity as well as in maximum discharge temperature compared to a standard heat pump cycle.

Although liquid injection does not offer the advantageous of an economizer flow chart with respect to efficiency and capacity, but it enlarges significantly the compressor envelope by lowering the compressor discharge temperature, which is of special interest in case of high condensation temperatures and low evaporation temperatures.

For the ejector system only ambient temperatures above 0°C were investigated but with the results that the ejector system with intercooler and internal heat exchanger can improve the COP by about 21% compared to a standard heat pump cycle at the considered conditions. However, further investigations should be done for lower ambient temperatures to verify its efficiency in cold climates.

4 CONTROL STRATEGY OF HEAT PUMPS

Conventional heat pumps are usually equipped with a constant-speed compressor, which are operated in on/off-mode to provide the energy that is necessary e.g. for space heating. Especially with ASHPs the thermal output increases at an increasing ambient air temperature, while the required heating capacity of the building decreases. Consequently the thermal output of the heat pump is much higher than the actual demand for the major part of the year causing a large number of on/off cycles of the heat pump. A heat pump with variable speed controlled compressor (VSD) can adjust its heating capacity to the currently required heating load during a large part of the heating season (Figure 36). This results in a reduction of the number of on/off cycles and an increased efficiency. Different researchers showed the potential of electric energy savings by using a VSD (e.g. Aprea et al., 2004 and Gasser et al., 2008).

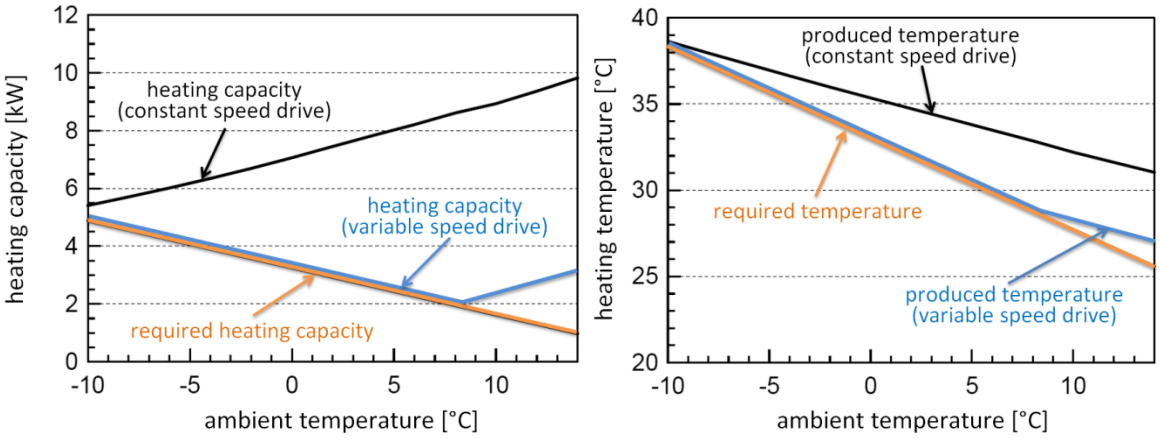

Figure 36: Heating capacity and heating temperature depending on the ambient temperature (modified from Gasser et al., 2011)

However, the study carried out by Gasser et al. (2011) deals with universally valid design and planning criteria for the realization of efficient, reliable and economic air/water heat pumps with continuous capacity control and economizer cycle. An optimized process control

depending on the applied control strategy of the heat pump has been developed using simulations as well as experiments (Figure 37 and Figure 38). The aim of this control strategy is that the compressor should operate at its highest COP if it is possible. The highest COP is not at the highest compressor speed so in case of higher heating capacity of the building the compressor increases its speed to match the required heating capacity, but the COP drops below its maximum. In case that the heating capacity of the building drops below the heating capacity of the compressor, where the highest COP occurs, the compressor switch its control strategy to an on/off strategy to stay at the compressor speed with the highest COP.

To verify the theoretical findings as well as to investigate different control strategies for a heat pump prototype with capacity control, a test facility for air/water heat pumps has been realized (Figure 39). The investigations show that the optimal control strategy and the efficiency of the capacity controlled heat pump strongly depend upon the part load efficiencies of the compressor and the fan (Figure 40). The experimental investigations approve the great potential of the capacity control. Figure 41 shows the control strategy for the heat pump with variable speed compressor and economizer.

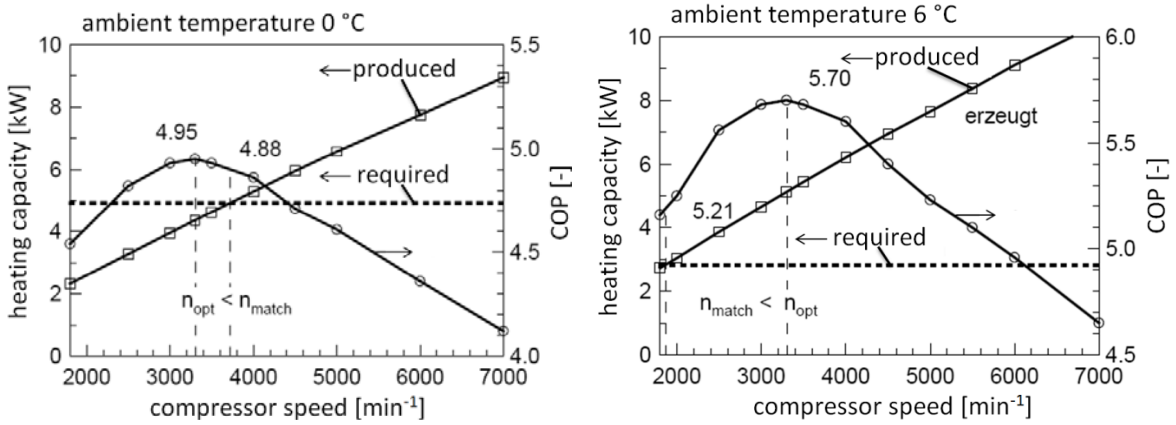

Figure 37: COP and heating capacity depending on the compressor speed for two different ambient temperatures (Gasser et al., 2011a)

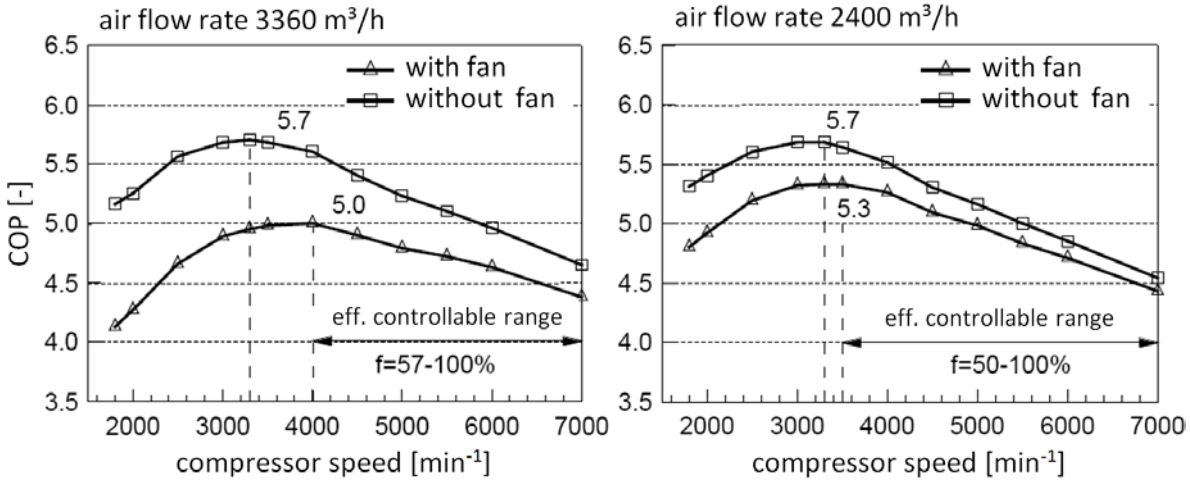

Figure 38: COP at different air flow rates (Gasser et al., 2011a)

As a result of the capacity control and using an economizer the Seasonal Performance Factor (SPF) can be increased by approximately 13% from 4.2 (standard ASHP) to 4.75 (advanced heat pump layout) (design supply/return temperature: 30°C/25°C at

$t_{ambient}$ = -10°C). For a retrofit building (design supply/return temperature: 41°C/35°C at $t_{ambient}$ = -10°C) the SPF could be increased by approximately 49%.

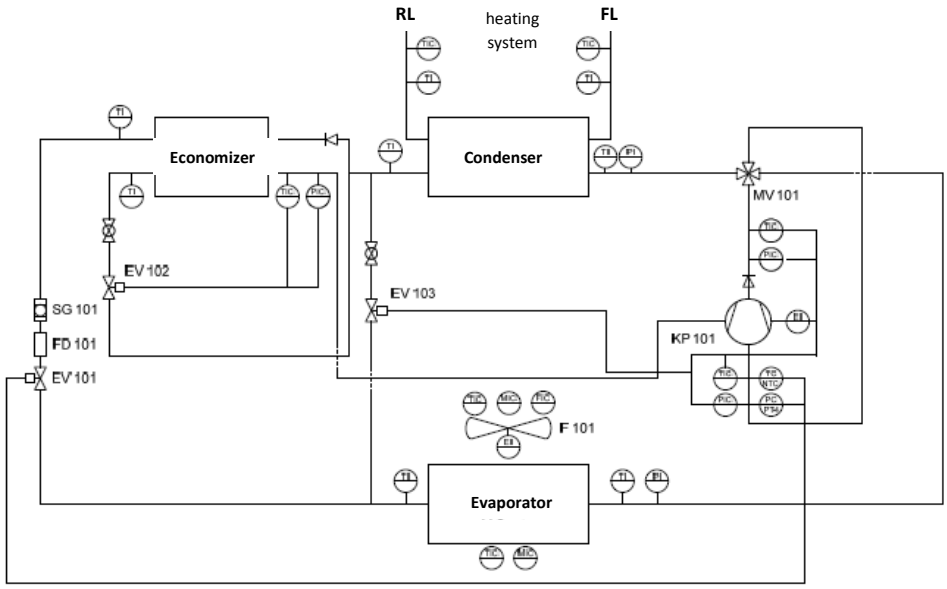

Figure 39: Scheme of the air/water heat pump prototype layout with inverter compressor technology and economizer (Gasser et al., 2011)

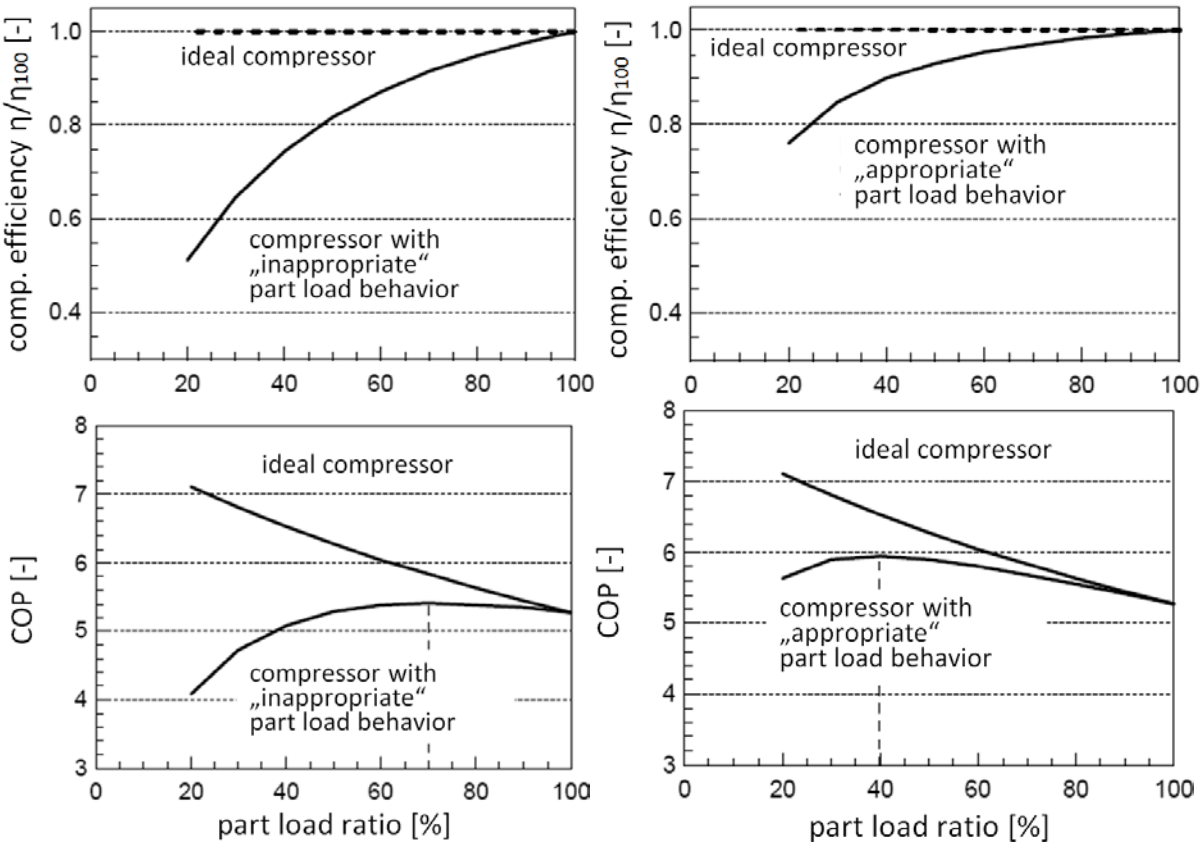

Figure 40: Load behavior of different compressor types (Supply Temperature: 30°C, Return Temperature: 25°C, Ambient Temperature: -10°C) (Gasser et al., 2011)

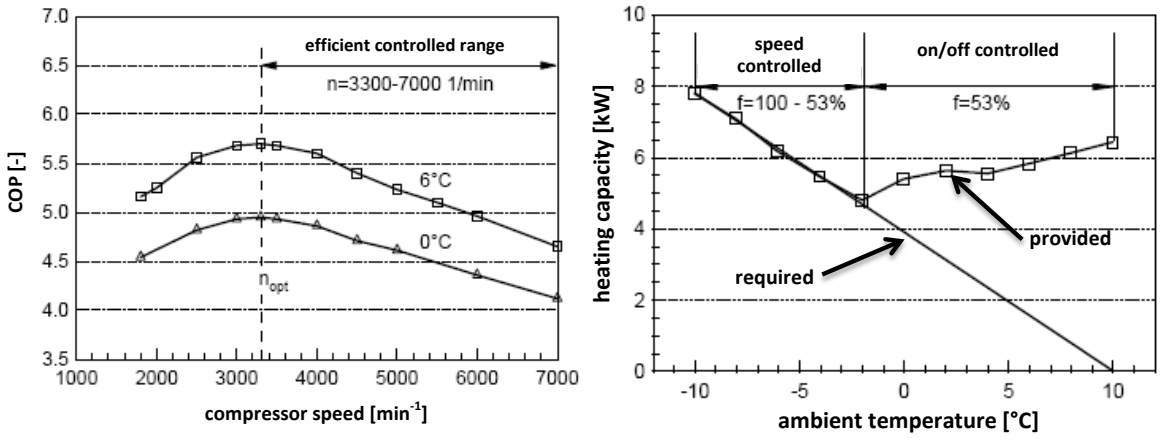

Figure 41: COP against compressor speed at ambient temperatures of 0°C and 6°C (volume flow rate through the evaporator: 3360 m³/h, humidity: 85%) (left) and the provided heating capacity of the heat pump against the ambient temperature (right) for a low energy house with a flow/return temperature of 30/25°C at -10°C ambient temperature (Gasser et al., 2011)

Another study concerning a heat pump system comprising a speed controlled compressor and an economizer cycle (CEV) by means of detailed measurements in the laboratory and simulations was done by Hengel et al. (2014). The measured data was used to parameterize and validate a detailed simulation model of the heat pump. Using this model, dynamic system simulations were performed to analyze the SPF of the heat pump system in comparison to a standard heat pump (CSD, i.e. Constant Speed Drive) for a retrofit building located in Zurich.

Figure 42 shows the assumed hydronic scheme for the annual simulations with the heat pump ("HP") and the hydronic system on the right side of the heat pump. The heat pump is responsible for the space heating of the building, which is split into two thermal zones (north and south) and for preparing domestic hot water (DHW), where priority is for DHW.

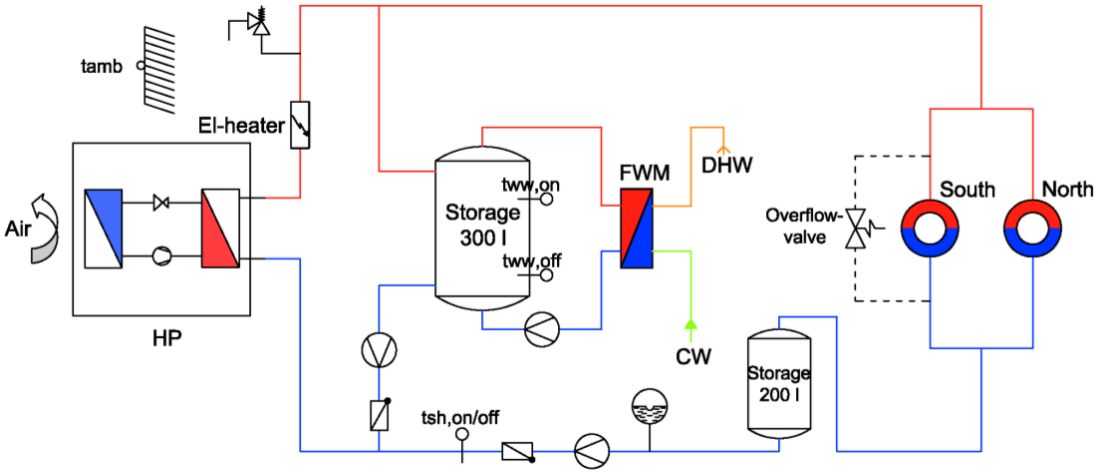

Figure 42: Hydronic scheme for the annual simulations (Hengel et al., 2014)

Table 1 depicts the climate and building definition for the simulation. The assumed building is an adaption of the IEA SHC TASK 44/HPP ANNEX 38 (T44A38) reference building, which is a single family house and has a heating demand of 100 kWh/(m²·a) for the climate Strasbourg (SFH100). The supply temperature of the radiator heating system is 55°C and the return temperature is 45°C at design ambient conditions (= -10°C).

Table 2 shows the technical data of the considered scroll compressors, with economizer and variable speed control (CEV, i.e. Combined Economizer and Variable speed drive) and constant-speed control only (CSD). Whereas the first compressor is used in the test rig and the experimental data is used for the validation of the heat pump model CEV. The model for the second compressor, CSD, is based on manufacturer data.

Table 1: Climate and building definition for the simulation (Hengel et al., 2014)

Climate			Building				
Location	Design temperature	Heating degree days	Heating system	Heating demand	Heating load	Heating area	Design room temperature
	[°C]	[Kd/a]		[kWh/(m²·a)]	[kW]	[m²]	[°C]
Zurich	-10	3406	Radiator system	154	7.87	140	20

Table 2: Technical data of the considered scroll compressors, with economizer and variable speed control (CEV) and constant-speed control only (CSD) (Hengel et al., 2014)

compressor		CEV	CSD
Swept volume (V_{swept})	ccm	15.56	49.44
Speed range	rpm	1800 - 7020	3000
Refrigerant		R410A	R410A
Heating capacity at t_{evap} = -15°C & t_{cond} = 55°C; ΔT_{sup} = 5 K, ΔT_{sub} = 0 K	kW	8.6	8.9

Both compressors meet the heating load of the building plus additional 0.5 kW for DHW preparation. In case of the CSD the capacity (8.9 kW) is slightly higher compared to the CEV (8.6 kW). Figure 43 shows the compressor efficiencies (overall isentropic $\eta_{is,over}$ and volumetric η_{vol} efficiency) for the CEV heat pump system which are obtained by measurements and additionally the compressor efficiencies for CSD which are assumed from manufacturer data.

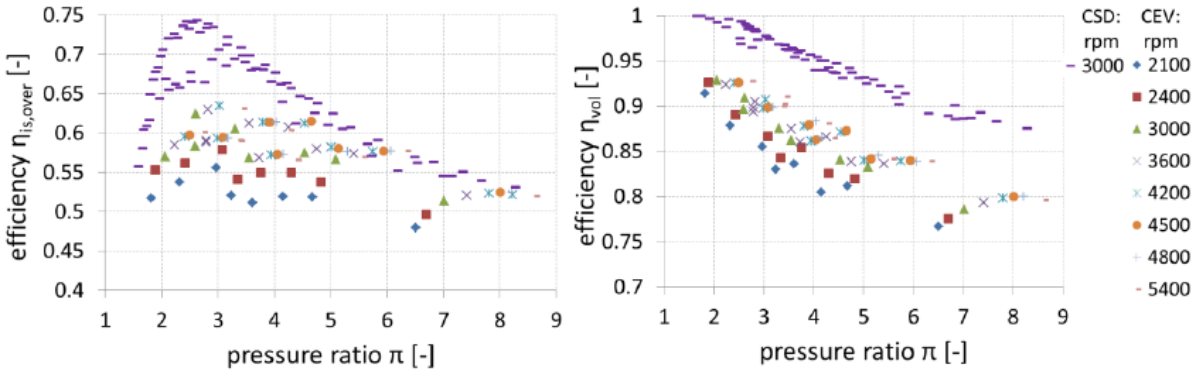

Figure 43: $\eta_{is,over}$ (left) and η_{vol} (right) for the speed controlled compressor with vapor injection CEV (data basis: laboratory measurements) and for the constant speed compressor CSD (data basis: manufacturer) (Hengel et al., 2014)

Figure 44 depicts the condenser inlet and outlet water temperatures over the provided energy of the heat pump for space heating for the CSD (left diagram) and for the CEV (right), obtained by annual system simulations. It can be observed that by using the CEV system the temperature at the outlet of the condenser is lower than the temperature of the CSD.

Further results of the dynamic system simulation for the standard heat pump cycle (CSD) show a seasonal performance factor SPF_{sys} of 2.63 and an annual electric energy consumption $W_{el,sys}$ of 9395 kWh (Table 3). The SPF_{sys} can be increased by about 14.8%, corresponding to electric energy savings of about 13.5%, with the advanced heat pump cycle (CEV). This is mainly due to lower water outlet temperatures at the condenser. The advanced heat pump cycle achieves a reduction of the start and stop losses of more than 50% compared to CSD.

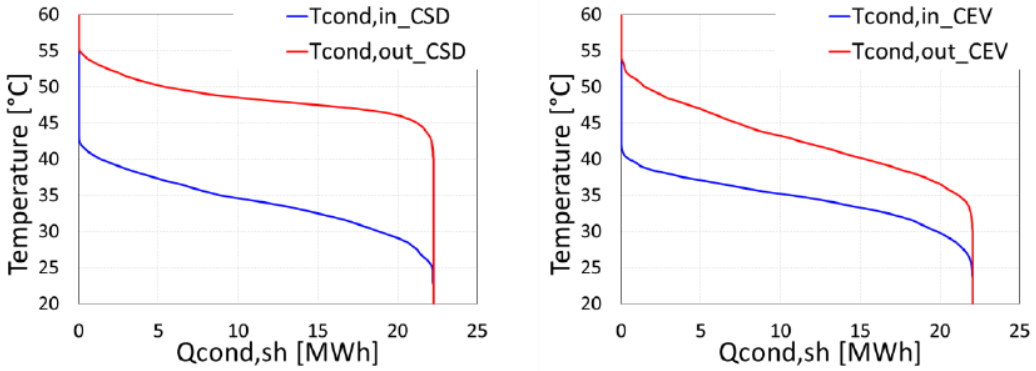

Figure 44: Heat provided by the heat pump condenser with different inlet and outlet water temperatures; left: without speed control (CSD), right: with speed control (CEV) (Hengel et al., 2014)

The authors concluded that there is a large energy saving potential, if an advanced heat pump cycle with an economizer and a speed controlled compressor is used instead of a single speed “standard” compressor.

Table 3: Detailed information for both heat pump systems (CEV and CSD)

System	SPF_{sys}	HP starts	avg. runtime per start	$W_{el,sys}$	$W_{el,comp}$	$W_{el,fan}$	$W_{el,pu}$	$Q_{start,losses}$
	[-]	[-]	[h]	[kWh/a]	[kWh/a]	[kWh/a]	[kWh/a]	[kWh/a]
CEV	3.02	1457	4.5	8133	6824	991	48	452
CSD	2.63	3354	1.2	9395	8342	600	48	880

All in all it can be said that by using an appropriate control strategy for the heat pump system as well as using the combination of a variable speed compressor and an economizer cycle the efficiency of an ASHP can be increased significantly. At cold ambient temperatures the use of an economizer cycle has its advantages and at higher ambient temperatures the variable speed control on the compressor. By considering these possibilities an increase in SPF of above 13% should be possible.

5 SYSTEM INTEGRATION OF HEAT PUMPS

This chapter shows exemplary the possibilities of heat pump system integration for the cold climate region of Davos in Switzerland by means of the simulation results from the Austrian project “Highly efficient combinations of solar thermal and heat pump systems (SolPumpEff)” (Lerch and Heinz, 2014). In this project different configurations of solar and heat pump systems were analyzed and compared through dynamic system simulations in TRNSYS. In the investigated systems solar thermal energy can be used on one hand directly to charge the buffer storage and on the other hand as heat source for the evaporator of the heat pump (HP). Systems, in which solar heat is only used directly (parallel operation of solar and HP), and systems using the collectors also as a heat source for the HP are analyzed and compared to conventional air HP systems. Glazed and unglazed collectors are considered for the solar thermal system.

5.1. Climate, Heat Load and Simulation Platform

The simulations have been carried with the reference boundary conditions from T44A38 and with the simulation program TRNSYS, Version V17.01.0025. Table 4 depicts the climate and building definition for the simulation. The supply temperature of the heating system is 35°C and the return temperature is 30°C.

Table 4: Climate and building definition according to Lerch and Heinz (2014)

Climate			Building SFH045				
Location	Design temperature	Heating degree days	Heating system	Heating demand	Heating load	Heating area	Design room temperature
	[°C]	[Kd/a]		[kWh/(m²·a)]	[kW]	[m²]	[°C]
Davos	-18	about 5600	floor heating system	77.5	6.01	140	20

5.2 Solar Thermal and Heat Pump Systems

System A (Baseline, w/o solar thermal collector and ASHP):
Figure 46 shows the hydronic layout of System A, which is an air/water HP system without any solar thermal system. According to the system Figure 45 shows the energy flow diagram. The HP provides heat to the buffer storage and directly to the heating system of the building. The buffer storage is divided into a domestic hot water (DHW) and a space heating (SH) volume. As backup an electrical heater is placed in the buffer storage (space heat volume), which provides heat at times when the performance of the HP is not sufficient to cover the heating demand. For the dimensioning of the HP the heat load of the building plus 0.5 kW was used, which is to be covered by the HP at the operation point A-7/W35, i.e. ambient outdoor temperature -7°C and supply temperature for the heating system 35°C. In this system without solar collectors the buffer storage has a volume of 0.3 m³. The domestic hot water (DHW) preparation takes place via an external heat exchanger.

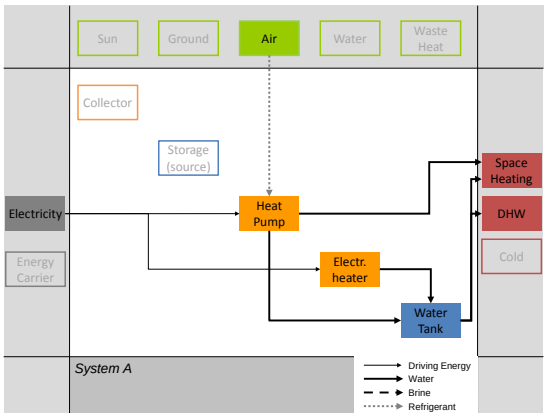

Figure 45: Energy low diagram System A

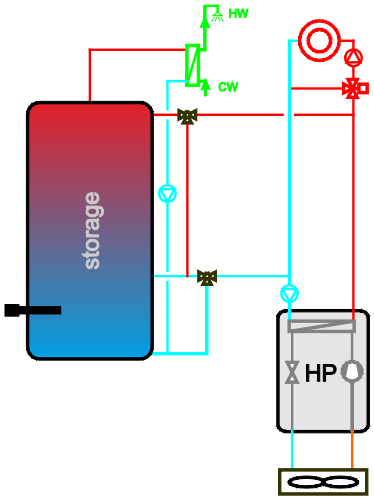

Figure 46: Hydraulic scheme System A

System B (with glazed solar thermal collector and ASHP):
In System B a solar system is installed in a parallel way, whereby 14 m² covered, selectively coated collectors are used, the buffer storage volume is increased to 1 m³. The energy flow diagram of the system is shown in Figure 47 and the hydraulic layout of System B is shown in Figure 48. The solar loop is integrated via an external plate heat exchanger and solar energy is only used to charge the buffer storage. As main energy source an air HP system is installed (dimensioning like in System A).

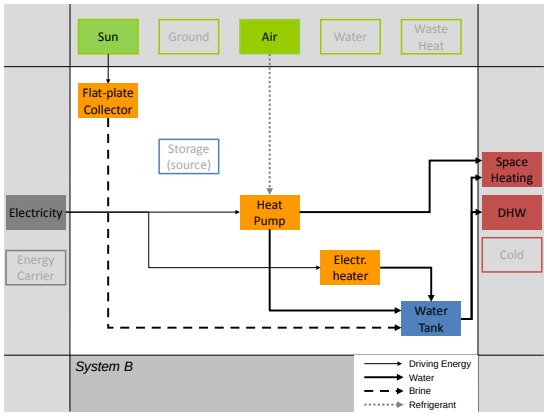

Figure 47: Energy flow diagram System B

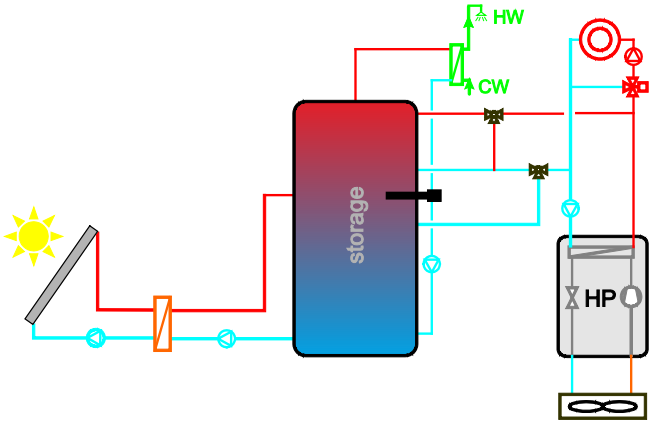

Figure 48: Hydraulic scheme System B

System C (with unglazed solar thermal collector and brine source HP):
As shown in Figure 50, in System C unglazed selectively coated collectors (30 m² collector area) are used as the only heat source for the HP. The according energy flow diagram is shown in Figure 49. Solar heat can either be used to charge the buffer storage or as heat source for the HP, a simultaneous operation is not possible.

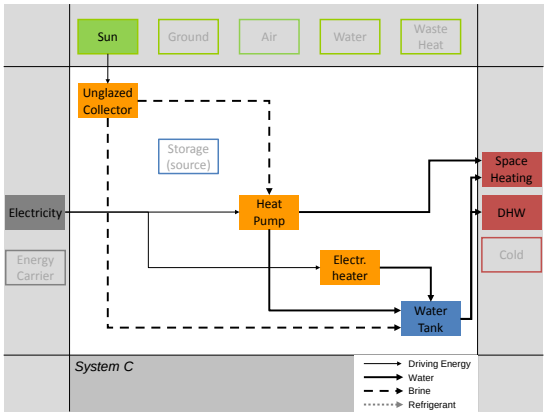

Figure 49: Energy flow diagram System C

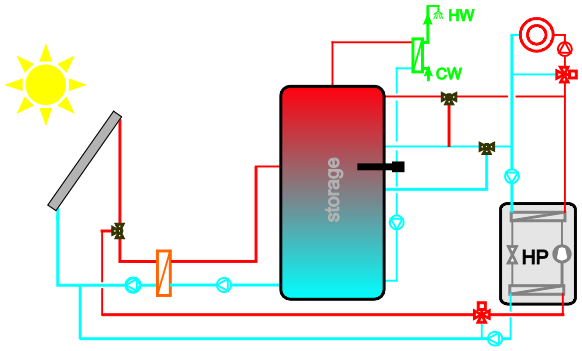

Figure 50: Hydraulic scheme System C

System D (with unglazed solar thermal collector, brine source HP and ice storage):
System D is similar to System C with the difference of an additional ice storage (0.6 m³) (Figure 51 and Figure 52), which is used as source for the evaporator of the HP. The buffer storage (water storage) is charged with priority. If the HP is operated and the solar thermal system supplies energy to the ice storage at the same time, then energy for the evaporator of the HP comes directly from the solar thermal system. In this case higher source temperatures can be achieved at the evaporator of the HP.

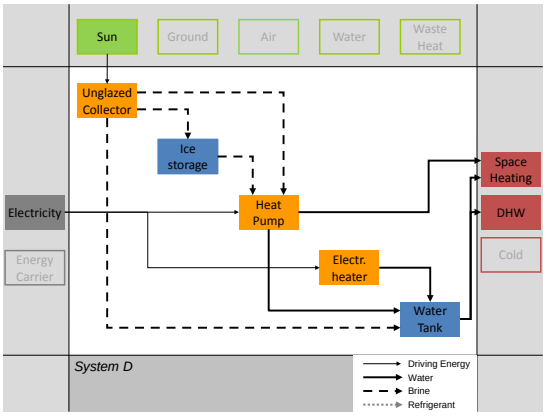

Figure 51: Energy flow diagram System D

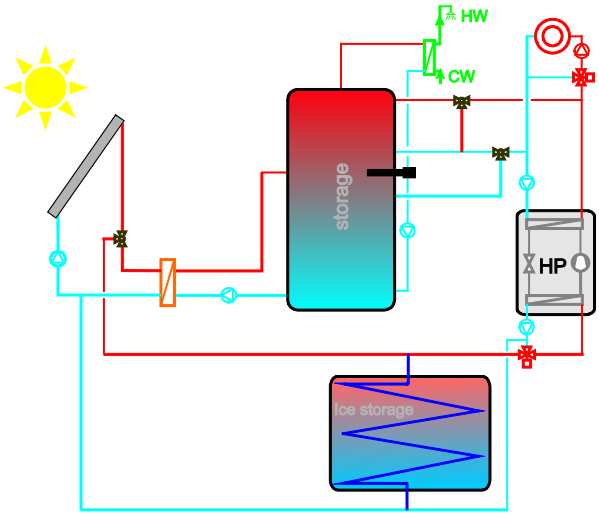

Figure 52: Hydraulic scheme System D

System E (with unglazed solar thermal collector and “air preheated evaporator” ASHP):
Figure 54 shows a solar air HP system, in which solar heat is used to charge the buffer storage on the one hand, and to preheat the temperature of the air entering the outdoor unit of the air HP on the other hand. Figure 53 depicts again the energy flow diagram for the system. For the solar system 14 m² glazed selectively coated collectors are used. If the HP has to provide heat and the collector temperature level is higher than the temperature of the ambient air, but lower than the temperature of the buffer store, then solar heat is used to preheat the ambient air. For this purpose a brine/air heat exchanger, which is connected to the solar loop, is installed in front of the evaporator.

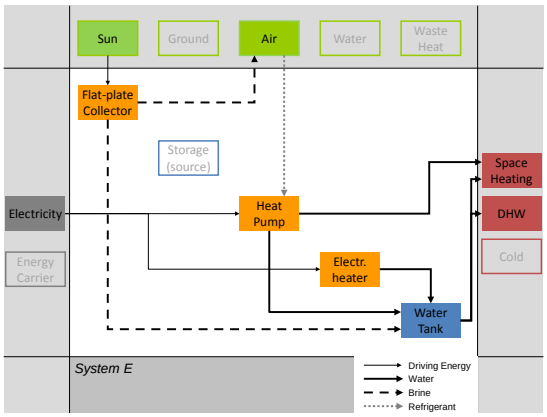

Figure 53: Energy flow diagram System E

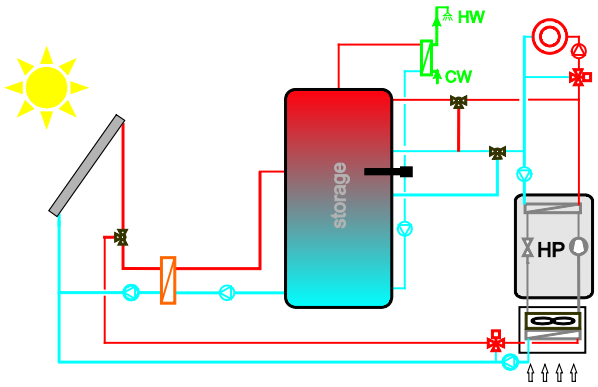

Figure 54: Hydraulic scheme System E

<u>System F (with unglazed solar thermal collector and dual source evaporator, ASHP and brine source HP):</u>
Also in System F solar heat is used to achieve higher evaporation temperatures (Figure 56, Figure 55 shows the energy flow diagram). The difference to System E is that the heat exchanger is directly integrated into the refrigerant cycle of the HP after the air source evaporator (in refrigerant flow direction). Solar heat supply to the evaporator is activated in the same way as in system E. Also here 14 m² glazed selectively coated collectors are used.

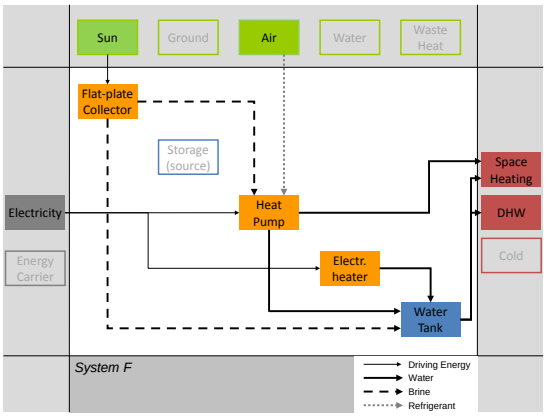

Figure 55: Energy flow diagram System F

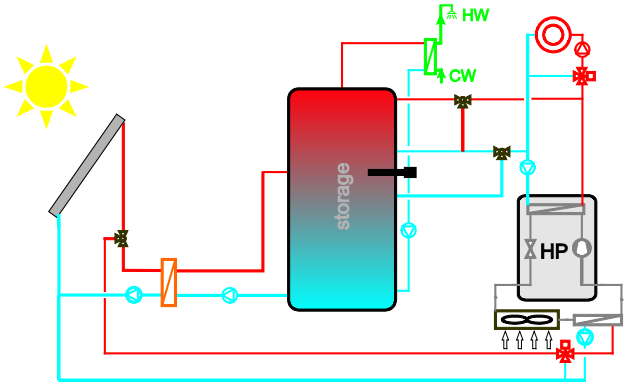

Figure 56: Hydraulic scheme System F

5.3 Results

To compare the systems together following key figures were defined (formula (2) to (4)).

$$P_{el,SHP+} = P_{el,HP} + P_{el,SC} + P_{el,EH} + P_{el,PU} + P_{el,PU,SH} + P_{el,Ctr} \quad (2)$$

With

HP heat pump – anything needed to run the heat pump (compressor, air ventilator, source pump(s), sink pump(s), heating elements, controllers, etc.)

SC Solar circuit – anything needed to run the solar circuit (pumps, controller - if additional to heat pump controller, valves, air ventilators for hybrid collectors, etc.)

EH electric heater elements (direct electric heating) that are not included yet in HP or SC

PU pumps that are not included yet in HP or SC, also including a primary DHW pump for an external DHW heat exchanger if present, but not the space heat distribution pumps

PU,SH space heat distribution pump

Ctr additional controllers that cannot be attributed to HP or SC alone

$$SPF_{HP} = \frac{\int_{t=0}^{8760h} \left(\dot{Q}_{COND}\right) \cdot dt}{\int_{t=0}^{8760h} \left(P_{el,HP}\right) \cdot dt} \quad (3)$$

With *COND* condenser of the heat pump

Some systems may not at all times provide domestic hot water at the required temperature level or they may not be able to maintain the room temperature of the building at all times above 19.5°C. In order to allow for a fair comparison between the simulation results of these systems and the simulation results of systems that maintained the defined comfort level of T44A38 at all times, penalties are added to the energy consumption based on proposals of the IEA SHC Tasks 26 and 32 (Jordan et al. 2003; Heimrath and Haller 2007).

$$SPF_{SHP+,pen} = \frac{\int_{t=0}^{8760h} \left(\dot{Q}_{SH} + \dot{Q}_{DHW}\right) \cdot dt}{\int_{t=0}^{8760h} \left(P_{el,SHP+} + P_{el,SH,pen} + P_{el,DHW,pen}\right) \cdot dt} \quad (4)$$

For System C and D simulations with different collector areas were performed. With System C and an unglazed collector area of 30 m² for the SFH045 a $SPFSHP+_{,pen}$ of 2.96 is reached. The electricity consumption of the electric heater is approximately equal to the electricity consumption of the compressor of the HP.

For System C and D simulations with different collector areas were performed. With System C and an unglazed collector area of 30 m² for the SFH045 a $SPFSHP+_{,pen}$ of 2.96 is reached. The electricity consumption of the electric heater is approximately equal to the electricity consumption of the compressor of the HP.

Table 5 depicts the overall system performance results for the SFH045 (definition compare chapter 4) building at the cold climate Davos for all configurations. It can be seen that system F shows the highest seasonal performance factor with 4.4 followed by system E and B, which reach a SPF of 4.38 and 4.37, respectively. The authors gave an explanation why the SPF is considerably lower for system C and D.

For System C and D simulations with different collector areas were performed. With System C and an unglazed collector area of 30 m² for the SFH045 a $SPF_{SHP+,pen}$ of 2.96 is reached. The electricity consumption of the electric heater is approximately equal to the electricity consumption of the compressor of the HP.

Table 5: Overall system performance table (building SFH45, climate Davos)

		Sys A	Sys B	Sys C	Sys D	Sys E	Sys F
$SPF_{SHP+,pen}$		***2.48***	***4.37***	***2.96***	***3.11***	***4.38***	***4.40***
SPF_{SHP+} without penalties		***2.49***	***4.40***	***2.96***	***3.12***	***4.41***	***4.43***
SPF_{HP}		***3.07***	***2.81***	***3.00***	***3.38***	***2.83***	***2.84***
Useful heat							
DHW	kWh/a	2556	2557	2557	2556	2556	2556
		Sys A	**Sys B**	**Sys C**	**Sys D**	**Sys E**	**Sys F**
space heat	kWh/a	10873	10823	10827	10826	10827	10832
Total	***kWh/a***	***13430***	***13379***	***13384***	***13382***	***13384***	***13389***
Used Electricity							
System	kWh/a	5393	3039	4515	4287	3036	3023
Penalty DHW	kWh/a	16.16	2.5	3.5	3.5	2.7	3.0
Penalty Space Heat	kWh/a	14.52	18.9	10.7	6.3	18.2	17.4
Total	***kWh/a***	***5424***	***3060***	***4529***	***4297***	***3057***	***3044***
Penalty Check							
not more than 2% respective		**O.K.**	**O.K.**	**O.K.**	**O.K.**	**O.K.**	**O.K.**

Compared to the parallel air HP system with glazed collectors the electricity consumption of the electric heater is about seven times as large as to the system with the unglazed collectors (30 m² instead of 14 m²). For this reason simulations are performed with higher collector areas. Through the increasing of the solar collector area the heat exchanger area for the evaporator of the HP is increased. Thereby the evaporator temperature level increases. By increasing of the collector area from 30 m² up to 60 m² the $SPF_{SHP+,pen}$ increases from 2.96 up to 3.87 and electricity consumption of the electric heater is approximately reduced to the half. Through the integration of additional ice storage (0.6 m³) the increase in system performance is very low (Figure 57).

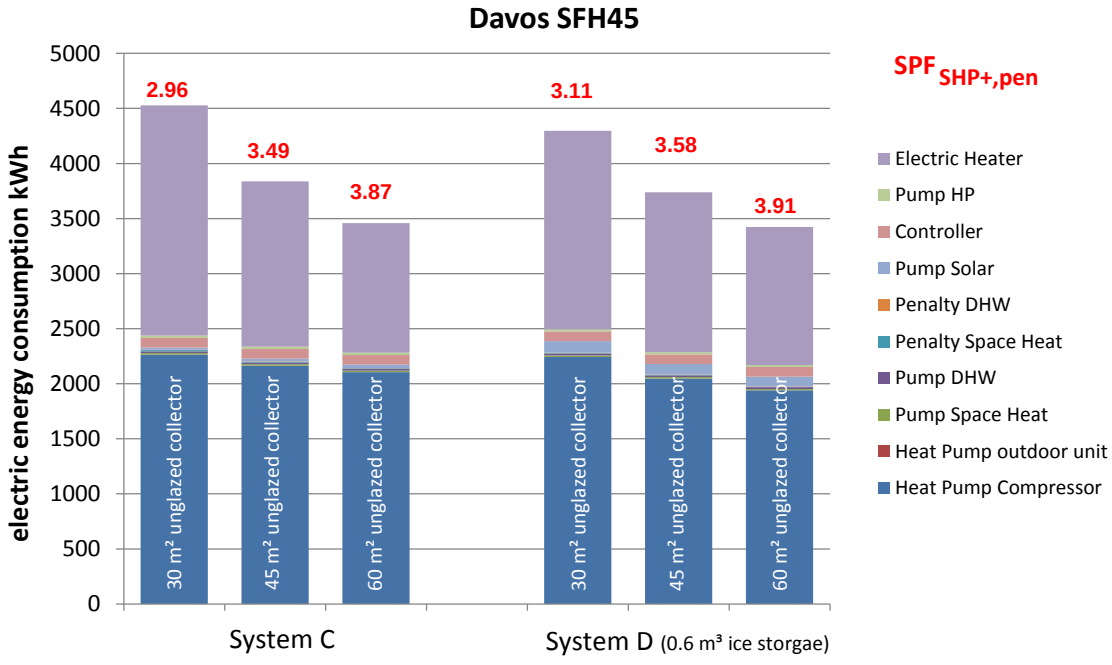

Figure 57: Comparison of results for System C and D under the same boundary conditions with different collector areas (climate, Davos, building SFH45)

6 HEAT PUMP COMPONENTS

Due to higher requirements to heat pump systems and the increasingly important ecological factor of reducing the greenhouse effect lead to developments of alternative refrigerants for heat pump systems and on the other hand some compressor types as well as heat exchangers are considered within this chapter.

6.1 Alternative Refrigerant – Carbon Dioxide (CO_2)

Using CO_2 as refrigerant for heat pump applications is quite long investigated by different institutions. Beside good physical properties (non-toxic, not flammable), it is cheap, has good heating transfer properties (Bresdesen et al., 1997) and a high isentropic compressed efficiency can be achieved (Neksa et al., 1999). Disadvantages of this refrigerant are higher pressures and a dropping efficiency of the heat pump at increasing heat sink inlet temperatures. Transcritical CO_2 cycles are an efficient option especially for hot water applications, because of the large temperature glide on the heat sink side combined with a low heat sink inlet temperature. Hot water temperatures up to 90°C without operational problems can be reached, which is quite important looking at demands of new sanitary regulations against legionnaires' disease. On the other side, the energy efficiency of such a transcritical CO_2 cycle strongly depends on the heat sink inlet temperature. In general, the COP of a CO_2 heat pump drops about 1% to 1.5% for each K increase in the inlet water temperature (Stene, 2004). Because of this, the concept of CO_2 heat pump systems is often combined with a temperature-stratified heat storage system.

Stene (2005) has investigated a CO_2 heat pump system in brine-to-water configuration with evaporation temperatures ranged from -10°C to 0°C, the supply/return temperatures of the space heating (SH) system were 33/28, 35/30 or 40/35°C and the domestic hot water (DHW) temperatures were 60, 70 or 80°C with an average water inlet temperature of about 6.5°C, and the evaporation temperature was -5°C. The measured COP for different supply/return temperatures of SH as well as for different DHW temperatures are shown in Figure 58. In Figure 59 three different modes are tested, DHW mode, SH mode and combined mode (DHW & SH).

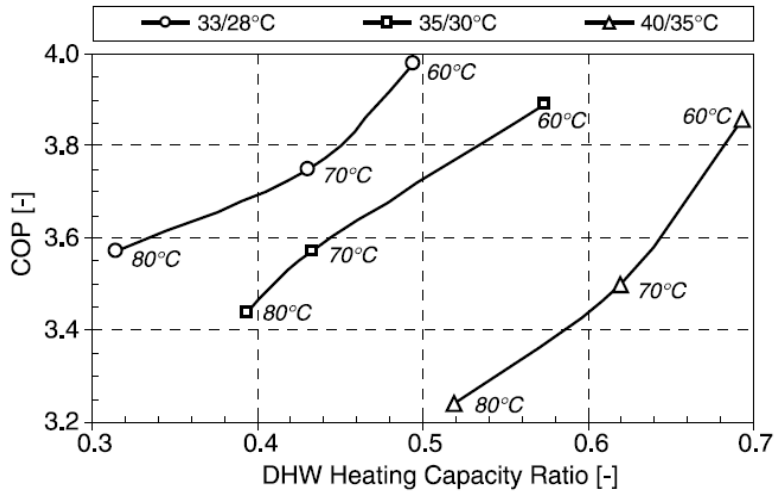

Figure 58: Measured relationship between the maximum COP and the DHW heating capacity ratio during testing in the combined mode with t_{evap} of -5°C (Stene, 2005)

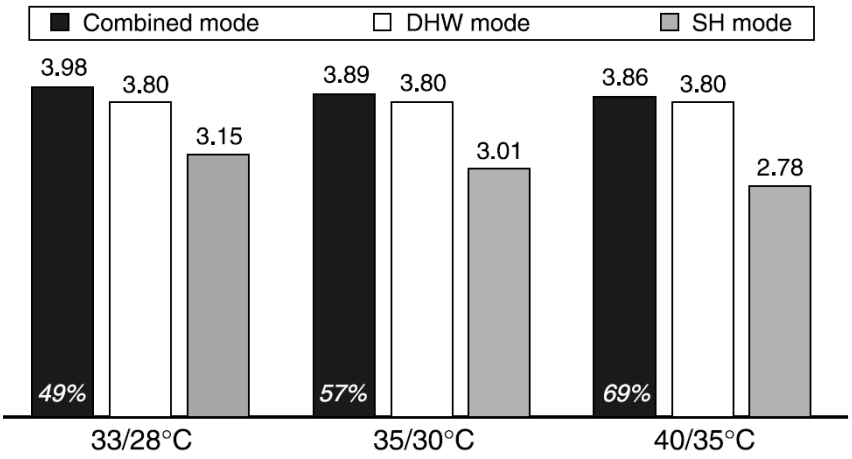

Figure 59: The measured maximum COP at 60°C DHW temperature and various supply/return temperatures in the space heating system during operation in the combined mode, DHW mode and SH mode with t_{evap} of -5°C (Stene, 2005)

In comparison to highly energy efficient brine-to-water heat pump systems, available on the market, the integrated CO_2 heat pump system achieved the same or higher SPF presupposed that, the ratio of the heating demand for the hot water production is at least 25% of the total annual heating demand, the return temperature for the space heating system is lower than 30°C, the city water temperature is lower than approximately 10°C and the thermal losses in the DHW tank are small. Further Stene (2008) has investigated different integrated CO_2 heat pump systems, focusing on the design of the heat rejection heat exchanger (gas cooler) and the DHW system. It was found that a counter-flow tripartite CO_2 gas cooler in combination with an external single-shell DHW tank (see Figure 60) and a low-temperature heat distribution system would enable production of DHW from 60 to 85°C without electric reheating, and contribute to the highest possible COP for the CO_2 heat pump system. At DHW heating demand ratios above approx. 50% (low-energy and passive houses), the CO_2 heat pump outperformed the most energy efficient heat pump systems on the market.

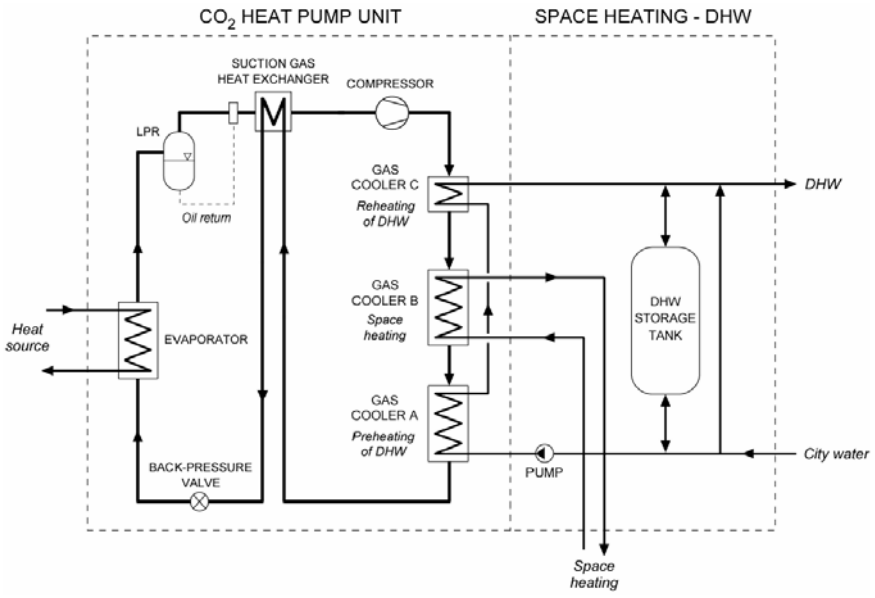

Figure 60: Principle design of the prototype brine-to-water integrated CO_2 heat pump system (Stene, 2008)

6.2 Types of Compressors

This subchapter is not only referring to cold climate condition rather to increase the compressor efficiency by means of innovative types of compressors.

One opportunity to reduce the energy consumption of a heat pump system is to know, which type of compressor is the best solution for the given situation. A high potential of existing compressors, which have been investigated in recent studies, considers scroll compressors, new designs of revolving vane compressors and rolling piston compressors. The first two compressor types are schematically shown in Figure 61. A schematically type of the rolling piston compressor is shown in Figure 62.

Winandy et al. (2002) have investigated scroll compressors and identified three reasons to increase the energy efficiency by approximately 10% compared to standard reciprocating compressors. First of all the suction process (chamber) is separated from the discharge process, which means that no heat is transferred to the suction gas, when it enters the compressor. Second, the process takes place in a 540 degree rotation versus a 180 degree rotation in a standard reciprocating compressor. Based on this, the driven torque by using the scroll compressor can be reduced by 10%, compared to conventional reciprocation compressors. Third, there are no valves included for the suction and the discharge process. Hence the pressure drop is lower for the scroll compressor.

Another compressor type has been investigated by Teh et al. (2009), who experimentally analyzed a new design of a revolving vane compressor including a rotating discharge valve (Figure 61, right). The leakage losses can be reduced by about 40% compared to conventional piston compressors.

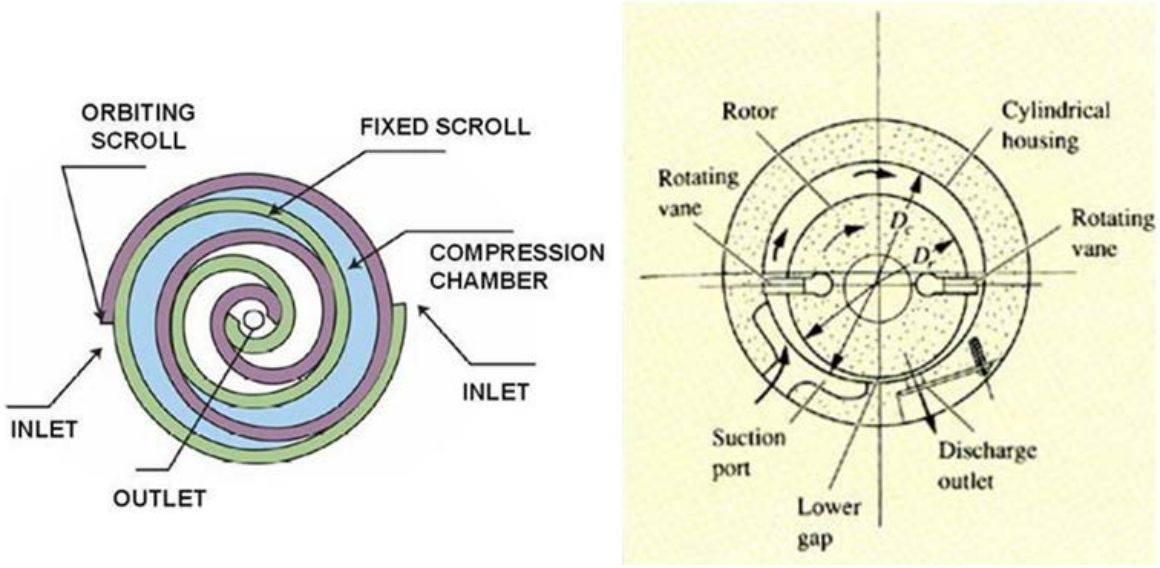

Figure 61: Compressor types, left: Scroll compressor (Gentech System Corp., 2008), right: Revolving vane compressor (Mukherjee, 2001)

A study about rolling piston compressors was done by Ooi (2005), who investigated the performance of this compressor type and opportunities to reduce mechanical losses to a minimum. Therefore he formulated a mathematical model including geometrical configurations, thermodynamical effects, etc. The accuracy of this model was verified with experimental data. Afterwards the optimal compressor performance, with minimal mechanical losses was found by feeding the available data to an optimization algorithm.

Theoretically mechanical losses were reduced about 50% and the compressor COP was improved by up to 14%.

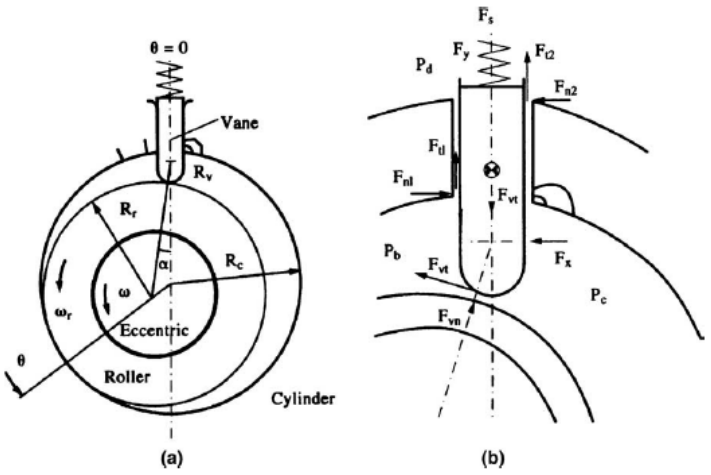

Figure 62: Rolling piston compressor (Ooi, 2005)

Wang et al. (2008) studied two methods of improving the performance behavior of compressors by keeping the compressor temperature low during operations. The first method is to keep the temperature of the compressor motor low by external measures, rather than by cooling with suction gas. The second option is to create an isothermal process by transferring heat from the compression process to an external cooling system. Figure 63 shows the saved compression work using two ideal types of compression processes (isothermal/isentropic).

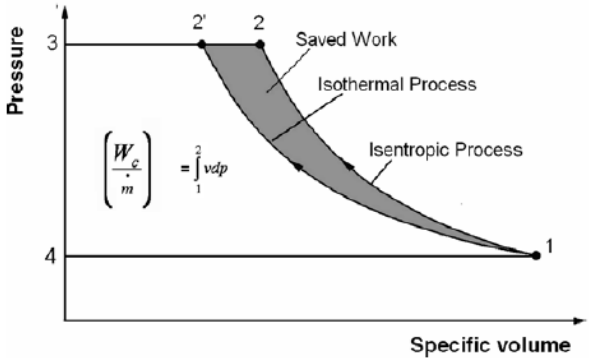

Figure 63: Isentropic and isothermal compression process in a pressure-specific volume-diagram (Wang et al., 2008)

Further the authors investigated a combined system of isothermal and isentropic compression to avoid wet compression. In case 1 first the isothermal compression takes place before and followed by an isentropic compression. In case 2 it was done inversely. The two cases are shown in Figure 64 for a R22-system exemplary.

Results showed that 14% (case 1) and 8.5% (case 2) compression work can be saved, compared to an isentropic process. For case 1 the conditions are better, because less heat has to be removed. However in case 1 the temperature of the cooling source must be lower than the discharge temperature, which could be a challenge to do it in an efficient way.

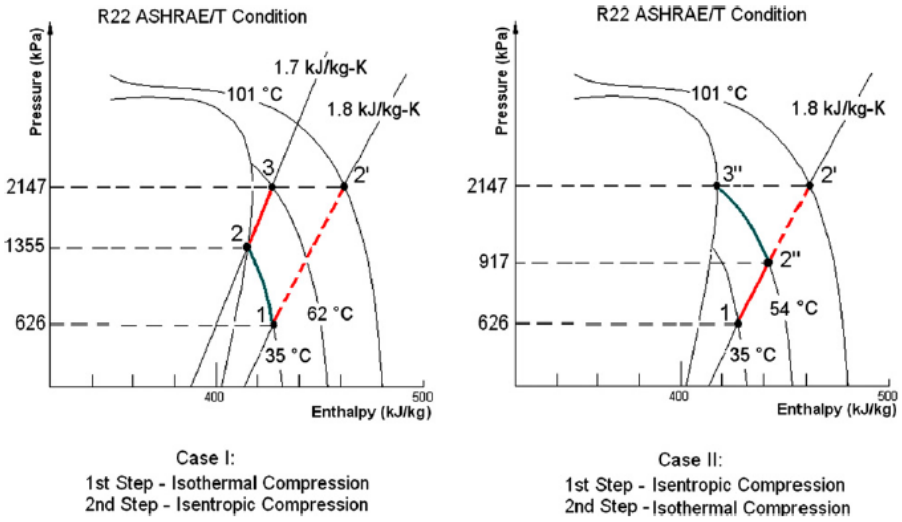

Figure 64: Combination of isothermal and isentropic compression (Wang et al., 2008)

6.3 Heat Exchanger

The heat exchanger of the heat pump evaporator unit faces the air side and therefore water accumulates on the cold heat exchanger surface in form of condensate and at low temperature in form of frost and ice, (Berlinger 2008). This ice starts to block the heat exchanger, which results in an increase of the airside pressure drop and with reducing air flow in a decrease of heat transfer and COP. Also the frost layer represents an additional thermal resistance but this effect has less influence than the obstructing of the free cross-section. In heat pump applications, the frost needs to be removed periodically to improve the efficiency of operation, (Hewitt 2008). The defrosting cycles are a highly energy consuming process and therefore different approaches are taken to optimise the defrosting performance and to reduce the frequency of the defrosting cycles by minimizing the ice and frost formation, (Albert 2008).

In Hewitt et al (2008), for example, the performance of hot gas bypass defrosting cycle for residential ASHPs, paying special attention to high humidity conditions, was investigated.

Figure 65: Fin heat exchanger at the air outlet side with partial ice accumulation (Berlinger 2008)

The evaporator coil was circular shaped. Performance optimisation was achieved through a series of experiments from which the best defrost initiation, defrost operating time and intervals between defrosts was noted.

Another approach for the icing problem was taken in Berlinger et al (2008). The scope of the investigations was fin heat exchangers used as evaporators for On/Off-controlled ASHP. To achieve a COP as high as possible despite ice and frost formation, investigations were carried out to improve the geometry of the fin heat exchanger and the process control. The main aim was to improve the efficiency by improving the geometry of the fin heat exchanger. One of the insights this work was that the changing of the geometry gave a moderate increase of the efficiency. However, a distinctive improvement could be reached if the difference between required and generated heating capacity of On/Off-controlled ASHP could be overcome with new control concepts.

In Sahinagic et al (2008) the precise prediction of the operation behaviour was investigated in order to further improve the efficiency of the overall system. A mathematical-physical simulation program was developed to calculate the non-stationary behaviour of ASHP with ice and frost formation in the evaporator for any geometry. The validation of the simulation program was carried out using the results of measurements made in experiments with a commercial ASHP at different air temperatures. The simulated heat capacity tended to be higher than the measured one. The discrepancies were about 8%, although the temporal profiles of the curves are nearly the same, (Albert 2008).

According to Heinz et al. (2012), micro-channels are heat exchangers in which fluid flows in channels with less than 1 mm sized. As depicted in Figure 66, they include horizontal tubes with a flattened surface that extend between two vertical headers. The flattened surface of the tubes is basically horizontal, and water does not shed from the fins effectively, which is a disadvantage of this innovative heat exchanger. Another disadvantage is if water stays on the tubes the heat transfer performance decreases, causes an increase in pressure drop, and allows a gradual built up of ice under frosting conditions (Kirkwood 2011).

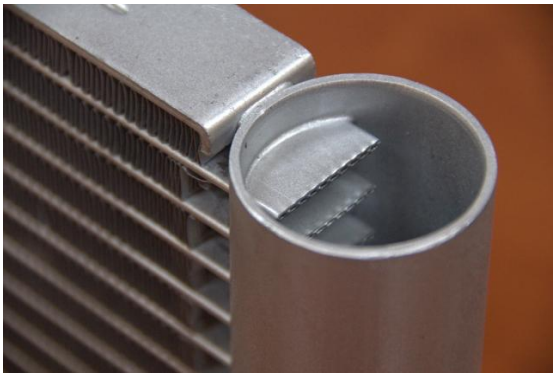

Figure 66: Micro-channel heat exchanger (Heinz et al., 2012)

But on the other hand, micro-channel heat exchangers are compact and offer higher performance per unit weight than conventional finned tube heat exchangers. Due to the fact they are made of aluminum, less material cost than finned-tube heat exchangers occurs. A further advantage is the refrigerant charge of such micro-channel heat exchanger systems because it is lower compared to conventional finned-tube heat exchangers.

In Fisher (2012) the frost growth on louvered folded fins in microchannel heat exchangers used as evaporators in ASHP was investigated. The research focused on the effects of surface temperature, fin geometry, fin surface coating and air psychrometric conditions on the performance of the heat exchanger under frosting conditions. Fins were cut out from

commercially available heat exchangers and assembled in a custom-made test apparatus to perform laboratory experiments. One part of the fin samples had different width, height and fin density, while other ones had the same geometry but difference surface coatings. Data showed that the frosting time and the frost growth rates were depended mainly on the local fins surface temperature. It seemed that the dominant factor that defined the frost time of a fin microchannel sample was first the fin surface temperature and then the geometry. It also turned out that the geometry effect seemed to influence the time of frost cycle much more than the effect of surface coating. The measurements showed that hydrophobic coated fins had slightly lower frosting performance after few defrost cycles compared to hydrophilic surface coated fins with the same geometry.

The effects of hydrophobic and hydrophilic surface coatings on louvered fin microchannel heat exchangers with same geometries under icing conditions were also studied in Moallem (2012). The experimental data showed that the hydrophilic and hydrophobic coated surfaces accumulated frost with visible difference in type, appearance and patterns of the frost. The duration of the frosting cycle, the heat transfer rate and air-side pressure drop were similar to the ones of a louvered fin microchannel heat exchangers with uncoated surfaces. For the operating conditions, hydrophobic and hydrophilic coatings affected the heat transfer capacity in frosting conditions up to 15%.

Due to the tendency of ice forming, micro-channel heat exchangers have not been widely applied as evaporators in air source heat pumps so far, but are generally used in automotive air conditioning.

Possibly, in future advanced micro-channel heat exchangers may play a more important role for ASHP as well.

7 SUMMARY

Some advanced heat pump systems were discussed. The literature study showed promising results for the economizer cycle, the cascade system, liquid injection and the ejector system. The first two layouts are suitable for low evaporation temperatures and their performance and heating capacity are satisfying for cold climates. The investigations show an improvement in efficiency and heating capacity as well as in maximum discharge temperature compared to a standard heat pump cycle. Although liquid injection does not offer the advantageous of an economizer flow chart with respect to efficiency and capacity, but it enlarges significantly the compressor envelope by lowering the compressor discharge temperature, which is of special interest in case of high condensation temperatures and low evaporation temperatures. For the ejector system only ambient temperatures above 0°C were investigated but with the results that the ejector system with intercooler and internal heat exchanger can improve the COP by about 21% compared to a standard heat pump cycle at the considered conditions. However, further investigations have to be done with lower ambient temperatures to verify its efficiency in cold climates.

Besides the advanced heat pump cycle this review depicted also some control strategies in case of using a variable speed controlled compressor and economizer. It can be said that by using an appropriate control strategy for the heat pump system as well as using the combination of a variable speed compressor and an economizer cycle the efficiency of an ASHP can be increased significantly. At cold ambient temperatures the use of an economizer cycle has its advantages and at higher ambient temperatures the variable speed control of the compressor. By considering these possibilities an increase in SPF of above 13% is possible. Also system integration of heat pumps in general was considered in chapter 5.

Lastly the literature survey dealt with some studies about heat pump components, especially with the alternative refrigerant carbon dioxide CO_2 (R744). To complete the chapter some types of compressors and an innovative heat exchanger (micro-channel) were introduced.

8 BIBLIOGRAPHY

Albert, M.; Sahinagic, R.; Gasser, L.; Wellig, B. & Hilfiker, K., 2008: Prediciton of ice and frost deformation in the fin tube evaporators for Air/Water heat pump, 9th International IEA Heat Pump Conference.

Afjei, T., Schonhardt, U., Wemhöner, C., Erb, M., Gagathuler, H.R., Mayer, H., Zweifel, G.; Achermann, M., von Euw, R., Stöckli, U., 2002. ”Standardschaltungen für Kleinwärmepumpenanlagen – Teil 2: Grundlagen und Computersimulationen”, final report, Bundesamt für Energie, Switzerland.

Aprea C., Mastrullo R., Renno C., Vanoli G. P., 2004: An evaluation of R22 substitutes performanc regulating continuously the compressor refrigeration capacity, Applied Thermal Engineering, 24(1),
pp. 127-139

Berlinger, L.; Imolz, M.; Albert, M.; Wellig, B. & Hilfiker, K., 2008: LOREF: Optimierung des Lamellenluftkühlers/Verdampfers von Luft/Wasser-Wärmepumpen, Teil 1: Theoretische und experimentelle Untersuchungen. Bundesamt für Energie.

Bertsch S. S., Groll E. A., 2008: Two-stage air-source heat pump for residential heating and cooling applications in norhern U.S. climates, International Journal of Refrigeration, 31(7),
pp. 1282-1292

Biermayr ,P., Eberl, M., Ehrig, R., Fechner, H., Kristöfel, C., Leonhartsberger, K., Martelli, S., Strasser, C., Weiss, W., Wörgetter, M., 2013. „Innovative Energietechnologien in Österreich Marktentwicklung 2012 – Biomasse, Photovoltaik, Solarthermie und Wärmepumpen“. Bundesministeriums für Verkehr, Innovation und Technologie, Report from R&D of Energy and Environment, 17/2013, Austria

Bredesen A.M., Aflekt K., Pettersen J., Hafner A., Neksa P., Skaugen G., 1997: Studies on CO_2 heat exchangers and heat transfers, CO_2 technology in refrigeration, heat pumps and air conditioning systems, IEA Heat Pump Centre, Trondheim, Norway, 1997, pp. 13-14

Chua K.J., Chou S. K., Yang W. M., 2010: Advances in heat pump systems: A review,
Applied Thermal Engineering 87, pp. 3611-3624

Fisher, D.; Moallen, E.; Hong, T. & Deokar, P., 2012: ASHRAE Research Project Report: Effects of Fin Design on Frost and Defrost Thermal Performances of Microchannel Heat Exchangers, ASHRAE Technical Commitee: TC8.4 Air-to-Refrigerant Heat Transfer Equipment, ASHRAE Project Number 1589-RP.

Gasser, L., Wellig, B. & Hilfiker, K., 2008. ”WEXA: Exergie-Analyse zur Effizienzsteigerung von Luft/Wasser-Wärmepumpen”, final report, Bundesamt für Energie, Switzerland.

Gasser L., Wyssen I., Albert M., Häusermann M., Kleingries M., Wellig B.,, 2011: Effiziente Luft/Wasser-Wärmepumpen durch kontinuierliche Leistungsregelung, Federal Office of Energy, Bern, Switzerland

Gasser L., Wellig B., 2011a, Effiziente Heizsysteme mit leistungsgeregelten Luft/Wasser-

Wärmepumpen, Horw, Switzerland

Gentech System Corp. 2008: Medical Air Compressor Technologies, http://www.gentecsys.com/Knowledge/KB04_comp_tech.htm , 08.01.2014

Gorris V., Stawiarski K. H., Hähnle K., 2011: Daten zum Wärmepumpenmarkt bis 2010 und Prognosen bis 2030, Federal Association of Heat Pumps, Berlin, Germany

Guoyuan M., Qinhu C., Yi J., 2003: Experimental investigation of air-source heat pump for cold regions, International Journal of Refrigeration 26, pp. 12-18

Halozan H., 1980: Die Außenluftwärmepumpenheizung – Spitzenlastabdeckung und Abtauproblematik, Institute of Thermal Engineering, Graz University of Technology, Austria

Halozan H., 2000: Heat Pumps in Low-Energy-Houses in Europe (Heating and Cooling), Institute of Thermal Engineering, Graz University of Technology, Austria

Heimrath, R. & Haller, M., 2007. Project Report A2 of Subtask A: The Reference Heating System, the Template Solar System - A Report of IEA SHC Task 32: Advanced Storage Concepts for Solar and Low Energy Buildings.

Hengel F., Heinz A., Rieberer R., 2014. „Analysis of an Air Source Heat Pump System with Speed Controlled Compressor and Vapor Injection". 11th International Energy Agency Heat Pump Conference, Montreal, Canada

Heo J., Jeong, M.W., Baek, C. & Kim, Y., 2011. "Comparison of the heating performance of air-source heat pumps using various types of refrigerant injection", International Journal of Refrigeration, 34(2),pp.444–453.

Hewitt, N. & Huang, M. J., 2008: Defrost cycle performance for a circular shape evaporator air source heat pump, International Journal of Refrigeration , 31, 444 – 452

IKZ Fachplaner: 40% höhere Energieeffizienz - Hotel in Bergamo heizt und kühlt mit Gas-Wärmepumpe und Solarenergie, http://www.ikz.de/nc/ikz-fachplaner/artikel/article/40-hoehere-energieeffizienz-brhotel-in-bergamo-0013.html, 09.01.2014

Jin X., Wang S., Zhang T., Zu F., 2012: Intermediate pressure of two-stage compression system under different conditions based on compressor coupling model, Int. J. Refrig. 2012, 35, pp. 827-840

Jordan U., Vajen, K., Streicher, W. & Letz, T., 2003. Performance of Solar Combisystems. In: W. Weiss, Ed. Solar Heating Systems for Houses - A Design Handbook for Solar Combisystems. James & James, London, pp. 125–162.

Kosowski K., Tegethoff W., Kühl L., 2009: CO_2-Wärmepumpen für Passivhäuser, Institute of Thermodynamics, Braunschweig University of Technology, Germany

Lammert S. (2013): „Optimierung von Luft/Wasser-Wärmepumpen durch Flüssigkeitseinspritzung in den Verdichter", VDI-Konferenz Wärmepumpen, Frankfurt, Germany.

Lerch W., Heinz A., 2014. "Annex G.3 - Simulation results from the national Austrian project SolPumpEff. Evaluation of combined solar thermal heat pump systems." In Haller M.Y. " Report C3 - System Simulation Reports for the IEA SHC Task 44 / HPP Annex 38"

Liegeois O., Winandy E., 2008: Scroll Compressors for Dedicated Heat Pumps: Developement and Performance Comparison, International Compressor Engineering Conference at Purdue University, Paper 1906, July 14 – July 17, 2008

Mader G., Tiedemann T., Palm B., 2012, Konzepte zur Erhöhung der saisonalen Leistungszahl einer Luft-Wasser-Wärmepumpe: Vergleich hinsichtlich Kosten und Nutzen, DKV-Tagung Würzburg, Germany

Mader G., Tiedemann T., Palm B., 2010, Konzepte zur Erhöhung der saisonalen Leistungszahl einer Luft-Wasser-Wärmepumpe: Vergleich hinsichtlich Kosten und Nutzen, DKV Conference, Magedeburg, Germany

Moallem, E.; Cremaschi, L.; Fisher, D. E. & Padhmanabhan, S., 2012: Experimental measurements of the surface coating and water retention effects on frosting performance of microchannel heat exchangers for heat pump systems, Experimental Thermal and Fluid Science , 39, 176 - 188

Mukherjee H. 2001: Air Conditioning and Refrigeration, http://www.ishrae.in/journals/2001apr/article02.html , 08.01.2014

Neksa P., Rekstad H., Zakeri G., Schiefloe P. A., Svensson M., 1999: Heat Pump Water Heaters with CO_2 as Working Fluid, 6th International Energy Agency Heat Pump Conference, "Heat Pumps – a Benefit for the Environment, Berlin, Germany, May 31 – June 2, 1999

Nowak T. (2013): „Heat pump market and statistics report 2013", European Heat Pump Summit, Oct. 15 – 16, 2013, Nuremberg, Germany.

Ooi K.T., 2005: Design optimization of a rolling piston compressor for refrigerators, Applied Thermal Engineering 2005, 25, pp. 813-829

Rieberer R., 2011: Unterlagen zur Vorlesung „Wärmepumpentechnik", Institute of Thermal Engineering, Graz University of Technology, Austria

Sahinagic, R.; Gasser, L.; Wellig, B. & Hilfiker, K. 2008: LOREF: Optimierung des Lamellenluftkühlers/Verdampfers von Luft/Wasser-Wärmepumpen, Teil 2: Mathematisch-physikalische Simulation des Lamellenluftkühlers mit Kondensat- und Frostbildung, Bundesamt für Energie

Sanaye, S., Asgari, H., 2013: Thermal modeling of gas engine driven air to water heat pump systems in heating mode using genetic algorithm and Artificial Neural Network methods, International Journal of Refrigeration, Vol. 36(8), pp. 2262-2277

Sanner B. et al., 2008: Wärmepumpen in Deutschland und Europa – ein Wachstumsmarkt, http://www.geothermie-nachrichten.de/erdgekoppelte-waermepumpen-ein-wachstumsmarkt , 09.01.2014

Schmidt M., Arold J., Klimke K., 2010: Regelstrategien zum Verbessern der Jahresarbeitszahl von Luft- und Wasserwärmepumpen, Institute of Building Energetics, University of Stuttgart, Germany, IGE 12-10

Shuxue X., Guoyuan M., 2014: Experimental study on two-stage compression refrigeration/heat pump system with dual-cylinder rolling piston compressor, Applied Thermal Engineering 2014, 62, pp. 803-808

Stene J., 2004: Residential CO_2 Heat Pump System for Combined Space Heating and Hot Water Heating, Doctoral thesis at the Norwegian University of Technology and Science (NTNU), ISBN 82-471-6316-0 (printed ver.), ISBN 82-471-6315-2 (electronic ver.)

Stene J., 2008: CO_2 Heat Pump System for Space Heating and Hot Water Heating in Low Energy Houses and Passive Houses, Paper at the First Nordic Conference on Passive Houses 2008, Trondheim, Norway, ISBN 978-82-90122-33-6

Steiner A., Rieberer R., 2012: Investigation of a reversible cooling and heating system for electric vehicles using CO_2 as working fluid under frosting conditions, 10 th IIR Gustav Lorenzen Conference on natural Refrigerants, Delft, Netherland

Tanaka N., Kotoh S., 2007: The current status of and future trends in heat pump technologies with natural refrigerants, Mitsubishi Electr. Adv. 2007, 120(2), pp. 1-4

Teh YL., Ooi KT., 2009: Experimental study of the revolving vane (RV) compressor, Applied Thermal Engineering 2009, 29(14-15), pp. 3235-3245

Teh YL., Ooi KT., 2009: Theoretical study of a novel refrigeration compressor – Part 1: Design of the revolving vane (RV) compressor and its frictional losses, Int. J. Refrig. 2009, 32(5), pp. 1092-1102

Teh YL., Ooi KT. 2009: Theoretical study of a novel refrigeration compressor – Part 2: Performance of a rotating discharge valve in the revolving vane (RV) compressor, Int. J. Refrig. 2009, 32(5),
pp. 1103-1111

Teh YL., Ooi KT. 2009: Theoretical study of a novel refrigeration compressor – Part 3: Leakage loss of the revolving vane (RV) compressor and a comparison with that of the rolling piston type, Int. J. Refrig. 2009, 32(5), pp. 945-952

Wang W., Ma Z., Jiang Y., Yang Y., Xu S., Yang Z., 2005: Field test investigation of a double-stage coupled heat pumps heating system for cold regions, Int. J. Refrig. 2005, 28(5), pp. 672-679

Wang X., Hwang Y., Radermacher R., 2008: Investigation of potential benefits of compressor cooling, Applied Thermal Engineering 2008, 28(14-15), pp. 1791-1797

Wang B., Shi W., Han L., Li X., 2009: Optimization of refrigeration system with gas injected scroll compressor, Int. J. Refrig. 2009, 32, pp.1544-1554

Winandy E., Lebrun J., 2002: Scroll compressors using gas and liquid injection: experimental analysis and modelling, Int. J. Refrig. 2002, 25(8), pp. 1143-1156

Yari M., Sirousazar M., 2007: Performance analysis of the ejector-vapour compression refrigeration cycle, Proc. Inst. Mech. Eng., J. Power Energy 2007, 221(8), pp. 1089-1098

Zehnder M., Favrat D., Zahnd E., Cizmar J., Trüssel D., 2000: Wärmepumpe mit Zwischeneinspritzung bei Scrollkompressoren, Federal Office of Energy, Switzerland

9 ACKNOWLEDGEMENT

The work on “IEA HPP Annex 41” is financially supported within the framework of the “IEA Research Cooperation” on behalf of the “Austrian Federal Ministry for Transport, Innovation and Technology” (bmvit) (FFG project number: 839560).

Austrian Team Report

IEA HPT TCP Annex 41
"Cold Climate Heat Pumps"

Task 2 – Simulation Models and Prototype Experiments

Submitted by:

Heinz Moisi
René Rieberer (contact: rene.rieberer@tugraz.at)

Graz University of Technology
Institute of Thermal Engineering
Inffeldgasse 25/B, 8010 Graz, Austria

Thomas Fleckl, Mirza Popovac, Christoph Reichl
(contact: thomas.fleckl@ait.ac.at
mirza.popovac@ait.ac.at
christoph.reichl@ait.ac.at)

AIT – Austrian Institute of Technology
Energy Department
Giefinggasse 2, 1210 Wien, Austria

May 11, 2016

TABLE OF CONTENTS

LIST OF TABLES

LIST OF FIGURES

1 INTRODUCTION

Based on the results of Task 1 (Hengel, et al., 2014) for different cycle modifications, simulation work has been carried out at the Institute of Thermal Engineering (IWT, Institut für Wärmetechnik) in order to investigate the potential of the different heat pump cycles for cold climate applications. This report is mainly based on the work of Zoier (2014) and Hengel et al. (2013). Zoier (2014) investigated several promising heat pump cycles by means of steady state simulation in EES (Engineering Equation Solver). Furthermore, estimations regarding ice formation based on a semi steady state approach and models derived from literature are discussed briefly. Zoier (2014) also performed more detailed calculations of a liquid injection-cycle and has carried out validation measurements on a heat pump test rig available at the IWT. Simulation based investigations of a heat pump cycle, using an economizer with internal heat exchanger (IHX) as well as a speed controlled scroll compressor, had been performed by Hengel et al. (2013). The boundary conditions, models and results are summarized in this report.

Frosting Performance of heat exchangers is covered in detail in chapter 4. First, different fin geometries are investigated experimentally (4.1) and fin frosting is performed using a computational method (4.2). Low temperature measurements of heat exchanger frosting are discussed in chapter 4.3.

2 PERFOMANCE OF AIR SOURCE HEAT PUMPS AT LOW AMBIENT TEMPERATURES

In this chapter, boundary conditions, system models and simulation methods used by Zoier (2014) are summarized. Furthermore, results of experimental work are presented and discussed.

2.1 Simplified Heat Pump Models

In order to show enhancement potential in terms of heating capacity and efficiency, as well as ways to extend the field of application of heat pumps in cold climates, steady state simulations in EES (F-Chart, 2014) have been carried out. At first, simple cycle models according to those already described in Hengel et al. (2014) have been set up. Based on the simplified models, more detailed simulations have been carried out for certain cycle modifications. The investigated cycle layouts are described briefly in the following sections. Main assumptions and simplifications taken are given as follows:

a) steady state operation in any operation point at any time
b) isenthalpic expansion
c) Heat transfer only in condenser and evaporator, no thermal losses due to piping, compressor, built in components etc.
d) Pressure losses neglected in condenser and evaporator (if not mentioned otherwise)
e) Refrigerant state of HP receiver is always saturated
f) Refrigerant chosen: R410A
g) Temperature glide of refrigerant during phase change is neglected (if not mentioned otherwise)

Table 1 gives an overview of the set up heat pump cycles. Additional parameters, which are necessary to those of the basic conventional cycle and the number of pressure stages are given in the table as well.

Table 1: Investigated cycle layouts and parameters (according to Zoier, 2014)

Model No.	Description	Stages	Additional parameters
01	Conventional cycle	1	-
02	Cycle with internal heat exchanger (IHX)	1	Efficiency of IHX
03	Cycle with flooded evaporator, low pressure (LP) accumulator (seperator)	1	Pump efficiency, Pressure drop in LP cycle
04	Two stage cycle with intercooler	2	Temperature difference to saturation curve, intermediate pressure level (IP)
05	Liquid injection cycle	1	Intermediate pressure level, injection massflow
06	Vapor injection with internal heat exchanger (IHX or Economizer_IHX)	2	Efficiency of IHX , intermediate pressure level
07	Vapor injection with receiver (Economizer_receiver)	2	intermediate pressure level
08	Cascade system	2	Temperature difference between low and high temperature (HT) cycle, refrigerant
09	Ejector cycle	1	Ejector efficiency

2.1.1 Conventional heat pump cycle (Model 01)

The conventional heat pump cycle layout, as shown in Figure 1, sets the base for comparison of the different cycle modifications. Heat from ambient air evaporates the refrigerant which is then compressed to high pressure level (HP) by the compressor. Afterwards heat is removed and the refrigerant is liquefied in the condenser. The liquefied refrigerant is then expanded to evaporation pressure level (LP) in the expansion valve.

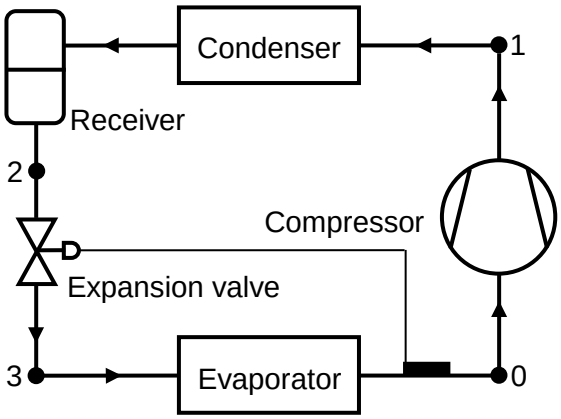

Figure 1: Layout of a conventional heat pump cycle (Zoier, 2014)

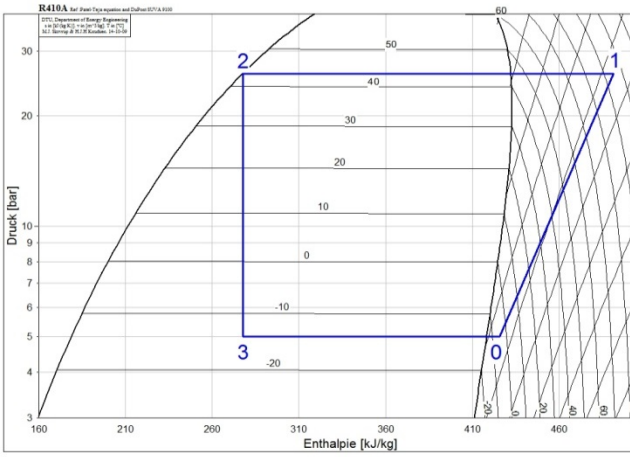

Figure 2: Conventional heat pump cycle illustrated in a log(p)-h diagram of R410A (Zoier, 2014)

The process can be illustrated in a log(p)-h diagram as shown in Figure 2. In order to determine the HP and LP level, evaporation and condensation temperatures (T_{evap} and T_{cond} respectively) are chosen in the simplified approach. Based on the property data base provided by EES, the pressure levels can be determined (p_{evap} and p_{cond}). No subcooling (ΔT_{sub}) after condensation has been considered (see Figure 2, point 2) but a temperature difference for superheating in the evaporator (ΔT_{sup}) is set. The compressor model is based on an isentropic efficiency ($\eta_{c,is}$), a mechanical efficiency ($\eta_{c,m}$), a volumetric efficiency (λ_{eff}), its swept volume (V_c), its speed (n) and follows the relations for the refrigerant massflow ($\dot{m}$) and the electrical power consumption (P_{el}) given in Eq. 2-1 and Eq. 2-2 respectively. Pressure ratio dependence of $\eta_{c,is}$ is not considered.

$$\dot{m} = \frac{\lambda_{eff} \cdot V_c \cdot n}{v_{c\_in}} \qquad \text{Eq. 2-1}$$

Using the specific volume at the compressor inlet $v_{c,in}$ and the enthalpy at the end of an isentropic compression ($h_{1,is}$) as well as the enthalpy at the compressor inlet (h_0).

$$P_{el} = \frac{\dot{m} \cdot (h_{1,is} - h_0)}{\eta_{c,m} \cdot \eta_{c,is}} \qquad \text{Eq. 2-2}$$

With $\eta_{c,is}$ given in the following expression.

$$\eta_{c,is} = \frac{(h_{1,is} - h_0)}{(h_1 - h_0)} \qquad \text{Eq. 2-3}$$

The evaporator and condenser heat capacity ($\dot{Q}_C$ and $\dot{Q}_H$) can then be calculated easily with Eq. 2-3 and Eq.2-4 as follows.

$$\dot{Q}_C = \dot{m} \cdot (h_0 - h_3)$$ Eq. 2-4

$$\dot{Q}_H = \dot{m} \cdot (h_1 - h_2)$$ Eq. 2-5

Using the enthalpy at the evaporator inlet (h_3), the enthalpy at the expansion valve inlet (h_2) and the enthalpy after non-isentropic compression (h_1) (compare to Figure 1 and Figure 2). Finally, the coefficient of performance for heating (COP_H) and cooling (COP_C) can be calculated according to equations Eq. 2-6 and Eq. 2-7.

$$COP_H = \frac{\dot{Q}_H}{P_{el}}$$ Gl. 2-6

$$COP_C = \frac{\dot{Q}_C}{P_{el}}$$ Gl. 2-7

The compressor discharge temperature (T_1) is then fully determined by h_1 (calculated via Eq. 2-3) and p_{cond} and can be obtained from the property data base.

2.1.2 Cycle with internal heat exchanger (IHX) (Model 02)

Figure 3 depicts the layout for a cycle IHX. The IHX increases the discharge temperature (point 2 in Figure 4) by increasing the compressor inlet temperature (point 1 in Figure 4) which results in a higher enthalpy difference at the condenser.

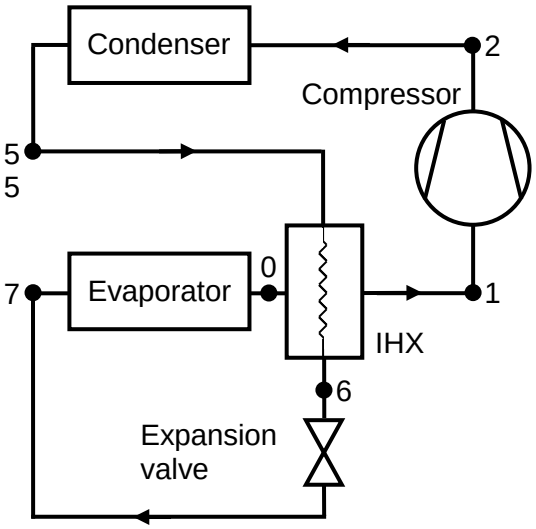

Figure 3: Layout with IHX, Zoier (2014)

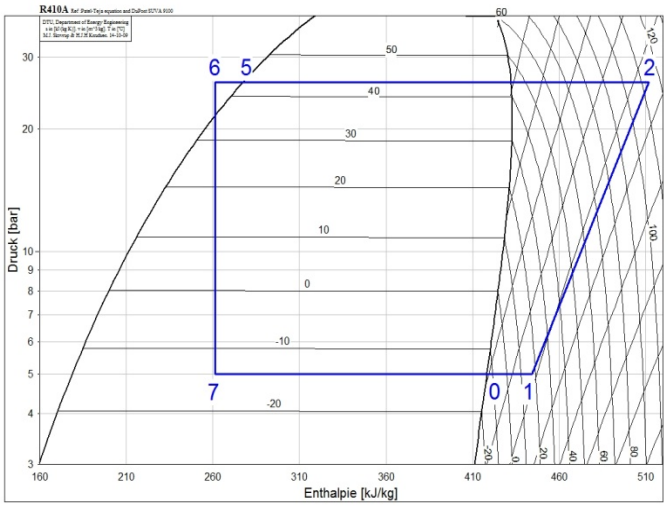

Figure 4: log(p)-h diagram for the IHX cycle, Zoier (2014)

However, the suction mass flow decreases with increasing inlet temperatures. Hence, in order to increase the heating capacity the advantage of an increased enthalpy difference has to compensate for the disadvantage of a reduced mass flow. The compressor model is the same as used for Model 01. The internal heat exchanger is modelled as a counterflow heat exchanger with an efficiency parameter η_{IHX} depending on the maximum achievable enthalpy difference in the LP stream. The parameter is defined in Eq. 2-8 according to Figure 4 as follows.

$$\eta_{IHX} \cdot (h_{1,max} - h_0) = h_1 - h_0 \qquad \text{Eq. 2-8}$$

With $h_{1,max} = f(p_{evap}, t_5)$.

2.1.2 Cycle with flooded evaporator (Model 03)

Model 03 describes a heat pump cycle with low pressure accumulator. The accumulator keeps the compression inlet state on the saturation line (point 3 in Figure 6). Liquid refrigerant is separated and pumped through the evaporator thus, if ideally controlled, the entire phase change enthalpy can be used. It is especially advantageous for cooling applications.

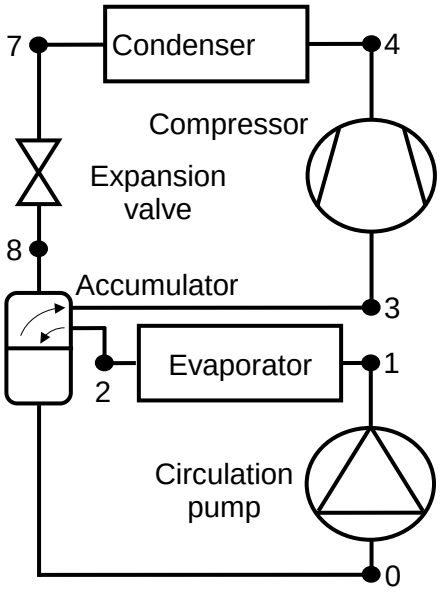

Figure 5: Heat pump with LP accumulator according to (Zoier, 2014)

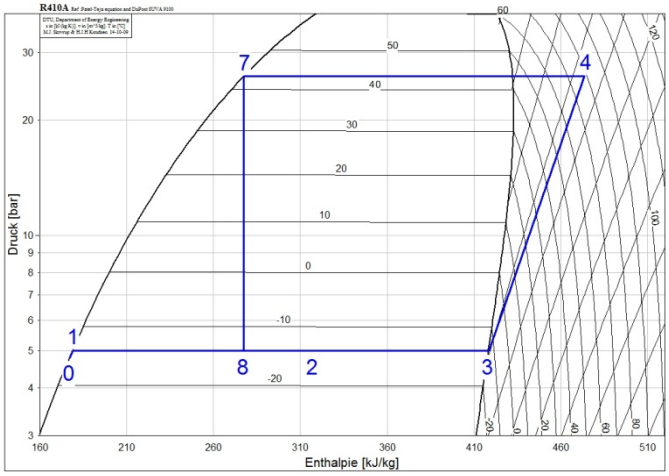

Figure 6: log(p)-h diagram of the accumulator cycle according to (Zoier, 2014)

The circulating pump of course decreases the COP slightly. The pump model uses similar parameters as the compressor with, a mechanical efficiency ($\eta_{p,m}$), a volumetric efficiency ($\lambda_{p,eff}$), its swept volume (V_c), its speed (n). Equation Eq. 2-9 provides the electrical power consumption of the pump ($P_{el,p}$) with an assumed pressure drop in the evaporator and piping ($\Delta p_{evap+piping}$).

$$P_{el,p} = \frac{\dot{m}_{LP} \cdot \Delta p_{evap+pipe}}{\eta_m \cdot \eta_{is}} \qquad \text{Eq. 2-9}$$

Finally the LP mass flow ($\dot{m}_{LP}$) can be obtained from energy balance at the accumulator.

2.1.3 Two stage cycle with intercooler (Model 04)

For cold climate applications, pressure ratios (π) and compressor outlet temperatures can reach unacceptable values. Therefore a two stage compression (swept volumes $V_{c,1}$ and $V_{c,2}$) provides the possibility to operate each compressor in an optimal efficiency area and the intercooler keeps the discharge temperature of the high stage compressor in an acceptable range. The intercooler is modelled with a given temperature difference from the saturation curve ($\Delta T_{IC,sat}$, see Figure 8 point 2).

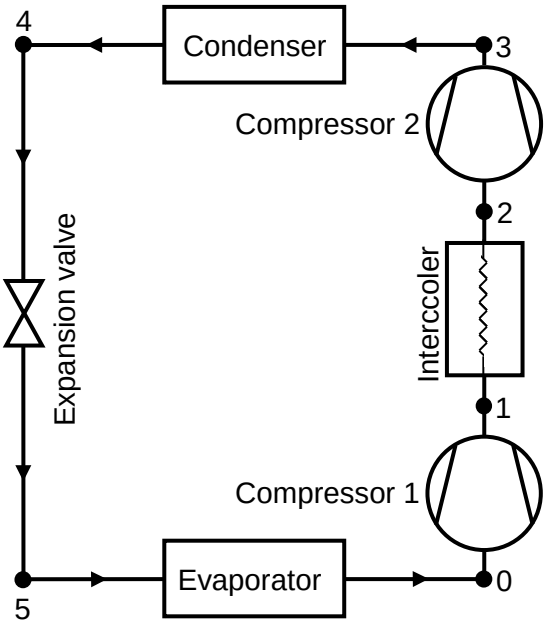

Figure 7: Layout for a two stage cycle with intercooler according to Zoier (2014)

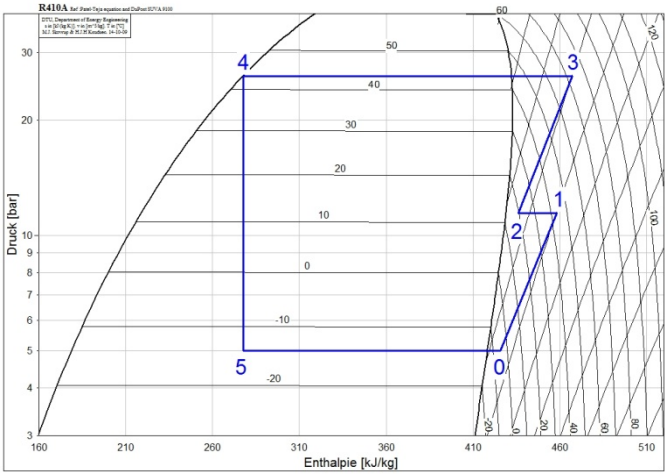

Figure 8: log(p)-h diagram of a two stage cycle with intercooler according to Zoier (2014)

Both compressors are calculated according to the equations given at the conventional cycle. The intermediate pressure level is defined by the assumption that the pressure ratios of both stages are identical, which results in equation Eq. 2-10.

$$p_{MP} = \sqrt{p_{evap} \cdot p_{cond}} \qquad \text{Eq. 2-10}$$

The removed heat between stages is not used and therefore not part of the COP calculation. This states a rather pessimistic approach since the removed heat may be used to preheat the air before it enters the evaporator.

2.1.4 Refrigerant injection cycle (Model 05)

In this cycle, a part of the refrigerant mass flow is expanded to an intermediate pressure level (MP, two phase region, Figure 10 point 5) and this mostly liquid refrigerant is injected via an MP inlet into the compressor. Primarily, the injected refrigerant cools down the compressor mass flow which results in lower discharging temperatures and thereby increases the range of application at low ambient temperatures. On the other hand, the additional MP mass flow influences the condenser heat capacity ($\dot{Q}_H$). The intermediate injection is modelled with two separate compressors (LP and HP) with identical isentropic efficiencies and an ideal mixing chamber in between. The intermediate pressure level follows again Eq. 2-10. A constant predefined ratio (x_{LI}) between HP mass flow ($\dot{m}_{HP}$) and injection mass flow ($\dot{m}_{LI}$) and the mass balance at the condenser outlet provide the injection mass flow (see Eq.2-11 and Eq.2-12).

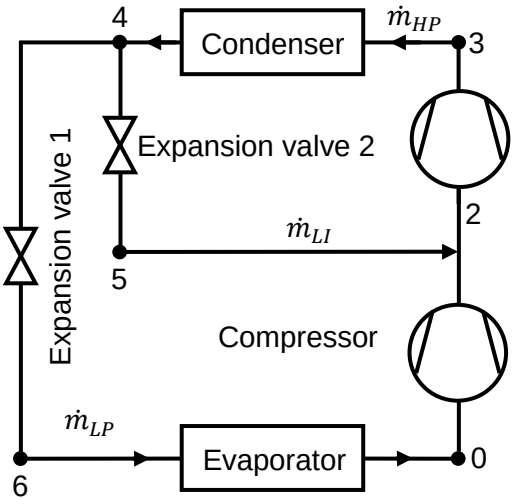

Figure 9: Layout of the injection cycle according to Zoier (2014)

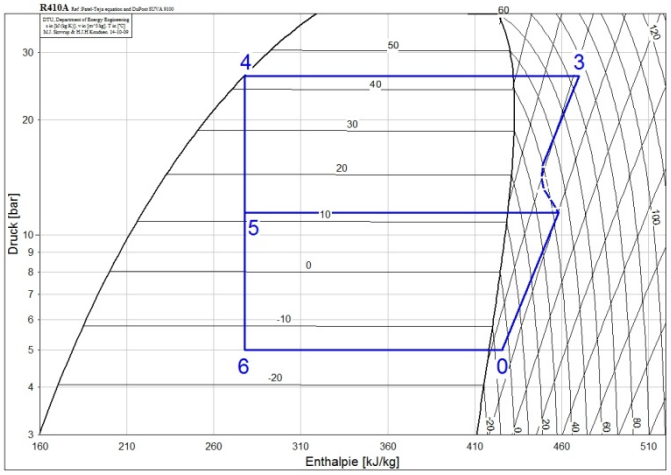

Figure 10: log(p)-h diagram for the injection cycle according to Zoier (2014)

$$\dot{m}_{LI} = \dot{m}_{HP} \cdot x_{LI} \qquad \text{Eq. 2-11}$$

$$\dot{m}_{HP} = \dot{m}_{LP} + \dot{m}_{LI} \qquad \text{Eq. 2-12}$$

The state for the HP compressor inlet can then be found with the energy balance of the ideal mixing process defined in Eq. 2-13.

$$\dot{m}_{HP} \cdot h_2 = \dot{m}_{LP} \cdot h_1 + \dot{m}_{LI} \cdot h_5 \qquad \text{Eq. 2-13}$$

With the enthalpy at the inlet of HP stage h_2, the outlet of the LP stage h_1, the LP mass flow $\dot{m}_{LP}$ and the enthalpy h_5 of injection mass flow at intermediate pressure.

2.1.5 Vapor injection with IHX (Model 06)

A vapor injection model with internal heat exchanger according to Figure 11 has been investigated. This modification makes it possible to extend the range of application for low ambient temperatures because of vapor injection between the compressors resulting in a lower discharge temperature of the second compressor. Furthermore the compressors can operate at with lower pressure ratios, i.e. better efficiency. The IHX states a simple method to decrease the HP inlet temperature (see point 2 in Figure 12). The compressors are modelled again according to the conventional cycle with identical isentropic and volumetric efficiencies.

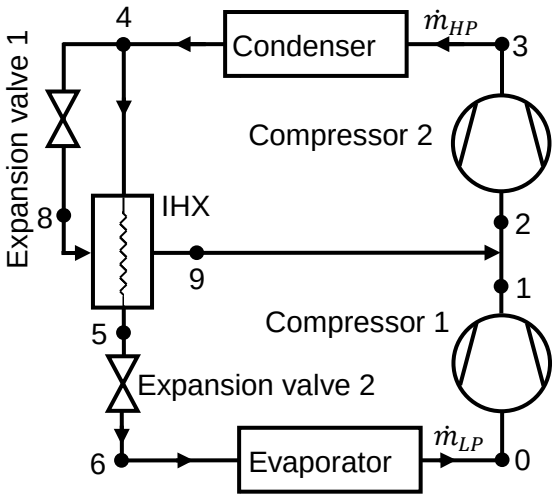

Figure 11: Layout of economizer with IHX according to Zoier (2014)

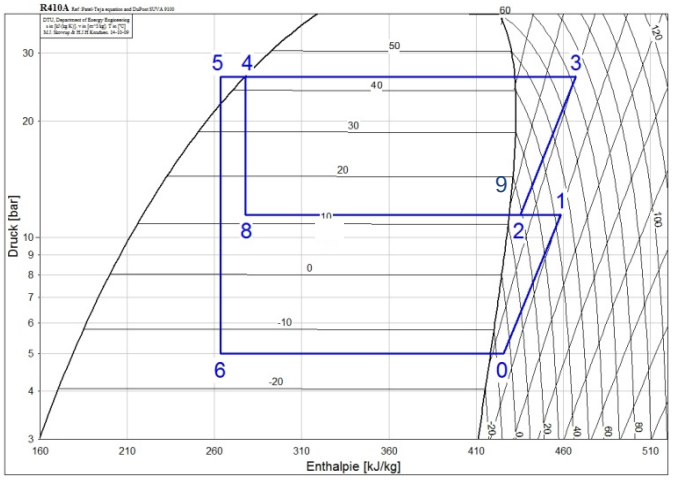

Figure 12: log(p)-h diagram of economizer cycle with IHX according to Zoier (2014)

The outlet state of the IHX has been set on the saturated vapor line at the intermediate pressure level which can be calculated by Eq. 2-8. The HP inlet state (Figure 12, point 2) can be calculated similar to Eq. 2-11. Considering the energy balance of the IHX, the condenser mass flow ($\dot{m}_{HP}$) and the injection mass flow ($\dot{m}_{inj}$) can be calculated according to Eq. 2-14 and Eq. 2-15.

$$\dot{m}_{inj} = \dot{m}_{HP} - \dot{m}_{LP} \qquad \text{Eq. 2-14}$$

$$\dot{m}_{inj} \cdot (h_9 - h_8) = \dot{m}_{LP} \cdot (h_4 - h_5) \qquad \text{Eq. 2-15}$$

With a defined heat exchanger efficiency η_{IHX} as given in Eq. 2-16 and $h_{5,min} = f(t_8, p_{cond})$

$$\eta_{IHX} \cdot (h_4 - h_{5,min}) = h_4 - h_5 \qquad \text{Eq. 2-16}$$

2.1.6 Vapor injection cycle with flash tank (Model 07)

In this application the economizer cycle is realised with a flash tank which sets point 5 from FigureFigure 12 on the liquid line at intermediate pressure. A flash tank separates saturated vapor from the liquid phase for the injection (see Figure 13).

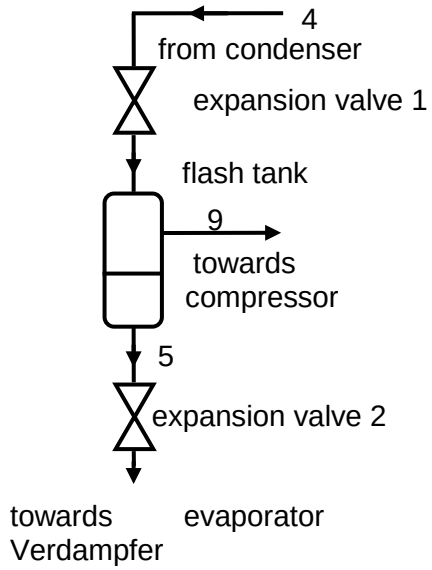

Figure 13: Economizer with flash tank according to Zoier (2014)

The two compressor stages are modelled identically to Model 06. Ideal mixing is assumed and the mass flow at intermediate pressure can be found via energy balance of the flash tank.

2.1.7 Cascade cycle (Model 08)

The cascade cycle combines two separate conventional cycles via a heat exchanger (HX). The process is divided into a high temperature (HT) and a low temperature cycle (LT) as depicted in Figure 14, which allows the compressors to operate within adequate pressure ratios and thus in an optimal operating range. Furthermore, two different refrigerants can be used. In this case only R410A has been used for each stage. The heat transfer between the HT and LT cycles has not been modelled in detail, instead a temperature difference ($\Delta T_{HT,LT}$) between HT evaporation temperature and LT condensation temperature in the HX has been assumed. Based on the intermediate pressure level found by Eq. 2-10 the condensation temperature on the LT side and the evaporation temperature on the HT side are determined by the following equations.

$$T_{1-2} = T_m + \frac{\Delta T_{HT,LT}}{2} \qquad \text{Eq. 2-17}$$

$$T_{8-5} = T_m - \frac{\Delta T_{HT,LT}}{2} \qquad \text{Eq. 2-18}$$

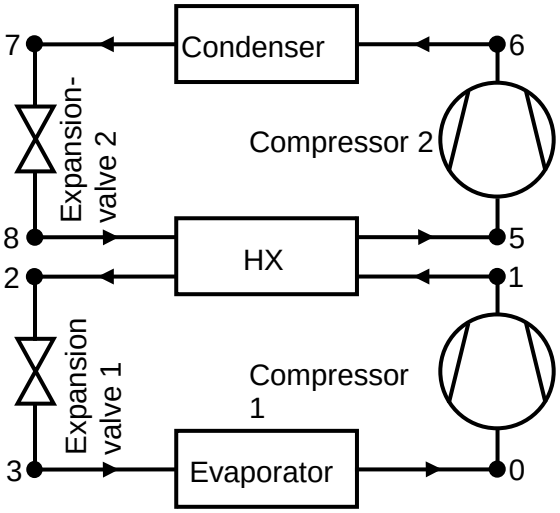

Figure 14: Cascade cycle layout according to Zoier (2014)

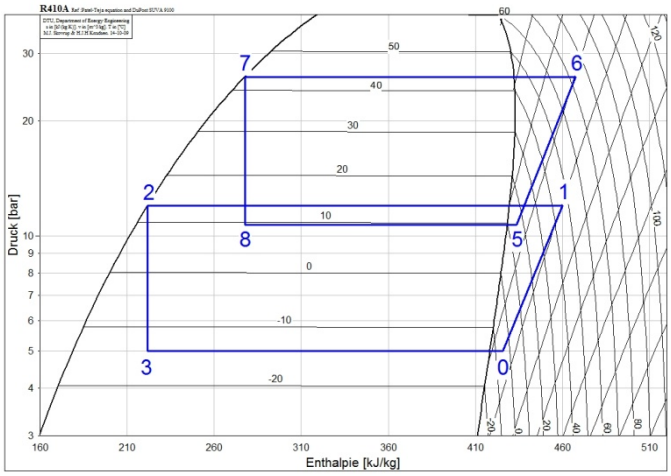

Figure 15: log(p)-h diagram of the cascade cycle according to Zoier (2014)

The intermediate temperature T_m is a function of p_{MP} (see Eq.2-10). Hence the HP level of the LT cycle and the LP level of the HT cycle can be obtained as a function of T_{1-2} and T_{8-5}, respectively. Compressors are modelled identical to the aforementioned systems. The refrigerant for both cycles in the simulation is R410A, in advanced calculations the refrigerant combination should be varied

2.1.8 Ejector cycle (Model 09)

The ejector cycle presents an interesting cycle modification where a part of the expansion work can be used to compress the refrigerant after the evaporator. This results in a higher inlet pressure for the compressor and thus lower pressure ratio and lower compression work.

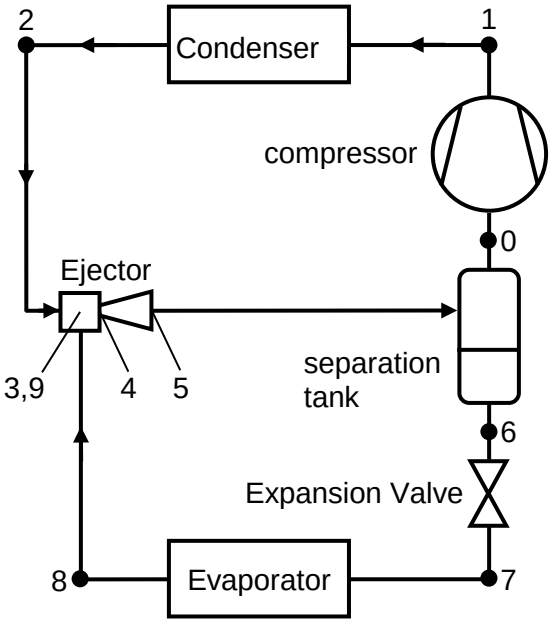

Figure 16: Ejector cycle layout according to Zoier (2014)

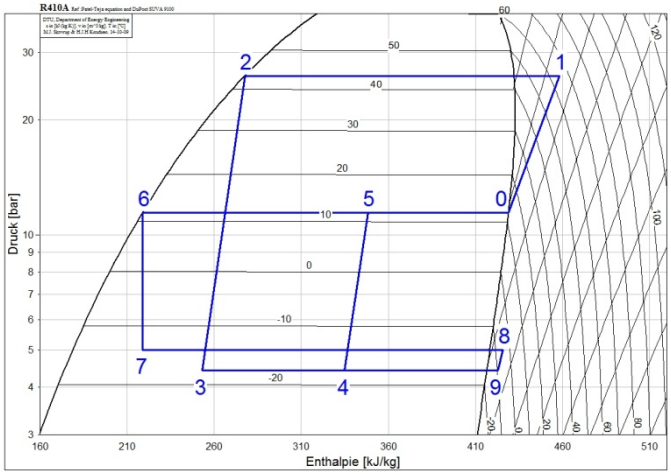

Figure 17: log(p)- h diagram for the ejector according to Zoier (2014)

The acceleration of HP flow stream in the ejector from point 2 to 3 causes an acceleration of the flow stream from the evaporator (8 to 9). This is followed by an isobaric mixing process (point 4). The refrigerant is then brought to an intermediate pressure level in a diffusor (point 5). The liquid and gaseous phase is separated in a tank. Figure 18 shows the utilized ejector model with designated areas corresponding to Figure 17.

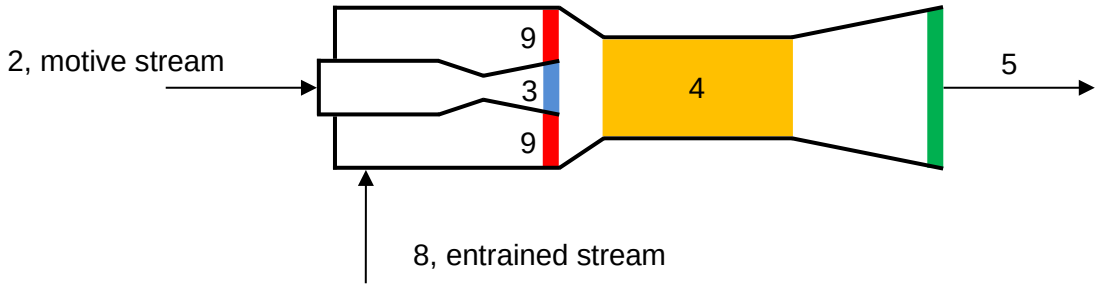

Figure 18: Ejector model according to Zoier (2014)

The following briefly described model used by Zoier (2014) is based on Li et al. (2014) and requires the following assumptions and simplifications.

- velocities at ejector inlet and outlet are neglected
- friction effects are considered with efficiencies
- homogenous one dimensional flow within the ejector
- motive and entrained refrigerant are not mixed before the mixing chamber (area 4 in Figure 18)
- no pressure difference of accelerated and drawn-in mass flow at mixing chamber inlet

Parameters like the ratio between accelerated and drawn-in mass flow (μ), pressure drop between point 3 and 8 (Δp), efficiencies for the acceleration nozzle (η_{acc}), the suction nozzle (η_{suc}), the mixing chamber (η_{mc}) and the diffusor (η_d) are assumed. At first the pressure in point 9 can be found with Eq. 2-19 considering the defined pressure drop.

$$p_9 = p_8 - \Delta p \qquad \text{Eq. 2-19}$$

As mentioned in the assumptions above the pressure at the acceleration nozzle outlet (point 9) is identical to the pressure in point 3 hence

$$p_3 = p_9. \qquad \text{Eq. 2-20}$$

The enthalpy in point 3 assuming an isentropic expansion ($h_{9,is}$) can be found as a function of the entropy in state 8 (s_8) and p_9. Therefore the enthalpy h_9 can be calculated considering η_{suc}, with Eq. 2-21.

$$h_9 = h_8 - \eta_{suc} \cdot (h_8 - h_{9,is}) \qquad \text{Eq. 2-21}$$

The enthalpy h_3 can be found similarly.

$$h_3 = h_2 - \eta_{acc} \cdot (h_2 - h_{3,is}) \qquad \text{Eq. 2-22}$$

The velocities at each outlet can be obtained from Eq. 2-23 and Eq.2-24.

$$c_3 = \sqrt{2 \cdot (h_2 - h_3)} \quad \text{Eq. 2-23}$$

$$c_9 = \sqrt{2 \cdot (h_8 - h_9)} \quad \text{Eq. 2-24}$$

With the mass flow ratio μ and the conservation of momentum and energy, the outlet state of the isobaric ($p_3 = p_4$) mixing chamber can be calculated as follows.

$$c_4 = \sqrt{\eta_{mc}} \cdot \left(\frac{1}{1+\mu} \cdot c_9 + \frac{\mu}{1+\mu} \cdot c_3 \right) \quad \text{Eq. 2-25}$$

$$h_4 = \frac{1}{1+\mu} \cdot \left(h_9 + \frac{{c_9}^2}{2} \right) + \frac{\mu}{1+\mu} \cdot \left(h_3 + \frac{{c_3}^2}{2} \right) - \frac{{c_4}^2}{2} \quad \text{Eq. 2-26}$$

$$s_4 = s(p_4, h_4) \quad \text{Eq. 2-27}$$

Finally the outlet state of the ejector can be obtained from equations Eq. 2-28 to Eq. 2-27.

$$h_5 = h_4 + \frac{{c_4}^2}{2} \quad \text{Eq. 2-28}$$

$$h_{5,is} = h_4 + \eta_{dif} \cdot (h_5 - h_4) \quad \text{Eq. 2-29}$$

$$p_5 = p(h_{5,is}, s_5) \quad \text{Eq. 2-30}$$

2.2 Results of Simplified Models

In order to compare the described cycle layouts in terms of cold climate application, discharge temperatures, heating capacity and COP have been calculated for operating conditions given in Table 2.

Table 2: Considered operating conditions for each system (Zoier, 2014)

t_{evap} [°C]	-30	-27	-23	-19	-15	-11	-7
t_{cond} [°C]	45						

Table 3 lists input parameters and boundary conditions utilized for the simulations.

Table 3: Boundary conditions and input parameter, Zoier (2014)

description	**symbol**	**value**
swept volume of each stage	V_c ; $V_{c,1}$; $V_{c,2}$	$5*10^{-5}$ m³
volumetric efficency of each stage	λ_{eff} ; $\lambda_{eff,1}$; $\lambda_{eff,2}$; $\lambda_{p,eff}$	0,8
isentropic efficiency of each stage	$\eta_{c,is}$; $\eta_{c1,is}$; $\eta_{c2,is}$	0,66
mechanical efficiency	η_m ; $\eta_{m,1}$; $\eta_{m,2}$; $\eta_{m,p}$	1
Compressor speed	n ; n_1 ; n_p	25 1/s
Superheating at evaporator outlet	ΔT_{sup}	5 K

Subcooling at condenser outlet	ΔT_{sub}	0 K
Swept volume of pump	$V_{c,p}$	$5*10^{-6}$ m³
pressure drop (used for all models where necessary)	Δp	0,5 bar
temp. diff. between cascade stages	$\Delta T_{HL,LT}$	5 K
injection masslfow ratio	x_m	20%
IHX efficency	η_{IHX}	0,5
efficiency of accelerating nozzle	η_{acc}	0,9
diffusor efficiency	η_{dif}	0,9
mixing chamber efficiency	η_{mc}	0,9
efficiency of suction nozzle	η_{suc}	0,9
ejector mass flow ratio	μ	0,2

Figure 19 shows the results of the heating COP calculations. The y-axis shows the COP and the x-axis shows the evaporation temperature in a range from -30°C to -7. The COP results of the conventional cycle (Model01) are marked by the red line. It stands out that the ejector model (09) shows by far the best COP values, however it has been considered highly theoretical and is therefore neglected in the following considerations.

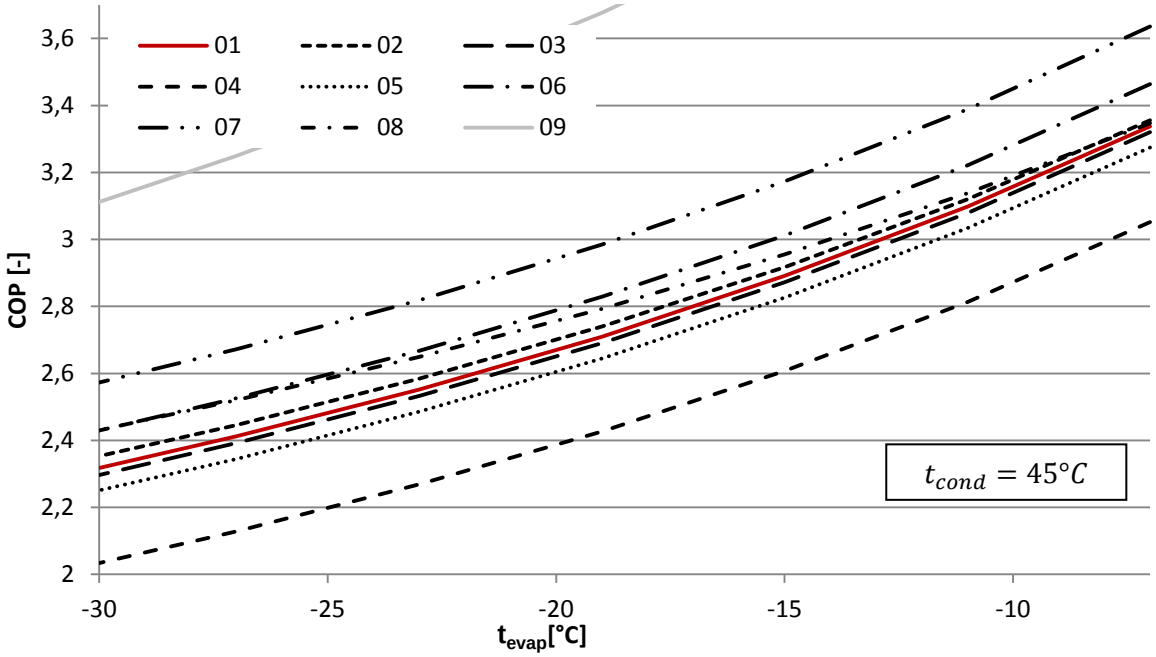

Figure 19: Comparison of COP/t_{evap} characteristics of each system (Zoier, 2014)

The second best performance is shown by the economizer with flash tank (07) with about +9 to 11% increase in COP compared to Model 01. The economizer with IHX (06) shows improvements in a range from 3.8 to 4.8% followed by the cascade cycle (08) with 0.3 to 4.8% compared to Model 01. On the other hand the cycle with intercooler results in with a COP decrease from -8.5 to -12.3%. A slight COP reduction can also be seen at the liquid injection cycle (05) with -2 to -3% compared to the conventional cycle.

The calculated condenser heat capacity over the evaporation temperature can be seen in Figure 20. Besides the ejector cycle, the cascade model (08) shows the highest increase in heating capacity compared to the conventional cycle (01) with 30 to 44% followed by 29 to

41% for the vapor injection with flashtank (07), Models 02 (IHX) and 03 (flooded evaporator) show no significant improvement and again the model with intercooling ranks last.

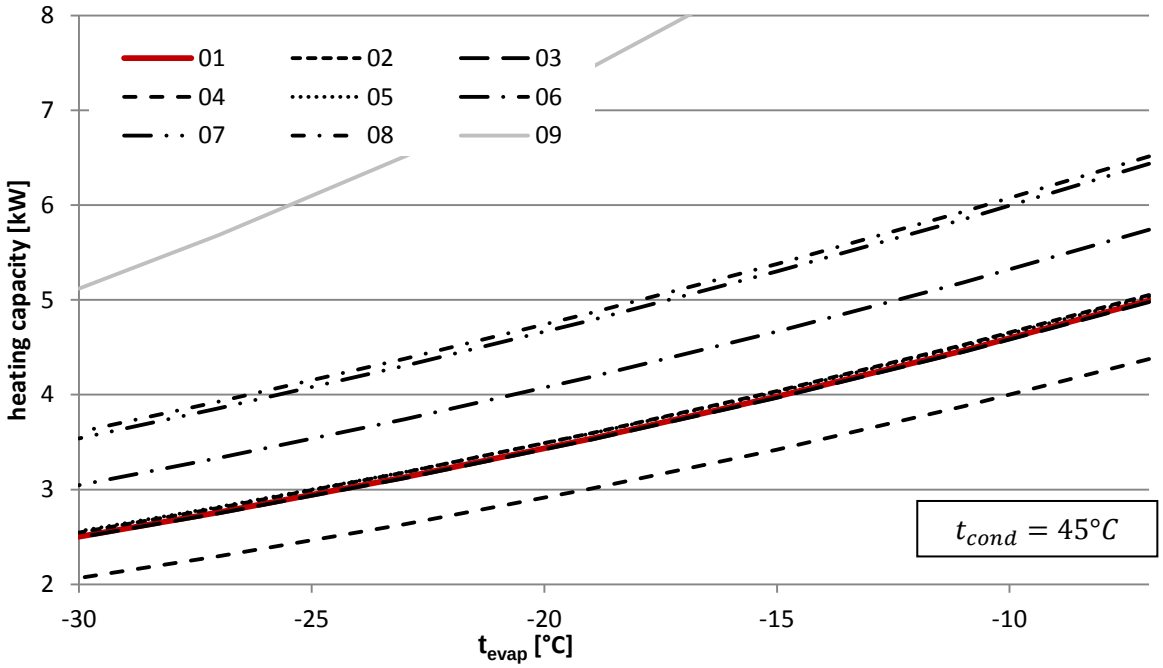

Figure 20: Condenser heating capacity depending on evaporation temperature for each system (Zoier, 2014)

All models are showing a decrease in discharge temperature except the cycle with IHX (02) as can be observed in Figure 21. Liquid injection (05) has the highest impact with a decrease of about -38 to -32 K due to the injection mass flow. Models 04 (intercooler) and 08 (cascade) are showing a significant decrease in discharge temperature with about -36 to -21 K and -34 to -19 K respectively.

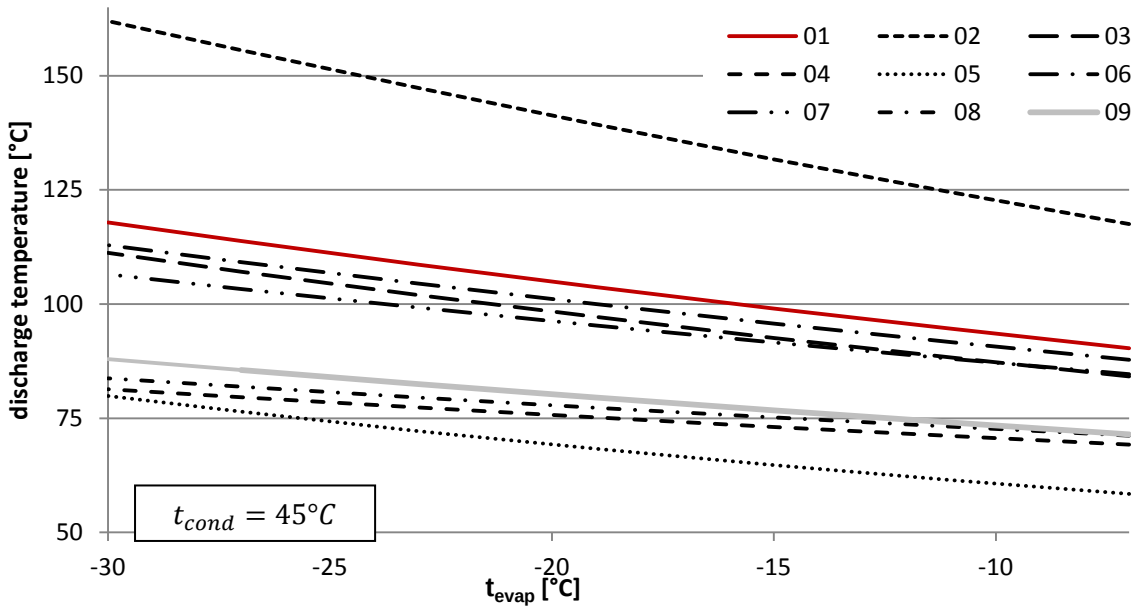

Figure 21: Compressor outlet temperature for each system (Zoier, 2014)

The highest combined potential for cold climate applications can be found in the cascade cycle and the vapor injection with flash tank cycle, with improvements in all three investigated parameters (COP, heating capacity, discharge temperature) as descried by the results above. However, these systems are more complex compared to the conventional cycle. An easier to implement alternative could be the liquid injection cycle. This cycle presents significant potential for decrease in compressor outlet temperature and similar heat capacities as the conventional cycle, the combination of which extends the range of application with a rather simple system.

2.3 A More Detailed Model for the Liquid Injection Cycle

Simplified models have been investigated to estimate their cold climate operating behavior as explained in the previous chapter. In spite of small efficiency losses, liquid injection can provide a simple way to extend the field of application for low ambient temperatures. Therefore, a more detailed simulation model of a liquid injection cycle using a scroll compressor has been developed based on an air source heat pump prototype tested at the IWT. Furthermore, ice formation at the evaporator has been considered. Measurements have been carried out in order to evaluate performance at low ambient temperatures and to verify simulation results. The simulation model, test rig and results are described briefly in the following sections.

2.3.1 Refrigerant Injection Cycle Model

The detailed injection cycle model is based on Figure 9 and Model 05. The major difference is that evaporation and condensation temperatures are not directly applied as boundary conditions anymore. The pressure levels are determined iteratively by considering heat transfer to the heat sink (water) and from the heat source (ambient air). A summary of input and iterative values are given in Table 4.

Table 4: Description of initial values and boundary conditions according to Zoier (2014)

Symbol	Description
R$=R410A	refrigerant
p_{evap_it} ; p_{cond_it} ; $m_{dot\_VI\_it}$; x_{cnt}	initial values for iteration
T_{amb} ; p_{amb}; relative humidity	state of ambient air
T_{w_in} ; T_{w_out}	Heating inlet and return temperature
ΔT_{sup} ; ΔT_{sub}	superheating evaporator outlet subcooling condenser outlet
T_{VI}	discharge temperature threshold for injection
V_{dot_a}	air volume flow
c_{p_w} ; c_{p_ma}	specific heat capacities of water (w) and air (ma)
A_{evap} ; A_{cond}	heat transfer areas
U_{evap_A} ; U_{evap_B}; U_{cond_A} ; U_{cond_B} ; U_{cond_C}	heat transmission coefficients

For the calculation of the heat transfer, the evaporator and condenser are divided into different sections considering phase transformation (gaseous, two phase and liquid). Estimated supplier provided U-values have been applied for each individual section. Moreover, area fractions of the heat exchangers for each section depending on the pressure level and temperatures are calculated to estimate the two-phase flow along the heat exchanger. Initial temperatures derived from ambient temperature and water outlet temperature are applied to start the pressure iteration process. The refrigerant mass flow as well as isentropic efficiencies for the high and low pressure stage can be calculated according to polynomial functions given by manufacturer data in dependence of p_{evap} and

p_{cond}. The air volume flow is also given by manufacturer data and remained constant. The state of ambient air has been defined by temperature, pressure and relative humidity. The injection is controlled by means to a temperature threshold. If the discharge temperature of the high stage compressor is below this threshold, injection is inactive. The injection mass flow can then be calculated iteratively by comparison of the current discharge temperature (T_{cond_in}) with the set maximum compressor outlet temperature (T_{VI}).

The following steps should explain the workflow of the cycle simulation according to Figure 22:

- In the beginning, necessary initial and input parameters are read and the iteration counter x_{cnt} is set to 1.
- The second step is an IF request in order to determine if injection is necessary ($T_{cond\_in} \leq T_{VI}$) or not. Is the compressor outlet temperature lower than the threshold and was the injection active in the previous iteration step, the injection also remains active (VI$=YES). If not, injection is switched off (VI$=NO)
- The driving temperature differences (ΔT) for heat transfer calculations are determined (Air to R410A and R410A to water). Heat fluxes ($\dot{Q}$) are calculated in two ways, as a function of massflow ($\dot{m}$) and enthalpy difference (Δh) and as a function of U-value, area (A) and the logarithmic mean temperature difference (ΔT_{log}). Since the logarithmic function is not defined for negative values, it has to be assured that ΔT is positive.
- The calculation jumps directly to the pressure iteration if negative or equal to zero temperature differences are found. If ΔT is positive, ΔT_{log} and the heat fluxes can be calculated. Now the area fractions for the heat transfer can be determined. Moreover, the arithmetic sign of heat flux difference sets the direction of pressure iteration.
- Finally, the heat fluxes have to meet the iteration criteria given in Figure 22.

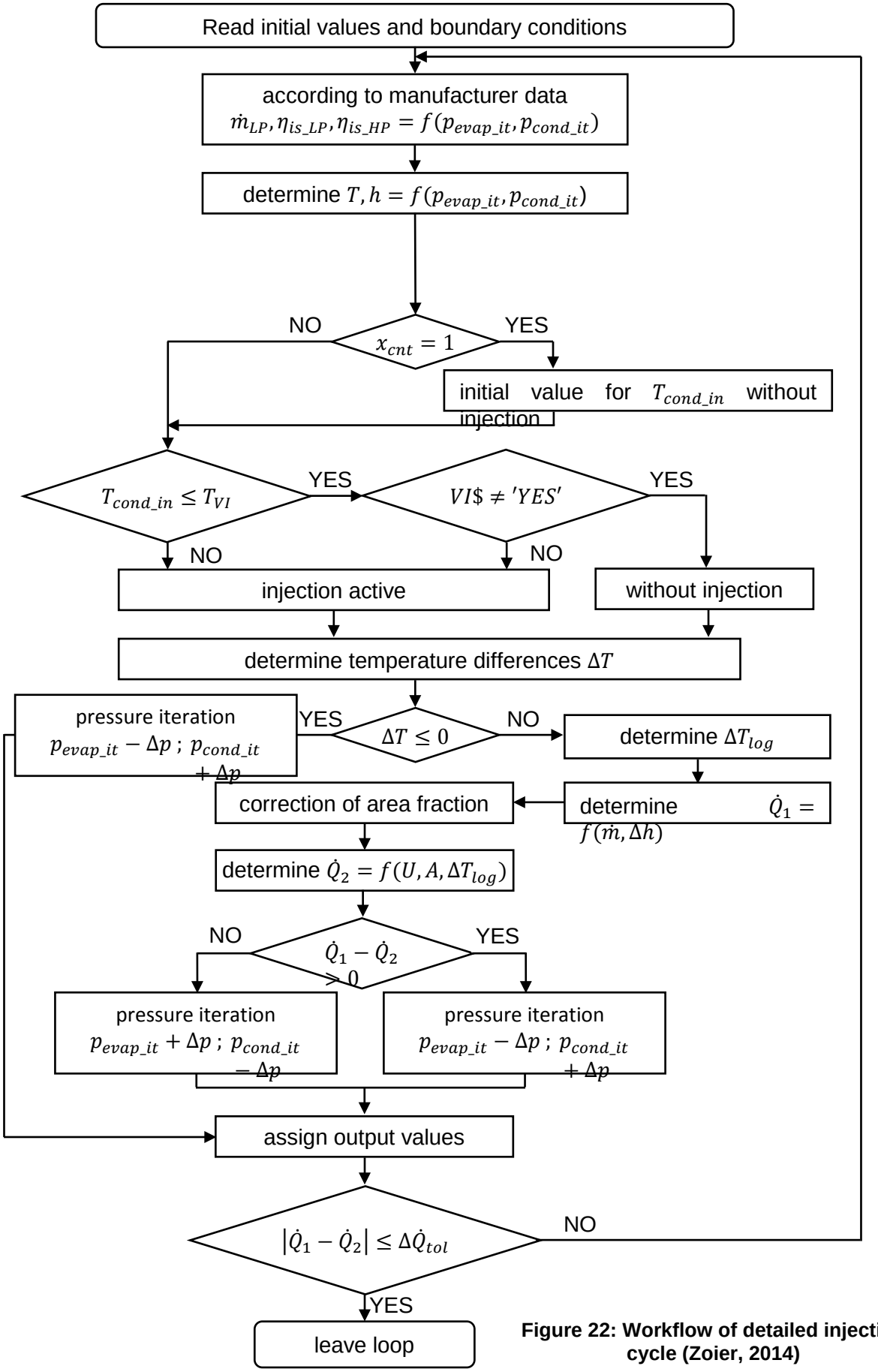

Figure 22: Workflow of detailed injection cycle (Zoier, 2014)

2.3.2 Ice formation

Within the detailed model, ice formation on a single evaporator fin is estimated with a quasi-steady state approach. Every variable is assumed constant in every time step. The model used in Zoier (2014) is based on equations given in Robinson et al. (2010) and Sankaranarayanan (2010). Briefly, the implementation of the frost model into the overall simulation should be described. The effect of ice formation within this simulation is a change in the heat transfer coefficient of the evaporator due to the ice layer. The interaction of the frost model with the heat pump cycle of Figure 22 is illustrated in Figure 23.

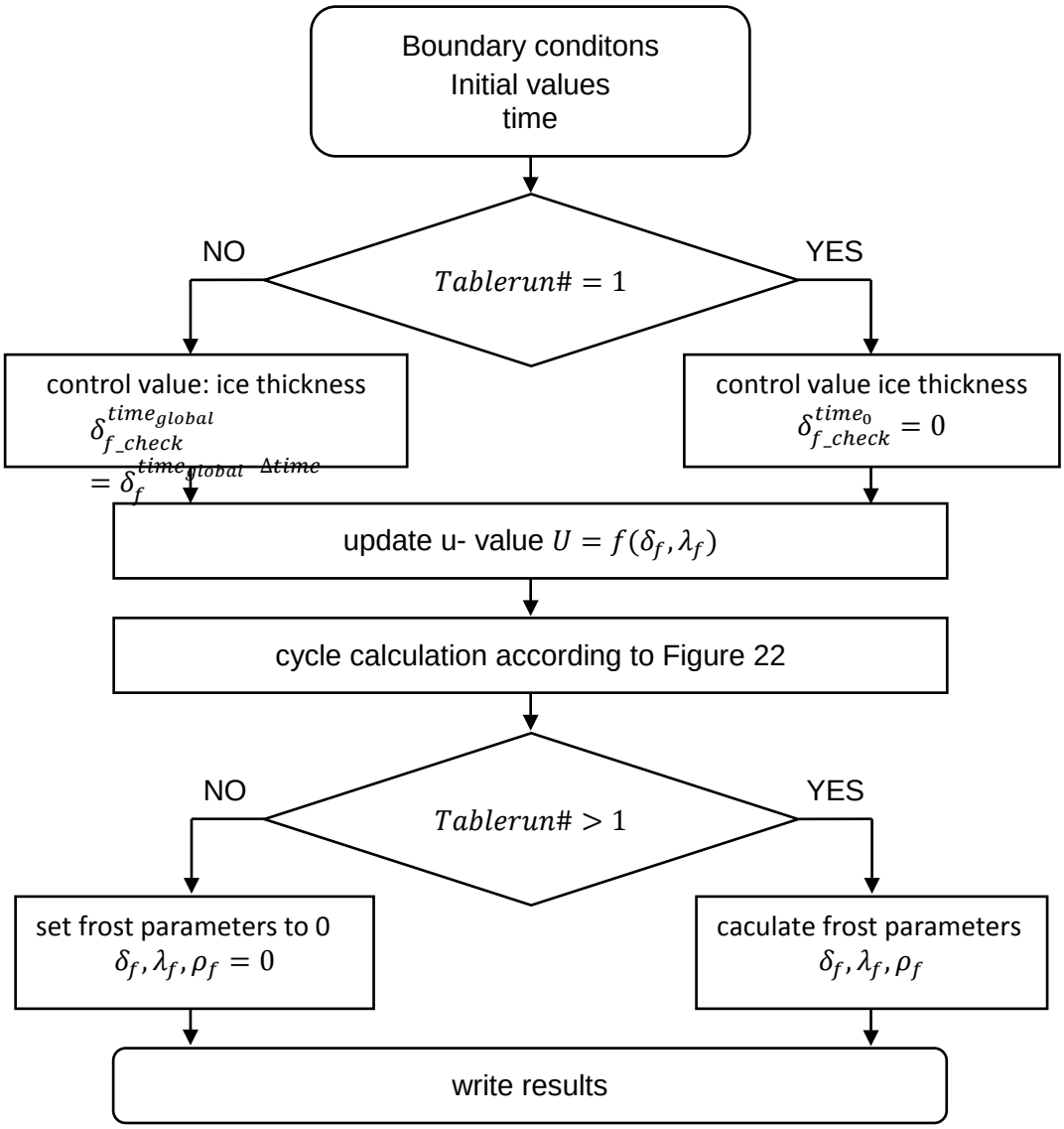

Figure 23: Overall simulation workflow including ice formation (Zoier, 2014)

In the first time step (Tablerun# = 1) no ice formation is considered. In the following time steps the frost parameters (δ_f= layer thickness, λ_f= thermal conductivity, ρ_f= density) of the previous steps are initial values. The heat transfer coefficient is then updated with the additional thermal resistance caused by the ice layer and the cycle procedure is calculated again with the corrected U-values.

2.4 Test Rig and Experiments

As mentioned before, the detailed model is based on a prototype tested at the IWT with a 22 kW condenser capacity (at t_{amb}=7°C and t_w=45°C). A scroll compressor with an injection inlet port (Pos. 1) is used. Figure 24 shows the layout of the test rig. An expansion valve (Pos. 16) regulates the injection mass flow. A detailed description of the cycle is given in section 2.1.

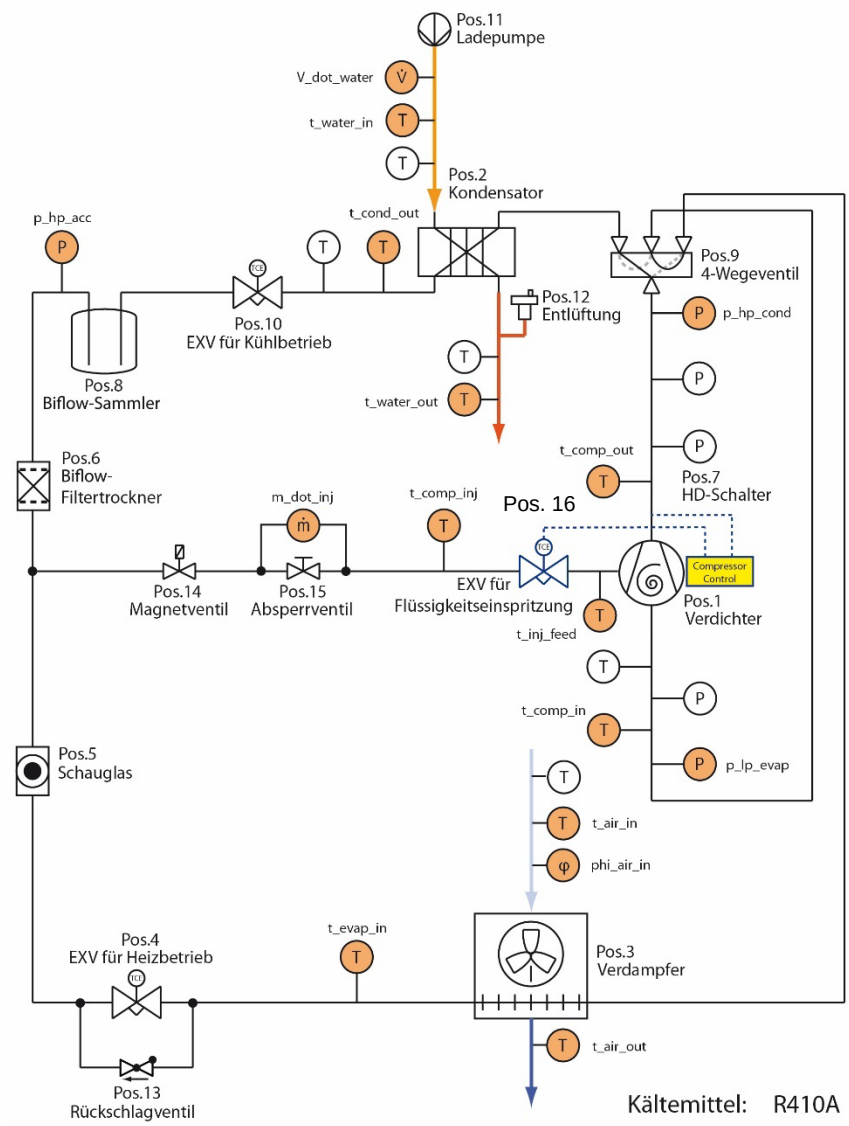

Position	Description
1	Scroll compressor
2	Condenser
3	Evaporator
4	Expansion valve
5	Inspection glass
6	Bi flow filter dryer
7	HP switch
8	Bi flow accumulator
9	4 way valve
10	Expansion valve
11	Pump
12	Venting valve
13	Check valve
14	Magnetic valve
15	Ball valve
16	Evaporation valve

Figure 24: Test rig layout of the liquid injection heat pump including applied sensors (orange and white circles), Zoier (2014)

A 4-way valve (Pos. 9) and an expansion valve (Pos. 10) for cooling operation provide the possibility to run defrosting cycles if necessary.

In order to simulate cold climate ambient conditions the climatic chamber at the IWT has been utilized. Figure 25 shows the layout of the test set up. Ambient conditions can be regulated within the climatic chamber in terms of air temperature and humidity in a range from -20 to 30°C and a maximum humidity of 95%. A thermal storage with a re-cooling system provides the necessary heat sink. The volume flow rate has been manually adjusted with the regulating valve. The return temperature is set and controlled by the mixing valve.

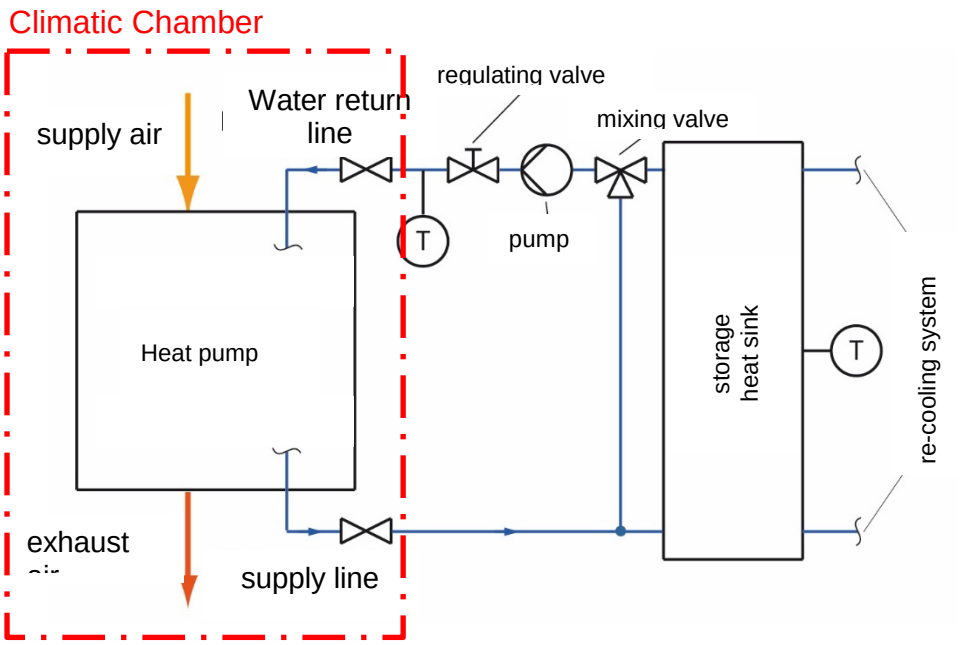

Figure 25: Test set up including climate chamber and heat sink according to Zoier (2014)

The measurement has been carried out based on standard EN 14511. The suggested measurement matrix obtained from EN-14522-2 (2007) has been extended with three additional operation points regarding the evaporator inlet air temperature at -2°C, -11°C and -19°C. Furthermore an additional operation point for the water outlet temperature with 60°C has been included. The modified measurement matrix is shown in Table 5 where “A” indicates the evaporator inlet air dry bulb temperature and “W” indicates the water outlet temperature.

Table 5: Modified measurement matrix translated in English from Zoier (2014)

abbrevation.	evaporator inlet air dry bulb temperature [°C]	evaporator inlet air wet bulb temperature [°C]	water outlet temperature [°C]	measured water inlet temperature[°C]
A7W35	7	6	35	29,8
A7W45	7	6	45	40,0
A7W55	7	6	55	50,2
A7W60	7	6	60	55,4
A2W35	2	1	35	30,5
A2W45	2	1	45	40,6
A2W55	2	1	55	50,7
A2W60	2	1	60	55,9
A-2W35	-2	-3	35	31,1
A-2W45	-2	-3	45	40,9
A-2W55	-2	-3	55	51,2
A-2W60	-2	-3	60	56,3
A-7W35	-7	-8	35	31,3
A-7W45	-7	-8	45	41,4
A-7W55	-7	-8	55	51,5
A-7W60	-7	-8	60	56,7
A-11W35	-11	-12	35	31,7
A-11W45	-11	-12	45	41,8
A-11W55	-11	-12	55	51,9
A-11W60	-11	-12	60	56,8
A-15W35	-15	-	35	32,0
A-15W45	-15	-	45	42,1
A-15W55	-15	-	55	52,1
A-15W60	-15	-	60	57,2
A-19W35	-19	-	35	32,1
A-19W45	-19	-	45	42,4
A-19W55	-19	-	55	52,3
A-19W60	-19	-	60	57,4

In Table 5 above, it can be seen that wet bulb temperatures for -15 and -19°C are not listed. At very low air temperatures it was not possible to maintain the required humidity with the given infrastructure. The operation point A7W45 (air temperature 7°C and water outlet temperature 45°C) has been defined as standard according to EN-14522-2 (2007). The water volume flow for this operation point has been set to 3.8 m^3/h. It results in a temperature lift of 5K on the water side and has been left constant for the following operating conditions. The speed of the evaporator fan is set constant which results in a temperature drift on the air side of 4K at A7W35. The experimental runs are divided into stationary and transient runs according to the standard. Tests A7W35 and A2W35 have been considered transient because of ice formation and defrosting cycles. The remaining points have been performed stationary.

With the obtained data, the mean condenser heat capacity ($\bar{\dot{Q}}_H$) and the mean coefficient of performance ($\overline{COP}$) could have been calculated with the following equations.

$$\bar{\dot{Q}}_H = \bar{\dot{V}}_{water} \cdot \overline{\rho_w} \cdot c_{p\_w} \cdot (\bar{t}_{water,in} - \bar{t}_{water,out}) \qquad \text{Eq. 2-31}$$

Where $\bar{\dot{V}}_{water}$, $\bar{t}_{water,in}$, $\bar{t}_{water,out}$, describe the calculated mean values for water volume flow, water inlet and outlet temperature over the entire measurement period. Finally the mean COP can be found with equation Eq. 2-32.

$$\overline{COP} = \frac{\bar{\dot{Q}}_H}{\bar{P}_{el}} \qquad \text{Eq. 2-32}$$

With $\bar{P}_{el}$ describing the mean electrical consumption derived from measured data.

2.5 Experimental Results

As explained in the previous section, different operation points have been investigated. The results are presented in the following.

Figure 26 shows the measured heating capacity at different ambient temperatures and different water outlet temperatures. It stands out that the heat capacity for W35 (blue characteristic) has a bend at 2°C which can be explained with necessary defrosting cycles. Moreover, W45 (red characteristic) shows the highest capacity at 7°C.

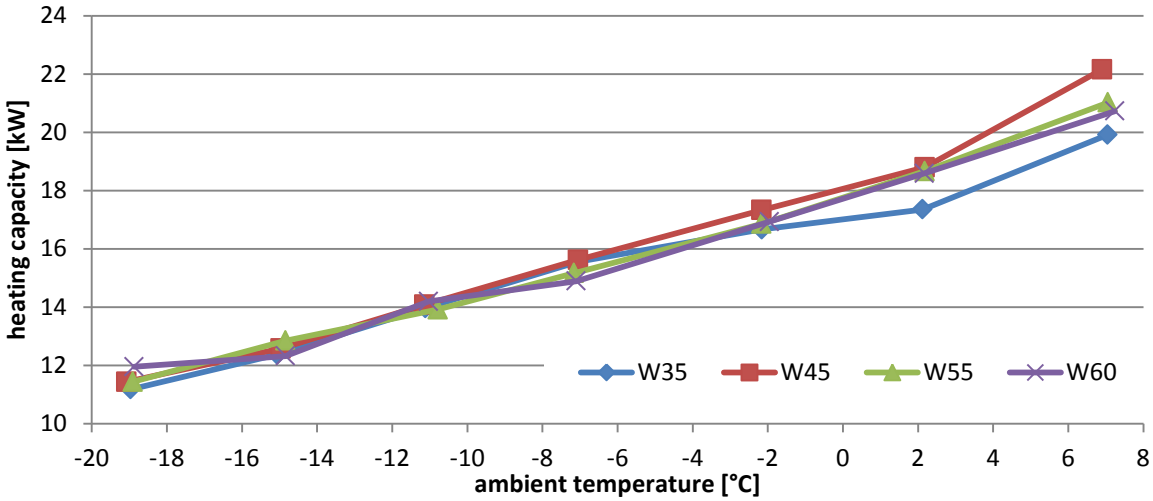

Figure 26: Measured heating heat capacities at different water outlet temperatures (35, 45, 55 and 60°C) depending on the ambient temperature according to Zoier (2014)

However, it is interesting to see that the characteristics are very close with a similar gradient. It shows that the impact of active injection and a rising condensation pressure due to higher water temperatures on the heating capacity is very pronounced. The general decrease in capacity for all water temperatures can be explained with a decrease of refrigerant mass flow due to low ambient temperatures. A comparison of the measured electric power consumption for each operation is depicted in Figure 27. Almost constant values over the ambient temperature range for each water outlet temperature can be observed. This is a consequence of the decreasing refrigerant density which compensates the increasing pressure ratios and enthalpy differences to the compressor.

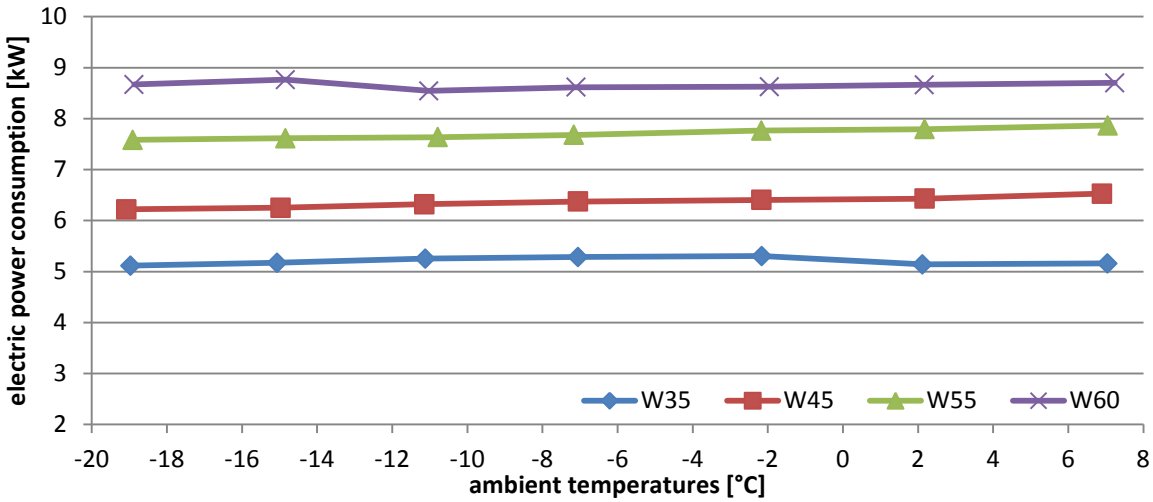

Figure 27: Electric power consumption of the compressor at different water outlet temperature according to Zoier (2014)

With the given condenser capacity and the electrical consumption of the compressor the mean COP for each operation point can be calculated and is shown in Figure 28. The incremental difference of the COP characteristics results from the electrical consumption depending on the water temperature (see Figure 27). The best performance can be of course achieved with low water outlet temperatures (blue characteristic).

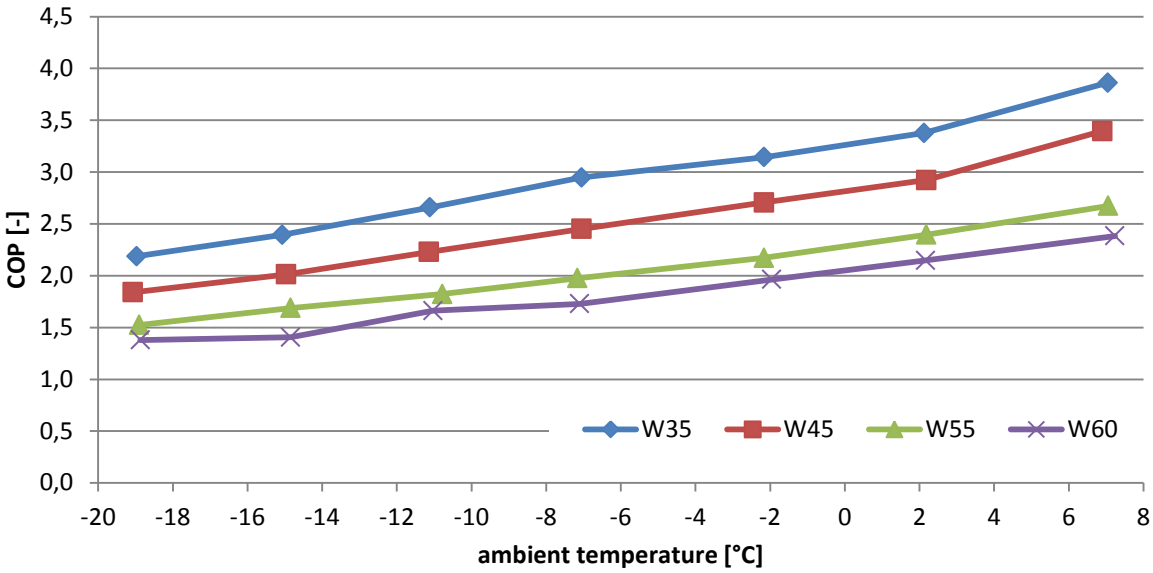

Figure 28: Resulting COP at the investigated operation points according to Zoier (2014)

The effect of the refrigerant injection becomes clear when discharge outlet temperatures are considered as illustrated in Figure 29. The injection allows an extension of application for low ambient temperatures, especially at high water temperatures and thus pressure ratios (purple and green characteristic in Figure 29). The discharge temperatures of W35 (blue) and W45 (red) was below the defined threshold (125°C) at all times hence the refrigerant injection was not active. However, the discharge temperature at -19°C and W45 was 126°C without injection activation which might be caused by a measurement error.

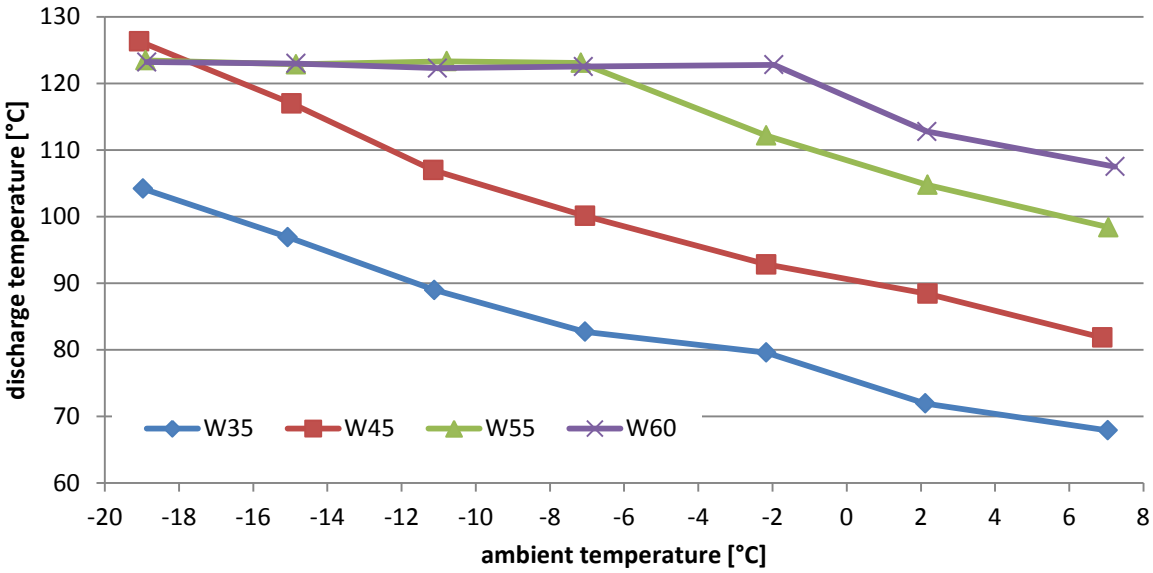

Figure 29: Discharge temperature in dependence of water outlet and ambient temperature according to Zoier (2014)

2.6 Comparison with Simulation Results

In order to achieve comparable results, data of the experimental set up have been used as boundary conditions and input parameters for the detailed simulation model. The utilized parameters are given in Table 6 and Table 7.

Table 6: Set up data used for the simulation model, Zoier (2014)

Description	variable	value
evaporator surface (air side)	A_{evap}	75 m²
condenser surface	A_{cond}	4,73 m²
Injection threshold temperature	T_{VI}	125°C
heat transmission coefficient condenser	U_{cond}	1900 W/(m² K)
heat transmission coefficient evaporator	U_{evap}	49,38 W/(m² K)

Table 7: Parameters derived from experiment according to Zoier (2014)

Description	variable	value
superheating evaporator outlet	T_{sup}	2 K
subcooling condenser outlet	T_{sub}	1,5 K
air volume flow rate	V_{dot_a}	3,45 m³/s

Here the operation points for W45 have been chosen for the comparison of COP, heating capacity and electric power consumption. Figure 30 shows the comparison between measured and simulated values of the COP (left) and the heating capacity (right) for W45 and different ambient temperatures. The deviation between measured and calculated data for the COP ranges between +17% and +24% and +9% to 18% for the heat capacity. As expected, the simulated results lie above the experimental data which can be explained by neglecting pressure drops and heat losses within the heat pump.

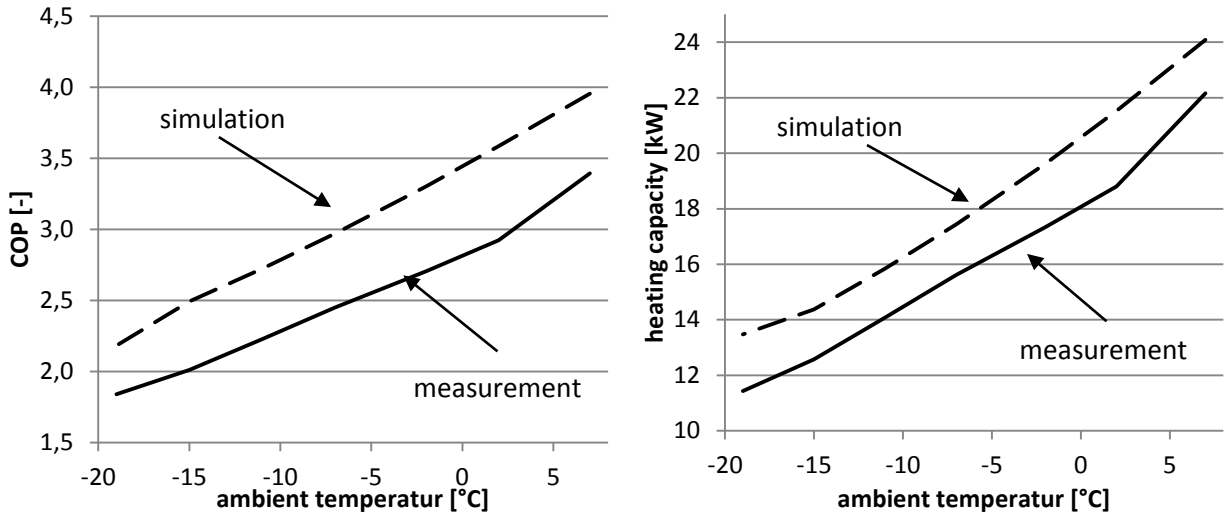

Figure 30: Comparison of COP (left) and heating capacity (right) between measured and simulated data for W45, Zoier (2014)

Another source of deviation comes from the prediction of the refrigerant mass flow and the compressor power consumption with the given correlations which have been derived from manufacturer data (see Figure 32). For example, the applied correlation for the mass flow in the low pressure stage shows a deviation in a range of +15% to +20% compared to the experimental results. This is found as the main reason for the differences since condensation and evaporation pressure show a rather good agreement as depicted in Figure 31.

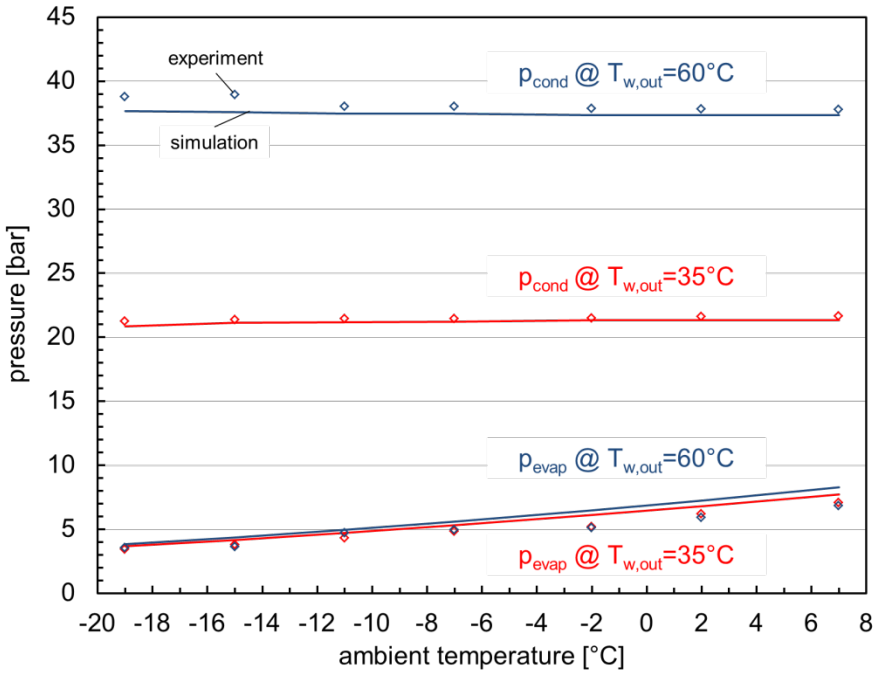

Figure 31: Comparison of measured and simulated condensation and evaporation pressure

As expected, a lower compressor power consumption has been calculated due to simplifications and assumptions taken (e.g. no pressure losses, ideal mixing chamber for injection). Therefore, higher COP values are reached in the simulation due to a lower electric power consumption and a higher heating capacity. The result at -19°C can be explained with an injection activation because of higher discharge temperatures in the simulation model. The disagreement between simulation and experiment is again, rather high.

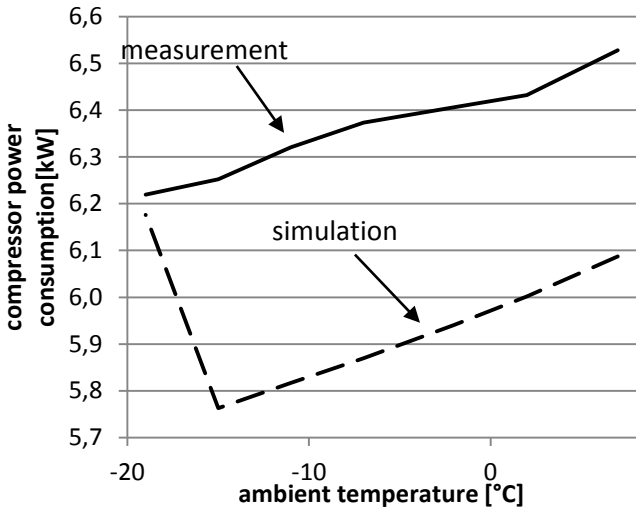

Figure 32: Compressor power consumption for W45 at different ambient temperatures, Zoier (2014)

Finally, the simulated and measured injection mass flow is compared in Figure 33 for W60 and different ambient temperatures. The red bars show the experimental data and the blue bars show the simulation results. It can be seen that the calculated values are higher than experimental data for all operating conditions.

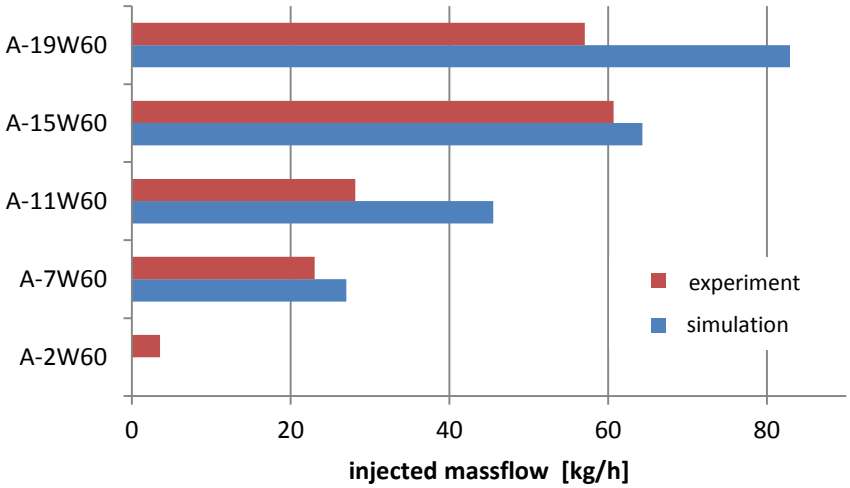

Figure 33: Injected massflow for W60 and different ambient temperatures according to Zoier (2014)

It will be necessary to improve the compressor model for a better agreement with experiment. In particular, the injection process has to be to reconsidered. Furthermore, the assumption of identical pressure ratios in each stage is not accurate enough. Figure 34 shows the comparison between the measured cycle (left) and the simulated cycle (right) for the operation point A-19W60 in a T/h diagram.

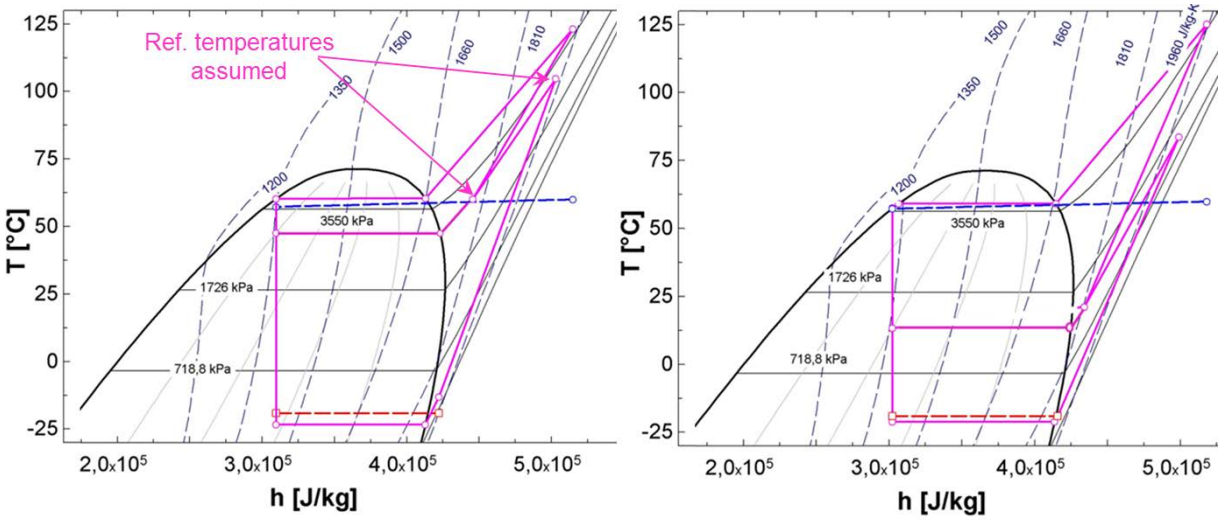

Figure 34: T/h diagrams of the measured (left) and simulated cycle (right) for A-19W60

It should be noted, that for the depiction of the measured cycle the temperatures after the first compressor stage and after the mixing process are assumed since no data has been available. However, the temperature of the injected mass flow has been measured and indicates the intermediate pressure level. Therefore the simulated intermediate pressure shows high deviations from the measured values, which contributes to the discrepancy of simulation and experiment.

3 PERFORMANCE OF AN AIR/WATER HEATPUMP USING A VARIABLE SPEED COMPRESSOR AND ECONOMIZER

Although not especially focused on cold climate applications, a theoretical analysis of an air-water heat pump using a variable speed scroll compressor and an economizer with an internal heat exchanger has been performed by Hengel et al. (2013). System simulations have been carried out in order to investigate the effect on the seasonal performance factor (SPF) caused by a variable speed compressor and the aforementioned economizer cycle (Model06, see section 2). Furthermore, steady state simulations down to -10°C air temperature have been performed, which are briefly summarized in this chapter.

3.1 Simulation Method and Model

An economizer with IHX cycle as depicted in Figure 11 of section 2.1 has been investigated. The calculations have been carried out with the transient system simulation program TRNSYS. As the heat pump model, the non-standard Type 887 (Heinz and Haller, 2012) has been used. The considered model is based on a semi physical approach. The refrigerant properties are estimated with two separate polynomial functions for the two- phase and the superheated region. The compressor model is either based on performance maps provided by manufacturer data or can be used with an overall isentropic efficiency and a volumetric efficiency (compare to section 2.1) as input parameters. These input parameters can be provided as polynomial functions in dependence on compressor speed and condensation temperature. For the economizer heat exchanger, the effectiveness- NTU approach has been chosen. Pressure losses of piping and heat losses of the heat exchangers are not taken into account.

The operation conditions, in terms of heating supply temperature have been modelled with a heating curve depending on ambient temperature and two different building types with an annual heating demand of 45 kWh/(m^2a) and 100 kWh/(m^2a) (SFH45 and SFH100 based on Task 32 (Heimrath and Haller, 2007)). A design ambient temperature of -10°C has been chosen.

3.2 Results

In addition to transient simulations and simulations with variable compressor speed, steady state simulations of an economizer cycle with IHX have been carried out. A conventional cycle has been calculated for comparison. Figure 35 shows the results for the COP of the SFH45 building with a design ambient temperature of -10°C. The blue diamonds show the conventional cycle (COP_conv) and the purple crosses show the economizer cycle (COP_ECO). The green triangles show the decreasing supply temperature (right y-axis) with increasing ambient temperature. A slight increase in COP for the economizer cycle can be observed since the heating capacity increases with a different rate for higher ambient temperatures than the compressor consumption.

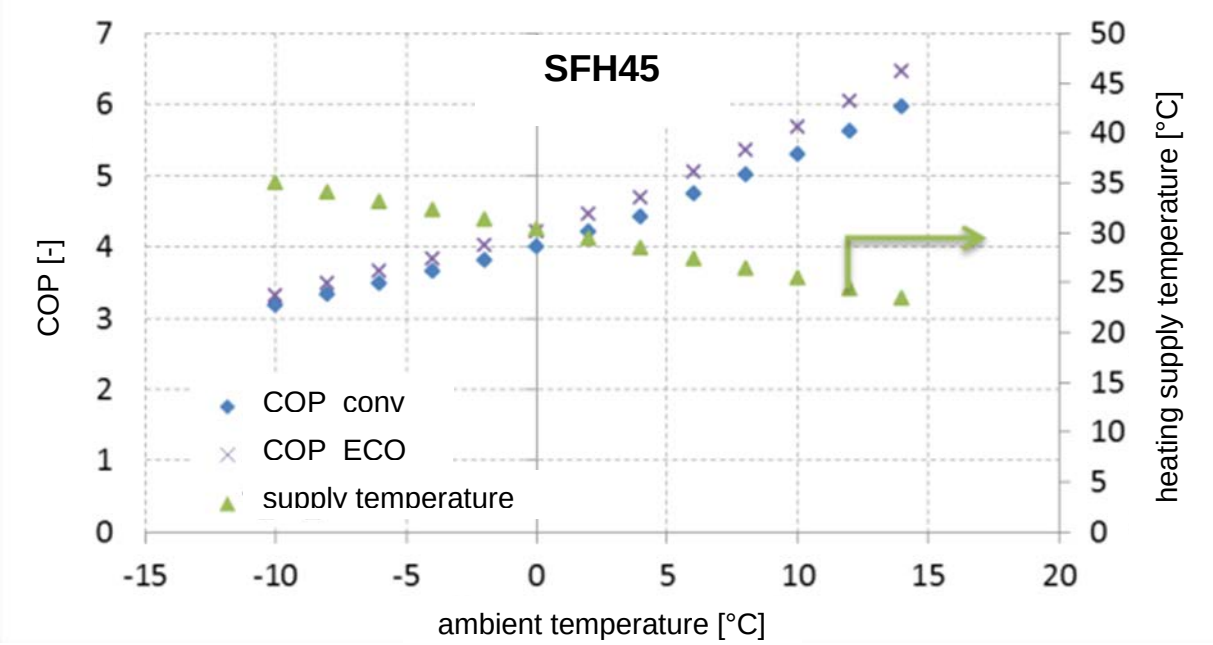

Figure 35: COP and heating supply temperature at different ambient temperatures for SFH45 (modified, Hengel et al., 2013)

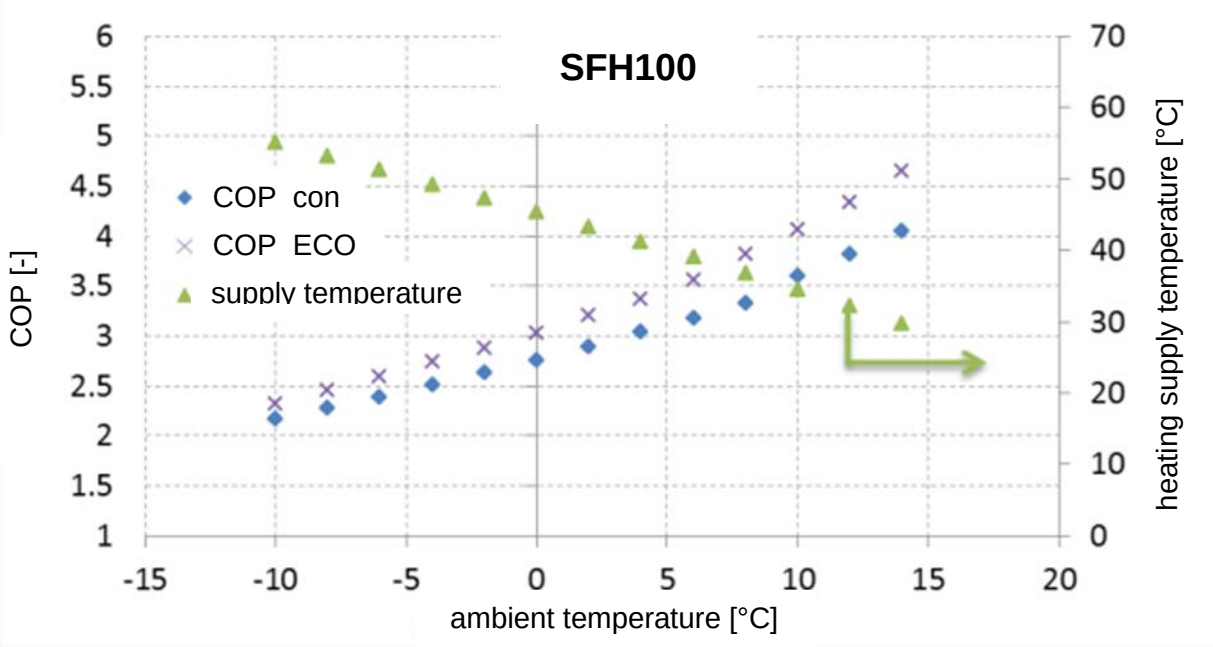

Figure 36: COP and heating supply temperature at different ambient temperatures for SFH100 (modified, Hengel et al., 2013)

Figure 36 above, shows the COP results for SFH100. A higher COP advantage for the ECO-system can be observed for higher supply temperatures, due to the increase of the pressure ratio. With an increasing pressure ratio, the effect of the economizer cycle increases compared to the results of SFH45. These results confirm the already observed tendencies in section 2.2, although in a smaller magnitude.

4 FROSTING PERFORMANCE OF HEAT EXCHANGERS

Typically the presence of frost is undesired in the heat pump's operation, since it implies a deterioration of the equipment performance or even critical safety problems. As this problem is particularly interesting for the heat pump operation at very low ambient temperatures, the understanding of the factors affecting the frost nucleation is very important. This chapter presents the results of the analysis of the frosting performance of a heat exchanger at three levels: the measurements of the frosting performance of different fin geometries (4.1), the numerical simulation of the frosting of selected fin geometries (4.2), and the frosting measurements of a total heat exchanger at low ambient temperatures (4.3).

4.1 Frosting measurements of different fin geometries

Both experimental and numerical methods have been used to characterize the frosting behavior of cooled fin samples and small heat exchanger packages. Experimental methods are based on a small scale wind tunnel placed in a climate chamber. The wind tunnel is equipped with both global and local measurement devices, whereas Computational Fluid Dynamics (CFD) simulations are used for analysis of the ice onset and growth under frosting conditions on fin samples and HEX packages.

4.1.1 Experimental methods

A small scale wind tunnel was built to be set-up in the AIT climate chambers, supporting typical cross sections (width x height) from 250x30 mm2 to 344x244 mm2. The wind tunnel is built as a modular setup in an open-loop configuration. Different devices can be examined in the test section allowing diagnostics of temperature, humidity, pressure and volume flow rate on the air-side and the measurement of temperature and volume flow rate on the coolant side. Mass growth of the fins and heat exchanger packages due to condensation and icing can be determined in real time: the devices are mounted on a scale which records the mass growth during the icing process.

The wind tunnel and especially the test section is built out of transparent materials allowing for the application of optical measurement methods like particle image velocimetry (PIV) and image capturing techniques. Figure 37 gives a schematic overview of the wind tunnel and the locations of global flow parameters. Figure 38 shows the experimental setup placed in one of the climate chambers at AIT.

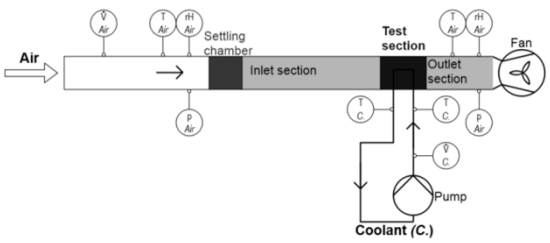

Figure 37: AIT small scale wind tunnel. The modular set-up allows for easy exchange of different heat exchanger devices through an adaptable test section

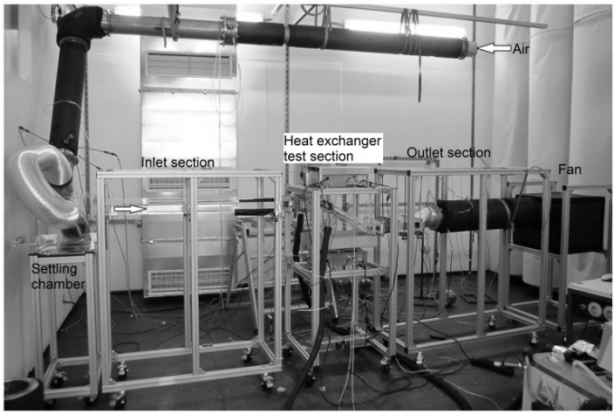

Figure 38: Setup showing from left to right: settling chamber, inlet section, heat exchanger test section with scales, outlet section and the fan

Particle Image Velocimetry measurements have been performed to assess velocity maps in the middle of the wind tunnel – these measurements have been done without a sample in the test section and show a uniform flow distribution at the end of the inlet section – proving that anisotropic components introduced in the settling chamber have negligible influence on the test section. Constant Temperature Anemometry (CTA) measurements indicate only slight disturbances, if samples are placed in the test section (see Figure 39).

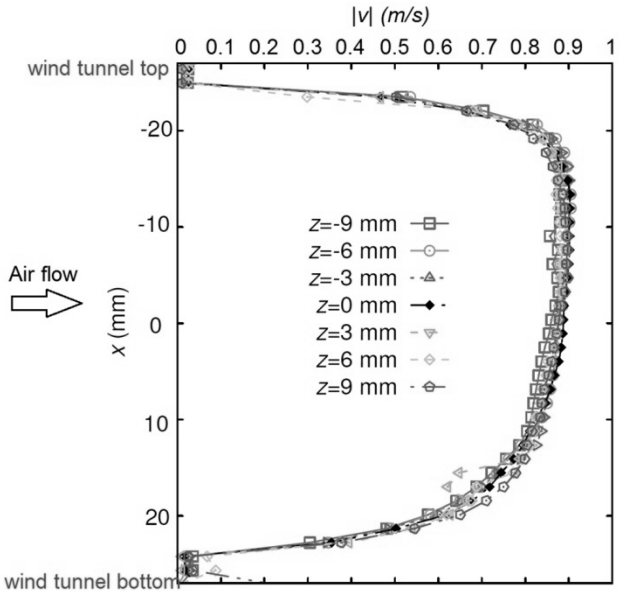

Figure 39: Velocity profile for different distances along the width of the inlet section upstream of the test section

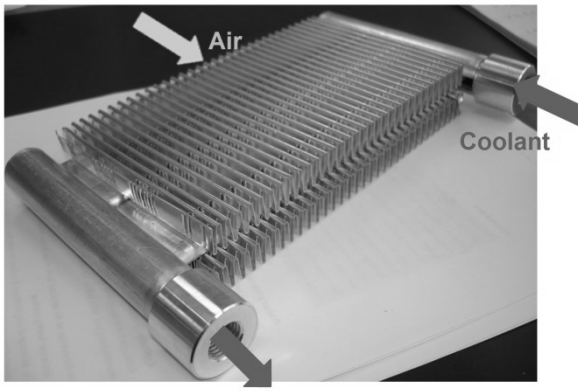

Figure 40: Typical fin sample with wavy fins mounted on a multi-port extrusion (MPE) tube

Fin / Name of the sample	Height	Pitch
Plain fin #1	10,4 mm	5,0 mm
Plain fin #2	10,4 mm	10,0 mm
Wavy fin #1	10,4 mm	5,0 mm
Wavy fin #2	10,4 mm	8,0 mm
Lanced fin #1	10,0 mm	4,8 mm
Louvered fin #1	10,4 mm	5,3 mm
Plain/louvered fin #1	10,4 mm	--

Figure 41: Summary of fin samples placed in the test section of the small scale wind tunnel facility. All fins characterized by structure, height and pitch have been mounted on MPE tubes

4.1.2 Experiments with fin samples

Different fin samples (plain, wavy, lanced and louvered) with different heights and pitches have been investigated. These samples have been mounted in multi-port extrusion (MPE) tubes and cooled by coolant solution. Figure 40 shows a typical fin sample and Figure 41 gives an overview of the fin samples under investigation.

The experiments were performed by changing the set points of the coolant temperature. During icing, the inlet air has been fixed at a temperature of -0.8 ± 0.4°C exhibiting a relative humidity of 71 ± 2%. The maximum volume flow rate is 62 m3/h which corresponds to a speed of 2.3 m/s. The coolant volume flow rate has been kept at 0.65 ± 0.01 l/min. Figure 42 shows a typical icing and defrosting cycle.

During icing, the air volume flow rate and the heat transfer decline, whereas the pressure difference over the fin samples increases. The time span, when the air volume flow rate has decreased from 100% to 75% of its start value has been defined as “icing time”. A mean heat transfer is calculated using:

$$\dot{Q}_{mean} = \frac{1}{t_{ICE}} \int_0^{t_{ICE}} \dot{Q}_{hex} \cdot dt$$
$$\dot{Q}_{hex} = \dot{V}_{coolant} \cdot \rho_{coolant} \cdot c_{p,coolant} \left(T_{out,coolant} - T_{in,coolant}\right) \quad (4.1.1)$$

Figure 43 shows the heat transfer decrease during icing for a typical measurement using plain fin #1 (see Figure 41). The inlet air temperature was set to -0.8°C with a relative humidity of 70%.

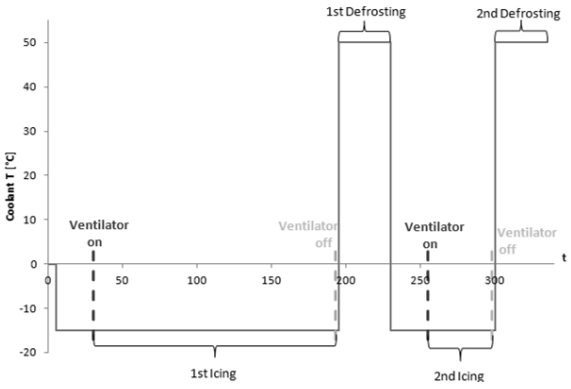

Figure 42: Typical icing and defrosting cycle showing the set point changes of the coolant liquid temperature versus time. Two defrosting stages are shown.

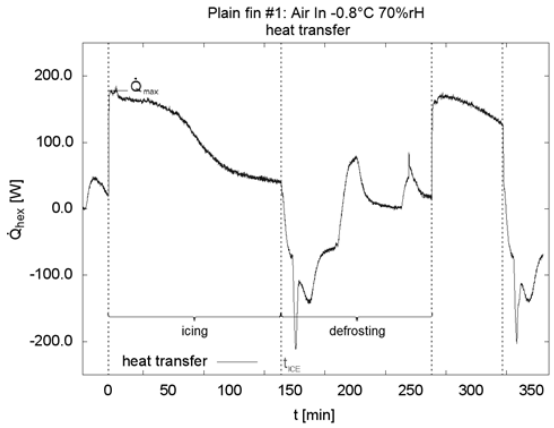

Figure 43: Heat transfer decrease during icing

During the experiments air pressure drops due to blocking of flow through the fins due to ice aggregation on the fin and MPE tube structures. Figure 44 gives an example of absolute pressure and pressure drop during a typical icing experiment. Icing times and mean heat transfer are summarized in Figure 45. Highest and lowest values are shown in gray. Icing time measurements are given with an error of around 20%, the inaccuracy of the mean heat transfer calculation can be estimated to be around 8%.

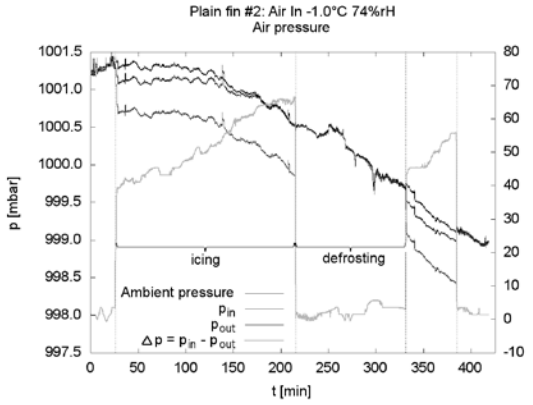

Figure 44: Absolute pressure (left scale, dark gray) and pressure difference (right scale, light gray) for a typical icing and defrosting experiment with plain fin #2 (see fig. 4.1.5).

Fin / Name of the sample		Mean values t_{ICE}	Mean values $\dot{Q}_{mean}$
Plain fin #1		3059 s	156 W
Plain fin #2	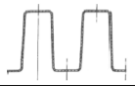	4688 s	104 W
Wavy fin #1	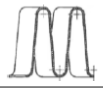	2380 s	166 W
Wavy fin #2	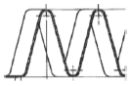	3767 s	135 W
Lanced fin #1		1300 s	163 W
Louvered fin #1		1766 s	167 W
Plain/louvered fin #1	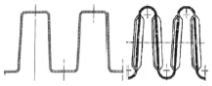	883 s	117 W

Figure 45: Icing times and heat transfer for various fin samples. Gray fields mark the highest and lowest values respectively.

Fins showing long icing times exhibit lower mean heat transfer compared to the other fins. Fins with equal geometry showed longer icing times if their pitch was larger – in this case the heat transfer has been also lower. Short icing times compared with good mean heat transfer can be seen in case of the louvered fin #1 and the lanced fin #1; a good balance between icing times and heat transfer has been found for wavy fins. These results led to the decision to focus on these fin structures for the small heat exchanger packages.

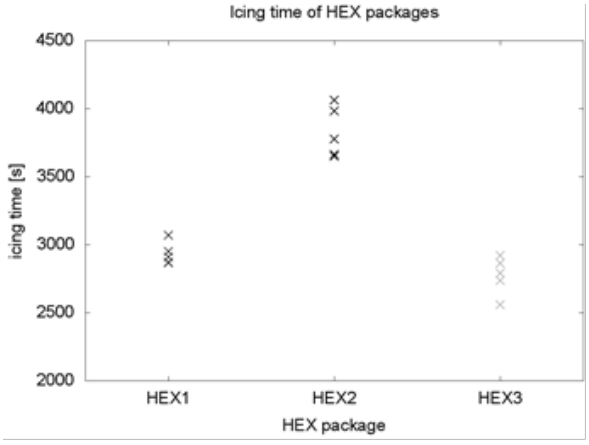

Figure 46: Typical icing times for three wavy fin heat exchanger packages with different heights, pitches and wave angles.

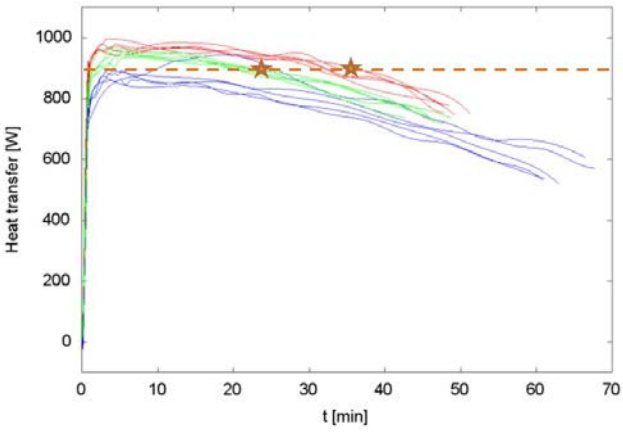

Figure 47: Typical heat transfer for the three heat exchanger packages during several measurement runs.

4.1.3 Experiments with small heat exchanger packages

Three different heat exchanger packages based on wavy fins pitch 5.0mm, height 10.4mm (HEX1), pitch 5.0mm, height 11.3mm (HEX2) and fin pitch 4.5mm, height 10.4mm (HEX3) have been built and measured in the wind tunnel facility. Inlet air temperature was set to 1.9 ± 0.3°C and conditioned with a relative humidity of 73 ± 2%. A volume flow rate of a maximum of 335 m3/h for the air flow and 2.11 ± 0.03 l/min for the coolant was used for the experiments.

Table 8: Icing time, maximum pressure loss and mean heat transfer for the three wavy fin heat exchanger packages

HEX	Icing time	Maximal p loss	Mean heat transfer
HEX1	2933 s ± 84 s	285 Pa ± 3 Pa	906 W ± 11 W
HEX2	3825 s ± 188 s	278 Pa ± 11 Pa	757 W ± 22 W
HEX3	2773 s ± 139 s	275 Pa ± 3 Pa	862 W ± 9 W

Icing times and heat transfer defined as given in section B are shown in Figure 46 and Figure 47 respectively, their mean values given in Table 8. HEX1 and HEX3 show nearly same icing time, HEX1 has a slightly higher mean heat transfer. HEX2 has a considerably longer icing time and mean heat transfer is lower by ~100W. Since HEX2 has the greatest pitch and the smallest wave angle of the 3 geometries this is in line with earlier experiments.

4.2 Numerical Simulation of Fin Frosting

For a detailed 3D frost simulation approach, the model of Hermes *et al.* (2009) for the frost growth and densification has been selected. Based on the fundamental principles of energy and mass conservation, this model represents a good balance between accuracy, simplicity and efficiency when dealing with the numerical analysis of frosting characteristics.

4.2.1 Frosting model

In order to derive the set of equations constituting the model of Hermes *et al.* (2009), the assumptions typical for the given application are invoked: the processes of mass and heat diffusion within the frost layer are treated as quasi-steady and one-dimensional, the frost thickness was assumed uniform along the surface, and the Lewis analogy is applicable. In the first step of this model, the overall mass flux is divided into the frost growth m_g flux and frost densification m_d flux:

$$m = m_g + m_d = \rho_f \frac{\mathrm{d}x_s}{\mathrm{d}t} + x_s \frac{\mathrm{d}\rho_f}{\mathrm{d}t} = h_m(\omega_\infty - \omega_s) \qquad (4.2.1)$$

where $\rho_f = a \cdot \exp[b \cdot (T_s - 273.15K)]$ is the frost density expressed through the empirical function ($a=650kg/m^3$, $b=0.277K^{-1}$) depending on the local frost surface temperature T_s (*Hayashi et al.,* 1977), x_s is the local frost thickness, h_m is the convection mass transfer coefficient, while ω_∞ and ω_s represent the humidity ratio (mass of vapour per mass of dry air) in the free-stream and at the frost surface respectively.

Analytical integration of the 1D equation of the diffusive mass transport through the frost layer, using abovementioned assumptions, yields the surface humidity ratio (assuming constant diffusivity properties and prescribed wall boundary conditions): $\cosh^{-1}(\omega_s/\omega_w) = Ha$, where the Hatta number *Ha* represents the ratio between the characteristic times of diffusion

and de-sublimation. The densification mass flux is derived from the empirical function assumed for the frost density:

$$m_d = x_s \dot{\rho}_f = b m_g x_s \left.\frac{\mathrm{d}T}{\mathrm{d}x}\right|_{x=x_s} \quad ; \quad \left.\frac{\mathrm{d}T}{\mathrm{d}x}\right|_{x=x_s} = \frac{q + m_g i_{sv}}{k_f} \tag{4.2.2}$$

whereby the temperature gradient at the frost surface is obtained from the local energy balance, including the latent heat of de-sublimation i_{sv}, and the local convective heat transfer $q = h\,(T_\infty - T_s)$.

The heat transfer coefficient h is obtained from the Nusselt analogy, whereas the frost properties (conductivity k_f, and the diffusivity parameter $D\varepsilon/\tau$) are empirically defined. By combining the abovementioned correlations, the frost growth mass flux is expressed in the form of the following 2nd order algebraic equation, supplemented by the analytical expression for the frost surface temperature T_s (also derived from the analytical integration of the 1D equation of the diffusive heat transport through the frost layer) in relation to the wall temperature T_w:

$$\begin{aligned} \frac{b x_s i_{sv}}{k_f} m_g^2 + \left(1 + \frac{b x_s q}{k_f}\right) m_g - m &= 0 \\ T_s = T_w + \frac{q + i_{sv} m}{k_f} x_s + \frac{i_{sv} \rho_a \omega_w}{k_f} \frac{D\varepsilon}{\tau} &(1 - \cosh \mathrm{Ha}) \end{aligned} \tag{4.2.3}$$

Finally, with the calculated m_g, the value of the instantaneous frost thickness is obtained using 1st order time integration: $x_s(t+\Delta t) = x_s(t) + \Delta t \cdot [m_g(t)/\rho_f(t)]$. Detailed derivation of the model equations is given in Hermes *et al.* (2009).

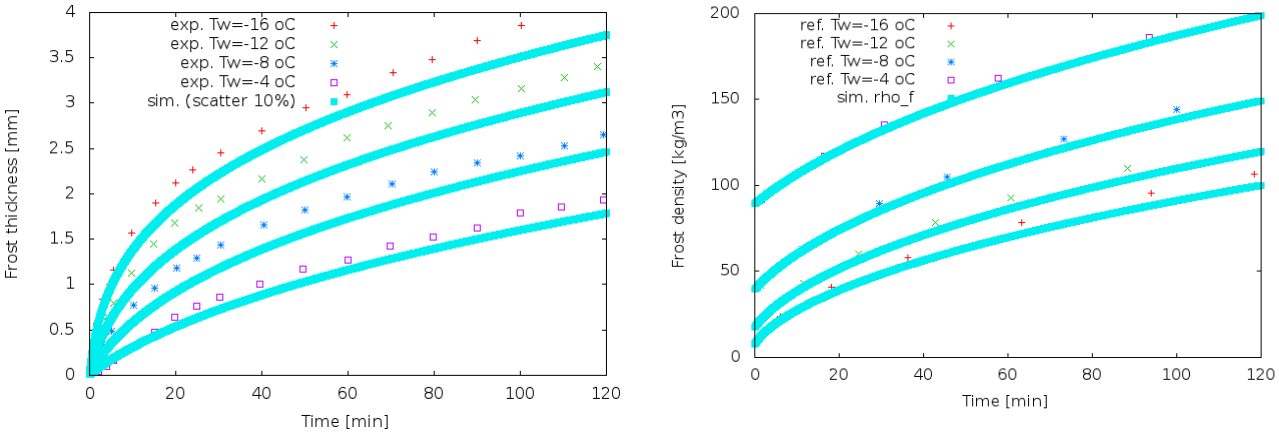

Figure 48: Comparison between the experiments and the Hermes et al. (2009) model simulations, showing the frost growth (left) and frost densification (right) for the reference case of the frost creation on a flat horizontal surface.

As a validation of the model, the results shown in Figure 48 give the comparison between the modelled frost creation and the reference experimental data for flat horizontal surface. One can see that for a range of frosting conditions the time development of the frost thickness and its characteristics agree well with the experiments. Although this reference case does not include any geometrical complexities, it can be concluded that the adopted

model is describing well the main physical phenomena of the frosting process, and hence it is able to reproduce its dynamics.

4.2.2 Model implementation

The selected model has been implemented into the general-purpose open source fluid flow solver, *OpenFOAM* (Weller et al., 1998), as it includes adequate representation of geometrical features (realistic geometry) and physical behaviour (flow pattern, temperature distribution, turbulence, etc.) which are relevant for the modelling of the air-side characteristics of heat pumps. Furthermore, the object oriented programming structure of the code offers an excellent platform for developing and implementing novel fluid flow related models.

The implementation is performed such that the creation of the frost is controlled by local flow characteristics, taking into account the spatial and temporal distribution of the relevant flow quantities. Namely, in addition to the frost growth described with Eqs. (4.2.1), (4.2.2) and (4.2.3), it is clear that for this frosting model the transport equations for velocity, temperature and relative humidity (including turbulent characteristics, as appropriate) need to be solved. These transport equations govern the flow of humid air through the domain, and the creation of frost is being represented through the growth of the porous zone which blocks the humid air flow, accompanied by the sink in temperature equation (i_{sv}) and the relative humidity equation (m_g).

The frost onset at a cooled surface is defined through the nucleation theory. However, after that initial frosting, a new solid surface will be created (the frost). As a consequence, the flow characteristics within the newly created frost layer are to be solidified (porous zone). Furthermore, all frost related correlations (heat and mass transfer coefficients, local velocities and temperatures, etc.) need to be calculated from the flow variables within the zone near the frost surface. This behaviour can be seen in Figure 49, which is depicting the reference experimental test case from Figure 48: the frost growth has been simulated for the 2D case of the flow of humid air over a cooled plate (here shown only for the initial phase of the frosting process), whereby the initial boundary layer velocity distribution (bottom) is being distorted due to the growth of the solid frost layer (top).

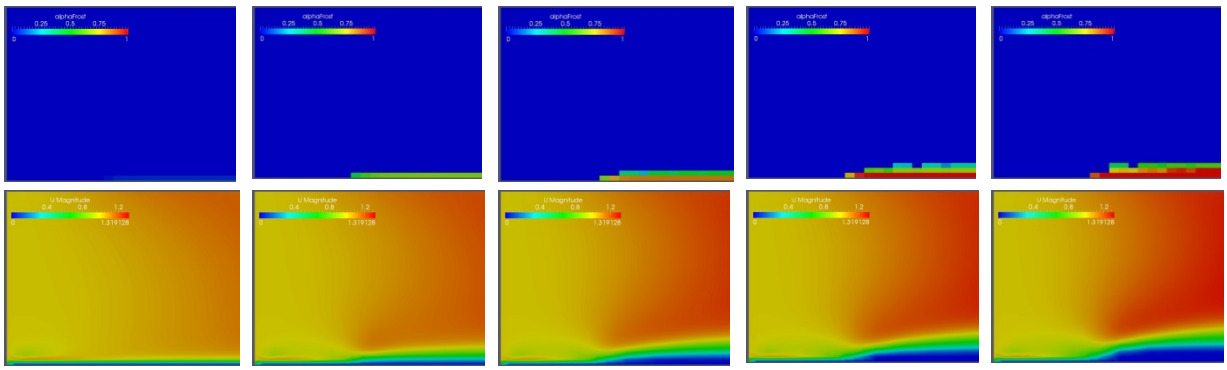

Figure 49: Frost growth: time development (left to right: t=0.016, 1, 2, 3, 4 minutes) of the frost volume fraction [m^3_f/m^3_{tot}] over a flat cooled plate (top), and the corresponding velocity magnitude [m/s] of the flow (bottom)

The most influential model quantity is the surface temperature T_s (as it is used to determine local properties), which is related to the wall temperature T_w. Hence, it is necessary to obtain the information throughout the domain about the temperature of the nearest wall boundary. In the present case, the distribution of the wall temperature throughout the domain (i.e. not

restricted only to the wall-adjacent cells) is obtained by solving the temperature diffusion equation, where the wall temperature is prescribed as the Dirichlet boundary condition at the cooled surfaces, zero Neumann boundary conditions at all other surfaces, and appropriate physical properties (humid air – frost) as the diffusivity coefficient throughout the domain.
Another important correlation which needs a careful consideration is the heat transfer coefficient, especially since it is also used to determine the mass transfer coefficient (by means of the Lewis boundary layer analogy $h_m = h/c_p \cdot Le$). The heat transfer coefficient is defined by the Nusselt analogy $Nu = hL/k = a1 \cdot Re^{b1}$ ($a1=0.034$, $b1=0.8$), based on the bulk Reynolds number $Re = \rho UL/\mu$. (ρ and μ are the fluid density and dynamic viscosity respectively, L is the characteristic length such as the fin height, and U is the bulk velocity). To arrive at the bulk velocity based on the local flow characteristics (velocity and turbulence adjacent to the frost surface), the Dean formula is deployed $c_f = a2 \cdot Re^{b2}$ (using $a2=0.073$, $b2=-0.25$), where for the friction factor $c_f = \tau_w/0.5\rho U^2$ the wall friction τ_w is expressed either by means of the turbulent friction velocity $u_K = (\tau_w/\rho)^{1/2} = c_\mu^{1/4} K^{1/2}$ ($c_\mu=0.09$ is the turbulence model constant, K is the turbulent kinetic energy) or directly as the product of the wall-normal velocity gradient and the dynamic viscosity of the fluid calculated at the surface $\tau_w = \mu \cdot \partial U/\partial x$ (depending whether or not the considered flow is turbulent, i.e. the turbulence model is applied).

4.2.3 Numerical simulations

In order to test the performance of the developed simulation approach, the frosting over the heat exchanger fins has been investigated with the consideration of industrial relevance. Shown in Figure 50 is a typical result of the frost build-up on a selected fin configuration of a heat exchanger. The presented case is showing how the analysis of the heat pump performance with respect to frost creation can be used to identify weak points of the construction, and also to indicate the possibilities for their improvements.

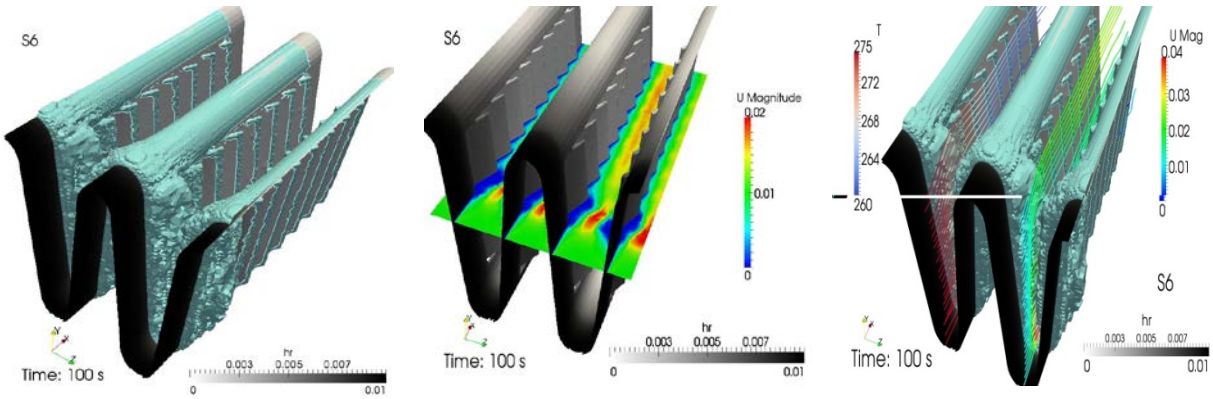

Figure 50: 3D distribution (iso-surface) of the frost accumulation after 100 s of simulation (left), the resulting velocity magnitude [m/s] contour plot between the fins (middle), and the contour plot of the humidity ratio [kg_v/kg_a] at the fins surface, together with the temperature [K] and velocity magnitude [m/s] distribution along the streamlines (right) for the selected fin configuration (S6).

From the obtained results one can see that, as the most intense frosting is taking place at the most exposed fin surfaces, the louvered fin passages are being blocked relatively quickly (although one needs to note that the frost growth is not uniformly distributed along the fin). Furthermore, as the strongest chunk of frost is being created at the entering section of the fins, the velocity is locally increasing whereas the pressure is locally decreasing. This will have an impact on the local frosting conditions through the change in local physical properties and humidity ratio. On the other hand, this entering section of the fins can be viewed as some sort of a “dehumidification filter” because the relative humidity is being

reduced in this frosted zone (m_g), together with the change in temperature due to the de-sublimation (i_{sv}). This is why the flow characteristics, and consequently also the frosting process, will be different in the remaining part of the fins after the entering section.

Another way of making use of the numerical frosting simulations is shown in Figure 51, where the influence of the density of the fin configuration (i.e the spacing between the fins) on the frost accumulation has been investigated by means of the parametric study. To that purpose, the basic wavy configuration (S7) has been modified to the half of the original spacing (S4) and to twice of the original spacing (S3). As can be seen from Figure 51, the distribution of the accumulated frost is increasing with the increase of the fin spacing. This can be explained by the resulting increase of the humid air which is penetrating deeper into the fin interior, thus extending the frosting process over a larger portion of the domain. As a consequence, though, the pressure drop is increasing for the higher density fins, since there is less space between the fins which gets easier blocked by the accumulated frost.

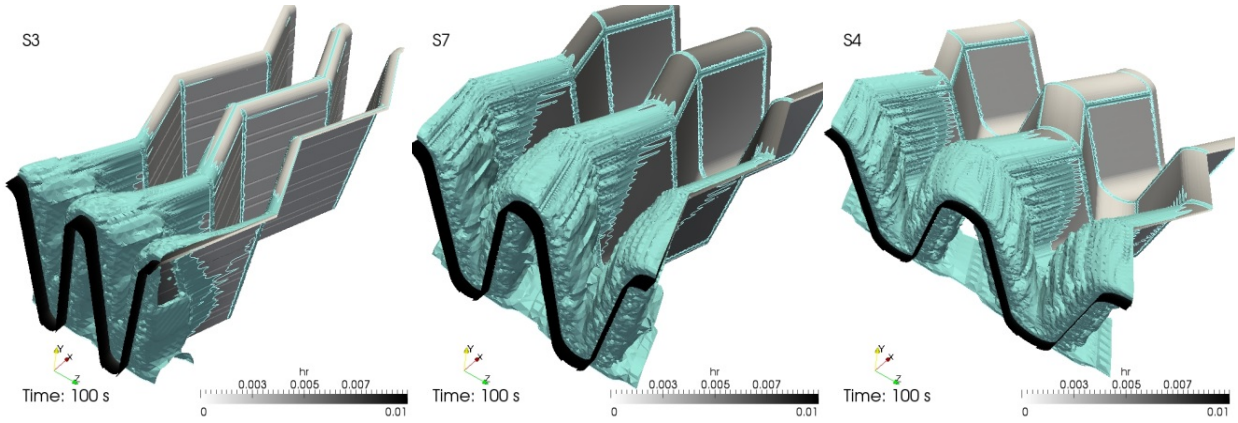

Figure 51: 3D distribution (iso-surface) of the frost accumulation after 100 s of simulation, for the high density (S3, left) moderate density (S7, middle) and low density (S4, right) fins configuration, together with the contour plot of the humidity ratio [kg_v/kg_a] at the fins surface.

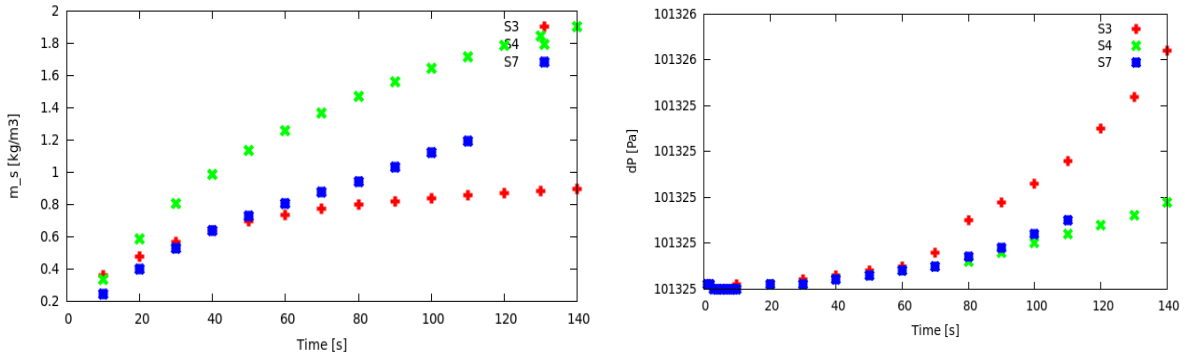

Figure 52: Time evolution of the integral values in the specific frost accumulation process [kg/m^3] for calculated fins geometries (left), and the area-averaged inlet pressure [Pa] indicating the pressure loss along the fins section (right).

For the quantification of the frosting, Figure 52 presents the integral values for the frosting process over different fin geometries (S3, S4, S7). Obviously, the pressure drop will increase (with a given exponent) as long as the frost blocking is increasing (Figure 52, right). On the other hand, looking at the slope of the total mass of created frost (Figure 52, left), one can distinguish between the phase of the fast frost accumulation (the time in which a substantial

part of the frosting surface is not covered with frost), and the phase of the slow frost accumulation (the time in which the frost is growing primarily over an initial layer of already existing frost). Since the presented calculations have been performed only for initial frosting phase (due to limited calculation time), the obtained values indicate a trend rather than actual frosting process.

4.3 Low Temperature Measurement of Heat Exchanger Frosting

For this final measurement campaign, the experimental setup used for analyzing individual fin geometries (Figure 38) is slightly modified in order to accommodate the whole heat exchanger. As shown in Figure 53, the experimental setup is located in the climatic chamber, in which the temperature and relative humidity are being controlled. In the experimental setup two circles are identified: the air side and the coolant side. The air side consists of the incoming pipe (S1), the settling chamber (S2), the straight channel (S3), the measurement box with the heat exchanger (S4), the outgoing pipe (S5) and the variable speed ventilator (S6) which drives the flow through the air circle. In the incoming tube the volumetric flow rate is measured by means of the pressure difference at the pipe orifice (A1), after the settling chamber the air flow is stabilized in the straight channel, entering the measurement box with the heat exchanger, and leaving through the outgoing pipe in which the temperature (A2) and relative humidity (A3) are being measured.

The core of the coolant side is the tempering device (Julabo), which can deliver the flow of thermo-oil at the given flow rate and with the given temperature. This device is connected to the heat exchanger's inlet and outlet with the flexible silicon pipe (in order to enable the weight measurement), whereby the temperature sensors (C1 and C2) have been located at these inlet and outlet points (in order to control the temperature values). The heat exchangers under investigation are located in the measurement box, which is hanging on the high-precision balance (C3).

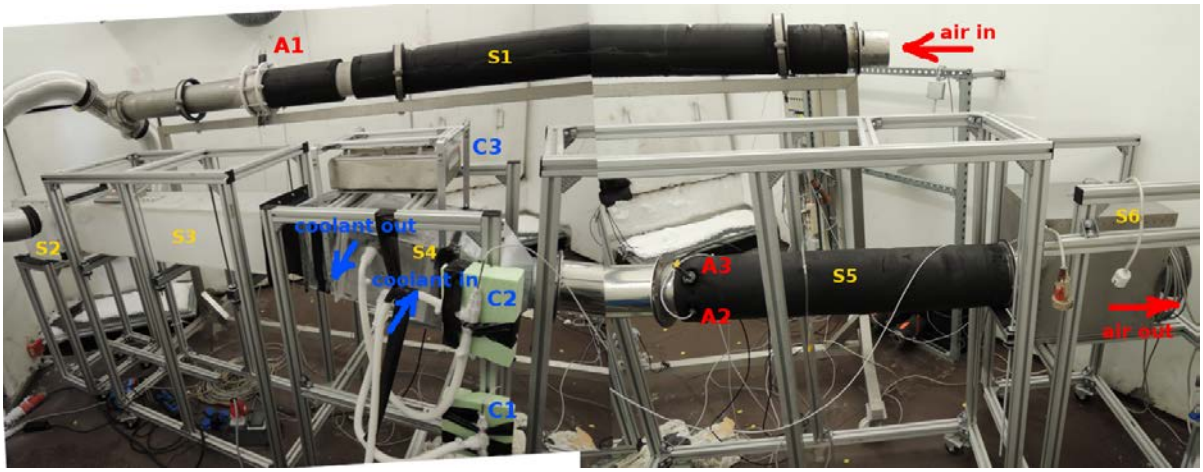

Figure 53: experimental setup for investigating the frosting performance of heat exchangers at low ambient temperatures

Figure 54 explains the measurement sequence: in the initial phase the thermal mass of the heat exchanger is accommodated to the tempering conditions (A to B1), and then the main frost growth takes place (B1 to B2). Afterwards, the rapid change of the heat exchanger thermal state (at air flow rate curve steepest gradient) takes place (B2), and frost creation continues until the heat exchanger is fully blocked and the temperatures do not change any more (C).

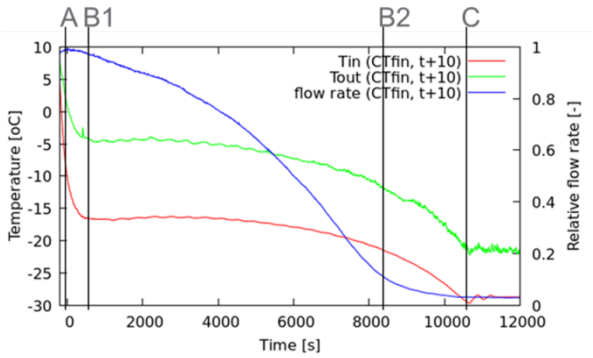

Figure 54: Frosting measurement sequence

Two types of heat exchangers have been investigated, as shown in Figure 55: the conventional tube fin heat exchanger (CTfin), and the multi-port extrusion fin heat exchanger (MPEfin). The aim was to compare two heat exchanger types with respect to the frosting performance, and the outcome indicates how the multi-port extrusion fin heat exchanger performs compared to the conventional tube fin heat exchanger CTfin, left) at low ambient temperatures.

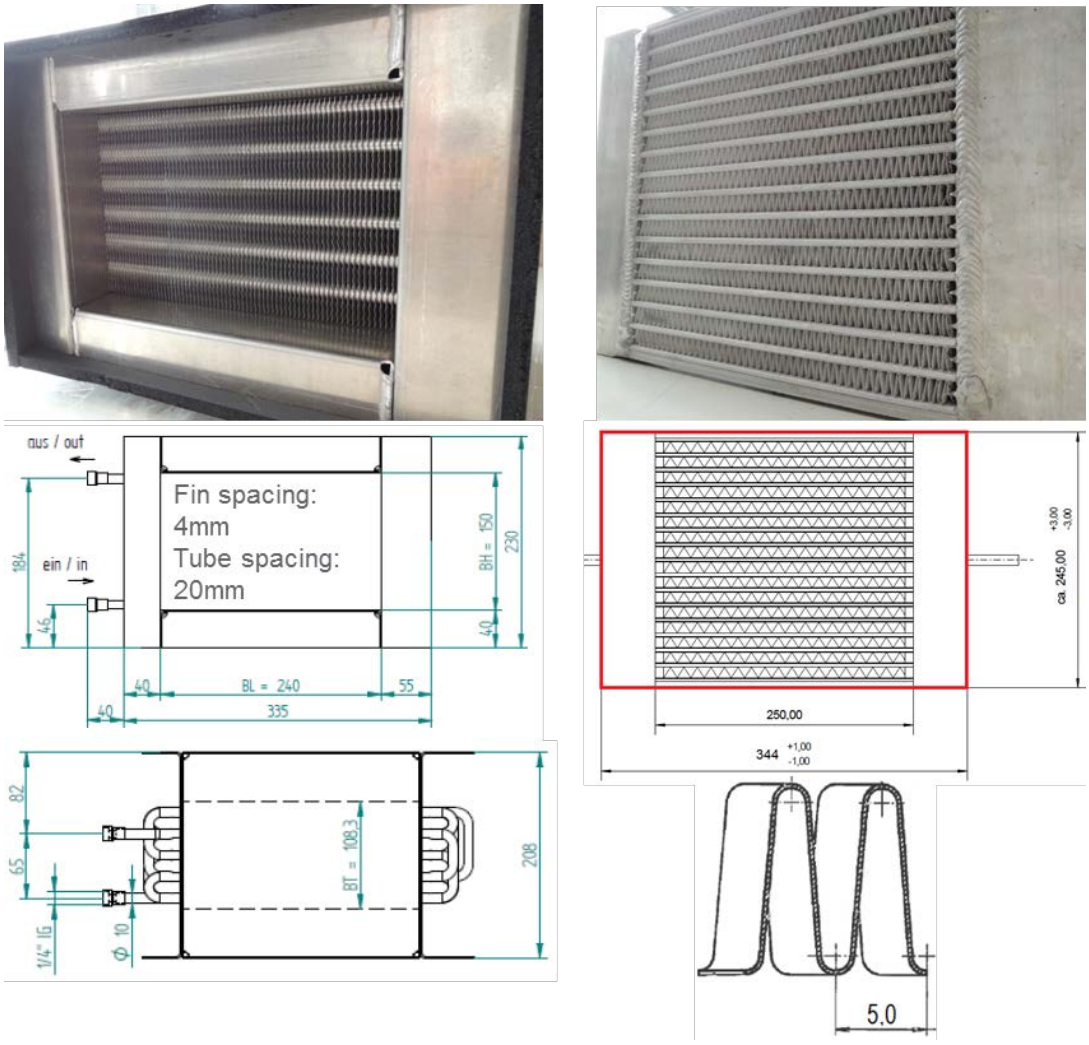

Figure 55: Geometrical characteristics of compared CTfin (left) and MPEfin (right) heat exchangers

The experimental comparison between CTfin and MPEfin frosting behavior is performed for two sets of operating conditions: the standard conditions (t+10: climatic chamber temperature 10 oC and RH 80%, Julabo temperature -30°C), and low temperature conditions (t-25: climatic chamber temperature -25°C and RH 80%, Julabo temperature -60°C). For both cases, the experiment was conducted so that the stable climatic chamber conditions are reached, then the tempering device is set to the desired temperature, and then the measured values are monitored until the air flow is blocked and the temperatures are stable again. The unfiltered results obtained from the temperature and accumulated frost measurements are being presented and discussed in the following paragraph, whereas for the discussion on the energy balances some more time will be required for post-processing.

Starting with the air side temperatures, shown in Figure 56, one can see that the inlet temperature (the temperature inside the climatic chamber) was varying between 7°C and 9°C during the experiment where the chamber set temperature was 10°C. The temperature difference which is reached on the air side for the t+10 experiment was approximately 7°C for both heat exchanger types, whereby the frosting time (the time period until the flow blockage is reached) for the CTfin heat exchanger time was approximately 4 times longer than the MPEfin type. For the t-25 experiment, shown in figure 4.3.5, the inlet temperature reached was -26°C, a temperature difference of 12°C was reached on the air side, and the difference in frosting times between the two heat exchanger types is approximately 1.5 times.

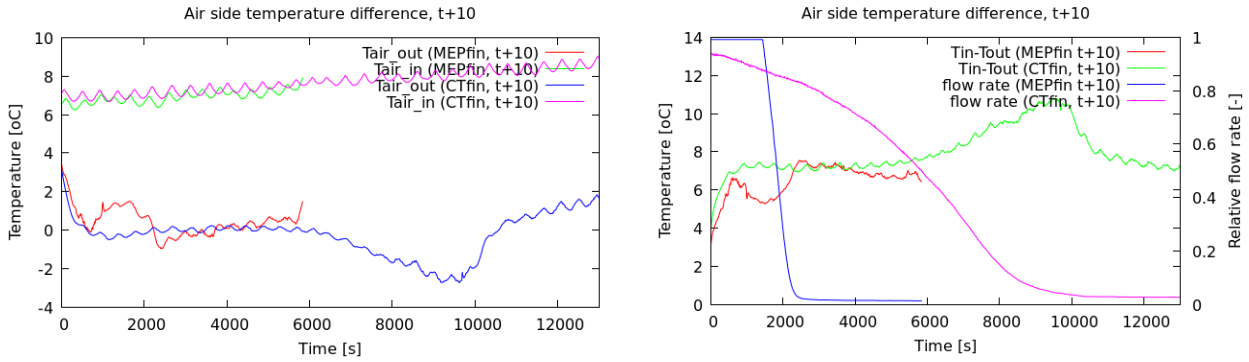

Figure 56: Transient air temperatures and relative volumetric flow signals, t+10 case

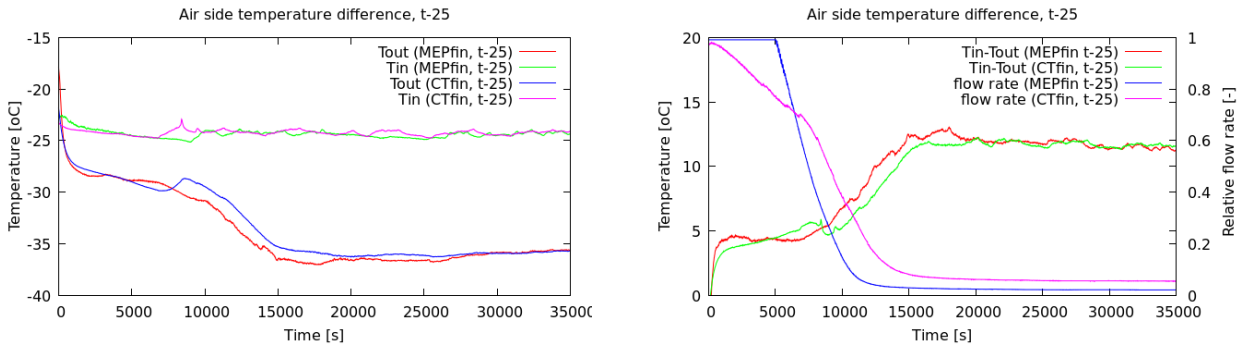

Figure 57: Transient air temperatures and relative volumetric flow signals, case t-25

From the coolant side, in the t+10 case shown in Figure 58, the inlet temperature which was reached was varying between -19°C for the MPEfin type and -21°C for the CTfin type. The difference between the set temperature and the reached temperature can be attributed to the thermal losses in the entire system, (both on the climatic chamber side, and the experimental setup side). The temperature difference between the heat exchanger inlet and

outlet, which was needed for this frosting, was between 11 and 12°C, and again the frosting times of MPEfin type is 4 times shorter than the CTfin type. The difference in the frosting times is the consequence of different overall geometry and dimensions of the two heat exchangers. From the coolant temperatures for the t-25 case, shown in Figure 59, one can see that the inlet temperature reached was between -53 and -51°C for the MPEfin and CTfin type respectively, with the limitation in the reached temperature dictated by the power of the tempering device (Julabo). The temperature difference needed for this frosting was approximately 10°C, with the difference in the frosting times for different heat exchanger types of 1.5 times, as seen previously.

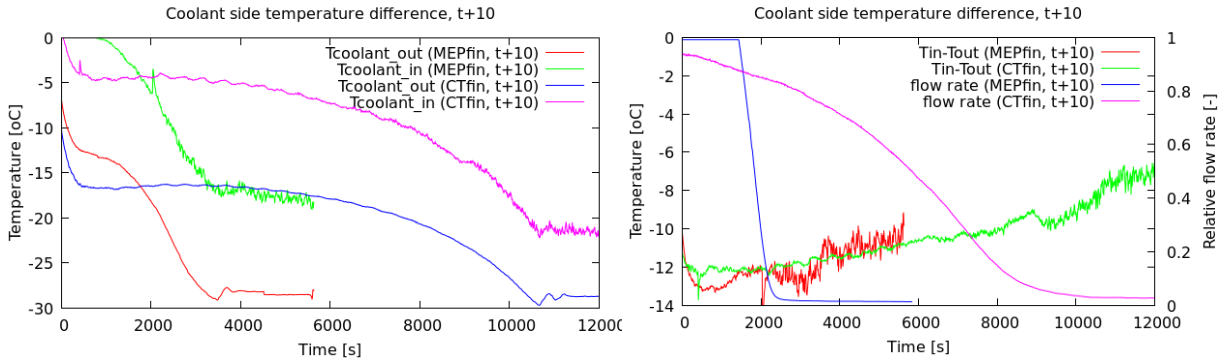

Figure 58: Transient coolant temperatures and relative volumetric flow signals, case t+10

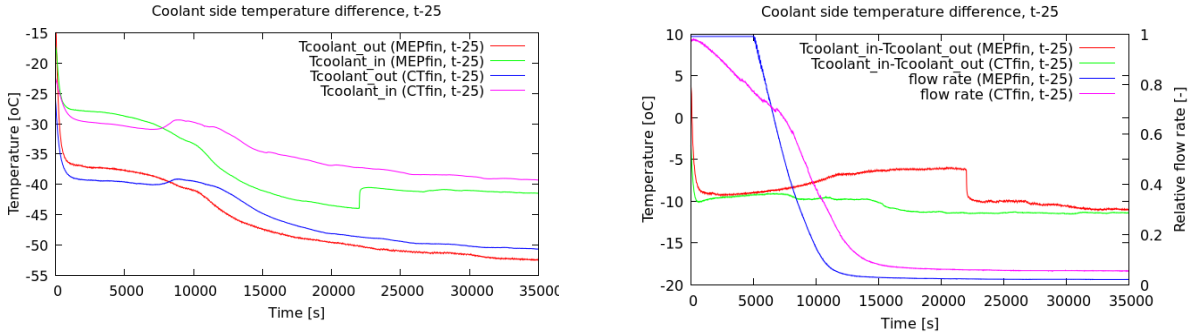

Figure 59: Transient coolant temperatures and relative volumetric flow signals, case t-25

The fin surface structure for the MPEfin is causing the frost mass gradient to be much lower as compared to the CTfin case. Therefore, a longer initial period before the frosting starts is observed for the MPEfin. Although it can be observed both in the t-25 case, as well as in the t+10 one, this behaviour is particularly pronounced at extreme ambient conditions. The frosting times can also be seen in the frost mass time signal, as shown in Figure 60, where the initial increase in the accumulated frost finishes with the plateau of nearly constant frost mass. In the initial phase, the properties of MPE show their efficiency: note the gradient of the frosting curve, and consequently the frost mass accumulated in the observed time interval. However, in the later stage, when the fin surface is mainly covered by the frost layer, the process is dominated by the main geometrical characteristics (fin spacing) and thus the frosting performance of both heat exchanger types is comparable.

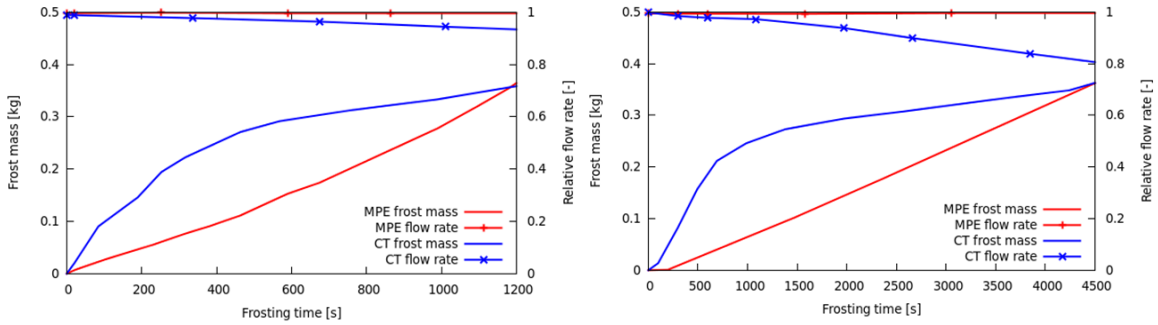

Figure 60: Frost mass growth of MPEfin and CTfin heat exchangers at t+10 (left) and t-25 (right)

5 SUMMARY

Simplified simulation models of promising heat pump layouts have been carried out with EES in order to increase the range of application and efficiency. The investigated refrigerant has been R410A. The heat pump cycle with ejector (09) to utilize the expansion work showed by far the best performance in terms of efficiency. However, because the model is highly theoretical and simplified, this cycle should be investigated in more detail to verify its advantages. The cascade cycle (08) has shown COP improvements up to 5% compared to the conventional cycle (01). Using R410A in both stages, the heating capacity showed an increase of up to 44% compared to the conventional cycle. Further investigation should be carried out in order to find an appropriate refrigerant couple. Further investigation has to be carried out in order to find an appropriate refrigerant couple. Vapor injection with flash tank (07) or with IHX (06) shows a COP increase in the range of 4% and 10%, respectively, at -30°C evaporation temperature. The work of Hengel et al. (2013) also showed slight COP improvements for the economizer with internal heat exchanger, especially at higher heating supply temperatures. Intercoolers (04) show a rather high decrease of COP and heating capacity if the heat removed from the intercooler is not used. The IHX cycle (02) resulted in similar values as the conventional cycle and showed no improvement in any category. The liquid injection caused minor COP losses in a range of 2% but identical heating capacity compared to the conventional cycle. The resulting compressor outlet temperatures could have been decreased within all models expect the IHX cycle. The most promising layouts in this regard are cascade, intercooling, and liquid injection, with a drop in compressor outlet temperatures of 19 K, 21 K and 32 K respectively compared to the conventional cycle. at an evaporation temperature of -30 K.

Based on the simplified calculations, a more detailed model of the liquid injection cycle has been set up. The liquid injection has been chosen because of its less complex layout compared to the cascade and economizer systems, while having the ability to increase the range of application for cold climate in terms of compressor outlet temperature. Furthermore, a liquid injection prototype was available to carry out experimental analysis. The detailed model considers heat transfers on the heat sink and heat source heat exchanger and calculates the resulting evaporation/condensation pressure level iteratively. Furthermore polynomial functions provided by manufacturer data are used to describe mass flow, electric power consumption and isentropic efficiencies based on evaporation and condensation temperature. Moreover a quasi-steady state ice formation model has been considered but not discussed in detail within this report.

A liquid injection prototype with a scroll compressor has beein investigated at the IWT. In order to simulate ambient conditions, a climatic chamber has been used. The heat sink has been provided by a thermal storage with re-cooling system. The measurement procedure

has been carried out according to EN-14511 for an ambient temperature range of -19°C to 7°C and different heating supply temperatures (35°C, 45°C, 55°C, 60°C). The analyzed data confirmed the statements of the simplified model that the injection has a minor influence on COP and heat capacity, but the range of application can be extended to low ambient temperatures for high supply temperatures. Furthermore it is interesting to see that the ambient temperature has almost no influence on the electrical consumption of the compressor.

The comparison with simulation results showed a major disagreement with the experimental data. Specifically, the electrical consumption of the compressor showed a high deviation, which is interesting since manufacturer data has been utilized. For example, results for the measured refrigerant mass flow are 15% to 20% lower than predicted with the compressor maps. Furthermore, the neglected pressure drops in heat exchangers and piping contribute to the disagreement. The simplified modelling of the injection process also has effects on the model accuracy and the assumption of equal pressure ratios and equal isentropic effciencies for each stage.

The frosting characterization of different fin geometries and surface structures (coatings) is possible by using a wind tunnel setup placed inside a climate chamber. With the distributor test-bench, new and existing flow distributing technologies can be characterized. Both experimental and numerical techniques are feasible for the pre-selection of fin types. Several techniques are readily developed to support any evaporator design. Some of the methods (PIV, Shadowgraphy, Video analysis) could also be used for investigations in the climate chambers and test-benches on full scale HEXs in heat pumps. Furthermore, with a careful implementation of the frost growth and densification model (which captures well the main physical phenomena of the frosting process) into the OpenFOAM fluid flow solver suite, 3D unsteady numerical simulations of the frosting performance over heat exchanger fins have enabled a deeper look at the spatial and temporal distribution of the flow characteristics that are relevant for the frosting process.

The experimental investigation of the heat exchanger frosting behavior revealed the interdependence between the icing time of a given fin geometry and the resulting mean heat transfer. Given that the fin geometry has an influence on the icing properties and the overall mean heat transfer, the wavy fins seem to be a good compromise between a good heat transfer and a proper icing time. Blocking takes place at the most exposed fin surfaces at the inlet area, which has been observed both by experiments and numerical simulations. When comparing advanced heat exchanger types with commonly available standard ones, it has been experimentally observed that the fin geometry design of MPEfin heat exchanger has a positive impact on the frost creation in the initial frosting phase. As the frost creation progresses over the entire fin surface, however, the process is further dominated by the main geometrical characteristics (fin spacing): here the advanced heat exchanger type characteristics have lower impact, as compared to a standard CTfin type. The observed effect is more pronounced at the ambient conditions with more absolute humidity.

The future work regarding the characterization of the heat exchangers is the measurement of the frost performance of the heat exchanger within the entire evaporator heat pump unit, including the quantification of the spatial frosting distribution.

6 BIBLIOGRAPHY

Albert M., R. Sahinagic, L. Gasser, B. Wellig, K. Hilfiker, Prediciton of ice and frost deformation in the fin tube evaporators for Air/Water heat pump, 9th International IEA Heat Pump Conference, 2008

EN-14511-2, 2007: Air conditioners, liquid chilling packages and heat pumps with electrically driven compressors for space heating and cooling -Part 2: Test conditions: Prüfbedingungen, European Committee for Standardization, Brussels, Belgium

EN-14511-3, 2007: Air conditioners, liquid chilling packages and heat pumps with electrically driven compressors for space heating and cooling -Part 3: Test methods, European Committee for Standardization, Brussels, Belgium

F-Chart, 2014, EES V9.699, F-Chart Software, Madison, Wisconsin, http://www.fchart.com/ees/

Heimrath, R, Haller, M., 2007: Project Report A2 of Subtask A: The Reference Heating System, the Template Solar System - A Report of IEA SHC Task 32: Advanced Storage Concepts for Solar and Low Energy Buildings

Heinz, A., Haller, M., 2012: Appendix A3 - Description of TRNSYS Type 877 by IWT and SPF. In: Models of Sub-Components and Validation for the IEA SHC Task 44 / HPP Annex 38 - Part C: Heat Pump Models - A technical report of subtask C Deliverable C2.1 Part C. Downloaded 11.04.2015 from http://www.task44.iea-shc.org/data/sites/1/publications/T44A38_Rep_C2_C_HeatPumpModels_Final_Draft_Revised_130610.pdf

Hengel, F.; Rieberer, R.; Heinz, A., 2013: Theoretische Analyse zur Effizienzsteigerung durch Drehzahlregelung und Economizer-Schaltung bei einer Luft/Wasser Waermepumpe, DKV-Tagung, Hannover, AA IV.10

Hengel, F.; Riedler, J.; Rieberer, R.; Heinz, A.; Fleckl T.; Reichl; Ch., 2014: HPP-Annex41, Task 1- Literature and Technology Review, Task-1 Report

Hermes C.J.L., R.O. Piucco, J.R. Barbosa Jr., C. Melo. 2009, A study of frost growth and densification on flat surface

Hewitt N., M. Jun Huang, Defrost cycle performance for a circular shape evaporator air source heat pump, International Journal of Refrigeration 3 (31), p. 444-452, 2008

Li H., Cao F., Bu X., Wang L., Wang X., 2014, Performance characteristics of R1234yf ejector-expansion refrigeration cycle, Applied Energy, Volume 121, S. 98-101

Popovac M., S. Seichter, P. Benovsky, T. Fleckl. Ch. Reichl. Numerical Analysis of the Frosting Performance of the air-side of a heat-pump, 24th IIR international congress of refrigeration, August 16-22, 2015, ICR2015, Yokohama, Japan

Popovac M., S. Seichter, C. Reichl, P. Benovsky. Implementation and application of the frost growth and densification model for numerical analysis of heat pump frosting performance Ammonia and CO_2 Refrigeration Technologies, April 16-18, 2015, Ohrid, Republic of Macedonia

Reichl Ch., A. Strehlow, T. Oltersdorf, S. Braungardt, M. Pröhl, P. Benovsky, M. Popovac, T. Fleckl, GreenHP: Next Generation Heat Pump for Retrofitting Buildings – new evaporator component for large capacity air-to-water heat pumps, Advanced HVAC & Natural Gas Technology Conference, May 6-9, 2015, Radisson BLU Hotel Latvija Conference Center, Riga, Latvia; DOI: 10.7250/rehvaconf.2015.015; page 100-109

Robinson C.M., Jacobi A.M., 2001: A Study of Frost Formation on a Plain Fin, Air

Conditioning and Refrigeration Center, University of Illinois - Mechanical & Industrial Engineering Dept., Urbana, Illinois, United States

Sankaranarayanan K.P., 2010: Study of frost growth on heat exchangers used as outdoor coils in air source heat pump systems, Dissertation, Graduate College of Oklahoma State University, Stillwater, Oklahoma, United States

Strehlow A., C. Martín-Callizo, T. Oltersdorf, M. Popovac, Ch. Reichl. GreenHP: Heat Exchangers for Next Generation Heat Pump, 4th International Congress and Exhibition on Aluminium Heat Exchanger Technologies for HVAC&R, 10-11 June, 2015, Hotel Radisson Blu Scandinavia, Düsseldorf, Germany

Weller H. G., G. Tabora, H. Jasak, C. Fureby. 1998, A tensorial approach to computational continuum mechanics using object-oriented techniques, Computers in Physics 12: 620 – 631. s, Experimental Thermal and Fluid Science 33: 371–379.

Zoier, H., 2014: Betriebsverhalten von Aussenluft-Waermepumpen bei tiefen Aussenlufttemperaturen, Masterthesis, Institute for Thermal Engineering, TU-Graz

7 ACKNOWLEDGEMENT

The work on “IEA HPP Annex 41” is financially supported within the framework of the “IEA Research Cooperation” on behalf of the “Austrian Federal Ministry for Transport, Innovation and Technology” (bmvit) (FFG project number: 839560). Furthermore, the activities on cold climate heat pumps at IWT were partly financed by the “Werner Hochegger Forschungsstiftung”.

Austrian Team Report

IEA HPT TCP Annex 41
"Cold Climate Heat Pumps"

Task 3 – Energy savings assessment of an ASHP with liquid injection for cold climate applications

Submitted by:

Heinz Moisi
René Rieberer (contact: rene.rieberer@tugraz.at)

Graz University of Technology
Institute of Thermal Engineering
Inffeldgasse 25/B, 8010 Graz, Austria

Graz University of Technology

Apr. 14, 2016

TABLE OF CONTENTS

LIST OF TABLES

LIST OF FIGURES

1 INTRODUCTION

As outlined in Task 2, an air-to-water heat pump using liquid injection (LI) can increase operational hours in cold climate regions by reducing compressor outlet temperatures. Thus, lubricant related problems can be avoided. The increased time of operation can also have positive effects on seasonal performance factors (SPF) depending on the kind of auxiliary heat preparation (direct electrical, oil, gas etc.). In order to quantify the effects of an LI-System compared to a conventional heat pump system, a simple methodology has been developed to estimate the seasonal performance in dependence of different locations and heat sink temperature levels. However, only space heating has been considered (domestic hot water preparation has been neglected). The following analysis is based on the heat pump model and the experimental work described in the ANNEX 41 Task 2 report (Moisi et al., 2015).

2 HEAT PUMP MODEL

In this section, the LI-cycle model and its implementation into the annual simulations is outlined. A detailed description of the heat pump prototype and the simulation model has been given in the ANNEX 41 Task 2 report (Moisi et al., 2015).

2.1 General Description

The LI system utilizes injection of refrigerant into the compressor to lower the compressor outlet temperature. The injected refrigerant is expanded to an intermediate pressure through an expansion valve (Expansion valve 2 in Figure 1) and subsequently injected into the compressor. The injected mass flow is then mixed with the current compressor charge. The mixings process cools down the compressor charge (dashed line in p-h diagram in Figure 1 and thus decreases the compressor outlet temperature. Figure 1 shows the hydraulic layout (left) and the corresponding log(p)-h diagram (right).

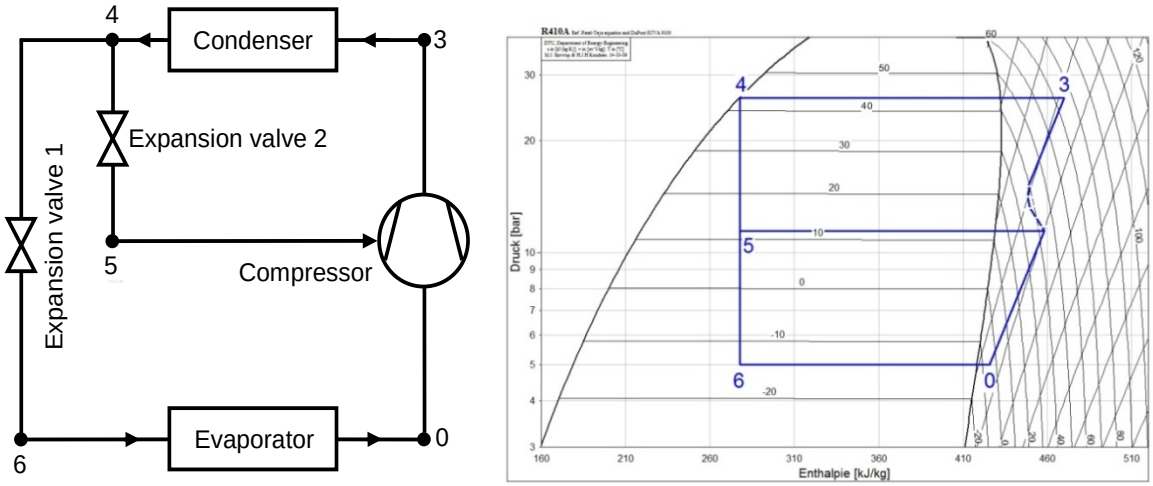

Figure 1: Layout (left) and log(p)/h diagram (right) of the LI injection cycle according to Zoier (2014)

The heat pump operates with an on/off control strategy. The set point for the compressor outlet temperature to activate the liquid injection has been defined to 125°C.

2.2 Heat Pump Characteristics

The seasonal performance estimation is based on a simple performance map approach. Therefore the results of the cycle simulations within Task 2 have been used to describe for example the heating capacity and the electrical consumption of the heat pump depending on the ambient temperature. The results for the heating capacity as a function of the ambient temperature and the heat sink outlet temperature (heating system supply temperature) are shown in Figure 2. The blue curve describes the capacity characteristic for a sink inlet temperature of 30°C and an outlet temperature of 35°C. The red line shows the characteristics for 40°C and 45°C respectively.

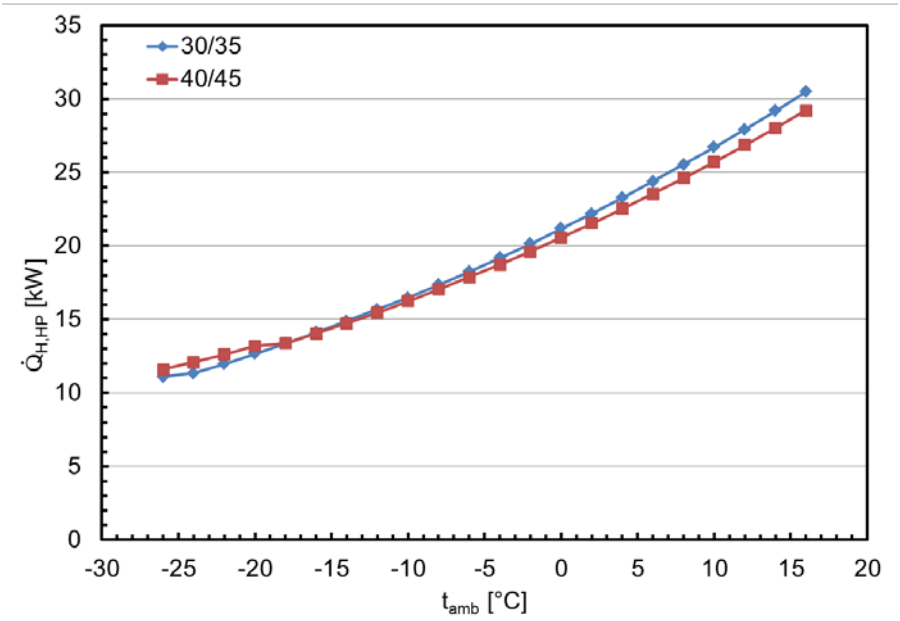

Figure 2: Heating capacity characteristics for two different heat sink temperature (30/35 and 40/45°C) levels of the LI-heat pump

For the annual performance simulation, the heating capacity is modelled by equation 2–1 in the form of a look up table where the heating capacity ($\dot{Q}_{H,HP}$) can be interpolated by providing the ambient temperature (t_{amb}).

$$\dot{Q}_{H,HP} = f(t_{amb}, t_{sink}) \qquad \text{Eq.: 2–1}$$

$$P_{el} = f(t_{amb}, t_{sink}) \qquad \text{Eq.: 2–2}$$

$$t_{comp,out} = f(t_{amb}, t_{sink}) \qquad \text{Eq.: 2–3}$$

For example, for an ambient temperature of -14°C the heating capacity results in approx. 15 kW (see Figure 2).

The same method is applied to describe the electrical consumption (P_{el}) which is displayed in Figure 3. The bend in the electrical consumption at an ambient temperature of approximately -20°C for the red line at approximately -24°C for the blue line indicates the threshold ambient temperature ($t_{amb,limit}$) where the liquid injection is activated to keep the compressor outlet temperature ($t_{comp,out}$) at a maximum of 125°C. According to the model the bend is caused by the additional compressor charge added due to the liquid injection.

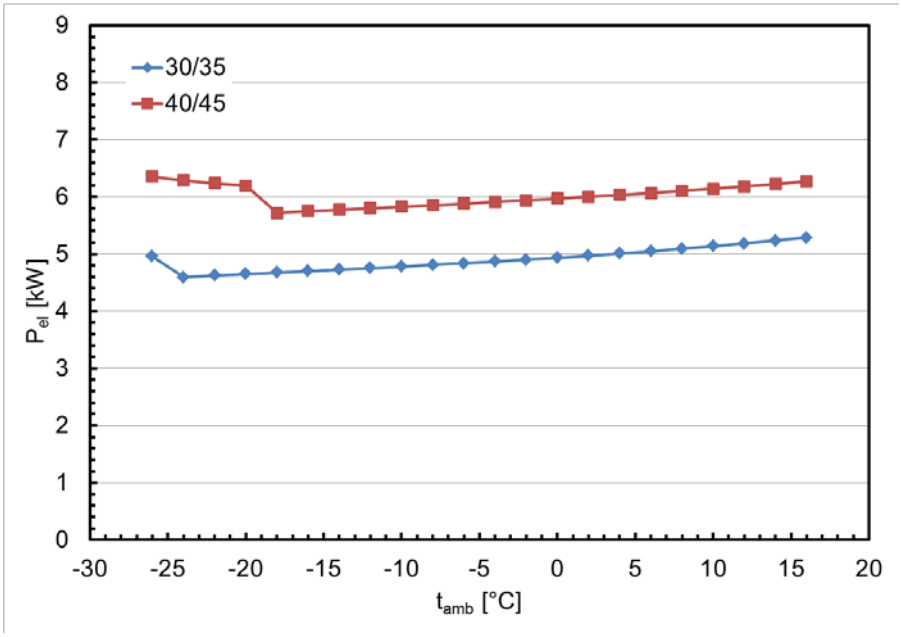

Figure 3: Characteristics for the electrical consumption of the LI-heat pump

The compressor outlet temperature provides the control variable and is depicted in Figure 4, as a function of the ambient and the heat sink temperature (see equation 2–3).

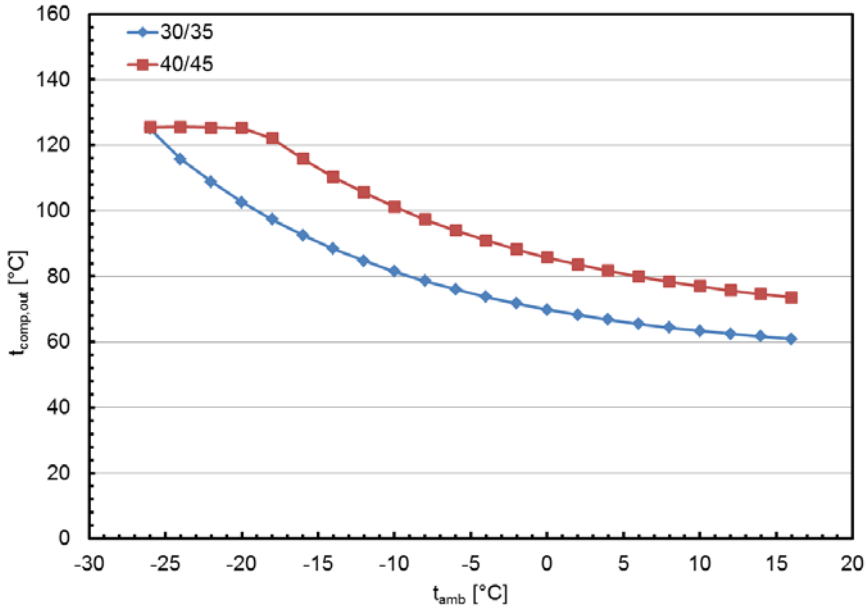

Figure 4: Compressor outlet temperature characteristics for the LI-heat pump

In the seasonal simulations (see section 4) the heat pump is represented by the three above described characteristics. The heat sink temperature represents the chosen heating system. For example a supply temperature of 35°C describes a floor heating system. The compressor outlet temperature serves as control variable for the injection. As mentioned above, each heating system (represented by t_{sink}) has a distinct minimum ambient temperature were the liquid injection is activated. At a given ambient temperature the compressor outlet temperature can be obtained from the provided characteristics.

Above the aforementioned ambient temperature threshold ($t_{amb,limit}$), the cycles are basically identical. Hence the characteristics for the conventional system (without LI) can be simply written as in equations 2–4 and 2–5.

$$\dot{Q}_{H,HP,con} = \dot{Q}_{H,HP}(t_{amb} \geq t_{amb,limit}, t_{sink}) \quad \text{Eq.: 2–4}$$

$$P_{el,con} = P_{el}(t_{amb} \geq t_{amb,limit}, t_{sink}) \quad \text{Eq.: 2–5}$$

If the outlet temperature rises above 125°C the heat pump is virtually switched off and the required heating capacity has to be provided by other means (e.g. direct electrical heating, see sections 3 and 4).

3 BOUNDARY CONDITIONS

In order to estimate the performance of the LI-System, boundary conditions in terms of required heating capacity and ambient temperature have to be defined. It is also necessary to define these conditions in a time variant manner to perform a seasonal estimation. This section describes briefly the climatic and building boundary conditions, chosen for the yearly simulations.

3.1 Climate

Since the cold climate regions are in the focus of this work, four locations have been selected with their minimum ambient temperature within one year of around -25°C. Additionally the location of Graz has been chosen for comparison although the minimum ambient temperature is rather high with -12°C. The locations are listed in Table 1 with their approximate minimum and maximum ambient temperatures as well as their heating limit temperature ($t_{heat,limit}$) derived from climate data.

Table 1: Estimated minimum, maximum ambient and heating limit temperatures of selected locations (Meteonorm, 2015)

Location	$t_{amb,min}$ [°C]	$t_{heat,limit}$ [°C]	$t_{amb,max}$ [°C]
Anchorage, USA	-24	14	26
Graz, Austria	-12	14	33
Helsinki, Finland	-22	15	29
Minneapolis, USA	-24	14	35
Moscow, Russia	-23	15	31

The climate data has been obtained from the Meteonorm Software (Meteonorm, 2015). The software has been used to generate climate data such as ambient temperatures for the above mentioned locations. The data can be obtained in the form of hourly values over a time span of a year. Furthermore it is possible to implement these data files as boundary conditions into the system simulation environment TRNSYS 17.02 (TRNSYS, 2015) to perform transient building simulations (see section 3.2). The climate data can then be used to derive the number of hours of the year with a certain ambient temperature for each location. The obtained curves are displayed in Figure 5 for the locations Anchorage (blue line) and Graz (red line).

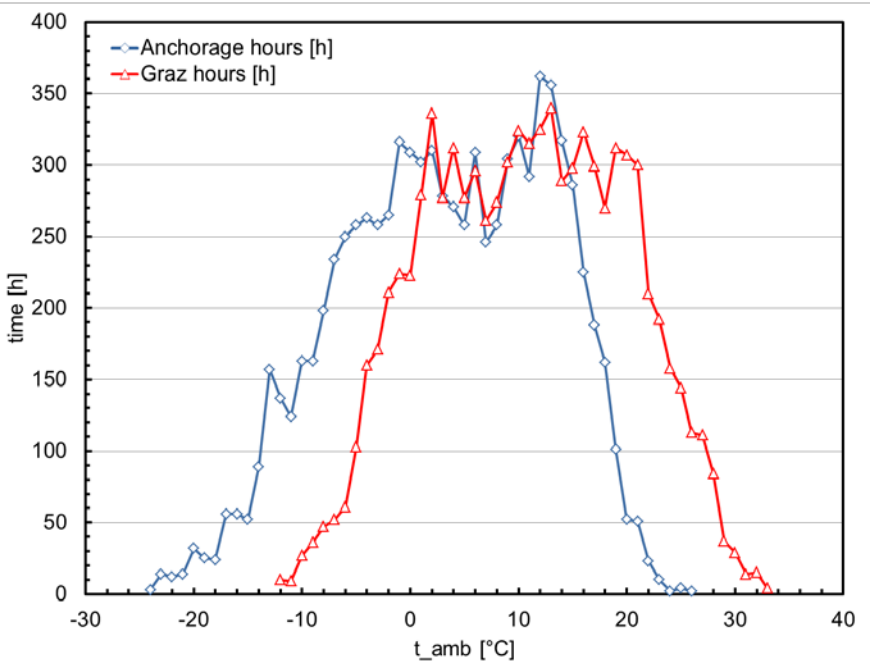

Figure 5: Number of hours over ambient temperature for the locations Anchorage and Graz

The number of hours (τ_{amb}) a certain ambient temperature occurs during the year can then be estimated for each temperature in discrete 1 K steps by the characteristics of Figure 5. For example, an ambient temperature of 0°C occurs approx. 223 hours a year in the City of Graz. The mathematical expression is given by equation 3–1.

$$\tau_{amb} = f(t_{amb}, location) \qquad \text{Eq.: 3–1}$$

The function τ_{amb} can then be used to calculate the annual energy demand as well as the supplied heating capacity and furthermore the seasonal performance factor (SPF) which is described in section 4.

3.2 Reference Building

In order to conduct an annual performance analysis the required heat demand must be determined. In this case, a reference building developed in the course of IEA SHC TASK 32 (Heimrath and Haller, 2007) has been selected. The building is defined as single family house with an annual heat demand of 100 kWh/(m^2a) calculated for the location of Zurich. Figure 6 shows the basic dimensions and the architectural design of the considered building.

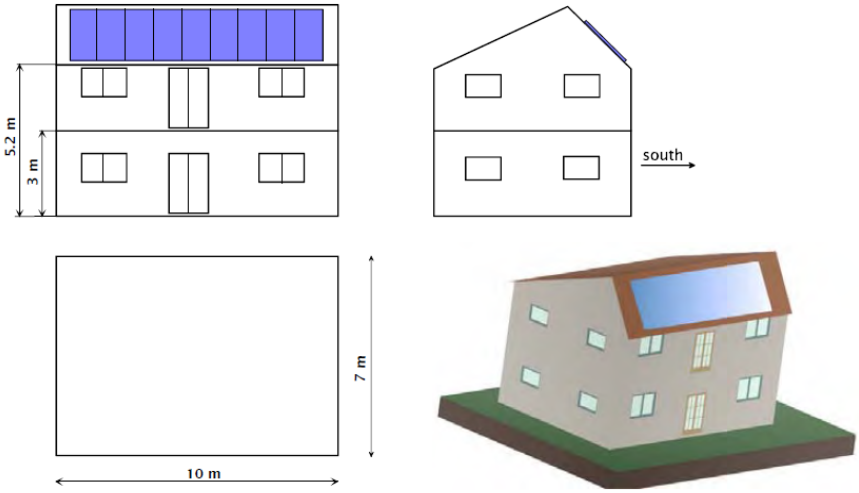

Figure 6: Basic dimensions and architectural design of the reference building (Heimrath and Haller, 2007)

The reference building has two stories with 70m^2 living space each. The total amount of the buildings glazed area is 12.7% of the total façade area. Main building parameters are summarized in Table 2.

Table 2: Main parameters of the reference building model (Heimrath and Haller, 2007)

Living Space $A_{LS}\ [m^2]$	Total façade area $A_F\ [m^2]$	U-value of wall construction $U_W\ [W/(m^2 \cdot K)]$
140	181	0.491

Further influences such as internal gains, occupancy and shading are considered within this building model. For a detailed description see Heimrath and Haller (2007).

A building model, implemented into the simulation environment TRNSYS 17.1 (TRNSYS 17, 2015) available at the Institute of Thermal Engineering of TU Graz has been used to evaluate the heat load of the building in dependence on the ambient temperature and location ($\dot{Q}_{load}(t_{amb}, location)$). Therefore the obtained climate data of the different locations has been utilized to derive heat load characteristics. Parameters for the calculations have been a set point room temperature of 21°C and the option “ideal heating”. The term “ideal heating” simply describes the amount of heating capacity that has to be supplied to the building in order to exactly meet the set point temperature of 21°C. The simulated period has been set to one year. Figure 7 shows the result of the building simulation for the example of Anchorage.

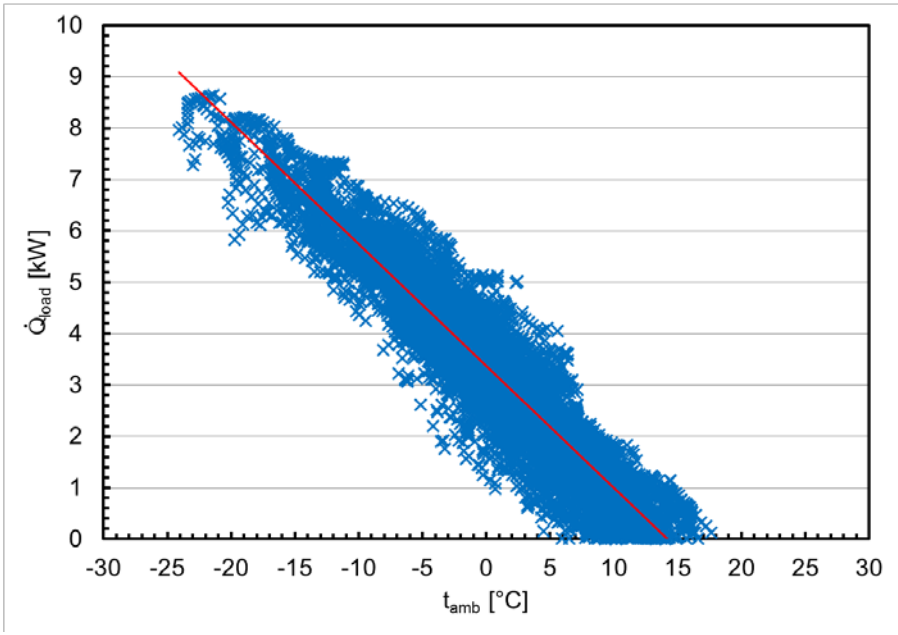

Figure 7: Building simulation results and linear fit for the building heat load in Anchorage

The blue crosses display the simulation results and the red line shows the linear heat load characteristic derived with the "least mean square" method. It can be observed the simulation results (blue) scatter around the red linear fit which is a consequence of solar radiation, internal gains and shading. The linear fit is therefore stating a rather simplified approach to model the required heat capacity. The simplified heat load can then be written as given in equation 3–2.

$$\dot{Q}_{load}(t_{amb}, location) = k \cdot t_{amb} + d \qquad \text{Eq.: 3–2}$$

Where k describes the slope of the linear fit and d the intercept. The results for k and d for the different locations mentioned in section 3.1 are summarized in Table 3.

Table 3: Parameters for the heat load characteristics

Locations	k [kW/°C]	d [kW]
Anchorage	-0,2372	3,3635
Graz	-0,2211	3,3063
Helsinki	-0,2261	3,4588
Minneapolis	-0,2071	2,9812
Moscow	-0,2226	3,4141

The further implementation into the annual performance estimation is described in section 4.1.

3.3 Heating System

For the heating system of the reference building only space heating has been considered. The system has been chosen to be monovalent with a direct electrical heater as a backup for ambient temperatures below the threshold already mentioned in section 2.2. A comparison between the heat load exemplary for Anchorage and the heat pump capacity for a 40/45 heating system is displayed in Figure 8.

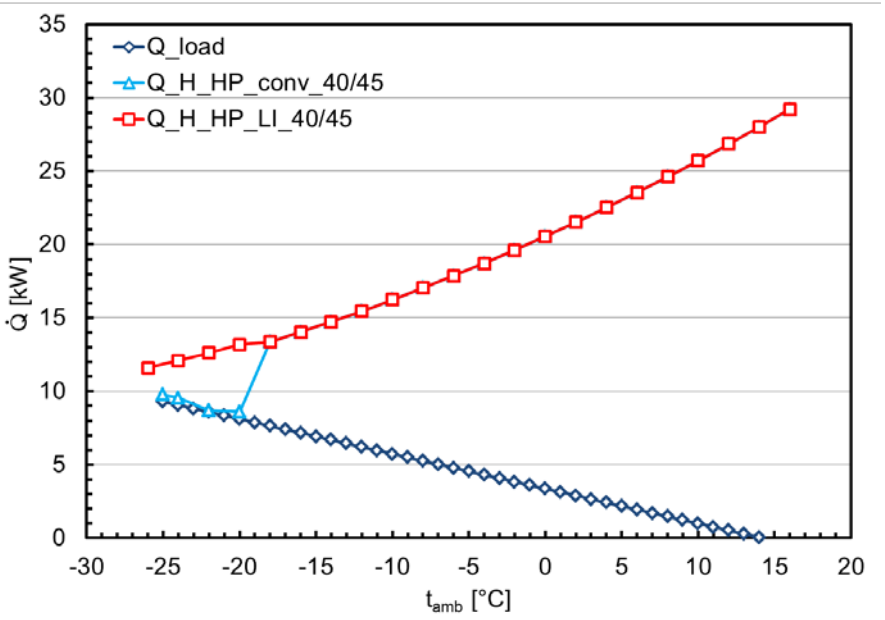

Figure 8: Comparison of building heat load (blue), LI heap pump capacity (red) and the characteristic of the conventional heat (light blue) pump as a function of the ambient temperature

It can be observed that the investigated heat pump is oversized for basically all considered climates especially for the climate of Graz. This fact influences the time in operation and the resulting on/off cycles of the heat pump. However, cycling losses have not been taken into account. For the annual simulation, constant return/supply temperatures of 30/35 and 40/45 are considered which states a major simplification since return temperatures can vary depending on the heat demand and ambient temperature. Furthermore, the electrical consumption of the circulation pump has not been considered.

As described before, an electrical backup heater (P_{aux}) is chosen to provide the required heat capacity if the compressor outlet temperature of the conventional heat pump system exceeds 125°C. Therefore, the auxiliary heating capacity must be equal to the building heat load at the given ambient temperature as stated in equation 3–3 (see Figure 8).

$$P_{aux}(t_{amb}) = \dot{Q}_{load}\left(t_{amb} \leq t_{amb,limit}, location\right) \qquad \text{Eq.: 3–3}$$

4 ANNUAL SIMULATIONS AND RESULTS

In this section the final simulation routine for the annual performance estimation is described. The calculations have been conducted throughout with the nonlinear equations solver EES v. 9.4 (EES, 2015).

4.1 Methodology

For the annual simulation, the LI-System and the conventional system are compared in terms of seasonal performance factor (SPF). As described in section 3.1, the number of hours at a distinct ambient temperature has been derived from climate data. With this information and the heat load characteristics, the energy demand for each discrete ambient temperature can be calculated combining equations 3–1 and 3–2 as follows.

$$Q_{load}(t_{amb}) = \tau_{amb}(t_{amb}, location) \cdot \dot{Q}_{load}(t_{amb}, location) \qquad \text{Eq.: 4–1}$$

The thermal energy required for space heating at a certain ambient temperature must be equal to the supplied energy by the heat pump. Since the heat pump operates with on/off control (see section 2.1) the time in operation (τ_{on}) can be simply calculated by equation 4–2.

$$\tau_{on}(t_{amb}) = \frac{Q_{load}(t_{amb})}{\dot{Q}_{H,HP}(t_{amb})} \quad \text{Eq.: 4–2}$$

The thermal energy ($Q_{H,HP}$) and the required electrical energy (E_{el}) of the heat pump can then be estimated as follows.

$$Q_{H,HP}(t_{amb}) = \tau_{on}(t_{amb}) \cdot \dot{Q}_{H,HP}(t_{amb}) \quad \text{Eq.: 4–3}$$

$$E_{el}(t_{amb}) = \tau_{on}(t_{amb}) \cdot P_{el}(t_{amb}) \quad \text{Eq.: 4–4}$$

As an example, the resulting energies of the 40/45 LI-System for the location of Anchorage are depicted in Figure 9. The effect of the liquid injection can be observed at an ambient temperature below -20°C since the heat pump is still operating (blue) while the conventional system is already switched off and the auxiliary heater is activated (compare to section 3.3).

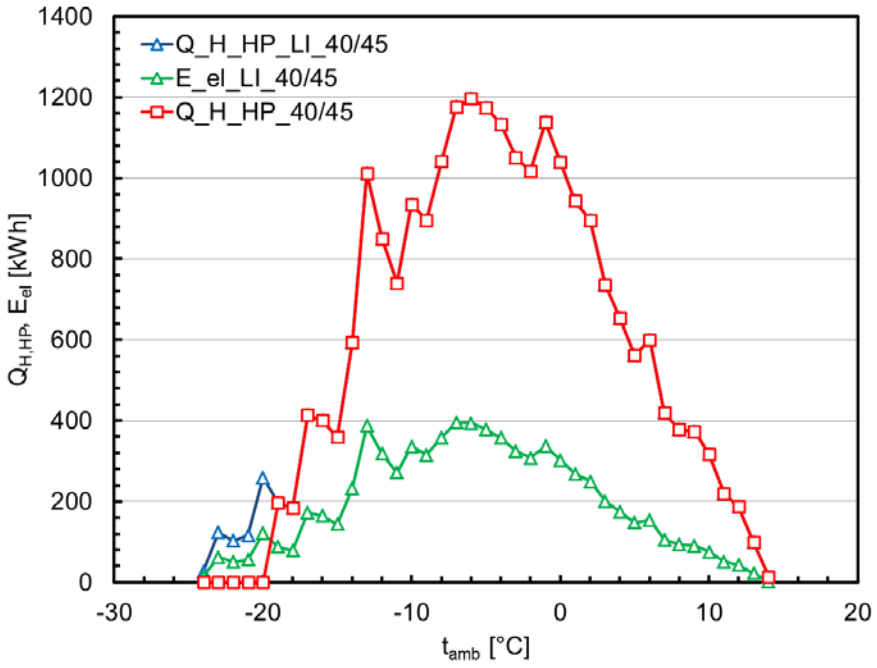

Figure 9: Simulation results for the supplied thermal energy and the esimated electrical consumption of the 40/45 LI-System (location Anchorage)

The above described control mechanism for the conventional heat pump is simply realized with an “if” condition considering the heat capacity of the heat pump (Eq.: 2–1), the compressor outlet temperature (Eq.: 2–3) and the auxiliary heating capacity (Eq.: 3–3) (see also section 2.2).

$$\dot{Q}_{H,HP,con}(t_{amb}) = \begin{cases} \dot{Q}_{H,HP}(t_{amb}) \;\; if \; t_{comp,out}(t_{amb}) \leq 125°C \\ 0 \;\; if \; t_{comp,out}(t_{amb}) > 125°C \end{cases} \quad \text{Eq.: 4–5}$$

In case the heat pump is switched off, the auxiliary energy is calculated according to equation 3–3 as described in section 3.3.

$$E_{aux}(t_{amb}) = P_{aux}(t_{amb}) \cdot \tau_{amb}(t_{amb} \leq t_{amb,limit})$$ Eq.: 4–6

Finally, the calculated energies can be cumulated (numerical integration) according to equations 4–6 to 4–9 to obtain their annual values.

$$Q_{H,HP,a} = \sum_{t_{heat,limit}}^{t_{amb}} Q_{H,HP}(t_{amb})$$ Eq.: 4–7

$$E_{el,a} = \sum_{t_{heat,limit}}^{t_{amb}} E_{el}(t_{amb})$$ Eq.: 4–8

$$E_{aux,a} = \sum_{t_{heat,limit}}^{t_{amb}} E_{aux}(t_{amb})$$ Eq.: 4–9

$$\tau_{on,a} = \sum_{t_{heat,limit}}^{t_{amb}} \tau_{on}(t_{amb})$$ Eq.: 4–10

With $Q_{H,HP,a}$ describing the annual heat supplied by the heat pump, $E_{el,a}$ as the annual electrical consumption, $E_{aux,a}$ describing the required auxiliary heat per year and $\tau_{on,a}$ as the total time in operation.

Using the obtained annual values, the annual seasonal performance factor (SPF_a) can be defined as follows.

$$SPF_a = \frac{Q_{H,HP,a}}{E_{el,a} + E_{aux,a}}$$ Eq.: 4–11

4.2 Results

The developed methodology has been used to estimate the seasonal performance of five different locations and two different heating system temperature levels. Furthermore, a comparison between the LI–System and the conventional system has been carried out. Figure 10 shows the comparison of the LI and the conventional system for a return/supply temperature of 30/35 in terms of the supplied thermal energy.

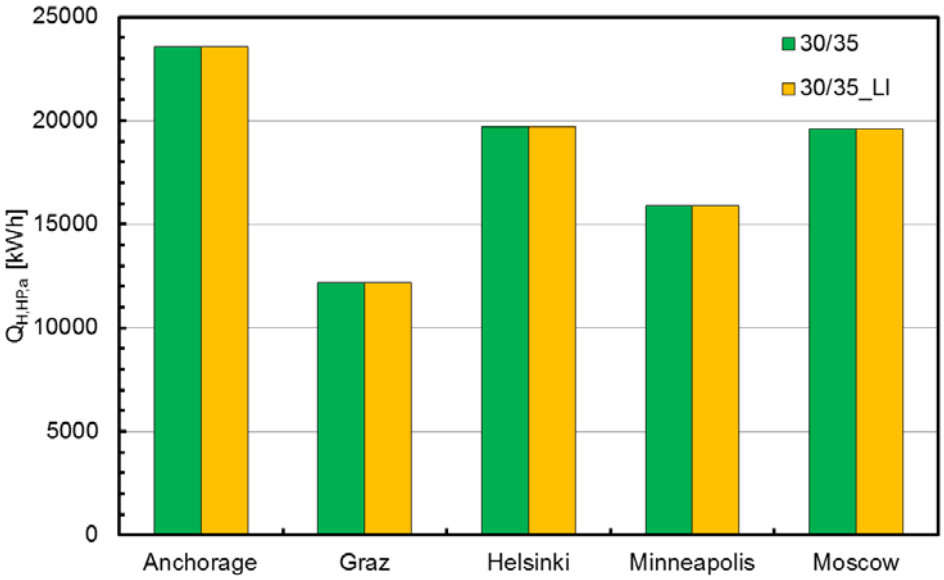

Figure 10: Comparison of the annual heat supplied for a 30/35 system

Anchorage shows the highest heat demand with approximately 24 MWh/a followed by Helsinki and Moscow with approx. 20 MWh/a. Minneapolis shows about 15 MWh/a in heat demand. The lowest value can be found in Graz which is clear considering the higher minimum ambient temperatures and a shorter heating season. However, no obvious difference occurs between the LI (orange) and the conventional system (green) since a liquid injection is not necessary in a 30/35 System for the considered locations. As stated in section 2.2, the limit ambient temperature for the considered heat pump in a low temperature system is -24°C. With none of the considered locations below this limit, no injection is needed. The simulation results for the annual performance are displayed in Figure 11.

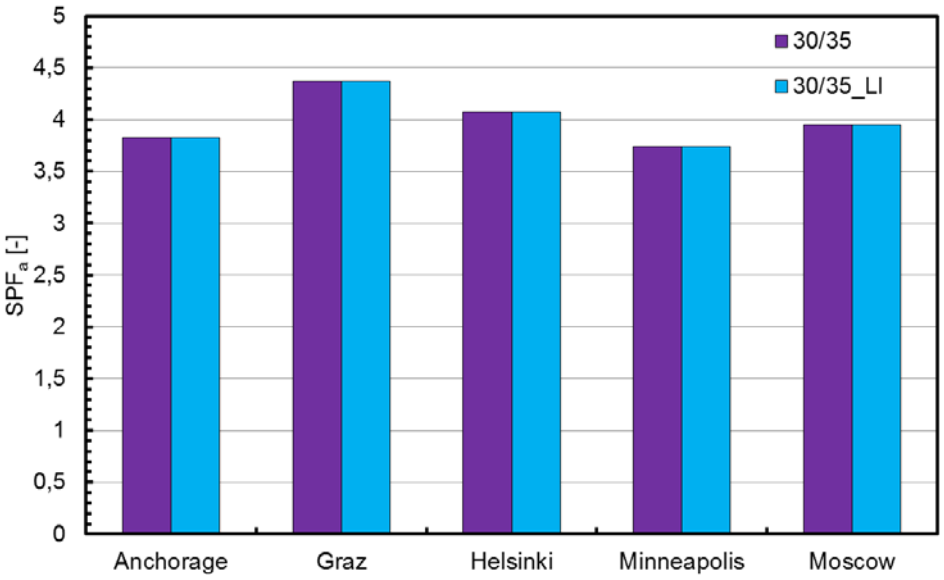

Figure 11: Comparison of the seasonal performance for a 30/35 system

The seasonal performance factors are in a range between 3.5 and 4.5. Graz shows the highest value since the heat pump operates mainly at higher ambient temperatures throughout the year compared to the other locations. Helsinki and Moscow show again similar values as well as Anchorage and Minneapolis. The climate of Minneapolis shows a

rather high number of hours with an ambient temperature below -20°C. In connection with a heating season as long as Graz as depicted in Figure 12, the fraction of heat pump operation with a low performance factor is rather high for the location of Minneapolis and thus a relatively low SPF_a results.

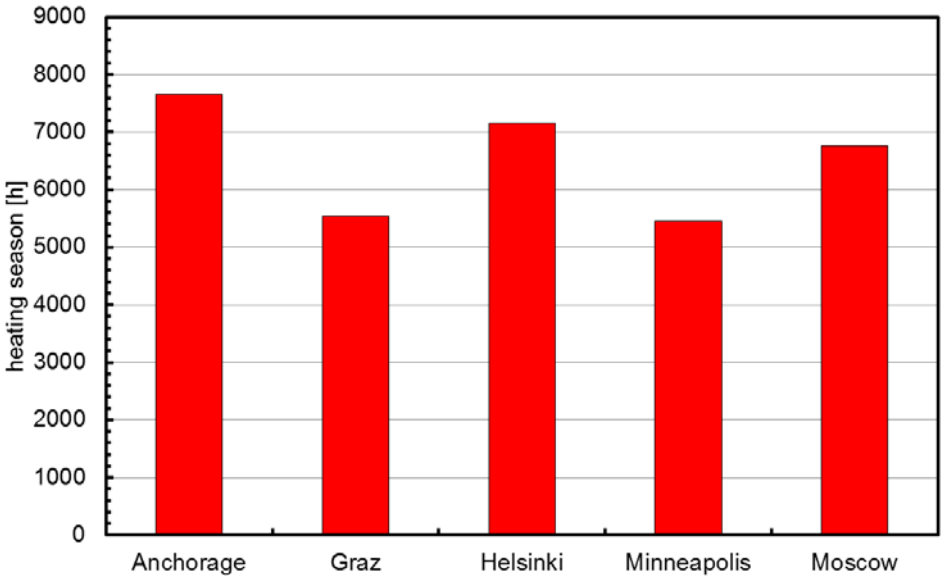

Figure 12: Estimated heating season hours of the considered locations

The 40/45 system shows clearly the influence of liquid injection on the supplied thermal energy as shown in Figure 13. Except for the location of Graz where the liquid injection has not been activated due to the high minimum ambient temperature, every location shows a higher energy supply with the LI-System, which is clear considering the assumptions taken in the previous sections.

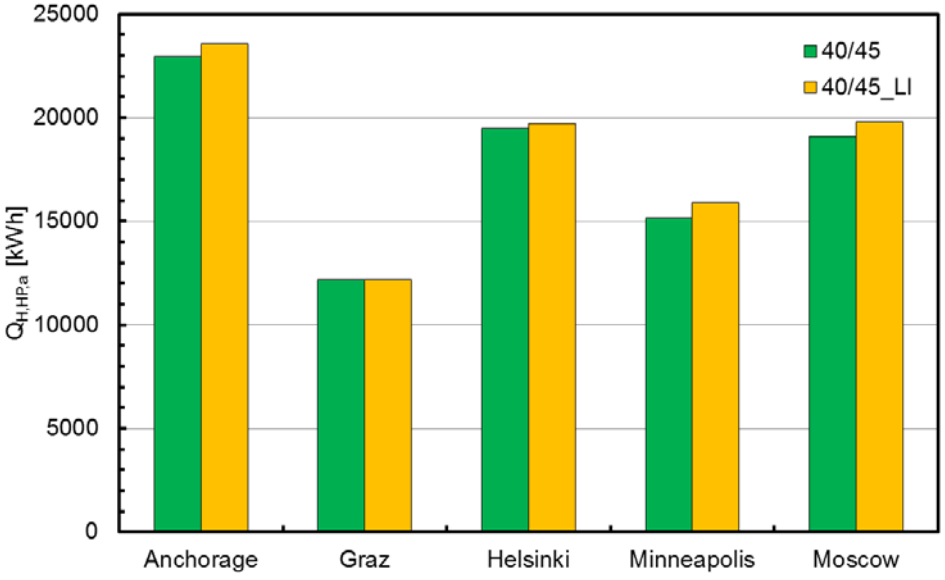

Figure 13: Comparison of the annual heat supplied for a 40/45 system

The reason for the difference is simply the time of operation, since the conventional heat pump is shut off at a certain ambient temperature. The remaining heat supply is then

provided by the electrical back up heater which of course has a negative influence on the SPF as depicted in Figure 14.

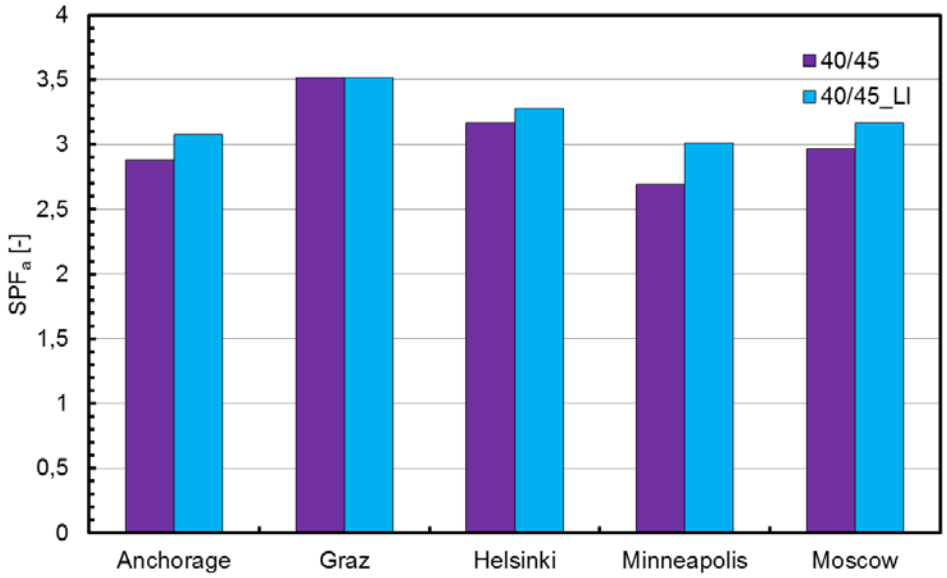

Figure 14: Comparison of the seasonal performance factor for a 40/45 System

The liquid injection shows an advantage in the cold climate locations due to the increase of time in operation and the fact that a backup heater is not necessary. The relative SPF improvement compared to the conventional system can be seen in Figure 15.

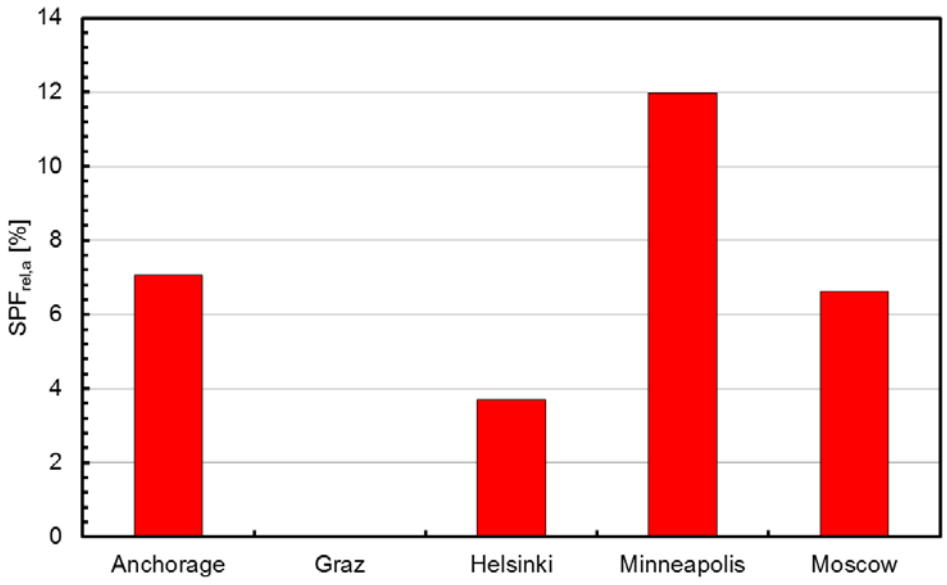

Figure 15: Relative SPF improvement for the 40/45 system

Minneapolis shows the biggest improvement potential with approximately 12% SPF increase. For the location of Anchorage and Moscow approx. 7% improvement can be achieved with the LI-System. The improvement potential is highly dependent on the number of hours of heat pump operation below a certain ambient temperature. This temperature again, depends on the heat pump system and/or the control strategy (max. compressor outlet temperature) as well as the temperature level of the heating system. An increase of the supply temperature level of the heating system will increase the improvement potential

compared to a conventional heat pump system with electrical backup heater since the threshold ambient temperature increases. However, larger time periods of low ambient temperatures are decreasing the overall SPF since the heat pump is operating with lower efficiency during these periods.

5 SUMMARY AND CONCLUSION

Based on the prototype testing and simulation of a Liquid-Injection air-to-water heat pump system in IEA HPP ANNEX 41 Task 2 (Moisi et al., 2015), characteristics for heating capacity, electrical consumption and compressor outlet temperature have been derived in order to carry out an annual performance estimation. A simple methodology has been developed to estimate the annual thermal energy and electrical consumption of a heat pump system with and without liquid injection. The heating system has been considered as monovalent with an electrical backup heater. A reference building based on IEA SHC Task 32 has been utilized to derive heat load characteristics for five different locations. Combining the climate data of the five locations with the heat pump and building characteristics, a seasonal performance factor has been estimated for two different heating system supply temperatures and a comparison of the LI-System to a conventional system has been carried out.

The results showed that, with a supply temperature of 35°C, no injection is needed at all. Therefore, no difference between the SPF results for the conventional and LI system occurred. The resulting SPF values are in a range of 3.8 (Anchorage) and 4.3 (Graz). The main influence on SPF has been the ambient temperature. The results are surely overestimated quantitatively according to the experimental data (Moisi et al., 2015), but can point out a qualitative trend., A difference between the conventional and the LI system in terms of performance can be observed at a supply temperature of 45°C. With increasing operation time of the LI-System at lower ambient temperatures (approx. below -20°C), the SPF improvement compared to the conventional system increases since the backup heater is required less often. In the case of Minneapolis for example, an SPF improvement of 12% can be achieved compared to the conventional system. On the other hand, Graz shows no effect at all since the minimum ambient temperature is too high for the activation of liquid injection (approx. -12°C). However, the threshold ambient temperature for the injection activation is dependent on the control strategy. Another fact is clear, that with an increasing heat supply temperature this threshold rises to higher ambient temperatures. Therefore, a liquid injection system can be interesting for more moderate climates and high temperature heating systems in the course of refurbishments in order to realize a monovalent heating system as well as for hot water production.

In conclusion, a liquid injection system can increase the range of application to lower ambient temperatures. Compared to a conventional air source heat pump system with a direct electrical backup heater, annual efficiencies can be improved depending on the time the heat pump operates at lower ambient temperatures.

6 BIBLIOGRAPHY

F-Chart, 2014: EES V9.699, F-Chart Software, Madison, Wisconsin, http://www.fchart.com/ees/

Heimrath, R, Haller, M., 2007: Project Report A2 of Subtask A: The Reference Heating System, the Template Solar System - A Report of IEA SHC Task 32: Advanced Storage Concepts for Solar and Low Energy Buildings

Meteonorm, 2016: Meteonorm Software V7.1.7, Meteotest, http://www.meteonorm.com/de/downloads

Moisi H., Rieberer R.; Fleckl T., Popovac M., Reichl Ch., 2015: IEA HPP-Annex41, Task 2-Simulation Models and Prototype Experiments, Task-2 Report, Graz, Vienna

TRNSYS, 2015: TRNSYS V17.02, Thermal Energy System Specialists, Madison, Wisconsin, http://www.trnsys.com/

Zoier, H., 2014: Betriebsverhalten von Aussenluft-Waermepumpen bei tiefen Aussenlufttemperaturen, Masterthesis, Institute for Thermal Engineering, TU Graz

7 ACKNOWLEDGEMENT

The work on “IEA HPP Annex 41” is financially supported within the framework of the “IEA Research Cooperation” on behalf of the “Austrian Federal Ministry for Transport, Innovation and Technology” (bmvit) (FFG project number: 839560).

Furthermore, the activities on cold climate heat pumps at IWT were partly financed by the “Werner Hochegger Forschungsstiftung”.

Austrian Team Report

IEA HPT TCP Annex 41
"Cold Climate Heat Pumps"

Task 4 – Proposed Future Work

Possible future work:

- Further experimental testing of other promising heat pump cycles: According to the simulation results of Task 2 promising measures to improve the heat pump cycle such as staged compression or the use of an economizer remain to be investigated in detail. However system complexity and investment costs are often obstacles to overcome in this regard. In order to determine the ratio between benefits and afford of the different cycle configurations further data is necessary. In this regard, real life monitoring of different cycle configurations can provide useful information. Based on this, simulation studies coupled with economic considerations can be carried out.
- Detailed evaluation of an ejector cycle due to the promising results of the simplified modelling: This includes a detailed literature research on modelling, design aspects and application of the ejector component. The part load behaviour of the ejector is of interest since very low ambient temperatures occur limited times of the year (depending on the location). In this regard, the fixed geometry of the ejector is an important aspect however variable injectors may improve the part load characteristics. The consideration to bypass the ejector if the ambient temperatures are higher should be investigated. Furthermore costs are an import issue. Detailed simulations and an experimental testing of an ejector cycle for cold climate applications should be carried out.
- Improved compressor model for the liquid injection cycle in order to improve the accuracy of the simulation results: Therefore it is necessary to reconsider the injection and subsequent mixing process in more detail. Performance maps of a scroll compressor with liquid injection can possibly be obtained via the cooperation with compressor manufacturers and their testing facilities or laboratory testing.
- The measurement of the frost performance of the heat exchanger within the entire evaporator heat pump unit, including the quantification of the spatial frosting distribution: This will be linked to the change of acoustic emissions due to subsequently icing of the heat exchanger. This topic will be covered in the newly established Annex 51 (Acoustic Signatures of Heat Pumps), which started in April 2017.

Canadian Team Final Country Report

IEA HPT TCP Annex 41
"Cold Climate Heat Pumps"

Submitted by:

Brice Le Lostec (contact: lelostec.brice@lte.ireq.ca)

Hydro Québec
Laboratorie des Technologies de l'Énergie (LTE)
Shawinigan, Québec

Daniel Giguère (contact: daniel.giguere@canada.ca)

Natural Resources Canada

CanmetENERGY
Natural Resources Canada
Varennes, Québec

November 2016

TABLE OF CONTENTS

EXECUTIVE SUMMARY

CANADA – PROJECTS ON ADVANCED HEAT PUMP CYCLES: VAPOR-INJECTION, VARIABLE-CAPACITY, CO_2 GROUND LOOP, SOLAR ASSISTED ICE SLURRY, AND REFRIGERANT MIXTURES

The country report details work in several independent areas of interest:

- Quantifying efficiency improvements of traditional air-source heat pumps, ASHPs, utilizing cycle enhancements – two-stage and variable-speed compressors and vapor-injection
- Analysis of the C656 standard (CSA (2006, 2014)), Canadian heat pump efficiency test standard, to understand its limits and identify areas for improvement
- Generating test bench results of a solar-assisted heat pump using ice-based latent storage to demonstrate the technology and validate simulation results in cold climates
- Measure benefits of a CO_2 ground loop to reduce installation costs of ground-source heat pumps, GSHPs
- Identify one or more refrigerant mixtures to improve the performance of a cold climate ASHP having an acceptable global warming potential, GWP

LTE (HYDRO-QUÉBEC)

Enhanced Air-Source Heat Pumps:
In order to foster the emergence of cold climate heat pumps on the market, efforts are being made at Hydro-Québec's energy technology laboratory (LTE) to characterize the equipment and propose solutions to promote the deployment of these technologies:

- Laboratory tests on four central heat pumps
- Heat Pump #1 is a conventional technology that is considered to be an upscale product and that can operate at temperatures as low as -25°C.
- Heat Pump #2 is a two-stage system specifically designed for cold climates. It includes a 2-piston compressor and a booster. The compressor functions depending on the needs – either with 1 piston (minimum displacement) or with 2 (maximum displacement).
- Heat Pump #3 leverages variable speed technology (compressor) with the injection of a refrigerant.
- Heat Pump #4 is a device designed for hydronic heating and the production of domestic hot water. This heat pump includes an outdoor unit and a storage tank. In this device, CO_2 is used as the refrigerant and the heat pump is known for its capacity to operate at an outdoor temperature as low as -20°C. It is based on a transcritical thermodynamic cycle and includes a variable speed compressor (refrigerant injection).
- A field measurement campaign on 22 heat pumps
- 16 houses were equipped with an air handling unit with a built-in heat pump assisted by an electric coil in the unit
- 10 sites have a single stage air source heat pump
- 6 sites have a cold climate air source heat pump (5 had variable speed compressors and 1 had a two-stage compressor)
- Remaining 6 sites were equipped with a ductless split heat pump system supplemented by independent electric baseboard heaters

A test bench was developed at the LTE to test central air-to-air heat pumps. The process was divided into several sections, and was regularly modified to meet the requirements of different tests. A second test bench was also developed to test an air-to-water heat pump. The outdoor unit of the heat pump was installed in the same section as the air-to-air heat.

The thermal load of both the heating and the domestic hot water was dissipated by cold water supplied by the municipal water utility. In this particular case, bypassing the storage tank is possible and allows an evaluation of the heat pump performance without the influence of this equipment.

The heating capacity of Heat Pump 1 decreased monotonously and the system operated at temperatures as low as -15°C. However, at that temperature, the heating capacity was low (5 KW) and could not meet the heating load of a house below this temperature. When a conventional back-up electric heater (ON/OFF) was used, the heat pump evidently could not operate normally at that temperature. The full load heating capacity of the variable speed and two-stage heat pumps evolved similarly. Indeed, two power levels are visible. This had the advantage of providing a considerably high heating capacity at low temperatures, which allowed to reduce the balance point temperature of the heat pumps. Their COP decreased based on the outdoor temperature. In the case of the VRF injection heat pumps, a significant decrease in the COP was observed between 5°C et 0°C, which corresponded to an increase in the compressor's speed ranging between 60% and 100%. It is normal for the COP of variable speed heat pumps to decrease with an increase in the speed of the compressor.

In the case of Heat Pump 1, because no frost occurred when the heat pump was operating at 10°C, its daily performance was not affected. It should be mentioned that, upon the formation of frost, the loss in capacity is relatively constant according to the temperature. The average capacity loss was 0.62 kW between 6°C and -14°C. In the case of Heat Pump 2, the capacity loss between 6°C and -5°C was 0.5 kW. As far as Heat Pump 3 was concerned, no defrosting activities occurred at temperatures above 0°C; its daily and instantaneous performance levels were therefore identical at these temperatures. When the temperature was below or equal to 0°C, the thermal capacity loss over a 24-hour period was an average of 0.61 kW, or 5.4% less than the instantaneous value. It was also observed that the difference between the instantaneous and daily values had a tendency to increase when the outdoor temperature decreased.

Measuring the bench top performance of various heat pumps (both air-to-air and water-to-air) allowed to obtain reliable and accurate information under controlled conditions on their heating capacity, their COP, the effects of the defrosting cycles and the effects of the air flow. This information not only helped to validate the specifications supplied by the manufacturers on the performance of the heat pumps but was also used in models to estimate the energy savings generated by the heat pumps.

The heating capacity of VRF injection heat pumps is interesting when the outdoor temperatures are low and significantly better than conventional heat pumps, including those that are rated as upscale. Their COP at full capacity is lower than the COP of conventional heat pumps. However, when the temperature rises above the heat pumps' balance point, it is expected that the COP should improve when the heat pump operates at a lower speed whereas conventional heat pumps tend to deteriorate because of the cycling impacts.

The field test results of this study demonstrate that heat pumps installed according to current practices allow to generate significant annual energy savings of between 25% and 30% in the case of conventional heat pumps and between 45% and 50% in the case of variable speed heat pumps as compared to resistive heating equipment. Variable speed heat pumps therefore generate greater energy savings than conventional heat pumps; however this remains difficult to quantify due to the number of samples. The difference in capacity at low temperatures, the coefficients of performance, the cut-off point, the sizing and the mode of operation (continuous ventilation, setpoint changes, control) remain criteria that can explain the difference in energy savings within a same category. It is important to mention that the quality of the installation of heat pumps has an impact on the performance of the overall heating system. The airflow, refrigerant load and heating equipment controls (or the

interaction between the various devices) are factors that should not be overlooked when they can have a significant impact on the generation of energy savings, and this applies for the entire life cycle of the equipment. Furthermore, unless a major problem occurs (a refrigerant leak for example), it is difficult for an individual to identify when a heat pump's operation is less than optimal because of poor installation practices.

Our measurement campaign also demonstrated that rated HSPFs as defined by CAN/CSA-C656-05 (similar procedure as AHRI 210/240) is not a criterion adapted to represent energy savings although there is a link between the average coefficient of performance of the systems we studied and the HSPF. It should be noted that the Office of Energy Efficiency (OEE) issued a publication in 2010, *Bulletin on Reporting Cold Climate Performance* (http://www.nrcan.gc.ca/energy/regulations-codes-standards/bulletins/7177), recommending modifications to CAN/CSA-C656-05 so that the performance of heat pumps used in cold climates is better represented in the standard. One requirement from this modification was additional standard testing to report heating capacity and COP at -17.8°C (0°F) be put in place by January 1, 2014. This would require that standardization labs be in a position to meet the criteria of the tests proposed by the OEE.

CAN / CSA C656 Standard

If the HSPF is a selection criterion for potential Program on heat pumps, it is important to know the limitations and work to close the gaps, either by modifying the calculation of HSPF and / or establishing criteria to meet the needs.

In general, the modification of a standard is relatively tedious. Different actors have different interests that must be taken into account. For example, when revising the Energy Star label, manufacturers where concerned about the workload that could represent the addition of low temperature standardized tests and taking into consideration regional weather conditions rather than national.

Therefore, if an amendment to the C656 standard should be carried out, it would be appropriate that these changes are also made to the American AHRI 260/240 in order not to create obstacles to the development of the Canadian market. One way not to be overlooked is the job of Annex 39 of the IEA, which aims to standardize internationally the heat pump performance criteria.

For electric utilities, changes in standards and the establishment of a representative performance criterion real savings is an important issue, however, this work is done on the long term which may prevent the establishment of a possible Energy-Savings Program. Proposed solutions such as the joint use of standardized criteria (HSPF) and technical parameters (e.g. variable speed, refrigerant injection), or the use of capacity and low temperature coefficients of performance (non-standardized) – as does Vermont currently for its commercial program – must be seriously studied whether a commercial program is implemented in the short term.

HSPF, which is a standardized performance criterion, do not calculate energy savings that are representative of what is observed in the field. Moreover, with the advent of new technologies such as heat pumps with variable speed compressor with or without refrigerant injection, the HSPF does not give a realistic energy saving difference between the different technologies. This is explained partly by the calculation assumptions which aim to idealize the operation of heat pumps below the balance point. For some heat pumps with variable speed, including wall units, low temperature standard capabilities (-8.3°C), are not always based on the maximum speed of the compressor. Therefore, it is difficult to rely on this criterion to identify the most efficient equipment.

According NEEP (Northeast Energy Efficiency Partnerships) barriers to the rapid introduction of “high performance” heat pumps would be:

- A lack of documentation on the impact of heat pumps on energy costs and peak consumption;
- A lack of standardized metrics that adequately describe the operation of the low-temperature heat pumps;
- A lack of knowledge among consumers and installers of new technologies;
- A lack of controls to manage different heating systems;
- A higher initial cost;
- A lack of support or disregard from the political level.

CanmetENERGY

Today, heat pumps are not the preferred appliance for space heating in Canada. The research work undertaken at Natural Resources Canada/CanmetENERGY–Varennes (Canmet) is aimed at improving the performance and first cost of heat pump technologies through simulation and experimental based research to make it them more attractive to the market.

This report describes four research projects conducted by Canmet to improve cold climate heat pump technologies. All these research projects are in progress and have started during the Annex 41 activities. The actual market situation of heat pumps is introduced in the Canadian context chapter.

Hybrid Ejector - Compressor Heat Pump

The hybrid ejector/compressor system is based on the appropriate integration of compressor and ejector technologies using air as a heat source. Work carried out under a previous R&D project on standard electrically driven heat pump (mechanical compression system) have shown that the replacement of the expansion device by the ejector component and a separator can improve the heat pump performance by up to 15% with a minimal incremental cost. While the system is simple, the main challenge lies in the two-phase-flow that takes place inside the ejector. The two-phase flow ejector is a very complex research field and research findings are not well described in the literature.

To gain a better understanding of the two phase flow ejector and integration, a hybrid ejector/compressor test bench for heating applications was constructed and some tests performed under a previous research project. The test bench uses a variable speed compressor combined with an electronic expansion valve for maximum flexibility of operation. Its nominal heating capacity is 10 kW, which corresponds to the typical capacity of residential and light commercial applications. This test bench has been upgraded for the purpose of this project with the refrigerant recently replaced from R410A to R-134a due to partial fractionation occurring in the separator. Preliminary results have shown appropriate compression ratios; however, entrainment ratios would need to be improved. Our efforts are now directed towards the development of a better ejector for R-134a (current ejector in test bench was designed for R410a) that will lead to higher entrainment ratios.

Coupled with the hybrid ejector/compressor test bench, a second test bench, dedicated solely to the study of the two phase ejector component was also constructed for this project. Capable of inducing a wide range of operating conditions, the two phase ejector test bench will generate in depth knowledge and experimental results used to validate numerical models.

These experimental activities, coupled with the modeling work and validation of results, will significantly improve our knowledge on the design of two-phase-flow ejector components and heat pump systems.

Solar-Assisted Heat Pump

Solar assisted heat pump systems, which rely on solar energy to supply or supplement heat pump operations, offer an attractive alternative to the air and ground source units more commonly found in the Canadian market. Solar based systems are often challenging to design and implement because they (i) require significant thermal storage capacity to bridge the temporal discrepancy between solar availability and thermal demand, and (ii) experience reduced collector efficiencies in the winter months when thermal demand in cold climates is highest. To address these issues, Canmet has worked extensively on the development of a new solar heat pump concept using ice-based latent storage.

Extensive simulation and experimental work has been undertaken to develop a novel solar heat pump system using ice-based thermal storage. Using validated energy models, it is estimated that such a system can reduce the energy use for space heating and DHW in high performance homes between 61% and 66%, depending on the location of the building.

Table ES-1 summarizes projected system sizing for typical existing homes in Eastern Canada (e.g. Montreal). Provided that the ice generation/storage technology can be sourced at a reasonable cost, the proposed system offers a cost-effective alternative to the current generation of ground-source heat pumps, and is particularly interesting for retrofit applications where it may be difficult to add ground heat exchangers.

Table ES-1: Suggested System Design Parameters for Typical Canadian Housing

Parameter	Suggested Value/Range
Solar Collector Area	30 m^2 to 35 m^2
Ice Storage Tank Volume	Approx. 10 m^3
Heat Pump/Ice Generator Capacity	3 tons (10 kW)

CO_2 Ground Source Heat Pump

Ground source heat pumps (GSHP) are one of the most efficient commercially available space heating systems in Canada. GSHPs use a constant ground source temperature throughout the year yielding a high annual COP (~3) reducing the space heating energy consumption by up to 65%. The main barrier for the market adoption is the first cost and thus the main objective of the project is to find ways to reduce the initial investment cost or further increase the efficiency of the system to make it a more attractive solution. Furthermore with the phase-out of HCFC refrigerants now in effect for new equipment and the next step phasing down HFC refrigerants, several projects are evaluating the feasibility of using CO_2 as the working fluid. CO_2 has a low global warming potential and the thermo-physical properties provide several advantages.

CO_2 as a phase change circulating fluid in the ground heat exchanger is seen as a promising alternative to synthetic refrigerants. CO_2 is a naturally occurring substance, has low cost, is not toxic or flammable, does not represent a threat for ground water contamination and has a global warming potential of 1. CO_2 does not require special material selection for corrosion prevention, and requires less circulation pumping energy. CO_2 as a phase change heat transfer fluid has been successfully applied in refrigeration technologies in Canada (and the world) such as in supermarkets and in ice rinks and heat pumping solutions are gaining increased interest.

The objective of this work is to contribute to the advancement of underground heat extraction technologies using CO_2 as a phase change fluid carrier, and to provide a cost effective and environmentally friendly alternative to GSHP systems commercially available today. The work consists of conducting experimental work on a new test bench at Canmet facility, and developing simulation models to support the optimization of CO_2 ground loop configuration and operation.

CO_2 is much less sensitive to pressure drop than synthetic refrigerants, which enables the downsizing of the borehole U tube diameter. The underground heat exchanger performance is 13.6 m/kW, which compares favorably to the conventional secondary fluid borehole that shows 17 to 26 m/kW with 20 mm to 50 mm pipe diameters. The seasonal COP of the heat pump increases by 21% for a 150% increase in borehole length. For the same scenario, the heating capacity of the heat pump increase by 15%. This demonstrates the importance of the borehole sizing on the efficiency of the heat pump.

This work shows the importance of the proper sizing of the heat pump capacity for a specific application. GSHPs show the lowest energy consumption, but ASHPs remain the most attractive heat pumping option for residential users. Future work on GSHPs should continue to address overcoming the high cost or achieving improved seasonal efficiency by meeting DHW loads in addition to space heating loads.

Refrigerant Mixtures

The use of refrigerant mixtures is becoming more and more common in air conditioning and refrigeration. In 1965, the ASHRAE Guide and Databook Fundamentals and equipment published three azeotropic refrigerant mixtures: R500, R501 and R502. In 2013, the 'ASHRAE Handbook Fundamentals' listed 65 zeotropic mixtures and 14 azeotropic mixtures. This number is growing each year. These new blends meet the need of the market which must deal with the phase-out and phase-down of CFCs, HCFCs and HFCs. To replicate the performance and characteristics of these refrigerants for specific applications it was necessary to create this diversity of mixtures.

One of the features of zeotropic blends is the temperature glide. At constant pressure, the mixture boiling temperature (bubble point) is lower than the condensing temperature (dew point).By matching the temperature glide of the refrigerant with the temperature glide of the fluid to cool in an air conditioning or chiller system, a 10 to 15% COP improvement can be achieved with a temperature glide of 5.5°C. If the application allows a temperature glide of 10°C, the COP of the heat pump could be improved by up to 30% theoretically.

A heat pump simulation model was developed, which was designed to permit changing/simulating a different refrigerant without modifying the main components of the heat pump: compressor, evaporator and condenser. Among all the mixtures studied, R-32/CO_2 (80/20) mixture presents better performance potential for the purpose of this study. The mixture is non-toxic with a GWP of approximately 540, which is 75% lower than the GWP of R-410A. Moreover, it is a zeotropic mixture with approximate temperature glides of 6°C and 8.5°C in the evaporator and condenser respectively.

To assess the performance of various refrigerant mixtures, the use of the residential building energy models were used. Five refrigerant cases were simulated using the same heat pump components:

- Case 1: (reference case) Standard R-410A air source heat pump, with a nominal heating capacity of 7.7 kW at 8°C outdoor temperature. This unit meets 75% of the total space heating load, so 25% of the load was provided by the auxiliary heating system.
- Case 2: Same as reference case with a variable speed compressor

- Case 3: Fixed mixture of 80% R32 and 20% CO_2
- Case 4: Variable composition (VC) mixture R32 - CO_2 with a reservoir located at the compressor suction to manage the concentration of CO_2
- Case 5: Fixed 80% R32 and 20% CO_2 with a variable speed compressor

The results of the simulation are summarized in Table ES-2 with the heat pump (HP) contribution indicating the percentage of the annual heating capacity met by the heat pump and the seasonal COP of the system.

Table ES-2: Simulation results for five refrigerant mixture cases

Refrigerant Case	Capacity	HP contribution	COP seasonal
	kW	kWh/kWh	kWh/kWh
R-410A	7.7	75%	2.16
R-410A VSD	7.7	91%	2.73
R32-CO2 80/20	8.1	84%	2.46
R32-CO2 VC	9.0	93%	2.81
R32-CO2 80/20 VSD	8.1	97%	2.98

These simulations show a potential COP improvement of ~14% (2.46 vs. 2.16) just by swapping the refrigerant in a heat pump with no important modifications to the basic mechanical design of the unit. But, the COP could be improved by ~30% (2.81 vs. 2.16) if the basic mechanical design of the heat pump was modified to include blend composition control capability. In other words, to get the total benefit of the refrigerant mixture glide, the air flow rates and the air coils' circuiting should be revised or redesigned. The design of refrigerant mixtures is a promising approach for heat pumps COP improvement. The next steps in this project will be to confirm experimentally the performances predicted by the model and to design a heat pump unit adapted to refrigerant mixtures with a strategic temperature glide.

Canadian Team Report

IEA HPT TCP Annex 41
"Cold Climate Heat Pumps"

CanmetENERGY Task 2 and 3 Efforts

Submitted by:

Daniel Giguère (contact: daniel.giguere@canada.ca)

Natural Resources Canada

CanmetENERGY
Natural Resources Canada
Varennes, Québec

December 2016

Disclaimer:

Neither Natural Resources Canada nor any of its employees makes any warranty express or implied, or assumes any legal liability or responsibility for the accuracy, completeness or usefulness of its contents. Reference in the report to any specific commercial product, process, service or organization does not necessarily constitute or imply endorsement, recommendation or favouring by Natural Resources Canada. The views and opinions of authors expressed in this report do not necessarily state or reflect those of Natural Resources Canada.

Funding for this work was provided by Natural Resources Canada through the Program of Energy Research and Development.

TABLE OF CONTENTS

LIST OF TABLES

LIST OF FIGURES

1 INTRODUCTION

Most of the energy consumed by Canadian buildings is used for space heating. Energy sources for space heating include electricity, natural gas, oil, propane and wood. As by-products of energy production and consumption, air pollutants and greenhouse gas emissions have an impact on the environment. Thus, by reducing a building's energy use, in addition to an economic benefit through less electricity and/or fuel consumption, savings will also contribute to a reduced environmental footprint. To achieve a significant reduction of a building's primary or secondary energy consumption, the use of renewable energy sources to meet space heating loads is necessary. While solar thermal energy can meet a portion if not all of a building's space heating load, not all building types or locations are suitable to harness this resource and often require a large thermal storage volume for non-coincident space heating loads. Heat pumping technologies on the other hand, by upgrading the available energy from the air, ground or water, are capable of meeting a building's space heating load with 50% or more of the energy coming from a renewable energy source. Heat pump systems are in addition much easier to adapt to a building than a large scale solar thermal systems and are thus one of the technologies, which can have a significant impact in reducing the space heating energy consumption of buildings.

Today, heat pumps are not the preferred appliance for space heating in Canada. The research work undertaken at Natural Resources Canada/CanmetENERGY–Varennes (Canmet) is aimed at improving the performance and first cost of heat pump technologies through simulation and experimental based research to make it them more attractive to the market.

This report describes four research projects conducted by Canmet to improve cold climate heat pump technologies. All these research projects are in progress and have started during the Annex 41 activities. The actual market situation of heat pumps is introduced in the Canadian context chapter. In this chapter, we present some statistics on heat pumps and we list market barriers for their adoption. Each research project is introduced through a short description followed by a rationale and finally a very short discussion of the findings or status of the project. A list of Canmet's scientific papers published during the Annex 41 is provided in the last chapter of this report.

Finally, the conclusion gives an overall summary of the research activities presenting and highlighting the cost and technological improvements currently being worked on to increase market adoption and performance of heat pump systems in Canada.

2 HEAT PUMPS IN THE CANADIAN CONTEXT

Space heating is the major energy end use in the Canadian building sector. In the residential sector space heating represents close to 62% of the secondary energy end use. For the commercial and institutional sector, over 46% of the secondary energy consumption is for space heating. Space heating design temperatures vary from -30°C to -20°C for the majority of populated regions in the country. Electricity and natural gas are the two main sources of energy used for space and water heating.

The use of heat pump technology is essential to reduce significantly and economically the energy consumption for residential and commercial building space heating. This is the only end use technology that shows efficiency (coefficient of performance or COP) greater than one. This high performance is possible because a part of the heat pump capacity comes from a renewable (and free) energy source such as: ambient air, ground, solar or water. The decarbonization of the electricity used to activate heat pumps can also support the adoption of this technology as greenhouse gas emissions to meet space heating loads would be lower

than conventional fuel fired space heating systems. However, unlike fuel driven boilers or electric baseboard heaters, the efficiency of air source heat pumps varies strongly with ambient temperature. At low ambient temperatures their COP and the capacity drop. While ground source and water source heat pump efficiencies and capacities do not rely on the ambient temperature, these types of systems have a much higher initial investment cost over conventional space heating systems.

In 2013, the stock of heat pumps for residential heating was 719 000 on a total of 15 million homes in Canada of which 100 000 installations are ground source heat pump systems. The stock of residential air source heat pumps increases only by 30,000 units per year (Natural Resources Canada, n.d.), with the Canadian GeoExchange Coalition estimating that close to 12 000 ground source heat pump systems are installed annually (Canadian GeoExchange Coalition, 2012). Interestingly, with the increased demand for comfort during the warm summer months, the split air conditioning market has grown exponentially over the past decade, with close to 300,000 split air conditioning systems having been sold in 2014 (HRAI, 2014). This provides an interesting opportunity to introduce reversible heat pumps in the Canadian sector through the space cooling market.

From a GHG emissions perspective, 36% of homes in Canada use electricity as the main source of space heating. Thus, regardless of the electricity generating source (hydro, nuclear, oil etc.) heat pumps with a seasonal efficiency close to 200%, can achieve significant GHG emission reductions. For the 10 million homes that use natural gas or oil as the main space heating fuel source, heat pump systems can also achieve significant GHG emission reductions; however the savings are highly dependent on the electricity generating source. For regions where coal or oil is the primary electricity generating fuel, the seasonal efficiency of a heat pump must be between 250% and 300% to achieve GHG emission reductions.However, several barriers exist, which limit market adoption of heat pump technologies. The barriers are:

- The high first cost of the heat pumps and auxiliary systems.
- The low energy cost and small ratio of fossil energy to electricity cost (in some regions natural gas is 8 times cheaper than electricity per unit of energy).
- The efficiency and capacity of conventional air source heat pumps diminish at low ambient temperatures.
- Air source heat pumps, the most affordable and common system in the market, requires a full capacity auxiliary heating system.
- Ground source heat pumps exceed the efficiencies of all other space heating technologies. However, the investment cost is too high to get a significant market acceptance.

As a result, it is important to develop specific technologies that can be integrated in heat pump systems in order to maintain high performance (capacity and efficiency) at low outdoor temperatures and decrease capital cost. Over the past five years, Canmet has performed simultaneous R&D on two fronts to address this issue – a simulation based approach to assess market barriers and experimental based to demonstrate the potential of improving a heat pumps performance in Canada's cold climate and high initial first costs.

With a database of residential and commercial building energy models, the simulation based analysis is used to identify promising combinations of renewable energy and heat pump systems across different Canadian regions in addition to identifying market barriers to make heat pump systems an economically viable solution in Canada. The simulation models are used to help guide the research in improving heat pumps.
The experimental based research projects conducted over the past five years and explained in more detail in this report are:

- Hybrid ejector - compressor heat pump

- Solar assisted heat pump system
- CO_2 ground source heat pump
- Refrigerant mixtures

3 HYBRID EJECTOR – COMPRESSOR AIR SOURCE HEAT PUMP

The hybrid ejector/compressor system is based on the appropriate integration of compressor and ejector technologies using air as a heat source. Work carried out under a previous R&D project on standard electrically driven heat pump (mechanical compression system) have shown that the replacement of the expansion device by the ejector component and a separator can improve the heat pump performance by up to 15% with a minimal incremental cost. The proposed concept is represented in Figure 1.

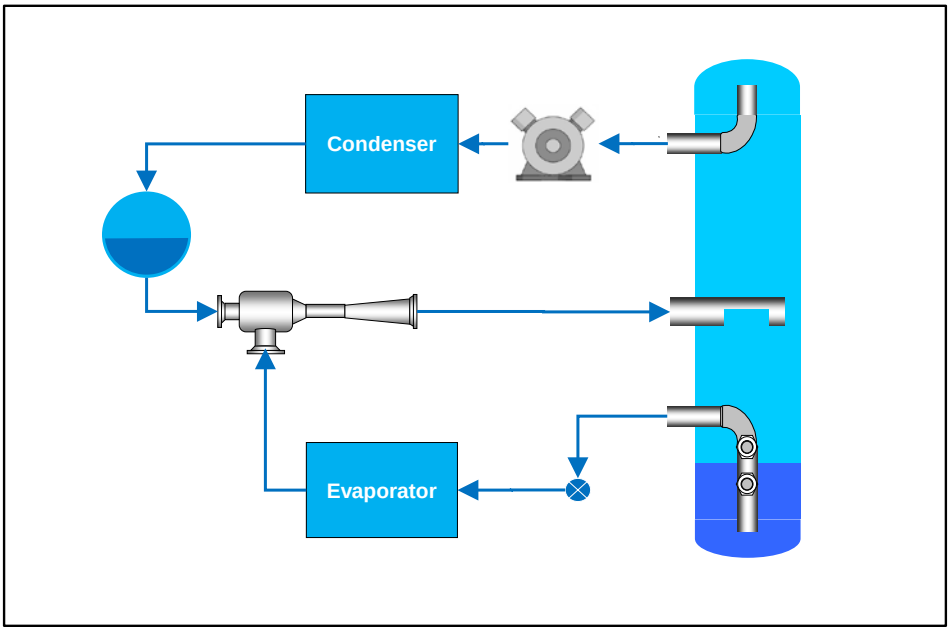

Figure 1: An example of a hybrid ejector/compression air-source HPs

While the system is simple, the main challenge lies in the two-phase-flow that takes place inside the ejector. The two-phase flow ejector is a very complex research field and research findings are not well described in the literature.

To gain a better understanding of the two phase flow ejector and integration, a hybrid ejector/compressor test bench for cooling applications was constructed and some tests performed under a previous research project. The test bench uses a variable speed compressor combined with an electronic expansion valve for maximum flexibility of operation. Its nominal heating capacity is 10 kW, which corresponds to the typical capacity of residential and light commercial applications. This test bench has been upgraded for the purpose of this project with the refrigerant recently replaced from R410A to R-134a due to partial fractionation occurring in the separator. Preliminary results have shown appropriate compression ratios; however, entrainment ratios would need to be improved. Our efforts are now directed towards the development of a better ejector for R-134a (current ejector in test bench was designed for R410a) that will lead to higher entrainment ratios.

Coupled with the hybrid ejector/compressor test bench, a second test bench, dedicated solely to the study of the two phase ejector component was also constructed for this project. Capable of inducing a wide range of operating conditions, the two phase ejector test bench

will generate in depth knowledge and experimental results used to validate numerical models.

These experimental activities, coupled with the modeling work and validation of results, will significantly improve our knowledge on the design of two-phase-flow ejector components and heat pump systems.

4 SOLAR ASSISTED HEAT PUMPS

Heat pumps are a critical tool for reducing building energy use because of their high efficiencies and ability to facilitate the integration of renewable energy sources with building mechanical systems. However, the selection of a heat pump system for cold climates is particularly challenging, as low ambient temperatures in the winter months can result in significant performance penalties for conventional air source units. While geothermal units offer a solution to this issue by using the relatively constant deep earth temperature as a thermal source/sink, associated capital costs with these systems represent a significant market barrier to widespread system adoption.

Solar assisted heat pump systems, which rely on solar energy to supply or supplement heat pump operations, offer an attractive alternative to the air and ground source units more commonly found in the Canadian market. Solar based systems are often challenging to design and implement because they (i) require significant thermal storage capacity to bridge the temporal discrepancy between solar availability and thermal demand, and (ii) experience reduced collector efficiencies in the winter months when thermal demand in cold climates is highest. To address these issues, Canmet has worked extensively on the development of a new solar heat pump concept using ice-based latent storage. This section of the report details both the heat pump concept and a corresponding test bench used to demonstrate the proposed technology.

4.1 Ice as a Latent Storage Material

Using ice-based storage has several advantages, including:

- Increased Energy Storage Densities. The latent heat available from the melting/solidification of ice (333 kJ/kg) is significantly higher than for other commonly used phase change materials. This results in higher energy storage densities and smaller tank sizes.
- Stable Heat Pump Source Temperatures. The phase change temperature of ice places a lower limit on source temperatures for the heat pump evaporator. This allows for more stable heat pump operations (especially in comparison to air source units), increasing the reliability and life expectancy of the heat pump.
- Improved Solar Collector Efficiencies. Using ice storage allows for a low temperature fluid to be circulated to the solar collectors. This improves collector efficiency, allowing for increased thermal gains per unit of collector area while also extending collector utilization periods. Figure 2 shows the impact of the inlet fluid temperature on solar collector efficiency for three values of incident solar radiation. Lower inlet temperatures significantly improve the solar collector efficiency, especially at reduced levels of incident radiation.

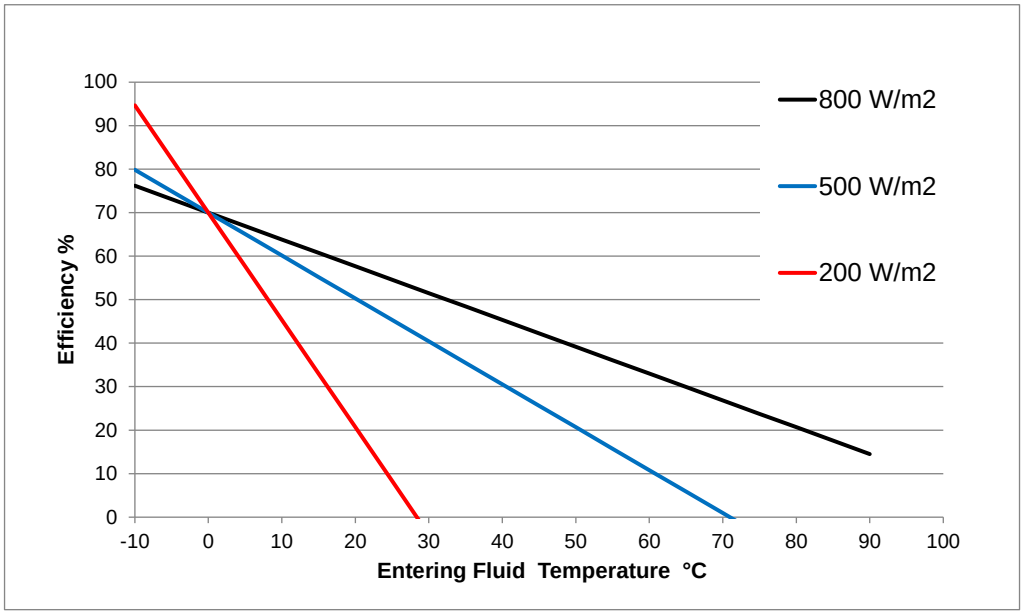

Figure 2: Glazed liquid flat plate collector efficiency at 0°C ambient temperature

4.2 Ice-based Solar Heat Pump Concept

Figure 3 shows the proposed solar heat pump concept in heating mode, as integrated into a Canadian home. Solar collectors operate against the ice tank, allowing for high collector efficiencies while extending the amount of time that the collectors can achieve useful thermal gains. This is particularly important in the winter months, where cold outdoor air temperatures often limit gains from typical solar combi-systems using warm water storage. A heat pump is used to upgrade the low temperature thermal energy from the collectors for use in the home. Depending on the configuration, the heat pump sink can include a low-temperature air handling unit, a radiant floor, or a hot water tank.

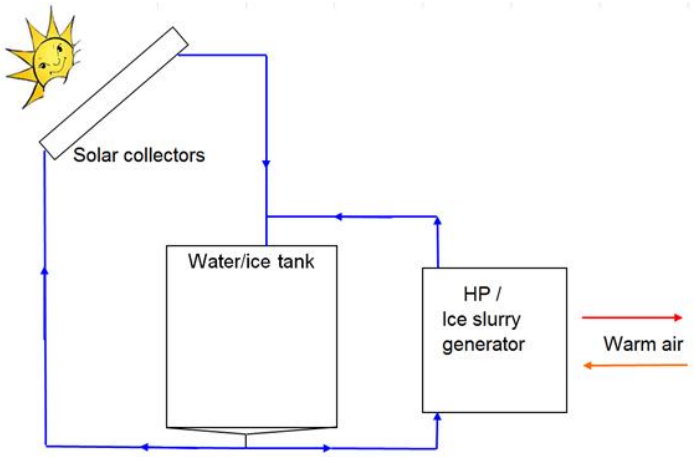

Figure 3: Solar-assisted heat pump system

Detailed annual simulations of these systems in TRNSYS have demonstrated the significant energy savings potential for heating and DHW in high performance Canadian housing (Tamasauskas et al., 2012). These energy use reductions can reach 66% in Montreal and Toronto, and 61% in Vancouver, in comparison to a home using electrical resistance elements for heating and DHW preparation.

4.3 Solar-assisted Heat Pump Test Bench

A test bench of the proposed system has been constructed at Canmet to more fully examine the potential of this system in reducing heating-related energy use. In addition to demonstrating the system concept, the test bench also served a number of additional purposes including validating the simulation models, identifying optimal operational strategies, and developing a deeper understanding of the system and its operations.

A simplified diagram of the developed test bench is provided in Figure 4, indicating all major equipment and measurement points. A propylene glycol mixture was used as the working fluid.

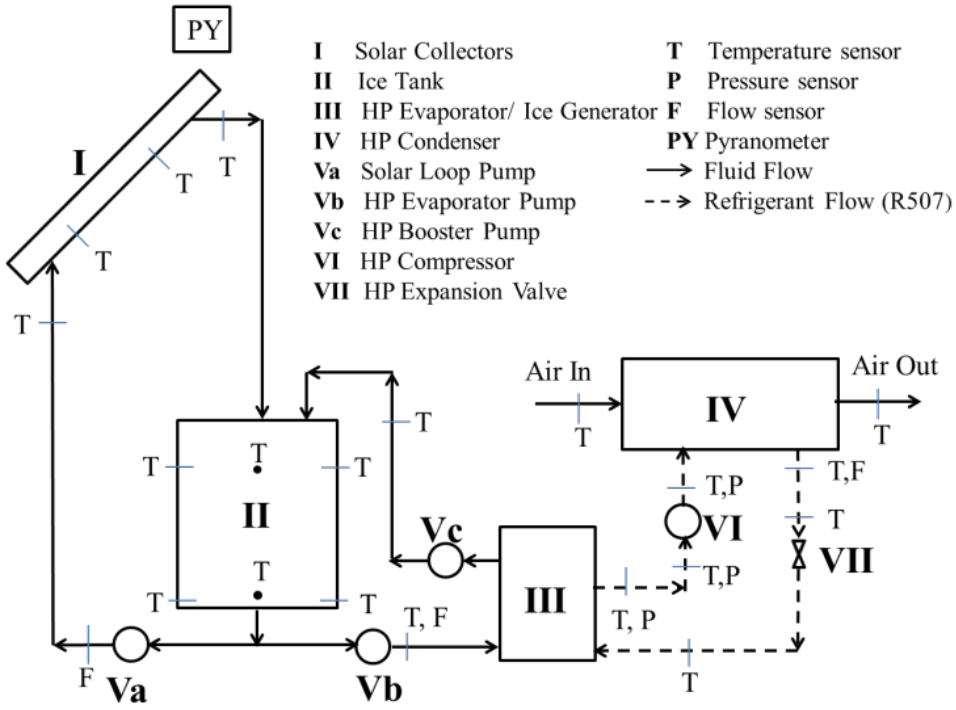

Figure 4: Solar-assisted heat pump test bench

4.3.1 Test bench components

The test bench consists of several key components:

- Solar Collectors: Four Thermo Dynamics G Series glazed flat plate collectors are used, with a total gross area of approximately 12 m^2. The collectors face directly south, with a title angle of 66°.
- Ice Tank: The ice tank has a total volume of approximately 5 000 L. The tank fluid mass is 3 695 kg, and consists of an initial 4% (by mass) propylene glycol/water solution with a freezing point of -1.1°C (30°F). The tank is not mixed: Ice and water are allowed to separate into separate layers via gravity.
- Heat Pump/Ice Generator: The heat pump is a Mueller E-STAR HIPERFORM, with a nominal heating capacity of 15 kW. The ice generator used is the Mueller MaximICE.
- Pumps: Two B&G 3530 circulation pumps are used, with each pump rated at 0.75 HP.

- Data Acquisition: Control and data acquisition are provided using a SCADA system Scadapack 334.

4.3.2 Test bench results

Table 1 provides a monthly summary of key metrics from the test bench from October 2015 to March 2016. It is clear that using a cold temperature working fluid significantly boosts the solar collector efficiency, with an average value over the heating season of 72%. The significant dip in collector efficiencies from January through March can be explained by a larger temperature difference between the inlet fluid and outdoor air, and a reduced amount of incident solar radiation due both to sun position and an increased number of cloudy days. The collectors captured approximately 4 600 kWh over the test period, which, if combined with a heat pump at a COP of 3.3, could supply up to 6 300 kWh of thermal energy for space heating and DHW. Heat pump performance is also improved by relatively constant average source temperatures of around 0°C, allowing for more stable heat pump operations (especially in comparison to air-source units).

Table 1: Solar panel performance combined with the propylene glycol/water tank

2015/2016	Oct.	Nov.	Dec.	Jan.	Feb.	March	Total/avg
*Average Ambiant Temperature (°C)	10.8	8.7	4.5	-3.3	-4.4	2.6	3.15
Average inlet Fluid Temperature (°C)	0.2	0.1	-1.1	-0.4	-0.3	-0.1	-0.3
Tfluid - Tamb (K)	-10.6	-8.6	-5.6	2.9	4.1	-2.7	-3.4
Solar energy (kWh)	1,300	1,074	425	946	1,035	1,597	6,377
Absorbed Solar energy (kWh)	1,082	873	346	554	629	1,096	4,580
Efficiency (%)	83%	81%	81%	59%	61%	69%	72%

* Note Average value during the operation of the test bench

4.4 Summary and Design Recommendations

Extensive simulation and experimental work has been undertaken to develop a novel solar heat pump system using ice-based thermal storage. Using validated energy models, it is estimated that such a system can reduce the energy use for heating and DHW in high performance homes between 61% and 66%, depending on the location of the building.

Table 2 summarizes projected system sizing for typical existing homes in Eastern Canada (e.g. Montreal). Provided that the ice generation/storage technology can be sourced at a reasonable cost, the proposed system offers a cost-effective alternative to the current generation of ground-source heat pumps, and is particularly interesting for retrofit applications where it may be difficult to add ground heat exchangers.

Table 2: Suggested system design parameters for typical Canadian housing

Parameter	**Suggested Value/Range**
Solar Collector Area	30 m^2 to 40 m^2
Ice Storage Tank Volume	Approx. 5 m^3
Heat Pump/Ice Generator Capacity	3 tons (10 kW)

5 CO_2 GROUND SOURCE HEAT PUMPS

Ground source heat pumps (GSHP) are one of the most efficient commercially available space heating systems in Canada. GSHPs use a constant ground source temperature throughout the year yielding a high annual COP (~3) reducing the space heating energy consumption by up to 65%. The main benefits of ground source heat pumps are:
Almost insensitive to ambient temperature variations

- High seasonal COP
- Almost constant heating capacity even during very cold ambient temperature
- Auxiliary heating system not required or with a low capacity
- High reliability

The main barrier for the market adoption is the first cost and thus the main objective of the project is to find ways to reduce the initial investment cost or further increase the efficiency of the system to make it a more attractive solution. Furthermore with the phase-out of HCFC refrigerants now in effect for new equipment and the next step phasing down HFC refrigerants, several projects are evaluating the feasibility of using CO_2 as the working fluid. CO_2 has a low global warming potential and the thermo-physical properties provide several advantages. The following sections describe in more detail to work undertaken.

5.1 A New Equation for Undisturbed Ground Temperature

For ground source heat pumps systems, the cost of the vertical boreholes is very high and contributes to hindering larger market adoption. The quantity and depth of these wells is estimated from models that depend on several factors including the undisturbed ground temperature. In general, the temperature deeper than 10 meters remains unchanged throughout the year (see Figure 5). Given that vertical boreholes have depths less than 300 m, most of the heat exchange surface depends on the ambient temperature of this region.

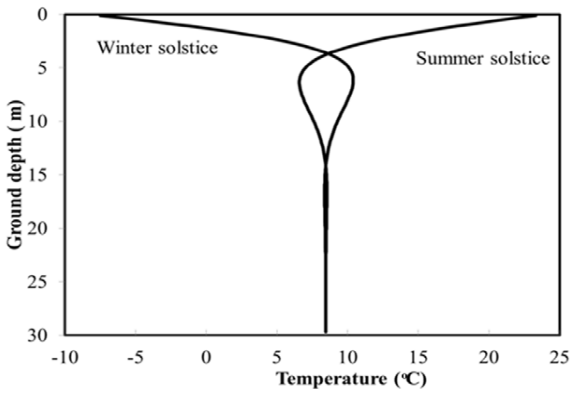

Figure 5: Typical ground temperature profile

The equation (1) published in 1965 (T. Kasuda et al., 1965) is often used to estimate the ground temperature profile. This equation is highly dependent on the annual average ground surface temperature, which is equivalent of the undisturbed ground temperature $\overline{T}s$. In absence of a measured value of the undisturbed ground temperature, the mean ambient temperature may be taken as $\overline{T}s$ in this equation to represent the undisturbed soil temperature. This assumption underestimates the actual undisturbed ground temperature and therefore overestimates the length or depth of the underground heat exchanger.

$$T(z,t) = \overline{T}s - As.e^{-Z/\delta}.\cos(\omega t - \emptyset s - Z/\delta) \quad (1)$$

A linear correlation between the undisturbed soil temperature and the annual average ambient temperature was developed based on the available data from several sites around the world. The new linear correlation (Figure 6) applies to all climates, ranging from the most northern permanently inhabited place in the world – Alert, Nunavut with mean ambient temperature of -17.7°C to Dhahran (Saudi Arabia) with mean ambient temperature of +25.9°C. The average error of the ground temperature correlation is less than 1°C and superimposing the undisturbed ground temperature isotherms on a geographical map of Canada (Figure 7) shows that the temperature ranges from 6 to 12°C in the most populated regions. Comparing this to the annual average ambient temperature typically used to calculate the borefield length (Equation (5) in ASHRAE HANDBOOK 2015 - p.34.15) the corresponding undisturbed ground temperature is 4°C higher. In Montreal, using the correct undisturbed ground temperature, the required borefield length would be 37% shorter resulting in significant drilling and material cost savings.

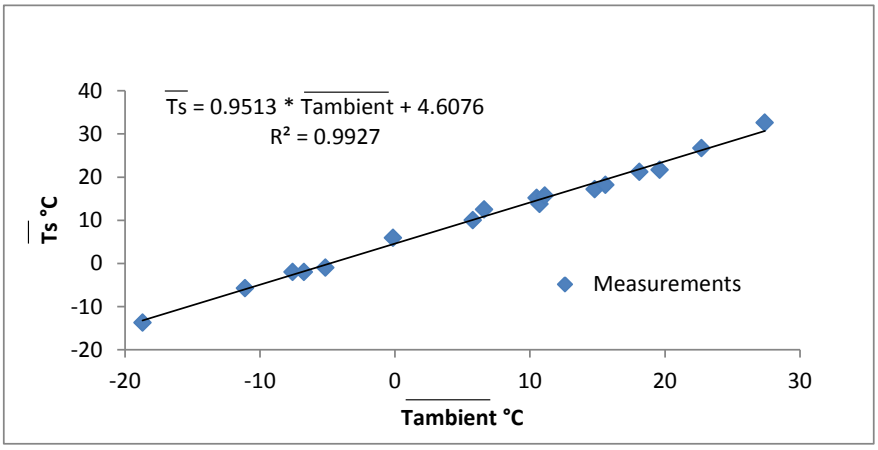

Figure 6: Undisturbed ground temperature correlation

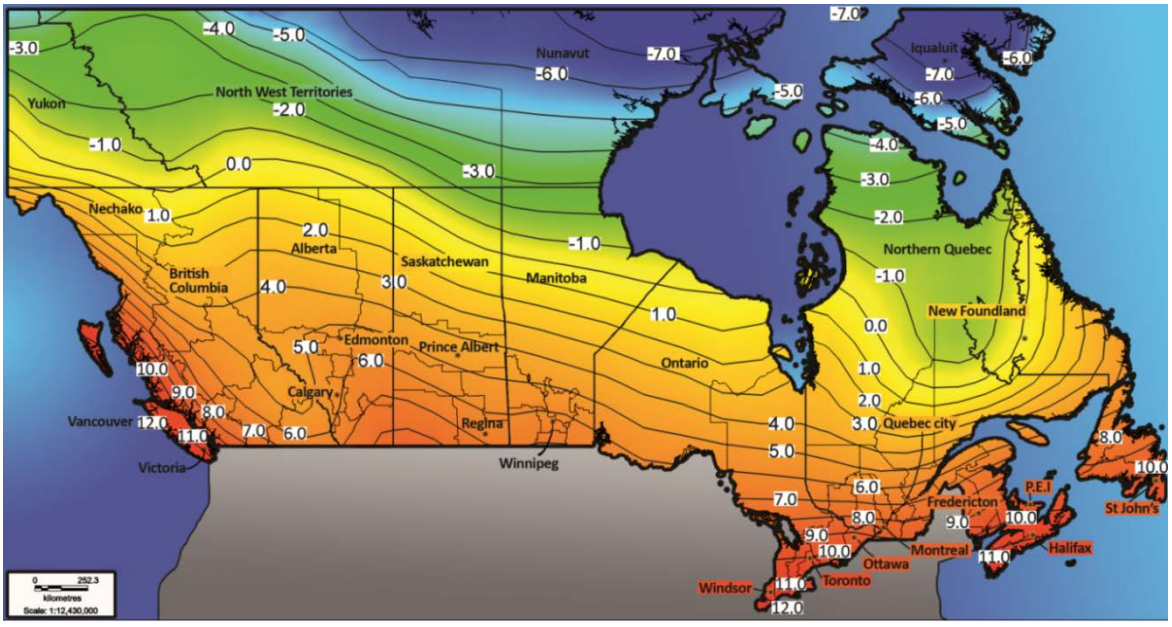

Figure 7: Undisturbed ground temperature isotherm Canada map (°C)

5.2 Investigation of CO_2 Ground Heat Exchanger

In the perspective of reducing ground loop cost and risk of underground contamination, one of the most promising technological solutions resides in the usage of an environmentally

friendly phase change circulating fluid in the ground coils instead of antifreeze solutions. The constant temperature of the phase change fluid in the boreholes pipe and the constant temperature of the ground below 10 meters result in constant heat transfer profile in the ground heat exchanger. Under this condition, the ground source heat pump efficiency and capacity is higher or for a given capacity a smaller (and cheaper) ground coil would be required.

The work performed consisted of investigating the replacement of synthetic refrigerants in DX systems by natural refrigerant, such as CO_2, and developing simulation and design tools for DX ground source heat pump applications.

CO_2 as a phase change circulating fluid in the ground heat exchanger is seen as a promising alternative to synthetic refrigerants. CO_2 is a naturally occurring substance, has low cost, is not toxic or flammable, does not represent a threat for ground water contamination and has a global warming potential of 1. CO_2 does not require special material selection for corrosion prevention, and requires less circulation pumping energy. CO_2 as a phase change heat transfer fluid has been successfully applied in refrigeration technologies in Canada (and the world) such as in supermarkets and in ice rinks and heat pumping solutions are gaining increased interest.

The objective of this work is to contribute to the advancement of underground heat extraction technologies using CO_2 as a phase change fluid carrier, and to provide a cost effective and environmentally friendly alternative to GSHP systems commercially available today. The work consists of conducting experimental work on a new test bench at Canmet facility, and developing simulation models to support the optimization of CO_2 ground loop configuration and operation.

- The work performed includes:
- Design and construction of a test bench including boreholes drilling
- Experimental work on the test bench
- Development of a simulation model for the hydrodynamic behaviour of CO_2 in ground coils. The experimental data will be used to validate the simulation model
- Identification of ground loop configuration and design parameters leading to better heat transfer performance

5.2.1 CO_2 vertical borehole numerical model

A new numerical model of a CO_2 vertical direct expansion borehole has been developed. The model was validated with experimental data (ground and circulating fluid temperatures) extracted from scientific literature. This model uses the finite volume method which allows calculating profiles of temperature, pressure and quality of the refrigerant along the U-tube. Figure 8 shows a schematic representation of the borehole section and the type of discretization used in the numerical model. The dimensions of this borehole correspond to the boreholes drilled and tested at Canmet facility. Note the tube diameters, 6.4 mm OD for the supply and 8 mm OD for the return. These diameters are very small compared to the 20 mm to 50 mm diameters used usually with secondary fluid.

For each element of volume, the model calculates the temperature, the pressure, the quality of the refrigerant and heat flux exchanged between the ground and the refrigerant.

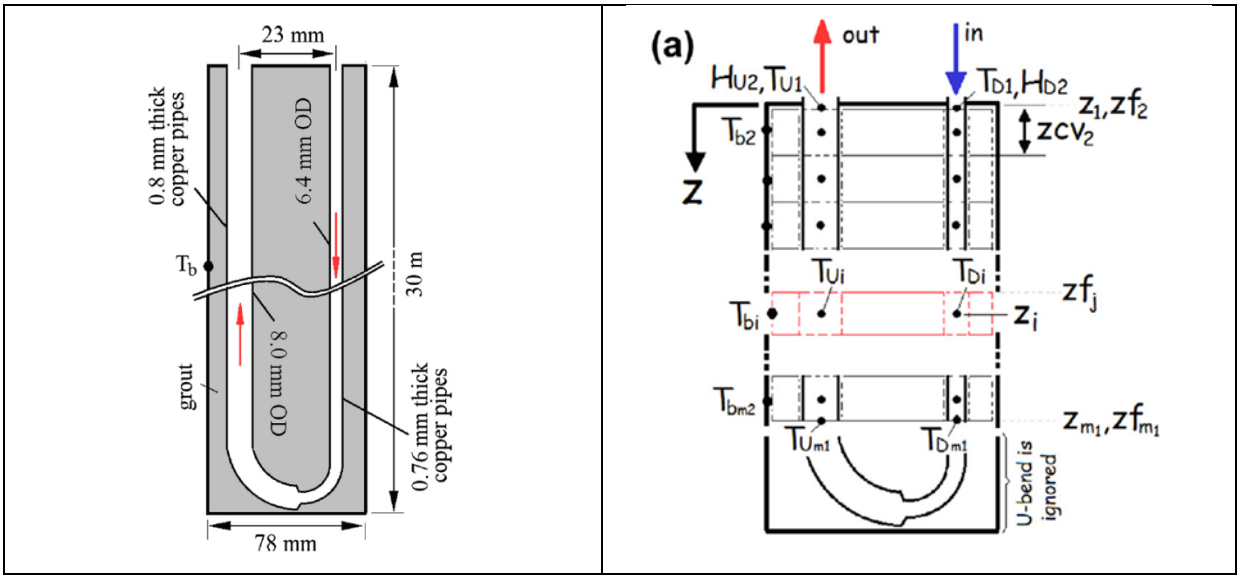

Figure 8: Schematic representation of the borehole divided into small control

Using the numerical model to simulate the system in heating mode (underground heat exchanger being the heat pump evaporator), the following observations and benefits of using CO_2 as the working fluid were found.

- The CO_2 pressure loss across the borehole U tube is 194 kPa. This pressure loss corresponds to a saturated temperature drop of 2.1°C. A similar pressure loss would cause a temperature drop of 14.3°C for R22 or 8.4°C for R410A. With such a temperature drop, the COP of the heat pump would be severely penalized. CO_2 is much less sensitive to pressure drop than synthetic refrigerants, which enables the downsizing of the borehole U tube diameter.
- The temperature of the ground near the surface is sometimes lower than the temperature of the CO_2 in the tube. Consequently, the CO_2 gas temperature decreases slightly in the first 3 meters of U tube. This temperature drop is a loss that can be reduced by insulating the first metres of tubes near the ground surface.
- The underground heat exchanger performance is 13.6 m/kW, which compares favorably to the conventional secondary fluid borehole that shows 17 to 26 m/kW with 20 mm to 50 mm pipe diameters (Natural Resources Canada, n.d.).

5.2.2 Effect of the number of boreholes

As part of the simulation R&D activity, Canmet has developed detailed building energy models representative of the Canadian residential building stock in TRNSYS v. 17. To evaluate the potential of ground source heat pump systems across Canada, a vertical ground source heat pump was incorporated into the model for comparison to other space heating systems. Using the energy model, the effect of the number of boreholes connected in parallel on the energy consumption for space heating of a 210 m^2 house located in Montreal, Canada was evaluated. Details of the housing model can be found in the publication by Kegel et al. with key characteristics summarized below:

- Annual space heating load 29 270 kWh
- Annual DHW load 5 340 kWh
- Peak space heating demand 14.3 kW

Simulating a direct expansion ground source heat pump using CO_2 as the working fluid the seasonal COP of the system was calculated for different borefield comprised of 2, 3, 4 or 5 30 m boreholes. The system provides a nominal heating capacity of 4 kW with Figure 9

showing the key elements that have been simulated. The heat pump operates in a transcritical cycle mode.

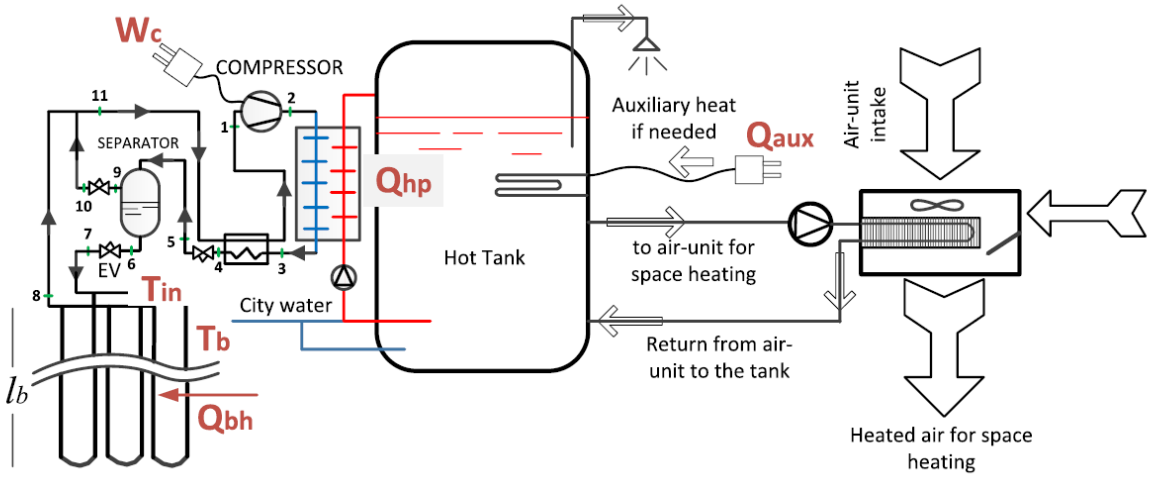

Figure 9: CO_2 GSHP-DX system

The simulation results are plotted in Figure 10 showing the seasonal coefficient of performance (compressor power only) versus the number of 30 m boreholes in the borefield.

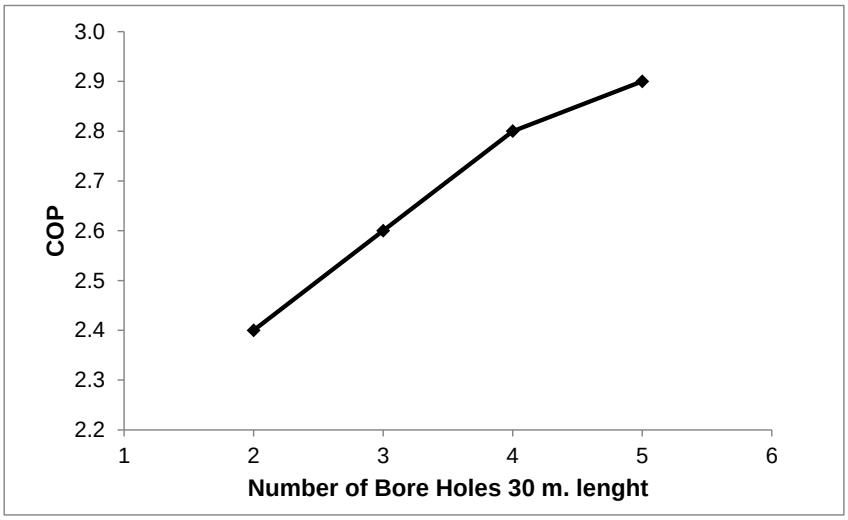

Figure 10: Seasonal COP of a DX-GSHP system

The seasonal COP of the heat pump increases by 21% for a 150% increase in borehole length. For the same scenario, the heating capacity of the heat pump increase by 15%. This demonstrates the importance of the borehole sizing on the efficiency of the heat pump.

5.2.3 Effect of heat pump type, heat pump capacity and number of boreholes

The aim of this work is to compare the seasonal COP of different cases of heat pumps by varying the number of boreholes and the heat pump capacity. Building upon the Montreal residential building energy model (Kegel et al., 2012), three types of heat pump systems were incorporated into the model and parametric studies conducted on nominal heat pump capacities and the number of boreholes.

- Systems: Direct expansion ground source heat pump (GSHP), air source heat pump (ASHP) and hybrid heat pump combining ground source and air source (HGSHP)
- The HGSHP takes advantage of the mild outdoor temperature at the beginning and end of the heating season
- Nominal capacities: 3.09 kW, 4.27 kW, 5.42 kW, 6.34 kW, 7.77 kW and 9.32 kW
- Number of boreholes: 1 to 5 depending on nominal GSHP capacity

A 10 year simulation for the typical Montreal house is run with the aim of taking into account the long term ground temperature profile evolution. The results of the simulation are shown in Figure 11. Further detail and description of the cases evaluated can be found in the technical paper by Eslami-Nejad et al. (2016). Overall, 6 ASHP, 13 GSHP, and 13 HGSHP systems were studied with 6 different compressor sizes with a 10 year space heating load of 293 MWh (29 270 kWh*10 years).

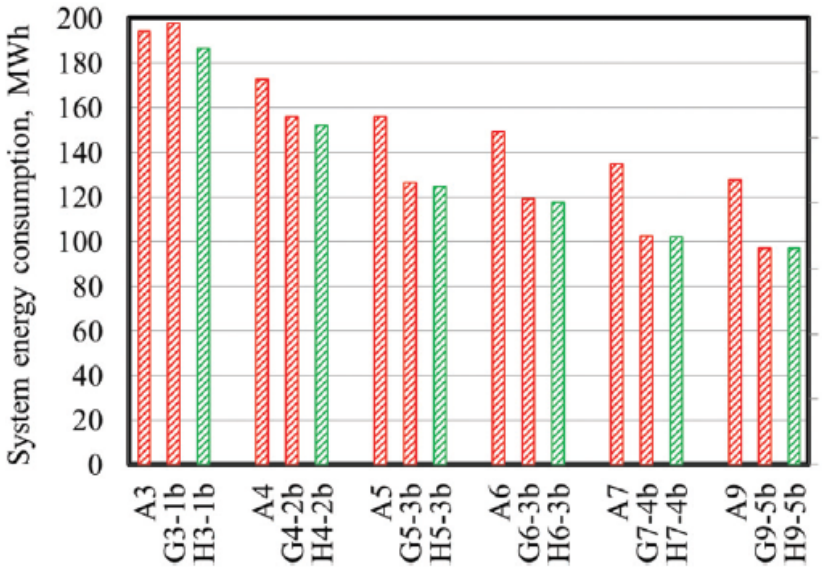

Code Nomenclature

- First Character – System Type - A: ASHP, G: GSHP, H: HGSHP
- Second Character – Nominal Capacity – 3: 3.09 kW, 4: 4.27 kW, etc.
- Last two Characters – No. of boreholes – 1b: 1 borehole, 2b: 2 boreholes etc.

Figure 11: System energy consumption during 10 years

The following conclusions were drawn from the simulation results:

- The capacity of the heat pump is an important factor for energy savings
- The ASHP system consumes more energy than the ground source heat pump except for the smallest capacity
- The ASHP A7 and A9 consume 30% more energy than the equivalent GSHP capacity. Since the first cost of ASHP is much lower than the GSHP, this 30% energy difference does not cover the extra cost of a GSHP installation. So, a properly sized ASHP is a good option
- The heat pump must have a nominal heating capacity of at least 5.5 kW to achieve a significant reduction of energy consumption. This minimum capacity is about 40% of the maximum heating demand of the residence (14.3 kW)
- In this graph, the case GSHP G7-4b with a nominal heating capacity of 7.7 kW and 4 boreholes of 30 meters deep, gives a good ratio of energy consumption reduction vs nominal capacity. This capacity is about 55% of the maximum heating demand of the residence (14.3 kW). G7 corresponds roughly to a nominal capacity 2 ½ tons or

30 000 BTU/h for the North American market. This value is close to the typical 3 tons capacity often used in ground source heat pump application for the residential sector
- The results show no significant benefit for the HGSHP cases

This work shows the importance of the proper sizing of the heat pump capacity for a specific application. GSHPs show the lowest energy consumption, but ASHPs remain the most attractive heat pumping option for residential users. Future work on GSHPs should continue to address overcoming the high cost or achieving improved seasonal efficiency by meeting DHW loads in addition to space heating loads.

6 REFRIGERANT MIXTURES

The use of refrigerant mixtures is becoming more and more common in air conditioning and refrigeration. In 1965, the ASHRAE Guide and Databook Fundamentals and equipment published three azeotropic refrigerant mixtures: R500, R501 and R502. In 2013, the 'ASHRAE Handbook Fundamentals' listed 65 zeotropic mixtures and 14 azeotropic mixtures. This number is growing each year. These new blends meet the need of the market which must deal with the phase-out and phase-down of CFCs, HCFCs and HFCs. To replicate the performance and characteristics of these refrigerants for specific applications it was necessary to create this diversity of mixtures.

One of the features of zeotropic blends is the temperature glide (Figure 12). At constant pressure, the mixture boiling temperature (bubble point) is lower than the condensing temperature (dew point). For most of the zeotropic mixtures the temperature glide is less than 1°C (like R410A). For other mixtures, such as R407C, it is 5.5 °C. By matching the temperature glide of the refrigerant with the temperature glide of the fluid to cool in an air conditioning or chiller system, a 10 to 15% COP improvement can be achieved with a temperature glide of 5.5°C. If the application allows a temperature glide of 10°C, the COP of the heat pump could be improved by up to 30% theoretically.

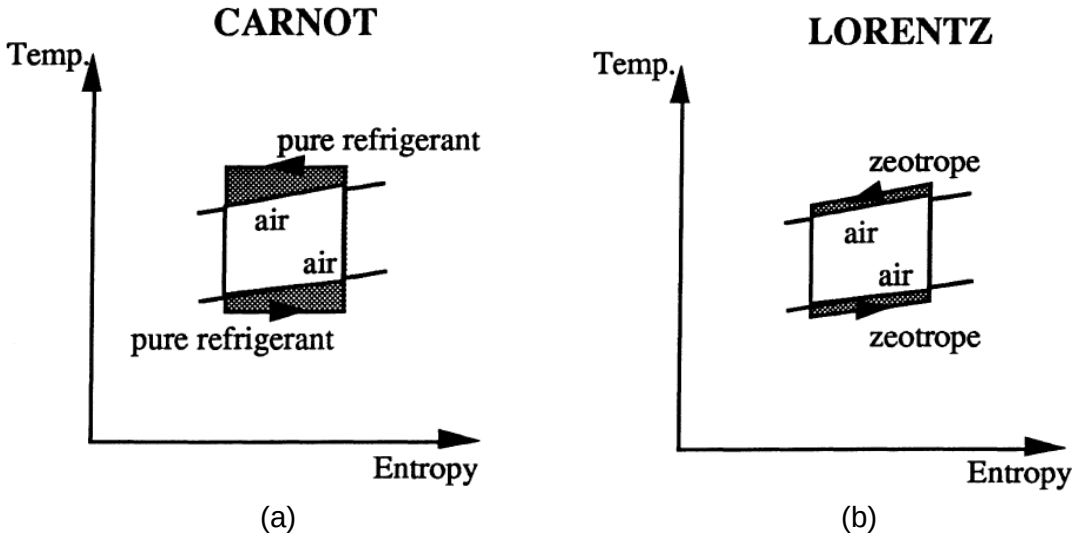

Figure 12: (a) Typical Carnot refrigeration cycle (b) Lorentz cycle demonstrating temperature glide

The majority of heat pumps use refrigerant HFC R410A which is a 50/50 mixture of R32 and R125. One of the components, R32, is an A2L class refrigerant according to safety standards. The 2L means it is lightly flammable and cannot therefore be used in residential

or commercial applications. The R32 offers better thermodynamic performances than the R410A mixture, but the addition of R125 changes the safety class to A1, non-toxic and non-flammable, so it may be used widely. However, R410a has a high global warming potential (GWP) of 2 100, and with upcoming requirements the use of this refrigerant will soon be restricted. There is therefore a strong need to identify new refrigerants, which have a low GWP, but also do not diminish the performance of these heat pump systems.

The main objective of Canmet's refrigerant mixture project is to identify one or more refrigerant mixtures to improve the performance of a cold climate air source heat pump with having an acceptable GWP. The research project is broken down into two phases:

- Phase I: Develop a detailed model of the heat pump to identify one or more mixtures of refrigerants to achieve the objective.
- Phase II: Conditional to the outcome of the Phase I, experimentally validate the theoretical results on a prototype.

This report reflects the results of the first phase only as phase II is currently underway.

Development of a Detailed Heat Pump Model to Evaluate Different Refrigerant Mixtures

A heat pump simulation model was developed, which was designed to permit changing/simulating a different refrigerant without modifying the main components of the heat pump: compressor, evaporator and condenser. The performance of the compressor is calculated from a polytropic model with a constant coefficient of polytropic efficiency. The condenser and the evaporator are two finned tubed air coils. The air coils are divided into several volume elements. The equations of heat and mass transfer, momentum, mass and energy balance are solved for each volume element in order to calculate the overall air coil performance.

Many refrigerant mixtures have been simulated with this model. Among all the mixtures studied, R-32/CO_2 (80/20) mixture presents better performance potential for the purpose of this study. The mixture is non-toxic with a GWP of approximately 540, which is 75% lower than the GWP of R-410A. Moreover, it is a zeotropic mixture with approximate temperature glides of 6°C and 8.5°C in the evaporator and condenser respectively.

Although, the R32 safety classification is A2L (2L for slightly flammable), the addition of CO_2 could mitigate the mixture flammability. Another aspect of this mixture is the operating pressure. The CO_2/R32 mixture would operate at a higher pressure than the R410A heat pump. Therefore, the heat pump mechanical design should withstand the pressures according to the concentration of CO_2.

Some refrigerant mixtures developed for the commercial market use hydrocarbons in low concentration but none, to the best of our knowledge, use CO_2. The addition of CO_2 to a refrigerant mixture decreases the GWP and improves the thermophysical properties such that for a specific capacity the components are smaller.

To assess the performance of various refrigerant mixtures, the residential building energy models presented in section 5 (Kegel et al., 2012) were used. Five refrigerant cases were simulated using the same heat pump components. The reference case (Case 1) is the standard R-410A air source heat pump, with a nominal heating capacity of 7.7 kW at 8°C outdoor temperature. This unit meets 75% of the total space heating load, so 25% of the load was provided by the auxiliary heating system.

The other cases evaluated are:

- Case 2: Same as reference case with a variable speed compressor
- Case 3: Fixed mixture of 80% R32 and 20% CO_2
- Case 4: Variable composition mixture R32 - CO_2 with a reservoir located at the compressor suction to manage the concentration of CO_2
- Case 5: Fixed 80% R32 and 20% CO_2 with a variable speed compressor

The results of the simulation are summarized in Table 3 with the heat pump (HP) contribution indicating the percentage of the annual heating capacity met by the heat pump and the seasonal COP of the system.

Table 3: Simulation results for five refrigerant mixture cases

Refrigerant Case	Capacity	HP contribution	COP seasonal
	kW	kWh/kWh	kWh/kWh
R-410A	7.7	75%	2.16
R-410A VSD	7.7	91%	2.73
R32-CO2 80/20	8.1	84%	2.46
R32-CO2 VC	9.0	93%	2.81
R32-CO2 80/20 VSD	8.1	97%	2.98

These simulations show a potential COP improvement of ~14% (2.46 vs. 2.16) just by swapping the refrigerant in a heat pump with no important modifications to the basic mechanical design of the unit. But, the COP could be improved ~30% (2.81 vs. 2.16) if the basic mechanical design of the heat pump was modified. In other words, to get the total benefit of the refrigerant mixture glide, the air flow rates and the air coils' circuiting should be revised or redesigned. The design of refrigerant mixtures is a promising approach for heat pumps COP improvement. The next steps in this project will be to confirm experimentally the performances predicted by the model and to design a heat pump unit adapted to refrigerant mixtures with a strategic temperature glide.

7 CONCLUSIONS

Heat pumps have long been recognized as critical components of energy efficient buildings. However, in Canada, market penetration remains low, with only 5% of buildings using a heat pump for space heating or DHW. This low figure underlines the challenges and opportunities in developing heat pump technologies for cold climates such as Canada.

The Canadian and North American markets are dominated by air-source heat pumps units. While these units generally exhibit strong performance in mild climates, capacity and overall performance tends to fall significantly below 0°C, requiring expensive, fully sized auxiliary systems. Conventional ground-source heat pump systems offer improved performance in cold climates by using near constant ground temperatures as a thermal source/sink. However, the high costs associated with the ground heat exchanger often limit the uptake of this technology. With these market barriers in mind, Natural Resources Canada/CanmetENERGY-Varennes (Canmet) has worked extensively to develop and promote heat pump technologies for improved performance in cold climates through parallel simulation and experimental based research.

While many market available air source heat pumps experience reduced performance at low ambient temperatures, the addition of new technologies has the potential to improve existing designs with minimal cost increases. Canmet has worked extensively on the integration of

two-phase flow ejectors as a replacement for more conventional expansion valves. Preliminary assessments have suggested an up to 15% improvement in system performance is possible, with minimal additional equipment costs. Additional work in Canada has focused on the potential of new refrigerant mixtures to improve low temperature heat pump performance. Simulated performance of heat pump cycles with identified mixtures have shown potential seasonal COPs exceeding 2.8, again with only small additional costs. Planned work will complement simulation work with experimental analysis to examine the full potential of these modifications.

Heat pump market barriers are also being addressed by extensive work on new ground-source heat pump technologies. By using CO_2 as a working fluid in ground heat exchangers, required borehole lengths can be reduced by between 15% and 45%. This represents a significant savings for building owners, especially when considering that the majority of ground source heat pump costs relate to the ground heat exchanger.

In addition to more established air source and ground source technologies, there is also extensive Canadian research into the use of solar assisted heat pump systems. These systems rely on solar energy to supplement heat pump operations, yielding strong energy savings. In order to address common issues such as storage capacity and collector performance, Canmet has been involved extensively in the development of a solar heat pump using ice-based latent storage using both simulation and a fully equipped test bench. The integration of ice storage offers numerous benefits, including smaller tank sizes, improved solar collector performance, and stable heat pump source temperatures. Heating energy savings of between 61% and 66% are estimated across Canada based on the use of validated simulation models. Provided that ice generation equipment can be sourced at reasonable cost, this system offers an interesting alternative to ground and air-source heat pump systems.

8 NATIONAL PUBLICATIONS IN CONTEXT OF IEA HPC ANNEX 41

M. Ouzzane, P. Eslami-Nejad, M. Badache, Z. Aidoun, New correlations for the prediction of the undisturbed ground temperature, Geothermics 53 (2015) 379-384.

M. Badache, P. Eslami-Nejad, M. Ouzzane, Z. Aidoun, L. Lamarche, A new modeling approach for improved ground temperature profile, Renewable Energy 85 (2016) 436-444

Badache M., Eslami-Nejad P., Ouzzane, M., Aidoun .Z, Lamarche L., Nouvelle approche pour l'évaluation du profil de température du sol, Proc. CIFQ, Sherbrooke, Juin 2015

M. Ouzzane, P. Eslami-Nejad, Z. Aidoun, L. Lamarche, Analysis of the convective heat exchange effect on the undisturbed ground temperature, Sol. Energy 108 (2014) 340e347.

P. Eslami-Nejad, M. Ouzzane, Z. Aidoun, Modeling of a two-phase CO_2-filled vertical, Applied Energy, Volume114, February 2014

Eslami-Nejad P., Ouzzane M., Aidoun Z., 2015. A Quasi-transient Model of a Transcritical Carbon Dioxide Direct-Expansion Ground Source Heat Pump for Space and Water Heating. Applied Thermal Engineering journal, 91, 259-269.

Badache, M., Ouzzane, Eslami-Nejad, P., M., Aidoun, Z., Experimental study of a transcritical carbon dioxide direct-expansion ground coupled heat pump. Energy and building, 2016. (in process)

Eslami-Nejad P., Badache M., Ouzzane M., Aidoun Z., (2017), Direct expansion ground source heat pump using CO_2 as refrigerant: Test facility and theoretical model presentation. Abstract submitted to IGSHPA 2017, Denver, CO, USA.

Eslami-Nejad P., Hakkaki-fard A., Aidoun Z., (2016), Ouzzane M., Technical assessment of ground source, air source and hybrid heat pumps for a single family building in cold climates, submitted to ASHRAE Transaction.

Eslami-Nejad P., Hakkaki-fard A., Aidoun Z., Ouzzane M, 2015. Direct Expansion Ground-Source vs Air-Source Heat Pumps: Is the "Hybrid" System a Solution to Expensive Ground Loop Installations in Cold Climates? 2015 ASME Power and Energy, San Diego, California, USA, 28 June to 2 July

Badache, M., Ouzzane, M., Aidoun, Z., Experiments on a CO_2 direct-expansion ground coupled heat pump. Proc. GSCE, ROME - ITALY, July 2016. (en cours)

Hakkaki-Fard, A., Z. Aidoun, P. Eslami-Nejad, (2016). Evaluation of refrigerant mixtures in three different cold climates residential air-source heat pumps, ASHRAE Transactions, Vol 122, Part 2, June 2016.

Hakkaki-fard A., Eslami-Nejad P., Aidoun Z., Ouzzane M., 2015. A techno-economic comparison of a direct expansion ground-source and an air-source heat pump system in cold climates. Energy journal, 87, 49-59.

Hakkaki-Fard, A., Aidoun, Z., and Ouzzane M., Applying refrigerant mixtures with thermal glide in cold climate air-source heat pumps, Appl. Therm. Eng., 62, 2014, pp. 714-722.

Hakkaki-Fard, A., Aidoun, Z., and Ouzzane M., Improving cold climate air-source heat pump performance with refrigerant mixtures, Appl. Therm. Eng., 78, 2015, pp. 695–703.

Hakkaki-Fard, A., Aidoun, Z., and Ouzzane M., 2014. Air-source heat pumps with refrigerant mixtures for cold climates, 11th International Energy Agency Heat Pump Conference, Montreal, May 12-16.

Hakkaki-Fard, A., Aidoun, Z., and Ouzzane M., Assessment of refrigerant mixtures performance with thermal glide for cold climate air-source heat pumps, HEFAT2014, 10th International Conference on Heat Transfer, Fluid Mechanics and Thermodynamics, 14 – 16 July, 2014, Orlando, Florida.

M. Poirier, J. Tamasauskas, Concept d'une thermopompe assistée par énergie solaire et stockage dans un réservoir eau/glace, CFIQ2015/ART-04-10

M. Poirier, J. Tamasauskas, Démonstration d'un système de récupération et de stockage d'énergie solaire thermique, 84e congrès de l'ACFAS, Colloque 202 : Efficacité énergétique industrielle, 2016

9 REFERENCES

Canadian GeoExchange Coalition, État de l'industrie canadienne de la géothermie 2011 – February 2012

Hakkaki-fard A., Aidoun Z., Eslami-Nejad, P., Ouzzane M., 2016. Technical assessment of ground source, air source and hybrid heat pumps for a single family building in cold climates, ASHRAE Transactions, Vol 122, Part 2, June.

HRAI 2014, http://www.hrai.ca/newsreleases.html

Kasuda T., P.R. Archenbach, Earth temperature and thermal diffusivity at selected stations in the United States, ASHRAE Trans. 71 (1965). Part1

Kegel M., J. Tamasauskas, R. Sunyé, A. Langlois, Assessment of a solar assisted air source and a solar assisted water source heat pump system in a Canadian household Energy proc. 30 (2012) 654-663

Natural Resources Canada, Commercial Earth Energy Systems: A buyer's Guide, ISBN 0-662-32808-6, Cat. No. M92-251/2002E

Natural Resources Canada, Comprehensive Energy Use Database, http://oee.rncan.gc.ca/corporate/statistics/neud/dpa/menus/trends/comprehensive_tables/list.cfm

Tamasauskas, J., Poirier, M., Zmeureanu, R., and Sunye, R., Modeling and Optimization of a Solar Assisted Heat Pump Using Ice Slurry as a Latent Storage Material Solar Energy, Solar Energy, 86(11), pp. 3316-3325, (2012).

Canadian Team Report

IEA HPT TCP Annex 41
"Cold Climate Heat Pumps"

Task 1 - Summary of Prior Activities on Residential Air Source Heat Pumps Undertaken at LTE (Hydro-Québec)

Submitted by:

Brice Le Lostec (contact: lelostec.brice@lte.ireq.ca)

Hydro Québec
Laboratorie des Technologies de l'Énergie (LTE)
Shawinigan, Québec

April 2015

August 2017

TABLE OF CONTENTS

LIST OF TABLES

LIST OF FIGURES

1 INTRODUCTION

Canada's total area is approximately 10 million km^2 and its population is 35.7 million inhabitants (3.57 per km^2). The country is divided into 10 provinces and 3 territories. Québec is one of the 10 provinces and represents 10% of the country's area and 23% of its population. The province's population is mainly located in the south of the province close to the St. Lawrence River. In Québec, heating represents approximately 50% of the energy requirements in the residential sector. Electricity, which is largely hydroelectric (>99%), is the primary energy source (78% in 2014) for residential heating and this ratio has tended to increase over the last decade. Electricity is used as the primary heating source in over 85% of the new houses built between 2005 and 2014. The cost of this energy and that of the resistive heating equipment partly explains the prominence of electricity for this application in Québec.

Hydro-Québec generates, transmits and distributes electricity. Its sole shareholder is the Government of Québec. Primarily, the utility uses renewable energy sources, in particular hydroelectricity; it also supports the development of other energy sources such as wind power and biomass through purchases from independent producers. It is also involved in Research and Development in the energy sector, including energy efficiency.

Heat pumps with electric or fuel-burning back-up devices have been on the Québec market for several decades. In recent years, heat pumps that can operate at very low outdoor temperatures (-25°C to -30°C) have appeared on the market. These so-called cold climate heat pumps are technologies that improve the energy efficiency of residential heating and reduce the power demand during peak winter consumption periods as compared to resistive heating. There are several obstacles to the deployment of these technologies on the market including the lack of criteria for the identification of the equipment, the bias regarding the comparison between energy savings depending on the technology (single stage, variable refrigerant flow (VRF) with injection, etc.) based on the HSPF and the lack of metrics to evaluate the impact on peak power demand.

In order to foster the emergence of cold climate heat pumps on the market, efforts are being made at Hydro-Québec's energy technology laboratory (LTE) to characterize the equipment and propose solutions to promote the deployment of these technologies. This document summarizes some of the work that has been undertaken at LTE:

- Laboratory tests on 4 central heat pumps
- A measurement campaign on 22 heat pumps

2 LABORATORY TESTS

To validate the energy saving potential of central heat pumps, it was necessary to better understand and document their operating modes and performance under different conditions and in different climates. This necessarily involved measuring their performance in the context of experimental laboratory tests. The specifications supplied by heat pump manufacturers cannot replace laboratory tests because the data does not include all the necessary information (defrosting cycle, outdoor temperature, etc.). Laboratory measurements allow to obtain reliable and accurate data in monitored conditions, which can then be compared to measured data in the context of pilot projects. Based on this, calculation models can be developed to estimate the energy savings associated with this type of heating device.

2.1 Tested Devices

The heat pumps were selected based on technologies intended to function under the climate conditions in Québec (Canada) in the winter. The LTE tested four technologies. The first three were air-to-air heat pumps and the fourth was an air-to-water heat pump.

- **Heat Pump #1** was a conventional technology that is considered to be an upscale product and that can operate at temperatures as low as -25°C. The device has two power levels, however its performance curve is similar to that of a conventional heat pump.
- **Heat Pump #2** was a two-stage system that was specifically designed for cold climates. It includes a 2-piston compressor and a booster. The compressor functions depending on the needs – either with 1 piston (minimum displacement) or with 2 (maximum displacement). The booster, which is lined up with the compressor, is activated when temperatures are lower than -8°C to increase the level of heating. An internal heat exchanger is used to inject a refrigerant between the two compression stages and increase the subcooling at the outlet of the condenser.
- **Heat Pump #3** was a variable speed technology (compressor) with the injection of a refrigerant. When the outdoor temperature is low, the compressor's speed increases to maintain the condensing pressure and the heating capacity at adequate levels. Generally, a speed increase can cause the compressor to overheat. The injection of the refrigerant into the compressor can overcome this problem.
- **Heat Pump #4** was a device designed for hydronic heating and the production of domestic hot water. This heat pump includes an outdoor unit and a storage tank. The outdoor unit corresponds to the heat pump itself including the gas cooler. The water from the storage tank circulates directly through the heat pump. The heat pump is controlled via the storage tank according to the operating parameters (particularly the water temperature and outdoor temperature). In this device, CO_2 is used as the refrigerant and this heat pump is known for its capacity to operate at an outdoor temperature as low as -20°C. It is based on a transcritical thermodynamic cycle and includes a variable speed compressor (refrigerant injection). This product is not available on the North American market.

Table 1: Tested air-to-air heat pumps – manufacturers' specifications

		Heat pump 1	**Heat pump 2**	**Heat pump 3**
Refrigerant		R410a	R410a	R410a
Cooling Capacity	kW	10.4	10.6	10.0
Heating Capacity (8.3°C)	kW	9.7	10.7	11.1
Heating Capacity (-8.3°C)	kW	6.1	12.9	11.1
SEER		15.85	14	15
EER		12.2	12.3	12
$HSPF_5$		8.5	8.5	7.8
Defrosting		Inversion	Inversion	Inversion
Compressor		Scroll – two-stage	Scroll – two-capacity With booster	DC Inverter-driven, With injection

Table 2: Tested air-to-water heat pumps – manufacturers' specifications

		Heat pump 4
Refrigerant		CO_2
Heating Capacity (25°C)	kW	9
Energy Consumption (25°C)	kW	2.2
Heating Capacity (7°C)	kW	9
Energy Consumption (7°C)	kW	2.9
Heating Capacity (-15°C)	kW	9
Energy Consumption (-15°C)	kW	5
Compressor		DC Inverter-driven, 2-stage rotary, with injection

With the emergence of variable speed ductless heat pumps and their low cost compared to more conventional technologies, it is most likely that their market share will increase significantly in the coming years. As a result, testing in the future will focus on this technology.

2.2 Description of the Test Bench

A test bench was developed at the LTE to test central air-to-air heat pumps. The process was divided into several sections (Figure 1) and was regularly modified to meet the requirements of different tests.

The first section, where the outdoor unit of the heat pump was installed, was conditioned so that the temperatures could be below -25°C. This section was cooled by the refrigeration equipment and the temperature was controlled by an electric resistance coil. A boiler with a capacity of 11.5 kW generated the desired humidity level within the chamber. The humidity level was modulated by way of controls, which were separate from the acquisition system, based on the readings of a humidity sensor in the test area.

The second section was used to create a thermal load with a significant level of inertia to represent a building. The air entering the ventilation unit could be entirely or partially supplied by this zone.

In the future and in order to better evaluate the performance of heat pumps, a semi-virtual test bench will be developed. It will allow to better understand the interaction between the heat pumps, the buildings where they are located and the resistive heating devices that are also present in the buildings (electric back-up, baseboards, etc.) as well as analyze the control algorithms implemented in the thermostats.

Measuring the performance of the heat pumps was carried out with an HP data acquisition system (model HP3852A) that allowed us to collect the various measurements while ensuring that all the components in the test bench functioned properly. A transition to Labview is underway, which will allow us to simplify the acquisition system, increase its functionality and migrate towards the semi-virtual test bench.

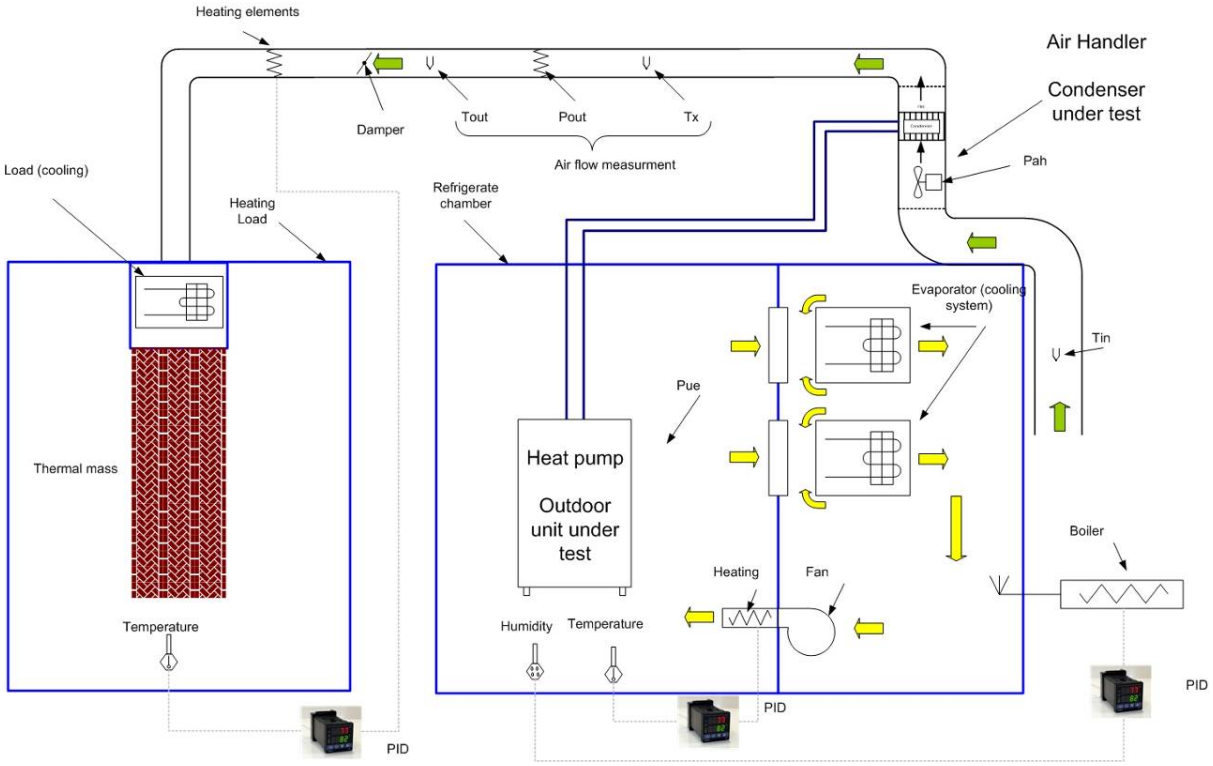

Figure 1: Simplified illustration of the test bench (air-air)

A test bench, illustrated on Figure 2, was also developed to test an air-to-water heat pump, The outdoor unit of the heat pump was installed in the same section as the air-to-air heat pump (see Figure 1). The thermal load of both the heating and the domestic hot water was dissipated by cold water supplied by the municipal water utility. In this particular case, bypassing the storage tank is possible and allows to evaluate the performance of the heat pump without the influence of this equipment (Figure 2).

Under normal operating conditions, that is to say when the storage tank was used, valves V3 and V12 were closed (Figure 2). Thus, a pump (P1), which is an integral part of the storage tank that controls it, circulated the water from the tank to the heat pump. The flow rate was measured by a flowmeter (D8) and the inlet and outlet temperatures of the heat pump were measured by thermocouples (T7 to T10). As far as the heating network is concerned, a pump (P2) circulated water from the municipal main to the storage tank. The heating capacity was induced by a mixture of the hot water drawn from the tank (linked to the heating network) and cold water via a mixing valve to obtain the water return temperature from the heating network. Different flow rates (D1, D3) and temperatures (T1 to T4) were measured in this circuit to perform thermal balances. This equipment is designed to heat domestic hot water, so a cold water supply along with a solenoid valve was provided. A flowmeter (D5) and thermocouples (T5, T6) were installed on the water circuit. Surface thermocouples were also placed at different levels in the tank in order to analyze any stratification. The electric power of the heat pump and the electric resistance coils located in the storage tank were also measured.

The circulation pump (P2) located on the heating system was a variable speed pump (rotation frequency) and could therefore be used to characterize the performance of the heat pump when the storage tank was bypassed. In this configuration, the flow rate of the pump (P2) was set so that it was similar to that of the P1 pump (constant value), and therefore P1 pump can be switched off.

The mixing valve on the heating circuit controlled the mixing temperature (T2), which corresponded to the water return temperature from the heating system or, when the storage tank was bypassed, to the heat pump's supply temperature.

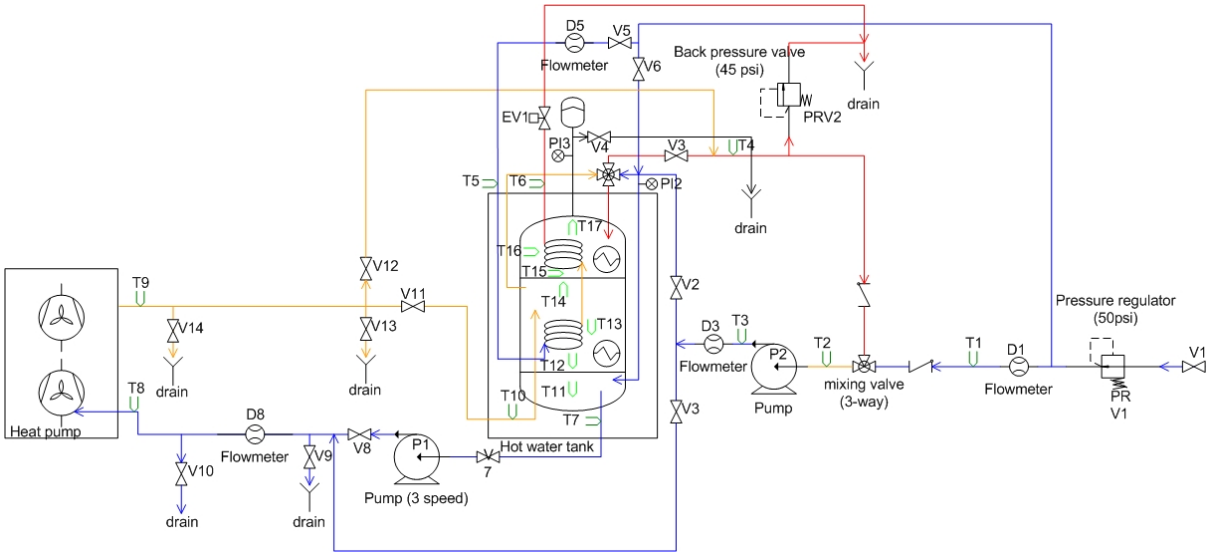

Figure 2: Simplified illustration of the test bench (air-to-water)

2.3 Description of the Tests

2.3.1 Air-to-air heat pumps

The tests were undertaken to evaluate the following:

<u>The performance under ideal conditions (**Heat Pumps 1, 2 and 3**)</u>
The performance of the heat pumps under ideal conditions was evaluated based on establishing an average over 30 minutes of operation. The defrosting cycle, the heat pumps' warm-up time or any other element that could affect the performance of the heat pumps were not taken into account in the tests.

<u>The performance of the heat pumps over a longer period of time (**Heat Pumps 1, 2 and 3**)</u>
The performance was determined by establishing an average based on the heat pumps' continuous operation over 24 hours. The purpose of these tests was to evaluate the performance of the heat pumps including the defrosting cycle and the accumulation of frost. It should be noted however that the warm-up period of the test bench (heat pumps and operating conditions) was specifically not taken into account in these tests.

<u>Effect of cycling on the performance of the heat pumps (**Heat Pumps 1 and 2**)</u>
An operating ratio was determined for a number of temperature levels and for both heat pump models. The ratios were obtained by dividing the heating load of a hypothetical house by the average heating capacity determined during the 24-hour tests at the same outdoor temperatures.

<u>The effect of the air flow on the heat pump's performance (**Heat Pump 3**)</u>
The impact of the air flow of the ventilation system on the performance of this heat pump was evaluated by conducting experimental tests over 24-hour periods. Different predefined air flows in the ventilation unit were tested in identical operating conditions.

2.3.2 Air-to-water heat pumps

The experimental tests were conducted in two steps. The first was aimed at characterizing the performance of the heat pump (outdoor unit) without using the storage tank. Different operating conditions (input water temperature and outdoor air temperature) were set to evaluate the heating capacity and the full load coefficient of performance (COP). The second step was aimed at characterizing the performance of the system including the heat pump and the storage tank based on programmed heating and domestic hot water needs.

Tests without the storage tank (**Heat Pump 4**)
Compared to a standard installation, the test bench was modified to bypass the storage tank. This allowed to control the temperature and the water flow into the gas cooler in order to determine the effect of these parameters on the COP of the thermodynamic cycle. Various tests were conducted based on two separate water flows (5.3 L/min and 3.5 L/min) and on three water temperatures flowing into of the gas cooler, namely 20°C, 30°C and 40°C.

Tests using the storage tank (**Heat Pump 4**)
In order to characterize the heating system and the production of domestic hot water, that is to say the heat pump and the storage tank, a heating load and a domestic hot water demand were imposed on the system.

- To conduct the tests, five on average 7-minute hot water draws per day at a flow rate of 6 L/min were imposed. This represented a daily consumption of 200 L, or the representative daily consumption of an average household in Québec. The water draws occurred at 8 a.m. (7 min.), 8:30 a.m. (7 min.), noon (5 min.), 7 p.m. (7 min.) and 7:30 p.m. (7 min.). It should be noted that the temperature of the water from the municipal main varies during the summer and the winter, which had an impact on the heating capacity required to produce domestic hot water. In our test bench, the temperature of the water was not controlled, which could have had an impact on our results.
- The temperature of the water supplied to the home's heating system was imposed by the storage tank. Because of the constraints in the test bench (maintaining the balance of the hydraulic network when the mixing valve was open or closed), the water flow in the heating system was approximately 10 L/min. The heating network's return temperature was therefore imposed in order to attain the heating capacity needed depending on the outdoor temperature.

2.4 Results

2.4.1 Air-to-air heat pumps

Comparing the operating characteristics of the different heat pumps is complex since they are all designed differently. Nevertheless, the exercise can be done by focussing on their operating differences and, as a result, on the advantages of each technology. However, the control factor, particularly in regards to the management of the partial load – especially in the case of **Heat Pump 3** (variable speed) and **Heat Pump 2** (two-stage) – and in regards to the management of the electric back-up, was not studied in depth in this exercise in spite of the fact that this factor can have an impact on the seasonal performance of the heat pumps. As a result, our comparison between the different technologies is not exhaustive and should not be the sole decisional factor.

Performance under ideal conditions (**Heat Pumps 1, 2 and 3**)

Figure 3 illustrates the full load heating capacity of all three technologies. Clearly, the heating capacity of **Heat Pump 1** decreased monotonously but the system did operate at

temperatures as low as -15°C. However, at that temperature, the heating capacity was low (5 KW) and could not meet the heating load of a house below this temperature. When a conventional back-up electric heater (ON/OFF) was used, the heat pump evidently could not operate normally at that temperature. The full load heating capacity of the variable speed and two-stage heat pumps evolved similarly. Indeed, two power levels are visible. This had the advantage of providing a considerably high heating capacity at low temperatures, which allowed to reduce the balance point temperature[1] of the heat pumps. Their COP decreased based on the outdoor temperature. In the case of the VRF injection heat pumps, a significant decrease in the COP was observed between 5°C et 0°C, which corresponded to an increase in the compressor's speed ranging between 60% and 100%. It is normal for the COP of variable speed heat pumps to decrease with an increase in the speed of the compressor.

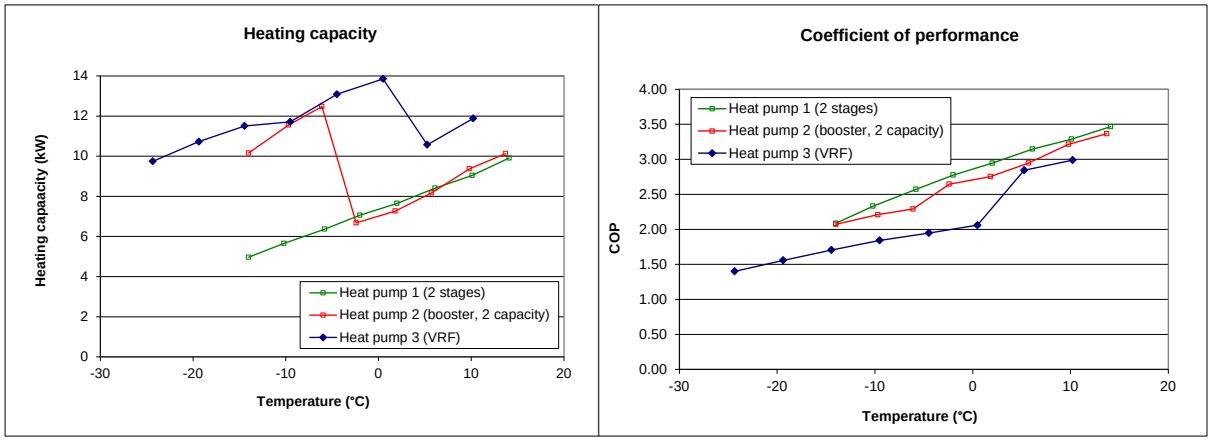

Figure 3: Average performance over 30 minutes

Performance over a longer period of time (**Heat Pumps 1, 2 and 3**)
In addition to reducing the heat pump's availability, the defrosting cycle added a thermal load to the building by absorbing part of the energy supplied to the building. In most installations, back-up heating devices are used to minimize the negative impact this process has on the comfort of the occupants. These auxiliary devices represent a use of energy with a lower performance than that normally obtained with a heat pump, which contributes to decreasing the performance of the global system. However, this was not part of our study because no back-up devices were used during the tests.

In the case of **Heat Pump 1** (Figure 4 and Table 3), because no frost occurred when the heat pump was operating at 10°C, its daily performance was not affected. It should be mentioned that, upon the formation of frost, the loss in capacity is relatively constant according to the temperature. The average capacity loss was 0.62 kW between 6°C and -14°C. In the case of **Heat Pump 2** (Figure 4 and Table 4), the capacity loss between 6°C and -5°C was 0.5 kW.

As far as **Heat Pump 3** was concerned (Figure 4 and Table 5), no defrosting activities occurred at temperatures above 0°C; its daily and instantaneous performance levels were therefore identical at these temperatures. When the temperature was below or equal to 0°C, the thermal capacity loss over a 24-hour period was an average of 0.61 kW, or 5.4% less than the instantaneous value. It was also observed that the difference between the instantaneous and daily values had a tendency to increase when the outdoor temperature decreased.

[1] Balance point temperature: Outdoor temperature at which the heating capacity of the heat pump is equal to the thermal load of the building.

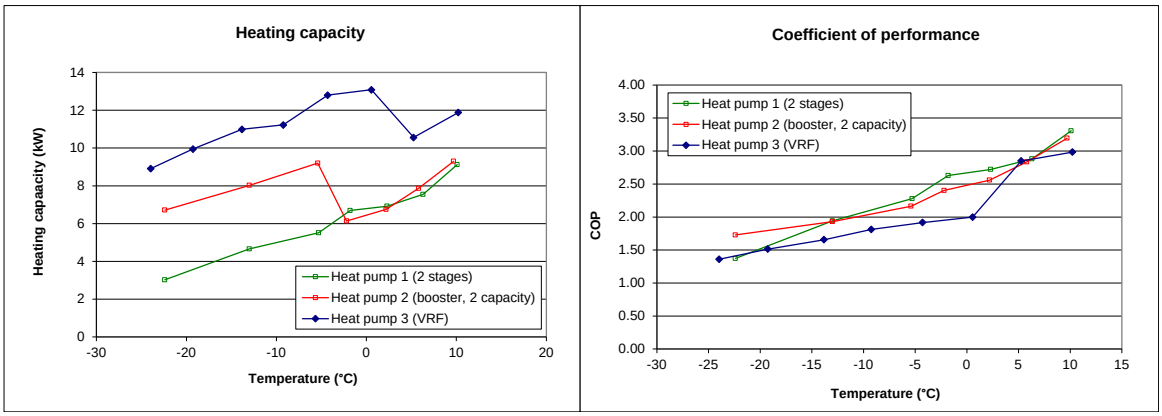

Figure 4: Average performance over 24 hours

Table 3: Comparison between the instantaneous values (baseline) and daily values – heat pump 1

Heat Pump 1						
Temperature	**Capacity Difference**		**COP Difference**		**Electric Energy Consumption**	
°C	kW	%		%	kW	%
10	-0.08	-0.9%	-0.02	-0.5%	-0.01	-0.3%
6	0.86	10.3%	0.27	8.4%	0.05	2.0%
2	0.73	9.5%	0.22	7.6%	0.05	2.1%
-2	0.37	5.3%	0.15	5.3%	0.00	0.0%
-6	0.85	13.3%	0.29	11.4%	0.05	2.2%
-14	0.30	6.1%	0.15	7.0%	-0.02	-0.9%
Average (<6°C)	0.62	8.9%	0.22	7.9%	0.03	1.1%

Table 4: Comparison between the instantaneous values (baseline) and daily values – heat pump 2

Heat Pump 2						
Temperature	**Capacity Difference**		**COP Difference**		**Electric Energy Consumption**	
°C	kW	%		%	kW	%
10.00	0.07	0.7%	0.02	0.6%	0.00	0.1%
6.00	0.30	3.7%	0.11	3.8%	0.00	-0.1%
2.00	0.51	7.1%	0.19	7.0%	0.00	0.0%
-2.00	0.54	8.1%	0.24	9.2%	-0.03	-1.2%
-6.00	3.27	26.2%	0.13	5.5%	1.19	21.9%
-14.00	2.14	21.0%	0.14	6.8%	0.75	15.3%
Average (<6°C et >-5°C)	0.45	6.3%	0.18	6.7%	-0.01	-0.4%

Table 5: Comparison between the instantaneous values (baseline) and daily values – heat pump 3

Heat Pump 3						
Temperature	**Capacity Difference**		**COP Difference**		**Electric Energy Consumption**	
°C	kW	%		%	kW	%
10.00	0.00	0.0%	0.00	0.1%	-0.01	-0.2%
5.00	0.01	0.1%	0.00	-0.1%	0.01	0.3%
0.00	0.77	5.5%	0.06	2.9%	0.18	2.7%
-5.00	0.29	2.2%	0.03	1.6%	0.04	0.6%
-10.00	0.49	4.2%	0.03	1.7%	0.16	2.5%
-15.00	0.52	4.5%	0.05	2.9%	0.11	1.7%
-20.00	0.78	7.3%	0.04	2.8%	0.32	4.6%
-25.00	0.83	8.6%	0.04	2.9%	0.40	5.8%
Average (<0°C)	0.61	5.4%	0.04	2.5%	0.20	3.0%

The frequency as well as the average and overall duration of the defrosting cycles (Figure 5) were longer at low temperatures in the case of **Heat Pump 3** than they were in the case of the other two. However, it seems that this process had less of an impact on the heat pump's daily performance. One hypothesis that would explain it, is that the value of the compressor speed was lower during the defrosting cycles than it was for heating. The lengthy duration of the defrosting cycles was compensated by the compressor's low energy consumption and the low cooling capacity in the air handler.

The defrosting frequency in the case of **Heat Pump 3** was constant even though it wasn't required. Indeed, no decrease in the heating capacity and in the COP was perceptible between two defrosting periods, which led to assume that the frequency of the process was often overestimated under the conditions tested. A loss in efficiency was caused by the process. However, the loss was relatively insignificant (5.4% of the heating capacity and 2.5% of the COP). As a result, it is felt that improving the defrosting strategy for this technology would not significantly improve its daily performance.

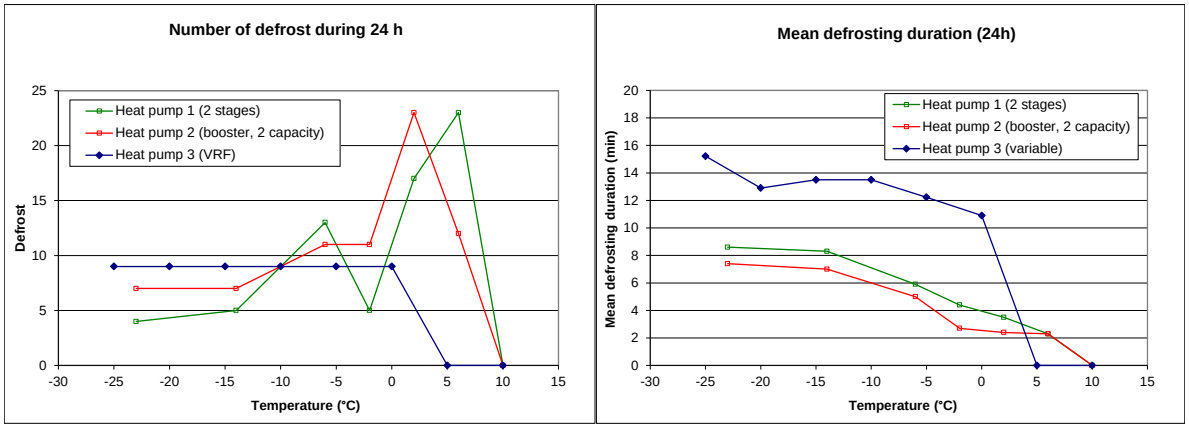

Figure 5: Defrosting over 24 hours

<u>The effect of cycling on the performance of the heat pumps (**Heat Pumps 1 and 2**)</u>
Because the heating load exceeded the thermal capacity of **Heat Pump 1** when the temperature was -10°C and below, this test was not applicable at those temperatures. This also applied to **Heat Pump 2**, the thermal capacity of which roughly corresponded to the heating needs at -6°C.

The tests were conducted using the control signal usually triggered by the thermostat by way of the data logger. The operating ratio on Table 6 was applied on an hourly basis. For example, the 30% operating ratio of **Heat Pump 1** was applied by the heat pump being activated for approximately 18 minutes in an hour. Its COP was calculated by dividing the amount of generated heat by the energy consumed by the heat pump and air handler. An adjustment was made to take into account the fact that the ventilation system was kept on even when the heat pump was switched off. This adjustment corresponded to the energy consumed by the air handler during the downtime, which was deducted from the measured overall electrical consumption and the heat that was produced.

The performance of both heat pump models decreased to an operating ratio of 15% (Table 6). The expected impact on their performance was greater when their operating cycle was short because the warm-up period of a heat pump is an important factor in its operating cycle. This result was not surprising. The difference in the COP of **Heat Pump 1** ranged from 5% to 20% whereas there was very little variation in the case of **Heat Pump 2**.

Table 6: Operating Ratios of the Heat Pumps in Tests with Cycles Depending on the Temperature

Temperature (°C)	**Heat Pump 1**			**Heat Pump 2**		
	Duty cycle (%)	COP_{24hr}	COP_{cycle}	Duty cycle (%)	COP_{24hr}	COP_{cycle}
10	15	3.31	2.68	15	3.19	2.65
6	30	2.88	2.73	25	2.84	2.81
2	45	2.72	2.43	45	2.56	2.56
-2	60	2.63	2.15	70	2.40	2.41
-6	85	2.28	2.01	-	-	-
-10	-			70	2.16	2.01
-14	-			85	1.93	1.91

The effect of the air flow on the heat pump's performance (**Heat Pump 3**)

Tests were conducted in order to identify the impact of the ventilation air flow on the performance of **Heat Pump 3**. The three flow rates tested were 800 cfm, 1000 cfm (baseline) and 1200 cfm. These were selected on the ventilation unit, but the measured flow rates were slightly different because of the pressure losses in ducts. It should be noted that the measured performance at 1000 and 1200 cfm was identical, which would indicate that an oversizing of the flow rate would not improve the performance of the equipment (Figure 6). However, at 800 cfm, the heating capacity decreased by about 10% to 20% depending on the weather conditions and the COP dropped by 2% to 15%. This clearly indicated that an undersized flow rate causes a significant decrease in the heat pump's performance.

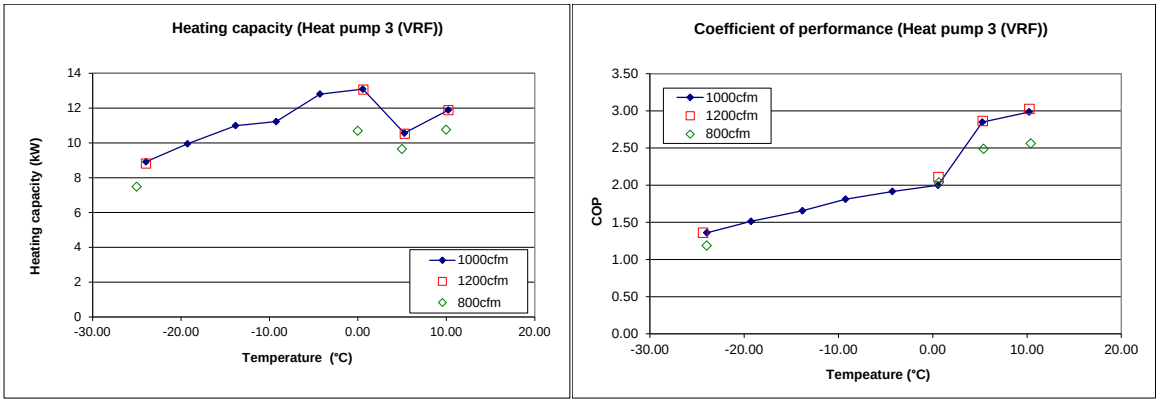

Figure 6: Effect of air flow on the heat pump's performance (24h)

2.4.2 Air-to-water heat pump

Tests without the storage tank (**Heat Pump 4**)

Figure 7 shows the effect of the outdoor temperature and the water temperature at the inlet of the heat pump on COP and on heating capacity. The graph shows two different slopes (above and below 0°C) resulting from the variation in the compressor's speed. In these tests, the outdoor temperature had a significant impact on the COP, especially when the water temperature was low and, logically, the COP had a tendency to decrease with the outdoor temperature. In addition, when the water temperature increased, the refrigerant (CO_2) was less cooled in the gas cooler. This therefore affected the heat pump's COP as well as its heating capacity. This demonstrated that it is important that the water storage tank be properly sized so that the water supplied to the heat pump is at the lowest possible temperature (stratification).

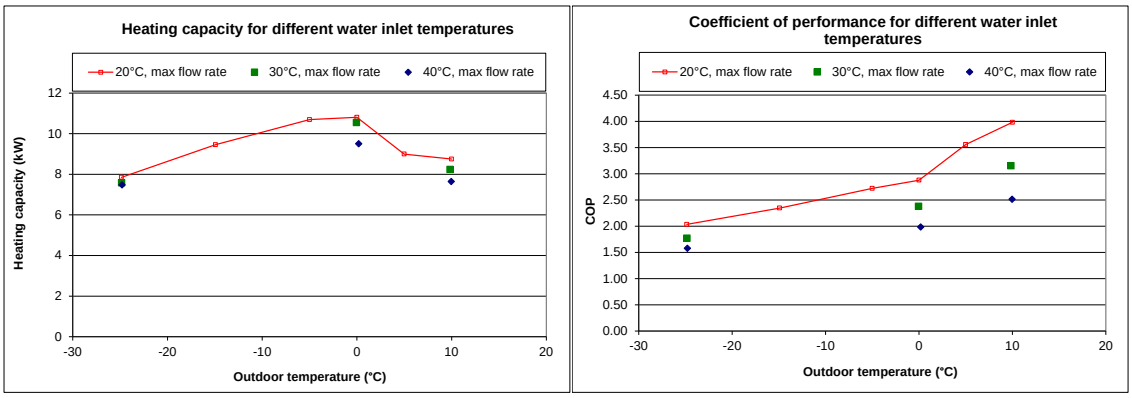

Figure 7: Performance without the storage tank

Figure 8 shows the effect of flow of water circulating in the heat pump on performance. Regardless of the operating conditions, the heating capacity and the COP were maximized when the flow rate was maximized. The impact of the flow in both rates that were tested was more significant when the outdoor temperature was high. The flow rates (D8) circulating in the gas cooler were 5.3 L/min and 3.6 L/min. At 10°C, a decrease in the flow rate (32%) triggered a decrease in the COP of 14% to 16% whereas at -25°C, the COP decreased to between 6% to 8%. This decrease in performance also included a slight decrease in the heating capacity provided by the heat pump and a slight increase in the electricity consumed. This phenomena was normal because a decrease in the water flow circulating in

the gas cooler caused an increase in the temperature of the CO_2 at the outlet of the cooler, which therefore affected the cycle's performance.

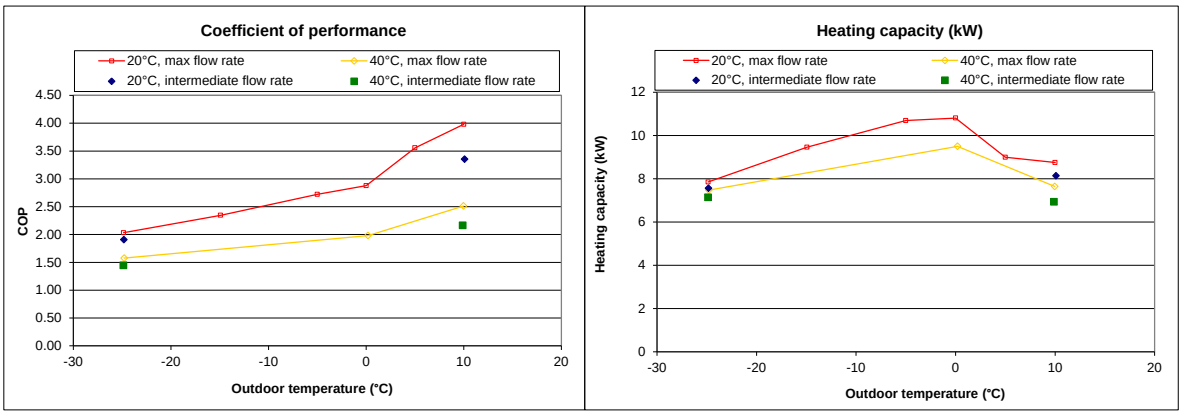

Figure 8: Effect of the water flow in the heat pump (without the storage tank)

Tests using the storage tank (**Heat Pump 4**)

On Figure 9, the results of the tests using the storage tank demonstrated that the temperature of the water being supplied to the heat pump (T11) was identical to that of the heating network's return water. The heat pump's COP was therefore directly influenced by this temperature. Therefore, in order to ensure the equipment's efficiency, it must be installed within a low-temperature heating network (low-temperature radiator, heated floor).

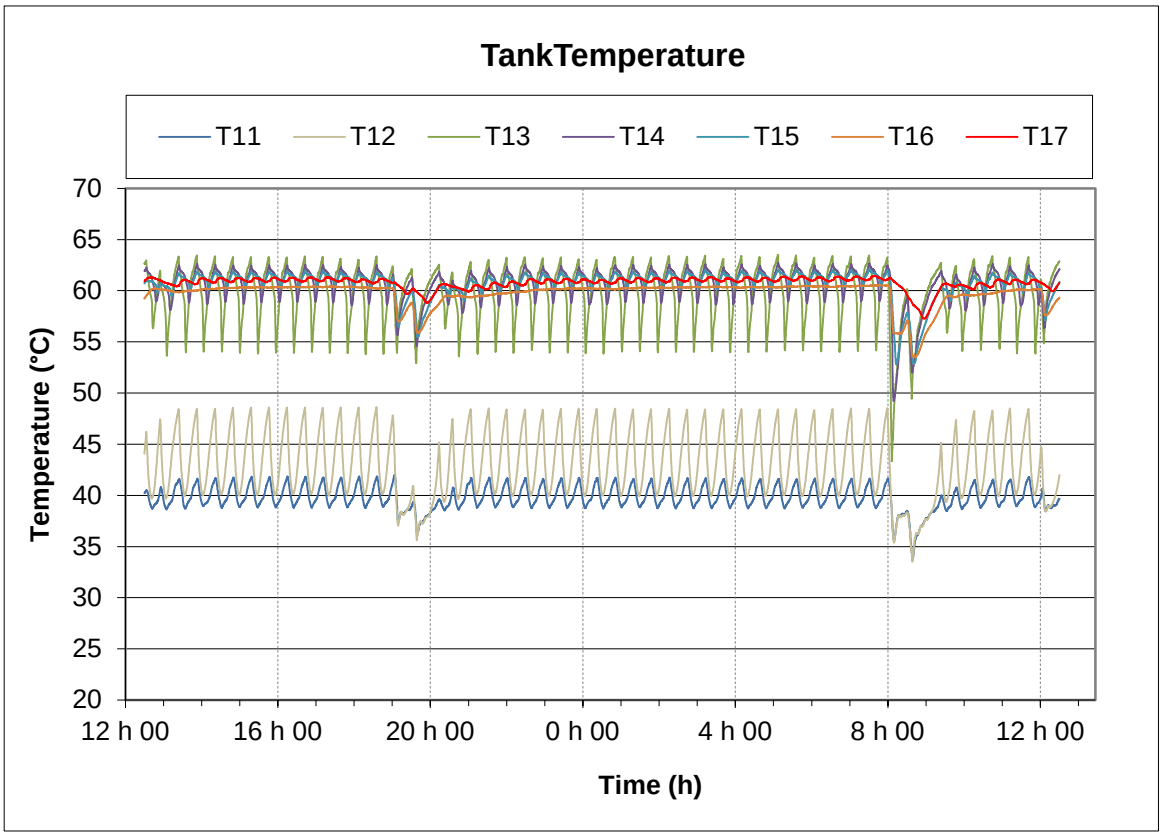

Figure 9: Temperature in the storage tank (-10°C test)

With an outdoor temperature of -10°C, the heating capacity of the heat pump was around 8 kW, which was similar (in identical conditions) to the capacity in steady state conditions

(without the reservoir). The energy consumed was similar to that measured in the tests without the storage tank. The tests demonstrated that using the storage tank had little impact on the COP of the heat pump. At that temperature, the utilization factor (or hours of operation) of the heat pump was 72.5% in the testing conditions.

When there was a demand for domestic hot water, the storage tank had the capacity to meet the needs. Nevertheless, we observed that there was a decrease (slight but not negligible of – 5°C) of the temperature of the hot water when it was drawn (Figure 10) that stabilized at the end of the draws. This can be explained by the fact that, when the water draws began, the water in the heat exchanger had the time to heat up before the hot water was needed. This type of equipment therefore requires using low-flow thermostatic valves in order to minimize this effect. In principle, several simultaneous calls for hot water could have an impact on comfort; however, to remedy such situations, the heat pump is equipped with controls that allow to increase the temperature in the storage tank when the option is selected.

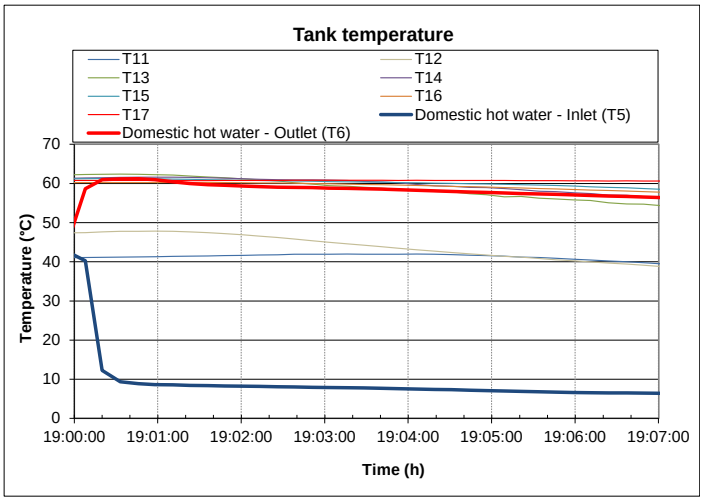

Figure 10: Temperature in the storage tank to produce hot water (tested at -10°C)

2.5 Discussion

Measuring the performance of various heat pumps (both air-to-air and water-to-air) allowed to obtain reliable and accurate information under controlled conditions on their heating capacity, their COP, the effects of the defrosting cycles and the effects of the air flow. This information not only helped to validate the specifications supplied by the manufacturers on the performance of the heat pumps but was also used in models to estimate the energy savings generated by the heat pumps.

The heating capacity of VRF injection heat pumps is interesting when the outdoor temperatures are low and significantly better than conventional heat pumps, including those that are rated as upscale. Their COP at full capacity is lower than the COP of conventional heat pumps. However, when the temperature rises above the heat pumps' balance point, it is expected that the COP should improve when the heat pump operates at a lower speed whereas conventional heat pumps tend to deteriorate because of the cycling impacts.

3 FIELD TESTS - SUMMARY

A pilot project consisting of 22 test sites was carried out in Quebec, Canada during the heating season to measure the energy savings associated with the use of heat pumps for space heating. The reference system for the energy saving is an electric resistance heating system. The sites participating in the project were divided into three different categories according to their respective space heating system. Sixteen houses were equipped with an air handling unit with a built-in heat pump (10 sites with a single stage air source heat pump and 6 sites with a cold climate air source heat pump, 5 of which had variable speed compressors and 1 had a two-stage compressor) assisted by an electric coil in the unit. The remaining 6 sites were equipped with a ductless split heat pump system supplemented by independent electric baseboard heaters. The 22 test sites were located in the Trois-Rivières and Montreal regions. Variable speed compressors were classified under the cold climate heat pump category. There were three sizes in all 5.25 kW (1.5 tons), 8.8 kW (2.5 tons), and 10.5 kW (3 tons). The systems were installed between 2005 and 2011. The single stage heat pumps were older than the others. They were installed in 2005 while those in the cold climate and ductless heat pump categories were installed more recently (2011). However, this study did not take the age of the systems into account. Any maintenance activities on the equipment were also not included in the study. However, the systems were tested to assess their adequate operation before the beginning of the measurements.

3.1 Data Acquisition

The purpose of the experiment was to acquire data from heat pumps in operation that provided information about their real performance. Thus, it was necessary to measure all the elements of the heating systems to be able to calculate the energy balance of each system, the electric power related to each system's operation as well as the temperature and airflow rate. The measured data therefore included:

- the electric energy consumed by the heat pumps for compression
- the electric energy consumed by the air handlers for air supply
- the electric heating power from auxiliary heaters
- the air velocity in the air handlers
- the temperature and relative humidity at the inlet and outlet of the air handlers
- the outdoor temperatures provided by the nearest weather stations (Montreal and Trois-Rivières)

All the measurement instruments were calibrated. The uncertainties in the energy consumption measurements were less than 1% and the uncertainties for the temperature ranges were about ±0.2°C, which resulted in a relative uncertainty of 1% to 10% on temperature difference.

Data was acquired at intervals of 88 seconds. For safety purposes, the minimal storage capacity of the data loggers was set at 3 weeks to provide enough time for any maintenance operations in the event of problems with the data acquisition system. The data was imported from the data loggers every week.

The electric consumption of the HVAC equipment was measured at the electric panel. For the air handler units, the air velocity was measured but not used for flow rate calculations because of difficulties in accurately calculating the flow rates. The method proposed by Johnson (2005) was used to determine the flow rates, whereby the heating capacity delivered by an electric heater with a known capacity was used to calculate the flow rate in the air handlers. This method has often been used in different studies (Johnson, 2005) because of its simplicity and precision. However, a radiation effect of the heaters on the temperature sensors was observed in some installations. This phenomenon led us to

exclude some sensors in the data treatment. It was suggested that the uncertainty of this method was less than 15% (5 to 15%). The air velocity was used to detect the type of ventilation (constant, controlled or intermittent) and therefore define an operation period.

All temperature and flow rate measurements were not carried out on the ductless heat pumps to avoid measuring equipment located in the living room. However, their heating capacity was estimated using the data on their performance, based on electric consumption measurements. The difference in the heating output between the manufacturer's curves and the laboratory tests was about 2% to 8% in the case of the 3-ton central variable speed compressor. We assumed that the error resulting from using manufacturer heating output curves for the ductless systems was less than 10%.

3.2 Results

The results show that the performance of single stage heat pumps provides similar energy savings regardless of their capacity. In Figure 11, the energy saving value for each system type is the arithmetic mean of the energy saving (kWh or %) of sites having the same heat pump technology. The energy savings of these heat pumps were about 28% compared to the heating demand. It was found that heat pumps designed for cold climates (VRF injection types) are more efficient than single stage heat pump systems. The energy savings of these heat pumps were about 45% compared to the heating demand. In the case of the ductless heat pumps, which operate with the same technology as cold climate heat pumps, energy savings of 25% were attained, compared to the heating demand.

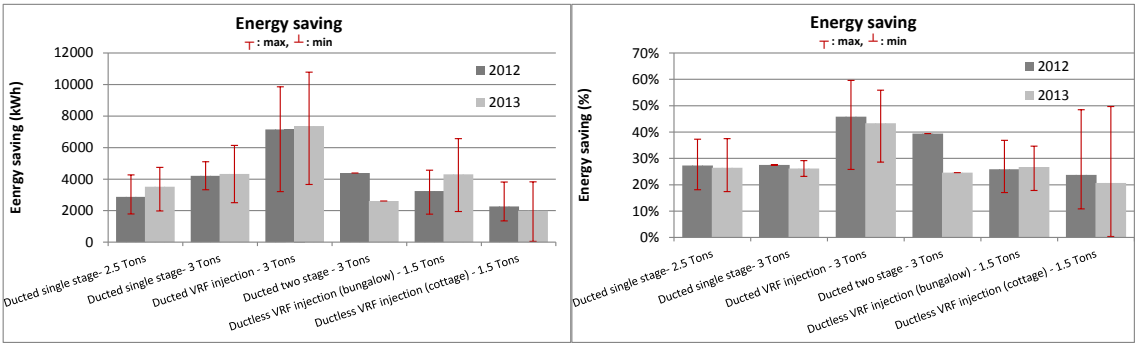

Figure 11: Energy savings by heat pump category

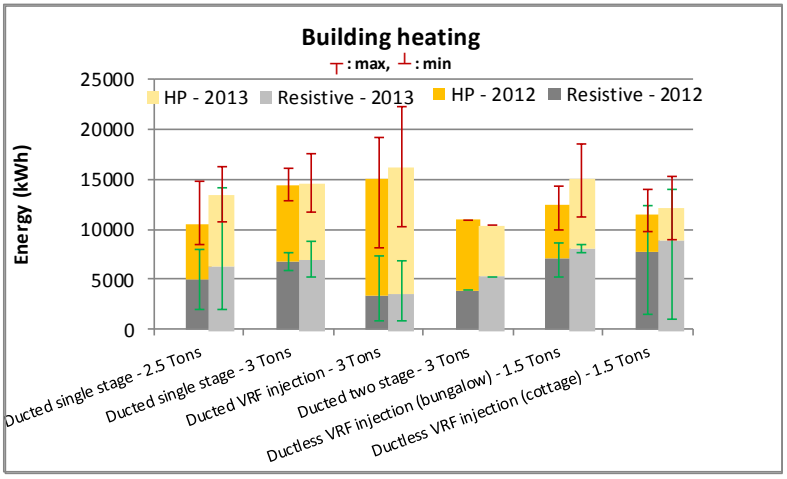

Figure 12: Heating by heat pump category

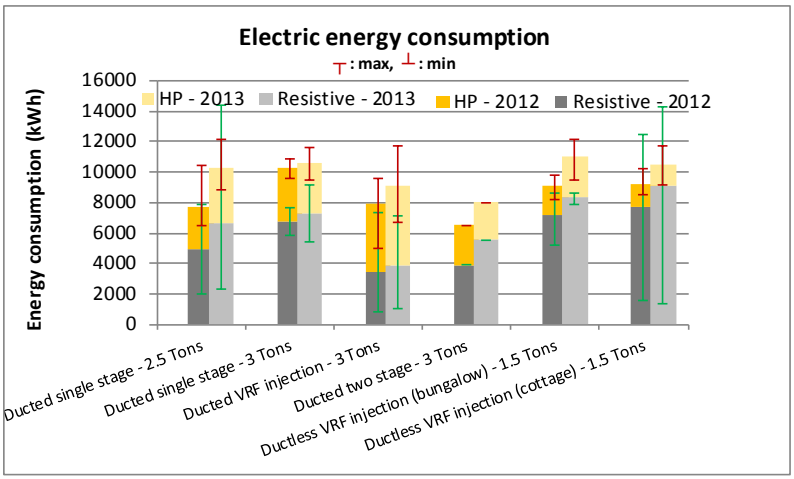

Figure 13: Electric energy consumption by heat pump category (heating)

The Heating Seasonal Performance Factor (HSPF) represents the rating of a heat pump in specific conditions, and is defined by the CAN/CSA-C656-05 standard. It is defined as the total space heating required during the heating season (BTU) divided by the total electric energy consumed (W) for space heating. The BTU/hr/W HSPF unit can be changed to a (W/W) COP unit by dividing the value by 3.413. A test procedure was defined within this standard to estimate the thermal capacity and the heating performance of the heat pumps at various temperature levels. This performance data was used in a BIN model to calculate the energy provided by the heat pumps to heat the houses in the experiment. Some variables such as the heating demand of the houses were estimated according to the capacity of the heat pumps and it was found that these variables could affect the HSPF.

In this study, the COP (global system COP) was defined as the total space heating measured during the space heating season (kWh) (mean value on Figure 12) divided by the total electric energy consumed (kWh) (mean value on Figure 13) for space heating (including back-up and baseboards). This coefficient of performance took into account the time required to defrost the equipment and the cycling behaviour of some of the heat pumps. It was therefore relevant to establish a comparison between the HSPF and COP. The COP value on Figure 14 for on system type is the arithmetic mean of the COP of sites having the same heat pump technology.

On Figure 14, our first observation was the difference in amplitude of the COP compared to the HSPF. The HSPF of the single stage heat pumps was about 7.5 (equivalent COP of 2.2) while the COP measured was 1.4. The HSPF of the cold climate and ductless heat pumps was respectively 8.2 and 8.9 (equivalent COP of 2.4 and 2.6). The COP of the cold climate heat pumps was 1.9 and even lower for the ductless heat pumps at 1.3. It can therefore be concluded that the HSPF always overestimates the heating performance of this type of equipment. In HSPF ratings, the equipment's operation was idealized because the HSPF criteria are the following:

- Heat pumps provide all the heating needs for temperatures over the balance point
- When below the balance point, auxiliary heating devices compensate by providing additional heat to the energy provided by heat pumps at their maximum operation
- Cut-off options provided by the installer are not considered
- The minimum design heating requirement (DHRmin) is used to calculate the HSPF. Note: This minimum requirement is not adequate for most heat pumps actually installed in Québec.

Based on our first observation, the HSPF of single stage heat pumps is more overestimated than the HSPF of cold climate heat pumps. The balance point of single stage heat pumps is higher (-10°C) than the balance point of cold climate heat pump (-25°C). In addition, the cut-off point is at about -12°C for single stage heat pumps while cold climate heat pumps can operate at temperatures as low as -28°C. It is therefore not recommended to compare the HSPF of the different technologies.

As a result of their basic criteria, the HSPF ratings are often overestimated. The HSPF calculation method does not take into account the equipment's operation at very low temperatures (including the use of auxiliary heating). In our study, the heating demand and the performance of the heat pumps were evaluated for an outside temperature of 8°C, 1.7°C and -8.3°C. A more accurate evaluation of cold climate heat pumps should include an evaluation at lower temperatures (-18°C for example). We therefore concluded that, in the context of Québec's cold climate, the HSPF is not an adequate method to evaluate the performance of heat pumps. However, it can provide a good basis for the classification of heat pumps based on similar technologies.

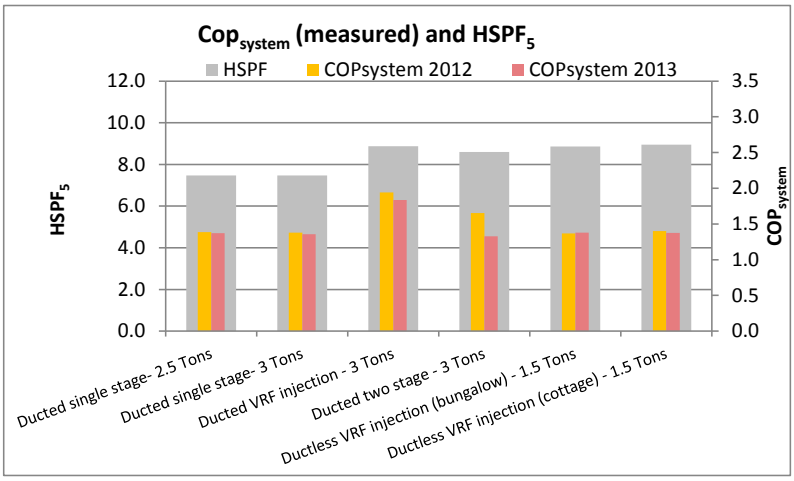

Figure 14: HSPF by heat pump category

3.3 Discussion

The main purpose of our study was to evaluate the energy saving potential associated with heat pumps in the Québec residential sector. A measurement campaign was conducted in homes located in the Montreal and Trois-Rivières regions to meet this objective. The chosen approach was based on measuring the power consumption of the resistive heating equipment and of the outdoor unit of heat pumps as well as measurements of the heating capacity provided by the heat pumps.

The results of this study demonstrate that heat pumps installed according to current practices allow to generate significant annual energy savings of between 25% and 30% in the case of conventional heat pumps and between 45% and 50% in the case of variable speed heat pumps as compared to resistive heating equipment. Variable speed heat pumps therefore generate greater energy savings than conventional heat pumps; however this remains difficult to quantify due to the number of samples. The difference in capacity at low temperatures, the coefficients of performance, the cut-off point, the sizing and the mode of operation (continuous ventilation, setpoint changes, control) remain criteria that can explain the difference in energy savings within a same category. It is important to mention that the quality of the installation of heat pumps has an impact on the performance of the overall heating system. The airflow, refrigerant load and heating equipment controls (or the interaction between the various devices) are factors that should not be overlooked when

they can have a significant impact on the generation of energy savings, and this applies for the entire life cycle of the equipment. Furthermore, unless a major problem occurs (a refrigerant leak for example), it is difficult for an individual to identify when a heat pump's operation is less than optimal because of poor installation practices.

Our measurement campaign also demonstrated that rated HSPFs as defined by CAN/CSA-C656-05 (similar procedure as AHRI 210/240) is not a criterion adapted to represent energy savings although there is a link between the average coefficient of performance of the systems we studied and the HSPF. It should be noted that the Office of Energy Efficiency (OEE) issued a publication in 2010, *Bulletin on Reporting Cold Climate Performance* (http://www.nrcan.gc.ca/energy/regulations-codes-standards/bulletins/7177), recommending modifications to CAN/CSA-C656-05 so that the performance of heat pumps used in cold climates is better represented in the standard. One requirement from this modification was additional standard testing to report heating capacity and COP at -17.8°C (0°F) be put in place by January 1, 2014. This would require that standardization labs be in a position to meet the criteria of the tests proposed by the OEE.

4 CONCLUSION

Measuring the performance of different heat pumps (air-air and air-water) allowed us to obtain reliable and accurate data under controlled conditions on the heating capacity, the COP, the effects of the defrosting cycles and the effects of the air flow. This information not only helped to validate the specifications supplied by the manufacturers on the performance of the heat pumps but was also used in modelling to estimate the energy savings generated by the heat pumps.

A measurement campaign was conducted in homes located in the Montreal and Trois-Rivières regions to evaluate the energy saving potential associated with heat pumps for the Québec residential sector. The results of this study demonstrate that heat pumps installed according to current practices allow to generate significant energy savings of between 25% and 30% in the case of conventional heat pumps and between 45% and 50% in the case of variable speed heat pumps as compared to resistive heating equipment.

The experimental tests and the measurement campaign demonstrated that the energy saving potential of VRF injection heat pumps is significant for the Québec context. Nevertheless, certain issues must be addressed to promote the deployment of these technologies in the residential sector. We observed a lack of regulated criteria for the identification of these heating devices, the calculation of energy savings and the calculation of the impact on peak power demand.

5 REFERENCES

Johnson R. K. 2005. "Monitoring of two air source cold climate heat pumps", Johnson Research, LLC, CEATI Report No. T041700-7014.

Canadian Team Report

IEA HPT TCP Annex 41
"Cold Climate Heat Pumps"

Task 3 - Study of the C656-14 standard for evaluating the performance of heat pumps in heating mode (HSPF)

Submitted by:

Brice Le Lostec (contact: lelostec.brice@lte.ireq.ca)

Hydro Québec
Laboratorie des Technologies de l'Énergie (LTE)
Shawinigan, Québec

March 2017

TABLE OF CONTENTS

LIST OF TABLES

LIST OF FIGURES

1 GENERAL CONTEXT

1.1 Barriers to the Development of the Market for Heat Pumps Called "Cold Climate"

1.1.1 Position of the *American Council for an Energy-Efficiency Economy* (ACEEE) - (Stover, A. & al 2013)

In this document, the ACEEE analyzes the cryptic barriers (hidden or unrecognized) that hamper the deployment of some energy efficiency technologies in the residential sector. This is a category of barriers rarely addressed and is generally not a policy or program target. These barriers are usually linked to the codes and / or standards and are the result of problems related to uncertainties in the regulations, archaic regulations or inaccurate classification criteria and standards. Regarding archaic regulations, ACEEE notes that they have not evolved with technologies, products and techniques that they regulate. When these regulations do not address the original purpose and that they are obstacles to technological development and innovation, we can consider them as barriers. In addition, a classification criterion should be done with the simplest tests that can reasonably foresee in-field performance of current and anticipated products. These barriers inhibit investments that could represent a public interest. To remedy this problem, the ACEEE argues that governments should intervene with policies (or change it in strengths which can be problematic) to ensure that actions promoting the public interest are not penalized.

Among the energy efficiency technologies in the residential sector have unrecognized barriers hindering their deployment; heat pumps (heat pumps classification criteria calculations) are identified by the ACEEE. For this organization, heat pumps are a good example to work on the cryptic barriers because the classification methods (e.g. AHRI 210/240) are partly inaccurate and partly obsolete. In addition to a questioning of certain technical aspects of the AHRI 210/240, ACEEE emphasizes that the HSPF and SEER of a heat pump are based on the climatic zone 4 for the United States for simplicity (Canada, zone 5). However, the original intent of the standard did not have standardized values determined for an average region and are being applied to all regions. These points result that consumers and manufacturers (and the market in general) are affected. If standardized criteria are not precise, they will not promote (or divert) purchases and investments. Manufacturers then are not interested in developing better products. On the other hand, too complicated and too long classification systems are not easy to use for the consumer.

A brief analysis of stakeholders proposed by ACEEE is as follows:

- Manufacturers: They are reluctant to support a change in the methods of standardization as more accurate normalization may require costs to adapt / optimize the equipment to the new criteria. To justify that the most efficient equipment can be sold more expensive, it is necessary that the performance criteria can differentiate these devices from a gap in standardized criteria. Therefore, modification of performance criteria could influence this classification and thus affect manufacturers. When standardized performance criteria are not consistent, a manufacturer may not be able to establish the real performance difference between two devices.
- Other market players: A small change in equipment efficiency, following revision of the standard, should not apply to distributors and contractors, as long as the energy efficiency labels do not change. Poor standardization can lead to significant problems for programs of public utilities / agencies. As long as the standard criteria do not reflect the actual operating performance, they represent an important issue. If the energy savings of a program are based on these criteria and that it is not confirmed, the program could be a failure with the consequences that may result.

- Owners: More specific standardized criteria would help the owners to choose more efficient equipment enabling them to save energy and money. Generally, owners are changing their equipment when they are defective so they are more concerned about a quick replacement than by the quality and / or effectiveness of the product. In this context, the owners are basing on the minimum performance requirement to ensure a quick alternative; economical while ensuring minimal performance.
- US Department of Energy (DOE): DOE is working as part of a legal requirement that says that testing procedures must be reasonably designed to produce results that reflect energy efficiency and the use of energy which estimates the operating costs for an average usage cycle. As part of test methods and existing standards, the DOE must comply with specific criteria for assessing the cost and benefits on the modification of a standard. This also includes the economic impact for manufacturers and consumers, the impact on total energy savings, the impact on the product's usefulness and the performance. So while their mission should lead interest in the most effective way to normalize, it turns out the complexity of their objectives complicates their interests.

1.1.2 Position of the Northeast Energy Efficiency Partnerships (NEEP) - (NEEP 2014)

To summarize, the NEEP raises the fact that the main barrier to the rapid market introduction of next-generation high efficiency air-to-air heat pump is a lack of documentation on:

- The impact of heat pumps on energy
- Cost
- The peak consumption

Other barriers have been identified including:

- A lack of standardized metrics that adequately describe the operation of the low-temperature heat pumps
- A lack of knowledge among consumers and installers on new technologies
- A lack of controls to manage different heating systems
- A higher initial cost
- A lack of support or disregard from the political level

The NEEP (Northeast Energy Efficiency Partnerships) also raised its interest with ENERGY STAR (NEEP 2014) so that additional metric is added to products. Thus,

- The NEEP supporting the addition of performance metrics to qualify cold climate heat pump
- The NEEP raise the fact that the HSPF is not an accurate indicator to characterize – and distinguish – the heating capacity of a heat pump in a cold climate
- The addition of the COP and the ability to operate at colder temperatures (i.e. <-8.3°C) could be a good solution to identify products operating at low temperature (e.g. commercial Program of Vermont).

To erase the barriers described above, the NEEP proposes the following strategy, Figure 1:

Near-Term 2014-2015 Regional Stakeholders work through coordinated efforts to:
1. Develop more accurate tools to predict energy and cost savings associated with ASHP installations, through collection of real world performance data
2. Develop standardized Metrics for Cold Climate ASHP Performance
3. Increase Consumer Awareness and Education
4. Expand HVAC Contractor Awareness and Education
5. Improve Integration of ASHPs with Other Heating Systems
6. Provide ASHPs at Affordable Costs to Consumers
7. Characterize policy implications of large scale deployment of ASHPs
Long-Term 2016-2018 Regional Stakeholders work through coordinated efforts to:
8. Clarify the policy case for broad-scale deployment of ASHPs
9. Support federal appliance efficiency standards that incorporate improved cold climate performance metrics
10. Support International Code Council recognition of ASHP in model energy codes

Figure 1: Actions suggested by NEEP

1.1.3 Position of Bonneville Power Administration (BPA) – (EPS 2011)

BPA has directed and participated in numerous technical studies on residential heat pumps. This organization suggests a roadmap outlining the barriers to the deployment of heat pumps with variable capacity (VCHP), actions to be taken, and resources that can participate. The following chart, Figure 2, outlines the action plan, noted that for each identified barrier, an action plan is proposed. For more details on these action plans, the reader may consult the reference document.

The main barriers identified are:

- Contractor: Ignorance of heat pumps with variable capacity
- Designer: Ignorance of heat pumps with variable capacity
- Client: Ignorance of heat pumps with variable capacity
- Lack of information to prioritize measures
- Uncertainty about energy savings, cost and profitability
- Difficulty in developing measures and incentive programs
- Standards and Regulations
- Other

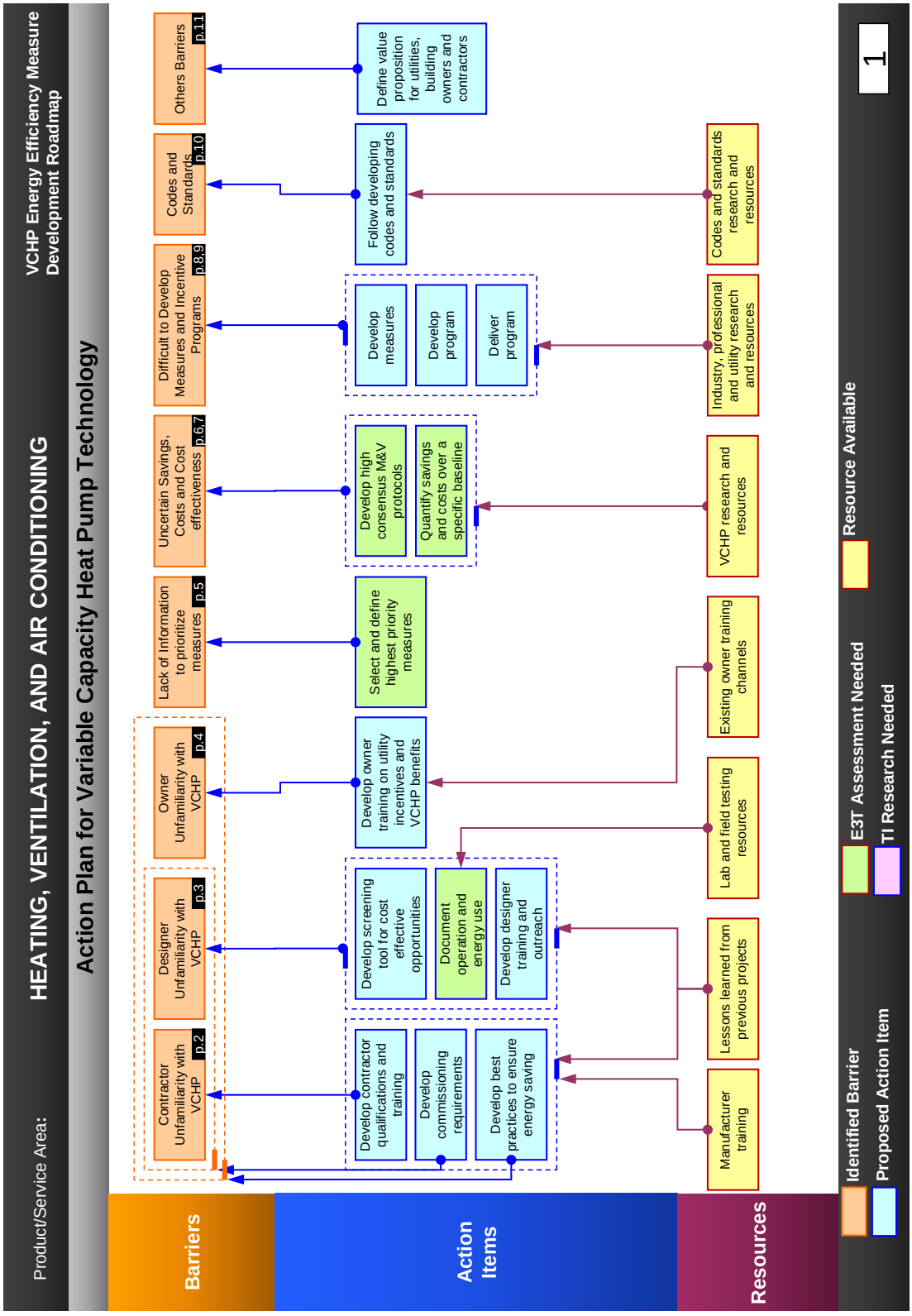

Figure 2: Barriers and actions (BPA)

1.2 Interventions to Modify the Standards and Regulations

1.2.1 Natural Resources Canada (NRCan), (NRCan 2004)

In 2004, NRCan has proposed making a mandatory report (not a qualifying standard, but simply to produce a report) on the energy efficiency ratio (EER). According to studies conducted by NRCan, the EER does not necessarily follow the seasonal energy efficiency ratio (SEER). There is a wide range of EER's for a given SEER. Many Canadian utilities are currently experiencing a peak in the summer. The EER will be of great importance to initiatives to reduce peak demand to delay the need to build more electricity-producing facilities. It is not considered that the production of a report with this information presents difficulties since some manufacturers already voluntarily provide this information to NRCan. Furthermore, EER ratings are required to assess the compliance of air conditioners and heat pumps for the ENERGY STAR® Label.

1.2.2 NRCan (2010)

During the revision of CSA C273.5 Standard – Installation of air source heat pumps and air conditioners – it became evident that additional information about the operation of these appliances in cold weather would be useful to choose a heat pump and determine the necessary capacity. Therefore, in 2010, NRCan has proposed additional requirements for the preparation of the report, Table 1.

Table 1: Modifications suggested by NRCan

Information to report	Calendar	Comments / justifications
COP (heating) at -8,3°C (17°F) Heating capacity at -8,3°C (17°F)	January 1, 2012	Value already measured during testing
COP (heating) at -17,8°C (0°F) Heating capacity at -17,8°C (0°F)	January 1, 2014	Value not measured; extra time to redo the test and report

If the energy efficiency ratio (EER) may be relevant for summer peaks, such capacity and COP could be relevant for winter peaks. It seems that there have been no developments since the publication of the draft regulation. Probably the manufacturers will not be more favorable to the proposed regulation (and perhaps even less) than for the preparation of the report on EER.

1.2.3 US EPA (US Environmental Protection Agency) - Revision of the qualification criteria ENERGY STAR (ENERGY STAR 2013)

On July 1st 2013, the U.S. EPA published a document (Framework 5.0) laying the foundations of the next version for qualifying Energy Star (US). In this document, EPA says it plans to set new performance parameters that would allow government agencies to differentiate products for the Northern Regions. After consultation with various stakeholders, EPA has concluded that the COP at 35°F (1.6°C) or at 17°F (-8.3°C) and the capacity at 17°F (-8.3°C) respond to this need. For the EPA, these performance parameters allow government organizations to characterize the performance during the winter peak on the power grid, like the EER does for the summer peak. In this document, EPA also proposes to require regional performance.

The public consultation on this document (Framework 5.0) indicates that manufacturers and AHRI are totally opposed to these changes. The main reasons for this opposition are the burden of additional work and a concern for national uniformity. Only NEEP supports these proposals. Therefore in the next version of EPA (Draft 1.0) published April 16, 2014, the low temperature performance parameters have been removed. Only regional specifications for SEER and EER were maintained, however, the comments received on regional specifications were in the majority, unfavorable.

EPA abandons the low temperature operating parameters for qualifying Energy Star but could be used for qualifying Energy Star Most Efficient Products, which strategically is not a bad idea.

1.2.4 International Energy Agency (IEA) - Annex 39 (HPC IEA 2010)

Annex 39 of IEA – A common method for testing and rating of residential HP AC and annual / seasonal performance – aims to establish methods of standardized tests and develop methods for calculating the seasonal coefficient of performance a heating system comprising a heat pump. Heating technologies with wood or gas would be taken into account in these methods. It is therefore relevant to monitor the evolution and the findings of this annex in order to validate that the current and future work carried out by LTE are consistent with the work of the various institutions of this annex.

2 CAN/CSA C656-14 STANDARD

2.1 Introduction

The CAN / CSA C656 Standard is based under Part 430 (Subpart B) of Appendix M of the Code of Federal US regulations "Uniform test method for measuring the energy consumption of air conditioner and central heat pump", itself based on ARI Standard 210 / 240-94.

2.1.1 Role and purpose of the standard

CAN / CSA standard C656-14 – *Performance standard for split-system and single-package central air conditioners and heat pumps* – is the recognized standard in Canada to evaluate the performance of heat pumps. This standard describes the procedure for calculating the HSPF (Heating Seasonal Performance Factor), SEER (Seasonal Energy Efficiency Ratio) and the EER (Energy Efficiency Ratio) which are three performance criteria, used in particular for ENERGY STAR Label. Essentially, it defines the tests, the conditions of tests, and the calculation procedure to calculate these performance criteria, for different types of heat pumps (Single-speed compressor speed, Two-stage compressor including cold climate heat pumps as defined in C656, and Variable-speed compressor).

- Seasonal energy efficiency ratio (SEER): The total energy (BTU) taken from the building to cool divided by the power consumption of the air conditioning unit (Wh);
- Heating seasonal performance factor (HSPF): The total energy required to heat the building (Btu) divided by the electric consumption of all heating equipment (Wh).

This standard applies to unitary air conditioners and heat pumps that are:

- Factory-made
- Air-source and/or air-sink
- Split-system matching assemblies (including mini-split and multi-split) or single package
- Of the type classified in Clause 1.2
- Intended for air-conditioning and space-heating applications in buildings

- Electrically driven, mechanical, vapour-compression-type systems
- Rated below 19.0 kW (65 000 Btu/h) heating or cooling at standard rating conditions, in accordance with Clause 5.2

This standard does not apply to the following:

- Burner-assisted air-source heat pumps
- Air-source/air-sink multi-function heat pump systems
- Integrated vapor-compression-type heat pump systems
- ”Direct Expansion Dedicated Outdoor Air Systems” (DX-DOAS)
- Water-cooled and evaporative-cooled unitary air conditioners and heat pumps.

This standard thus gives the minimum performance requirements applicable to the equipment in Canada. Moreover, the performance criteria achieved with the standard are used for ENERGY STAR. For the ENERGY STAR Label, heat pumps must meet the following criteria:

Table 2: Performance criterions to respect (CAN/CSA C656-14)

	Regulation	**ENERGY STAR**
$HSPF_V$	6.7	≥ 7.1
SEER	13	≥ 14.5
EER		≥ 12

2.2 Structure of the Standard

The standard consists of 9 Chapters and 2 Annexes:

Chapters:

1. Scope: This chapter describes the devices covered by this standard
2. Reference work: This chapter provides reference works (Mechanical Refrigeration Code, Canadian Electrical Code and heating and cooling equipment)
3. Definitions: This chapter provides some general definitions such as COP, HSPF, or SEER. The definitions that call more techniques are in Appendix B.
4. General requirements: Construction, design and assembly
5. Nominal characteristics: This chapter gives the definition of the rated power of equipment and the way to calculate it
6. Sampling Plan: Referred to in Annex A
7. Performance characteristics required: This chapter provides the minimum SEER and HSPF of different types of equipment and the SEER, EER, and HSPF minimum to be considered high-efficiency
8. Tests: Refers to Annex B gives some tests and parameters
9. Calculation of SEER and HSPF V: Refers to Annex B

Annexes:

1. Understanding the sampling plan
    - This Annex provides the steps confidence limit and gives a sample calculation
2. Uniform test method for measuring the energy consumption of central air conditioners (Including heat pumps)
    - This Annex is the basis of the standard. First, there is the experimental protocols for measuring the performance of equipment and second, the calculation procedure for calculating the SEER and HSPF.

2.3 Methodology of the Standard

2.3.1 Brief methodology of the standard

HSPF and SEER are calculated from the results of standardized experimental tests. Overall, these experimental tests and the method of calculation of performance criteria (air conditioning and heating) are adapted to the type of compressor used in the heat pump.

- One-stage compressor
- Two-stage compressor
- Variable-speed compressor

For each technology, the procedure of calculation and parameters of the experimental design (for HSPF) are given in the sections below).

For the HSPF, experimental tests are done at 62°F, 47°F, 35°F and 17°F as well as for some technologies. From the heating capacity and the measured power consumption, linear interpolations and extrapolations are made to estimate parameters for operating temperatures covering the climate zone referred. The method of calculating the HSPF is based on the BIN method, so for each temperature range of 5°F from 62°F to -23°F, the heating demand is met by the heat pump and / or electrical backup. The procedure assumes that the heat pump can heat the residence entirely a temperature above the balance point of the heat pump, while below the balance point an auxiliary electric system supplies the remaining heating.

2.3.2 The HSPF

The HSPF (Btu / hr / W) is equivalent to an average annual coefficient of performance, so it can be converted to an annual average COP when divided by 3.413. The calculation of HSPF is an estimate of the energy saving potential for a home with heating needs sized according to the standard capacity of the heat pump.

2.3.3 Referenced climatic conditions

According to CAN / CSA C656-14 Standard and Part 430 (Subpart B) of Appendix M of the U.S. *Code of Federal Regulations*, Zone V is characterized by a design temperature of -10°F, with 2 750 hours of heating. This number is used to calculate the annual heating load based on the DHR. It is determined from the following equation.

$$C \times DHR \times HLH = \frac{C \times DHR}{(65 - T_{OD})} \times \sum_{j=1}^{j} \frac{n_j}{N}(65 - T_j) \times HSH$$

Or:

$$HLH \times (65 - T_{OD}) = HSH \times \sum_{j=1}^{j} \left[\frac{n_j}{N}(65 - T_j)\right]$$

With:
HLH: Heating Load Hours (2750, zone 5, Table 3)
T_{OD}: Outdoor design temperature of the region (-10°F)
HSH: Heating Season Hours (6956, zone 5)
$\frac{n_j}{N}$: Fractional bin hours for the heating season, Table 4
T_j: Outdoor bin temperature
C: Correction factor (0.77)
DHR: Design heat load (Btu/hr) DHR

Table 3: Heating hours and air-conditioning hours for each climatic region (CAN / CSA C656-05)

Region	*CLHR*	HLH_R
I	2400	750
II	1800	1250
III	1200	1750
IV	800	2250
V	400	2750
VI	200	2750

The indoor design temperature is 65°F (18.3°C) in the CAN / CSA C656-14 Standard. For the C656 Standard, it is preferable to use the balance point of the house, with solar and internal gains considered to best represent the useful heating load.

Table 4: Information on Climate Regions (CAN / CSA C656-05)

Region Number		I	II	III	IV	V	VI
Heating Load Hours, *HLH*		750	1250	1750	2250	2750	2750*
Outdoor Design Temperature, T_{OD}		37	27	17	5	−10	30
j	T_j (°F)	Fractional Bin Hours, $\frac{n_j}{N}$					
1	62	.291	.215	.153	.132	.106	.113
2	57	.239	.189	.142	.111	.092	.206
3	52	.194	.163	.138	.103	.086	.215
4	47	.129	.143	.137	.093	.076	.204
5	42	.081	.112	.135	.100	.078	.141
6	37	.041	.088	.118	.109	.087	.076
7	32	.019	.056	.092	.126	.102	.034
8	27	.005	.024	.047	.087	.094	.008
9	22	.001	.008	.021	.055	.074	.003
10	17	0	.002	.009	.036	.055	0
11	12	0	0	.005	.026	.047	0
12	7	0	0	.002	.013	.038	0
13	2	0	0	.001	.006	.029	0
14	−3	0	0	0	.002	.018	0
15	−8	0	0	0	.001	.010	0
16	−13	0	0	0	0	.005	0
17	−18	0	0	0	0	.002	0
18	−23	0	0	0	0	.001	0

**Pacific Coast Region.*

2.3.4 Sizing and heating load

Chapter 28 of the ASHRAE 1985 – *Fundamentals Handbook - Energy Estimating methods* – proposes a calculation method to estimate the heating load required by a house. Details on this method are no longer available in Ashrae Handbooks (correction factor C, for example). The Degree-Day Method, which is used in the C656-14 Standard, is based on the assumptions that the heating load is proportional to the temperature difference between the outside temperature and 18.3°C and the solar and internal gains are a fraction of this heating load so that they are proportional to the temperature difference between the outside temperature and 18.3°C. According to Chapter 28 of the ASHRAE 1985 this procedure for calculating the heating load is used because of its simplicity and speed of calculation but that the difference between the calculation and the real need for home, which is influenced by the habits of the occupant, may be as much as 30% to 40%.

For the calculation of HSPFV, CAN / CSA C656-14 Standard states that the heating power required in the design (DHRmin) associated to an equipment, and this, at the external reference temperature, is equal to the heating capacity of the standard heat pump to 47°F (V region). For two-stage compressors, cold climate heat pumps, (see definition of the standard) it is possible to take the capacity of the first stage. So this would lead to lesser DHR, hence oversizing compared to a single-stage heat pump – which makes sense – and allowed by C273.5. For variable-speed heat pumps, it is possible to consider the heat capacity at 47°F for a compressor speed that corresponds to the maximum speed in **cooling mode**. This means that the calculation of the HSPF provides a dimensioning of the heat pump in relation to the need of heating and not in relation to those of air as specified by the CAN / CSA F280-12 / CSA C273.5-11.

CAN / CSA C656-14 standard provides for the calculation of a DHRmax, which corresponds to the Region V, at 2.2 times the DHRmin. The Federal Code CFR subpart C-430.32 (c) provides that for Region IV 4, the HSPF is calculated for DHRmin[2]. It would be interesting to have the recommendations of the Government of Canada on the choice of DHR necessary for calculating the HSPF for Region V. Although there is no official document to confirm this, it seems that for Canada the DHRmin is used (Cane, D. 2013). For Quebec, it would be interesting to analyze the DHR that would be the most representative of the situation, considering the actual design methods. It is important to note that the standard does not clearly specify whether the HSPFV is given for the DHRmin or on DHRmax, but it is highly likely to be calculated from the DHRmin (maximizing HSPF).

The procedure for calculating the HSPF through the use of a correction coefficient (C = 0.77) that weights the heating load for each temperature range ***i***. This correction factor is intended to get a better match between the calculated heating load and heating load typically measured. The difference there is between these two values is mainly internal and solar gains and thermal capacity of the building.

In the CAN / CSA C656-14 Standard, the heating load is calculated with the following equation. As explained previously, the DHR is directly proportional to the standard capacity of the heat pump

$$BL(T_i) = \frac{65 - T_i}{65 - T_{OD}} \times C \times DHR$$

With :

$BL(T_i)$	Building heating load (Btu/hr)
T_i	Outdoor bin temperature (Btu/hr)
T_{OD}	Outdoor design temperature of the region. Note that for Region V, the temperature considered is -10°F. This temperature is equivalent to that of Montreal and the warmest for Quebec. A small change in temperature will have a small effect on HSPF.
C	Correction factor (0.77)
DHR	Design heating requirement (Btu/hr)

2.3.5 Filling of heating needs

The HSPF calculation procedure assumes that the heat pump can heat the residence entirely for a temperature above the balance point of the heat pump, while below the balance

2 *Central air conditioners and heat pumps : The energy conservation standards defined in terms of the heating seasonal performance factor are based on Region IV, the minimum standardized design heating requirement, and the sampling plan stated in § 430.24(m)*.

point an auxiliary electric heating fills the remaining load. The heat pump always operates when the outside temperature is above its shutdown temperature. The CAN / CSA C656-14 assume that:

- There is no resistive power consumption above the balance point, even during defrosting. Only the heat pump is used
- The performance degradation during operation of the heat pump at part load is taken into account
- Below the balance point, the heat pump operates at full load. The remaining heat is then filled by an electrical element. Therefore, the electrical element is modulating.
- There is no defrosting below 17°F (-8.3°C)

2.3.6 Performance of heat pump at part load

When the heat pumps operate at partial load, i.e. above the balance point, a correction factor (PLFi≤1) on its power consumption is used to represent the performance degradation associated with cycling On/Off of the heat pump. The power consumption is equal to the consumption determined based on performance curves (therefore tests) divided by the correction factor. The PLF_i is calculated for each of the temperature ranges and it depends on the load of the heat pump represented by the ratio between the heating load and capacity of the heat pump. It is evaluated using the following equation:

$$PLF_i = 1 - C_D^h \bullet \left(1 - X\left(T_j\right)\right)$$

With;

$$X\left(T_j\right) = \begin{cases} BL\left(T_j\right) / Q_h\left(T_j\right) \\ or \\ 1 \end{cases} \quad \text{(minimum of both values)}$$

C_D^h, default value : 0.23

For the two-stage heat pump when the heating load is between the two capacities, a weighting on the heating output and power consumption is applied to assess the operating time on each stage. No correction factor (PLFi) is then applied for consumption.

For heat pumps with variable speed operation at a speed between the maximum speed and minimum speed, uses a specific calculation procedure. This procedure is based on the calculation of the balance point temperatures of the heat pump at the minimum and maximum speeds as well as the calculation of the COP at these temperatures. A second degree equation is established to calculate the COP for a compressor speed between the two extrema. This COP is then used to calculate the power consumption of the equipment, from the heating load.

2.3.7 Performance curves for single-stage heat pumps

For heat pump with one-speed compressor, the required tests (optional tests excluded) are at temperatures of 47°F (8.3°C) (high temperature, not in defrost mode), 35°F (1.7°C) (effect of defrost mode) and 17 ° F (-8.3°C) (low temperature, not in defrost) as noted in Table 5. These three tests are used to evaluate the performance curve of the heat pump between 62°F and -23°F (16.7°C to -30.6°C).

Between 47°F and 17°F, a linear interpolation between the test data at 47°F and 17°F is used to represent the performance of the heat pump.

$$Q_h(T_j) = \begin{cases} Q_h(17°F) + \dfrac{Q_h(47°F) - Q_h(17°F)}{47-17}(T_j - 17), T_j \geq 45°F \text{ or } T_j \leq 17°F \\ Q_h(17°F) + \dfrac{Q_h(35°F) - Q_h(17°F)}{35-17}(T_j - 17), 17°F \prec T_j \prec 45°F \end{cases}$$

$$E_h(T_j) = \begin{cases} E_h(17°F) + \dfrac{E_h(47°F) - E_h(17°F)}{47-17}(T_j - 17), T_j \geq 45°F \text{ or } T_j \leq 17°F \\ E_h(17°F) + \dfrac{E_h(35°F) - E_h(17°F)}{35-17}(T_j - 17), 17°F \prec T_j \prec 40°F \end{cases}$$

Table 5: Heating mode test conditions for single-speed or single-stage heat pumps (CAN / CSA C656-05)

	Air Entering Indoor Unit		Air Entering Outdoor Unit		
	Temperature (°F)		Temperature (°F)		Heating Air Volume Rate
Test Description	Dry Bulb	Wet Bulb	Dry Bulb	Wet Bulb	
H1 Test (required, steady)	70	60(max)	47	43	Heating Certified(1)
H1C Test (optional, cyclic)	70	60(max)	47	43	(2)
H2 Test (required)	70	60(max)	35	33	Heating Certified(1)
H3 Test (required, steady)	70	60(max)	17	15	Heating Certified(1)

(1) *Defined in Section 3.1.4.4.*
(2) *Maintain the airflow nozzle(s) static pressure difference or velocity pressure during the ON period at the same pressure difference or velocity pressure as measured during the* H1 *Test.*

Next, Figure 3 shows how the HSPF Region V is calculated according to Standard C656 for a heat pump with a one-speed compressor and for which the operation would not be restricted based on the outdoor temperature (no “stop” temperature or cut-off). It may be noted that the balance point of the heat pump can vary significantly depending on the DHR (min or max). This causes a variation in the resulting HSPF, which variation is however mitigated by the fact that below the balance point, the heat pump operates continuously at full load and the electric backup fills the remaining requirements.

If the heat pump operation should be restricted (“stopped” or cut-off) to the balance point of the heat pump[3], the change of HSPF, resulting from a change of DHR (min or max) would be larger.

[3]The heat pump does not work continuously under its balance point, especially when the auxiliary heat is not modulating and represents an important power, often greater than or equal to the design heat losses.

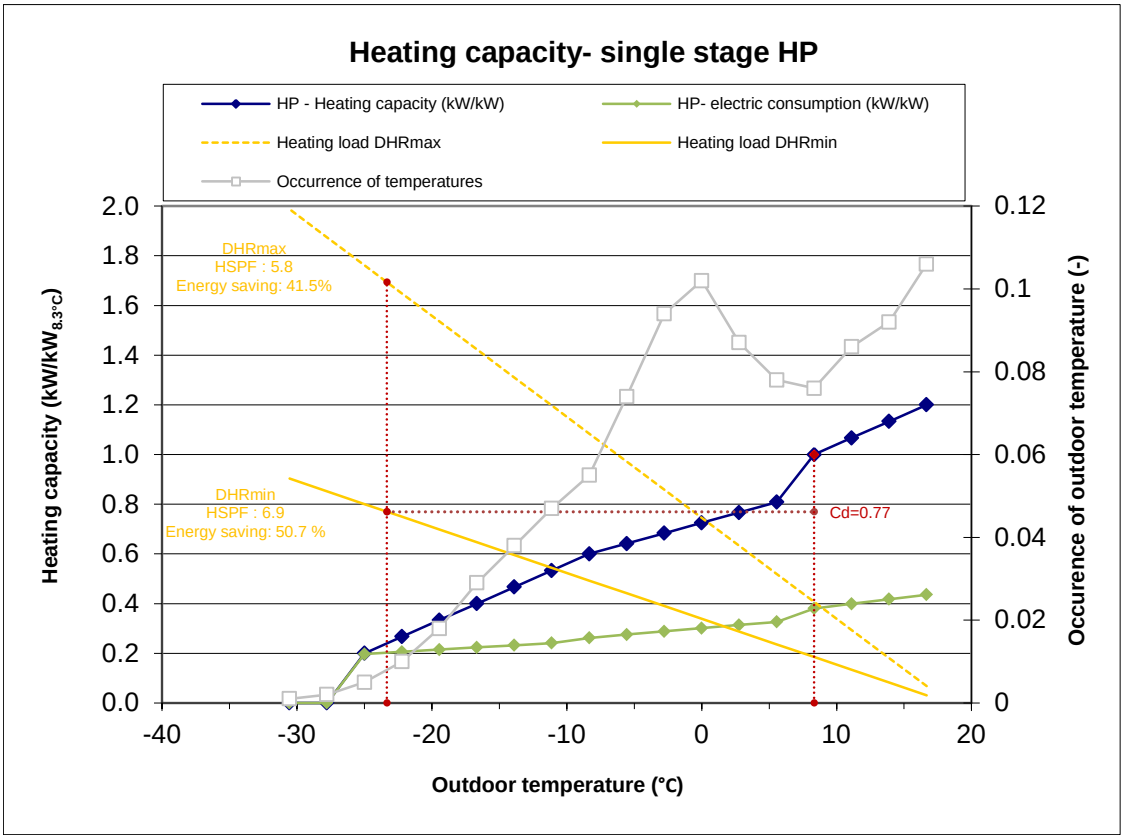

Note: The reference system for the energy saving is an electric resistance heating system.

Figure 3: Heating capacities – Single stage heat pump according to C656

2.3.8 Performance curves of the two-stage heat pump

For two-stage compressor heat pump, required tests (optional tests excluded) are at temperatures of 62, 47, 35 and 17°F with lower capacity and 47, 35 and 17°F at higher capacity as noted in Table 6. Tests at 35°F include the effect of defrost. To assess the performance curve of the heat pump of 62°F to -23°F, a similar procedure is applied to the single-stage heat pumps.

When the heat pump is operating at full capacity (on both stages, k = 2), the equations of conventional (one-stage) heat pump are used with the values of standardized tests for both stages in operation (k = 2). When a single stage is used, then the following equations are used:

First stage operation (k=1)

$$Q_h^{k=1}(T_j)=\begin{cases} Q_h^{k=1}(47°F)+\dfrac{Q_h^{k=1}(62°F)-Q_h^{k=1}(47°F)}{62-17}(T_j-47), T_j \geq 40°F \\ Q_h^{k=1}(17°F)+\dfrac{Q_h^{k=1}(35°F)-Q_h^{k=1}(17°F)}{35-17}(T_j-17), 17°F \leq T_j \prec 40°F \\ Q_h^{k=1}(17°F)+\dfrac{Q_h^{k=1}(47°F)-Q_h^{k=1}(17°F)}{47-17}(T_j-17), T_j \prec 17°F \end{cases}$$

$$E_h^{k=1}(T_j)=\begin{cases} E_h^{k=1}(47°F)+\dfrac{E_h^{k=1}(62°F)-E_h^{k=1}(47°F)}{62-17}(T_j-47), T_j \geq 40°F \\ E_h^{k=1}(17°F)+\dfrac{E_h^{k=1}(35°F)-E_h^{k=1}(17°F)}{35-17}(T_j-17), 17°F \leq T_j \prec 40°F \\ E_h^{k=1}(17°F)+\dfrac{E_h^{k=1}(47°F)-E_h^{k=1}(17°F)}{47-17}(T_j-17), T_j \prec 17°F \end{cases}$$

Second stage operation (k=2)

$$Q_h^{k=2}(T_j)=\begin{cases} Q_h^{k=2}(17°F)+\dfrac{Q_h^{k=2}(47°F)-Q_h^{k=2}(17°F)}{47-17}(T_j-17), T_j \geq 45°F \text{ or } T_j \leq 17°F \\ Q_h(17°F)+\dfrac{Qk=2_h(35°F)-Q_h^{k=2}(17°F)}{35-17}(T_j-17), 17°F \prec T_j \prec 45°F \end{cases}$$

$$E_h^{k=2}(T_j)=\begin{cases} E_h^{k=2}(17°F)+\dfrac{E_h^{k=2}(47°F)-E_h^{k=2}(17°F)}{47-17}(T_j-17), T_j \geq 45°F \text{ or } T_j \leq 17°F \\ E_h^{k=2}(17°F)+\dfrac{E_h^{k=2}(35°F)-E_h^{k=2}(17°F)}{35-17}(T_j-17), 17°F \prec T_j \prec 45°F \end{cases}$$

Table 6: Heating mode test conditions for two-speed or two-stage heat pumps (CAN / CSA C656-05)

Test Description	Air Entering Indoor Unit Temperature (°F) Dry Bulb	Air Entering Indoor Unit Temperature (°F) Wet Bulb	Air Entering Outdoor Unit Temperature (°F) Dry Bulb	Air Entering Outdoor Unit Temperature (°F) Wet Bulb	Compressor Capacity	Heating Air Volume Rate
$H0_1$ Test (required, steady)	70	60(max)	62	56.5	Low	Heating Minimum(1)
$H0C_1$ Test (optional, cyclic)	70	60(max)	62	56.5	Low	(2)
$H1_2$ Test (required, steady)	70	60(max)	47	43	High	Heating Certified(3)
$H1_1$ Test (required, steady)	70	60(max)	47	43	Low	Heating Minimum(1)
$H2_2$ Test (required)	70	60(max)	35	33	High	Heating Certified(3)
$H2_1$ Test(4) (required)	70	60(max)	35	33	Low	Heating Minimum(1)
$H3_2$ Test (required, steady)	70	60(max)	17	15	High	Heating Certified(3)
$H3_1$ Test(4) (required, steady)	70	60(max)	17	15	Low	Heating Minimum(1)

(1) *Defined in Section 3.1.4.5.*
(2) *Maintain the airflow nozzle(s) static pressure difference or velocity pressure during the ON period at the same pressure difference or velocity pressure as measured during the* $H0_1$ *Test.*
(3) *Defined in Section 3.1.4.4.*
(4) *Required only if the heat pump's performance when operating at low compressor capacity and outdoor temperatures less than 37 °F is needed to complete the Section 4.2.3* HSPF *calculations.*

The same observations as in Figure 3 can be made to Figure 4 and Figure 5. For the two-stage cold climate heat pump (Figure 4) the effect of DHR (sizing as anticipated in C656) on energy savings is less than for single-stage heat pump (Figure 3) and the two-stage "non-cold climate" heat pump (Figure 5) because the sizing is based on the heating capacity on the first stage. Therefore the balance point (DHRmin and DHRmax) are relatively low, and

this allows the heat pump to cover a significant part of the heating (low temperatures occurrences is low). In addition, the operation on the first stage at partial load also limits the performance penalty during cycling (On / Off).

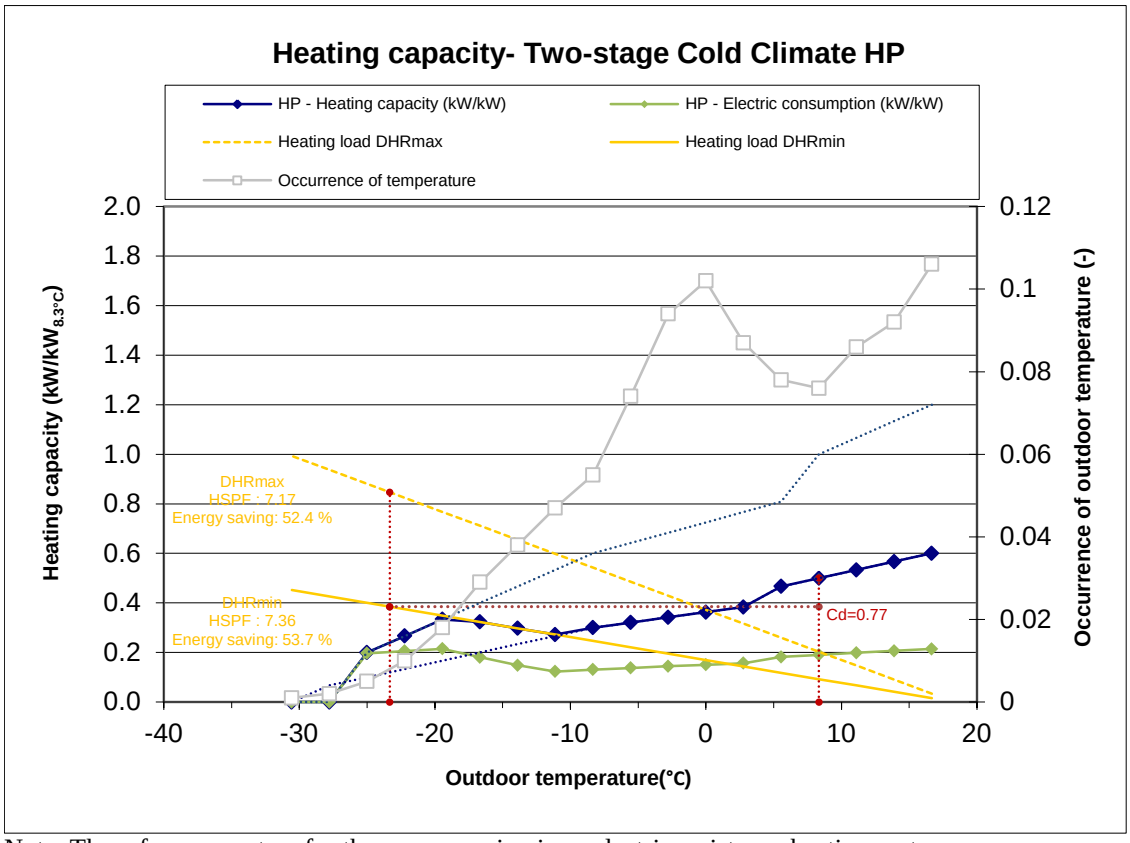

Note: The reference system for the energy saving is an electric resistance heating system.

Figure 4: Standard heating capacities – Two-stage "Cold climate" heat pump according to C656

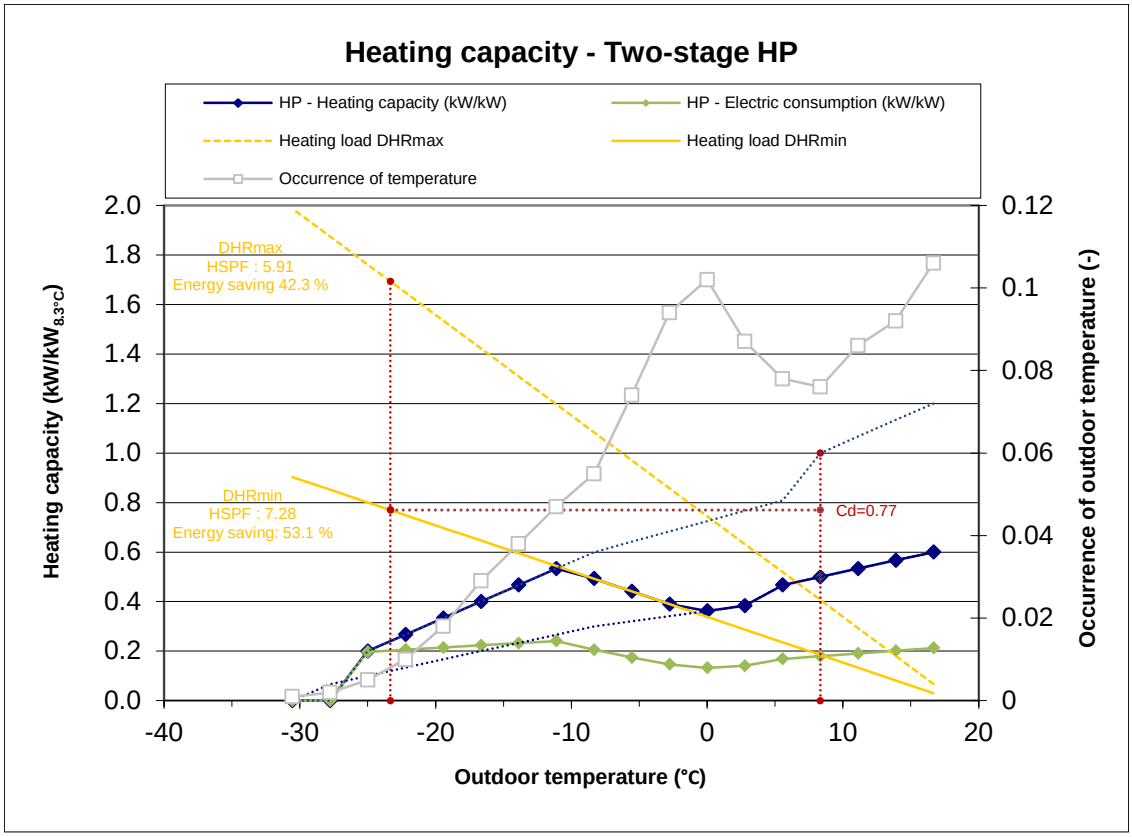

Note: The reference system for the energy saving is an electric resistance heating system.

Figure 5: Standard heating capacities – Two-stage "Non-Cold climate" heat pump according to C656

2.3.9 Performance curves for variable-speed heat pumps

For variable speed heat pumps, the required tests (optional tests excluded) are at 62 and 47°F temperature at the minimum speed, at 35°F at an intermediate speed and at 47 and 17°F at maximum speed as noted in Table 7. The test at 35°F includes the effect of the defrosting.

According to laboratory tests, the maximum speed of the compressor at 47°F is less than the maximum speed at 17°F (-60%), which is also observed on manufacturer's data. Therefore, $Q_h^{k=2}(47°F)$ was calculated using an extrapolation of data at low temperature in order to be consistent with equations (9) and (10) expressed below. Note that it is important to have the same speed for $Q_h^{k=2}(17)$ and $Q_h^{k=2}(47)$ in order that the calculation of high-speed performance and in particular at temperatures below 17 °F is consistent (equations (9) and (10) below). Regarding the sizing, as the compressor speed seems constrained at 47°F, it is reasonable to assume that the capacity used for the sizing is the actual capacity (constrained) at 47°F, therefore the capacity given by experimental tests or by the manufacturer. Probably for sizing based on CAN / CSA C656, the optional H_{1N} test is performed in order to have the nominal capacity required for sizing. Data for this test are not available.

The intermediate speed is calculated from the maximum speed and minimum speed:

$$v^{k=v} = v^{k=1} + \frac{v^{k=2} - v^{k=1}}{3}$$

For variable-speed heat pumps, the method of calculation of performance curves is more complex than for other technologies. Nevertheless it can be summarized as follows:

Operation at minimum speed

$$Q_h^{k=1}(T_j) = Q_h^{k=1}(47°F) + \frac{Q_h^{k=1}(62°F) - Q_h^{k=1}(47°F)}{62-17}(T_j - 47) \quad (1)$$

$$E_h^{k=1}(T_j) = E_h^{k=1}(47°F) + \frac{E_h^{k=1}(62°F) - E_h^{k=1}(47°F)}{62-17}(T_j - 47) \quad (2)$$

Operation at intermediate speed

$$Q_h^{k=v}(T_j) = Q_h^{k=v}(35°F) + M_Q(T_j - 35) \quad (3)$$

$$E_h^{k=v}(T_j) = E_h^{k=v}(35°F) + M_E(T_j - 35) \quad (4)$$

With M_Q and M_E that represent the slope (or change) of the performance of the heat pump at the intermediate speed. These parameters are calculated from a weighting of medium and high speed performance.

$$M_Q = \left[\frac{Q_h^{k=1}(62°F) - Q_h^{k=1}(47°F)}{62-47}(1 - N_Q)\right] + \left[\frac{Q_h^{k=2}(35°F) - Q_h^{k=2}(17°F)}{35-17}N_Q\right] \quad (5)$$

$$M_E = \left[\frac{E_h^{k=1}(62°F) - E_h^{k=1}(47°F)}{62-47}(1 - N_Q)\right] + \left[\frac{E_h^{k=2}(35°F) - E_h^{k=2}(17°F)}{35-17}N_Q\right] \quad (6)$$

The parameters N_Q and N_E represent the ratio of performance for different speeds. They are used to weight the performance in the preceding equations.

$$N_Q = \frac{Q_h^{k=v}(35°F) - Q_h^{k=1}(35°F)}{Q_h^{k=2}(35°F) - Q_h^{k=1}(35°F)} \quad (7)$$

$$N_E = \frac{E_h^{k=v}(35°F) - E_h^{k=1}(35°F)}{E_h^{k=2}(35°F) - E_h^{k=1}(35°F)} \quad (8)$$

Operation at maximum speed

At the maximum speed of equations similar to one-speed (conventional) heat pumps are used.

$$Q_h^{k=2}(T_j) = \begin{cases} Q_h^{k=2}(17°F) + \frac{Q_h^{k=2}(47°F) - Q_h^{k=2}(17°F)}{47-17}(T_j - 17), T_j \geq 45°F \text{ or } T_j \leq 17°F \\ Q_h(17°F) + \frac{Qk=2_h(35°F) - Q_h^{k=2}(17°F)}{35-17}(T_j - 17), 17°F \prec T_j \prec 45°F \end{cases} \quad (9)$$

$$E_h^{k=2}(T_j) = \begin{cases} E_h^{k=2}(17°F) + \dfrac{E_h^{k=2}(47°F) - E_h^{k=2}(17°F)}{47-17}(T_j - 17), T_j \geq 45°F \text{ or } T_j \leq 17°F \\ E_h^{k=2}(17°F) + \dfrac{E_h^{k=2}(35°F) - E_h^{k=2}(17°F)}{35-17}(T_j - 17), 17°F \prec T_j \prec 45°F \end{cases} \quad (10)$$

Table 7: Heating mode test conditions for variable-speed heat pumps (CAN / CSA C656-05)

	Air Entering Indoor Unit		Air Entering Outdoor Unit			
	Temperature (°F)		Temperature (°F)			
Test Description	Dry Bulb	Wet Bulb	Dry Bulb	Wet Bulb	Compressor Speed	Heating Air Volume Rate
$H0_1$ Test (required, steady)	70	60(max)	62	56.5	Minimum	Heating Minimum(1)
$H0C_1$ Test (optional, cyclic)	70	60(max)	62	56.5	Minimum	(2)
$H1_2$ Test (required, steady)	70	60(max)	47	43	Maximum	Heating Certified(3)
$H1_1$ Test (required, steady)	70	60(max)	47	43	Minimum	Heating Minimum(2)
$H1_N$ Test (optional, steady)	70	60(max)	47	43	Cooling Mode Maximum	Heating Nominal(4)
$H2_2$ Test (optional)	70	60(max)	35	33	Maximum	Heating Certified(3)
$H2_V$ Test (required)	70	60(max)	35	33	Intermediate	Heating Intermediate(5)
$H3_2$ Test (required, steady)	70	60(max)	17	15	Maximum	Heating Certified(3)

(1) *Defined in Section 3.1.4.5.*
(2) *Maintain the airflow nozzle(s) static pressure difference or velocity pressure during the ON period at the same pressure difference or velocity pressure as measured during the* $H0_1$ *Test.*
(3) *Defined in Section 3.1.4.4.*
(4) *Defined in Section 3.1.4.7.*
(5) *Defined in Section 3.1.4.6.*

The same observations as in Figure 3, Figure 4, and Figure 5 can be made to Figure 6.

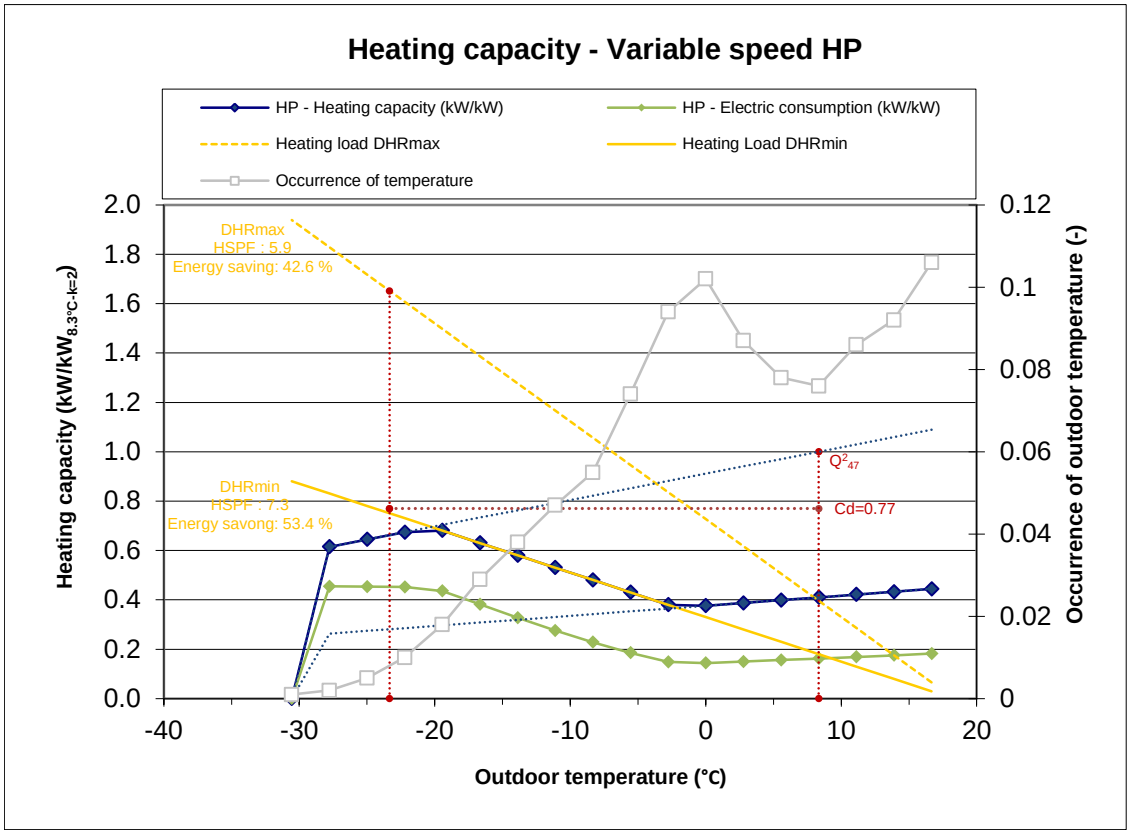

Note: The reference system for the energy saving is an electric resistance heating system.

Figure 6: Standard heating capacities – Variable-speed heat pump according to C656

2.4 Conclusion

The Standard C656 allows establishing the performance of heat pumps with different technologies either for heating or air conditioning. This standard is based on laboratory performance measurements at different temperatures (62°F, 47°F, 35°F and 17°F for HSPF) which are subsequently used in a calculation model.

3 PROBLEMS ENCOUNTERED WITH STANDARD CAN/CSA C656-14

3.1 Introduction

A field measurement campaign was conducted in 2011-2013 by Le Lostec (2014) in order to measure the performance of heat pumps in real situations. This study highlights an important difference between the measured performance and the HSPF of heat pumps. Some results of this study are presented in order to highlight the difference observed between the measurement and the HSPF, and identified causes that can explain them.

Figure 7 shows the average coefficient of performance (COP) of heat pumps on the heating period. It characterizes the ratio of the thermal energy supplied by the heat pump and the electrical energy it consumes during the entire heating period. Therefore, this coefficient of performance depends on the operating time of the heat pump to the different outdoor temperatures. It reflects the heat pump stops and starts, and the energy consumption associated to defrost. It is between 1.5 (single stage heat pumps) and 2.5 (other heat pumps). The coefficient of performance is an equipment performance criterion which is independent of the building's characteristics.

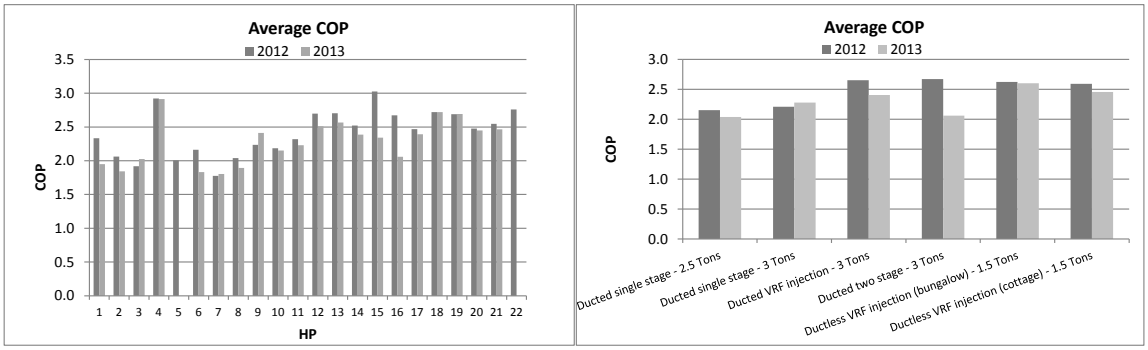

Figure 7: Average Coefficient of Performance (COP) of heat pumps

The HSPF is compared to the average coefficient of performance of the global heating system (COPsystem) obtained from the measured values during the pilot project and for the entire heating season. The COPsystem is equivalent to the ratio between the heating needs of the house and the total power consumption of the various heating equipment. The fan energy consumption is included in the calculation of the COPsystem when a heating system, included into a central system, is in operation. The fan energy consumption is excluded from the calculation of the COPsystem when the heat pump and the electric back-ups are not activated. Figure 8 shows that the HSPF is not adapted to estimate the energy savings associated with the use of a heat pump.

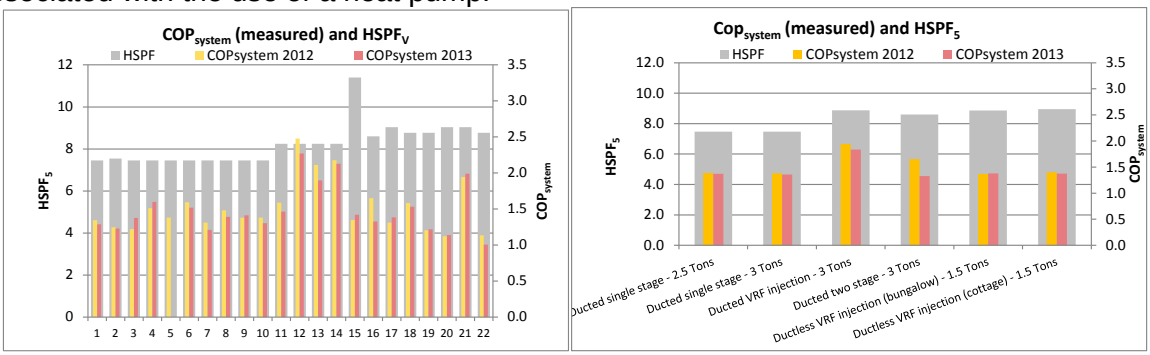

Figure 8: HSPF of heat pumps

The difference between the HSPF and the COPsystem is caused by various factors, which result primarily from the very objective of the HSPF. This criterion is used to characterize the performance of a device, not a heating system. This performance must be calculated / evaluated in optimal operating conditions that are to say without the influence of other equipment such as electrical backup. Therefore, the HSPF is representative of the energy savings in an ideal system (modulating back-up, no cut-off added to the installation, ideal thermostat, sizing corresponding to that used in calculating the HSPF ...) which is certainly not the situation in Quebec. Thereby the HSPF can be used to classify equipment of similar technologies. To better represent the situation in Quebec, the HSPF minimally should consider:

1. The “stop” temperatures installed by contractors
2. The non-modulation back-up heat below the balance point
3. A sizing according to current standards, that depends on the cooling load. This should be addressed by national regulations because the Standard C656 allows a sizing range that seems realistic.

Various studies questioned some of the assumptions and parameters used in calculating the HSPF. For example, the study of Ecotope (2011) on behalf of the Northwest Energy Efficiency Alliance (NEEA) states clearly that the HSPF and SEER are not criteria that

determine the performance of heat pumps. The most problematic elements are discussed in the following sections.

3.2 Referenced Climatic Conditions

According to CAN / CSA C656-14 Standard and Part 430 (Subpart B) of Appendix M of the U.S. Federal Code of Regulations, the Region V is characterized by a design temperature of -10°F and 2 750 hours of heating. But according to CAN / CSA F280-M90, the design temperature in Quebec varies among cities and is between -10°F (Montreal) and -23°F (Roberval) for Northern Quebec. A sensitivity analysis of the HSPF at this design temperature should show that this criterion is of little influence. A decrease in the design temperature should cause an increase in the HSPF because it causes an oversizing of the heat pump in compared to the calculated value in the standard or a decrease in the load for a constant capacity heat pump. The potential for energy efficiency (HSPF) can then be improved.

At first glance, the distribution of the dimensionless heating hours for climatic Zone V, as seen in Figure 9, compared to the total annual dimensionless heating hours for Montreal (temperature range of 5°F from 62°F to -23°F), is very similar, according to Dumont (2009).

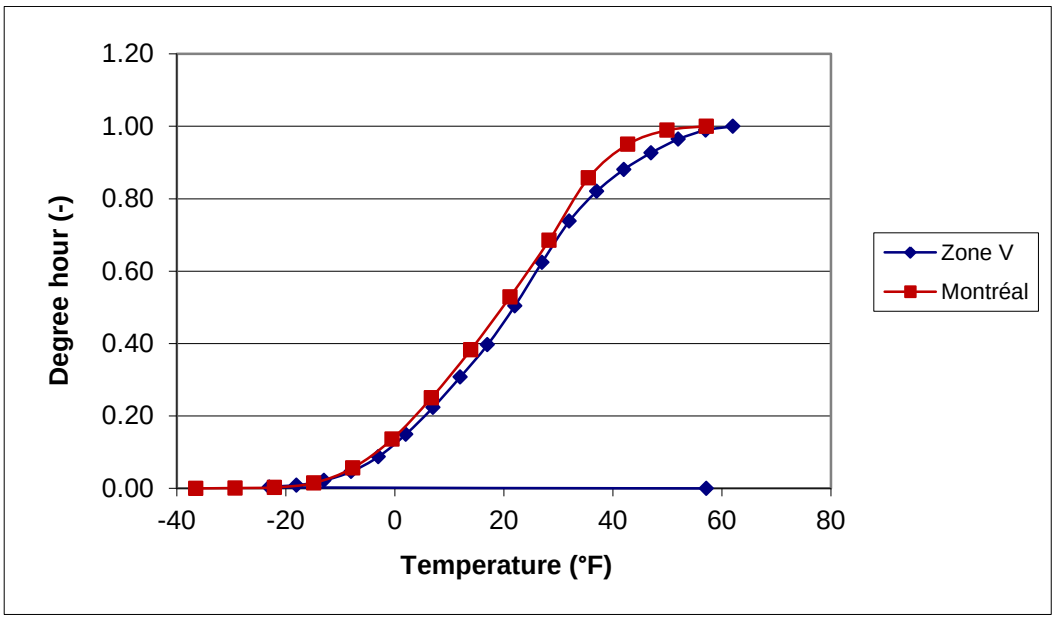

Figure 9: Summation as a function of temperature normalized Degree-hours (Dumont 2009)

In Table 8 the fractional bin hours for Montreal is set for the heating season only and the fractional bin hours for Zone V comes from Figure 10. Results for Montreal give a significant decrease in the number of hours between 40°F and 60°F. So we can ask ourselves, namely whether the distribution of temperatures above 40°F is actually representative of the heating period.

Table 8: Number of cooling and heating hours for each Region (CAN/CSA C656-05)

Region	*CLHR*	HLH_R
I	2400	750
II	1800	1250
III	1200	1750
IV	800	2250
V	400	2750
VI	200	2750

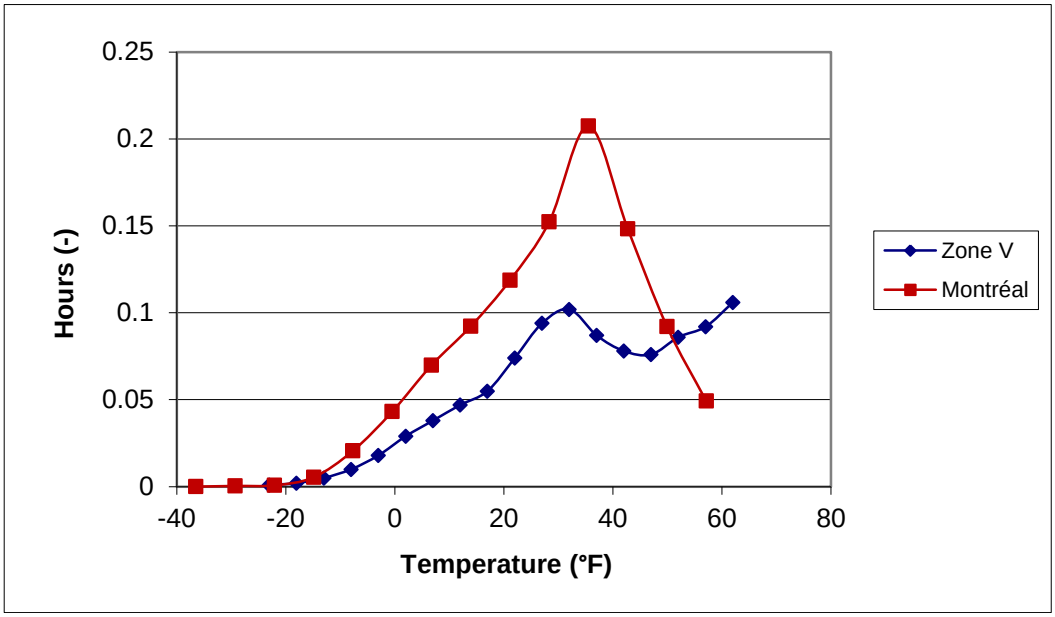

Figure 10: Fractional bin hours (Dumont 2009)

The indoor calculation temperature, from CAN / CSA F280-M90 Standard, is 22°C (71.5°F) against 65°F (18.3°C) in the CAN / CSA C656-14 Standard. The F280 Standard, regarding the sizing of heating equipment, has the advantage to use a higher (warmer) indoor design temperature to avoid undersized heating equipment. For the C656 Standard, it is preferable to use the house balance point, with solar and internal gains considered to best represent the useful heating load. Francisco W (2004) and Erbs (1986) propose a house balance point between 55°F and 60°F (12.6°C to 15.6°C), which, according to them, would probably be more representative of the current housing stock.

Region Number		I	II	III	IV	V	VI
Heating Load Hours, *HLH*		750	1250	1750	2250	2750	2750*
Outdoor Design Temperature, T_{OD}		37	27	17	5	−10	30
j	T_j (°F)	Fractional Bin Hours, $\frac{n_j}{N}$					
1	62	.291	.215	.153	.132	.106	.113
2	57	.239	.189	.142	.111	.092	.206
3	52	.194	.163	.138	.103	.086	.215
4	47	.129	.143	.137	.093	.076	.204
5	42	.081	.112	.135	.100	.078	.141
6	37	.041	.088	.118	.109	.087	.076
7	32	.019	.056	.092	.126	.102	.034
8	27	.005	.024	.047	.087	.094	.008
9	22	.001	.008	.021	.055	.074	.003
10	17	0	.002	.009	.036	.055	0
11	12	0	0	.005	.026	.047	0
12	7	0	0	.002	.013	.038	0
13	2	0	0	.001	.006	.029	0
14	−3	0	0	0	.002	.018	0
15	−8	0	0	0	.001	.010	0
16	−13	0	0	0	0	.005	0
17	−18	0	0	0	0	.002	0
18	−23	0	0	0	0	.001	0

**Pacific Coast Region.*

Figure 11: Weather Data for Climatic Regions (CAN/CSA C656-05)

3.3 "C" Coefficient

According to Fancisco, PW (2004), the seasonal performance factors are often used to forecast annual consumption and energy savings associated with the replacement or installation of equipment. However, the actual performances of equipment depend on a variety of factors such as the climate in which it is used or building heat loss. In addition, the overall energy consumption for heating and seasonal performance of the heating system can be heavily influenced by factors such as the sizing of the equipment, the control strategy, and losses in distribution ducts. For specific projects, the authors recommend to calculate the HSPF with the actual values of the site weather and building heating load. However, this requires knowledge of the degradation factor and some changes to the method of calculating the HSPF. This study revealed several inconsistencies between the performance of calculated heat pumps with the Standard, and that we can expect to get in a real situation. Thus, the authors propose to modify the "C" Factor (internal gain and balance point).

Fairey, P. et al. (2004) also stresses that the" C" coefficient is a correction factor (0.77) which corrects the heating load in the BIN model to get closer to the experimental values, Figure 12. Nevertheless, the authors report the results of a 1980 EPRI study (the study is no longer available) where it is demonstrated that the "C" coefficient can range from 0.4 to 1.2 in the homes of those years. Didon, DA (1979) proposed the procedure which is based on calculating the HSPF; however the author explicitly states that the "C" coefficient is set to 0.77 (in 1979) and that it can be adjusted in the future, which was not done.

For a heat pump with a known heating capacity, the HSPF is calculated for a house with a fixed gross heating load (DHR). To take account of gains (internal, solar ...), the net heating load is assumed to be 0.77 ("C" factor) times the gross load for each temperature ranges. According to the authors, the fact of using a correction factor is due to the fact that the calculated gross heating load does not match the measured load (internal and solar gains) and the balance point of the house (calculated) is higher than the measured balance point. Nonetheless the authors stress that assuming that these gains are equal to 0.23 times the gross load means that the gains increase as the outdoor temperature decreases. The authors propose using an absolute value of heat gains in order, firstly to better represent the reality and on the other hand to reduce the balance point of the house.

Note: Additional information is available on the "C" factor in the ASHRAE1985 (Chapter 28) and ASHRAE 1989 (Chapter 28)

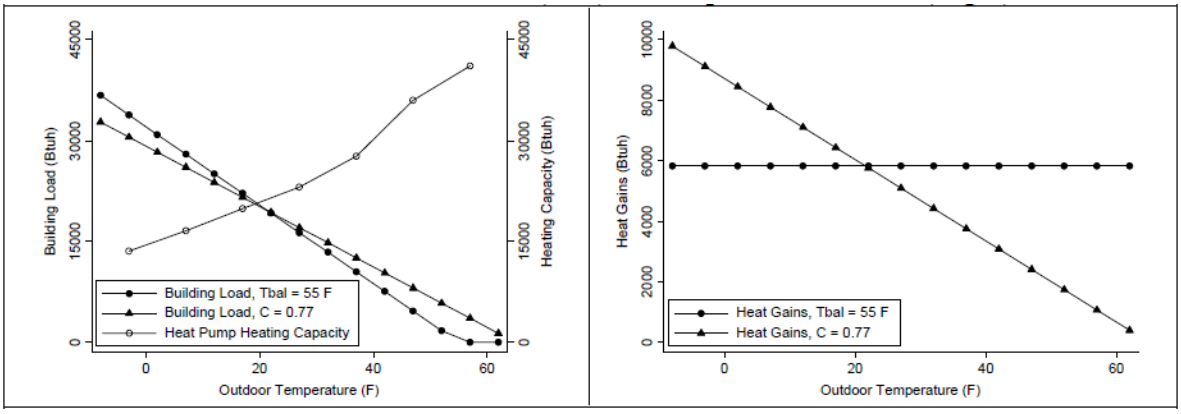

Figure 12: Effect of "C" Factor on the heating slope

Prior to this study, Cane, D. (1979) proposed to use constant internal gains in the BIN method of ASHRAE.

3.4 Degradation Coefficient

To calculate the performance of a heat pump operating at partial load, when the outside temperature is above the balance point, a degradation coefficient (C_d) is used. Its default value is 0.25, and can be calculated from optional tests. For Francisco, PW (2004), this factor should be published to enable calculations and compare the performance in part load operation. Since this parameter is not known, it is necessary to use the default value to make the calculation of HSPF, which does not allow differentiating the equipment with the best coefficients of degradation. In addition, it is currently difficult to identify characteristics (technical, control ...) that achieve a good coefficient of degradation, since that they are not known.

3.5 Modulation and Cut-off

In Quebec, the heat pump installers prevent equipment operation when the outdoor temperature is below -12°C. There are different ways to disable the heat pump; however, the most common is to install a thermostat in the outdoor unit of the heat pump:

- Adding a thermostat in the outdoor unit
- Integrated option by the manufacturer in the outdoor unit
- Parameter integrated directly into the thermostat setting

The main reason for this are:

- Economic profitability (COP> 1, including defrost)
- Maintain comfort (minimum supplied air temperature to be respected)
- Limits maintenance during extreme winter conditions
- Limits premature wear of the heat pump
- Installation practice related to Hydro-Québec's Rate DT (usually, with an oil-fired back-up heating system)

The CAN / CSA C656-14 Standard assumes that heat pumps can operate below the balance point as long as the COP is greater than 1 or that a temperature sensor does not shut down the equipment. Below the balance point, the heat pump is supposed to operate continuously and a backup heating supplements the required heat between the capacity of the heat pump and the total heating needs. Now, according to Dumont (2009):
"*…in fact, the system installed often prevented such operation. If the heat pump's condenser coil is installed downstream of the furnace, which is always the case of fuel systems to avoid condensation on the heat exchanger of the generator during the cooling season, it is impossible to compensate for the lack of power by a partial operation of the furnace for raising the temperature upstream of the condenser would reduce possible heat exchange therewith. Furthermore, most fuel-fired supplemental (back-up or auxiliary) heater does not allow operation at reduced power. In the cases where the heat pump and the auxiliary heater may operate simultaneously (usually systems using electric coils), the power of the auxiliary heater is usually not modulated. It thus operates in priority and responds quickly to heating demand, thus reducing the contribution of the heat pump. Furthermore, a probe with a switch normally avoids the operation of the heat pump below a certain threshold temperature which may vary from one installation to another…"* This stop temperature for the conventional heat pump is usually between -10°C and -12°C.

Above the balance point, the heat pump is supposed to fill all of the heating needs. The calculation of the HSPF based on these assumptions, highlights that the HSPF corresponds to a situation that maximizes energy savings (ideal operation), which seems logical, since it is a performance criterion of an equipment, and not of a system (heat pump and auxiliary heating), but has some limitations.

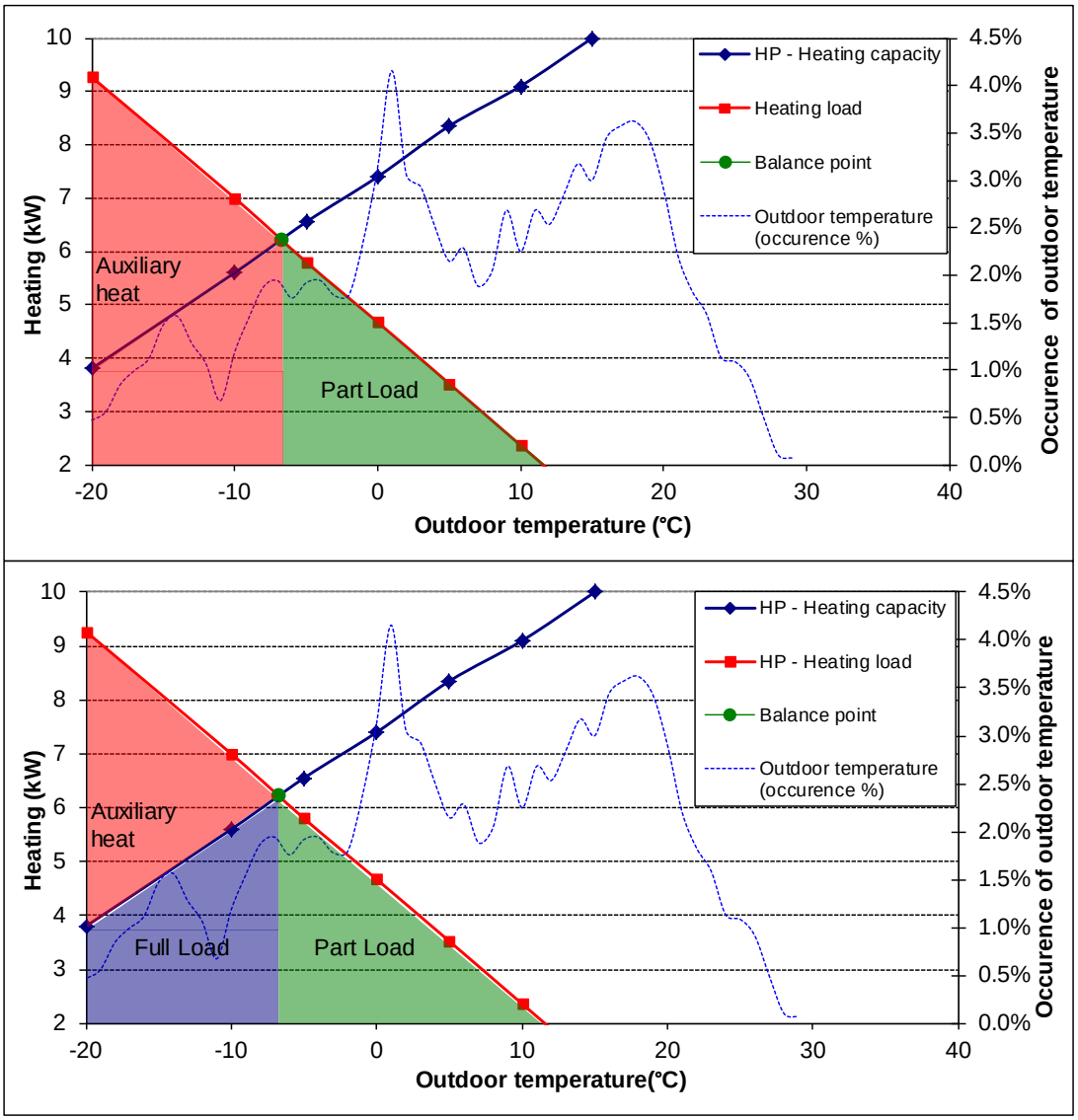

Figure 13: Example of operation – Modulation of the auxiliary heater or shut down of the heat pump at the balance point

In Quebec, the installation of cut-off (-12°C) on conventional heat pumps ensures that the stop temperature of the heat pump is close to the balance point. Furthermore the use of a non-modulating electric backup tends to fill quickly the heating demand which in consequence is limiting the energy savings from a heat pump. As part of a furnace system with fuel oil, it is very rarely used in parallel with the heat pump; it is therefore not relevant to consider the energy savings below the balance point. Note that in the standard, the auxiliary is implicitly a resistive equipment because its energy consumption is equal to its heating capacity (efficiency is 100%).

The cut-off is usually configured to disable the heat pump between -8°C and -12°C, except for heat pumps called "cold climate" where no cut-off is installed. Since the cut-off is not installed by the manufacturer, the HSPF of this equipment does not account for this “cut-off” and its effect on the operation of the heat pump. It would be appropriate to propose a method of calculating the HSPF taking into account the cut-off.

The report of Le Lostec (2013a) shows the effect of modulation and the cut-off on the HSPF, and this for various DHR. Essentially, the relative energy savings decrease with under-sizing

of the heat pump whether or not the electric backup is modulating. This tendency is accentuated when operating with a stop at equilibrium. This is logical in so far because below the balance point, the heat pump cannot meet all needs, and this is accentuated when the heating load for a given heat pump increases. For a large oversizing the opposite effect is observed, which is explained by the large share of operating above the balance point generating a part load operation and therefore a degradation of performance due to cycling (on-off) of the heat pump (on the first stage or on low speed). In this case, the balance point is low, the number of hours of heating below this point is very low and therefore the effect of modulating or not have little impact on energy savings. For conventional or "non-cold climate two-stage" heat pumps, the same finding can be said for modulation. Generally, the cut-off tends to decrease the energy savings whether there is modulation or not. When the balance point is higher than the stop temperature, energy savings are identical for scenarios without modulation. When the sizing decreases, the energy savings tend to approach, for both scenarios having a modulation.

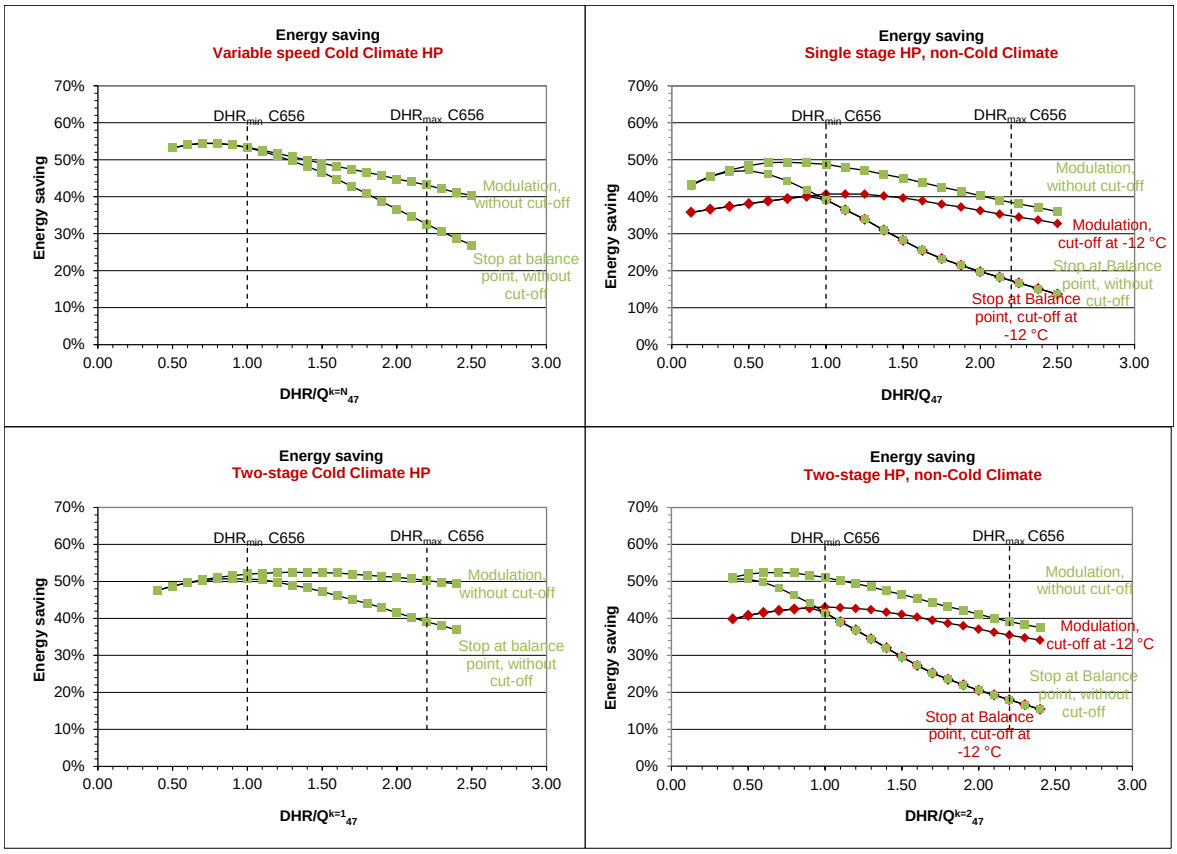

Figure 14: Effect of DHR, modulation (of electric back-up) and cut-off on relative energy savings

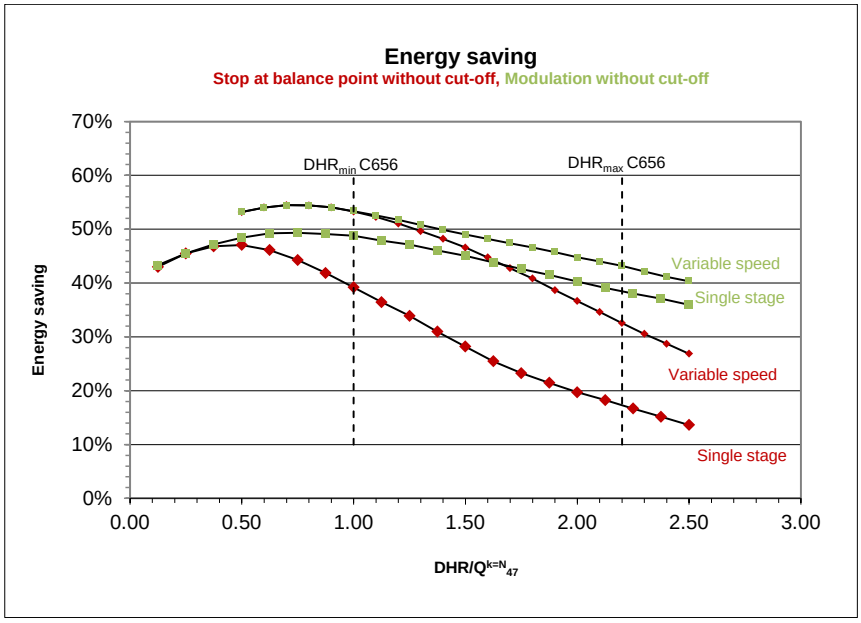

Figure 15: Comparison between variable-speed and conventional heat pumps

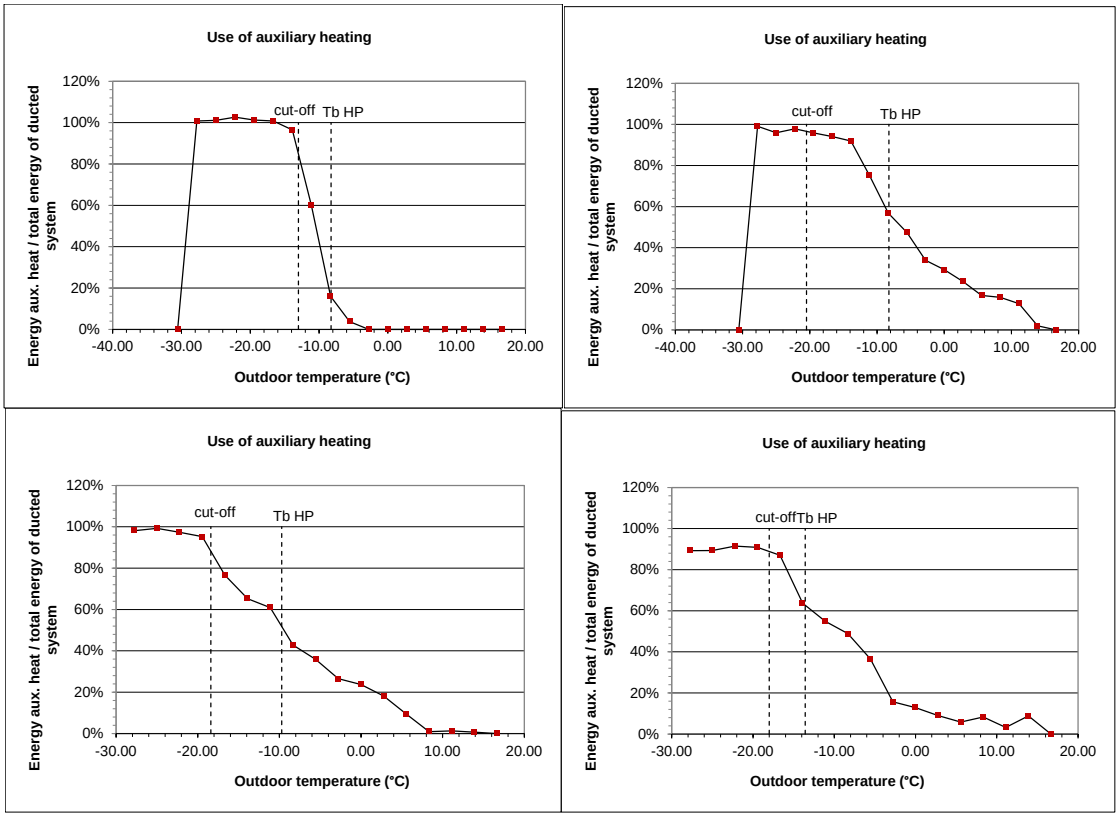

Figure 16: Use of electric backup – Conventional heat pump (experimental data - 4 installations)

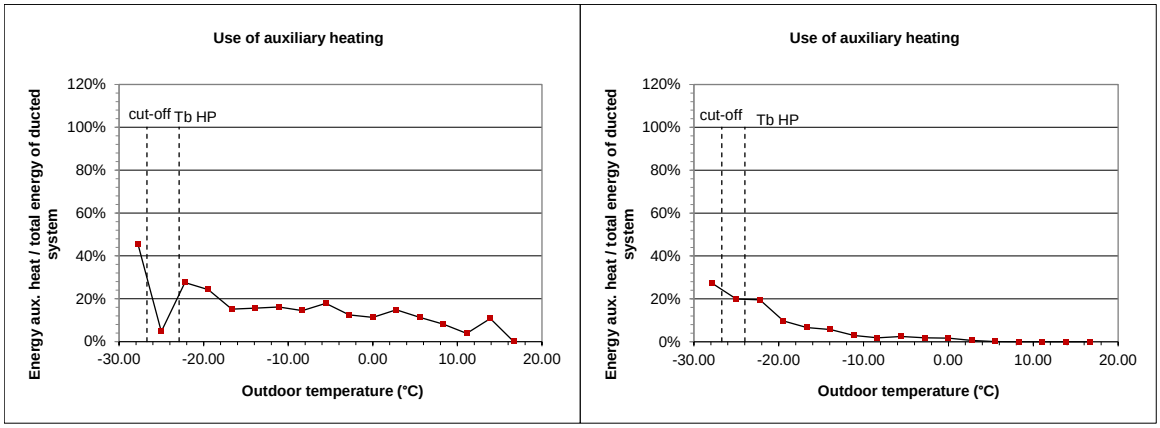

Figure 17: Use of electric backup – Variable-speed heat pump (experimental data - 2 installations)

For more information, the effect of the cut-off on energy savings is also discussed in the Technical Report of Le Lostec, B. (2013b).

A study conducted in Switzerland by Wemhöhner, C. (2003) present different methods of calculating the performance of an air-water heat pump for domestic hot water and space heating. The authors of this study suggest a mode of operation of the back-up called "alternate operation" which is to turn off the heat pump below the balance point and just use the back-up to meet the needs.

Since the HSPF is based on a BIN model, the thermostat operating characteristics (conditions for activating the back-up for example) are not documented / measured in standardized tests. This could be useful in a time simulation model to better reflect the operation close to and below the balance point.

3.6 Defrost

Fairey, P (2004) present various experimental studies (dating from 1970-1980) that show the performance of the heat pumps is often less than the performance calculated with standards.

The authors focus on the effect of climate on calculating the HSPF and SEER. They conclude that HSPF can that vary from +40% to -50% depending on the winter weather. In general, the calculation method overestimates the HSPF for the following reasons:

- While the defrosting operation is usually based upon compressor run time in real systems, the calculation procedure of the HSPF assumed that there is no defrosting operation below 17°F (-8°C). However, below this temperature, the defrosting is often triggered due to prolonged operation of the compressor.

Note: tests conducted by LTE (Le Lostec 2011) shows that the number of defrosting cycles does not increase in all cases, but the defrost duration may significantly increase as the outdoor temperature decreases.

- During the defrosting process (thus reversing the operating cycle to cooling mode), the auxiliary heating system can be activated to avoid blowing fresh air into the house. According to the authors, the procedure ARI-210/240 explicitly states that the auxiliary heater must not be activated during the defrosting process. Thus, calculating the HSPF therefore does not count the energy consumed by the auxiliary heating.
- The sizing of heat pumps is not consistent between different climate zones.

Note: Canadian Standards stipulate that the design must be made according to the air-conditioning load while the C656 Standard suggests a sizing range that depends on the heating load.

- A lower air flow rate to the nominal flow rate affects the performance of the heating system and increases the use of electrical resistances.

Note: Tests have been carried out by the LTE (Le Lostec 2011) to quantify this effect.

3.7 Performance at -17.8°C

Note that the Office of Energy Efficiency issued a bulletin (NRCan 2010) proposing to require publication of capacities and COP at -8.3°C (which is already established in the C656 Standard). In addition, this agency suggested that tests to -17.8°C be added to the standard. This would require that standardisation laboratories can meet the criteria of tests proposed in this newsletter.

The NEEP (Northeast Energy Efficiency Partnerships) also raised its interest with ENERGY STAR (NEEP 2014) so that additional metric is being added to products. Thus:

- The NEEP supports the addition of performance metrics for qualifying cold climate heat pumps
- The NEEP raises the fact that that the HSPF is not an accurate indicator to characterize the heating capacity of a heat pump in a cold climate
- The addition of the COP and the capacity at colder temperatures (e.g. <-8.3°C) could be a good solution to identify products operating at low temperature (example: commercial program of Vermont)

3.8 Sizing

The choice of sizing is partially addressed in the standard because it allows a broad sizing range (can be from “100%” to “doubled”). National regulations set the value to use for calculating the HSPF; however it might be interesting to validate this value for Québec. Given that there is a gap between what the standards provide sizing air conditioning systems (thermal calculation of the building) and what is actually done on the ground (rule of thumb), an analysis must be conducted to understand the Quebec and Canadian situation.

3.8.1 Sizing of heat pumps – Standards

The technical report of Le Lostec (2013a) presents an analysis of the sizing of heat pumps. This study shows that the sizing of the heat pump must be made according to the air conditioning needs, Figure 18. The main points mentioned are:

- In Canada, the sizing of residential heating and cooling equipment are regulated by CAN / CSA-F280-12 "Determining the Required Capacity of Residential Space Heating and Cooling Appliances". In this Standard (Version M90), it is specified (Section 5.3.5) that the net output of an air-source heat pump should not be included in the output of the heating system unless the operation is not restricted by a heating limit. It is specified in the comments appended to this standard (Section 2.2) that the purpose of this restriction is to exclude from calculations all the output capacity of heat pumps part of a heating system arranged to depend exclusively on the auxiliary heat at the design temperature. Generally, the air-source heat, regardless of the technology, are therefore not included in the output of the heating system and must not meet the design constraints of the heating system under by this standard.
- In this standard (CAN / CSA F280), it is specified that the nominal power of the cooling system of a building is equal to 1.3 times the sum of sensible heat gain calculation. Based upon the comments appended to this Standard, this sizing method is based on the fact that most residential cooling appliances on the market have a

latent power of about 30% of their power sensitive (23% of the total power (0.3 / 1.3)). An oversizing of the cooling equipment is accepted. In general, this standard (CAN / CSA F280), and therefore CAN / CSA C273.5-11 so allow, with few exceptions the values shown in the following Figure 18.

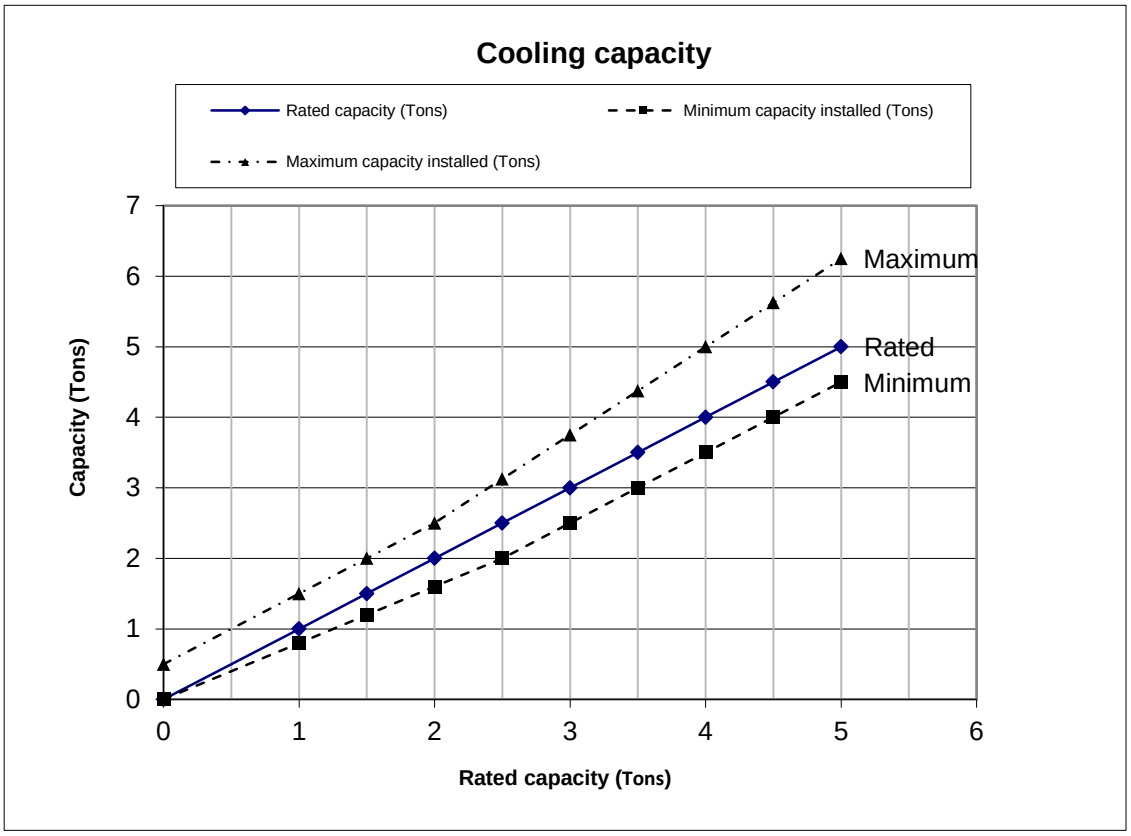

Figure 18: Sizing of cooling systems based on the CAN / CSA F280, air-to-air heat pump

- It would be very relevant to assess the sizing of heat pumps in Quebec (C656, F280, C273.5, rule of thumb, land characterization, market analysis ...) so that the sizing proposed by the C656 Standard is as representative of Quebec situations and Canada. A more complete study (CEATI data, HOT2000 ...) might also better describe the issue of sizing.
- To calculate the HSPFV, CAN / CSA C656-14 Standard assumes that the minimum heating power required in the design (DHRmin), associated with equipment at the external reference temperature, is equal to the standardized heating capacity of the heat pump at 47°F. This standard also provides for the calculation of an equivalent DHRmax for Region V to 2.2 times the DHRmin. This standard does not give a definition or an equation of DHR to use in calculating the HSPF; however, the US Code of Federal Regulation, CFR subpart C-430.32 (c) provides that for Region IV, the HSPF is calculated with DHRmin. It would be interesting to have the recommendations of the Government of Canada on the choice of DHR necessary for calculating the HSPF Region V. It is logical to assume that the DHRmin is used since it tends to maximize the HSPF. For Quebec, it would be interesting to analyze which of the two DHR would be most representative of the situation, and this considering the actual sizing methods (sizing by air conditioning) as specified by the F280 Standard

3.9 IEA Annex 39

The Annex 39 of the IEA HPC (2010) aims to establish methods of standardized tests and develop methods for calculating the seasonal performance factor of a heating system comprising a heat pump. Heating technologies with wood or gas would be taken into account in these methods. It is therefore relevant to monitor the evolution and the findings of this annex in order to validate that the current and future work carried out by LTE are consistent with the work of the various institutions of that annex.

The main objectives of the annex are:

- Establish common calculation methods for SPF (Seasonal Performance Factor) using a generalized and transparent approach. The focus is on a fair comparison between the different types of heat pumps, but also on the comparison between the various competing technologies, such as wood pellet boilers and gas boilers.
- Establish comprehensive test methods based on the development of current testing standards. Standard test methods must include the test conditions necessary for future calculations of SPF.

Deliverables from annex will be:

- Recommendation for a transparent calculation method / common tool for SPF combined operation, which can then be incorporated into standardization. This method takes into account the combined operation and part-load operation. Calculations must be based on laboratory measurements.
- Recommendation for further improvements of existing test methods
- National analysis reports of existing test methods and calculation methods for SPF
- The reports from countries summarizing the history, development and the reason for using the existing methods at National level
- An alternative method for evaluating the heat pump performance
- A summary of 2 pages freely distributed and popularizing the results of the annex
- A final report from the annex summarizing the progress reports.

3.10 Conclusion

The HSPF can probably be representative of the energy savings in an ideal system (modulating of the auxiliary heat, no cut-off added to the installation, ideal thermostat, sizing corresponding to the one used in calculating the HSPF ...) which is not representative of the situation in Quebec. It can be used to classify similar technology equipment and probably different technologies (to be validated), but it should be limited to that use. The objective of this analysis is to understand the limits of HSPF and identify the reasons for the gap between the real and HSPF and the real COP_{system}.

4 SUMMARY AND CONCLUSION

In general, the modification of a standard is relatively tedious. Different actors have different interests to be taken into account. For example, when revising the Energy Star Label, manufacturers were concerned about the workload that could represent the addition of low temperature standardized tests and taking into consideration regional weather conditions rather than national.

Therefore, if an amendment to the C656 Standard should be carried out, it would be appropriate that these changes are also made to the American AHRI 260/240 in order not to create obstacles to the development of the Canadian market. One way not to be overlooked

is the content of Annex 39 of the IEA, which aims to standardize internationally the heat pump performance criteria.

Changes in standards and the establishment of a performance criterion representative of real savings is an important issue; however, this work is done on the long term which may prevent the establishment of a possible commercial program. Proposed solutions, not retained in the past, such as the joint use of standardized criteria (HSPF) and technical parameters (variable speed, injection, for example), or the use of capacity coefficients of performance at low temperature (non-standardized), as does Vermont currently for its commercial program, must be seriously studied whether a commercial program is implemented in the short term.

HSPF, which is a standardized performance criterion, does not calculate savings of energy representative of what is observed in the field. Moreover, with the advent of new technologies such as heat pumps with variable speed compressor with or without refrigerant injection, the HSPF does not give a realistic energy saving difference between the different technologies. This is explained partly by the calculation assumptions which aim to idealize the operation of heat pumps below the balance point. For some heat pumps with variable speed, including wall units, low temperature standard capabilities (-8.3°C), are not always based on the maximum speed of the compressor. Therefore, it is difficult to rely on this criterion to identify the most efficient equipment.

5 REFERENCES

This Section is intentionally left in French.

ASHRAE (1985) Fundamentals Handbook, Ashrae.

ASHRAE (1989) Fundamentals Handbook, Ashrae.

ASHRAE (2006) 2003 Standard for Unitary Air-Conditioning & Air-Source Heat Pump Equipment - ARI Standard 210/240-2003, Ashrae.

BPA (2011) VHCP Energy Efficiency Measure Development Roadmap, Bonneville Power administration.

Cane, D. (2013) communication personnelle.

Cane, R. L. D. (1979) A ‘Modified’ bin method for estimating annual heating energy requirments of residential air source heat pumps, Conseil national de recherches Canada (publié également dans : Ashrae journal vol. v 21, n 9. pp. 40 – 44, 1979).

CSA (2006) ‘’Évaluation des performances des climatiseurs centraux et des thermopompes biblocs et monoblocs,” CAN/CSA-C656-05.

CSA (2011) Installation des thermopompes à air et des climatiseurs - C273.5-11.

CSA (2012) Determining the required capacity of residential space heating and cooling appliances - F280-12.

CSA, (2014) Performance standard for split-system and single-package air conditioners and heat pumps, C656-14.

Department of Energy, (2013) Electronic code of federal regulations appendix M to subpart B of Part 430-Uniform test Method for measuring the energy consumption of central air conditioners and heat pumps, DOE.

Didon, D.A., Kelly, G.E. (1979) New testing and rating procedures for seasonal performance of heat pumps, Ashrae journal vol. v 21, n 9. pp. 40 – 44, 1979.

Dumont, E., Chénard, S., Baribeault, J. (2009) Étude des normes et modèles de calcul des thermopompes air-air et comparaison en laboratoire d'une thermopompe basse température avec un modèle courant, Rapport technique, LTE-RT-2009-0212.

Ecotope (2011) Ductless heat pump impact & process evaluation lab-testing report, rapport E11-225, Ecotope.

Energy Star (2013) Central Air Conditioner and Air Source Heat Pump Specification Version 5.0.

Erbs, D.G., Sanford, A. K., Beckman, W.A. (1983) Estimation of degree-days and ambient temperature bin data from monthly-average temperatures, Ashrae Journal June 1983.

Fairey, P., Parker, D., Wilcox, B., Lombardi, M. (2004) Climate Impacts on Heating Seasonal Performance Factor (HSPF) and Seasonal Energy Efficiency Ratio (SEER) for Air Source Heat Pumps, Florida Solar Energy Center, Berkley Solar Group, FSEC-PF-413-04.

Francisco, P. W., (2004) Understanding Heating Seasonal Performance Factors for Heat Pumps, Building Research Council, Ecotope.

Francisco, P. W., Baylon, D., Davis, B., Palmiter, L. (2004) Heat Pump System Performance in Northern Climates, ASHRAE Trans., vol. 110, no. 1, pp. 442–451.

IEA HPC (2010) Annex 39 – A common method for testing and rating of residential HP and AC annual/seasonal performance, IEA Heat pump centre.

Le Lostec, B., (2013a) Évaluation de l'impact en puissance et en énergie des thermopompes au Québec, Rapport technique LTE-RT-2013-0131.

Le Lostec, B., (2013b) Effet de la température d'arrêt (« cut-off ») sur la performance des thermopompes conventionnelles, Rapport technique LTE-RT-2013-0130.

Le Lostec, B. Nouanegue, H.F. (2011) Performances d'une thermopompe centrale à vitesse variable, LTE-RT-2011-0093.

Le Lostec, B. Nouanegue, H.F. (2014) On-site performance of air source heat pumps, 11th IEAHP comference, 2014, Montreal, n.O.2.4.3.

NEEP (2014) Northeast/Mid-Atlantic air source heat pump market strategies report, Northeast Energy Efficiency Partnerships.

RNCan (2004) Bulletin sur la modification de la norme, Climatiseur et les thermopompes d'une capacité de moins de 19 kW (65000 Btu/h) – Août 2004 (http://www.rncan.gc.ca/energie/reglements-codes-standards/7004).

RNCan (2010) Bulletin sur le rapport de rendement dans un climat froid, Thermopompe à air – Juin 2010 (http://www.rncan.gc.ca/energie/reglements-codes-standards/bulletins/7178).

Stover, A., Sachs, H., Lawenberger, A. (2013) Cryptic barriers to energy efficiency, American council for an energy efficiency economy ACEEE, Report number A135.

Canadian Team Report

IEA HPT TCP Annex 41
"Cold Climate Heat Pumps"

Task 4: Future Research Work

Submitted by:

Brice Le Lostec (contact: lelostec.brice@lte.ireq.ca)

Hydro Québec
Laboratorie des Technologies de l'Énergie (LTE)
Shawinigan, Québec

Daniel Giguère (contact: daniel.giguere@canada.ca)

CanmetENERGY
Natural Resources Canada
Varennes, Québec

December 2016

TABLE OF CONTENTS

1 LTE

Heat pumps with electric or fuel-burning back-up devices have been on the Québec market for several decades. In recent years, heat pumps that can operate at very low outdoor temperatures (-25°C to -30°C) have appeared on the market. These so-called cold climate heat pumps are technologies that improve the energy efficiency of residential heating and reduce the power demand during peak winter consumption periods as compared to resistive heating.

Several obstacles exist to the deployment of these technologies on the market including the lack of criteria for the identification of the equipment, the bias regarding the comparison between energy savings depending on the technology (single stage, VRF injection, etc.) based on the HSPF and the lack of metrics to evaluate the impact on peak power demand. In order to foster the emergence of cold climate heat pumps on the market, efforts are being made at Hydro-Québec's energy technology laboratory (LTE) to characterize the equipment and propose solutions to promote the deployment of these technologies.

In the future and in order to better evaluate the performance of heat pumps, a semi-virtual test bench will be developed. It will allow better understanding of the interaction between the heat pumps, the buildings where they are located and the resistive heating devices that are also present in the buildings (electric back-up, baseboards, etc.) as well as analyze the control algorithms implemented in the thermostats.

Comparing the operating characteristics of the different heat pumps is complex since they are all designed differently. Nevertheless, the exercise can be done by focusing on their operating differences and, as a result, on the advantages of each technology. However, the control factor, particularly in regards to the management of the partial load – especially in the case of Heat Pump 3 (variable speed) and Heat Pump 2 (two-stage) – and in regards to the management of the electric back-up, was not studied in depth in this exercise in spite of the fact that this factor can have an impact on the seasonal performance of the heat pumps. As a result, our comparison between the different technologies is not exhaustive and should not be the sole decisional factor. Future work could entail accounting for these factors in determining the HSPF.

In addition to reducing the heat pump's availability, the defrosting cycle added a thermal load to the building by absorbing part of the energy supplied to the building. In most installations, back-up heating devices are used to minimize the negative impact this process has on the comfort of the occupants. These auxiliary devices represent a use of energy with a lower performance than that normally obtained with a heat pump, which contributes to decreasing the performance of the global system. However, this was not part of our study because no back-up devices were used during the tests. Considering the impact of these devices could be explored in future investigations.

A pilot project consisting of 22 test sites was carried out in Quebec, Canada during the heating season to measure the energy savings associated with the use of heat pumps for space heating. However, this study did not take the age of the systems into account. Any maintenance activities on the equipment were also not included in the study. However, the systems were tested to assess their adequate operation before the beginning of the measurements. Exploring the impact of these factors on the HSPF would provide an assessment on the degradation of the equipment over its useful life. Also, a more accurate evaluation of cold climate heat pumps should include an evaluation at lower temperatures (-18°C for example).

The results of this study demonstrate that heat pumps installed according to current practices allow to generate significant annual energy savings of between 25% and 30% in

the case of conventional heat pumps and between 45% and 50% in the case of variable speed heat pumps as compared to resistive heating equipment. Variable speed heat pumps therefore generate greater energy savings than conventional heat pumps; however this remains difficult to quantify due to the number of samples. Researching current literature with field results would provide further clarification on the amount of savings when using variable speed heat pumps.

The experimental tests and the measurement campaign demonstrated that the energy saving potential of VRF injection heat pumps is significant for the Québec context. Nevertheless, certain issues must be addressed to promote the deployment of these technologies in the residential sector. We observed a lack of regulated criteria for the identification of these heating devices, the calculation of energy savings and the calculation of the impact on peak power demand. Proposed solutions such as the joint use of standardized criteria (HSPF) and technical parameters (e.g. variable speed, refrigerant injection), or the use of capacity and low temperature coefficients of performance (non-standardized) – as does Vermont currently for its commercial program – must be seriously studied whether a commercial program is implemented in the short term .

To better represent the situation in Quebec, the HSPF minimally should consider:

- The “stop” temperatures installed by contractors
- The non-modulation back-up heat below the balance point
- A sizing according to current standards, that depends on the cooling load. This should be addressed by national regulations because the Standard C656 allows a sizing range that seems realistic

It would be very relevant to assess the sizing of heat pumps in Quebec (C656, F280, C273.5, rule of thumb, land characterization, market analysis ...) so that the sizing proposed by the C656 Standard is as representative of Quebec situations and Canada. A more complete study (CEATI data, HOT2000 ...) might also better describe the issue of sizing.

Therefore, if an amendment to the C656 Standard should be carried out, it would be appropriate that these changes are also made to the American AHRI 260/240 in order not to create obstacles to the development of the Canadian market. One way not to be overlooked is the content of Annex 39 of the IEA, which aims to standardize internationally the heat pump performance criteria.

Moreover, with the advent of new technologies such as heat pumps with variable speed compressor with or without refrigerant injection, the HSPF does not give a realistic energy saving difference between the different technologies. This is explained partly by the calculation assumptions which aim to idealize the operation of heat pumps below the balance point. For some heat pumps with variable speed, including wall units, low temperature standard capabilities (-8.3°C), are not always based on the maximum speed of the compressor. Therefore, it is difficult to rely on this criterion to identify the most efficient equipment.

2 CANMETENERGY

2.1 Hybrid Ejector - Compressor Heat Pump

The hybrid ejector/compressor heat pump is based on the appropriate integration of compressor and ejector technologies using air as a heat source. Simulations show that this low cost technological improvement can increase the performance of the heat pump by 15%.

Effort is now directed towards the development of a better ejector for R-134a (current ejector in test bench was designed for R410a) that will lead to higher entrainment ratios. Coupled with the hybrid ejector/compressor test bench, a second test bench, dedicated solely to the study of the two phase ejector component was also constructed for this project. Capable of inducing a wide range of operating conditions, the two phase ejector test bench will generate in depth knowledge and experimental results used to validate numerical models. These experimental activities, coupled with the modeling work and validation of results, will significantly improve our knowledge on the design of two-phase-flow ejector components and heat pump systems.

2.2 Solar-Assisted Heat Pump

Extensive simulation and experimental work has been undertaken to develop a novel solar heat pump system using ice-based thermal storage. Using validated energy models, it is estimated that such a system can reduce the energy use for heating and DHW in high performance homes between 61% and 66%, depending on the location of the building. Provided that the ice generation/storage technology can be sourced at a reasonable cost, the proposed system offers a cost-effective alternative to the current generation of ground-source heat pumps, and is particularly interesting for retrofit applications where it may be difficult to add ground heat exchangers.

Several future steps are planned for this project. First, a new ice-on-coil method of ice generation will be examined, offering the potential to lower initial equipment costs and increase maximum possible ice fractions. System simulations will also be expanded to larger buildings (multi-unit residential, office buildings) to examine different ratios of collector and storage area to building thermal loads. Multi-objective analysis is also planned to examine the trade-off between lifecycle cost and energy for several regions in Canada. Finally, the potential of ice storage combined with liquid-based Building Integrated Photovoltaic/Thermal (BIPVT) will also be studied as an extension of the current concept. The BIPVT configuration has the potential to expand the system market, while also addressing a number of important technical issues (stagnation temperatures, long-term reliability) common with higher temperature liquid-based PVT systems.

2.3 CO_2 Ground Source Heat Pump

Ground source heat pumps (GSHP) are one of the most efficient commercially available space heating systems in Canada. The main barrier for the market adoption is the first cost and thus the main objective of the project is to find ways to reduce the initial investment cost or further increase the efficiency of the system to make it a more attractive solution. Furthermore with the phase-out of HCFC refrigerants now in effect for new equipment and the next step phasing down HFC refrigerants, several projects are evaluating the feasibility of using CO_2 as the working fluid. CO_2 has a low global warming potential and the thermo-physical properties provide several advantages.

Future work on GSHPs should continue to address overcoming the high cost or achieving improved seasonal efficiency by meeting DHW loads in addition to space heating loads.

2.4 Refrigerant Mixtures

The simulations show a potential COP improvement of 38% just by swapping the refrigerant in a heat pump with no important modifications to the basic mechanical design of the unit. But, the COP could be improved if the basic mechanical design of the heat pump was modified. In other words, to get the total benefit of the refrigerant mixture glide, the air flow rates and the air coils' circuiting should be revised or redesigned. The design of refrigerant mixtures is a promising approach for heat pumps COP improvement. The next steps in this

project will be to confirm experimentally the performances predicted by the model and to design a heat pump unit adapted to refrigerant mixtures with a strategic temperature glide.

Although, the R32 safety classification is A2L (2L for slightly flammable), the addition of CO_2 could mitigate the mixture flammability. Further research is needed to verify this potential. The CO_2/R32 mixture would operate at a higher pressure than the R410A heat pump. Therefore, the heat pump mechanical design should withstand the pressures according to the concentration of CO_2.

From an efficiency and GHG emission reduction potential, heat pumps should be more widely used in Canada. However, several barriers exist, which limit market adoption of heat pump technologies. As a result, it is important to develop specific technologies that can be integrated in heat pump systems in order to maintain high performance (capacity and efficiency) at low outdoor temperatures and decrease capital cost. Over the past five years, Canmet has performed simultaneous R&D on two fronts to address this issue – a simulation based approach to assess market barriers and experimental based to demonstrate the potential of improving a heat pumps performance in Canada's cold climate and high initial first costs.

Japan Team Final Country Report

IEA HPT TCP Annex 41
"Cold Climate Heat Pumps"

Submitted by:

Waseda University, Tokyo, Japan

Lead: Prof. Masafumi Katsuta, Waseda University (contact: katsuta@waseda.jp)

Contributors:

Annex 41 Japanese Company and Research Institute Members

- CRIEPI
- NEDO
- Mitsubishi Electric
- Toshiba Carrier Corporation
- Daikin
- Kansai Electric Power Co. Inc.
- Chubu Electric Power Co. Inc.
- Hitachi Appliance, Inc.
- Mitsubishi Heavy Industries

Observers

- Hokkaido Electric Power Co. Inc.
- Tohoku Electric Power Co. Inc.

January 2017

TABLE OF CONTENTS

EXECUTIVE SUMMARY

TASK 1 – COMPREHENSIVE LITERATURE REVIEW

A comprehensive literature review was performed in the area of cold-climate heat pumps and fundamental research on frost formation in heat exchangers. The cold-climate heat pump review encompassed several publications that focused on the functionality and improvement of heat pumps and air conditioners working in cold climates (-25 C). Emphasis was given to novel architecture and packaging as well as heat exchanger modifications to improve performance. For example, a novel two stage compressor heat pump cycle was considered for its improvements in heating capacity at low ambient temperature operation. The novel architecture also provided additional reliability in the high pressure operation. These overall improvements were considered in the scope of residential application and feasibility. Another reviewed concept was that of a Flash injection (or vapor injection, VI) cycle which boosted heating capacity by 25% in ambient temperatures of -15 C. This improvement stemmed from an increase in heat gain from ambient by using an injection cycle during the compression process thereby increasing mass flow in the condenser. An additional component of the review in cold-climate heat pumps was a review of improved heat exchanger design that minimizes frost formation in cold-climate operation. The literature provided experimental data proving that addition of anti-freeze pipes at the base of the heat exchanger significantly affected the frost formation on a heat exchanger utilized in a heat pump application. Finally, the heat pump review widened to include heat pump technology utilized for water heating applications. New variable ejector refrigeration cycle technology helped improve water heating capacity and COP of the cycle by 20% over conventional designs.

The second component of the literature review focused on fundamental frost formation simulations and calculations as well as experimental results for validation and discussion of various setup regimes that affect heat exchanger performance. The literature went on to detail models for frost formation and heat flux at different frosted conditions. Conclusions were drawn that wettability of the cooling surface significantly affected the physical force required for removal. In Tasks 2 and 3 the frost model was developed further and incorporated into an ASHP system model for use in analysis and design of future heat pump systems.

Finally recent measurements and development of models for isobaric heat capacity (c_p) for R32 was summarized.

TASK 2 – INITIAL WORK

Three principal areas of research were explored: frost formation simulation and validation, usage of thermosiphons to collect heat from ground layers, and frost free heat pump for water heating. All areas focus on improvement of refrigeration cycles in cold-climate operations by utilizing novel technology or architecture.

A detailed analysis of frost formation in heat pump heat exchangers was performed in order to generate and validate a numerical model. Experimentation utilizing controlled inlet air temperature, inlet absolute humidity, cooling surface temperature, and initial flow rate was performed to analyze the frost formation and density across various geometries. In analyzing various parameters and their effect on frost formation, a numerical model was built to predict frost formation given different operating schemes. Yamashita's crystal growth stage model was applied to predict growth in different flow scenarios. Finally, the model was validated against experimental results and shown to predict mean frost layer density and height within 3%, 7% and 10% in respective cases. Additionally, frost formation amount and frost layer

surface temperature could be calculated within 10% of experimental values. Overall, the model has demonstrated capability to predict the influence of various factors on frost formation.

A novel method for collecting energy from surface ground layers was investigated as a possible improvement for cold-climate heat pumps. Different configurations and constructions of the thermosiphons were investigated for their heat transfer characteristics. It was found that smooth construction demonstrates better heat transfer due to lack of corrugated reinforcement acting as a thermal barrier. Additionally, the length and number of thermosiphons was analyzed showing their improved effectiveness in different setups. Empirical relations were also used to explain the performance of the thermosiphon. The novel technology provided ample increase in COP in heat pump simulations.

A hot gas defrosting system is proposed to improve air source heat pump water heaters. By dehumidifying incoming gas, the formation of frost on heat exchangers is significantly mitigated. The effectiveness of this system is analyzed experimentally and numerically and demonstrated a 30% boost in COP at relative humidity of 60-80%.

TASK 3 – CONTINUED WORK

In continuation of the research performed in Task 2, numerical models and experiments were conducted to further delve into the effectiveness of the proposed modifications to the heat pump setups.

The first area of continuation focused on in-depth modeling of a heat pump and all its components, including frost formation on heat exchangers. The modeling was conducted system wide on all components of the heat pump in order to incorporate the previously created frost formation model. This study was based on a modular analysis theory utilizing numerical solvers to converge a non-steady solution to non-linear equations. In parallel to the modeling efforts, an experimental setup was created to validate the numerical model and also to perform optimization and apply improvements.

Paired with the continuation of modeling study and experimentation is an evaluation of a cold-climate heat pump in comparison to its commercially available predecessor. The evaluation was performed for the city of Minneapolis, USA and the primary investigation was into cost to operate per year. Japanese heat pumps were evaluated using APF (Total Load/Total Power Consumption), calculated using the bin method, and compared to the equivalent systems currently in use. Tested at varying temperatures and humidity for heating and cooling schemes, the system significantly reduced energy consumption compared to combustion type heaters.

Japan Team Report

IEA HPT TCP Annex 41
"Cold Climate Heat Pumps"

Task 1 – Comprehensive Literature Review

Submitted by:

Waseda University, Tokyo, Japan

Lead: Prof. Masafumi Katsuta, Waseda University (contact: katsuta@waseda.jp)

Contributors:

Annex 41 Japanese Company and Research Institute Members

- CRIEPI
- NEDO
- Mitsubishi Electric
- Toshiba Carrier Corporation
- Daikin
- Kansai Electric Power Co. Inc.
- Chubu Electric Power Co. Inc.
- Hitachi Appliance, Inc.
- Mitsubishi Heavy Industries

Observers

- Hokkaido Electric Power Co. Inc.
- Tohoku Electric Power Co. Inc.

November 2016

TABLE OF CONTENTS

LIST OF TABLES

LIST OF FIGURES

1 INTRODUCTION OF HEAT PUMPS FOR COLD CLIMATE AREAS

In cold climate areas, air-source heat pumps which utilize ambient heat are less efficient than those in warmer areas. In the past, when the heat pump technology was not so advanced as today, the heating performance of some pieces of heat pump equipment drastically declined when the outside air temperature became low. Therefore, air-source heat pumps were rarely introduced for heating purposes, while fossil fuel combustion boilers were mainly used under such cold climate.

However, the performance of air-source heat pumps has been remarkably improved in recent years, and some products newly born have sufficient heating performance even at an outside air temperature of -25°C due to the enhanced performance of compressors and heat exchangers.

For example, an air-source heat pump water heating system for residential use that was invented by Daikin Industries, Ltd. in 2006 can supply sufficient heat in a climate below freezing point, and its specifications are reliable enough for use in cold climate areas such as Northern Europe. In 2007, approximately 10,000 units were shipped to Europe. At present, they are exported to China and North America in addition to Europe, and the annual shipment is more than 50,000 units.

Another air-source heat pump room heater and water heater that Mitsubishi Electric Corp. started producing in 2009 in the U.K. have also captured a new market. The expectations for air-source heat pumps are rapidly growing.

As it is easy to replace existing boilers with these air-source heat pumps, they foster the demand not only for new installation but also for the replacement of boilers.

Up to now, approximately 6 million boilers are sold annually in Europe. Air to water heat pumps are expected to account for about 1 million of these 6 million units in the coming years. Moreover, France and several other European countries are offering subsidies as an incentive to purchase heat pump equipment, which are providing a needed boost to heat pump water heating market expansion.

For reference, high-efficiency multi type air-conditioners with heat pumps for buildings, which were commercialized by Daikin Industries, Ltd. in 2007, achieved a level of COP3 or higher at an outside air temperature of -10°C.

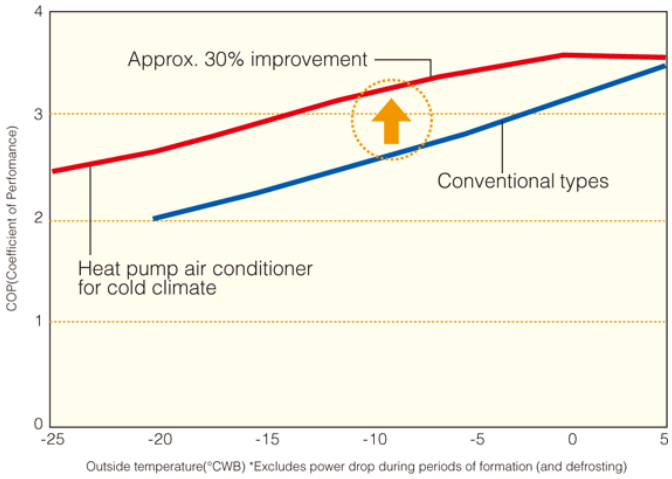

Figure 1: Air-source heat pump air conditioner for cold climate COP characteristics in cold ambient temperatures *(Outdoor unit, COP of a 40kW system)

2 COLD CLIMATE HEAT PUMP APPLICATIONS

2.1 CO_2 Two Stage Compressor for Commercial Heat Pump Water Heater

2.1.1 Introduction

A household heat pump water heater using CO_2 refrigerant has become widespread from a viewpoint of environment conservation. On the other hand, there are some issues to be solved, including compressor reliability against high operating pressure and reduction of the heating capacity in low ambient temperature operation.

MHI developed a novel two stage compressor which can solve the above issues. The developed compressor obtained substantial efficiency improvement by two stage compression using a combination of scroll and rotary mechanisms.

2.1.2 Structure of the developed two stage compressor

By comparison of efficiency and reliability as against of structure of the compressor (Table 1), the basic structure of the new compressor is determined as below.

- Two stage compression using a combination of scroll and rotary mechanisms
- Intermediate pressure housing and intermediate gas injection between first and second stage

Structure of the developed two stage compressor is shown in Figure 2.

Table 1: Performance comparison

Number of stage	Shell pressure *1	Type of compression		Shell thickness	Gas injection	Reliability		Efficiency	
		1st stage	2nd stage			1st stage	2nd stage	1st stage	2nd stage
Single stage	HP			-	-	-		-	
	LP			+	-	-		-	
Two Stage	HP			-	+ *2				
	MP	Scroll	Scroll	+	++	+ *3	+ *3	+	++
		Scroll	Rotary	+	++	++	-	+	+
		Rotary	Scroll	+	++	++	++	++	++
		Rotary	Rotary	+	++	++	-	++	+
	LP	Scroll	Scroll	+	+ *2	+ *3	+ *3	+	++
		Scroll	Rotary	+	+ *2	++	-	+	+
		Rotary	Scroll	+	+ *2	-	++	++	++
		Rotary	Rotary	+	+ *2	-	-	++	+

*1 LP: Suction pressure, MP: Intermediate pressure, HP: Discharge pressure
*2 Connection pipe between 1st and 2nd stage is required.
*3 Oil pump needs to be placed in the middle of crankshaft

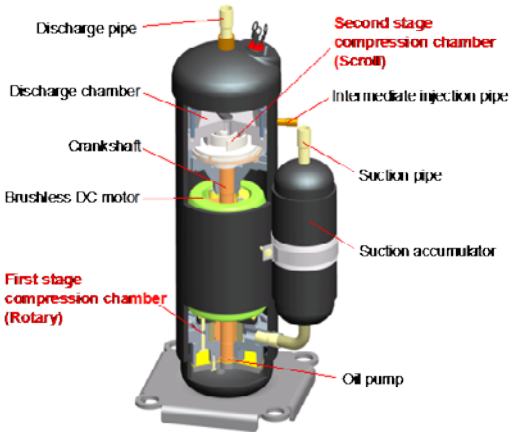

Figure 2: Structure

2.1.3 Efficiency of the developed compressor

Figure 3 shows efficiency comparison between the conventional and the developed two stage compressor. For the conventional compressor, the efficiency dropped drastically with increasing of operating pressure ratio. On the other hand, for the developed compressor, there is little decline in efficiency because of employment of the two stage compression mechanism. The developed compressor resulted in 15% improvement of efficiency on Pd/Ps=3 and more than 30% improvement on Pd/Ps>4 as against conventional single stage scroll compressor.

Figure 4 shows the improvement in heating capacity and COP in a two-stage intermediate gas injection cycle with the developed two-stage compressor compared with a conventional

single-stage cycle. The performance is substantially improved especially in the low ambient temperature condition. This made it possible to introduce heat pump water heaters in cold regions, which have been previously-unattainable.

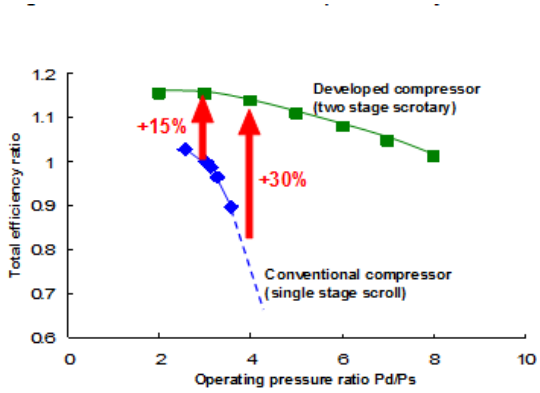

Figure 3: Efficiency variation against operating pressure ratio

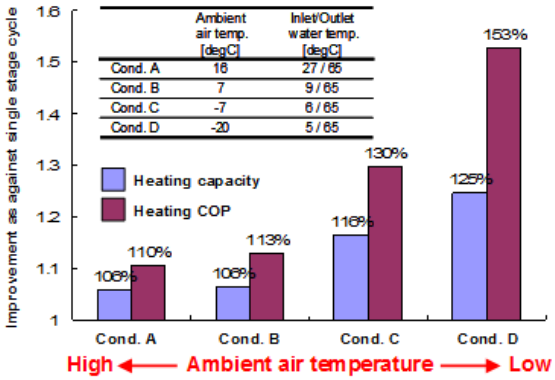

Figure 4: Improvement of heating capacity and COP as against single stage cycle

2.1.4 Application to Commercial Heat Pump Water Heater

The developed two-stage compressor is installed on our recently developed commercial CO_2 heat-pump water heater, “Q-ton ESA30” (Figure 5). The developed system can supply 90°C hot water even in ambient air temperature as low as -25°C, and the COP on rated conditions of OD temperature 12 C(WB) reaches 4.3, which is the highest level in the industry (Figure 6). The heating capacity at -25°C is ~70% of the nominal rated capacity at 12°C(WB) (Figure 6).

Figure 5: Q-ton ESA30

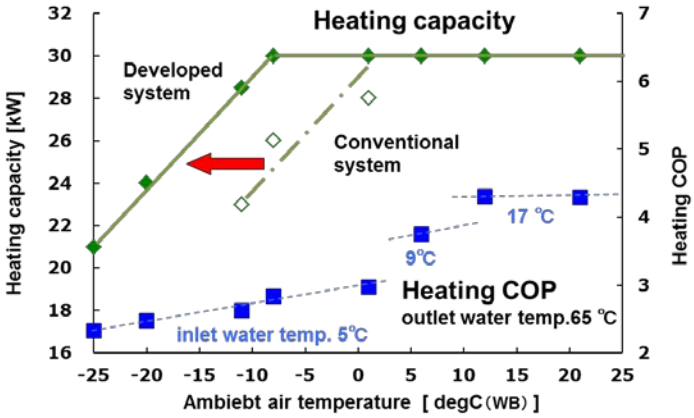

Figure 6: Q-ton ESA30 Variation of Heating capacity and COP against ambient air temperature

*This report is quoted from the PosterSession of JRAIA INTERNATIONAL SYMPOSIUM 2012.

2.2 Development of Packaged Air Conditioner for Cold Climate Application

2.2.1 Abstract

A refrigerant cycle ‘FLASH injection cycle’ which two-phase high-quality refrigerant injects into compressing process was developed. The maximum heating capacity was increased by

25% under the condition of ambient temperature at -15°C. In order to achieve its high performance, the heat inter changer was applied to the cycle to increase the heat gain from ambient where inlet refrigerant to the evaporator is cooled by the injection flow. Moreover, the discharge temperature of the compressor is easily controlled by the two-phase injection which allows the compressor to run at maximum speed even under the condition of high compression ratio in low ambient temperature.

2.2.2 Introduction

In cold area such as Hokkaido Japan, the minimum ambient temperature is approximately -15°C in winter and heating capacity of an electrical heat pump (EHP) under the condition has been said to be insufficient. What mainly used for heating in those areas are indoor unit with a built-in electric heater or heating systems using combustion heat by oil or gas. Although EHP is better in safety, easier setting and maintenance than the combustion type heating facilities, EHP in cold regions is highly required and the built-in heater type costs a lot, EHP has not become popular in cold climate application because of its insufficient heating capacity under low ambient temperature.

We have successfully developed a packaged air conditioner for commercial use which can develop enough capacity in heating mode under -15°C ambient temperature by injecting two-phase refrigerant into compressing process. In addition, the technology provides high energy-saving and eco-friendly products.

This report introduces the new refrigerant cycle and its characteristics.

2.2.3 Refrigeration Cycle for Cold Regions

Refrigeration Cycle Configuration
The configuration of refrigeration circuit of the packaged air conditioner which has been developed for cold climate application is shown in Figure 7. In the outdoor unit, the refrigerant circuit equips a receiver (Asai 2001) at middle pressure with suction pipe inside for heat recovery which cools high pressure refrigerant. A part of liquid refrigerant diverged from the receiver is reduced its pressure, and then exchanged heat with the main liquid refrigerant flow at high pressure from the receiver. The diverged refrigerant is injected into the compressor as high-quality two-phase refrigerant.

The conventional refrigerant curcuit increases discharge temperature of compressor as the ambient air temperature becomes lower, therefore the rotation speed of compressor becomes lower and heating capacity also becomes lower because the discharge temperature of compressor reaches a high-limit. While the new refrigerant circuit can adjust discharge temperature without restriction by controlling injecting flow rate of refrigerant.

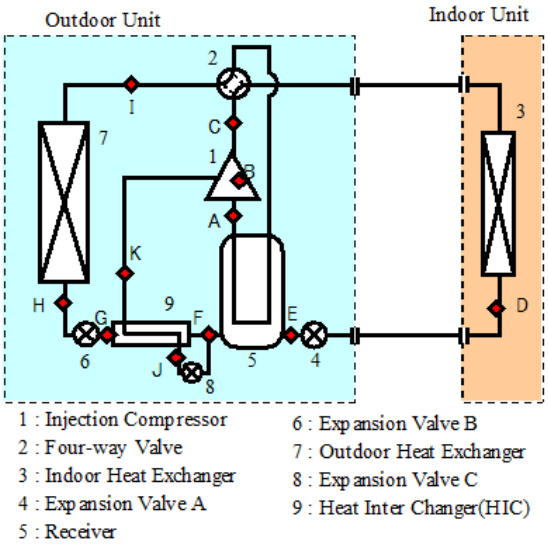

Figure 7: Refrigeration cycle of package air conditioner for cold regions

Refrigeration Cycle Operation

P-h diagram is shown in Figure 8 to illustrate the refrigerant cycle operation. Symbols from A to K in the diagram correspond to those in Figure 7. The refrigerant cycle has two internal heat exchangers. The first one exchanges heat between E-F and I-A, and the second one - heat inter changer (HIC) - exchanges heat between F-G and J-K. The refrigerant cycle is called 'FLASH Injection Cycle' because the injected refrigerant (marked with K) into the compressor is two-phase and high-quality.

In this refrigerant cycle, injecting two-phase refrigerant into middle of compressing process reduces discharge temperature when the compression ratio is very high, and increases heating capacity due to increased refrigerant flow rate in the condenser. In order to increase heating capacity, it is important to maintain the discharge temperature of compressor at just below the maximum allowed temperature and large enthalpy difference of condensing refrigerant. For this purpose, high flow rate and high quality of injecting refrigerant is desirable.

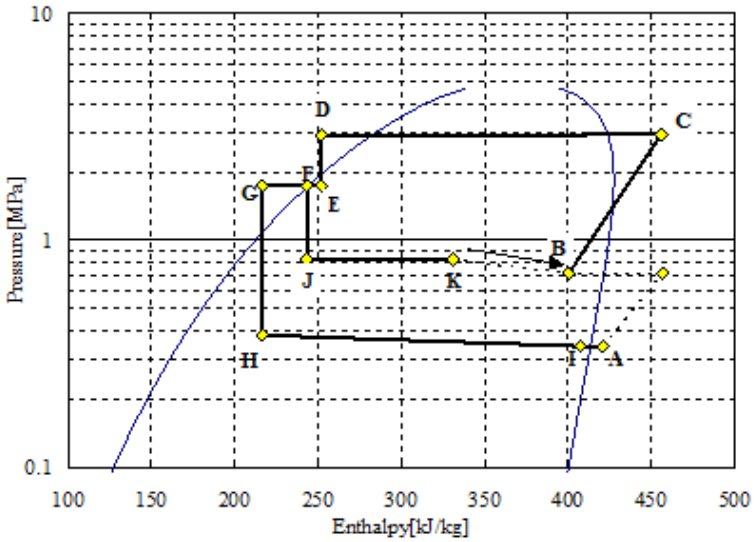

Figure 8: Typical refrigerant cycle on P-h diagram

2.2.4 Theoretical Cycle Characteristics

Calculation Method
Figure 9 shows P-h diagram in theory for calculating efficiency of 'Flash Injection Cycle'. In this calculation, heat exchange function in the receiver and effect of expansion valve on upper stream of the receiver are omitted. The symbol α indicates ratio of injecting flow rate Gi against evaporating refrigerant flow rate Ge.

Table 1 shows the calculation conditions to calculate temperature efficiency ε, injection flow ratio α and theoretical COP for 'FLASH Injection Cycle'. Discharge pressure Pd, injection pressure Pm and suction pressure Ps are premised to be constant in the calculation. Compression process with symbols 1-2 and 3-4 is premised to be equal entropy compression. Expansion process with symbols 5-6 and 7-8 is premised to be equal enthalpy expansion. The status at point 7 is derived from HIC temperature efficiency ε, the status at point 9 is calculated by heat balance at HIC, and the status at point 3 is calculated by average calorific value which is derived from the calculation that each refrigerant flow rate multiplied by enthalpy at the point 2 and 9 respectively.

In this calculation model, a conventional single refrigerant cycle characteristics is described as the injection flow ratio α at 0, and a liquid injection cycle is described as the temperature efficiency ε at 0.

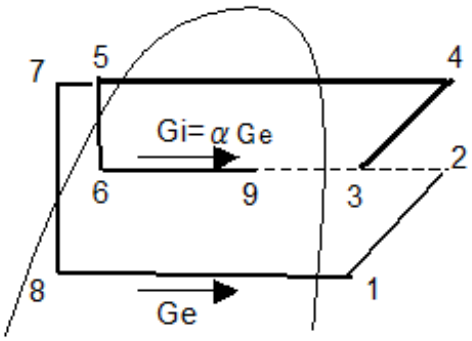

Figure 9: Theoretical Cycle Model of Flash Injection

Table 2: Theoretical Calculation Conditions

Refrigerant	R410A
Condensing Temp.(CT)	50℃ (Pd=3.063MPa)
Evaporative Temp.(ET)	-30℃ (Pe=0.269MPa)
Injection Pressure	$Pm=(Pd\cdot Ps)^{1/2}$ =0.908MPa
SubCool(SC)	10deg
Suction SuperHeat(SHs)	10deg
Temp. efficiency of HIC	ε=(T5-T7)/(T5-T6)
Injection Flow ratio	α=Gi/Ge

2.2.5 Calculation Result

Influence of Injecting Flow
Figure 10 shows the characteristics of the refrigerant cycle against the injection flow ratio α which changes from 0 to 1 where HIC temperature efficiency ε is constant at 0, 0.6 and 1.0 respectively. The upper figure shows coefficient of performance – COP - and lower one

shows capacity ratio in heating mode. The overheating condition of injection refrigerant at point 3 is not calculated in this case.

When the evaporating refrigerant flow Ge is constant, heating capacity ratio compared with the condition of α=0 hardly changes against changes of the injection flow rate. And COP in heating mode changes by only 2% at the maximum. Consequently, the injecting flow rate gives almost no effect on heating capacity and COP at constant rotation speed of compressor in the theoretical refrigerant cycle.

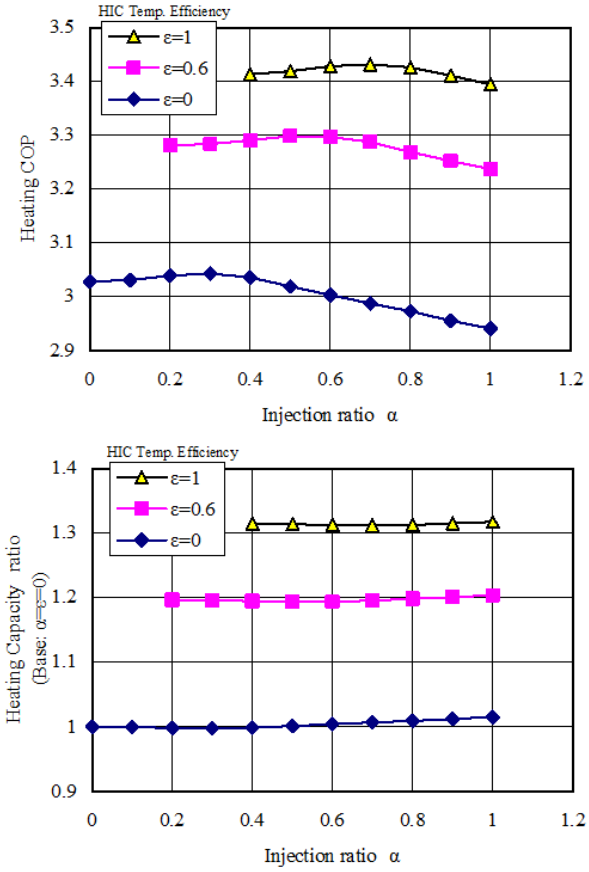

Figure 10: Influence of Injection Flow Ratio

Influence of HIC Heat Transfer Performance

Figure 11 shows ratio of heating COP, heating capacity and power consumption compared with the condition of ε=0 under the condition of HIC temperature efficiency ε changes from 0 to 1 where evaporating flow rate Ge is constant and injection flow ratio α is also constant at 0.5. Both COP and heating capacity increase monotonically as HIC temperature efficiency ε increases. HIC temperature efficiency ε decides temperature difference between outlet temperature of high pressure liquid refrigerant, injecting refrigerant, and quality of injecting refrigerant at HIC. As the temperature efficiency ε increases, outlet temperature of high pressure liquid refrigerant from HIC becomes lower, quality of injection refrigerant increases and discharge temperature at compressor becomes higher. Therefore the enthalpy difference at the evaporator and condenser becomes large, and consequently, both heating capacity and COP increase.

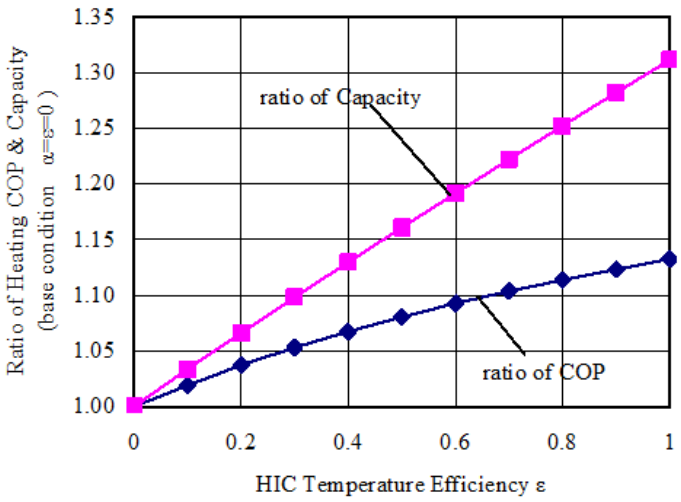

Figure 11: Influence of HIC temperature efficiency

2.2.6 Unit characteristics

Method and Conditions of Experiment

Table 3 shows the experimental conditions. The testing equipment was prepared with HIC and injection compressor added to a 4HP Mitsubishi packaged air conditioner. Suction volume of the compressor and specification of the heat exchanger and fans for both indoor and outdoor units were kept same as the original ones.

Figure 12 shows the experimental equipment configuration. Symbols T and P in this figure indicate temperature and pressure to be measured. Two mass flow meters were equipped on the refrigerant circuit. The injecting flow rate is calculated by the difference between the measured flow rate at condenser and evaporator. For the three different lengths - 0 m, 1.5 m and 3 m - of heat transfer tubes in HIC, characteristics of injection flow ratio α was evaluated.

Table 3: Experimental Conditions

Outdoor AirTemp.	℃	-15℃DB
Indoor Air Temp.	℃	20℃DB
Rotation Speed of Comp.	r/sec	118 (maximum)
Indoor Unit Fan Speed	r/min	680
Outdoor Unit Fan Speed	r/min	700
Subcool	deg	15
Suction SuperHeat	deg	10
HIC Length	m	0, 1.5, 3.0(3 patterns)
Injection Flow ratio		0.1～0.8

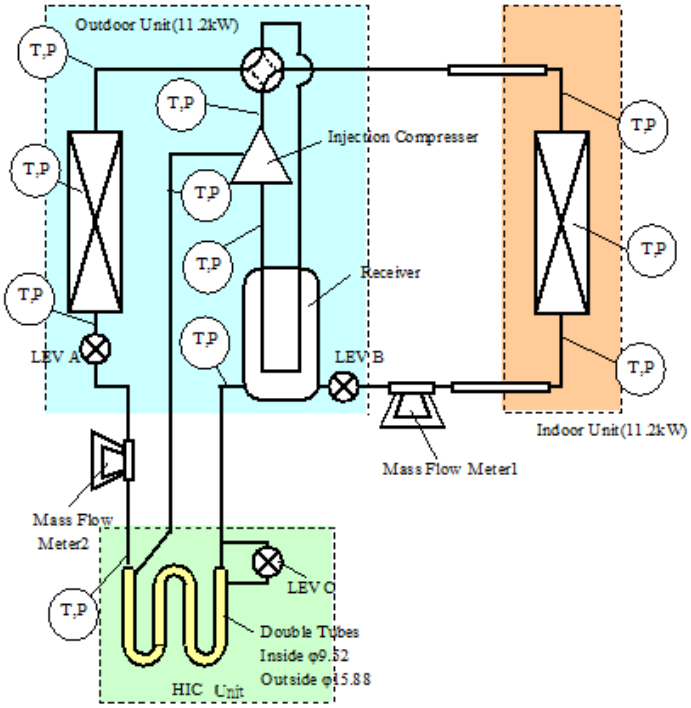

Figure 12: Experimental equipment

2.2.7 Experiment result

Figure 13 shows results of the experiment. Discharge pressure, outlet liquid temperature at HIC, heating capacity ratio and heating COP ratio compared with those under the condition of injection flow ratio α is constant at 0. According to the theoretical calculation result in the chapter 3, influence of injection flow rate on heating capacity was limited. While heating capacity increases as the injection flow rate increase in the actual unit. This is because that discharge pressure rises in proportion to injection flow rate and compressing work increases to contribute increasing heating capacity though the discharge pressure is assumed to be constant in theory. Heating COP tends to decrease as injection flow rate increases because pressure loss at each part of the cycle increases and discharge pressure increases as the refrigerant flow rate increases.

As for influence of HIC length, because the outlet temperature of liquid from HIC becomes lower as HIC becomes longer, the longer HIC provides the bigger maximum capacity and COP in heating mode under the same injection flow rate.

For HIC length at 0m which simulates liquid injection cycle, COP decreases monotonically as the injection flow rate increases while the capacity increases by from 10% to 15%. On the other hand, for ‘FLASH injection cycle’, heating capacity increases by more than 25% though COP keeps constant or better under the condition that injection flow ratio α is less than 0.4.

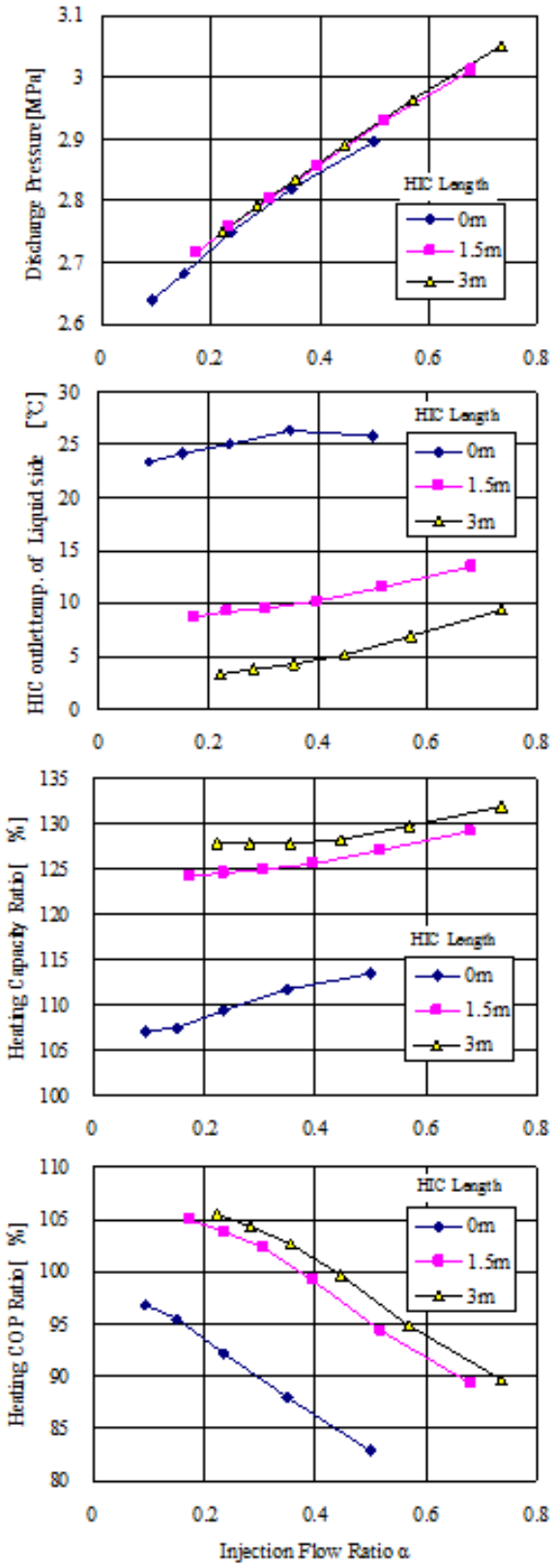

Figure 13: Results of experiment

2.2.8 Summary

‘FLASH injection cycle’ fulfilled air source heat pump which can develop adequate heating capacity even under the condition of very low ambient air temperature. This paper reported its characteristics for both theory and practice. The summery of the development is as follows:

(1) According to the theoretical characteristics under the condition of constant operating pressure, increase of heating capacity and improvement of COP are subjected by performance of heat exchanger of HIC on ‘FLASH injection cycle’.
(2) It is confirmed that condensing pressure increases as injecting flow rate increases, and consequently, increased compressing work contributes towards increasing heating capacity for performance of practical air conditioner with ‘FLASH injection cycle’.
(3) ‘FLASH injection cycle’ is proved to increase heating capacity by more than 25% under the condition of ambient temperature at -15°C without increasing power consumption compared with the conventional air source heat pump.

Mitsubishi Electric Corporation (MEC) developed a system called ZUBADAN featuring the ‘FLASH injection cycle’ (or vapor injection, VI, refrigeration cycle) as illustrated schematically in Figure 14. Figure 15 shows the system heating capacity vs. outdoor temperature - at -25°C the capacity ranges from ~71-75% of the rated heating capacity.

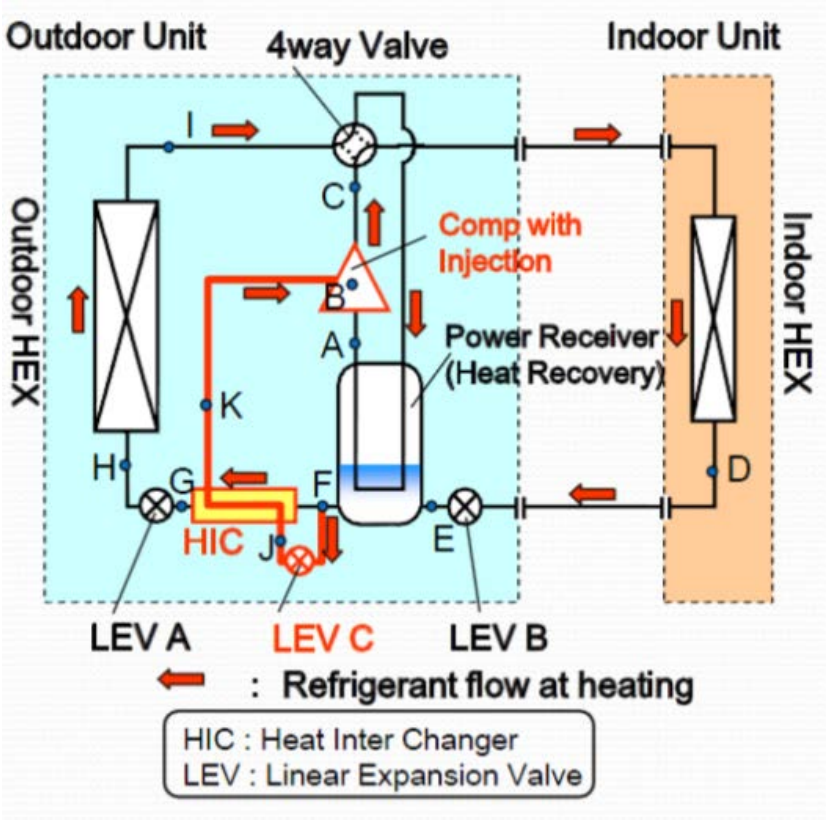

Figure 14: MEC “ZUBADAN” system refrigeration cycle schematic

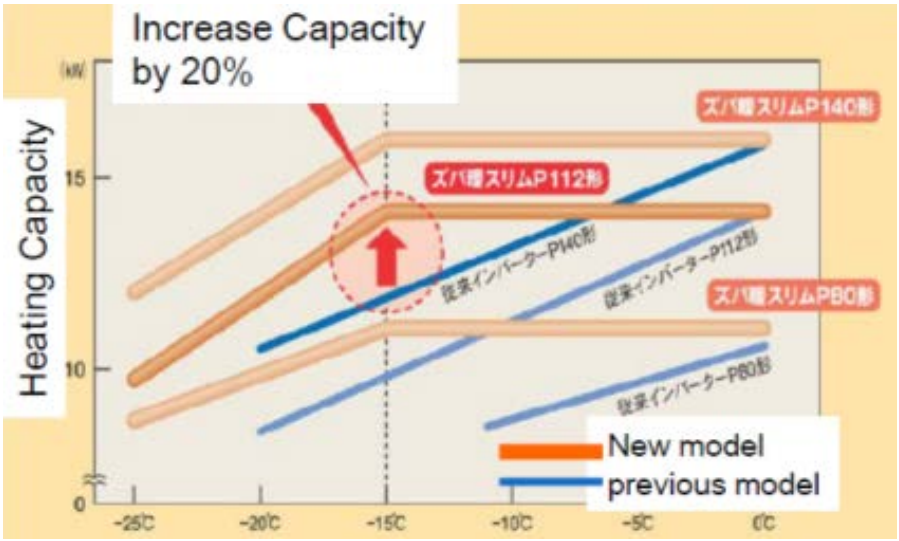

Figure 15: ZUBADAN heating capacity vs. previous product (Katsuta, 2013b)

*This report is quoted from a paper submitted at 2005 JSRAE Annual Conference held on 25 Oct, 2005.

2.3 Air Conditioner with Liquid Injection for Cold Regions

2.3.1 Introduction

Although air source heat pumps are widely used as air conditioners for offices and retail buildings in warm regions, they are not extensively used in cold regions. The reason is that the heating capacity and outlet air temperature from indoor units decreases as the outdoor temperature becomes lower, and that they have a defrost operation that is unpleasant for users. Nevertheless, social demand for low-maintenance all-electric heat pumps is getting higher year by year, and cold regions are no exception. This paper presents an overview of an air conditioner for cold regions featuring liquid injection.

2.3.2 Features

This air conditioner for cold regions has the following features:

- Wide range heating operation and non-decrease heating capacity down to -15℃ - By using a liquid injection (LI) compressor and refrigeration cycle, heating operation in outdoor temperatures as low as -25℃ is possible, and heating capacity can be non-decreased down to -15℃. The capacity ratio at -25℃ OD ranges from ~75% to 80% vs. rated capacity (Figure 17 at right).
- Energy saving operation and low running cost - Owing to the high efficiency compressor, the heat exchanger, and the refrigeration cycle control, heating COP becomes 2.11 at the outdoor temperature of -15℃.
- Easy installation and compact, space-saving cabinet - It is easy to install an all-electric driven system and it is stored in a compact, space-saving cabinet.

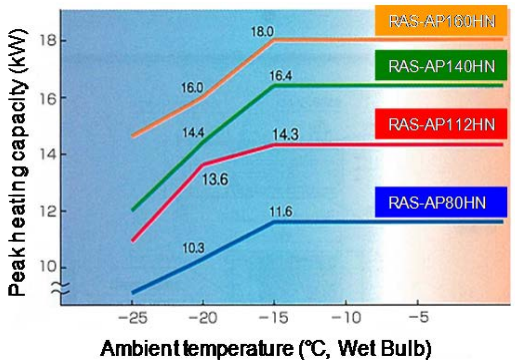

Figure 16: Heating characteristics

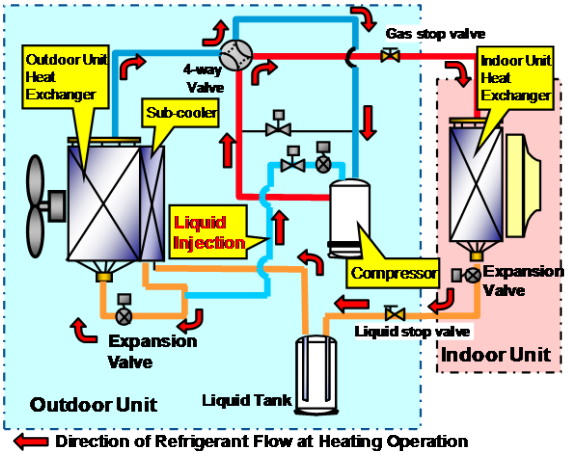

Figure 17: Diagram of liquid injection refrigeration cycle

2.3.3 Technical expertise

The features mentioned above are realized by the following technologies.

Liquid injection refrigeration cycle

Figure 18 shows a diagram of the liquid injection refrigeration cycle. The refrigerant is condensed at the indoor unit in heating operation, and the liquid refrigerant is by-passed and injected into the intermediate pressure port of the scroll compressor. The pressure fluctuation is suppressed with a capillary tube and silencer to prevent refrigeration flow noise. This injection refrigeration cycle, which has already been used in a refrigerator that has an evaporating temperature lower than the air conditioner, is effective for suppressing the discharge temperature of the compressor and improving heating capacity by increasing the refrigeration flow rate to the condenser and by raising the discharge pressure (Figure 18). In addition, the accumulator is removed to improve the efficiency.

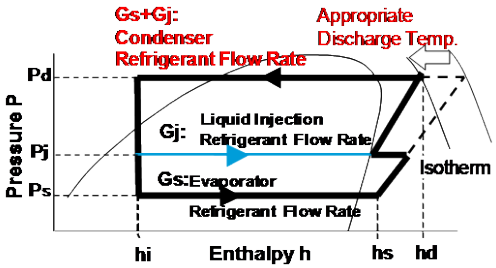

Figure 18: Mollier chart of liquid injection refrigeration cycle

Liquid injection compressor

For the development of this product, a liquid injection compressor has been exclusively designed for the air conditioners. Its cross-section diagram is shown in Figure 19. The location of the liquid injection port is optimized according to operating conditions, and asymmetry scroll wraps are introduced. The lubricant oil path is adjusted properly and a lower bearing is added to reduce friction loss. A DC motor is used to improve reliability, and the scroll stiffness and its back pressure are optimized against the high pressure ratio.

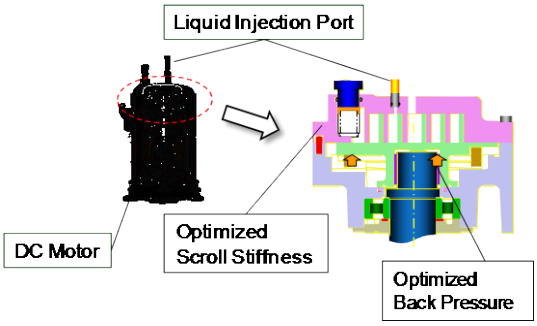

Figure 19: Liquid injection compressor

High efficiency heat exchanger
For the outdoor heat exchanger, corrugated fins (Figure 20) are used to improve the performance at the start of heating operation due to better draining at the defrosting operation. The heat transfer area is enough for heating capacity.

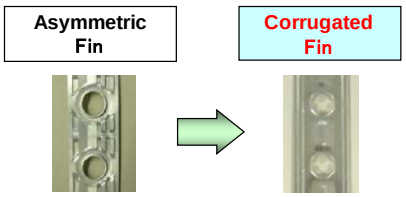

Figure 20: Fins of outdoor heat exchanger

Defrost operation control at low outdoor temperature
For improving the defrost performance, the defrost starting control is designed specifically for cold regions and for the avoidance of decision errors. The interval time for defrost operation is changeable according to the defrosting time to decrease the frequency of the defrost operation. In addition, the indoor fan starting control is varied for user's comfort.

2.3.4 Product line-up

Currently, we have 11 series products with nominal cooling capacities ranging from 6.3 kW to 56.0 kW in our line-up. These include multiple indoor units and can be operated individually.

2.3.5 Conclusion

We have presented an overview of an air conditioner for cold regions that has been developed with a combination of air conditioning and refrigeration technologies. We wish to express our gratitude to the Hokkaido Electric Power Co., Inc. and to the Tohoku Electric Power Co., Inc. for this product development.

Hitachi has developed product using a liquid injection (LI) refrigeration cycle for cold regions, based on the cycle illustrated in Figure 3, above.

2.4 High Heating Capacity Packaged Air-conditioners with Heat Exchanger for Cold Climates

In general, heating capacity of the air conditioner decreases with decreasing outdoor temperature. Conventionally, it was necessary to supplement the heating capacity by the combination, such as a stove or electric heater at very low temperature. Therefore, with the aim of disseminating air-conditioners in cold climates, we improved the heating performance of air-conditioners at low temperature in extremely cold regions, and developed anti-freezing functions for air-conditioners used in cold climates.

2.4.1 Technology for outdoor units in cold climates

The following are the main technical issues for air-conditioner use in cold climates:
- Ensuring heating capacity at very low temperature
- Expanding operational range in cold climates
- Improving defrosting performance
- Improving defrost water drainage and developing anti-freezing functions

Ensuring Heating Capacity at Very Low Temperature
In order to improve the heating capacity of air-conditioners at low temperature, it is necessary to ensure adequate heat exchanger capacities at low temperature. By approximately 15% larger face area of the heat exchanger, heating performance is improved at low temperature. In addition, its components were designed to enhance heating performance shown in Figure 21. The heat exchanger has a greater number of refrigerant paths compared to conventional heat exchangers in the same capacity in order to reduce

pressure loss during heating operations. Moreover, an anti-freezing component has been equipped at the bottom of the heat exchanger to prevent frost formation during heating operations. We also used a high-static pressure fan to prevent airflow reductions due to increased airflow resistance caused by frost formation.

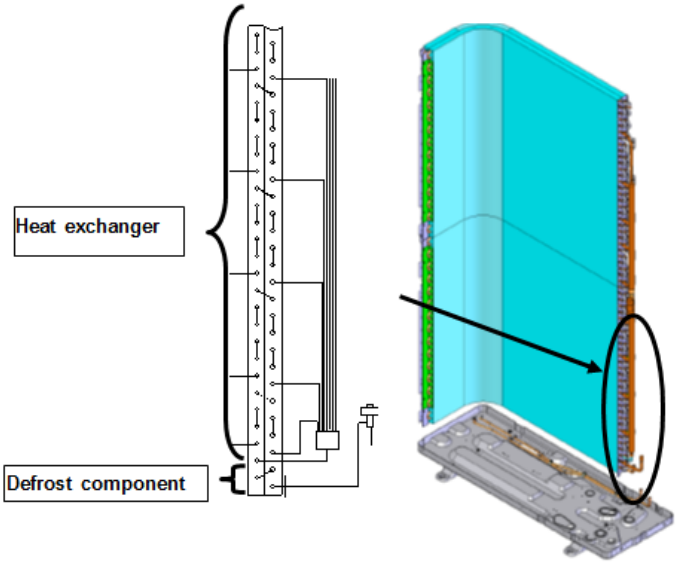

Figure 21: Structure of heat exchanger

Expanding Operational Range in Cold Climates

During heating operations, the high-pressure side of the compressor is related to the temperature of blowing to the air-conditioned room to make a comfort temperature, while the low-pressure side is determined by outdoor temperature and outdoor heat exchanger performance. For this reason, the conventional air-conditioner's compressor were operated using high compression ratio at very low temperature in cold climates, which reduced operational efficiency, increased the stress on the compressor itself and possibly reduced long-term reliability.

Therefore, by improving the performance of the outdoor heat exchanger, even when the outdoor temperature is low, it is possible to operate the low-pressure side comparatively highly. With ensuring heating capacity, it is possible to operate efficiently by reducing the compression ratio. In addition, if the heating operation is stopped, it is possible to keep the temperature higher than outdoor temperature by energizing a portion of the electrical components. And we selected the bearing grease that can be used at very low temperature in the bearing of the motor. Thus, the heating operation is ensured at temperature as low as -25℃.

Improving Defrosting Performance

Defrosting performance for air-conditioners were required in order to quickly resolve the capacity reduction due to frost formation in cold climates. The heat sources for defrosting are heat in highly-pressurized refrigerants immediately before defrosting, and heat generated through the compressor's power consumption during defrosting operation. It is necessary to use them effectively. To this end, we added a circuit bypassing the indoor unit in order to ensure the refrigerant flow rate during defrosting. This configuration allows for efficient defrosting.

Figure 22 shows a schematic diagram of the refrigeration cycle that features the bypass circuit, including a solenoid valve that opens during defrosting. If the connecting pipes are long, the defrosting performance of the conventional air-conditioners deteriorates due to

pressure drops between the indoor unit and the insufficient refrigerant amounts. However, our air-conditioners enable efficient defrosting while ensuring circulation flow rates. Thus, defrosting time is reduced by 25% compared to conventional heat exchanger under the same conditions.

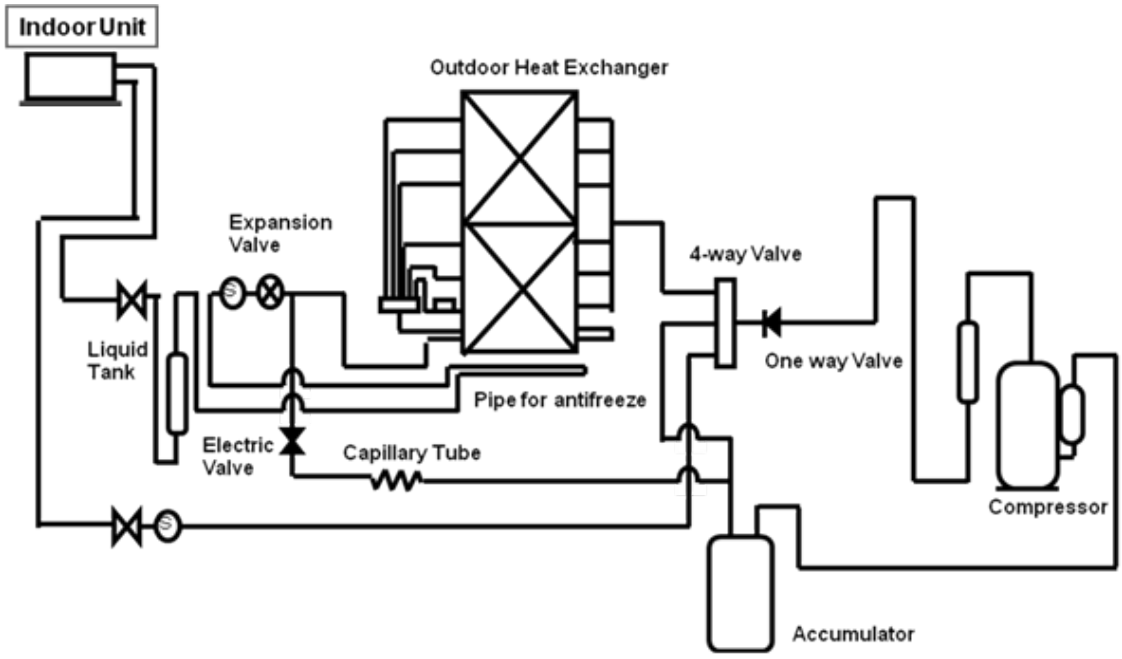

Figure 22: Schematic diagram of refrigeration cycle

Improving Defrost Water Drainage and Developing Anti-freezing Functions

When the conventional air-conditioner are used at very low temperature, the defrost water collected in drain-pan—at the bottom of outdoor heat exchanger—often refreezes. As the ice in the drain-pan repeatedly melts and re-forms, the ice spreads gradually throughout the lower part of heat exchangers. And there is a possibility to cause damage to the tubes of the heat exchanger bottom. This drainage of the defrost water is important in cold climates. One conventional approach to address this problem is to maintain the tubes of the heat exchanger bottom at temperature that prevent frost formation. This measure has proven to be successful based on market performance results.

Another mechanism that has been integrated into the air-conditioner is placing the outlet pipe of the condenser near outlets of the drain-pan, thereby preventing defrosted water from freezing (Figure 22). Figure 23 shows the layout of an anti-freeze pipe. Figure 24 is a photo of the heat exchanger, which was operated continuously for three weeks under high humidity at -20℃. The lower part of the heat exchanger is free of frost, indicating that defrosted water was properly drained.

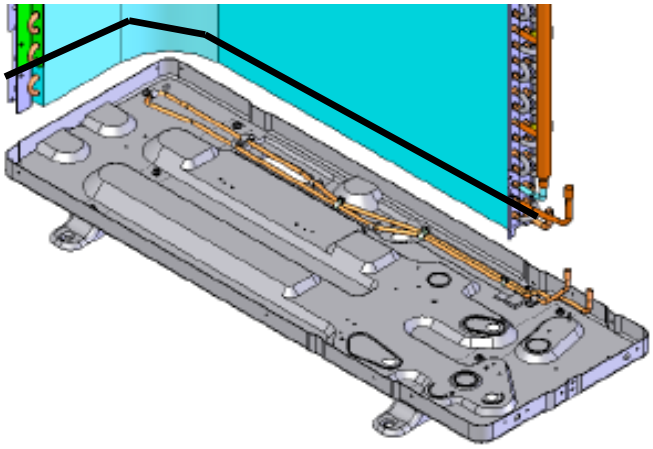

Figure 23: Lower part of heat exchanger: defrost area and anti-freeze pipes

Figure 24: Lower part of heat exchanger that was operated continuously for three weeks under high humidity at -20℃

2.4.2 Actual systems

Figure 25 shows the air-conditioner developed for stores and offices in cold climates. The main specifications of such air-conditioners are summarized in Table 4 below. The heating capacity of the air-conditioners remains unchanged up to -15℃. This has been achieved by controlling the maximum compressor speed according to outside temperature. As suction pressure and power consumption decrease when outside temperature are low, the compressor rotates at high speeds. Because of this, although the maximum current of the air-conditioners is the same as that of conventional air-conditioners, the heating capacity can be ensured even at low temperature.

Figure 25: Air-conditioner for shops and offices
(Super Power Eco Dantaro by Toshiba Carrier Corporation)

Table 4: Main specifications when connected to 4-way cassette type indoor unit

		3 HP	4 HP	5 HP	6 HP
Rated heating capacity	(kW)	8.0	11.2	14.0	16.0
Rated heating COP		4.42	4.36	4.47	4.00
Rated heating capacity at low temperature (outside temperature: 2℃)	(kW)	11.5	14.2	16.3	16.8
Heating capacity at low temperature (outside temperature: -15℃*)	(kW)	11.5	14.2	16.3	16.8
Heating capacity at low temperature (outside temperature: -20℃*)	(kW)	10.3	12.0	14.3	14.8
Outdoor unit dimensions	(mm)	1340 H×900 W×320 D		1540 H×900 W×320 D	
Outdoor unit weight	(kg)	95		116	

*Conditions were set by the manufacturer. Heating capacities are peak values and do not include defrost functions.

The heating capacity ratio at -20C vs. low temperature (2C) rated capacity ranges from about 85% to 90% for these products (Table 4 above).

2.5 High-Efficiency Heat Pump using Two-Stage Compression System for the Cold Area

2.5.1 Introduction

Presently, although the heat pump technology has been developed, introduced and popularized, the combustion-type heating is still generally applied in the cold area. The heat pump is not popularized due to the degradation of its heating capacity and the lack of comfort at low ambient temperature. Therefore, it is very important to improve the performance of the air source heat pump for cold area. As a solution, a highly efficient and comfort providing two-stage compression variable refrigerant volume (VRV) system was

developed by Daikin. The features of this product are outlined below.

2.5.2 Features

The "two-stage compression VRV system" designed for the cold area adopts the newly developed two-stage compression technology. With this technology, the heating efficiency at low ambient temperature is significantly improved, and both the heating capacity and heating rapidity at low ambient temperature are enhanced.

In the system, the functional module of the two-stage compression refrigerant circuit is additionally equipped with the outdoor unit module, so we have four models: 10HP, 14HP, 16HP and 20HP. Figure 26 shows the outlook of the representative model.

Figure 26: Outlook (14HP)

Two-stage compression technology

The two-stage compression VRV adopts the two-stage compression technology, which divides the compression process into high-pressure stage and low-pressure stage and additionally incorporates an intercooler (flash tank) and a bypass circuit. Figure 27 shows the schematic diagram of two-stage compression technology. The functional module for the outdoor unit consists of the high-stage compressor and the intercooler. Figure 28 shows P-h diagram of two-stage compression technology. The refrigerant which flows out of the condenser enters into the intercooler (flash tank). The refrigerant is separated into gas and liquid in the intercooler. The liquid refrigerant goes into an evaporator, evaporates and enters into the low-stage compressor. On the other hand, the gas refrigerant separated by the intercooler flows into the bypass circuit, mixed with the refrigerant compressed by the low stage side compressor, and enters into the high-stage compressor. The two-stage compression technology makes the amount of circulation of the refrigerant which passes a condenser increase. In addition, this technology reduces the discharge temperature of the refrigerant. The reduction of discharge temperature has an effect in the heat loss decrease to the exterior space from high temperature piping.

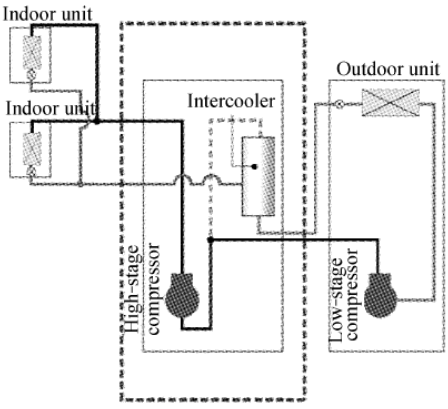

Figure 27: Schematic diagram of two-stage compression technology

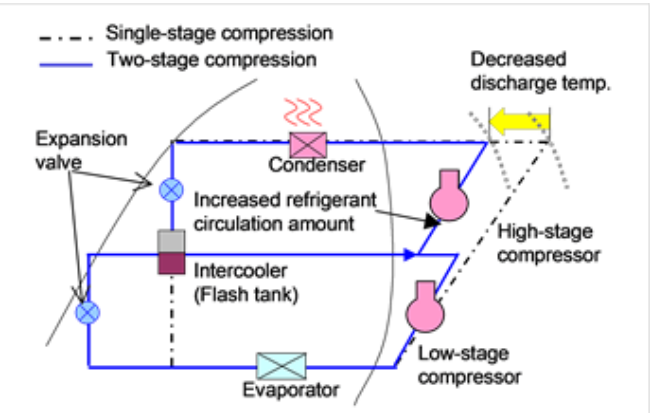

Figure 28: P-h diagram of two-stage compression technology

2.5.3 Enhanced heating capacity and COP

Figure 29 shows the relationship between the heating capacity and ambient temperature.

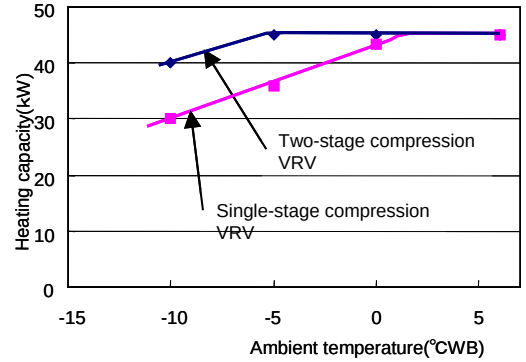

This value does not include the capability degradation with frost generation

Figure 29: Heating capacity enhancement

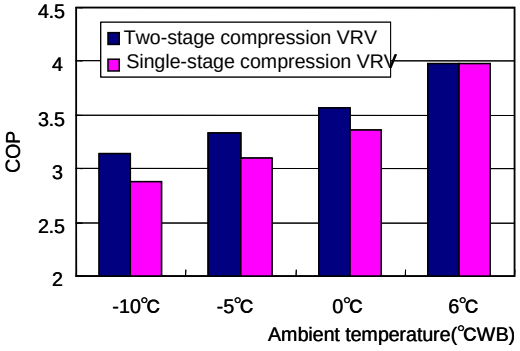

Figure 30: COP enhancement

For the traditional single stage compression system, the heating capacity degradation is mainly due to the reduced mass flow rate of the refrigerant under low temperature conditions. The gas refrigerant, instead of entering the evaporator, is separated in the intercooler, resulting to increase the flow rate of the refrigerant entering the indoor unit, thus enhances the heating capacity. Figure 30 shows the relationship between the COP and ambient temperature. The two-stage compression technology reduces the input power for refrigerant compression, and enhances the COP of the entire system. The heating capacity ratio at -10C (14F) vs rated capacity at 5C is 90% (Figure 29).

*This section is a summary of the above paper.

2.6 Development of Ejector Refrigeration Cycle Technology for Co_2 Heat Pump Water Heater

2.6.1 Outline

As an environmental protection measure, public attention is now focusing on improving the energy savings of residential water heating, which accounts for about one-third of total household energy consumption. One practical solution is to promote expanded use of "EcoCute," a high efficiency heat pump water heater using a natural refrigerant (CO_2). As part of our efforts to increase the popularity of EcoCute, Denso has developed the world's first variable ejector refrigeration cycle technology for CO_2 refrigerants. This technology enables more efficiently designed, larger-capacity water heating systems that can supply hot water for floor heating and other purposes as well as standard hot water systems.

2.6.2 Contents of techniques

In a conventional refrigeration cycle, the refrigerant loses part of its kinetic energy in the expansion valve since energy is wasted as heat in generating a vortex in the decompression-expansion process. Among its physical properties, CO_2 refrigerant loses larger amounts of energy compared with usual fluorocarbon refrigerants. We devised a refrigeration cycle that effectively recovers the wasted energy, and thus improves coefficient of performance (COP).

An ejector is used in place of a conventional expansion valve, and an accumulator located downstream from the ejector, it should be possible to realize a refrigeration cycle in which liquid refrigerant can continuously be supplied to an evaporator. The ejector itself consists of a nozzle, mixing unit, and diffuser, Figure 31.

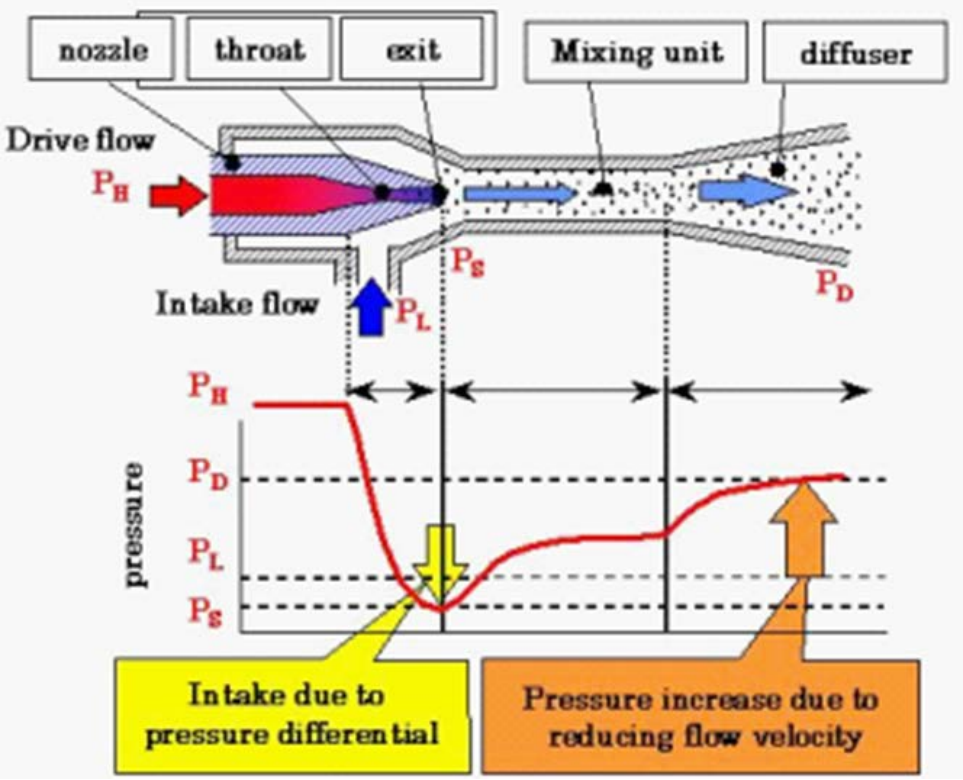

Figure 31: Principle of ejector

The refrigerant flowing into the nozzle (drive flow) is decompressed at the nozzle to draw the refrigerant from the evaporator (intake flow). The drive flow and intake flow are mixed until they are homogenized in the mixing unit, reducing the flow velocity and increasing the pressure of the mixture. The mixture further reduces velocity when it passes through the diffuser with its larger passage, further increasing the pressure. The new ejector refrigeration cycle thus uses the kinetic energy of the refrigerant to increase the pressure, thereby supplementing the power of the compressor.

The following are key points for ensuring the ejector refrigeration cycle of a heat pump water heater under a wide range of operating conditions (atmospheric temperature, feed water temperature, hot water temperature, etc.).

The first point is to maintain a heating capacity that will ensure the required discharge temperature of the compressed refrigerant, the basic function of a heat pump water heater. One of the features of the ejector refrigeration cycle is that the heating capacity tends to drop because the refrigerant discharge temperature decreases as the refrigerant pressure rises. Increasing the refrigerant pressure at the discharge port is one way to maintain the required discharge temperature. However, this measure will impair the result of ejector refrigeration cycle. To secure the required discharge temperature by absorbing heat into the refrigerant, we combined the features of an external heat exchanger and internal heat exchanger by positioning them downstream from the accumulator, Figure 32.

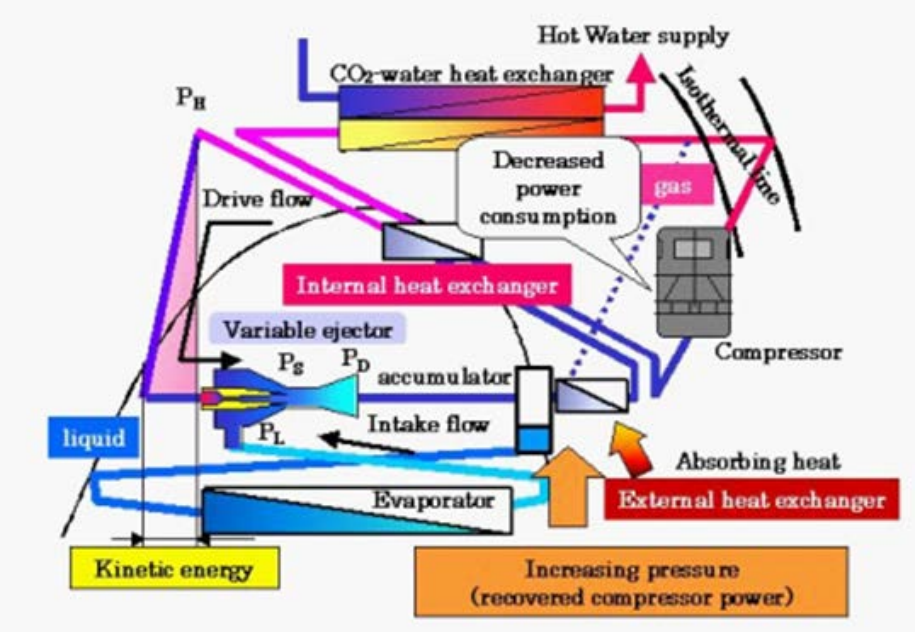

Figure 32: Ejector refrigeration cycle constitution

The external heat exchanger absorbs heat in the air whereas the internal heat exchanger exchanges heat with the high-side pressure refrigerant. The external heat exchanger functions most effectively when the feed water temperature is low, whereas the internal heat exchanger is more effective for high temperature feed water.

The second point is to maintain a high COP. Optimal control of high-side pressure is essential for CO_2 refrigerant cycle, as has already been introduced in conventional CO_2 heat pump water heater. For the new ejector refrigeration cycle, the high-side pressure should also be optimally controlled to realize a high energy without decline energy recovery efficiency of ejector (ejector efficiency). The ejector efficiency is influenced mainly by its nozzle. An ejector nozzle includes a "throat" and an "exit." The throat adjusts the refrigerant flow rate to assure the required heating capacity and maintains a high-side pressure for high COP, while the exit has a large effect on ejector efficiency. We have developed a unique flow restriction mechanism that optimally controls the cross-sectional areas of the throat and exit simultaneously, Figure 33.

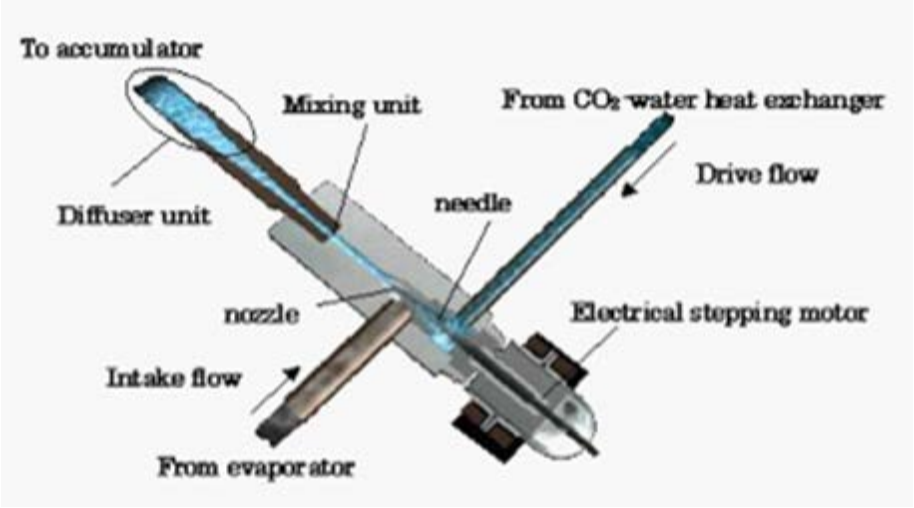

Figure 33: Variable ejector construction

The ejector is designed so that its flow path configuration is best suited to the physical properties of CO_2 refrigerant.

The new ejector design discussed above has expanded the range of applications of the ejector refrigeration cycle, which previously was only available in a restricted operating range, to heat pump water heater that have to operate all year round.

2.6.3 Conclusion

Alongside our development of the new variable ejector refrigeration cycle technology, we also improved the compressor and CO_2-water heat exchanger designs. As a result, we succeeded in realizing a new CO_2 heat pump water heater with 30% heating capacity and a COP approximately 20% higher than conventional type.

*This report is quoted from http://www.jsme.or.jp/English/awardsn03-3.html, JSME News on WWW.

3 FUNDAMENTAL RESEARCH

In this chapter, fundamental technologies such as measurement technologies, material property evaluation technologies, evaluation of the frost phenomena on the heat exchanger's surface are explained. These technologies help to design properly for cold climate.

3.1 Isobaric Heat Capacity of R32

3.1.1 Introduction

R32 (difluoromethane, CH_2F_2) is used as one component of important refrigerant mixtures, e.g., R 407C [R32/125/134a (23/25/52 mass%)] and R410A [R32/125 (50/50 mass%)] that are alternatives to replace conventional R 22. Ozone depletion potential (ODP) of R32 is zero, and global warming potential (GWP) is 675, which is much smaller than that of R22 (GWP=1500), R407C (GWP=1307), and R410A (GWP=1725) currently used as refrigerants.

In order to use a refrigerant, the thermophysical property information about the refrigerant is required. Among the information, isobaric heat capacity (c_p) is one of the fundamental thermodynamic property data which are used to design application systems. However, available thermophysical property data for R32 are still limited, especially for caloric properties. Hozumi et al. (1994) reported speed of sound of gaseous R32 at temperatures from 273 K to 343 K and at pressures from 0.02 MPa to 0.25 MPa. Kubota et al. (1995) reported c_p of R 32 in the gas phase where 18 c_p measurements were obtained from 303 K to 343 K and from 0.12 MPa to 0.5 MPa by using a flow calorimeter. And also, the authors reported 32 c_p measurements obtained from 274 K to 353 K and from 0.65 MPa to 2.4 MPa by using a flow calorimeter (Kagawa, 2012).

In this work, cp data of R32 in the gas phase close to the saturation curve were obtained by using a flow calorimeter. The measurements were obtained at temperatures from 282 K to 319 K and at pressures from 1.0 MPa to 2.4 MPa. The previous data from 274 K to 353 K and from 0.65 MPa to 2.4 MPa in the gas phase and the present data are used to evaluate equations of state. And also, curves of the isobaric ideal-gas heat capacity, $c_{p,0}$, and the vapour saturation (c_p") of R32 are specified by using the data.

3.1.2 Measurements

Experimental Procedure

A flow calorimeter was used for these measurements; it has been described previously in detail by Mukoyama et al. (1998) and the authors (2009). A stable and steady flow of sample gas is provided, and heat flux is generated by a microheater inserted in the calorimeter tube. The calorimeter tube is surrounded with an evacuated thermal shield. The tube and shield are placed in a well-stirred water bath which is controlled at the target temperature within ±10 mK. Each c_p datum is determined by measuring the temperature increment, ΔT, and mass flow rate, $\dot{m}$, of R32.

To measure the temperature increment, two calibrated standard platinum resistance thermometers (PRTs) are located at both ends of the microheater in the sample flow. To measure the mass flow rate, a three-way solenoid valve, a timer, and a sampling cylinder were used. During one minute, the sample is permitted to flow into the cylinder that was cooled by liquefied nitrogen. The cylinder mass was measured with an electronic balance with an uncertainty of 0.1 mg.

By measuring the heat input to the heating element, $\dot{Q}$, and mass flow rate, $\dot{m}$, experimental values of $c_{p,\mathrm{app}}$ are obtained from

(1)

$$c_{p,\mathrm{app}} = \frac{\dot{Q}}{\dot{m}\Delta T} = \frac{\dot{Q}_\mathrm{R}}{\dot{m}\Delta T} + \frac{\dot{Q}_\mathrm{L}}{\dot{m}\Delta T} = c_p + \frac{\dot{Q}_\mathrm{L}}{\dot{m}\Delta T}$$

Part of the heating energy, $\dot{Q}_\mathrm{L}$, is released from the sample and the calorimeter to the surroundings even though the calorimeter is thermally shielded. In order to determine the value of $\dot{Q}_\mathrm{L}$, more than four $c_{p,\mathrm{app}}$ data were measured by changing the mass flow rate from 2.3 to 5.1 g•min^{-1} with ΔT = 2 K at the same temperature and pressure. By plotting a $c_{p,\mathrm{app}}$ curve versus $\dot{m}^{-1}$ and extrapolating the curve to $\dot{m}^{-1} \rightarrow 0$, the actual c_p value can be determined.

To establish a stable sample flow in the calorimeter tube during measurements, a condenser with a bellows-type liquid pump, an evaporator, and a nozzle (needle valve) are used for the apparatus. The mass flow can be adjusted by the needle valve and an electronic controller. The sample pressure at the calorimeter outlet was measured with a quartz crystal pressure transducer (Paroscientific, Model 31K-101).

Materials

A sample of R 32 of a minimum purity of 99.98 mol% was obtained for this study. The sample supplied in a bottled cylinder was filled into the apparatus. The total mass of the charged sample was about 1 kg.

Results and Discussion

Figure 34 shows the c_p -T diagram of the present measurements and the former measurements for R32 (Kagawa, 2012a, b). Vertical error bars in the figure indicate the uncertainties of the experimental data. In this figure, the isobaric data along 0.65, 1.0, 1.5, 2.0, and 2.4 MPa seem to be reasonable.

The behavior of isobars, the saturation curve, and ideal-gas heat capacity calculated by the available equations of state (EOS), which have been formulated by Outcalt and McLinden (1995), Tillner-Roth and Yokozeki (1997), Piao and Noguchi (2001), and Astina and Sato (2004) based on experimental thermodynamic property data, are also shown in Figure 34.

Based on the behavior of the present and previous measurements and isotherms of R32, eight data of the isobaric ideal-gas heat capacity, $c_{p,0}$, of R32 were graphically determined.

Vertical error bars in the figure indicate the uncertainties of the experimental data. The $c_{p,0}$ data were correlated with an equation.

$$\frac{c_{p,0}}{R} = 2.4550 + 3.0874\,T_r + 0.12407T_r^2 \qquad (2)$$

where, $c_{p,0}$ is molar heat capacity, kJ•kmol^{-1}•K^{-1} and R is the universal gas constant, 8.314472 kJ•kmol^{-1}•K^{-1}. The applicable temperature range of the correlation is from 293 K to 353 K corresponding to the measurement range. The uncertainty in the calculated results with eq. (2) is estimated to be less 3.5% because the maximum deviation of the values from the $c_{p,0}$ data is 0.28% and the maximum estimated uncertainty of the $c_{p,0}$ data is about 3.2%. The calculated $c_{p,0}$ with eq. (2) are also shown in Figure 34.

Furthermore, five c_p on the saturation curve (c_p") were determined from the isobars in Figure 34, and also four c_p" were done from behavior of isotherms. The c_p" data were correlated with an equation.

$$\frac{c_p''}{R} = -0.43986 + 1.7206\,T_r - 2.2346T_r^2 + 0.97813T_r^3 \qquad (3)$$

where c_p" is molar saturated gaseous heat capacity, kJ•kmol^{-1}•K^{-1} and R is the universal gas constant, 8.314472 kJ•kmol^{-1}•K^{-1}. The applicable temperature range of the correlation is from 266 K to 313 K. The uncertainty in the calculated results with eq. (3) is estimated to be less than 4.0% of the 0.76% of the maximum deviation of the values from the c_p" data and 3.2% of the maximum estimated uncertainty of the c_p" data. The calculated values with eq. (3) are also shown in Figure 34.

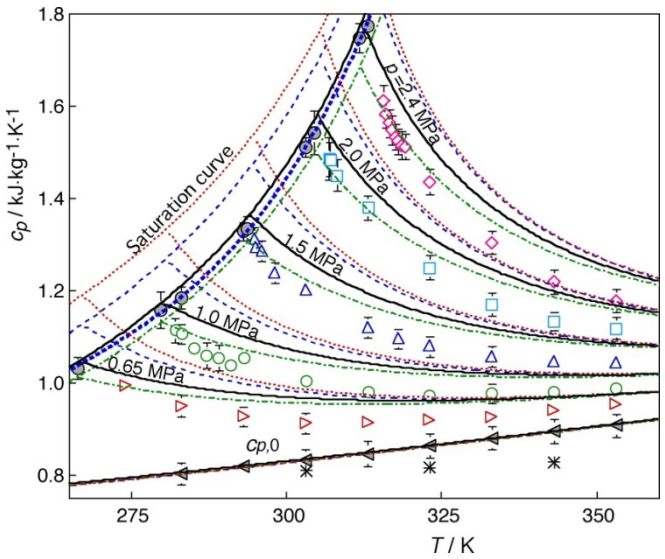

Figure 34: Experimental data (points) compared to several equations of state (lines); ◁ : $c_{p,0}$, ◎:saturation, ▷ :0.65 MPa, ○:1.0 MPa, △: 1.5 MPa, □: 2.0 MPa, ◇:2.4 MPa, closed: present measurements, open: previous, shaded: graphically determined values, *: Kubota et al. (1995), 0.5 MPa, ——— : Outcalt and McLinden (1995), ·····: Tillner-Roth and Yokozeki (1997), —·—·— : Piao and Noguchi (2001), – – – – – : Astina and Sato (2004), ▪▪▪▪▪▪ : saturation curve by eq. (3).

3.2 Heat Transfer and Flow Characteristics in a Plate Heat Exchanger

3.2.1 Introduction

Plate heat exchanger (PHE) is widely used in industrial process as a liquid-liquid heat exchanger. Recently, plate heat exchangers are applied to an evaporator or a condenser of refrigerating or heat pump cycle or the compactness and heat transfer performance improvement. Higher heat transfer coefficient and larger heat transfer area can lead to a reduction of temperature difference between fluids, moreover the reduction leads to an improvement in COP. Therefore, plate heat exchanger is much effective for water heat source heat pump system.

PHE for heat pump system is made by brazing wavy thin stainless steel sheets. Each fluid flows between the sheets alternately, that is, a PHE has parallel channels. Each channel has netlike conduits formed by wave configuration of sheets. The configuration leads to larger heat transfer area and higher heat transfer coefficient, but also induces larger pressure loss. Therefore, the number of parallel channels is generally designed larger. For evaporator or condenser, since a working fluid flows as a gas-liquid two-phase mixture, the dynamic behaviors of gas-liquid two-phase flow strongly affect on the heat transfer performance. In order to design or improve the heat transfer performance, it is important to understand liquid distribution not only in each channel but also into parallel channels. In particular, in the case where the inlet flow is wet vapor, the effects of inlet flow conditions and inlet configuration on liquid distribution characteristics should be clarified.

This study deals with the relationship between boiling heat transfer performance and flow pattern for a single channel PHE. This is especially the case for the effect of flow direction, such as vertically upward and downward, on the flow and heat transfer characteristics. Flows were visualized by neutron radiography[(1)].

3.2.2 Experimental apparatus and method

Neutron radiography is a visualization technique by using the difference in attenuation rate of neutron ray to irradiated materials. Since the attenuation coefficient of thermal neutron ray is high for hydrogen, and is low for metallic elements, neutron radiography is efficient for the visualization of fluids including hydrogen in a metallic vessel. HCFC-142b (CH_3CFCl_2) was used as the working fluid. FC-3283 without hydrogen was selected as heating medium because of its low neutron attenuation. Neutron radiography experiments were performed using real-time neutron radiography facility in the research reactor JRR-3 of Japan Atomic Energy Agency.

The detail of plate configuration is shown in Figure 35. The heat transfer area of a plate is 0.0123 m^2, and the volume of single channel is 0.02 L. The average hydraulic diameter of the single channel was calculated to 3.36 mm. Tested PHE has three channels by 4 thin SUS wavy sheets. The working fluid in the center channel was heated by the heating medium in the both sides channel. The PHE was placed vertically. Neutron beam was irradiated vertically to plates, and boiling behaviors were visualized. The flow direction of the working fluid, vertically upward or downward, was set by four-way ball valves. On the other hand, the heating medium was supplied to the PHE from a constant temperature bath in the opposite direction of the working fluid.

Original radiographs of the test section with the liquid single phase flow and without the working fluid are shown in Figure 36 (a), (i) and (ii), respectively. From these two images, only liquid can be visualized by image processing. Processed image is shown in Fig.(b). Brightness becomes lower with thicker liquid thickness.

The system pressure was at atmospheric pressure. As experimental conditions, the mass flow rate of the working fluid G_f was varied from 0.0052 to 0.026 kg/s for 3 inlet conditions, subcooling liquid with the subcooling degree ΔT_{subin} of 10 K, saturated liquid, and wet vapor with the quality x_{in} of 0.01.

3.2.3 Experimental results and discussion

Experimental results of heat transfer rate and overall heat transfer coefficient are plotted in Figures 37 and 38 against mass flow rate G_f, respectively. The results for upward flows and downward flows are plotted by open and closed symbols, respectively. It can be seen from Figure 37 that heat transfer rate decreased with increasing mass flow rate of the working fluid, and was higher for the inlet subcooling condition than the inlet wet vapor condition. These reasons might be on temperature difference between the working fluid and the heating medium. The effect of the flow direction could not be clearly observed in heat transfer rate. To evaluate heat transfer performance, overall heat transfer coefficient was calculated by using logarithmic mean temperature difference defined with the terminal temperatures of both fluids. Since the temperature gradient in the flow direction for inlet subcooling condition will change at incipient boiling point, the logarithmic mean temperature difference was corrected according to the flow condition, liquid flow or boiling flow. The detail of the calculation method had been reported by L. Jiang, et al.

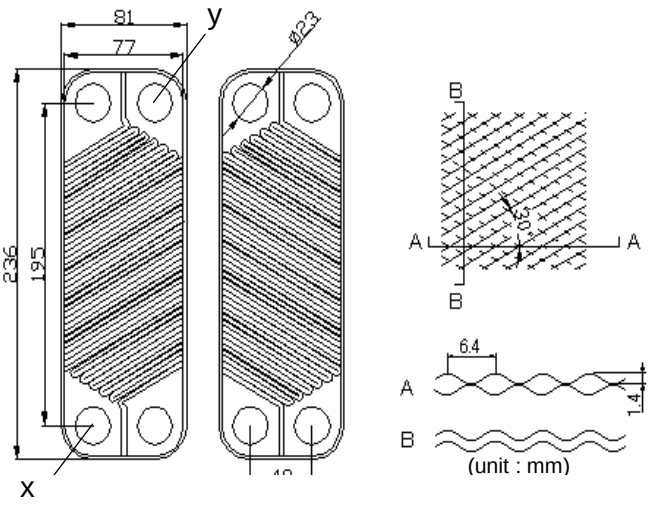

Figure 35: Plate configuration
Figure 35: Plate

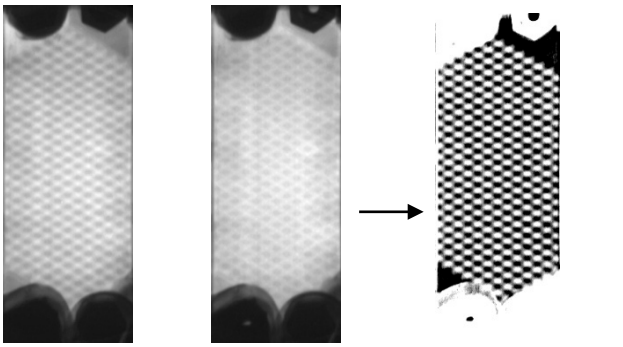

(i) Liquid single-phase (a) Original image. (ii) Without liquid. (b) Processed image for liquid visualization.

Figure 36: Image processing to visualize liquid behavior

Calculated results of overall heat transfer coefficient are plotted in Figure 38 with the same symbols with those in Figure 37. The downward flow produced higher heat transfer performance than the upward flow. Since the effect of the flow direction should be little in single-phase flow region, heat transfer coefficients in two-phase flow were affected by the flow direction.

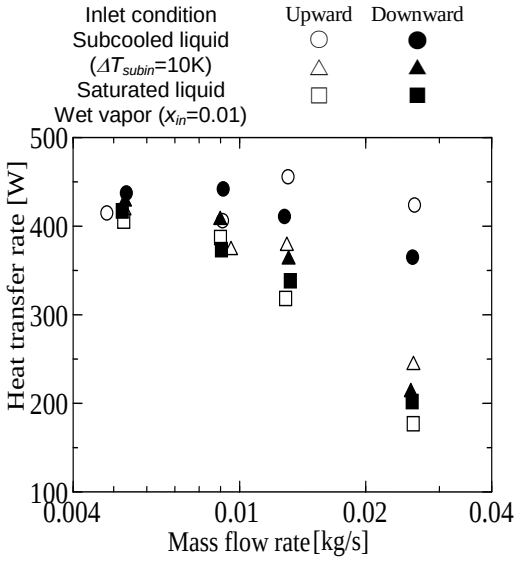

Figure 37: Heat transfer rate

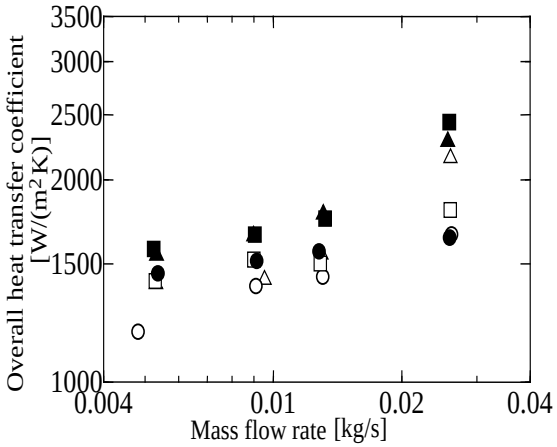

Figure 38: Overall heat transfer coefficient

Visualized images of liquid behaviors are shown in Figure 39. Figs.(i) are boiling behavior for inlet subcooling condition, and Figs. (ii) are those for inlet wet vapor condition for the upward flows in Figs.(a) and the downward flows in Figs.(b), respectively. Three continuous frames with the interval of 2/30 seconds are shown for each figure. Darker part shows thicker liquid thickness. The detail of image processing method is reported by H. Asano, et al.

For the inlet subcooling condition, the area where boiling occurred could be clearly observed. Single-phase flow area was larger at the center of channel for each direction. The reason might be on liquid flow rate distribution, that is, liquid flow rate along the center might be higher. Boiling two-phase flow area for the downward flow was larger than that for upward flow. In this case, there is little difference in overall heat transfer ere coefficient.

For the upward flow with the inlet wet vapor condition, vapor flowed into the test section intermittently. Liquid stagnation was observed at the both side around the inlet. Heat transfer might be lower in the area with liquid stagnation. On the other hand, for the downward flow with inlet wet vapor condition, though vapor flowed into the test section intermittently, liquid stagnation was not observed. The difference in flow pattern leaded to the difference in heat transfer coefficient.

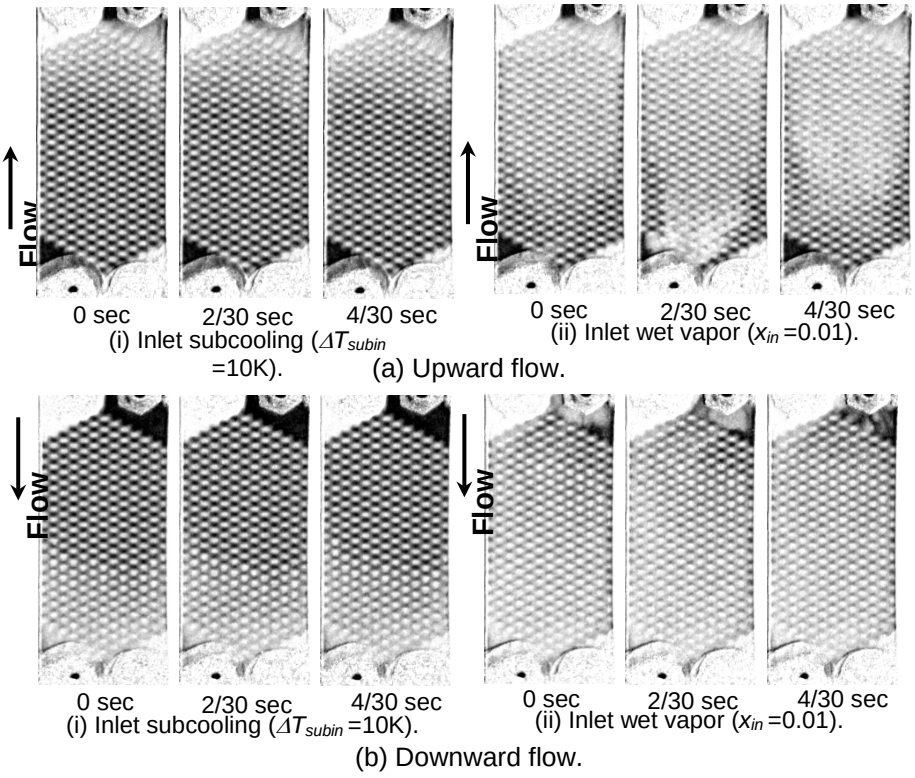

Figure 39: Liquid flow behaviors in boiling two-phase flow. Effect of inlet condition and flow direction (Mass flow rate：0.026 kg/s)

3.2.4 Conclusion

Boiling flows in a single-channel commercial brazing plate heat exchanger were visualized and void fractions were measured by thermal neutron radiography. Effect of flow direction on heat transfer performance was investigated. It was shown from the results, heat transfer of downward flow was higher that of upward flow because liquid stagnant area was larger for upward flow.

3.3 A New Defrosting Method for Utilization of Frost

3.3.1 Introduction

Frost formation occurs on a cooling surface, when the surface temperature is maintained below 0°C. A frost layer consists of a mixture of layers of ice and voids, which are filled with wet air. The frost formation phenomenon is a transient process in which frost crystals undergo changes with time, while both heat and mass transfer take place simultaneously. The frost formation needs to be prevented because frost acts as a layer of thermal resistance deteriorating the thermal performance. In most cases, the operation of low-temperature devices has to be temporarily stopped to remove the frost layers deposited on the surfaces of heat exchanges of the devices, by raising the surface temperature above 0°C. Due to this defrosting operation, the cooling surface has to undergo cycles of cooling and heating, which is a cause for the performance deterioration. To address the above issue, we propose here a new mechanical defrosting method, in which the defrosting can be done with the surface temperature of the heat exchanger maintained below 0°C. This method requires the determination of the adhesive force so that frosting can be reduced.

Fukiba et al. (K.Fukiba et al, 2009) applied one mechanical method of defrosting known as the jet defrosting method for removing the frost formed on heat exchangers with the view to use it in supersonic jet planes, and were successful in increasing the heat transfer and reducing the drag force. However, the cooling surface of their jet-defrosting method was at a cryogenic temperature of -200°C, when the adhesion of the frost layer onto the cooling surface is very weak. The objective of the research here is to investigate the removal of frost from heat exchangers of heat pump systems used in cold regions, where the jet-frost removal method would not be a good option. With the above background in mind, we investigated the effect of the cooling surface characteristics on the amount of frost formed and frost layer thickness. To evaluate the frosting process, we used in this experimental investigation a new parameter, which is the force required scrap off the frost from the cooling surface.

3.3.2 Experimental apparatus and method

Figure 40 shows the schematic diagram of the experimental apparatus. The apparatus can be considered as mainly consisting of the following sub-systems: an apparatus that maintains the test room and test chamber at constant temperature and humidity, measuring devices, devices for observation and a heat transfer section. In the test chamber, the temperature and humidity were controlled by using an air-conditioner, a humidifier, a dehumidifier and a heater, which were measured by a ventilated Asman hygrometer.

We have previously proposed a new method for mechanically removing the frost formed on cooling surfaces by using an impinging jet of air. To be able to use this method, it will be required to evaluate the cohesiveness of frost by some means. However, to the knowledge of the authors', research on the frost cohesion is mostly not reported in the literature, although there are numerous publications on the cohesion of ice. Further, it should be stated that defining an appropriate adhesive force for frost is also not clear at this stage. Therefore, we define here the force required to scrape the frost layer off a cooling surface with a blade as the adhesive force of frost, which was measured in the present work and referred to as the scraping force below. Figure 41 shows the schematic diagram of the apparatus for the measurement of the scraping force. After continuing the frost deposition process for a pre-determined time interval, a part of the frost layer was scraped off for up to 10 mm from the leading edge of the cooling surface. Then the tip of an acrylic scraper was brought into contact with the edge formed on the frost layer. The scraper has a sharp edge at its tip with an angle of 15°. The scraper was fixed at right angle to a stand or shelf made of SUS304, with weights made of stainless steel being mounted on this stand to move the scraper. A weight is spherical and can have masses of the three types, 4g, 1g or 0.5g.

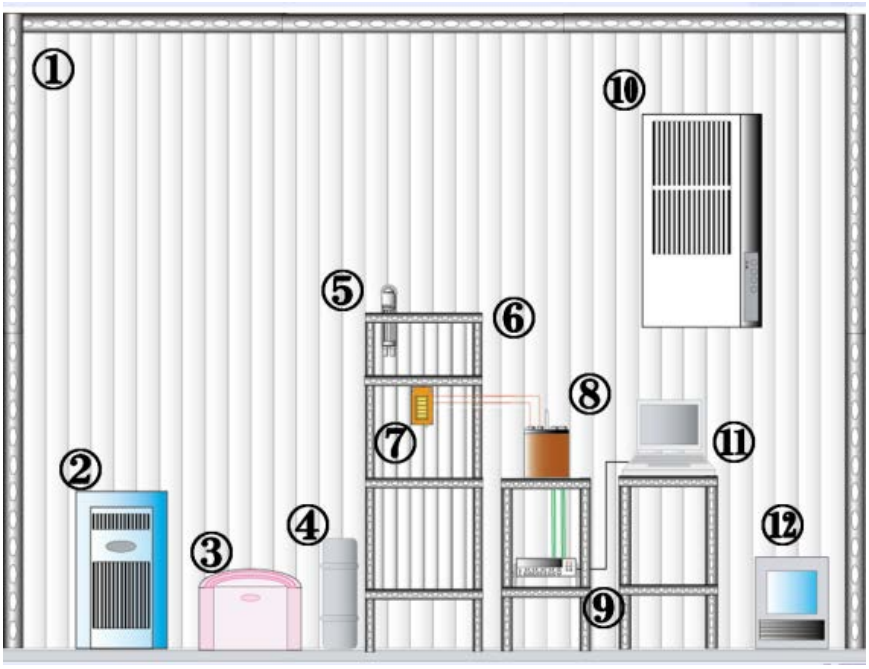

① Test room ② Dehumidifier ③ Humidifier ④ Dewar vessel ⑤ Asman hygrometer ⑥ Test chamber ⑦ Cooling surface ⑧ Cold junction ⑨ Digital voltmeter ⑩ Cooler ⑪ Computer ⑫ Heater

Figure 40: Schematic diagram of experimental apparatus I

This stand is attached to a movable mechanism, which consists of pulleys, rollers, wires and rails, the spherical weights on the stand being gradually increased until the mechanism started to move under the total of the added weights. The total weight m_T [g] was recorded when, on the addition of a last weight of 0.5 g, the mechanism started to move completely. It should be noted that the mechanism (shown in Figure 41) remained stationary even without a frost layer on the surface, due to friction. Therefore, in a preliminary test, the total mounted weight m_0 [g] that initiated motion in the mechanism was measured when there was no frost on the surface, and the scraping force per unit blade length F [N/m] was defined as in the following equation. Some minute amount of frost crystals would still remain on the cooling surface after the scraping, but its quantity is very small so as to reveal the copper color of the heat transfer surface.

$$F = (m_T - m_0) \times \frac{g}{l} \qquad (1)$$

Here, m is mass of the weight used [kg], g is acceleration due to gravity [m/s^2] and l is the width of the cooling surface.

Next, the measurement of the heat flux during the process of frost deposition is described, which is a process involving both simultaneous heat and mass transfer. Figure 41 shows a schematic diagram of the heat transfer section, which consists of 5 oxygen-free copper blocks, each with a mirror-surface finish and of the size, 40mm in width, 17mm in length and 10 mm in thickness. The sides and underneath of these blocks are insulated with fabric-reinforce Bakelite. To start the experiment, the heat transfer section was first dipped in liquid nitrogen in a Dewar vessel to cool it to a fixed temperature, and after maintaining the temperature steady for 5 mins, it was then fixed vertically in the test chamber. The frosting phenomenon is a transient process in that the thickness of the frost layer varies with time, but there are many research works that assume the temperature of the heat transfer surface

to be constant and the frosting to be a pseudo-steady state process. The present work is different from the reported ones in that the experiments were conducted under the condition that the temperature of the heat transfer surface also changed with time. In the experiments, we recorded the history of the temperature rise of the heat transfer surface, and obtained the heat flux q [W/m^2] using the lumped-thermal mass approximation as follows:

$$q = \rho \, c_p \delta \frac{dT}{d\tau} \qquad (2)$$

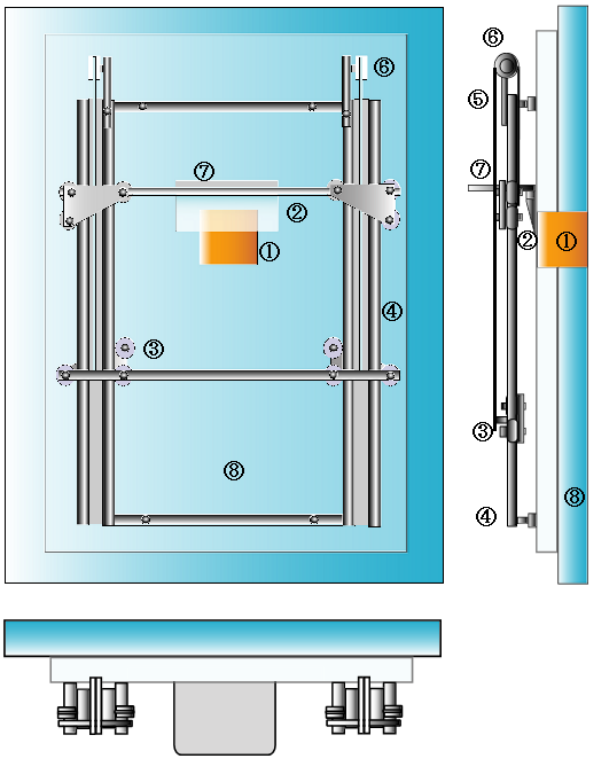

① Heat transfer plate ② Scraper ③ Roller ④ Rail ⑤ Wire ⑥ Pulley ⑦ Shelf ⑧ Insulation

Figure 41: Schematic diagram of experimental apparatus II

Here, ρ [kg/m^3] and c_p [kJ/kg·K] are the density and specific heat capacity of oxygen-free copper, respectively; δ [mm] is the thickness of the heat transfer section; T [K] is the temperature of the heat transfer surface; τ [sec] is time.

To evaluate the heat flux, it the heat loss needs to be considered, which was measured under each experimental condition by conducting the experiment with the heat transfer section covered with an insulation covering. The surface temperature of frost layer was measured using a commercial radiation thermometer (Minolta HT-11). The conditions of the experiments are as follows: air temperature t_a = 25^{o}C, absolute humidity x_a = 0.0099 kg/kg', initial temperature of heat transfer surface t_{w0} = -190 ^{o}C, and temperatures are measured at the distances y= 34.5, 53.5, 72.5 and 91.5mm from the leading edge.

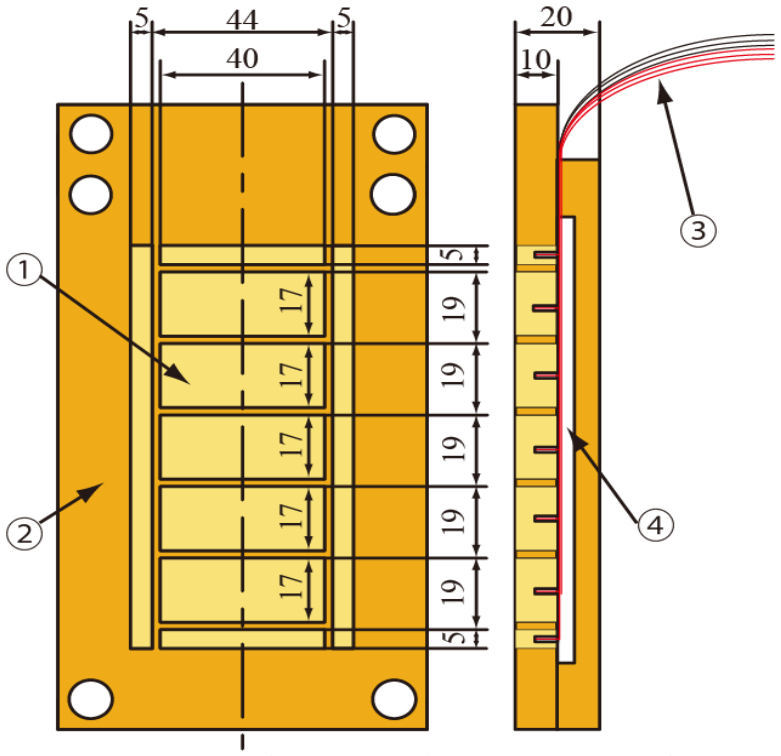

① Heat transfer plate ② Bakelite ③ Thermocouple ④ Insulation

Figure 42: Front and sectional-side views of the heat transfer plate

3.3.3 Experimental results and discussion

Figure 43 shows the frosting curve for frost layer thickness. It also shows the existing measurements and predictions of Eq.(3), reported previously (H.Ohkubo , 2010). In the case of region I see below, it was confirmed that the frost layer thickness reduces when the cooling surface becomes less wettable.

$$\begin{aligned} \boldsymbol{l}_f &= (-0.00028\Delta\boldsymbol{T}_w{}^2 + 0.087\Delta\boldsymbol{T}_w + 1.2)\boldsymbol{\tau}^{\boldsymbol{b}} \\ &\quad \times \left(6.52\times10^5\,\boldsymbol{x}_a{}^3 - 2.71\times10^4\,\boldsymbol{x}_a{}^2 + 3.79\times10^2\,\boldsymbol{x}_a - 0.75\right)\times 2.07\boldsymbol{t}_a{}^{-0.226} \\ \boldsymbol{b} &= \left(\frac{0.015}{\boldsymbol{x}_a{}^{0.25}}\right)\times \boldsymbol{y} \qquad\qquad \tau \leqq 1.0\text{hr} \end{aligned}$$

(3)

$$\begin{aligned} \boldsymbol{l}_f &= (-0.00028\Delta\boldsymbol{T}_w{}^2 + 0.087\Delta\boldsymbol{T}_w + 1.2)\boldsymbol{\tau}^{0.45} \\ &\quad \times \left(6.52\times10^5\,\boldsymbol{x}_a{}^3 - 2.71\times10^4\,\boldsymbol{x}_a{}^2 + 3.79\times10^2\,\boldsymbol{x}_a - 0.75\right)\times 2.07\boldsymbol{t}_a{}^{-0.226} \\ &\qquad\qquad \tau > 1.0\text{hr} \end{aligned}$$

Here, ΔT_w is the degree of superheat of the cooling surface (K), τ is time (hr), Δx is the difference in absolute humidity (kg/kg') and y is the distance from the leading edge (mm).

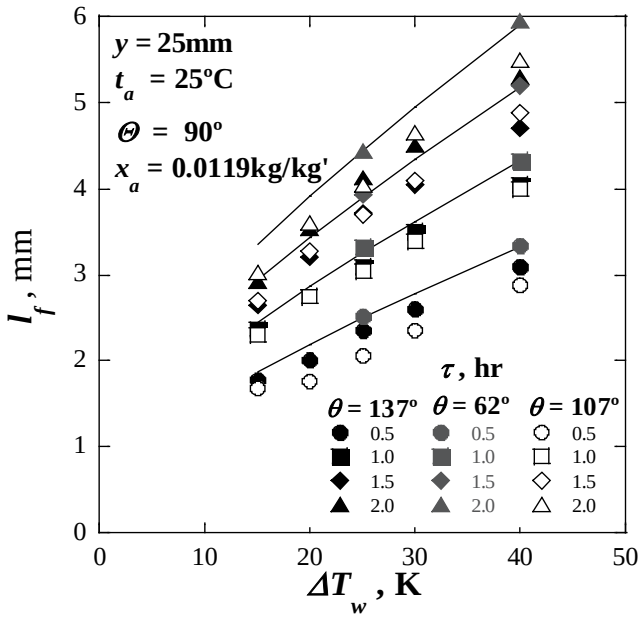

Figure 43: Frosting curve for frost layer thickness (In region I)

Figure 44 shows the frosting curve for the amount of frost deposited. It also shows the values for the surface wettability of θ=62° and the predictions from the following equation (H.Ohkubo, 2009).

$$m_f = (0.000257\Delta T_w{}^2 + 0.238\Delta T_w + 170) \times 65L^{-0.25} x_a \tau \qquad (4)$$

Here, m is the amount of frost deposited (g/m^2), ΔT_w is the degree of superheat of the cooling surface (K), τ is time (hr) and x_a is the absolute humidity (kg/kg').

The figure shows that the effect of wettability becomes apparent as the time passes, and the amount of frost deposition decreases the poorer the wettability of the surface. Figure 45 shows the time traces of the cooling surface temperature, heat flux and surface temperature of the frost layer in the case of absolute humidity x_a =0.0099kg/kg'. When measuring the surface temperature, it was found that emissivity ε_f = 0.98. However, the frost surface temperature in the initial deposition period is not shown here because it is difficult to determine the emissivity for this period. The cooling surface temperature increases with time, and when it reached 0°C, the experiment was stopped. The figure shows that the temperatures of both the cooling surface and frost layer increase gradually with time. On the other hand, the heat flux increased initially with time, but reached a peak, after which it decreased with time. Note that the heat flux values shown in the figure are those found by deducting the corresponding heat loss value from the measured heat flux values.

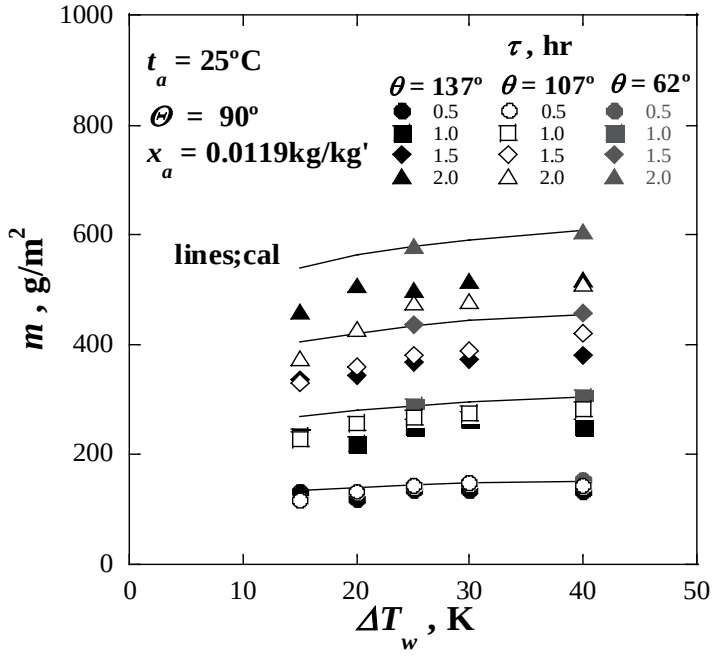

Figure 44: Frosting curve for the amount of frost deposition (Region I)

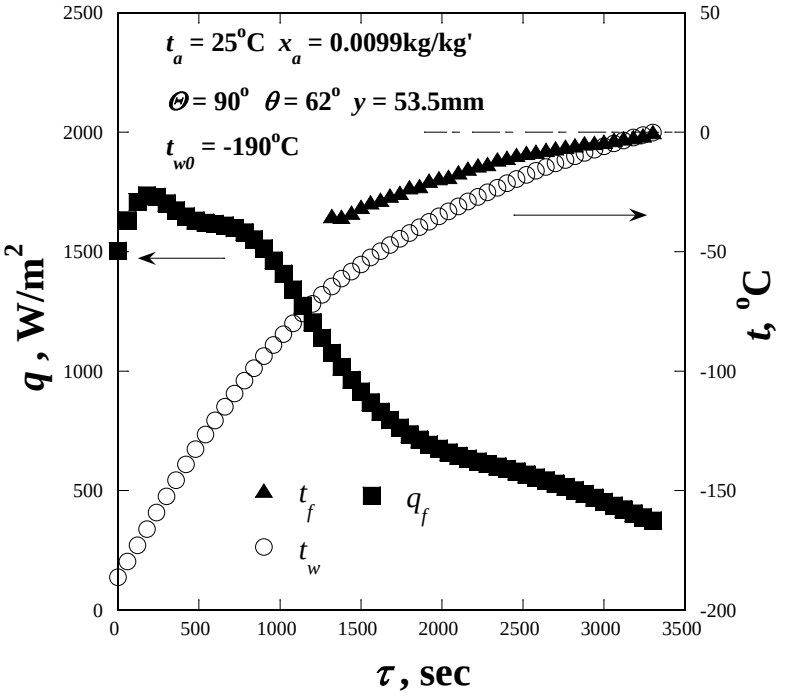

Figure 45: Variations of q, t_f and t_w as a function of time, τ

Figure 46 shows a typical experimentally obtained relationship between the heat flux and cooling surface temperature. The figure also includes the calculated values of the heat flux. Further, it also shows the total heat flux q_f obtained using the predictive relationship described below for every 10°C rise of the cooling surface temperature when the jet defrosting is taking place. Figure 46 shows the relationship between various heat fluxes and cooling surface temperature for an initial cooling surface temperature of -190°C and absolute humidity of 0.0099kg/kg'. If we define the total heat flux during the frost deposition as q_f, it

can be expressed approximately as the summation of the heat fluxes resulting from convection q_c, mass transfer q_m and radiation heat transfer q_r as below (H.Ohkubo, 2004).

$$q_f \approx q_c + q_m + q_r \quad (5)$$

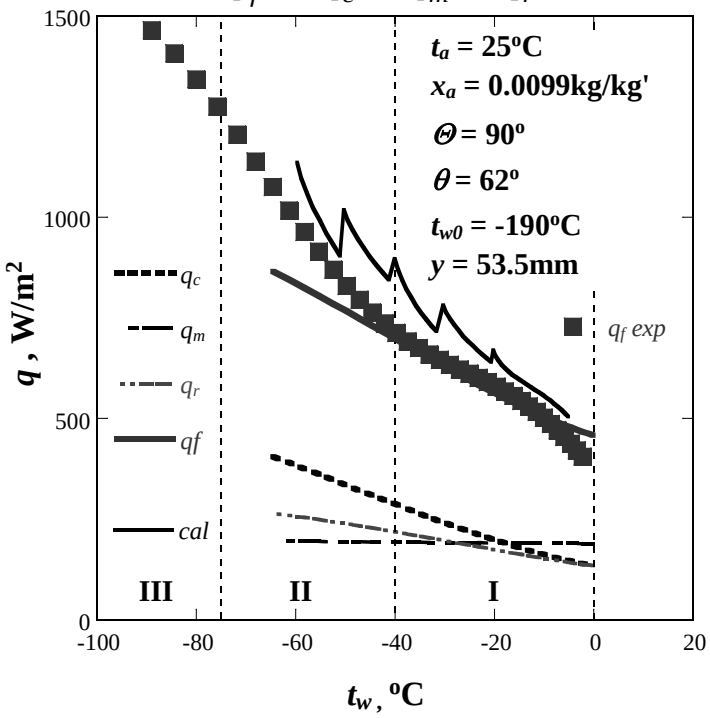

Figure 46: Relationship between the heat flux and cooling surface temperature

The figure shows that whenever the jet defrosting occurs, the heat flux increases due to the removal of the frost layer. In the range of -10°C≦ t_w < -45°C, the experimental and calculated results on q_f agree reasonably well, and therefore, it can be expected that the predictive relationship of the present work for q_f will apply in this range.

Figure 47 shows the relationship between the weights needed to move the blade, m[g] and temperature of the cooling surface, with wettability □/as the parameter. Here, m[g] is the difference between the total weights m_T[g] and m_0[g], which are the total weights needed to initiate the blade movement with and without frost on the cooling surface respectively. The figure shows that the scraping force decreases when the cooling surface temperature decreases. Further, the force decreases with a reduction in the surface wettability.

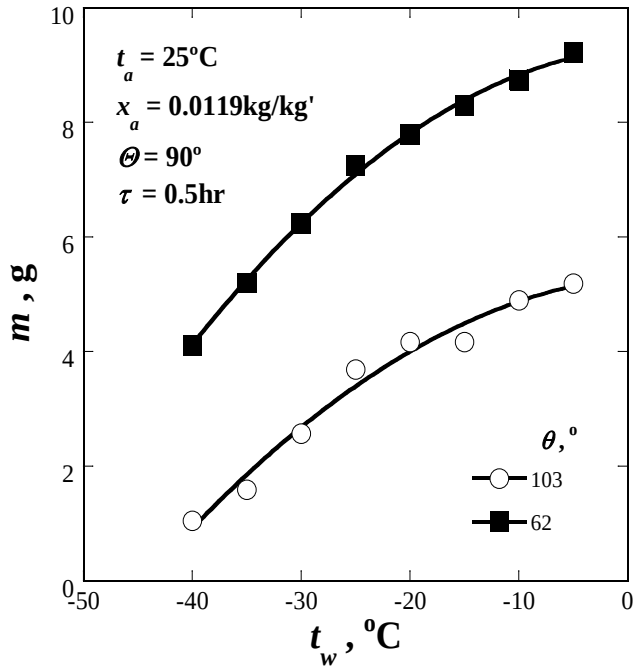

Figure 47: Relationship between *m* and t_w at different wettabilities

Figure 48 shows the frosting curve of the scraping force per unit blade length, *F*[N/m] obtained using Eq.(1); note that x-axis here is converted to the degree of supercooling of the cooling surface ΔT_w(=0-t_w), [K]. Figures 46 and 47 both show that poor surface wettability (i.e. a large contact angle θ in the static state) causes the scraping force to decrease drastically.

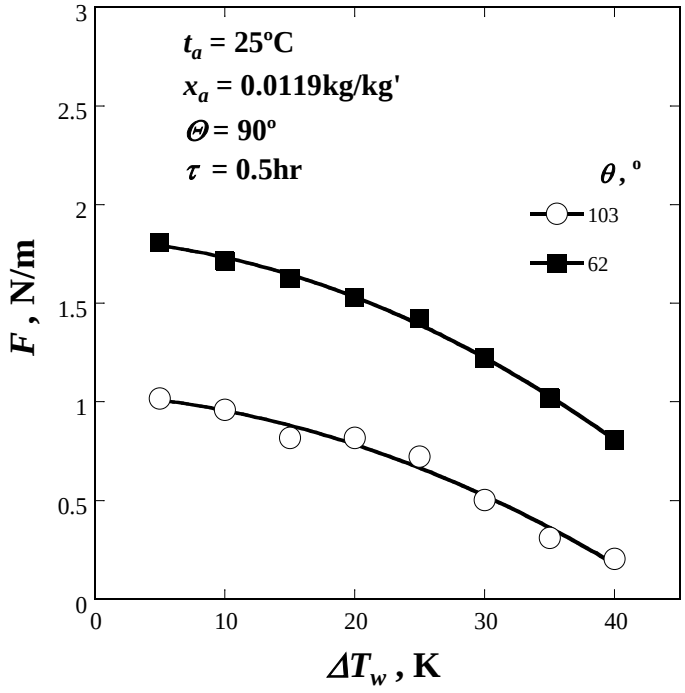

Figure 48: Relationship between *F* and ΔT_w at different wettabilities

3.3.4 Concluding remarks

Frost deposition phenomenon was investigated with the aim of reducing the frost deposition on a cooling surface by changing the cooling surface characteristics. Effects of the surface characteristics were investigated using the frost layer thickness, frost deposition, apparent frost layer density and force required to scrape frost.The following conclusions are drawn:

- The effect of the wettability of the cooling surface is such that there are no drastic differences in the frost layer thickness, frost deposition and apparent frost layer density due to the wettability change, but the force required to scrape off the frost shows a drastic change. The scraping force decreased with the cooling surface temperature and poor surface wettability.
- A jet stream was used to remove frost mechanically, and it was shown that the heat transfer improved on removal of frost from the cooling surface.

*This report is quoted from the IIR Proceedings Series 'Refrigeration Science and Technology', 2012/X: 1-8 (10th IIR Conference on PCMs and Slurries for Refrigeration and Air Conditioning, Kobe, Japan).

3.4 An Experiment on the Frosting of Laminar Humid Air Flow on a Flat Aluminum Plate

3.4.1 Introduction

When humid air contacts cold surfaces of heat exchanger used in heat pumps or air-conditioners, there might happen frosting on the surfaces, if the surface temperature is below the freezing temperature of water. Then the thermal performance of the heat exchanger becomes lower due to the thermal resistance of the frost layer as well as the decrease of airflow area. Relevant to the frost research, many studies have been reported. O'Neal and Tree (1985) reviewed some frost research and classified them into three categories: the frost properties, the frost growth process, and heat transfer measurement in simple geometries or in overall heat exchangers. They pointed out that there were no data available for flows in laminar regions for internal flow. Because the flow between the fins of heat exchanger is often laminar, these kinds of research are very important. For the frost properties such as frost thickness, density, and conductivity, many researchers (Sami and Duong 1989, Schneider 1978, Dietenberger 1983, Sahin 2000, Yun et al. 2002, Lee and Ro 2001) reported their experimental and/or theoretical results of frosting in very simple geometries. But, their results show quite discrepancy due to the complicated structure of frost. As to the frost growth process, Na and Webb (2004) recently suggested a super-saturation model for frost growth rate, and showed the prediction capability of the model was better than those of the previous models (Jones and Parker 1975, Sanders 1974) by comparing some experimental data available in open literature. Related to the heat transfer measurement in simple geometries or in overall heat exchangers, Senshu et al. (1990) experimentally investigated the performance of the test heat exchangers under frosting conditions, and based on the results an analytical method to predict frost formation speed was developed. Yang and Lee (2004) reported the frosting test of heat exchangers, and suggested correlations of frost properties on a cold plate. Most of the previous experimental work focused on frosting on the heat exchanger itself, or on simple geometry with constant temperature cooling conditions, usually using brine-type refrigerator.

According to the literature survey, the study on frosting of laminar airflow with locally being cooled down has been lacking, especially for air temperature to be near $0^{\circ}C$, which would be the standard test conditions for evaporator of heat pumps in winter season. Therefore, the objective of this study is to clarify the heat and mass transfer characteristics of laminar

airflow in a small duct having local cooling devices under the standard frosting test conditions.

3.4.2 Experimental apparatus

Figure 49 shows the experimental apparatus for the present frosting study. The humid air was controlled to be 2°C/1°C (dry and wet bulb air temperature: DB/WB) for frosting test by using a constant temperature and humidity chamber, and then the air was supplied to the inlet of the test section. The test section has 4mm x 100mm rectangular cross sectional passage. The cooling surface of aluminum was installed at the bottom side of the test section. Nine Peltier cooling modules (each has 4W maximum power) were used for the cooling of the aluminum plate. The dry and wet bulb air temperatures were measured by using 0.5mm O.D. K-type sheathed thermocouples at the inlet of the test section. For the outlet position, there might be severe temperature gradient of the airflow due to the cold aluminum plate at the bottom side. A mini-temperature sensor consisting of three 0.1 mm O.D. thermocouples was, therefore, manufactured to measure the temperature distribution of vertical direction at the outlet flow passage. For the measurement of humidity at the outlet, the dry and wet bulb temperatures were also measured.

For the temperature distribution of the aluminum plate, sixteen 0.1 mm O.D. K-type thermocouples were installed flush to the aluminum surface. For the airside pressure drop distribution, six differential pressure drops were measured by using a differential pressure manometer (0.002mmAq/5mmAq) and a rotary valve system. The overall mass of frost at each test run was measured with an electronic balance (1mg resolution). Also, a telescope system is used in order to determine the frost thickness at the specified positions. Figure 50 is the schematic of the frost thickness profile and the positions where the thickness was measured. The positions are shown in Table 5. Table 6 shows the test conditions of the present study.

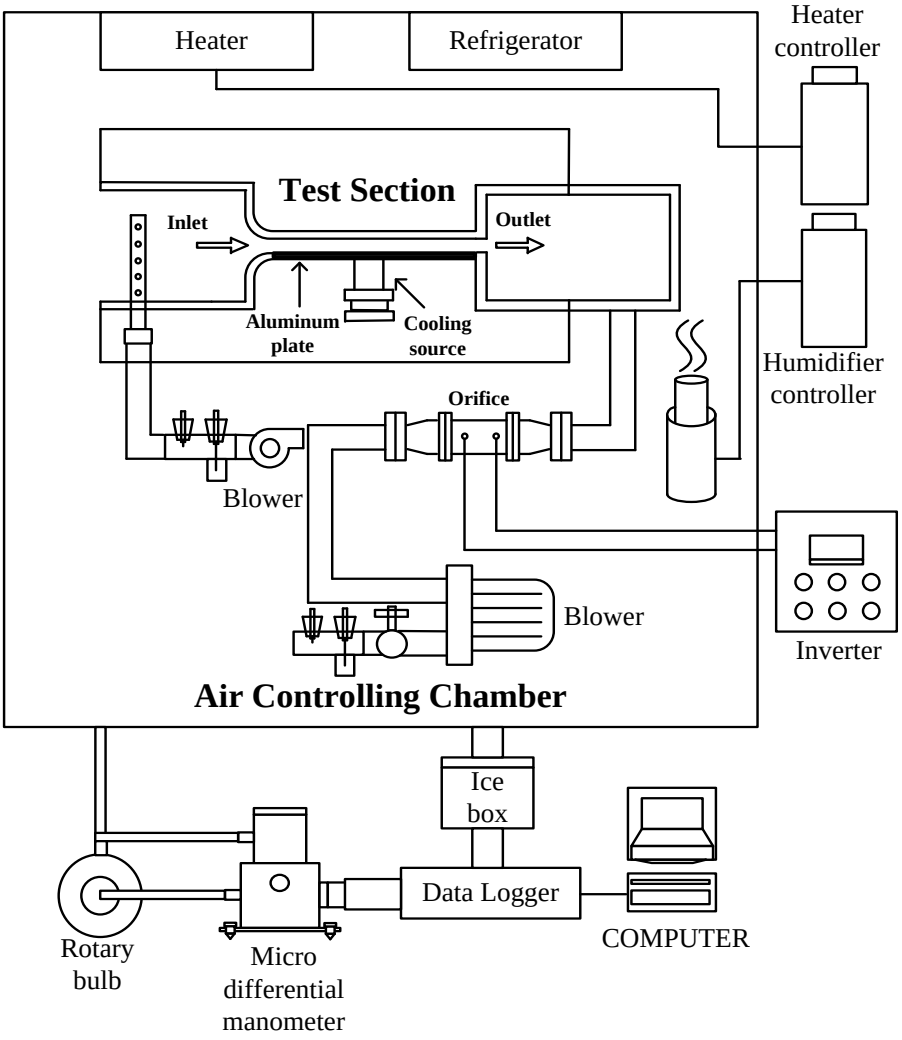

Figure 49: Schematic of experimental apparatus

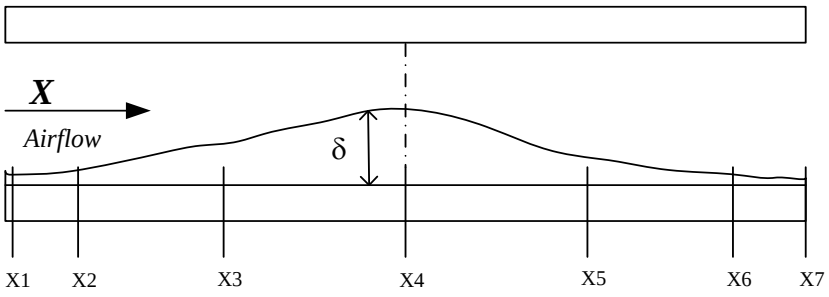

Figure 50: Schematic of typical frost thickness profile

Table 5: Positions where frost thickness measured

T_wall	1	2	3	4	5	6	7	8	9	10	11	12	13	14	15	16	17
X[mm]	1	8	15	22	29	36	43	46.5	55	60	67	74	81	88	95	102	109
P	1		2		3		4		5		6		7				
X[mm]	-38		5		12.5		25		45		65		142				
δF	1		2		3		4		5		6		7				
X[mm]	1		10		30		55		80		100		110				

Table 6: Test conditions

Test type	$T_{air,in}$[°C]	$V_{air,in}$[m/s]	T_{root}[°C]	Peltier device	Time [min]	Measured quantities
Frost test	2/1 (DB/WB)	1.5	-9	I=22.5A E=0.78V	30, 60, 120, 180	T, P, δ_{frost}, W_{frost}

3.4.3 Data reduction method

Figure 51 shows the schematic of the physical model for the analysis. The data reduction procedure is as follows:

(a) Calculate the x-directional heat flux $q_{w,x}$ in the fin plate from the fitting equation of wall temperature. The fitting equation was obtained from the measured wall temperature as a 3rd order polynomial function.

$$q_{w,x} = -k_w \frac{\partial T_w}{\partial x} \quad (1)$$

(b) Calculate the y-directional heat flux $q_{w,x}$ that flows from the air-side to fin-side.

$$q_{w,y} = -tk_w \frac{\partial^2 T_w}{\partial x^2} \quad (2)$$

(c) Develop the frost thickness δ correlation as a function of position x at each time step from the measured value of frost thickness. Then the local frosting mass flux can be express as

$$G_w = G_{w,avg} \frac{dV}{V} = \frac{L_z \delta dx}{L_z \int_0^{L_x} \delta dx} \quad (3)$$

under the assumption of uniform frost density and span-wise (z-directional) uniform frost distribution, where the $G_{w,avg}$ is the average mass flux obtained the measured value of frost weight W_F divided by the plate surface area and the time interval as follows:

$$G_{w,avg} = \frac{W_F\big|_{\tau+\Delta\tau} - W_F\big|_{\tau}}{A \cdot \Delta\tau} \quad (4)$$

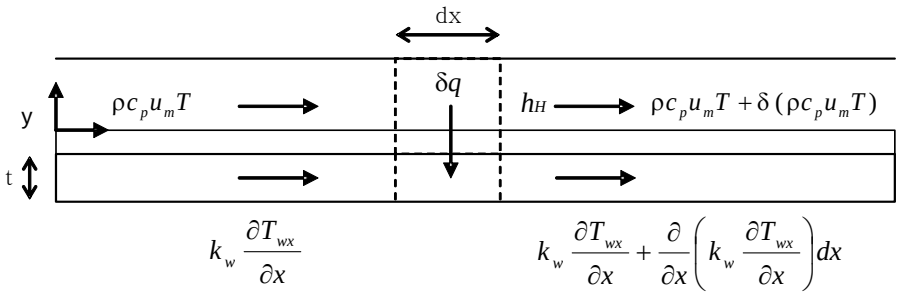

Figure 51: Physical model for the analysis

(d) For the convective heat transfer coefficient h_H , Kays' correlation for laminar developing flow was used as follows:

$$Nu = \frac{h_H d_h}{k} = 4.36 + \frac{0.036[(x/d_h)/Pe]^{-1}}{1 + 0.0011[(x/d_h)/Pe]^{-1}} \qquad (5)$$

where d_h is the hydraulic diameter and *Pe* is the Peclet number which is defined as: $Pe=Re \cdot Pr$

(e) The finite difference form of the air-side heat balance is expressed as

$$\frac{\dot{m}_a c_{pa} + \dot{m}_w c_{pw}}{L_z} \frac{T_{b2} - T_{b1}}{\Delta x} = (h_H - G_w c_{pw})(T_b - T_i) \qquad (6)$$

where T_i is the frost temperature (air-frost interfacial temperature) and T_b is the air bulk mean temperature as defined as

$$T_b = \frac{T_{b1} + T_{b2}}{2}$$

(f) Frost-side heat balance is as follows:

$$q_{w,y} = q_{sens} + q_{lat} \qquad (7a)$$

or

$$q_{w,y} = h_H (T_b - T_i) + L_{SG} G_w \qquad (7b)$$

where q_{sens} is the sensible heat flux and q_{lat} is the latent heat flux, which are defined as

$$q_{sens} = h_H (T_b - T_i) \qquad (7c)$$

and

$$q_{lat} = L_{SG} G_w \qquad (7d)$$

respectively.

(g) We have now two equations (equations (6) and (7b) with two unknowns T_{b2} and T_i. Guess T_i and determine the T_{b2} so that both values satisfy the two equations above. Once T_{b2} and T_i obtained at the first section, move to the next section until the final section arrives.

3.4.4 Experimental results

Figure 52 represents the temperature distributions of aluminum plate under the present frosting conditions, i.e., the inlet air temperature is 2°C/1°C (DB/WB) and inlet air velocity is 1.5m/s during the three hour test. The root temperature, which is measured at the center region in the x-direction, i.e., the airflow direction, was controlled to be nearly -9°C. The corresponding y-directional heat flux is shown in Figure 53. It was clearly confirmed that the characteristics in the upstream region differs very much from that in the downstream area. It is noted that, on average, the y-directional heat flux in the upstream is almost twice that in the downstream area.

Figure 54 and Table 7 represent the frost thickness profiles and the frost weight measured at various time steps. The central region, where the cooling sources were located, had the highest frost thickness as expected. It is, also, confirmed that the leading edge had the higher values than those of the right following region.

Figure 55 shows the local distribution of air, frost and wall temperatures at the time of 30 minutes. From the measured values of wall temperature and inlet air temperature, the local air bulk temperature and frost temperature (air-frost interface temperature) were calculated by the data reduction method prescribed in Section 3. It is found that the frost temperature profile shows very interesting features. The frost temperature decrease in the flow direction until the air meets the central region (x=55mm) where the cooling source exists.

After the cooling source region, the frost temperature increase dramatically right after the central region and then soon decrease gradually mainly due to the prominent change of wall temperature and wall heat flux near central region. The central region distinguishes the upper stream characteristics from the downstream ones.

Figure 56 shows the local heat flux distribution corresponding to the temperature profile at the time of 30 minutes. The total heat flux was decomposed as sensible and latent heat fluxes. Latent heat flux was shown very similar to the corresponding frost thickness profile. It is natural that the latent heat flux was calculated from the measured values of frost thickness and frost weight based on the assumption of quasi-steady transfer process. The sensible heat flux distribution shows quite interesting characteristics: there is a dramatic decrease of sensible heat flux across the central region and after that gradual increase occurs. The sensible heat flux is larger than 3 times latent heat flux at the very upper stream region, but approaching into the central region the latent heat flux grows nearly 75% of the values of sensible heat flux. Downstream region shows quite different characteristics: even though the average value of sensible heat flux is almost the same value to that of latent heat flux, the trend is opposite. The sensible heat flux is gradually increasing while the latent heat flux is decreasing.

The local sensible and latent heat flux at the time of 30, 60, 120 and 180 minutes were integrated at each test time to investigate the heat flux characteristics with respect to time as shown in Figure 57.

Figure 58 shows the pressure drop characteristics of humid air in frosting test. According to the result, the pressure drop increases during frost test, and it can have 20-30% higher values that those of dry test.

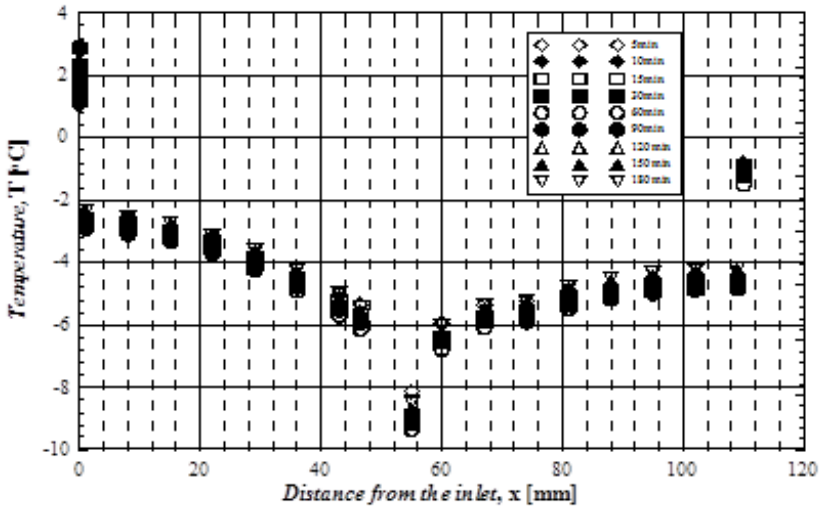

Figure 52: Temperature distributions in x-direction

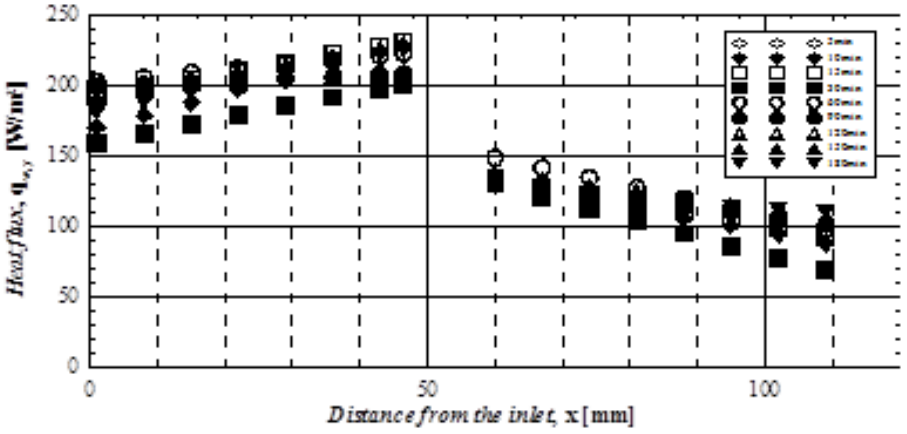

Figure 53: Heat flux distributions in y-direction

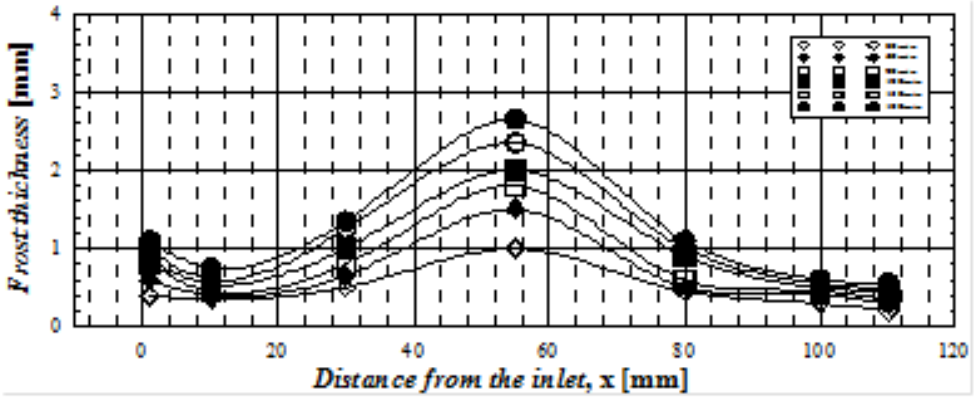

Figure 54: Frost thickness distribution

Table 7: Frost thickness and weight data at the specified positions

Time	Position x[mm]							Weight
[min]	1	10	30	55	80	100	110	[g]
30	0.40	0.35	0.50	1.00	0.45	0.30	0.20	0.42
60	0.60	0.40	0.65	1.50	0.50	0.40	0.30	0.66
120	0.85	0.55	1.00	2.00	0.90	0.50	0.45	1.223
180	1.10	0.75	1.35	2.65	1.10	0.60	0.55	1.707

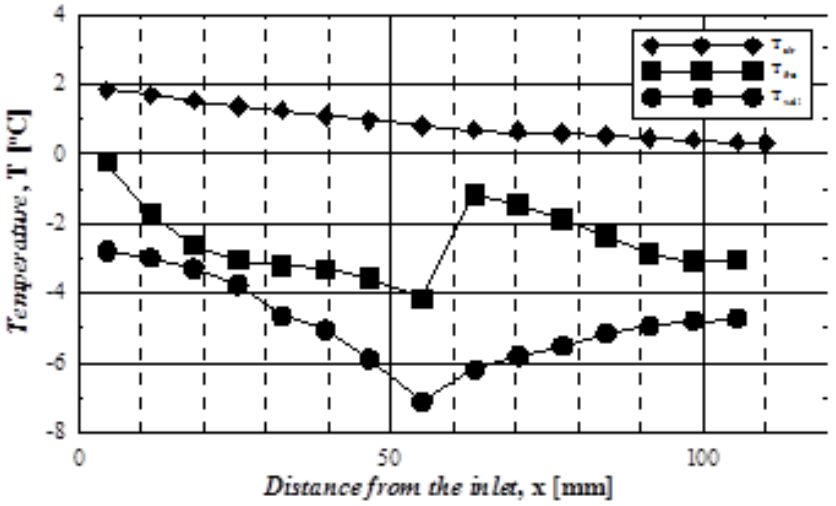

Figure 55: Local temperature distributions at time of 30 minutes

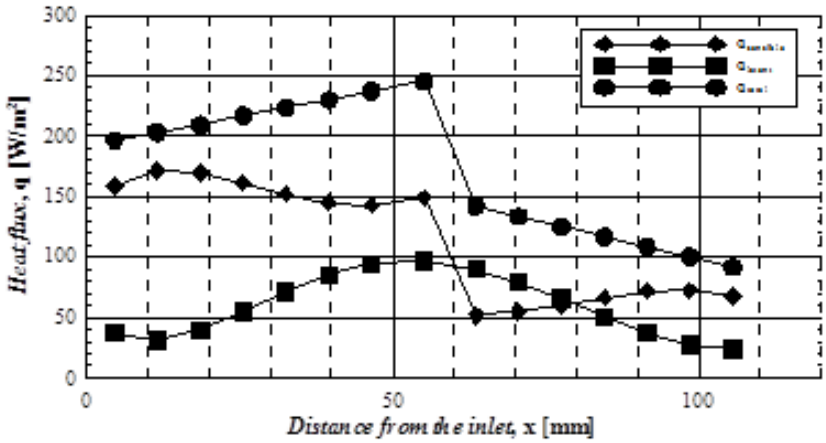

Figure 56: Local heat flux distributions at time of 30 minutes

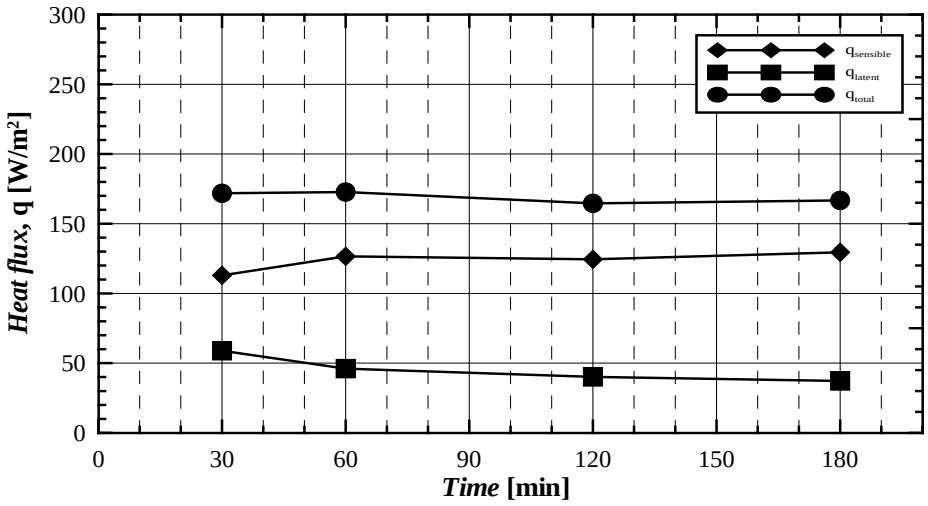

Figure 57: Average values of sensible, latent and total heat fluxes at standard frosting test conditions

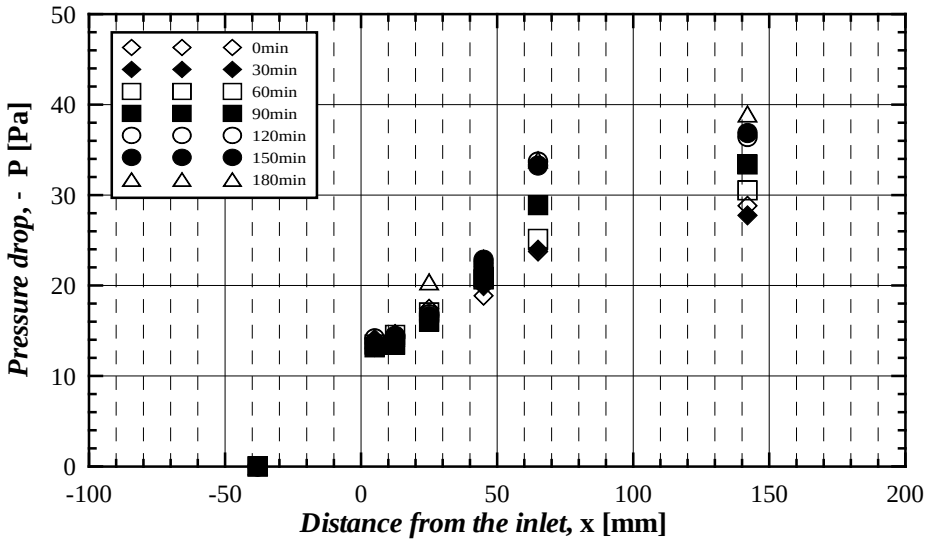

Figure 58: Pressure drop characteristics of humid air in frosting conditions

3.4.5 Conclusions

The heat and mass transfer characteristics of the humid airflow in frosting conditions have been experimentally investigated. From the present study, the followings are drawn:

1) On average, y-directional heat flux of upstream region was about 2 times higher than that of downstream area.
2) The latent heat flux distribution was very similar to the frost thickness profile.
3) The sensible heat flux distribution dramatically changed across the central region where the cooling source exists.
4) The frost thickness shows the mountain shape having its peak at the central region.
5) For the frost thickness distribution, the leading edge effect was confirmed.

6) Even though the total heat flux was invariant during the test, the sensible and latent heat flux ratio changed a lot.
7) The frosting caused higher value of air-side pressure drop than the non-frosting case by about 20-30%.

3.4.6 Main nomenclature

c_p : isobaric specific heat capacity, $kJ \cdot kg^{-1} \cdot K^{-1}$
h_H : heat transfer coefficient, $W \cdot m^{-2} K^{-1}$
h : specific enthalpy, $kJ \cdot kg^{-1}$
k : thermal conductivity, $W \cdot m^{-1} K^{-1}$
L : length, m
p : pressure, Pa
q : heat flux, $W \cdot m^{-2}$
T : temperature, K
u : local flow velocity, $m \cdot s^{-1}$

4 SUMMARY

This report is intended to summarize the activities performed by the IEA annex 41 Japanese team in 2012. This team has been collected from the national organization of the professional heat pump technology research. They are experts in the compressor, heat exchanger, refrigerant, natural refrigerant, two-phase flow and frost/defrost phenomena.

4.1 Background

The annual energy consumption per household in the cold climate area (Hokkaido in Japan) is about 1.7 times as high as compared to that in mild temperature area (for example, Tokyo). As shown in Figure 59, heating and hot water supply accounts for about 80%. Due to the energy conservation, it is necessary to spread heat pump equipment. Therefore, heat pump for cold climate area was developed relatively early and has already been marketed in Japan. Considered from many experiences, Japan team can collaborate with IEA Annex 41 suggested project.

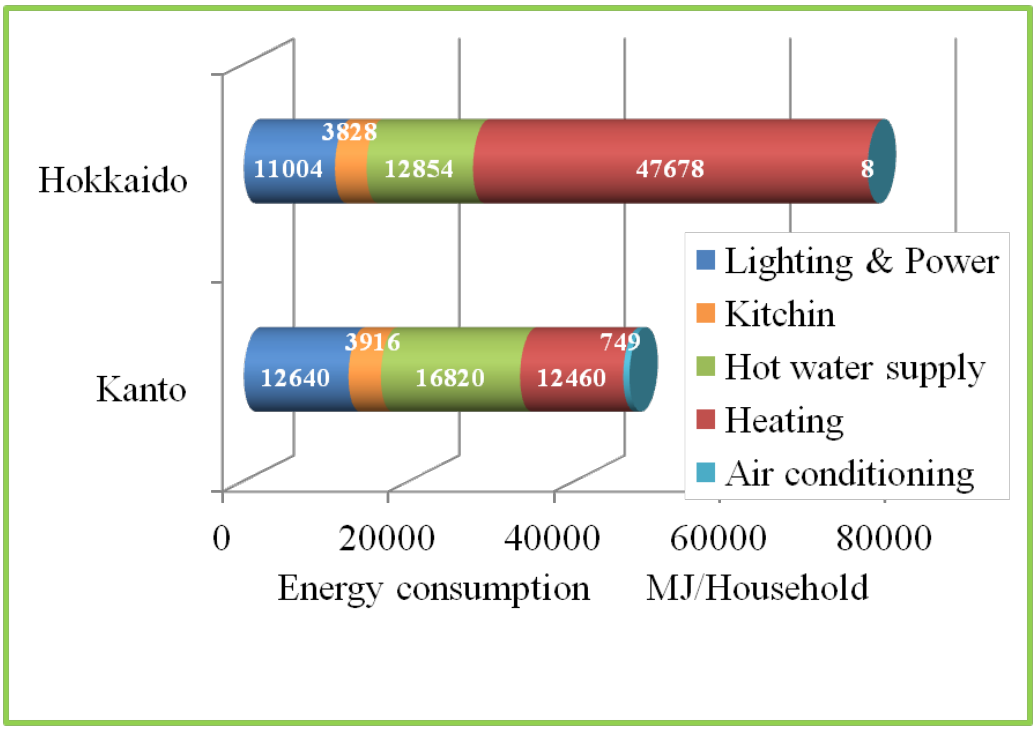

Figure 59: Annual energy consumption per household in the cold climate area

4.2 Progress

We had four meetings, including the Executive Committee meeting as follows;

- On June 20 - Executive Committee meeting
  - Participants: Prof. Koyama, Fukuda, Kagawa, Dr. Hashimoto, Mr. Matsubayashi, Mr. Hikawa and Prof. Katsuta
  - At first, the introduction and the proposal of the IEA Annex from the secretariat were made. Towards the kick-off meeting to be held in San Antonio, and arranged with contents of Japanese efforts and plans. Japanese decision to participate in the task was based on the legal text, the determination complete contents of the spreadsheet have been made. We have chosen the Japan team members from industries as well.
- On August 30, 2012 - First Committee meeting
- First round of meeting was held in response to the kick-off meeting in San Antonio. The meeting was participated by heat pump manufacturers and electric power companies. Since the international conference was held in the summer period, notable presentations from system side and from the compressor side has been reported on the international conference held at Purdue University by Prof. Koyama and Prof. Fukuda.
- At the same time, the committee had hearing from the electric power company side and the manufacturer on the status and development of heat pump for cold climate area. We also discussed on the presentation contents of Japan team for forthcoming Chillventa meeting.
- On October 3, 2012 - Second Committee meeting
  - Impressive presentations special focus on refrigerant from the Asian international conference held in Xi'an, China (ACRA) reported by Prof. Kagawa.
  - Prof. Fukuda gave us an introduction of the contents of the state- of- art and future prospects of the compressor technology. Special lecture on the reduction of frost and mechanical defrosting was made by Prof. Ohkubo.

  - Prof. Saitoh reported the contents of the IEA Annex 41 second meeting held in Chillventa, Germany.
- On January 8, 2013 - Third Committee meeting
- We had two special lectures in this meeting. One was entitled “Development of CO_2 heat pump and technologies for cold climate area (ejector cycle)” from Denso (Mr.Taira) and the other was “ Evaluation of refrigerant stability by using highly dispersed specimens” by Dr. Suzuki.
- Discussion items were as follows: Country reports, Research plan for next year (task 2).

5 REFERENCES

Asai, T. et al.: Proc. of 35th Joint Conf. on Air-conditioning and Refrigeration, (2001)69-72

Asano, H. et al., Experimental Thermal and Fluid Science, 28, pp.223-230 (2004).

Asano, H. et al., Nuclear Instruments and Methods in Physics Research-A,542, pp.154-160 (2005).

Asano, H. et al., Proc. 5th Int. Conf. on Multiphase Flow on CD-Rom, Paper No.172 (2004).

Asano, H., N. Takenaka, T. Fujii, H. Hayashi, T. Wakabayashi, "Visualization and Void Fraction Measurement of Gas-Liquid Two-Phase Flow in a Commercial Plate Heat Exchanger by Thermal Neutron Radiography", IEEE Trans. Nuclear Science, 52-1, pp.280-284 (2005).

Astina, I.M., Sato, H., 2004, “A Rational Helmholtz Fundamental Equation of State for Difluoromethane with an Intermolecular Potential Background,” Int. J. Thermophys., Vol. 24, pp. 963-990.

Baba, T. et al., Nuclear Instruments and Methods in Physics Research-A, 605, 1-2, pp. 142-145, (2009).

Baba, T., S. Harada, H. Asano, K. Sugimoto, N. Takenaka, K. Mochiki, "Nondestructive Inspection for Boiling Flow in Plate Heat Exchanger by Neutron Radiography", Nuclear Instruments and Methods in Physics Research-A, 605, pp.142-145 (2009).

Dietenberger, M.A.: *Int. J. Heat Mass Transfer*, **26**(4), (1983).

Fukiba, K., Inoue, S., Sato, H., Ohkubo, H. (2009).Journal of Thermophysics and Heat Transfer Volume 23, Number 3, Jul.-Sep. 2009.pp. 533-542.

Hotta, Y., et al., 2012, Development of R744 Two Stage Compressor for Commercial Heat Pump Water Heater, Proc. Of international compressor engineering conference at Purdue, Perdue University, 1162.

Hozumi, T., Sato, H., Watanabe, K., 1994, “Speed of Sound in Gaseous Difluoromethane, J. Chem. Eng. Data,” 39, pp. 493-495.

Jiang, L., H. Asano, N. Takenaka, K. Sugimoto, "Heat Transfer Characteristics of Boiling Two-Phase Flow in a Plate Heat Exchanger", Proc. of Int. Conf. on Power Engineering (ICOPE-07), pp.455-461 (2007).

Jiang, L. et al., Proc. of Int. Conf. on Power Engineering (ICOPE-07), pp.455- 461 (2007).

Jones, B.W. and J.D. Parker: *J. Heat Transfer*, **97**, (1975).

Kagawa, N., Matsuguchi, A., Watanabe, K., 2009, “Measurement of Isobaric Heat Capacity for R 134a and Carbon Dioxide by Using a Flow Calorimeter,” Trans. JSME, Vol. 75 B, pp. 1491-1496 (in Japanese).

Kagawa, N., Matsuguchi, A., Watanabe, K., 2012a, “Measurements of Isobaric Heat Capacity of R32”, Int. J. Refrig., Vol. 35, pp. 1014–1020.

Kagawa N, Matsuguchi A, Yamaya K, Watanabe K. Behavior of isobaric heat capacity of r 32 in the gas phase, 2012b, Proc. the 6th Asian Conference on Refrigeration and Air Conditioning Paper No.2954 (Xi’an, 8/27/2012).

Kawai, N., Kubo, T. Tani, T. “The High Heating Capacity Packaged Air-conditioners Carrying the Heat Exchanger Suitable for the Cold District” Journal of Refrigeration, Vol. 82, No. 952, pp. 23–27.

Kobayahsi, H., et al., 2012, Commercial use CO_2 Heat Pump Water Heater with Scrotary compressor, MITSUBISHI HEAVY INDUDTRIES, LTD,. The International Symposium on New Refrigerants and Environmental Technology 2012, P.53.

Kubota, H., Sotani T., Kunimoto Y., 1995, “Isobaric Specific Heat Capacity of Difluoromethane at Pressure up to 0.5MPa”, Fluid Phase Equilibria, Vol. 104, 413-419.

Lee, Y.B. and S.T. Ro: *Int. J. Refrigeration*, **24**, (2001).

Mukoyama, K., Sato, H., Watanabe, K., 1998, “Measurements of Gaseous Isobaric Specific Heat Capacity of R-134a and R-143a”, Proc. Int. Conf. High Press. Sci. Tech., M. Nakaiwa, ed., pp. 158-164.

Na, B. and R.L. Webb: *Int. J. Heat Mass Transfer*, **47**, (2004).

Nakamura, K., 2006. “High Heating Capacity Packaged Air Conditioners with Liquid Injection Cycle”, *REFRIGERATION,* Vol.82, pp.124—128

Ohkubo, H. (2010).Proceedings of Thermal Engineering Conference ’10, 7-8.

Ohkubo, H., et al. (2004).Proceedings of the 1st International Forum on Heat Transfer,97-98.
Ohkubo, H. et al. (2009).Proceedings of Thermal Engineering Conference ’09, 59-60.

O’Neal. D.L., F.G. and D.R. Tree: *ASHRAE Trans.*, **91**(2), (1985).

Outcalt, S.L., McLinden, M.O., 1995, “Equations of State for the Thermodynamic Properties of R32 (Difluoromethane) and R125 (Pentafluoroethane),” Int. J. Thermophys., Vol. 16, 79-89.

Piao, C.-C., Noguchi, M., 2001. “Thermodynamic Properties of HFC-32 (Difluoromethane),” Int. J. Refrig., Vol. 24, pp. 519-530.

Sahin, A Z.: *Int. J. Heat Mass Transfer*, **43**, (2000).

Sami, S.M. and T. Duong: *ASHRAE Trans.*, **95**(1), (1989).

Sanders, C.T.: *"The Influence of Frost Formation and Defrosting on the Performance of Air Coolers,"* 2Ph.D. Thesis, Delft Technical University, (1974).

Schneider, H.W.: *Int. J. Heat Mass Transfer*, **21**, (1978).

Senshu, T., H. Yasuda, K. Oguni and K. Ishibane: *ASHRAE Trans.* **96**(1), (1990).

Takenaka, N. and H. Asano, Experimental Thermal and Fluid Science, 29, pp.393-402 (2005).

Tillner-Roth, R., Yokozoki, M., 1997, "An International Standard Equation of State for Difluoromethane (R-32) for Temperatures from the Triple Point at 136.34 K to 435 K and Pressures up to 70 MPa," J. Phys. Chem. Ref. Data, Vol. 25, pp. 1273-1328.

Yamamura S. and Zhong M., Development of the High efficiency Heat Pump-Two-stage Compression System for the Cold Area, Cryogenics and Refrigeration - Proceedings of ICCR 2008 (2008).

Yang, D.K. and K.S. Lee: *Int. J. Refrigeration*, **27**, (2004).

Yun, R. et al. : *Int. J. Refrigeration*, **25**(4), (2002).

Japan Team Report

IEA HPT TCP Annex 41
"Cold Climate Heat Pumps"

Task 2 – Initial Work

Submitted by:

Waseda University, Tokyo, Japan

Lead: Prof. Masafumi Katsuta, Waseda University (contact: katsuta@waseda.jp)

Contributors:

Annex 41 Japanese Company and Research Institute Members

- CRIEPI
- NEDO
- Mitsubishi Electric
- Toshiba Carrier Corporation
- Daikin
- Kansai Electric Power Co. Inc.
- Chubu Electric Power Co. Inc.
- Hitachi Appliance, Inc.
- Mitsubishi Heavy Industries

Observers

- Hokkaido Electric Power Co. Inc.
- Tohoku Electric Power Co. Inc.

November 2016

TABLE OF CONTENTS

LIST OF TABLES

LIST OF FIGURES

1 FROST FORMATION BETWEEN CONCAVE- AND CONVEX-PATTERNED FLAT PLATES UNDER FORCED CONVECTION: DEVELOPMENT OF ANALYTICAL AND PREDICTIVE TECHNIQUES FOR FROST LAYER GROWTH

1.1 Purpose of This Study

This study is intended to observe closely and measure frost formation under forced convection, which hampers performance improvement of heat pumps in cold climates. Based on the analysis of frost layer growth, this study develops a technique to predict frost formation.

The following are the background of this study and NEDO's future prospects for heat exchangers.

In this study, we investigated basic characteristic of frost formation of the flow path between flat plate with concavity and convexity under forced convection. Test section is a flow path that is placed opposite to a flat plate having a periodic concavity and convexity groove on the surface. Experiment was conducted using structure of concavity and convexity as a parameter. By visualizing the frost formation, the relationship of time to passage blockage and structure of concavity and convexity became clear. And it is possible to optimize of concavity and convexity.

1.2 Future Prospects for Heat Exchangers Used for Automotive Air Conditioners and How This Study is Positioned in the Prospects

With the increasing development of hybrid electric vehicles (HEVs) and electric vehicles (EVs), air conditioners are expected to be improved to higher performance levels. It is particularly important to reduce their impact on driving range and to secure heat source for cabin space heating. From the standpoint of electricity consumption, cabin space heating by a heat pump system is thought to be most effective. However, when such a heat pump system is operated in cold climates, frost formation in the outdoor heat exchanger is expected to cause various problems, such as a decrease in heat-transfer coefficient and an increase in pressure drop.

For multi-pass heat exchangers with corrugated louvered fins, which are today’s mainstream automotive heat exchangers, fins and tubes are more closely packed to improve their heat-exchange performance. As a result, the structure tends to increase the amount of trapped condensed water between the fins, which raises concerns that it may deteriorate defrosting performance. Proposed as countermeasures to solve this problem are finless heat exchangers, which suppress the amount of trapped condensed water.

This study is intended to demonstrate the advantages of finless heat exchangers over existing heat exchangers in terms of resistance to frost formation and defrosting performance, by analyzing the mechanism of frost formation in finless heat exchangers.

1.3 Experimental Procedure

The test equipment consists of a temperature-controlled air supply unit, blower, volume flow meter, test section, and ducts that connect these main units. In the temperature-controlled air supply unit, air temperature and humidity are adjusted to certain levels. The air is fed by the blower to the cooled test section, where frost forms between two flat plates. The air that has passed the test section returns to the temperature-controlled air supply unit for recirculation. The condition of air before and after the test section and the heat flux into the test section are measured. At the same time, frost layer heights are measured by means of image processing. From digital microscope images, the diameters and intervals of frost pillars are measured, and the frost transition time is also specified.

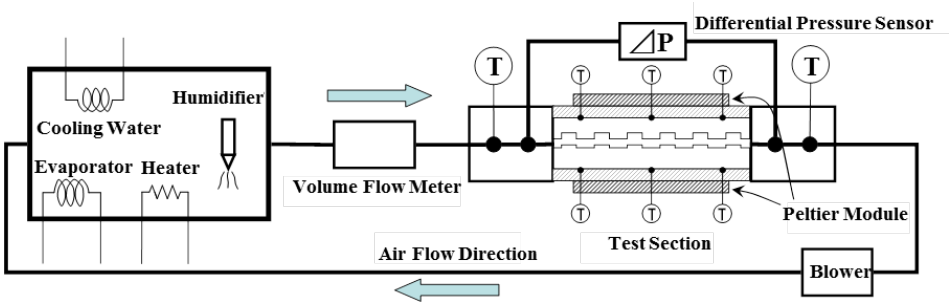

Figure 1: Schematic view of test equipment

Table 1: Test conditio

Inlet air temperature T_a	°C	7.0
Inlet absolute humidity X_a	kg/kg'	0.0053
Cooling surface temperature T_w	°C	–10.0
Initial flow rate	m³/h	5.0

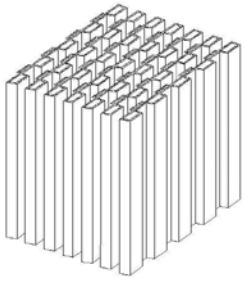

Figure 2: Overall view of heat exchanger

A finless heat exchanger that has the shape as shown in Figure 2 was designed. This study uses an aluminum test section that duplicates one of the air-side flow paths in the heat exchanger. Table 2 represents the design parameters of the test section.

Table 2: Design parameters

		No.1	No.2	No.3
(1) Height of convex a_l	mm	2.0	1.2	2.8
(2) Depth of concave a_u	mm	2.8		
(3) Width of concave/convex l	mm	8.0		
(4) Pitch of convex/concave L	mm	16.0		
(5) Angle of convex/concave α	deg.	10		
(6) Number of convex/concave	N	6		

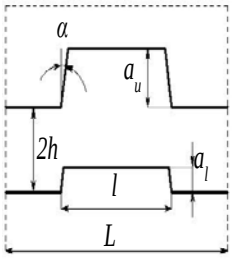

Figure 3: Test section details

1.4 Experimental Results

Measurement of frost layer growth

The image along the whole test section flow path was taken with a camera from above. After the image was processed and photo image distortion was corrected, the area of the frost layer was measured. The interface between the frost layer and the aluminum plate, and the interface between the frost layer and the air layer, were identified. Then the area surrounded by the interfaces was obtained as the area of the frost layer.

The volume of the frost layer was obtained from the area of the frost layer measured on the image. The mean frost layer density was calculated by dividing the amount of frost formation by the area of the frost layer. Similarly, the mean frost layer height was calculated by dividing the area of the frost layer by the length of frost formation (wet length). Figure 4 and Figure 5 show the calculation results of mean frost layer densities and mean frost layer heights, respectively.

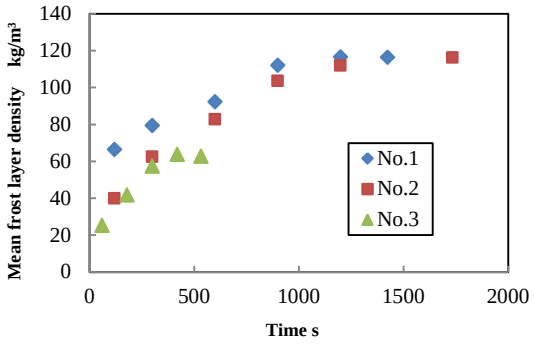

Figure 4: Mean frost layer densities

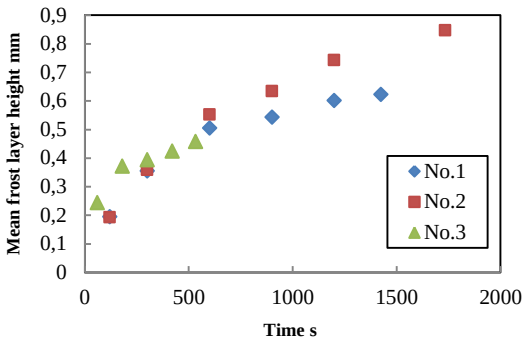

Figure 5: Mean frost layer heights

The higher the mean frost layer density in the early part of the test results , the smaller the overall change in frost layer density. The difference in flow path shape did not have a significant effect on mean frost layer heights.

Observation of frost layer growth

Images of frost layer growth were captured with a digital microscope in the flow path of the test section, with an acrylic plate on one side. A heater film was included with the transparent acrylic plate to prevent formation of frost that would inhibit visualization of the test surface. The maximum resolution capability of this observation system depends on the magnification of microscope. We looked for the optimum observation condition for the tests we ran and at this condition the maximum resolution is 0.02mm (20μm). Figure 6 shows details of the microscope and the test section set up. A high-speed camera was included to capture detailed video recordings of ice crystal growth.

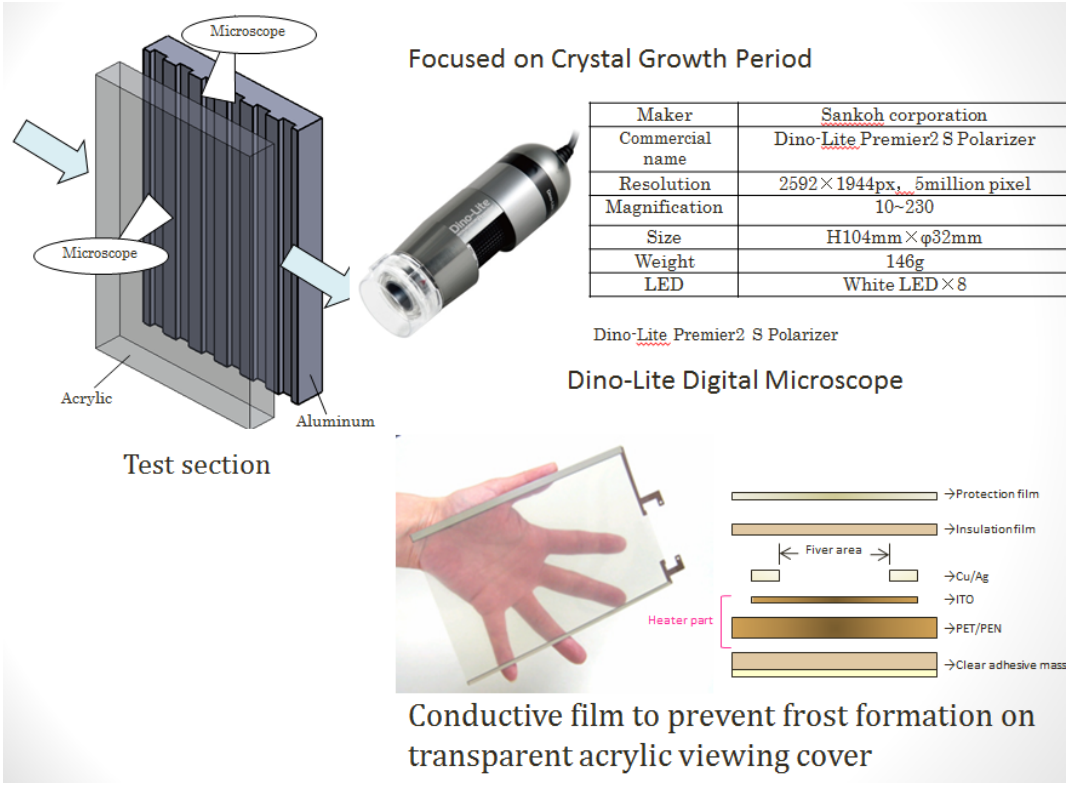

Figure 6: Frost crystal growth visualization set up

From the photo images, initial frost pillar diameters, frost pillar intervals, and the time of frost pillar formation in the crystal growth stage were measured. The taller the convex height became, the higher the initial air velocity (the Reynolds number) became at the point where the flow path was narrow. As a result, initial frost pillar diameters and frost pillar intervals became smaller, indicating that the difference in initial air velocity (the Reynolds number) had an influence on the mode of frost pillar formation. The photo images captured the scene of the crystal growth stage, in which needle crystals formed from droplets of ice as nuclei, grew in the direction perpendicular to the cooling surface, and formed frost pillars. The photo images also captured the scene of the frost layer growth stage, in which lateral branches formed from the sides of a frost pillar and grew three-dimensionally. In flow paths No. 1 and No. 2, frost pillars were seen growing against the direction of air flow.

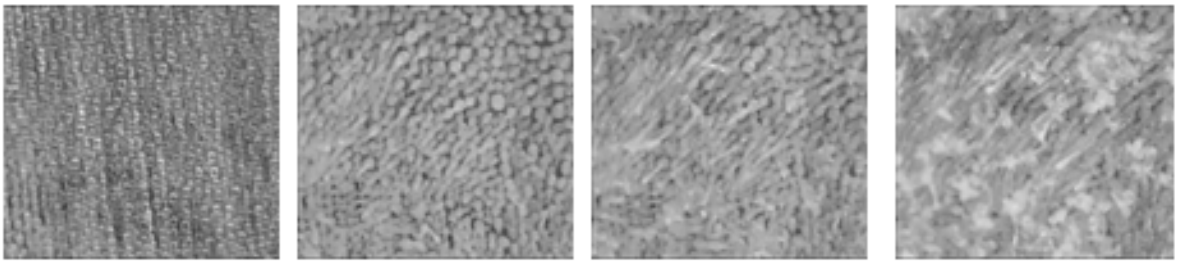

(a) 2min (b) 4min (c) 5min (d) 7min

Figure 7: Process of frost layer growth (No. 2)

Table 3: Data of ice pillars

	Initial air velocity m/s	Initial ice pillar diameter mm	Ice pillar intervals mm	Time of ice pillar formation s
No. 1	4.34	0.023	0.075	80
No. 2	3.10	0.024	0.076	160
No. 3	7.23	0.016	0.056	35

1.5 Analysis of Frost Layer Growth

The analysis of frost layer growth was conducted based on the calculation model suited for each frost layer growth process. Frost layer growth process is classified into three stages: "crystal growth stage," "frost layer growth stage," and "frost layer full growth stage." Because this test was not designed to analyze frost pillars melting on the frost layer surface, the analysis of the frost layer growth process was conducted based on the crystal growth stage and the frost layer growth stage. To the analysis of the crystal growth stage, the model developed by Yamashita (2009) was applied. This model is fundamentally based on the model developed by Tao, et al. (1994), which simulates frost pillars growing one-dimensionally, but multiplied by a coefficient.

$$\frac{\partial L_f}{\partial t} = C_1 \times \frac{h_D}{\rho_I} \times \left(X_a - X_{fs}\right) \tag{1.1}$$

$$\frac{\partial d}{\partial t} = C_2 \times 2 \times \frac{h_D}{\rho_I} \times \left(X_f - X_I\right) \tag{1.2}$$

$$\rho_f = \frac{\int_0^{L_f} \left[\frac{\pi}{4} d^2 \rho_I + \left(l^2 - \frac{\pi}{4} d^2\right) \times \rho_a\right] \times dz}{l^2 \times L_f} \tag{1.3}$$

L_f: frost layer height *m*, ρ: density *kg/m*^{3}
d: ice pillar diameter *m*
l: ice pillar intervals *m*
h_D: mass transfer coefficient *kg/m*^{2} *sΔX*
X: absolute humidity *kg/kg'*
C_1*C_2: coefficient

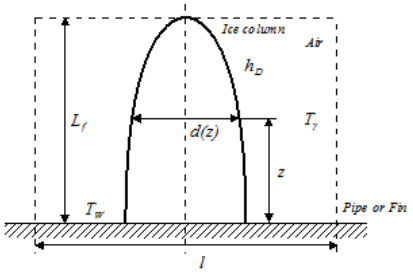

Figure 8: Calculation model by Tao, et al.

In the frost layer growth stage, water vapor is divided into two components: one component contributes to increasing frost layer density, and the other component contributes to increasing frost layer height. The analysis model used for the component that increases frost layer density is based on the assumption that frost layers are porous, and that water vapor diffuses along its concentration gradient in the air path between ice particles according to Fick's law of diffusion.

$$\dot{m} = \dot{m}_d + \dot{m}_h = h_D \times (X_a - X_{fs}) \tag{1.4}$$

$$\dot{m}_d = D_{eff} \times \frac{d\rho_v}{dz} = D_{eff} \times \frac{M_v}{RT_f} \times \frac{dP_v}{dz} \tag{1.5}$$

$$D_{eff} = \mu \times D_v = \frac{\varepsilon}{\tau} \times D_v \ , \ \varepsilon = \frac{\rho_i - \rho_f}{\rho_i - \rho_a} \tag{1.6}$$

$$\frac{\partial \rho_f}{\partial t} \times \left(L_f \times A_w\right) = \dot{m}_d \times A_w \tag{1.7}$$

$\dot{m}$: mass flux *kg/m²s*, $\dot{m}_d$: mass flux that increases frost layer density *kg/m²s*, D_{eff} : effective diffusion coefficient *m²/s*, $\dot{m}_h$: mass flux that increases frost layer height *kg/m²s*, *Aw*: cooling surface area *m²*
μ: diffusion resistance coefficient, *ε*: porosity, *τ*: tortuosity, D_v: diffusion coefficient *m²/s*

Based on the comparison with its experimental data, the tortuosity used in this study was calculated from the equation by Le Gall, et al. (1997), one of the previously proposed correlaions.

$$\tau = \frac{\varepsilon}{\frac{\varepsilon}{1 - 0.58 \times (1 - \varepsilon)} + F \times 10 \times (1 - \varepsilon) \times \varepsilon^{10}} \tag{1.8}$$

Between the concave- and convex-patterned flat plates, the transition from water vapor to frost pillars occurs first in the upstream area and gradually moves toward the downstream area. Taking this phenomenon into consideration, the time between the start of the transition in the upstream area and the end of the transition in the downstream area is set as a theoretical transition period. Based on frost growth observation results, a transition period is practically defined as the time between the point when the mean frost layer height becomes about 0.10 mm and 80% of the time when the flow path becomes completely blocked. The point of the transition is calculated to shift linearly from the start to the end of the transition period. Figure 9 shows the comparison results of calculated and measured mean frost layer densities. Likewise, Figure 10 shows the comparison results of calculated and measured mean frost layer heights. Table 4 represents the calculation parameters used for each of the flow paths tested.

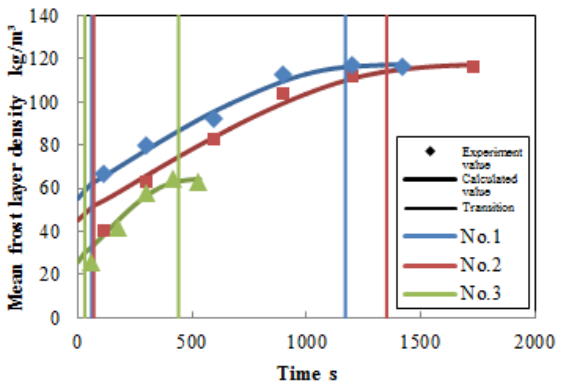

Figure 9: Comparison of mean frost layer density

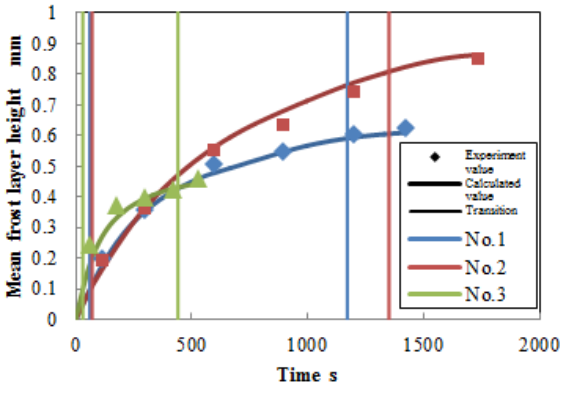

Figure 10: Comparison of mean frost layer height

Table 4: Calculation parameters

No.	Transition period		Frost pillar formation stage			Frost layer growth stage
	Transition start time	Transition end time	Initial ice pillar diameter	Ice pillar intervals	Mass transfer coefficient	Tortuosity
No. 1	60s	1170s	0.020mm	0.073mm	52g/m^{2}sΔX	Equation by La Gall, et al. (F=1)
No. 2	70s	1350s	0.021mm	0.085mm	36g/m^{2}sΔX	Equation by La Gall, et al. (F=1)
No. 3	30s	440s	0.012mm	0.065mm	65g/m^{2}sΔX	Equation by La Gall, et al. (F=1)

Figure 11 shows the deviations of calculated mean frost layer density from their experiment values. In a similar fashion, Figure 12 shows the deviation of calculated mean frost layer height from their experiment values. Table 5 lists mean error ratios for each of the flow paths tested.

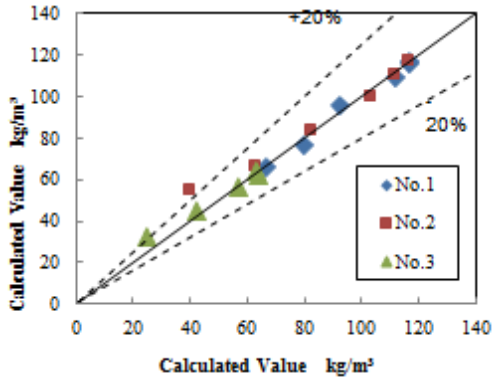

Figure 11: Mean frost layer density deviation

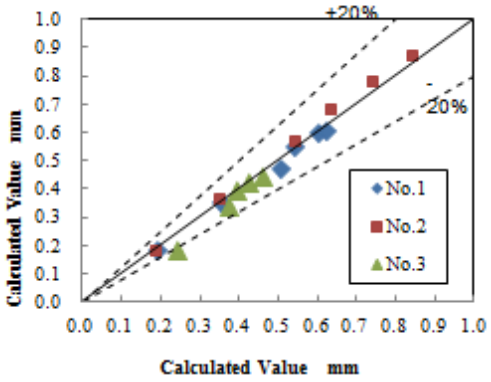

Figure 12: Mean frost layer height deviation

Table 5: Mean error ratios

	No. 1	**No. 2**	**No. 3**
Mean frost layer density	1.61%	6.69%	7.48%
Mean frost layer height	2.33%	4.86%	10.1%

For each of all flow paths tested, the differences between calculated and measured initial ice pillar diameters were less than 0.01 mm. The same applied to ice pillar intervals. Similarly, the differences between calculated and measured mean frost layer density were not more than about 10%. The same applied to mean frost layer height.

1.6 Prediction of Frost Layer Growth

The prediction of frost layer growth was conducted using flow path No. 1, which showed the smallest differences between calculation and measurement values in the analysis of frost layer growth. Predictive calculation is made using input parameters such as air temperatures, air humidity, cooling surface areas, and volumetric air flow rate. Table 6 lists

the values used as input parameters.

Table 6: Input parameters

Air temperature	ºC	6, 7, 8
Absolute air humidity	kg/kg'	0.0051, 0.0053, 0.0055
Cooling surface temperature	ºC	-9, -10, -11
volumetric air flow rate	m³/h	5

As with the analysis of frost layer growth, the model used to predict frost layer growth analyzes the process based on the transition in the crystal growth stage and the frost layer growth stage. The calculation parameters used in this predictive calculation, such as initial ice pillar diameters and ice pillar intervals, were similar to those used for the analysis of frost layer growth.

Figure 13 through Figure 16 show the comparison between the calculation results using experiment values as input parameters and the experiment values.

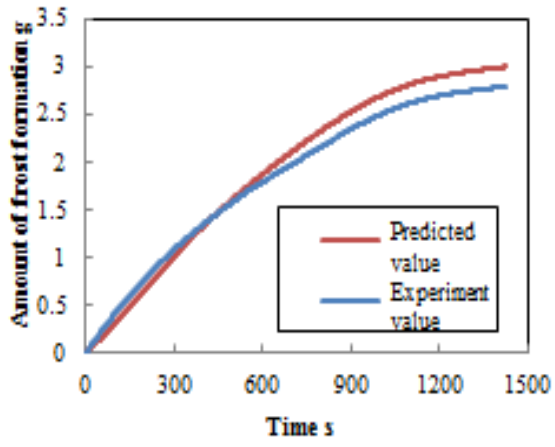

Figure 13: Comparison of frost formation amount

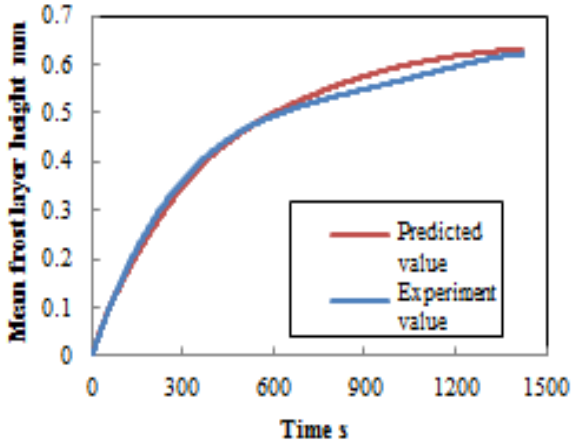

Figure 14: Comparison of mean frost layer height

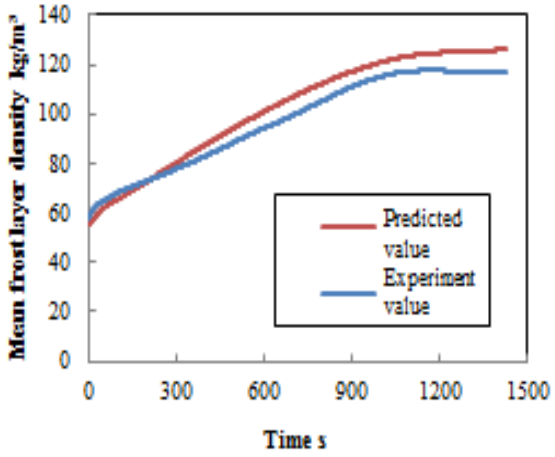

Figure 15: Comparison of mean frost layer density

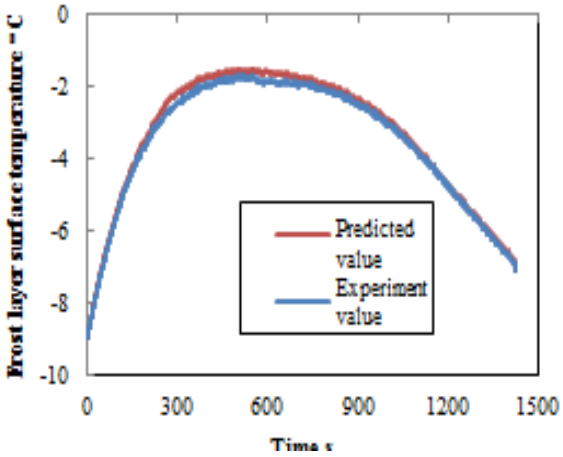

Figure 16: Comparison of frost layer surface temperature

Table 7 lists mean error ratios between predicted and experiment values.

Table 7: Mean error ratios between measured and predicted values

Frost formation amount	Mean frost layer height	Mean frost layer density	Frost layer surface temperature
8.7%	3.4%	5.6%	5.8%

The measured and predicted values agreed well with each other in the amount of frost formation, mean frost layer height, mean frost layer density, and frost layer surface temperature, and maximum error did not exceed 10%.

Based on the predictive model developed as described above, the influence of various factors on frost layer growth was studied.

With air humidity X_a set at 0.0053 kg/kg' and cooling surface temperature T_w set at –10ºC as two parameters other than air temperature, Figure 17 shows the predicted amount of frost formation when air temperature T_a is changed from 6ºC to 8ºC. Likewise, Figure 18 shows the predicted mean frost layer height when air temperature T_a is changed from 6ºC to 8ºC.

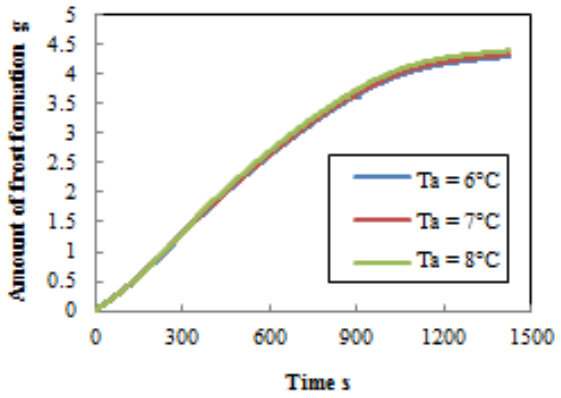

Figure 17: Predicted amount of frost formation with varying air temperature

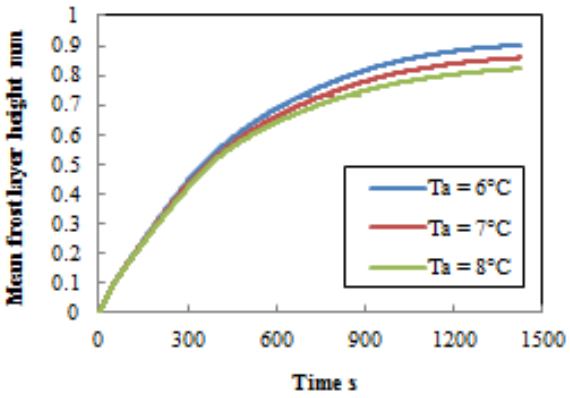

Figure 18: Predicted mean frost layer height with varying air temperature

Figure 17 indicates that a change in air temperature does not have significant impact on the amount of frost formation. On the other hand, Figure 18 indicates that increase in air temperature decreases mean frost layer height.

With air temperature T_a set at 7ºC and cooling surface temperature T_w set at –10ºC as two parameters other than air humidity, Figure 19 shows the predicted amount of frost formation when air humidity X_a is changed from 0.0051 kg/kg' to 0.0055 kg/kg'. Similarly, Figure 20 shows the predicted mean frost layer height when air humidity X_a is changed from 0.0051 kg/kg' to 0.0055 kg/kg'.

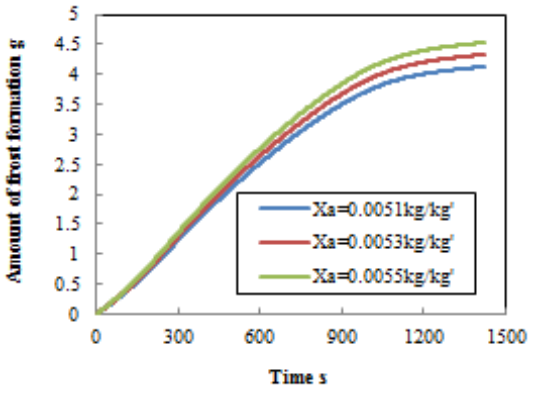

Figure 19: Predicted amount of frost formation with varying air humidity

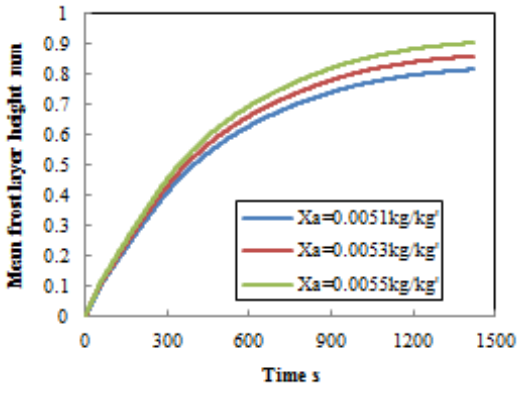

Figure 20: Predicted mean frost layer height with varying air humidity

Figure 19 indicates that increase in air humidity increases the amount of frost formation. This finding agrees qualitatively with the test results of the previous study in FY2012 using this test equipment. Similarly, Figure 20 indicates that an increase in air humidity increases mean frost layer heights.

With air temperature T_a set at 7ºC and air humidity X_a set at 0.0053 kg/kg' as two parameters other than cooling surface temperature, Figure 21 shows the predicted amount of frost formation when cooling surface temperature T_w is changed from –9ºC to –11ºC. In a similar fashion, Figure 22 shows the predicted mean frost layer height when cooling surface temperature T_w is changed from –9ºC to –11ºC.

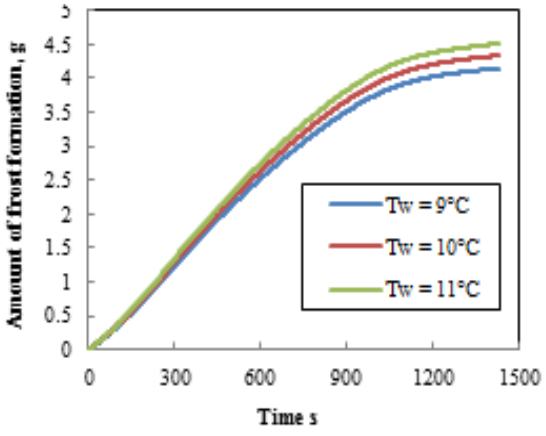

Figure 21: Predicted amount of frost formation with varying cooling surface temperature

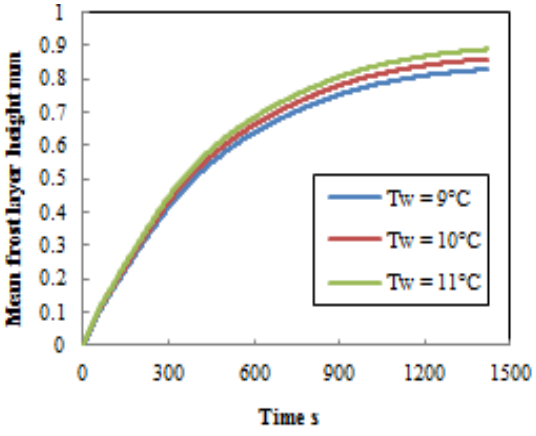

Figure 22: Predicted mean frost layer height with varying cooling surface temperature

Figure 21 indicates that decrease in cooling surface temperature increases the amount of frost formation. This finding agrees qualitatively with the test results of a previous study using this test equipment, in which cooling surface temperature was varied as a parameter. Similarly, Figure 22 indicates that a decrease in cooling surface temperature increases mean frost layer heights.

Based on the results described above, this predictive model has demonstrated its capability to quantitatively predict the influence of various factors on frost layer growth. However,

evaluating the influence of volumetric air flow rate on frost growth, and predicting and evaluating frost growth in a much colder environment, are considered difficult to accomplish within the scope of this experiment. The challenges NEDO should solve in the near future include predicting the change in a flow path, and estimating the time when the flow path is blocked.

2 THERMOSIPHONS WHICH COLLECT HEAT FROM SURFACE GROUND LAYERS FOR CO_2 REFRIGERATION CYCLE IN COLD CLIMATES: EFFECT OF ARTERY TUBE ON PERFORMANCE

2.1 Background and Purpose of This Study

In Hokkaido, where temperatures are very low in winter, the energy used for space heating accounts for about 42% of annual energy consumption per household. Energy consumed for space heating and hot water supply combined exceeds 80%. On the other hand, the utilizationof heat pumps in the region remains as low as 5%. This is because low outdoor temperatures in cold climates cause various problems such as reduction in heat pump efficiency. For this reason, the development of high-efficiency heat pumps used in cold climates for space heating and hot water supply is considered an effective measure at households for energy saving and CO_2 emission reductions. In this study, thermosiphons with a new shape have been designed and evaluated to collect heat from surface ground layers. The new thermosiphons utilize underground heat as a heat source for evaporators in order to prevent a reduction in heat pump efficiency. In addition, heat pump simulations have been conducted by incorporating the test results of the thermosiphons.

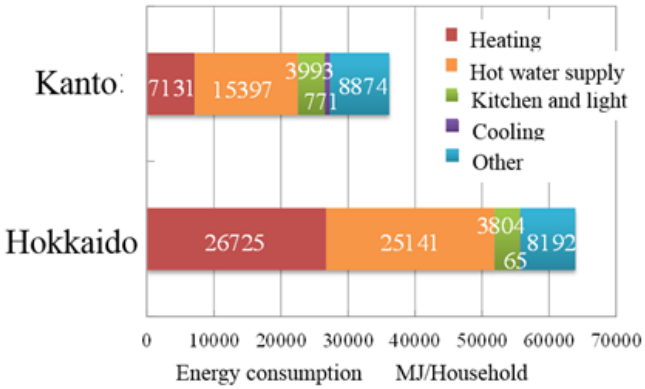

Figure 23: Regional comparison of energy consumption at households

Table 8: Percentage of heat pump installations at new all-electric homes in Hokkaido

Hot water supply		Space heating		Actual sales in FY2010 (households)	Percentage (%)
Heat source	APF	Heat source	SPF		
EcoCute	2.3	Heat pump	2.3	800	5
		Heater on snow melting power	1	1532	10
		Heater on midnight power	1	553	4
Heater	1	Heat pump	2.3	693	4
		Heater on snow melting power	1	8766	56
		Heater on midnight power	1	3172	20
Total				15516	100

2.2 Experimental Procedure

The performance of two types of thermosiphons, a 1-m-long corrugated tube and a 1-m-long smooth tube, has been evaluated. The corrugated tube is designed to increase its heat-transfer area and give it the effect of preventing flooding by having the wall surface trap the working fluid. The corrugated tube is covered with a stainless steel net reinforcement on the external wall to ensure its pressure resistance. The smooth tube has a smaller heat-transfer area than the corrugated tube, but has a higher heat-transfer coefficient because there is no need to cover the tube with a metal net reinforcement. A plate heat exchanger is set up above a thermosiphon. The whole thermosiphon area works as an evaporator, and the plate heat exchanger works as a condenser. In this test, an artery tube is inserted inside each thermosiphon. The artery tube is inserted inside the thermosiphon to facilitate the recirculation of the working fluid from the condenser.

Leading the condensate of working fluid into the artery tube can separate the gaseous flow path from the liquid flow path, which is expected to prevent flooding from incidence. Four types of artery tubes were used in this study, three of which were showering tubes. Each showering tube is blocked on the bottom, with three holes opened on the side wall. The recirculated working fluid is distributed through these holes like showering, which was expected to prevent localized dry out. Three types of artery tubes were prepared with different hole positions: 1) the three holes face in one direction, 2) face alternately in two directions at the intervals of 180 deg., and 3) face in three directions at the intervals of 120 deg. In addition, another artery tube was prepared, whose bottom was not blocked, and which had no holes on the side wall. This artery tube was named “double tube”.

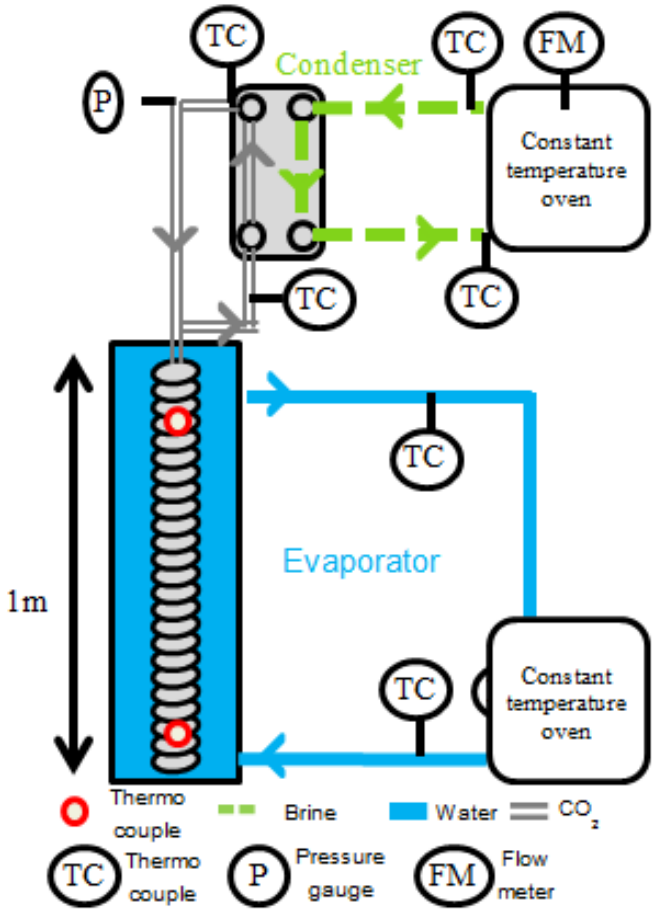

Figure 24: Test equipment

Table 9: Dimensions of corrugated tubes

Corrugated tube	Length	mm	900	Wall thickness	mm	0.25
	ID (min. ID)	mm	10	Inner heat-transfer area	m^2	0.0882
	OD	mm	15.0	Volume	m^3	10.5×10^{-5}
	Groove pitch	mm	2.4	Material		SUS316L
	Groove depth	mm	2.25			
Straight portion (edges)	Length	mm	30,70	Wall thickness	mm	1.0
	OD	mm	12.7	Material		SUS304
Total	Length	mm	1000	Volume	m^3	11.4×10^{-5}
	Inner heat-transfer area	m^2	0.0916			

Table 10: Dimensions of smooth tubes

Heat exchanger	Length	mm	930	Wall thickness	mm	1.2
	ID	mm	14.9	Heat-transfer area	m^2	0.0509
	OD	mm	17.3	Volume	m^3	10.5×10^{-5}
	Material		SUS304			
Heat exchanger joint area (edges)	Length	mm	70	Wall thickness	mm	1.2
	OD	mm	12.7	Material		SUS304
	ID	mm	10.3			
Total	Length	mm	1000	Volume	m^3	16.7×10^{-5}
	Heat-transfer area	m^2	0.0537			

Table 11: Dimensions of artery tubes

Length	mm	1170
ID	mm	4.4
OD	mm	6.4
Hole height, hole diameter	mm	250, 0.5
		570, 1.0
		890, 2.0

2.3 Experimental Results

As a result of performance evaluation, the smooth tube showed higher performance than the corrugated tube. This is attributable to the fact that the corrugated tube has a lower heat-transfer coefficient than the smooth tube. For the purpose of making it flexible, the corrugated tube used in this test is designed to have a very thin wall thickness. The corrugated tube is covered with a metal net reinforcement on the external surface to be able to withstand its internal pressure. It is thought that this construction made the tube's heat-transfer resistance higher than intended.

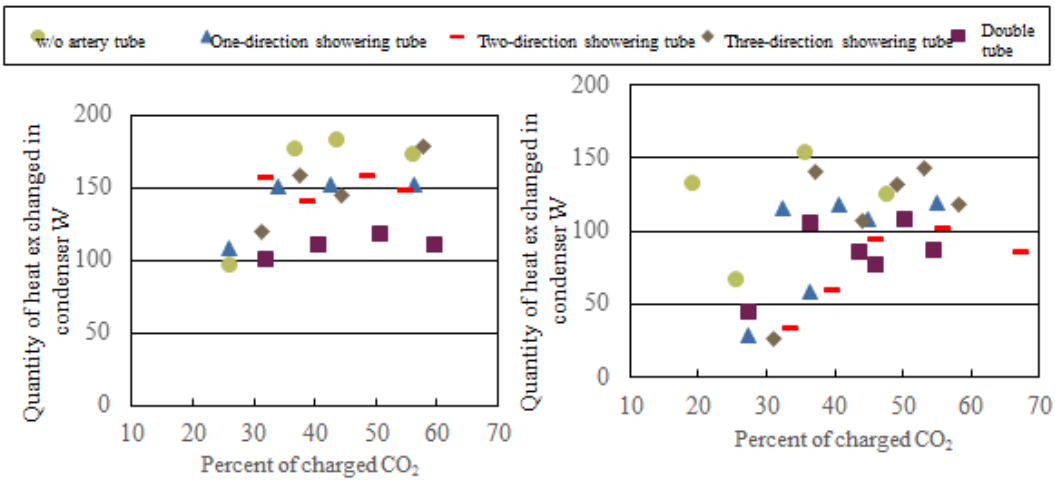

Figure 25: Quantity of heat exchanged (smooth tube)

Figure 26: Quantity of heat exchanged (corrugated tube)

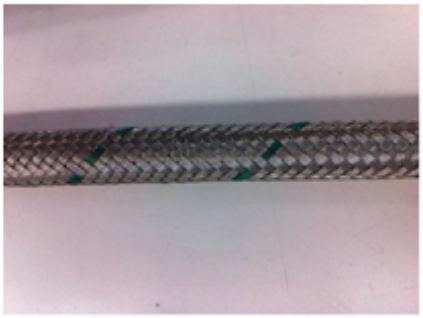

Figure 27: Metal net reinforcement on corrugated tube

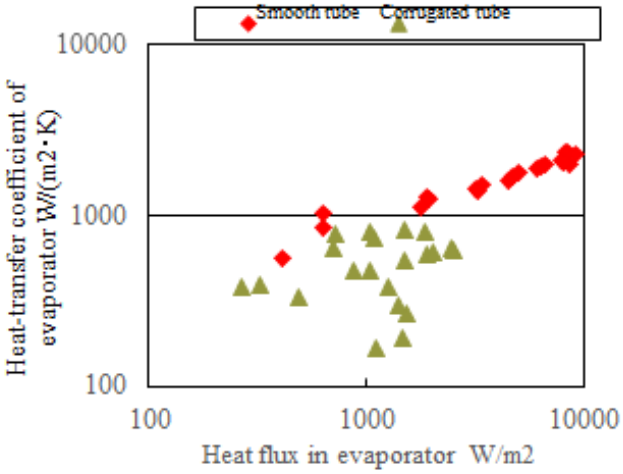

Figure 28: Heat-transfer coefficient of evaporator

With respect to the smooth tube that showed higher performance than the corrugated tube, its internal state has been examined. Shown in the following figures are the relationships in smooth tubes between the evaporator's heat flux and the degree of superheat of the evaporator wall surface. In the three cases where a one-direction showering tube, a two-direction showering tube, and a double tube were used, the heat flux in the evaporator peaked out at around 7000 W/m^2, which indicated that dry out happened. On the other hand, in the cases where no artery and a three-direction showering tube were used, the heat flux in the evaporator increased up to at around 9000 W/m^2. Although dry out started at around 1000 W/m^2 in the case where no artery tube was used, such dry out was not observed in the case where a three-direction showering tube was used. Based on these results, it was found that the use of a three-direction showering tube is most effective where smooth tubes are used.

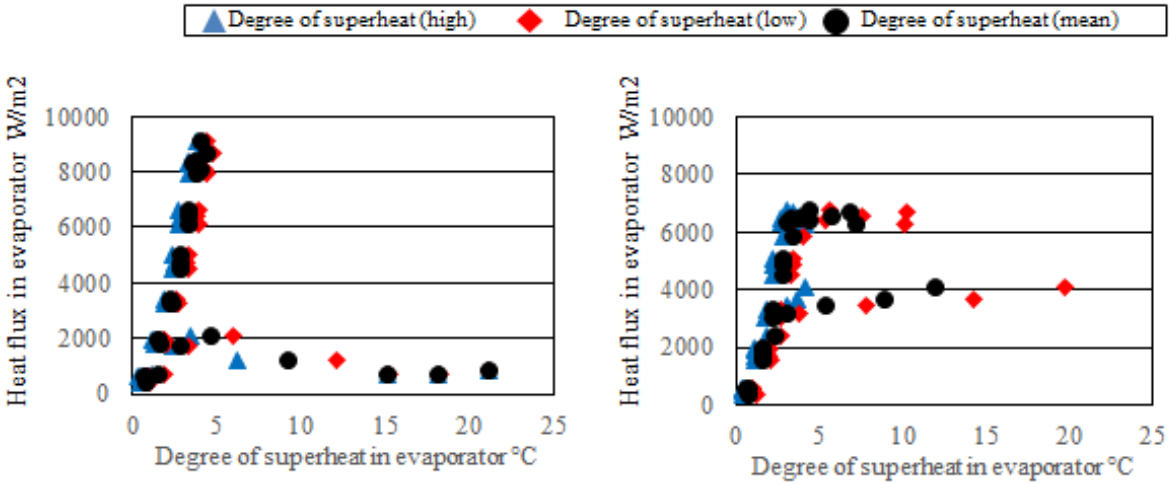

Figure 29: Degree of superheat on evaporator wall surface (w/o artery tube)

Figure 30: Degree of superheat on evaporator wall surface (one-direction)

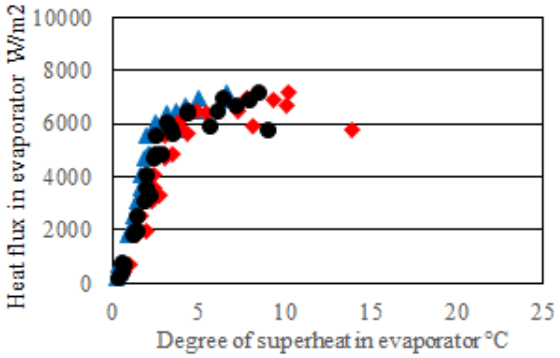

Figure 31: Degree of superheat on evaporator wall surface (two-direction)

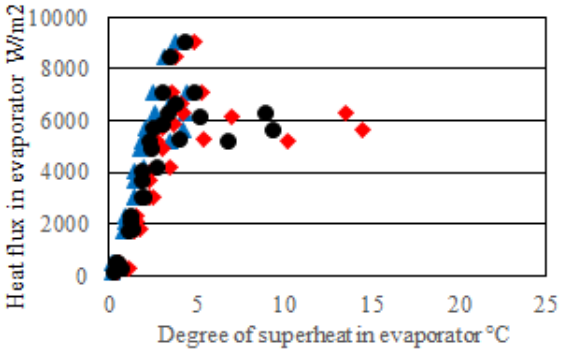

Figure 32: Degree of superheat on evaporator wall surface (three-direction)

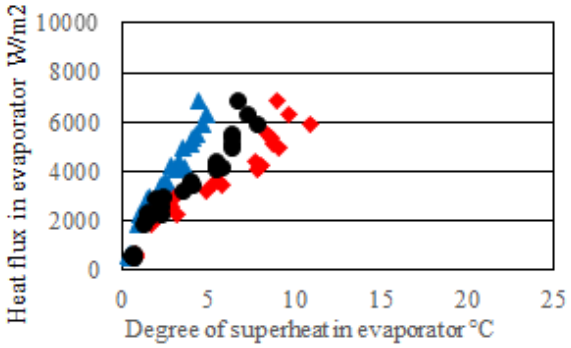

Figure 33: Degree of superheat on evaporator wall surface (double tube)

Based on the test results showed above, an empirical correlation of heat-transfer coefficients was developed, and then integrated into heat pump simulations. In this study, the experimental equation was developed based on the experimental data obtained from the smooth tube without an artery tube, and the smooth tube with a three-direction showering tube, both of which showed the highest test performance. The following is the empirical

correlation for heat-transfer coefficients of two-phase closed thermosiphons developed by Imura, et al. (1978).

$$h_e = 0.32 \frac{\rho_l^{0.65} \lambda_l^{0.3} c_{pl}^{0.7} g^{0.2} q_h^{0.4}}{\rho_g^{0.25} L^{0.4} \mu_l^{0.1}} \left(\frac{P_{in}}{P_a} \right)^{0.3} \quad (2.1)$$

ρ_l	: Liquid density *kg/m^3*	ρ_g	: Vapor density *J/kgK*	C_{pl}	: Specific heat *J/kgK*
G	: Acceleration of gravity *m/s^2*	L	: Evaporative latent heat *J/kg*	μ_l	: Viscosity coefficient *kg/ms*
λ_l	: Thermal conductivity *W/mK*	q_h	: Heat flux in evaporator *W/m^2*	P_{in}	: Internal pressure *Pa*
P_a	: Atmospheric pressure *Pa*	h_e	: Heat-transfer coefficient *W/m^{2}K*		

Where

$$X = \frac{\rho_l^{0.65} \lambda_l^{0.3} c_{pl}^{0.7} g^{0.2} q_h^{0.4}}{\rho_g^{0.25} L^{0.4} \mu_l^{0.1}} \quad (2.2)$$

Using the above equations, empiricalcorrelations for heat-transfer coefficients have been developed for the smooth tube without an artery tube, and the smooth tube with a three-direction showering tube.

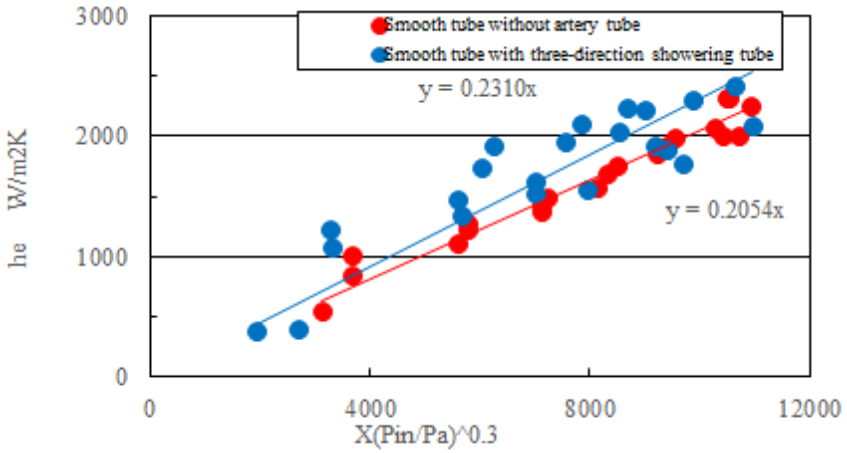

Figure 34: Experimental equations for heat-transfer coefficients

The empirical correlations were developed by altering the slope of the equation developed by Imura, et al (1978). The following are the empirical correlations for the cases where no artery tube and a three-direction showering tube are used.

$$h_e = 0.2054 X \left(\frac{P_{in}}{P_a} \right)^{0.3} \quad (2.3)$$

$$h_e = 0.231X\left(\frac{P_{in}}{P_a}\right)^{0.3} \quad (2.4)$$

The following are the results of heat pump simulations for the smooth tube without an artery tube, and the smooth tube with a three-direction showering tube. In the case where no artery tube is used, the number of thermosiphons required to achieve the targeted COP 2.8 is 14 for the tube length of 10 m, and 9 for 15 m. Similarly, in the case where a three-direction showering tube is used, the number of thermosiphons required is 13 for the tube length of 10m, and 9 for 15 m. Based on these results, in the case where 10-m-long thermosiphons are used, the use of a three-direction showering tube successfully reduced the number of thermosiphons required (in this connection, note that COP was calculated as APF here).

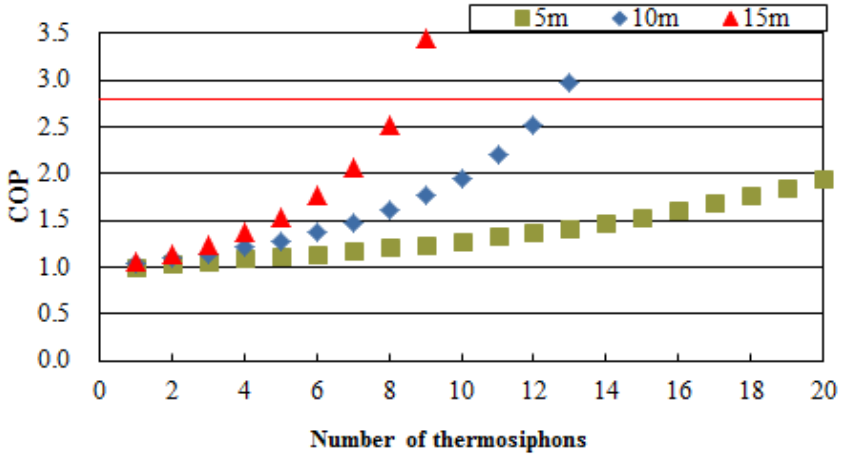

Figure 35: Results of heat pump simulations (smooth tubes without artery tube)

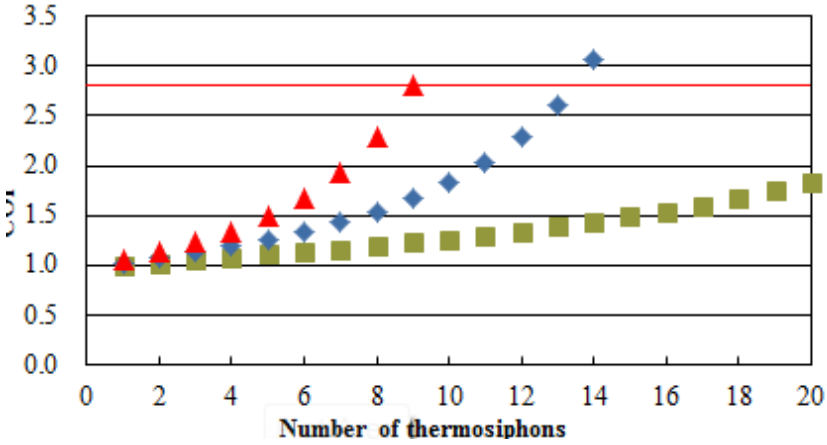

Figure 36: Results of heat pump simulations (smooth tubes with three-direction showering tube)

3 FROST-FREE AIR SOURCE HEAT PUMP WATER HEATER SYSTEM INTEGRATED WITH SOLID DESICCANT

3.1 Introduction

Air source heat pump water heaters (ASHPWHs) are widely applied as an economic form of heating. One of the largest problems in ASHPWHs is evaporator frosting, and the subsequent need for defrosting at a low ambient temperature and high relative humidity.

We proposed a frost-free air source heat pump water heater system with integrated solid desiccant, in which frosting can be retarded by dehumidifying air before it enters the ASHPWH evaporator.

3.2 System Description

A schematic diagram of the frost-free ASHPWH system is shown in Figure 37. This system consists of a desiccant-coated heat exchanger (1), an air heat exchanger (2), a compressor (3), a water heat exchanger (4), a water storage tank (5), a pump (6), two expansion valves (7, 8), a fan (9) and three valves (10, 11, 12). With respect to the moisture moving in the desiccant, the operation process of the ASHPWH system can be classified into two modes: adsorption mode (AD mode) and desorption mode (DE mode).

While the system works in AD mode, the refrigerant is vaporized in two evaporators (1, 2) at two different temperature levels by controlling the two expansion valves (7, 8). Hot water is produced at the water heat exchanger (4). Valves (11, 12) are opened and the valve (10) is closed. Outside air (OA) is blown in by a fan (9) across the desiccant-coated heat exchanger (1) and the air heat exchanger (2), and then is exhausted at state EA. The process air follows the two processes. OA→AA: OA is dehumidified at (1), and leaves as dry air (state AA). The adsorption heat is used to vaporize one part of the refrigerant. AA→EA: AA is then passed through (2), in which refrigerant is completely vaporized by obtaining sensible heat from AA, and finally, the air is exhausted at state EA. Because the dew point of the air (AA) is lower than the evaporation temperature of the refrigerant at (2), frost-free operation could be realized in this system. When the moisture content of the desiccant becomes relatively high so that the vapor partial pressure of the desiccant is higher than that of the OA, the desiccant should be regenerated, whereupon the system will be operated in desorption mode.

During DE mode, the expansion valve (7) is opened and another expansion valve (8) throttled. Therefore (1) and (4) are condensers, and (2) is evaporator. Simultaneously, the valve (10) is opened and valves (11, 12) closed to form an air cycle between (1) and (2). The refrigerant exiting from compressor (3) initially removes part of the heat into the water at (4), and then dissipates the remaining heat at (1), in which the desiccant is regenerated and the return air (RA) gets heat and moisture from the refrigerant and desiccant. The hot and humid air (DA) is then passed through (2), in which the refrigerant is vaporized by obtaining heat from DA, and finally, leaves at state RA. Therefore, the total heat load added to DA in (1), including sen ible and latent heat, could be completely recycled in (2). As a result, the zero heat loss at the air side and continuous heat output to water are realized. Because drain is exhausted at (2), the evaporation temperature of the refrigerant in (2) must exceed $0^{O}C$ while in DE mode. A single period is ended when this moisture adsorbed by the desiccant in AD mode is completely discharged in DE mode.

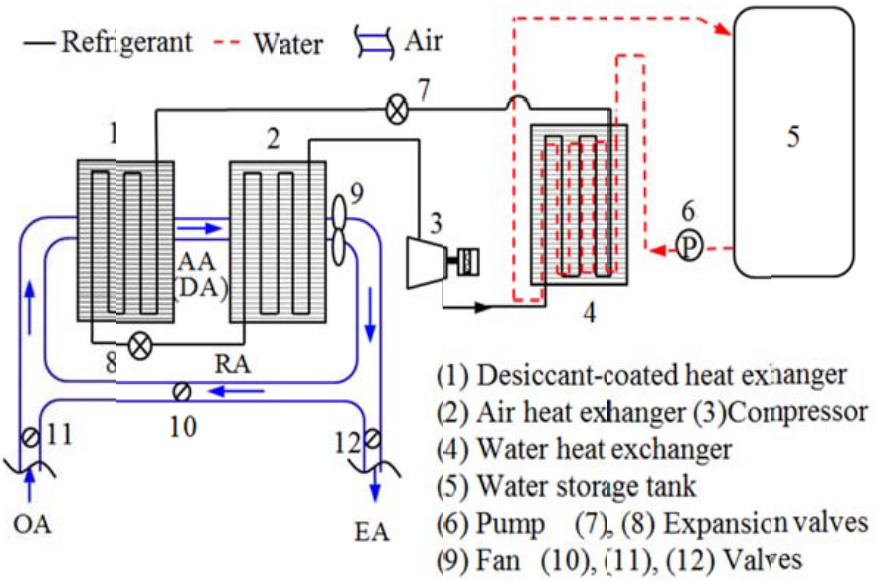

Figure 37: Schematic diagram of the frost-free A HPWH system

The coefficient of performance of the system (COP_{system}) is defined as the ratio of the water heating capacity to the electrical consumption of the compressor in a single period. It can be expressed as:

$$\frac{1}{COP_{system}-1} = \frac{1}{COP_{ad}-1} + \frac{1-SHF_{ad}}{1-SHF_{de}} \cdot \frac{1}{COP_{de}-1} \quad (3.1)$$

Here, COP_{ad} and COP_{de} are coefficients of performance of the heat pump unit in AD and DE modes, separately; SHF_{ad} and SHF_{de} are the sensible heat factors (SHF) of air in AD and DE modes, respectively.

3.3 Simulation Results

Calculations are carried out for a frosting climate: air temperature (T_{OA}) = -7 ~ 5.5 ℃, air relative humidity (RH_{OA}) = 60 ~ 80%. Simulation results of COP_{system} are shown in Figure 38. It is found that the high T_{OA}, or low RH_{OA}, contributes to the high COP_{system}. Furthermore, Figure 38 shows a comparison of COP_{system} between the frost-free ASHPWH system proposed in this work and a hot–gas defrosting ASHPWH system. Results show that the COP_{system} of the frost-free ASHPWH system is higher than that of the hot-gas defrosting ASHPWH system for any frosting temperature and humidity condition. In particular, the COP_{system} of the frost-free ASHPWH system is increased by 25-30% at low temperature (-7℃) or low relative humidity (60%) conditions compared to the hot-gas defrosting ASHPWH system.

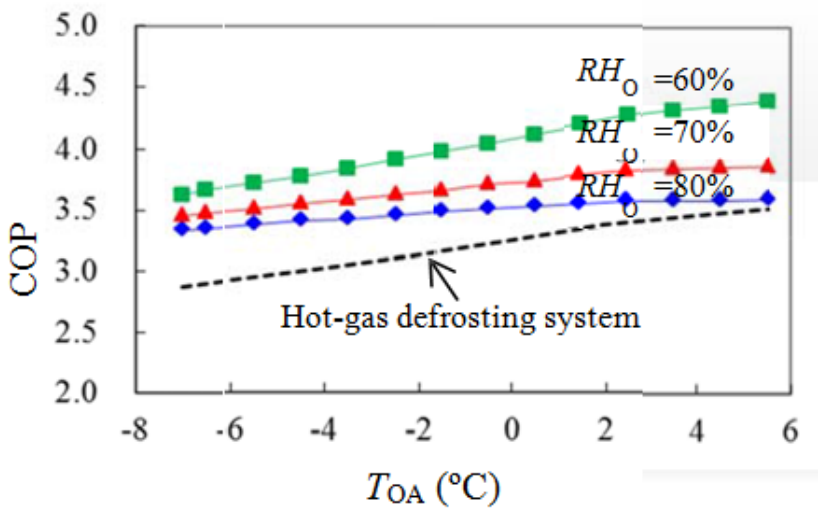

Figure 38: Simulation results of COP_{system}

3.4 Conclusions

In conclusion, the frost-free ASHPWH system proposed in this work has a solid desiccant coated heat exchanger and an air cycling flow path. So it can produce hot water continuously and its COP_{system} is estimated to be higher than that of a conventional system by 30% under frosting ambient air conditions. This technology is also applicable to other air source heat pumps for heating, etc.

4 REFERENCES

Imura, H. “Heat transfer inside Two-phase Closed Thermosiphon” Bulletin of JSME, B, (1978), pp.712-722. (in Japanese).

Le Gall, R., J.M. Grillot and C. Jallut, “Modelling of Frost Growth and Densification”, Int. J. of Heat Mass Transfer. 28,(7) (1997), 3177-3187.

Tao, Y. X., Mao, Y., and Besant, R. W., 1994, “Frost Growth Characteristics on Heat Exchanger Surfaces: Measurement and Simulation Studies,” Proceedings of the 1994 ASME International Mechanical Engineering Congress and Exposition, Chicago, IL, Nov. 1994, HTD-Vol 286 , pp. 29–38.

Yamashita, K. “Frost phenomena under the Low Temperature Environment” Ph.D. Thesis, Tamagawa University, (2009) (in Japanese).

Japan Team Report

IEA HPT TCP Annex 41
"Cold Climate Heat Pumps"

Task 3 – Continued Work

Submitted by:

Waseda University, Tokyo, Japan

Lead: Prof. Masafumi Katsuta, Waseda University (contact: katsuta@waseda.jp)

Contributors:

Annex 41 Japanese Company and Research Institute Members

- CRIEPI
- NEDO
- Mitsubishi Electric
- Toshiba Carrier Corporation
- Daikin
- Kansai Electric Power Co. Inc.
- Chubu Electric Power Co. Inc.
- Hitachi Appliance, Inc.
- Mitsubishi Heavy Industries

Observers

- Hokkaido Electric Power Co. Inc.
- Tohoku Electric Power Co. Inc.

November 2016

TABLE OF CONTENTS

LIST OF TABLES

LIST OF FIGURES

1 SIMULATION OF HEAT PUMP PERFORMANCE TAKING FROST FORMATION INTO CONSIDERATION

1.1 Background

In the air conditioning field, one of the elements that have high energy-saving potential is compression heat pumps. Based on the reverse Carnot cycle, compression heat pumps are widely used for air conditioners, refrigerators and freezers, water heaters, and the like. In addition, a number of technological developments are currently under way to improve the performance of these compression heat pumps. When operated in cold climates for space heating, however, compression heat pumps cause the problem of frost formation on the surface of their outdoor heat exchangers. The problem will increase draft resistance and thermal resistance, deteriorating operating performance. For this reason, a compression heat pump requires defrosting on the outdoor heat exchangers. But in a defrosting operation, the heat pump needs to be switched from the heating mode to the cooling mode to warm up the outdoor heat exchanger. In this process, comfort in the room will be lost. Additionally, total efficiency will decrease because of extra power consumption during defrosting. Therefore, it is expected that further energy saving can be obtained by finding the properties of heat pumps that take frost formation into account, and studying how to control them. However, the phenomenon of frost formation is too complex to understand, and the influence of frost formation on heat pump characteristics is largely unknown.

There are many previous studies on frost growth and the influence of frost on heat exchangers. For example, Jones, et al. (1975) regarded a frost layer as a porous layer, claiming that water vapor migrates through the layer according to Fick's law, and it diffuses along its concentration gradient. Aoki, et al. (1990) analyzed the characteristics of a fin and tube heat exchanger, taking frost growth into consideration. They figured out how the characteristics of a heat exchanger are affected by the difference in frost layer growth on the fins, taking some examples of parallel current and counter current. In addition, Kondepudi, et al. (1989) studied the frost formation characteristics of heat exchangers with louvered fins, claiming that the greater air humidity, wind velocity, and fin density are, the greater frost layer growth and pressure loss become.

However, these past studies did not expand their scope all the way to a whole heat pump system. There have been few studies that clarified the influence of frost growth on the dynamic behavior of a whole heat pump by means of numerical simulations. Given this background, this study is intended to analyze the compression refrigerating cycle of a whole heat pump system using numerical simulations and experiments.

1.2 Scope of This Study

A compression heat pump is a refrigeration cycle, made up of a compressor, a condenser, an expansion valve, and an evaporator. In the cooling operation, the outdoor heat exchanger works as a condenser, and the indoor heat exchanger works as an evaporator. A compressor heat pump mechanically creates pressure distribution in the refrigerant inside (the high-pressure side and the low-pressure side). The compressor heat pump absorbs heat by making the evaporation temperature of the low-pressure side refrigerant lower than the ambient temperature, and radiates heat by making the condensation temperature of the high-pressure side refrigerant higher than the ambient temperature. Figure 1 shows the process of a compression refrigerating cycle.

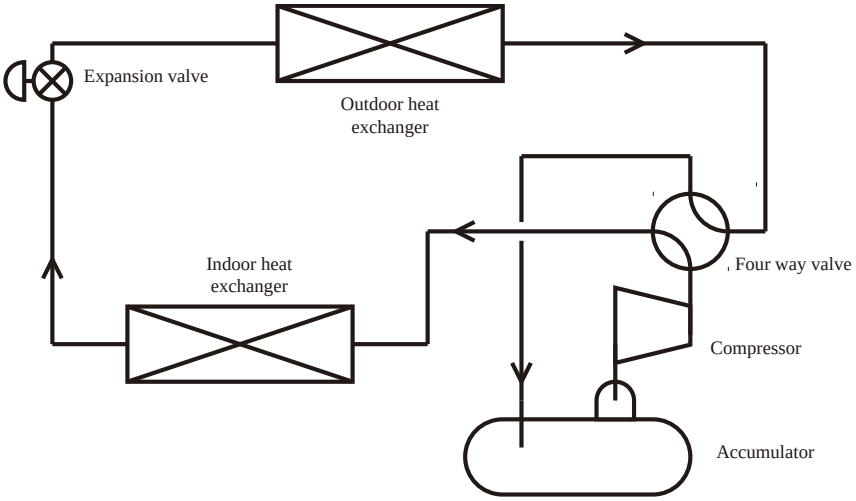

Figure 1: System flow

1. Refrigerant vapor is supplied into the compressor, and the compressed refrigerant vapor enters the condenser.
2. The high-pressure refrigerant exchanges heat with outside ambient air. Since the temperature of the refrigerant is higher than the outside air temperature at this point, the refrigerant radiates heat and is cooled. The refrigerant becomes a saturated liquid or in a supercooled state by the latent heat of condensation.
3. Then the pressure of the refrigerant is reduced in the expansion valve, becoming low-temperature, low-pressure wet vapor. The vapor enters the evaporator.
4. In the evaporator, the temperature of the refrigerant is lower than outside air temperature, and the refrigerant absorbs heat from the ambient air. The refrigerant becomes dry vapor by the latent heat of evaporation, with no pressure change involved. At the end of this cycle, the accumulator separates vapor from liquid, and supplies only refrigerant vapor to the compressor again.

Installed in indoor and outdoor air conditioner units, heat exchangers exchange heat between their refrigerant and outside air. If a gas-phase refrigerant condenses in a heat exchanger radiating its heat into the air, that heat exchanger is working as a condenser. If a refrigerant evaporates in a heat exchanger taking heat from the air, that heat exchanger is working as an evaporator. In the cooling operation, an indoor air conditioner unit works as an evaporator, taking heat in the room into the refrigerant. And an outdoor unit works as a condenser, radiating the heat of the room outdoors.

In this study, heat pump performance was simulated using a fin and tube heat exchanger. The heat exchanger has a structure that combines multiple heat exchanger tubes and plate fins, which is suited for air-to-refrigerant heat exchange. The advantage of this heat exchanger is that a larger heat-transfer area can be obtained in a limited space. For this reason, this type of heat exchanger is most widely used for air conditioners.

1.3 Numerical Simulations

The following is the mathematical model of an expansion valve.

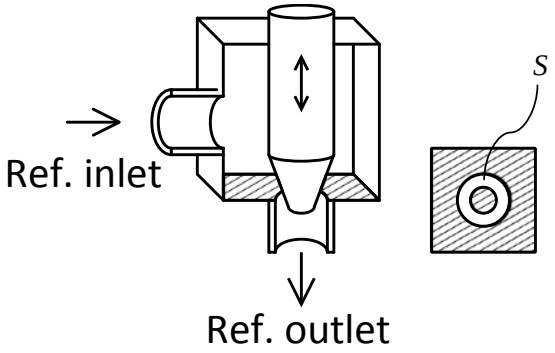

Figure 2: Electric expansion value

Equation of continuity

$$\rho_{R,O} v_{R,O} S_{R,O} - \rho_{R,I} v_{R,I} S_{R,I} = 0 \quad (1.1)$$

Energy equation

$$\rho_{R,O} v_{R,O} h_{R,O} S_{R,O} - \rho_{R,I} v_{R,I} h_{R,I} S_{R,I} = 0 \quad (1.2)$$

Relationship between differential pressure and flow volume

$$G_{R,I} = \begin{cases} c_V S \sqrt{2\rho_{R,I}\left(P_{R,I} - P_{R,O}\right)} & \left(0 < P_{R,I} - P_{R,O}\right) \\ -c_V S \sqrt{2\rho_{R,O}\left(P_{R,O} - P_{R,I}\right)} & \left(P_{R,I} - P_{R,O} \le 0\right) \end{cases} \quad (1.3)$$

Equation of state

$$s_{R,I} = f_s\left(P_{R,I}, h_{R,I}\right) \quad (1.4)$$

$$\rho_{R,I} = f_\rho\left(P_{R,I}, h_{R,I}\right) \quad (1.5)$$

Relationship between pulse and opening.

$$S = c_p p \quad (1.6)$$

The following is the mathematical model of a compressor.

The compressor model simulates a scroll compressor, which is calculated from the following equations.

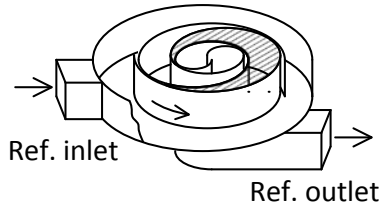

Figure 3: Compressor

Equation of continuity

$$\rho_{\mathrm{R,O}} v_{\mathrm{R,O}} S_{\mathrm{R,O}} - \rho_{\mathrm{R,I}} v_{\mathrm{R,I}} S_{\mathrm{R,I}} = 0 \quad (1.7)$$

Energy equation

$$\rho_{\mathrm{R,O}} v_{\mathrm{R,O}} h_{\mathrm{R,O}} S_{\mathrm{R,O}} - \rho_{\mathrm{R,I}} v_{\mathrm{R,I}} h_{\mathrm{R,I}} S_{\mathrm{R,I}} = W \quad (1.8)$$

Suction flow volume

$$\rho_{\mathrm{R,I}} v_{\mathrm{R,I}} S_{\mathrm{R,I}} = 2\pi n \eta_{\mathrm{V}} \rho_{\mathrm{R,I}} V \quad (1.9)$$

Ideal outlet entropy

$$s_{\mathrm{R,O,ad}} = s_{\mathrm{R,I}} \quad (1.10)$$

Adiabatic efficiency

$$\eta_{\mathrm{ad}} = \frac{h_{\mathrm{R,O,ad}} - h_{\mathrm{R,I}}}{h_{\mathrm{R,O}} - h_{\mathrm{R,I}}} \quad (1.11)$$

Power consumption

$$E = \frac{W}{\eta_{\mathrm{INV}}} \quad (1.12)$$

Shaft power

$$W = \frac{G_{R,I}\left(h_{R,O} - h_{R,I}\right)}{\eta_{\mathrm{M}}} \quad (1.13)$$

Equation of state

$$\rho_{\mathrm{R}} = f_{\rho}\left(P_{\mathrm{R}}, h_{\mathrm{R}}\right) \quad (1.14)$$

$$\rho_{\mathrm{R,I}} = f_{\rho}\left(P_{\mathrm{R,I}}, h_{\mathrm{R,I}}\right) \quad (1.15)$$

$$\rho_{\mathrm{R,O}} = f_{\rho}\left(P_{\mathrm{R,O}}, h_{\mathrm{R,O}}\right) \quad (1.16)$$

$$s_{\mathrm{R,I}} = f_{\mathrm{s}}\left(P_{\mathrm{R,I}}, h_{\mathrm{R,I}}\right) \quad (1.17)$$

$$s_{\mathrm{R,O,ad}} = f_{\mathrm{s}}\left(P_{\mathrm{R,O}}, h_{\mathrm{R,O,ad}}\right) \quad (1.18)$$

$$T_{\mathrm{R}} = f_{\mathrm{T}}\left(P_{\mathrm{R}}, h_{\mathrm{R}}\right) \quad (1.19)$$

Amount of charged refrigerant

$$M_R = \rho_R V \quad (1.20)$$

Other equations

$$G_{R,I} = \rho_{\mathrm{R,I}} v_{\mathrm{R,I}} S_{\mathrm{R,I}} \quad (1.21)$$

$$G_{R,O} = \rho_{\mathrm{R,O}} v_{\mathrm{R,O}} S_{\mathrm{R,O}} \quad (1.22)$$

Inlet and outlet boundary conditions

$$P_R = P_{R,I} \quad (1.23)$$

$$h_R = h_{R,I} \quad (1.24)$$

Variables

$G_{R,I}, G_{R,O}, P_R, P_{R,O}, h_R, h_{R,O}, h_{R,O,ad},$
$\rho_R, \rho_{R,I}, \rho_{R,O}, s_{R,I}, s_{R,O,ad}, T_R,$
$v_{R,I}, v_{R,O}, W, E, M_R$

The following is the mathematical model of a heat exchanger in consideration of frost formation.

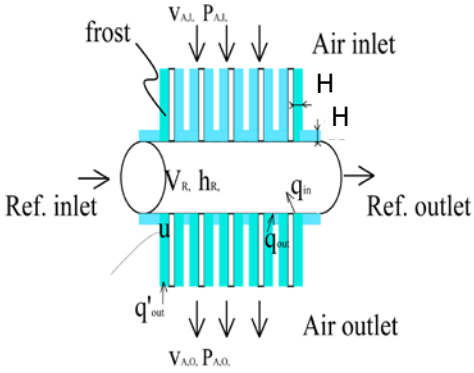

Figure 4: Frost phenomenon

Refrigerant-side equation of continuity

$$\frac{\partial \rho_R}{\partial t} + \frac{\partial (\rho_R v_R)}{\partial z} = 0 \tag{1.25}$$

Refrigerant-side pressure loss

$$\frac{\partial P_R}{\partial z} = -f_R \frac{1}{d_{In}} 2\rho_R v_R^2 \tag{1.26}$$

Refrigerant-side energy equation

$$\frac{\partial (\rho_R u_R)}{\partial t} + \frac{\partial (\rho_R v_R h_R)}{\partial z} = -\frac{Lc_{In}}{S_{In}} q_{In} \tag{1.27}$$

Piping-side energy equation

$$\rho_M C_M \frac{\partial T_M}{\partial t} = \frac{Lc_{In}}{S_M} q_{In} - \frac{A_{Pipe} + \eta_{FIN} A_{FIN}}{S_M L} (q_{Out} + j_{Out} h v_{Wat}) \tag{1.28}$$

Air-side equation of continuity

$$\rho_{A,O} v_{A,O} L_{x,O} - \rho_{A,I} v_{A,I} L_{x,I} = \frac{A_{Pipe} + \eta_{FIN} A_{FIN}}{L} j_{Out} \tag{1.29}$$

Air-side pressure loss (in this case primary mesh physical properties are used)

$$P_{A,O} - P_{A,I} = -f_A \frac{2L_x \rho_A V_{ac}^2}{D_{ec}} \tag{1.30}$$

Air-side energy equation

$$\rho_{A,O} v_{A,O} X_{A,O} L_{x,O} - \rho_{A,I} v_{A,I} X_{A,I} L_{x,I} = \frac{A_{Pipe} + \eta_{FIN} A_{FIN}}{L} j_{Out} \tag{1.31}$$

Air-side water vapor balance

$$\rho_{A,O} v_{A,O} h_{A,O} L_{x,O} - \rho_{A,I} v_{A,I} h_{A,I} L_{x,I} = \frac{A_{Pipe} + \eta_{FIN} A_{FIN}}{L} (q_{Out} + j_{Out} h v_{Wat}) \tag{1.32}$$

j is calculated assuming that if air outlet temperature reaches the dew point, air will be dehumidified so that the air outlet temperature and the dew point will be kept equal from that point afterward. If air outlet temperature is higher than the dew point, air will not be dehumidified.

$$j_{\mathrm{Out}} = \begin{cases} 0 & T_{\mathrm{DP,A,O}} < T_{\mathrm{A,O}} \\ f\left(P_{\mathrm{A,O}}, h_{\mathrm{A,O}}, T_{\mathrm{DP,A,O}}\right) & T_{\mathrm{DP,A,O}} = T_{\mathrm{A,O}} \end{cases} \quad (1.33)$$

Heat transfer

$$q_{\mathrm{In}} = \alpha_{\mathrm{In}}\left(T_{\mathrm{R}} - T_{\mathrm{M}}\right) \quad (1.34)$$

$$q_{\mathrm{Out}} = \alpha_{\mathrm{Out}} \frac{\left(T_{\mathrm{M}} - T_{\mathrm{A,I}}\right) - \left(T_{\mathrm{M}} - T_{\mathrm{A,O}}\right)}{\ln \dfrac{\left(T_{\mathrm{M}} - T_{\mathrm{A,I}}\right)}{\left(T_{\mathrm{M}} - T_{\mathrm{A,O}}\right)}} \quad (1.35)$$

Equation of state

$$hv_{Wat} = f_{\mathrm{Wat,hv}}\left(T_{A,O}\right) \quad (1.36)$$

$$x_{\mathrm{R}} = f_{\mathrm{x}}\left(P_{\mathrm{R}}, h_{\mathrm{R}}\right) \quad (1.37)$$

$$u_{\mathrm{R}} = f_{\mathrm{u}}\left(P_{\mathrm{R}}, h_{\mathrm{R}}\right) \quad (1.38)$$

$$\rho_{\mathrm{R}} = f_{\rho}\left(P_{\mathrm{R}}, h_{\mathrm{R}}\right) \quad (1.39)$$

$$T_{\mathrm{R}} = f_{\mathrm{T}}\left(P_{\mathrm{R}}, h_{\mathrm{R}}\right) \quad (1.40)$$

$$T_{\mathrm{A}} = f_{\mathrm{T}}\left(P_{\mathrm{A}}, h_{\mathrm{A}}, X_{\mathrm{A}}\right) \quad (1.41)$$

$$\mu_{R} = f_{\mu}\left(P_{R}, h_{R}\right) \quad (1.42)$$

$$\lambda_{\mathrm{R}} = f_{\lambda}\left(P_{\mathrm{R}}, h_{\mathrm{R}}\right) \quad (1.43)$$

$$\lambda_{\mathrm{R,Liq}} = f_{\lambda,Liq}\left(P_{\mathrm{R}}\right) \quad (1.44)$$

$$\lambda_{\mathrm{R,Vap}} = f_{\lambda,Vap}\left(P_{\mathrm{R}}\right) \quad (1.45)$$

$$Cp_{\mathrm{R,Liq}} = f_{Cp,Liq}\left(P_{\mathrm{R}}\right) \quad (1.46)$$

$$Cp_{\mathrm{R,Vap}} = f_{Cp,Vap}\left(P_{\mathrm{R}}\right) \quad (1.47)$$

$$Cp_{\mathrm{R}} = f_{Cp}\left(P_{\mathrm{R}}, h_{\mathrm{R}}\right) \quad (1.48)$$

Others

$$Lc_{\mathrm{In}} = \pi d_{\mathrm{In}} \tag{1.49}$$

$$S_{\mathrm{In}} = \frac{\pi D_{\mathrm{In}}^2}{4} \tag{1.50}$$

$$S_{\mathrm{M}} = \frac{\pi D_{\mathrm{Out}}^2}{4} - \frac{\pi D_{\mathrm{In}}^2}{4} \tag{1.51}$$

Refrigerant-side inlet and outlet conditions
When z=0

$$G_{\mathrm{R,I}} = \rho_{\mathrm{R}} v_{\mathrm{R}} S_{\mathrm{In}} \tag{1.52}$$

$$P_{\mathrm{R,I}} = P_{\mathrm{R}} \tag{1.53}$$

$$h_{\mathrm{R,I}} = h_{\mathrm{R}} \tag{1.54}$$

When z= L_{HEX}

$$G_{\mathrm{R,O}} = \rho_{\mathrm{R}} v_{\mathrm{R}} S_{\mathrm{In}} \tag{1.55}$$

$$P_{\mathrm{R,O}} = P_{\mathrm{R}} \tag{1.56}$$

$$h_{\mathrm{R,O}} = h_{\mathrm{R}} \tag{1.57}$$

Air-side inlet and outlet conditions

If the heat exchanger is an evaporator, air-side inlet and outlet conditions can be expressed as follows.

Upstream

$$G_{\mathrm{A,EVA,I}} = \rho_{\mathrm{A,I}} v_{\mathrm{A,I}} L_x L \tag{1.58}$$

$$P_{\mathrm{A,EVA\ I}} = P_{\mathrm{A,I}} \tag{1.59}$$

$$h_{\mathrm{A,EVA,I}} = h_{\mathrm{A,I}} \tag{1.60}$$

$$X_{\mathrm{A,EVA,I}} = X_{\mathrm{A,I}} \tag{1.61}$$

Downstream

$$G_{\mathrm{A,EVA,O}} = \rho_{\mathrm{A,O}} v_{\mathrm{A,O}} L_x L \tag{1.62}$$

$$P_{\mathrm{A,EVA\ O}} = P_{\mathrm{A,O}} \tag{1.63}$$

$$h_{\mathrm{A,EVA,O}} = h_{\mathrm{A,O}} \tag{1.64}$$

$$X_{\mathrm{A,EVA,O}} = X_{\mathrm{A,O}} \tag{1.65}$$

To obtain tube flow pressure loss, the Blasius equation is used for single-phase flows, and the Chisolm equation (1967) using the Lockhart-Martinelli parameter is applied to two-phase flows. Note that the Fanning friction factor is used in this case.

$$f_R = \begin{cases} 0.079\,\mathrm{Re}_R^{-0.25} & (\chi_B < 0 \text{ or } 1 < \chi_B) \\ 0.079\,\mathrm{Re}_{R,Liq}^{-0.25}\,\phi_{Liq}^2 & \left(0 \le x_R \le 1\right) \end{cases} \tag{1.66}$$

Reynolds number

$$\mathrm{Re}_R = \begin{cases} \dfrac{G_R D_{In}}{S_{In}\mu_{R,Liq}} & \left(x_R < 0\right) \\ \dfrac{G_R D_{In}}{S_{In}\mu_{R,Vap}} & \left(1 < x_R\right) \end{cases} \tag{1.67}$$

$$\mathrm{Re}_{R,Liq} = \frac{(1-x_R)G_R D_{In}}{S_{In}\mu_{R,Liq}} \qquad \left(0 \le x_R \le 1\right) \tag{1.68}$$

Density

$$\rho_{R,Liq} = f_{SAT,Liq,\rho}(P_R) \tag{1.69}$$

$$\rho_{R,Vap} = f_{SAT,Vap,\rho}(P_R) \tag{1.70}$$

Viscosity coefficient

$$\mu_{R,Liq} = f_{SAT,Liq,\mu}(P_R) \tag{1.71}$$

$$\mu_{R,Vap} = f_{SAT,Vap,\mu}(P_R) \tag{1.72}$$

The Lockhart-Martinelli correlation (both gas and liquid phases are in the state of turbulent flow classified by the Lockhart-Martinelli correlation, and from Chisolm's parameter C)

$$\phi_{Liq}^2 = 1 + \frac{20}{X_{tt}} + \frac{1}{X_{tt}^2} \tag{1.73}$$

Lockhart-Martinelli parameter

$$X_{tt} = \left(\frac{1-x_R}{x_R}\right)^{0.9}\left(\frac{\rho_{R,Vap}}{\rho_{R,Liq}}\right)^{0.5}\left(\frac{\mu_{R,Liq}}{\mu_{R,Vap}}\right)^{0.1} \tag{1.74}$$

Equation of tube flow heat transfer coefficients

For single-phase flows, tube flow heat transfer coefficients are calculated using the Dittus-Boelter equation, tube flow evaporative heat transfer coefficients are calculated using the equation by Yoshida, et al. (1983), and tube flow condensing heat transfer coefficients are calculated using the equation by Nozu, et al.

$$\alpha_{In} = \frac{\mathrm{Nu}_R \lambda_R}{D_{In}} \tag{1.75}$$

Single-phase flows

$$\mathrm{Nu}_R = 0.023\,\mathrm{Re}_R^{0.8}\,\mathrm{Pr}_R^n \tag{1.76}$$

$n = 0.3$ The inside of the tube is cooled

$n = 0.4$ The inside of the tube is heated

$$\mathrm{Pr}_R = \frac{\mu_R \cdot Cp_R}{\lambda_R} \tag{1.77}$$

The equation by Yoshida, et al. is used for two-phase evaporation.

$$\frac{\alpha_{In}}{\alpha_{In,Liq}} = 3.7\left\{ Bo\times 10^4 + 0.23\left(Bo\times 10^4\right)^{0.67}\left(\frac{1}{X_{tt}}\right)^2\right\}^{0.44} \tag{1.78}$$

$$Bo = \frac{q_{In}}{\frac{G_R}{S_{In}} h v_R} \tag{1.79}$$

$$\alpha_{R,Liq} = 0.023\,\mathrm{Re}_{R,Liq}^{0.8}\,\mathrm{Pr}_{R,Liq}^{0.4}\,\frac{\lambda_{R,Liq}}{D_{In}} \tag{1.80}$$

The equation by Nozu, et al. is used for two-phase condensation.

$$Nu_R = \begin{cases} Nu_{R,b} & \left(Nu_{R,f} < Nu_{R,b}\right) \\ Nu_{R,f} & \left(Nu_{R,b} \le Nu_{R,f}\right) \end{cases} \tag{1.81}$$

$$Nu_{R.f} = 0.018\left(\mathrm{Re}_{R,Liq}\sqrt{\frac{\rho_{R,Liq}}{\rho_{R,Vap}}}\right)^{0.9}\left(\frac{x_R}{1-x_R}\right)^{0.1x_R+0.8}\left(\mathrm{Pr}_{R,Liq}+\frac{8.0\times 10^3}{\mathrm{Re}_{R,Liq}^{1.5}}\right)^{1/3}\left(1.0+\frac{C_1 H_{R,Liq}}{\mathrm{Pr}_{R.l}}-\frac{0.2H_{R,Vap}}{\mathrm{Pr}_{R,Vap}}\right) \tag{1.82}$$

$$Nu_{R.b} = 0.725\left(\frac{Ga\,\mathrm{Pr}_{R,Liq}}{H_{R,Liq}}\right)^{0.25}\left\{1.0+0.003\sqrt{\mathrm{Pr}_{R,Liq}}C_3^{\,3.1-\frac{0.5}{\mathrm{Pr}_{R,Liq}}}\right\}^{0.3}\left(1.0+C_2C_4\right)^{-0.25} \tag{1.83}$$

Dimensionless flow volume

$$\bar{G}_{R,Liq} = \frac{G_R}{D_{In}\mu_{R,Liq}} \tag{1.84}$$

Galileo number

$$Ga = \frac{gD_{In}^3}{\upsilon_{Liq}^2} \tag{1.85}$$

Latent heat of evaporation

$$hv_R = h_{R,Vap} - h_{R,Liq} \tag{1.86}$$

Sensible heat/latent heat ratio

$$H_{R,Vap} = \frac{Cp_{R,Vap}\left(T_R - T_w\right)}{hv_R} \qquad \left(0 \le x_R \le 1\right) \tag{1.87}$$

$$H_{R,Liq} = \frac{Cp_{R,Liq}\left(T_R - T_w\right)}{hv_R} \qquad \left(0 \le x_R \le 1\right) \tag{1.88}$$

$$C_1 = 0.071\mathrm{Re}_{R,Liq}^{0.1}\left(\frac{\rho_{R,Liq}}{\rho_{R,Vap}}\right)^{0.55}\left(\frac{x_R}{1-x_R}\right)^{0.2-0.1x_R}\left(\mathrm{Pr}_{R,Liq} + \frac{8\times10^3}{\mathrm{Re}_{R,Liq}^{1.5}}\right)^{\frac{1}{3}} \tag{1.89}$$

$$C_2 = \frac{\left\{1+1.6\times10^{11}\left(\frac{H_{R,Liq}}{\mathrm{Pr}_{R,Liq}}\right)^5\right\}^{\frac{1}{4}}}{\sqrt{\frac{\rho_{R,Liq}}{\rho_{R,Vap}}}} \times \left\{\frac{\left(\frac{Ga\cdot\mathrm{Pr}_{R,Liq}}{H_{R,Liq}}\right)^{\frac{1}{4}}}{\bar{G}_{R,Liq}\frac{x_R}{1-x_R}}\right\}^{1.8} \tag{1.90}$$

$$C_3 = 0.47\sqrt{\frac{\rho_{R,Liq}}{\rho_{R,Vap}}}\left(\frac{H_{R,Liq}}{\mathrm{Pr}_{R,Liq}}\right)^{\frac{1}{12}}\frac{\left(\mathrm{Re}_{R,Liq}\frac{x_R}{1-x_R}\right)}{\left(\frac{Ga\,\mathrm{Pr}_{R,Liq}}{H_{R,Liq}}\right)^{\frac{1.1}{4}}} \tag{1.91}$$

$$C_4 = 20\exp\left(-\frac{\bar{G}_{R,Liq}}{3\times10^3}\right) \tag{1.92}$$

$$\mathrm{Pr}_{R,Liq} = \frac{\mu_{R,Liq}\cdot Cp_{R,Liq}}{\lambda_{R,Liq}} \tag{1.93}$$

$$\mathrm{Pr}_{R,Vap} = \frac{\mu_{R,Vap}\cdot Cp_{R,Vap}}{\lambda_{R,Vap}} \tag{1.94}$$

The equation of Seshita, et al. is used to obtain air-side heat-transfer coefficients and pressure loss.

$$\alpha_{Out} = \frac{Nu_A \lambda_A}{D_{ec}} \tag{1.95}$$

To obtain the physical properties of air, the arithmetic mean value of the inlet and outlet temperatures of the heat exchanger is used.

$$\rho_A = f_\rho\left(\frac{P_{A,In}+P_{A,Out}}{2}, \frac{T_{A,In}+T_{A,Out}}{2}\right) \tag{1.96}$$

$$\mu_A = f_\mu\left(\frac{P_{A,In}+P_{A,Out}}{2}, \frac{T_{A,In}+T_{A,Out}}{2}\right) \tag{1.97}$$

$$\upsilon_A = \frac{\mu_A}{\rho_A} \tag{1.98}$$

$$\lambda_A = f_\lambda\left(\frac{P_{A,In}+P_{A,Out}}{2}, \frac{T_{A,In}+T_{A,Out}}{2}\right) \tag{1.99}$$

Fin heat-transfer area taking frost into consideration

$$A_{FIN,s} = 2\frac{L}{F_P}\left(L_x \cdot L_y - \left(\frac{D_C+2H}{2}\right)^2\right) \tag{1.100}$$

Face area A_f

$$A_f = L_y \cdot F_p \tag{1.101}$$

Tube flow heat-transfer area A_{In}

$$A_{In} = L \cdot D_{In}\pi \tag{1.102}$$

Fin collar diameter D_c

$$D_c = D_{out} + 2F_t \tag{1.103}$$

Tube heat-transfer area $A_{Pipe,s}$

$$A_{Pipe,s} = \frac{\theta}{\pi}\cdot(D_c+2H)\cdot\pi\left(L - \frac{L}{F_P}(F_T+2H)\right) \tag{1.104}$$

Total heat-transfer area $A_{Out,s}$

$$A_{Out,s} = A_{FIN} + A_{Pipe} \tag{1.105}$$

Free passage volume $V_{c,s}$

$$V_{c,s} = \left(F_p - F_t - 2H\right)\left(L_y \cdot L_x - \frac{\pi}{4}(D_C + 2H)^2\right) \quad (1.106)$$

Mean free passage cross section $A_{c,s}$

$$A_{c,s} = \frac{V_{c,s}}{L_x} = \frac{\left(F_p - F_t - 2H\right)\left(L_y \cdot L_x - \frac{\pi}{4}(D_C + 2H)^2\right) \cdot A_f}{L_y \cdot L_x \cdot F_p} \quad (1.107)$$

Face velocity $v_{A,f}$

$$v_{A,f} = \frac{G_{A,I}}{\rho_{A,I}\left(L_y \cdot L\right)} \quad (1.108)$$

Representative wind velocity based on mean free passage cross section Ac $v_{A,Cha,s}$

$$v_{A,Cha,s} = \frac{A_f \cdot \rho_{A,I} \cdot v_{A,f}}{A_{c,s} \cdot \rho_A} \quad (1.109)$$

Representative dimension based on mean free passage cross section Ac $D_{ec,s}$

$$D_{ec,s} = \frac{4A_{c,s} \cdot L_x}{A_{Out,s}} \quad (1.110)$$

Reynolds number Res is defined by the following equation.

$$\mathrm{Re}_{A,s} = \frac{v_{A,Cha,s} \cdot D_{ec,s}}{\upsilon_A} \quad (1.111)$$

Figure 5 shows free passage volume.

Figure 6 shows mean free passage cross section.

Figure 7 shows face area.

Figure 8 shows inner, outer, and collar diameters.

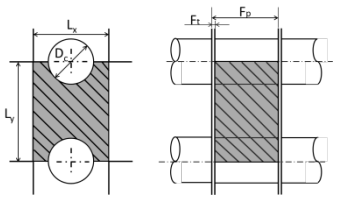

Figure 5: Free passage volume Vc

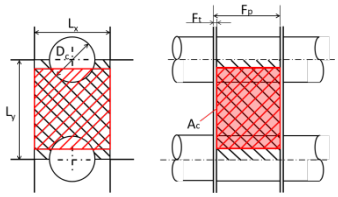

Figure 6: Mean free passage cross section Ac

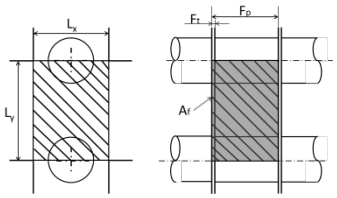

Figure 7: Face area A_f

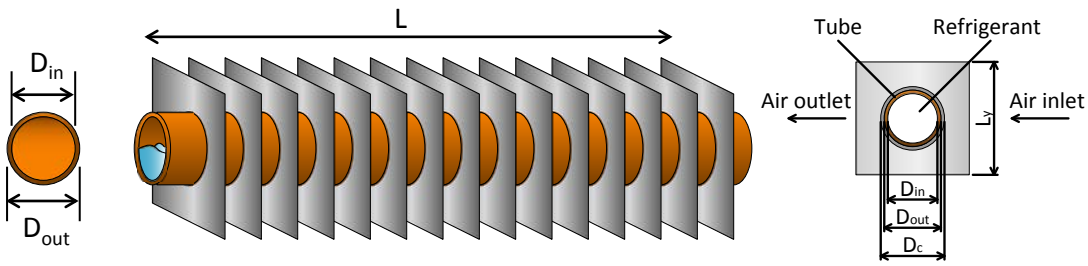

Figure 8: Heat exchanger

$$Nu_{A,s} = \begin{cases} 2.1\left(\dfrac{\mathrm{Re}_{A,s}\,\mathrm{Pr}_A\,D_{ec,s}}{L_x}\right)^{0.38} \\ \text{(for the first row)} \\ 2.1\left(\dfrac{\mathrm{Re}_{A,s}\,\mathrm{Pr}_A\,D_{ec,s}}{L_x}\right)^{0.47} \\ \text{((for the second row or backward)} \end{cases} \quad (1.112)$$

$$\eta_{FIN,s} = \frac{1}{1+\dfrac{\dfrac{1}{\dfrac{1}{\alpha_A}+\dfrac{1}{\lambda_s}}\left(D_{FIN}-D_c\right)^2\left(D_{FIN}/D_c\right)^{0.5}}{6\lambda_{FIN}F_t}} \quad (1.113)$$

$$D_{FIN} = \sqrt{\frac{4L_xL_y}{\pi}} \quad (1.114)$$

Air-side pressure loss is obtained from the equation by Seshita, et al.

$$f_{A,s}\frac{L_x}{D_{ec,s}} = \begin{cases} 0.43+3.51\left(\mathrm{Re}\dfrac{D_{ec,s}}{L_x}\right)^{-1.07} \\ \text{(for the first row)} \\ 0.83+24.7\left(\mathrm{Re}\dfrac{D_{ec,s}}{L_x}\right)^{-0.89} \\ \text{(for the second row or backward)} \end{cases} \quad (1.115)$$

To the frost growth model in this study, a growth model proposed by B. J. Jones, et al. is applied. In this model, frost layer density changes with time, and the thermophysical property of the frost layer remains constant in the direction of frost height.

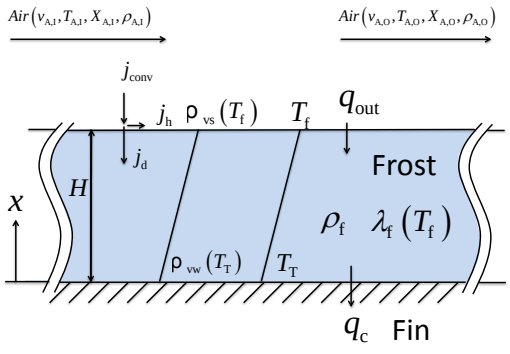

Figure 9: Frost model

Mass balance in a frost layer is expressed as shown below. In the equation, j_{conv} is the water vapor mass flux from mainstream air, j_d is the water vapor mass flux that permeates the frost layer and increases frost density, and j_h is the water vapor mass flux that increases frost height.

$$\frac{d\rho_f}{dt}H + \frac{dH}{dt}\rho_f = j_{conv} \tag{1.116}$$

The change of frost layer density with time is defined as follows.

$$j_d \equiv \frac{d\rho_f}{dt}H \tag{1.117}$$

The change of frost layer height with time is defined as follows.

$$j_h \equiv \frac{dH}{dt}\rho_f \tag{1.118}$$

The migration of water vapor into the frost layer is calculated using Fick's law of diffusion.

Assuming that the concentration of water vapor changes linearly in the perpendicular direction to the fin surface, the distribution of water vapor concentration shall be linearly determined by the concentration of water vapor on the frost surface and that on the fin surface. When frost porosity and tortuosity are factored in, the migration and diffusion of water vapor in the frost layer can be expressed as follows.

$$\frac{d\rho_f}{dt}H = D_s\frac{(1-\rho_f/\rho_{ice})}{\tau}\frac{\rho_{vs}-\rho_{vw}}{H} \tag{1.119}$$

$$\tau = 1.1 \tag{1.120}$$

In this study, heat-transfer coefficients and pressure loss coefficients are calculated using the equations proposed in the reference. Each of the heat transfer between refrigerant and heat exchanger tube, heat exchanger tube and frost, and frost and air is defined as follows.

$$q_{In} = \alpha_{In}(T_R - T_T) \tag{1.121}$$

$$q_C = \frac{\lambda_f}{H}(T_f - T_T) \tag{1.122}$$

$$q_{Out} = \alpha_{Out}\frac{(T_f - T_{A,I}) - (T_f - T_{A,O})}{\ln\left(\frac{T_f - T_{A,I}}{T_f - T_{A,O}}\right)} \tag{1.123}$$

The clearance δ, which is an air flow path between fins, is expressed as follows.

$$\delta = L_{FIN,pit} - L_{FIN,T} - 2H \tag{1.124}$$

The influence of frost formation will be seen as an increase in thermal resistance in Equation (1.122), and as a decrease in air flow volume in Equation (1.124) because of a narrowed air flow path.
The following is the mathematical model of an accumulator.

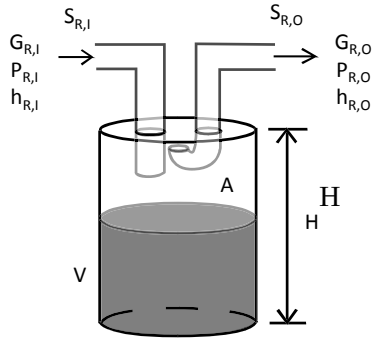

Figure 10: Accumulator

Equation of continuity

$$V\frac{d\rho_{\mathrm{R}}}{dt}+\rho_{\mathrm{R,O}}v_{\mathrm{R,O}}S_{\mathrm{R,O}}-\rho_{\mathrm{R,I}}v_{\mathrm{R,I}}S_{\mathrm{R,I}}=0 \tag{1.135}$$

Energy equation

$$V\frac{d\left(\rho_{\mathrm{R}}u_{\mathrm{R}}\right)}{dt}+\rho_{\mathrm{R,O}}v_{\mathrm{R,O}}S_{\mathrm{R,O}}h_{\mathrm{R,O}}-\rho_{\mathrm{R,I}}v_{\mathrm{R,I}}S_{\mathrm{R,I}}h_{\mathrm{R,I}}=0 \tag{1.136}$$

Equation of pressure loss

$$P_{\mathrm{I}}=P \tag{1.137}$$

$$P_{\mathrm{O}}=P \tag{1.138}$$

If there is a liquid in the accumulator (when the degree of dryness is between 0 and 1), saturated vapor shall flow out of the accumulator outlet.

$$h_{\mathrm{R,O}}=\begin{cases}h_{\mathrm{R}} & \left(x_{\mathrm{R}}=0,x_{\mathrm{R}}=1\right)\\ h_{\mathrm{R,sat,Va}} & \left(0<x_{\mathrm{R}}<1\right)\end{cases} \tag{1.139}$$

Equation of state

$$\rho_{\mathrm{R}}=f_{\rho}\left(P_{\mathrm{R}},h_{\mathrm{R}}\right) \tag{1.140}$$

$$\rho_{\mathrm{R,I}}=f_{\rho}\left(P_{\mathrm{R,I}},h_{\mathrm{R,I}}\right) \tag{1.141}$$

$$\rho_{\mathrm{R,O}}=f_{\rho}\left(P_{\mathrm{R,O}},h_{\mathrm{R,O}}\right) \tag{1.142}$$

$$x_{\mathrm{R}}=f_{\mathrm{x}}\left(P_{\mathrm{R}},h_{\mathrm{R}}\right) \tag{1.143}$$

$$u_{\mathrm{R}}=f_{\mathrm{u}}\left(P_{\mathrm{R}},h_{\mathrm{R}}\right) \tag{1.144}$$

$$h_{\mathrm{R,sat,Va}}=f_{\mathrm{sat,Va}}\left(P_{\mathrm{R}}\right) \tag{1.145}$$

Others

$$G_{R,I}=v_{R,I}S_{R,I} \tag{1.146}$$

$$G_{R,O}=v_{R,O}S_{R,O} \tag{1.147}$$

Variables

$G_{R,O}, P_R, P_{R,O}, h_R, h_{R,O}, h_{R,SAT,Va},$
$\rho_R, \rho_{R,I}, \rho_{R,O}, x_R, u_R, v_{R,I}, v_{R,O},$

Equation of discretization

Equation of continuity

$$V\frac{\rho_{\mathrm{R}}^{t}-\rho_{\mathrm{R}}^{t-\Delta t}}{dt}+\rho_{\mathrm{R,O}}^{t}v_{\mathrm{R,O}}^{t}S_{\mathrm{R,O}}^{t}-\rho_{\mathrm{R,I}}^{t}v_{\mathrm{R,I}}^{t}S_{\mathrm{R,I}}^{t}=0 \tag{1.148}$$

Energy equation

$$V\frac{\rho_{\mathrm{R}}^{t}u_{\mathrm{R}}^{t}-\rho_{\mathrm{R}}^{t-\Delta t}u_{\mathrm{R}}^{t-\Delta t}}{dt}+\rho_{\mathrm{R,O}}^{t}v_{\mathrm{R,O}}^{t}S_{\mathrm{R,O}}^{t}h_{\mathrm{R,O}}^{t}-\rho_{\mathrm{R,I}}^{t}v_{\mathrm{R,I}}^{t}S_{\mathrm{R,I}}^{t}h_{\mathrm{R,I}}^{t}=0 \tag{1.149}$$

The following is the mathematical model of a piping.

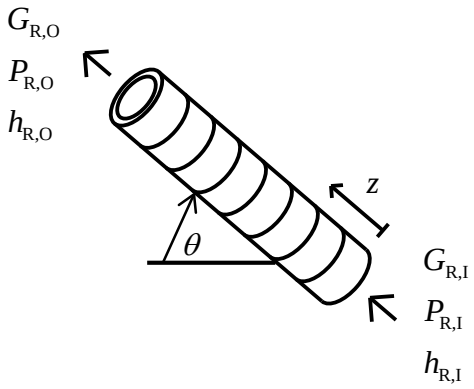

Figure 11: Pipe

Refrigerant-side equation of continuity

$$\frac{\partial\rho_{\mathrm{R}}}{\partial t}+\frac{\partial\left(\rho_{\mathrm{R}}v_{\mathrm{R}}\right)}{\partial z}=0 \tag{1.150}$$

Refrigerant-side pressure loss

$$\frac{\partial P_{\mathrm{R}}}{\partial z}=-f_{\mathrm{R}}\frac{1}{d_{\mathrm{In}}}2\rho_{\mathrm{R}}v_{\mathrm{R}}^{2}-\rho_{\mathrm{R}}g\sin\theta \tag{1.151}$$

Refrigerant-side energy equation

$$\frac{\partial\left(\rho_{\mathrm{R}}u_{\mathrm{R}}\right)}{\partial t}+\frac{\partial\left(\rho_{\mathrm{R}}v_{\mathrm{R}}h_{\mathrm{R}}\right)}{\partial z}=-\frac{Lc_{\mathrm{In}}}{S_{\mathrm{In}}}q_{\mathrm{In}} \tag{1.152}$$

Piping-side energy equation

$$\rho_{\mathrm{M}}C_{\mathrm{M}}\frac{\partial T_{\mathrm{M}}}{\partial t}=\frac{Lc_{\mathrm{In}}}{S_{\mathrm{M}}}q_{\mathrm{In}} \tag{1.153}$$

Heat transfer

$$q_{\mathrm{In}}=\alpha_{\mathrm{In}}\left(T_{\mathrm{R}}-T_{\mathrm{M}}\right) \tag{1.154}$$

Others

$$L_{\mathrm{In}} = \pi d_{\mathrm{In}} \tag{1.155}$$

$$S_{\mathrm{In}} = \frac{\pi d_{\mathrm{In}}^2}{4} \tag{1.156}$$

Equation of state

$$T_{\mathrm{R}} = f_{\mathrm{T}}(P_{\mathrm{R}}, h_{\mathrm{R}}) \tag{1.157}$$

$$\rho_{\mathrm{R}} = f_{\rho}(P_{\mathrm{R}}, h_{\mathrm{R}}) \tag{1.158}$$

$$u_{\mathrm{R}} = h_{\mathrm{R}} - \frac{P_{\mathrm{R}}}{\rho_{\mathrm{R}}} \tag{1.159}$$

Inlet and outlet conditions
When z=0

$$G_{\mathrm{R,I}} = \rho_{\mathrm{R}} v_{\mathrm{R}} S_{\mathrm{In}} \tag{1.160}$$

$$P_{\mathrm{R,I}} = P_{\mathrm{R}} \tag{1.161}$$

$$h_{\mathrm{R,I}} = h_{\mathrm{R}} \tag{1.162}$$

When z= L_{HEX}

$$G_{\mathrm{R,O}} = \rho_{\mathrm{R}} v_{\mathrm{R}} S_{\mathrm{In}} \tag{1.163}$$

$$P_{\mathrm{R,O}} = P_{\mathrm{R}} \tag{1.164}$$

$$h_{\mathrm{R,O}} = h_{\mathrm{R}} \tag{1.165}$$

The following is the mathematical model of a branch pipe.

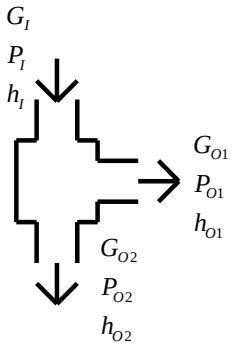

Figure 12: Branch pipe

Equation of continuity

$$\rho_{\mathrm{R,O1}} v_{\mathrm{R,O1}} S_{\mathrm{R,O1}} + \rho_{\mathrm{R,O2}} v_{\mathrm{R,O2}} S_{\mathrm{R,O2}} - \rho_{\mathrm{R,I}} v_{\mathrm{R,I}} S_{\mathrm{R,I}} = 0 \tag{1.166}$$

Energy equation

$$\rho_{\mathrm{R,O1}} v_{\mathrm{R,O1}} h_{\mathrm{R,O1}} S_{\mathrm{R,O1}} + \rho_{\mathrm{R,O2}} v_{\mathrm{R,O2}} h_{\mathrm{R,O2}} S_{\mathrm{R,O2}} - \rho_{\mathrm{R,I}} v_{\mathrm{R,I}} h_{\mathrm{R,I}} S_{\mathrm{R,I}} = 0 \tag{1.167}$$

Differential pressure balance

$$P_{\mathrm{I}} = P_{\mathrm{O1}} \quad (1.168)$$

$$P_{\mathrm{I}} = P_{\mathrm{O2}} \quad (1.169)$$

Inlet and outlet flow volumes

$$G_{\mathrm{R,I}} = \rho_{\mathrm{R,I}} v_{\mathrm{R,I}} S_{\mathrm{R,I}} \quad (1.170)$$

$$G_{\mathrm{R,O1}} = \rho_{\mathrm{R,O1}} v_{\mathrm{R,O1}} S_{\mathrm{R,O1}} \quad (1.171)$$

$$G_{\mathrm{R,O2}} = \rho_{\mathrm{R,O2}} v_{\mathrm{R,O2}} S_{\mathrm{R,O2}} \quad (1.172)$$

Equation of state

$$\rho_{\mathrm{R,I}} = f_{\rho}\left(P_{\mathrm{R,I}}, h_{\mathrm{R,I}}\right) \quad (1.173)$$

$$\rho_{\mathrm{R,O1}} = f_{\rho}\left(P_{\mathrm{R,O1}}, h_{\mathrm{R,O1}}\right) \quad (1.174)$$

$$\rho_{\mathrm{R,O2}} = f_{\rho}\left(P_{\mathrm{R,O2}}, h_{\mathrm{R,O2}}\right) \quad (1.175)$$

Other

$$h_{\mathrm{R,O1}} = h_{\mathrm{R,O2}} \quad (1.176)$$

Variables

$G_{R,O1}, G_{R,O2}, P_{R,O1}, P_{R,O2}, h_{R,O1}, h_{R,O2},$

$\rho_{R,I}, \rho_{R,O2}, \rho_{R,O2}, v_{R,I}, v_{R,O1}, v_{R,O2},$

The following are the conditions used for simulations.

Table 1: Simulation conditions

Outdoor temperature, ^{o}C	2(Dry)/1(Wet)
Indoor temperature, ^{o}C	20(Dry)/14(Wet)

Table 2: Driving conditions

Outdoor air flow volume	Experimental data
Indoor air flow volume	Constant
Compressor rotational speed	Constant
Expansion valve opening	Super heat control

Table 3: Frost first conditions

Frost thickness, mm	0.01
Frost density, kg/m^3	10

The analysis technique used in this study is based on a modular analysis theory. This specifically means discretizing the governing equations of composing elements. Based on the flow volume, pressure, and enthalpy of the fluid that flows into and flows out of each composing element, the conditions for connecting these elements, and the boundary conditions for the entire system, are determined so that these physical properties will be the

same at each connecting point. By doing so, the mathematical structure of a thermohydrodynamic system can be clearly defined, and then the governing equations for the entire system can be completed. These equations are nonlinear equations. By providing solution-finding algorithms that conduct convergence calculations, nonsteady solutions can be derived.

1.4 Experiment

This experimental equipment is a refrigerating cycle, made up of a compressor, a heat exchanger, and an expansion valve connected in a loop. The refrigerant is recirculated in the equipment. Figure 13 shows the outdoor heat exchanger. Table 4 lists the equipment's range of operating conditions.

Figure 13: Outdoor heat exchanger

Table 4: Experimental equipment

Equipment name		Operating range
Outdoor testing	Air conditioner	Temperature:

room		–20ºC to +52ºC Humidity: 30 to 90%RH
	Air flow volume measurement device	10.5－137㎥/min
Indoor testing room	Air conditioner	Temperature: 0ºC to +52ºC Humidity: 30 to 90%RH Amount of humidification: 15 Lt/H

The following is a description of measurement using this experiment equipment.

The following temperatures are measured: the compressor's suction and discharge temperatures, the outdoor heat exchanger's inlet, outlet, and intermediate refrigerant temperatures, the outdoor supercooling heat exchanger's inlet and outlet temperatures, the expansion valve's inlet and outlet temperatures, the indoor heat exchanger's inlet and outlet refrigerant temperatures, the outdoor heat exchanger's air discharge and suction temperatures, and the indoor heat exchanger's air discharge and suction temperatures.

The following pressures are measured: the compressor's inlet and outlet pressures, the expansion valve's inlet and outlet pressures, the outdoor heat exchanger's inlet and outlet pressures, pressure before the accumulator, and the indoor heat exchanger's inlet and outlet pressures.

In frost formation/defrosting experiments, the whole outdoor heat exchanger is placed on a weight scale to measure weight changes. By doing so, an increase or decrease of frost can be observed.

The following is the method for the frost formation experiment.

1. To remove frost from the heat exchanger, operate the heat pump as follows. After operating the heat pump in the low-temperature frost heating mode, stop the heating operation. Then operate the heat pump in the cooling mode for about 30 min for defrosting.
2. Set the compressor's frequency at a value for the no frost operation mode. Operate the heat pump in the heating mode for about an hour and stabilize the system.
3. Change the compressor's frequency to a value for the frost formation mode. Operate the heat pump in the heating (frost formation) mode for 35 min.
4. Stop the heating operation, and operate the heat pump in the cooling mode for about 30 min. After defrosting, measure the amount of drainage.
5. Same as 2.
6. Change the compressor's frequency to a value for the frost formation mode, and operate the heat pump in the heating (frost formation) mode for 25 min.
7. Same as 4.
8. Same as 2.
9. Change the compressor's frequency to a value for the frost formation mode, and operate the heat pump in the heating (frost formation) mode for 10 (5, 15, 20, 35) min. Measure the dynamic increment of frost formation.
10. Same as 4.

The following is the method for a frost formation/defrosting experiment.

1. Continue raising the compressor's frequency step by step, and keep the fan rotating speed constant in both the indoor unit and the outdoor unit.
2. When the temperature detected by the TE sensor meets a specific condition, the heat pump automatically enters the defrosting mode. The fans stop in the defrosting mode.

3. After returning the defrosting mode, the heat pump starts the heating operation about 50 seconds after the compressor and the outdoor fan stopped.
4. In this experiment, measure five frost formation/defrosting cycles, and use the data obtained from the last three cycles.
5. Calculate the arithmetic mean value for each of the measured data to obtain corresponding experiment value.

1.5 Experimental Conditions

Table 5 shows indoor suction air temperature and outdoor suction air temperature. These are the standard rating conditions (low temperature) for heating performance tests specified in Japan Industrial Standard JIS B 8615-1 (Non-ducted air conditioners and heat pumps - Testing and rating for performance).

Table 5: Experimental conditions

Outdoor temperature, °C	2(Dry)/1(Wet)
Indoor temperature, °C	20(Dry)/14(Wet)

1.6 Results and Discussion

The following are the results of numerical simulations.

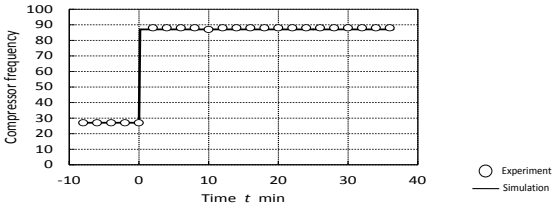

Figure 14: Compressor frequency input

Figure 14 shows compressor frequency input results. Figure 15 shows the results of frost weight changes, indicating that frost weight almost linearly increases with time. Note that the increase of frost weight lags behind the elapsed time. This phenomenon is considered attributable to the time lag between when the compressor's frequency was raised step and step, and when evaporation temperature began to decrease. Or the phenomenon may have occurred because the moisture that adhered to the fin surface remained supercooled water drops without freezing.

Figure 16 shows refrigerant temperatures at the outlet of the evaporator. The figure shows that raising the compressor's frequency step by step decreases refrigerant temperatures. The figure also indicates that the temperature of frost declines as it grows more. This phenomenon is considered attributable to the following. When frost begins to adhere to the fin surface, the quantity of heat exchanged on the evaporator becomes smaller, and the heat pump begins to squeeze the expansion valve to keep the degree of superheat constant. As a result, both evaporation temperature and evaporating pressure decline. As shown in Figure 17, the numerical calculation of power consumption agreed with its experiment result relatively well.

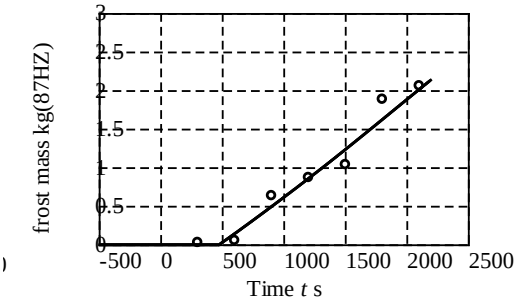

Figure 15: Frost mass

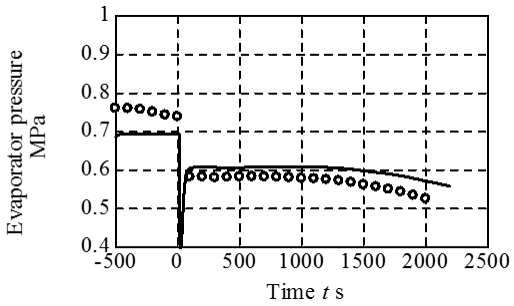

Figure 16: Evaporator pressure

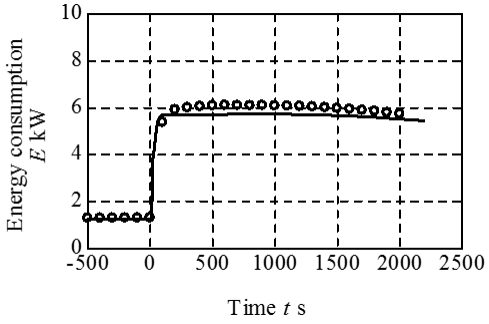

Figure 17: Energy consumption

Figure 18, Figure 19, and Figure 20 show the results of frost formation/defrosting experiments. These results show that the weight of the evaporator increased after the compressor's frequency was raised, and that the weight decreased during the defrosting mode. Immediately after the compressor started, the weight of the evaporator decreased. The moment the heat pump was switched to the defrosting mode, the weight of the evaporator increased. This phenomenon is considered attributable to the following. Immediately after the compressor started, the outdoor heat exchanger worked as an evaporator, decreasing the pressure of refrigerant inside, and decreasing the total weight temporarily. On the other hand, when the heat pump is switched to the defrosting mode, the refrigerant in the outdoor heat exchanger begins to flow backward, now working as a condenser. As a result, the pressure of the refrigerant inside the outdoor heat exchanger increased, which is considered to increase the total weight.

Figure 21 shows the ph diagrams of the refrigeration cycle. The figure shows that as frost grows more, the whole diagrams move downward. When frost begins to adhere to the fin surface, the quantity of heat exchanged on the evaporator becomes smaller, and the heat pump begins to squeeze the expansion valve to keep the degree of superheat constant. As a

result, both evaporation temperature and evaporating pressure decline, and the whole diagrams are considered to move downward.

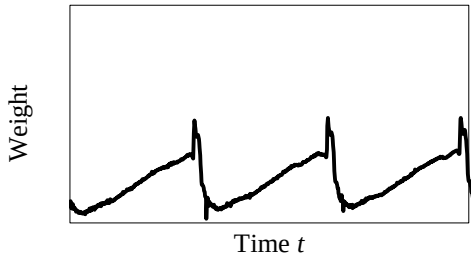

Figure 18: Weight

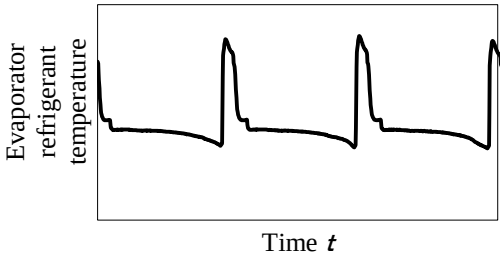

Figure 19: Evaporator refrigerant temperature

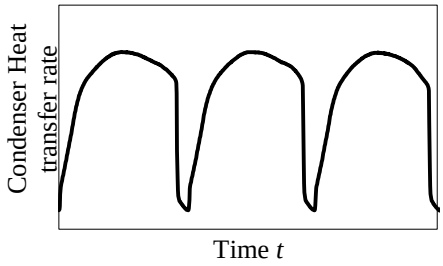

Figure 20: Condenser heat transfer rate

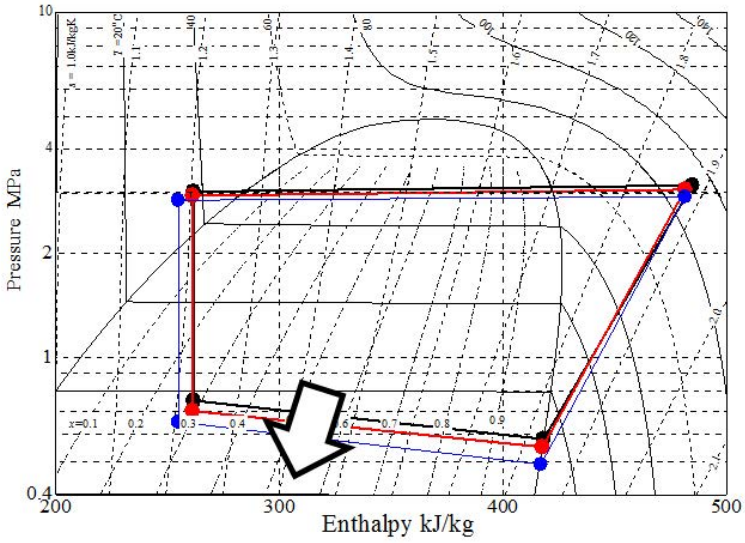

Figure 21: Ph diagram

1.7 Conclusion

In this study, NEDO conducted numerical simulations for each composing element of a heat pump, taking into consideration frost growth on a heat exchanger. At the same time, in order to ensure the validity of the NEDO-developed frost model, experiments were conducted using a compression heat pump under the same conditions as for the numerical simulations, and the experimental results and the simulation results were compared. The results of simulated frost weight, evaporation temperature, and power consumption agreed well with their respective simulation results.

In addition, an experiment which repeated frost formation and defrosting cycles studied the influence of frost growth on a heat pump cycle, and clarified the behavior of the heat pump cycle during a defrosting operation.

It is thought that conducting numerical simulations on repeated frost formation/defrosting cycles could facilitate the study on heat pump operational methods, which will lead to further heating performance improvements in the future.

1.8 Denotations

Ds : diffusion factor, m^2/s
G : mass flow rate, $kg \cdot s^{-1}$
f : fanning friction factor, -
h : specific enthalpy, $J \cdot kg^{-1}$
j : mass flux, $kg \cdot m^{-2} \cdot s^{-1}$
M : mass, kg
L : length, m
F : length, m
D : length,-
A : area, m^2
P : pressure, Pa
X : absolute humidity, kg/kg(D.A.)
q : heat flux, $W \cdot m^{-2}$
t : time, s
T : temperature, ℃
U : wetted perimeter, m
u : specific internal energy, $J \cdot kg^{-1}$
v : velocity, $m \cdot s^{-1}$
H : frost layer thickness, m
α : heat transfer coefficient, $W \cdot m^{-2} \cdot K^{-1}$
λ : thermal conductivity, $W \cdot m^{-1} \cdot K^{-1}$
τ : flexibility, -
ρ : density, $kg \cdot m^{-3}$
δ : gap, m
Re : reynolds number,-

SUBSCRIPT
A : air
conv : convection
d : increase of density
f : frost
t : tube

FIN : fin
ice : ice
I : inlet
In : inside
O : outlet
Out : outside
p : pitch
t : thickness
R : refrigerant
s : frost surface
T : tube
v : vapor
w : fin surface
max : maximum
cha : characteristic

2 ANNUAL SPACE HEATING PERFORMANCE OF THE LATEST HEAT PUMP MODEL

2.1 Background

Task 3 in Annex 41 describes a quantitative perspective that energy performance of air conditioners can be improved in cold area.

Firstly, Figure 22 was presented at a workshop of Atlanta EXPO in fall 2011 and it compared space cooling/heating by heat pump equipment with a combination of space cooling by conventional air-conditioning equipment in summer and space heating by combustion type heaters in winter, in terms of annual primary energy consumption, annual operating cost and CO_2 emissions. The evaluation work was conducted for Minneapolis, a city in cold area of the United States, which is located up north from Chicago. The heat pump equipment for evaluation was a two-stage compressor for use in cold area with HSPF of 8.42 (or 2.47 in terms of space heating SPF) in Region V, a cold area in the United States.

The left figure shows that the heat pump equipment is less efficient than the combination of conventional air-conditioning equipment and combustion type heaters in respect of annual primary energy consumption, under the weather conditions in Minneapolis. From this result, it is mentioned here that heat pump equipment with a higher performance are needed for use in cold area.

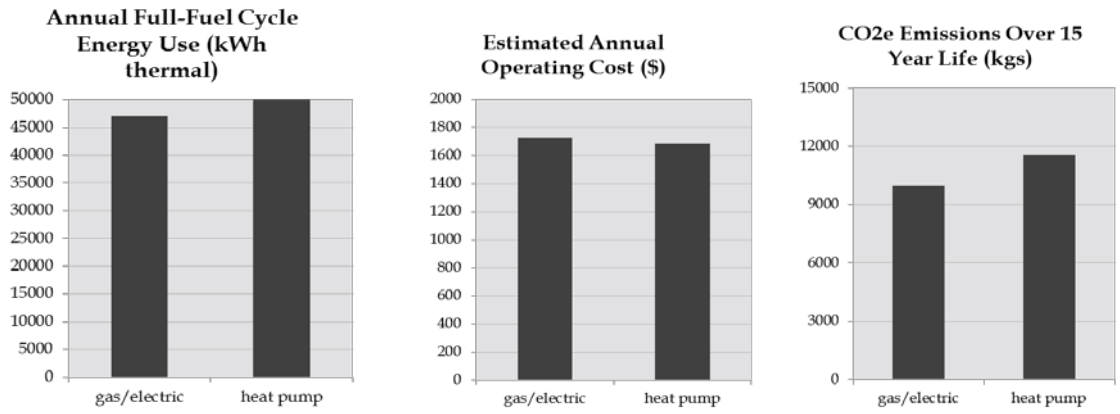

Figure 22: Comparison of "Best" HVAC Alternatives: Minneapolis, MN

"Best" Equipment Specifications:
Gas Furnace + Electric AC ≡ 98 AFUE and 13 SEER (3.8 cooling SPF)
Heat pump (2 Stage Heat Pump) ≡ 8.42 Region V HSPF and 17.4 SEER
(2.47 & 5.10 heating & cooling SPFs, respectively)

2.2 Evaluation Conditions

The Japan team has examined what level of performance improvement can be achieved by Japanese heat pump products in cold area with using APF, an annual performance indicator for heat pump equipment in Japan.

APF values are calculated with using the bin method, as is the case with EN14825 in Europe and ANSI/AHRI 210/240 in the United State. The bin method calculates annual performance based on the appearance time of each outdoor temperature in evaluation areas, characteristics of outdoor temperature and load, and characteristics of outdoor temperature and energy consumption.

$$\text{Power Consumption} = \frac{\text{Heating Capacity(Load)}}{\text{COP}}$$

To obtain energy consumption by using the above equation, it is clear that characteristics of outdoor temperature and COP according to load are required. The methods to derive characteristics of outdoor temperature and COP according to load are slightly different among respective indicators such as APF, SPF and SCOP. However, such methods basically derive an approximate curve method for outdoor temperature and COP from rated conditions or intermediate conditions. APF calculations are made by using this approximate curve method. For determination of APF in Japan, data of the five conditions in Table 6 below are necessary.

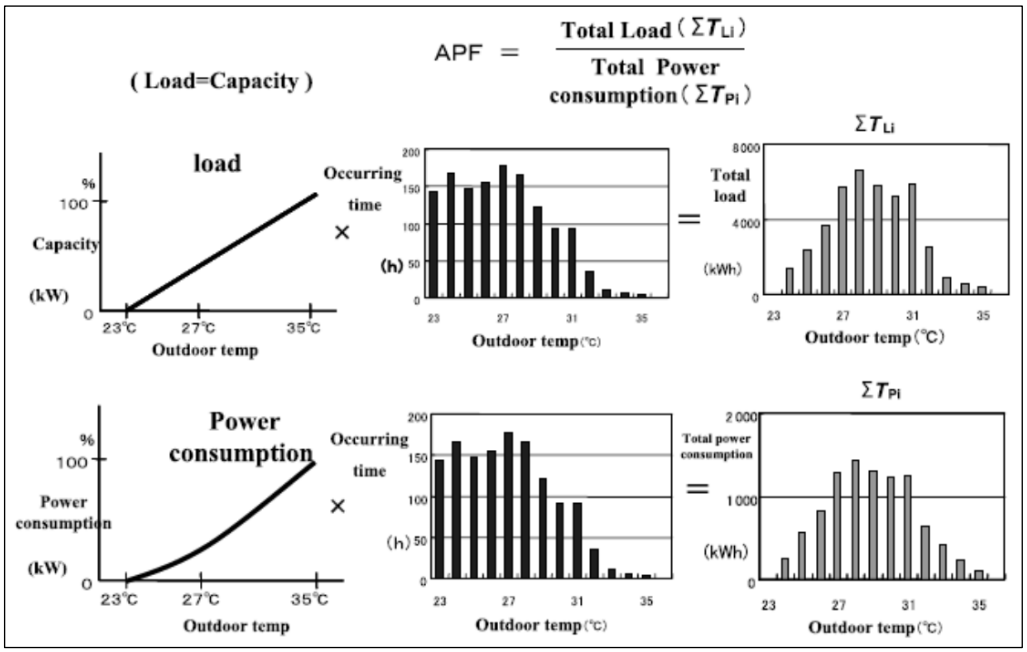

Figure 23: APF calculation concept

Table 6: Temperature and humidity conditions for calculating APFs

		Indoor		Outdoor	
		Dry Bulb (°C)	Wet Bulb (°C)	Dry Bulb (°C)	Wet Bulb (°C)
Cooling Condition	Rated capacity	27	19	35	24
	Intermediate Capacity	27	19	35	24
Heating Condition	Rated capacity	20	15	7	6
	Intermediate Capacity	20	15	7	6
	Maximum Capacity	20	15	2	1

2.3 Equipment Types Evaluated

Annual performance evaluation of the latest equipment types (Figure 24) with APF of 6.7 for annual space cooling/heating has been carried out in cold area in Japan this time as shown below. Table 7 gives the results of performance test on the above-mentioned five conditions for APF calculation.

Feature and specification
Rating heating capacity : 4kW
Seasonal performance(APF)
(Heating & cooling) : 6.7
Operating range : above -25℃
No additional heater is required

Figure 24: Evaluation heat pump model

Table 7: Performance measurement for APF calculation

		Measurment value				Measurement condition			
						Indoor		Outdoor	
		Capacity (kW)	Comsumption Electricity (kW)	COP		Dry Bulb (°C)	Wet Bulb (°C)	Dry Bulb (°C)	Wet Bulb (°C)
Cooling Condition	Rated capacity	3.6	0.773	4.66		27	19	35	24
	Intermediate Capacity	1.7	0.236	7.2		27	19	35	24
Heating Condition	Rated capacity	4	0.8	5		20	15	7	6
	Intermediate Capacity	1.8	0.258	6.98		20	15	7	6
	Maximum Capacity	5.1	1.61	4.83		20	15	2	1

2.4 Weather Conditions

Evaluation work has been conducted in Tokyo as well as Sendai, Sapporo and Asahikawa which are colder than Tokyo. Figure 25 below indicates changes in monthly average temperature and it is found that the monthly changes in Asahikawa and Minneapolis are similar.

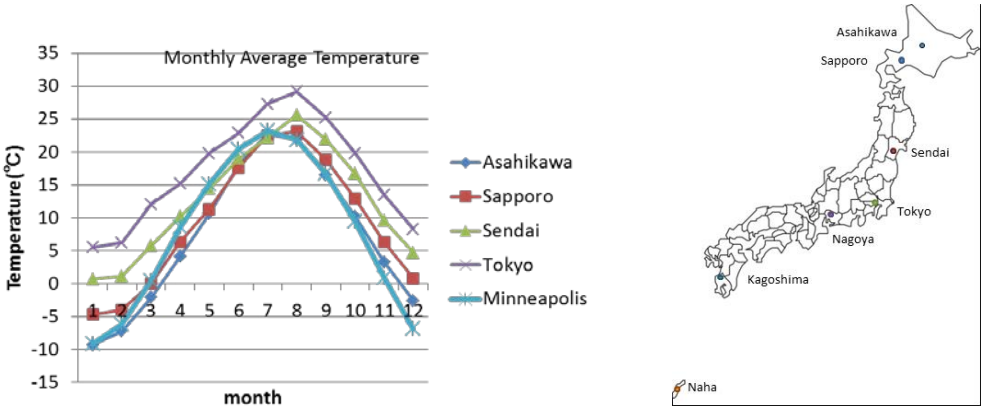

Figure 25: Meteorological data of several cities in Japan

2.5 Evaluation Result

The results of APF calculations are shown below in Table 8. The APF for annual space heating by this heat pump equipment is 3.05 in Asahikawa under similar weather conditions to those in Minneapolis, which is more excellent than that of combustion type heaters in terms of primary energy performance in the both cities.

Table 8: APF calculation results

location	Tokyo	Sendai	Sapporo	Asahikawa		Minneapolis
APF (for heating)	6.25	5.15	3.91	3.05		2.47(SPF for heating) 8.42(BTU/Wh)(HSPF)

2.6 Conclusion

In summary, annual space heating performance of the latest equipment with APF of 6.7 (Tokyo) has been evaluated in cold area. As a result, APF for space heating by this equipment is 3.05 in Asahikawa (Hokkaido) whose outdoor temperature conditions are quite similar to those in Minneapolis, the United States. Consequently, it is found that primary energy consumption is highly reduced compared to that consumed in combustion type heaters in this cold weather conditions.

3 REFERENCES

Aoki, K. Japan Society of Refrigerating and Air Conditioning Engineers, (1990) (in Japanese).

Chisholm, D. International Journal of Heat and Mass Transfer, 10 (12), 1767 (1967).

Jones, B.J., et. al., Trans ASME, Journal of Heat Transfer, 97, 255, (1975).

Kondepudi, S.N.and D.L.O'Neal, Int.J, Refrigeration, 12(3),151 (1989).

Nozu, S. (in Japanese).

Uselton, D. and Baxter, V. "Residential Heat Pump Life Cycle Climate Performance (LCCP) in North America." Lennox Industries Inc., Oak Ridge National Laboratory. IEA Heat Pumping Technology Work Shop at Atlanta 2011.

Yoshida, S., K.Nishikawa, et al., Refrigeration, 58 (666), 331 (1983) (in Japanese).

Japan Team Report

IEA HPT TCP Annex 41
"Cold Climate Heat Pumps"

Task 4 – Suggested/Recommended Future Work

April 2017

TABLE OF CONTENTS

LIST OF FIGURES

1 SUGGESTIONS FOR TASK 2, CHAPTER 1

The following suggestions apply to Chapter 1 of Task 2, entitled "Frost Formation between Concave- and Convex-Patterned Flat Plates under Forced Convection: Development of Analytical and Predictive Techniques for Frost Layer Growth."

- The predictive model has demonstrated its capability to quantitatively predict the influence of various factors on frost layer growth. However, evaluating the influence of volumetric air flow rate on frost growth, and predicting and evaluating frost growth in a much colder environment, are considered difficult to accomplish within the scope of this experiment. The challenges NEDO should solve in the near future include predicting the change in a flow path, and estimating the time when the flow path is blocked. (Task 2). Continued modeling efforts will include:
- Comparison of frost formation on corrugated fins with this research data (to ensure the anti-frost stiffness).
- In addition, we will manufacture a heat exchanger prototype for automobiles as soon as possible and aim at practical application.
- We will provide a model to the simulation calculation of Task 3 and investigate whether it is possible to reproduce the actual phenomenon.
- Following the modeling and experimentation performed in Task 3, it is thought that conducting numerical simulations on repeated frost formation/defrosting cycles could facilitate the study on heat pump operational methods, which will lead to further heating performance improvements in the future. (Task 3). Specific areas for improvement include:
- Efficient defrosting operation study is possible through heat pump simulation by switching the operation mode to unsteady state.
- In addition, it is possible to predict the amount of frost through the data reduction of the relationship between the amount of frost and the heat pump temperature from the actual data of the heat pump.

2 SUGGESTIONS FOR TASK 2, CHAPTER 2

The following suggestions apply to Chapter 2 of Task 2, entitled "Thermosiphons Which Collect Heat from Surface Ground Layers for CO_2 Refrigeration Cycle in Cold Climates: Effect of Artery Tube on Performance."

- We have a plan as the future work as follows: The experiments corrugated tube without metal net reinforcement conducts to make sure the further detailed performance characteristics. After this, we will propose the feasibility research on the commercial practical use in Hokkaido to embed heat pipes and try heat recovery using foundation piles. The building under construction and renovation will be a target for this research.
- High performance heat pumps providing both high efficiency and large heating capacity for cold climate areas will be developed in the future.

3 SUGGESTIONS FOR TASK 2, CHAPTER 3

The following suggestions apply to Chapter 3 of Task 2, entitled "Frost-Free Air Source Heat Pump Water Heater System Integrated with Solid Desiccant."

- Experiments have been carried out to measure the adsorption and desorption characteristics of the desiccant-coated heat exchanger (DCHE), the key component of the frost-free system, and confirm whether frost-free can be realized and how long to keep it, whether the DCHE can be effectively regenerated under the condensation temperature of the heat pump. Experimental results show that frost-free operation can be realized and the frost-free operation times are 17, 20 and 42 mins at air

temperatures of 5, 2 and -7°C. And the DCHE can be regenerated at low temperature (around 50°C), so the condensation heat of the heat pump can be used to regenerate the DCHE. Furthermore, design calculation based on those experimental results was conducted to determine the physical characteristics of the DCHE and evaporator, the layout and dimensions of the heat pump unit. Results show that the heat pump unit at the dimensions of 700(height) x 1000 (width) x 300 (depth) mm, has a water heating capacity of 4.5 kW under ambient air conditions of 2°C and 80% (relative humidity). The next step in the research is to design and make a prototype of the heat pump unit, and test its performance.

- A flow chart of one cycle for the simulation is given in the Fig. 1. For adsorption mode (AD mode), there are two evaporators in the heat pump cycle: a desiccant-coated heat exchanger (1st evaporator) and an air-heat exchanger (2nd evaporator). Their evaporation temperatures ($T_{eva,1}$ and $T_{eva,2}$) differ, and can be determined in terms of the outside air temperature (T_{OA}) and dew point (DP) of the dehumidified air (AA), respectively, as follows:

$$T_{eva,1} = T_{OA} - \Delta T_1 \quad (1)$$

$$T_{eva,2} = DP + \Delta T_2 \quad (2)$$

For desorption mode (DE mode), the air-heat exchanger works as an evaporator and its evaporation temperature (T_{eva}) is determined based on the return air temperature (T_{RA}) as

$$T_{eva} = T_{RA} - \Delta T_3 \quad (3)$$

CO_2 is used as a working fluid in the proposed frost-free ASHPWH system. The minimum temperature difference method is adopted to determine the discharge pressure of the compressor (P_{high}) in the current work. For AD mode, P_{high} is a function of $T_{eva,2}$, the inlet and outlet water temperatures of the water-heat exchanger ($T_{w,in}$, $T_{w,out}$): P_{high}= P($T_{eva,2}$, $T_{w,in}$, $T_{w,out}$), while P_{high} is a function of T_{RA} and the outlet air temperature of the desiccant-coated heat exchanger (T_{DA}) for DE mode: P_{high}=P(T_{eva},T_{RA},T_{DA}). The electrical consumptions of the compressor are obtained by the following expressions, respectively,:

For AD mode: w_{ad}=w($T_{eva,2}$, P_{high}, η_{comp}, $q_{w,ad}$) [kW] (4)
For DE mode: w_{de}=w(T_{eva}, P_{high}, η_{comp}, $q_{a,heat}$) [kW] (5)

where, η_{comp} is the isentropic efficiency of the compressor; $q_{w,ad}$ represents the water heating load in AD mode, [kW], $q_{a,heat}$ is the required air heating load to regenerate the desiccant in DE mode, [kW].Note that the water heating load during DE mode ($q_{w,de}$) is equal to the electrical consumption of the compressor (w_{de}).

The moisture removal rate between the DCHE and evaporator during AD (mvap,ad) and DE modes are obtained by Eqs.(6) and (7), respectively,

$$m_{vap,ad} = m_{OA}(X_{OA} - X_{EA}) \quad [g/s] \quad (6)$$

$$m_{vap,de} = m_{RA}(X_{DA} - X_{RA}) \quad [g/s] \quad (7)$$

In following, the four factors (SHFad, SHFde, COPad and COPde) influencing the COP of the system are calculated by Eqs. (8-11), separately,

$$SHF_{ad} = \frac{\int_0^{\tau_{ad}} m_{OA}(T_{OA}-T_{EA})d\tau_{ad}}{\int_0^{\tau_{ad}}(m_{OA}(T_{OA}-T_{EA})+m_{vap,ad}\cdot\gamma)} \quad (8)$$

$$SHF_{de} = \frac{\int_0^{\tau_{de}} m_{RA}(T_{DA}-T_{RA})d\tau_{de}}{\int_0^{\tau_{ad}}(m_{RA}(T_{DA}-T_{RA})+m_{vap,de}\cdot\gamma)} \quad (9)$$

$$COP_{ad} = \frac{\int_0^{\tau_{ad}} q_{w,ad}d\tau_{ad}}{\int_0^{\tau_{ad}} w_{ad}d\tau_{ad}} \quad (10)$$

$$COP_{de} = \frac{\int_0^{\tau_{de}} q_{w,de}d\tau_{de}}{\int_0^{\tau_{ad}} w_{de}d\tau_{de}} \quad (11)$$

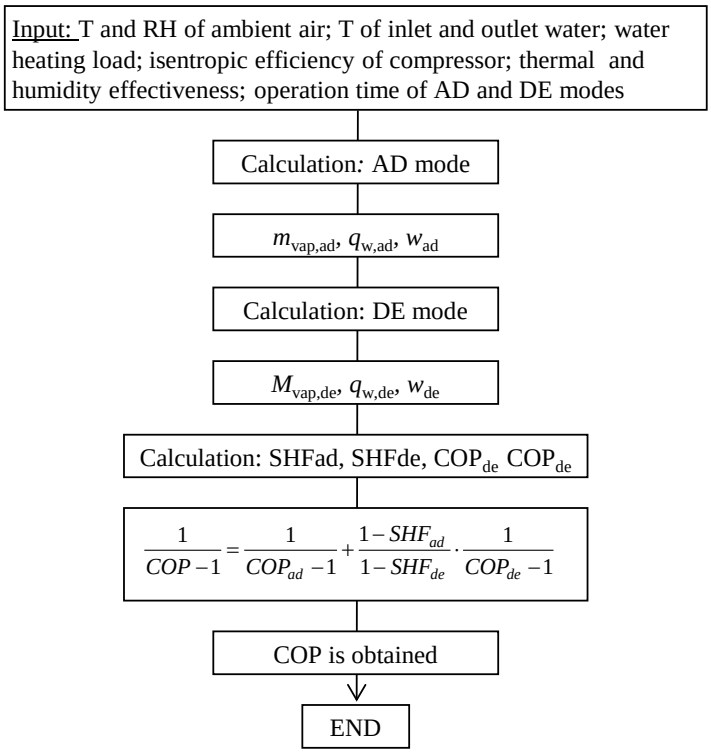

Figure 1: Flow chart of the simulation

U.S. Team Final Country Report

IEA HPT TCP Annex 41
"Cold Climate Heat Pumps"

Submitted by:

Ray Herrick Laboratories, Purdue University
Lead: Eckhard A. Groll (contact: groll@purdue.edu)
Contributors: Christian K. Bach (contact: cbach@okstate.edu)
Stephen L. Caskey (contact: scaskey@purdue.edu)
Alejandro C. Lavernia (contact: alaverni@purdue.edu)
Nicholas Salts (contact: nsalts@purdue.edu)

Oak Ridge National Laboratory
Lead: Van Baxter (contact: vdb@ornl.gov)
Contributors: Bo Shen
Omar Abdelaziz
C. Keith Rice
Gerald Groff, consultant
Gannate Khowailed, CSRA Inc.
Karen Sikes, CSRA Inc.

January 2017

TABLE OF CONTENTS

EXECUTIVE SUMMARY

In 2012 the International Energy Agency (IEA) Heat Pump Programme (now the Heat Pump Technologies (HPT) program) established Annex 41 to investigate technology solutions to improve performance of heat pumps for cold climates. Four IEA HPT member countries are participating in the Annex – Austria, Canada, Japan, and the United States (U.S.). The principal focus of Annex 41 is on electrically driven air-source heat pumps (ASHP) since that system type has the lowest installation cost of all heat pump alternatives. They also have the most significant performance challenges given their inherent efficiency and capacity issues at cold outdoor temperatures. Availability of ASHPs with improved low ambient performance would help bring about a much stronger heat pump market presence in cold areas, which today rely predominantly on fossil fuel furnace heating systems. US Annex 41 team activities focused on air-to-air ASHP system technologies using central air circulation as the heating energy distribution approach.

World energy consumption is projected to increase by 53% from about 530 EJ (505 quads) in 2008 to 810 EJ (770 quads) in 2035 (Conti et al., 2011). Energy consumption by OECD member countries is projected to increase by only 18% while that by non-OECD countries is projected to increase by 85% over this time span. Due to the increase in demand from non-OECD countries, it is expected energy prices will continue to increase from 2008 levels in spite of new developments in extraction methods such as fracking for natural gas or unconventional reserves such as oil tar sands. For the United States, current forecasts project the increase of energy prices (in 2011 dollars); Brent spot oil from $111 per barrel in 2011 to $163 per barrel in 2040, Henry Hub spot natural gas below $4 per million BTU through 2018 to $7.83 per million BTU in 2040, and mine mouth price of coal from $2.04 per million BTU in 2011 to $3.08 per million BTU in 2040 (EIA, 2013). In percentages, the predicted increase in the cost of energy is 47% for oil, roughly 90% for natural gas, and 51% for coal. These projected increases in fossil fuel prices could lead to increases in electricity prices of similar magnitude as well. With increases in consumption and costs of this magnitude, the urgency for reductions in U.S. energy consumption becomes evident.

The buildings sector in the United States accounted for about 42 EJ (40 quads) of primary energy consumption (~41% of the U. S. total) in 2010, making it the sector accounting for the largest consumption. The U.S. Energy Information Administration (EIA) projects this will increase by 17% by 2035. Space heating is responsible for ~22.5%, or roughly 9.5 EJ (9 quads) of this consumption (DOE, 2011). Fossil fuels account for about 6.7 EJ (6.3 quads) or 70% of the space heating energy consumption leaving a large potential for alternative heating methods employing electricity. Offsetting the consumption of fossil fuels on-site with electricity presents an opportunity to utilize renewable sources for power generation. Heat pumps are efficient technologies that employ electricity to achieve space heating where the heat output is a multiplier of the power consumption.

U.S. HEAT PUMP SHIPMENTS & TRENDS

U.S. heat pump shipments, along with most HVAC shipments, were significantly impacted by the economic recession and associated housing market decline, beginning in 2007 and intensifying over the next few years. When new single-family home construction drops (63 percent reduction in four years), the demand for new heat pumps is also depressed. The resulting steep drop in heat pump shipments between 2007 and 2009 is seen in Figure ES-1 (AHRI, 2010-2017; AHRI, 2012).

Since construction of new houses fell considerably during this time period, only 22% of heat pumps sold were installed in new homes during 2009; this indicates growing heat pump sales for add-on and replacement applications that usually require lower investments (Lapsa

and Khowailed, 2011). Furthermore, high energy prices led some consumers and businesses to make upgrades by replacing inefficient equipment, including older heat pumps, which assisted sales.The heat pump market has shown somewhat more resilience to the housing crisis and economic downturn compared to competing space heating technologies. Figure ES-2 displays how heat pump shipments compared to those of gas- and oil-fired warm air furnaces for the period 1990 to 2015. Compared to the market peaks in 2005-2006, heat pump shipments dropped by ~17% during the 2009-2012 period while combined gas and oil furnace shipments fell by ~35%. ASHP shipments rebounded starting in 2013 and exceeded the 2005-2006 levels in 2014-2015.

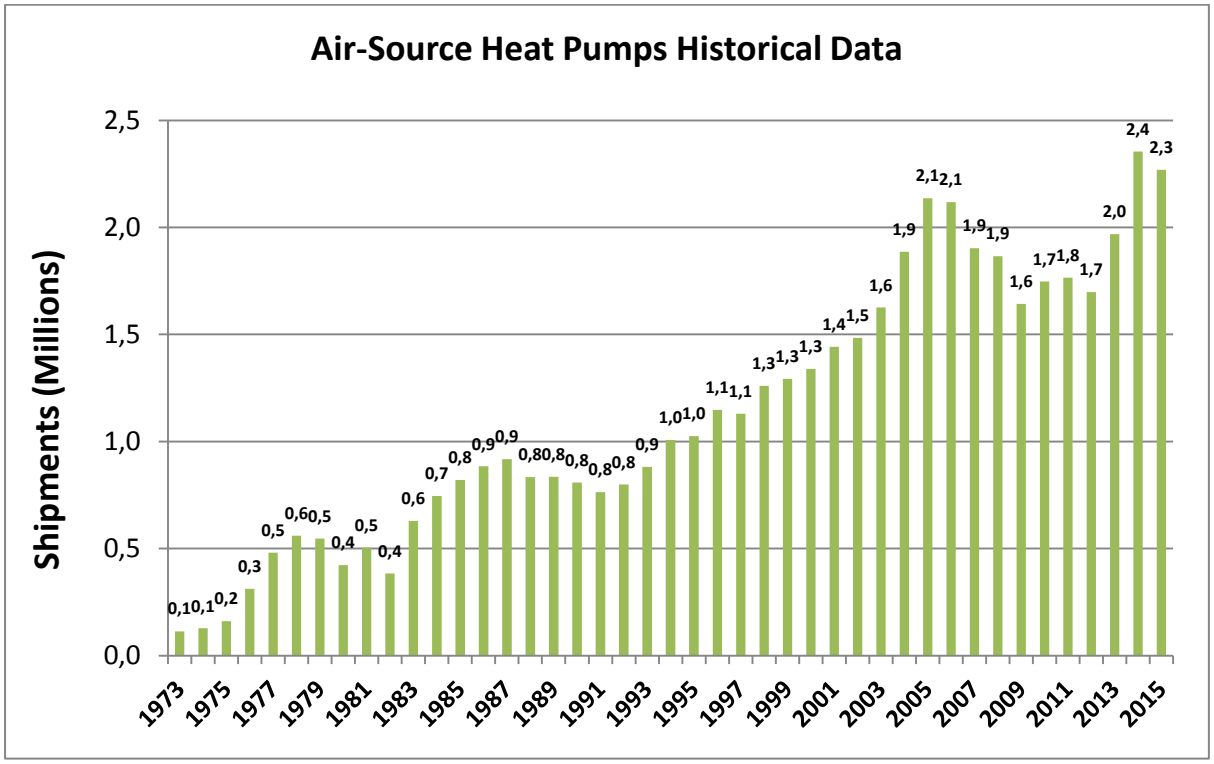

Figure ES-1: U.S. air source heat pump shipments (AHRI, 2010-2017)

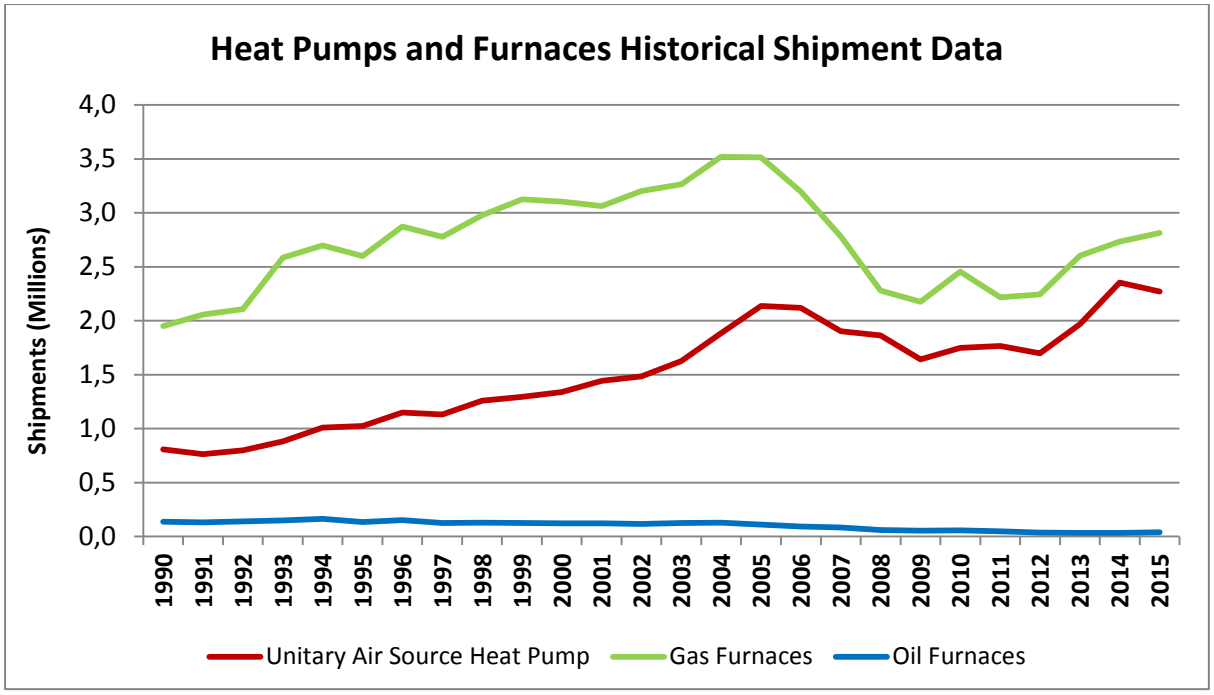

Figure ES-2: Unit shipments of heating equipment in the United States

PRELIMINARY CCHP MARKET ESTIMATE - 2010

As described by Khowailed et al. (2011), Cold climate heat pump (HP) technology is relevant to a substantial portion of the U.S. population, especially with more than one-third of U.S. housing stock concentrated in colder regions of the country (blue-shaded areas in Figure ES-3, below) and another 31% in the mixed-humid climate region (green-shaded area).

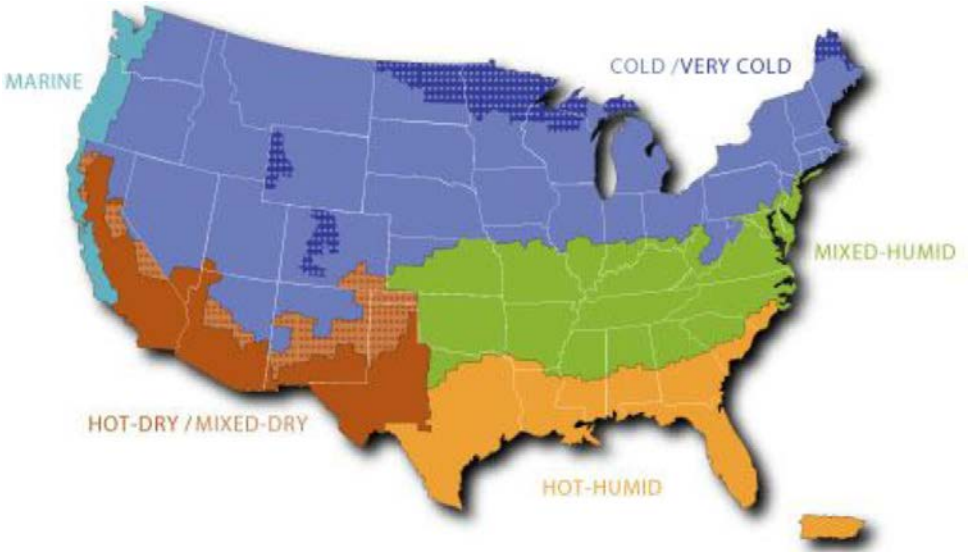

Figure ES-3: Building America Climate Regions adopted in RECS2009 (U.S. EIA, 2011)

The primary target market for CCHPs is the 2.6 million U.S. homes using electric warm air furnaces and HPs in the cold/very cold regions (U.S. EIA, 2011). Secondary markets for CCHPs are comprised of 1) homes in the mixed-humid region of the country with conventional ASHPs or electric furnaces, and 2) homes in the cold/very cold region and the

mixed-humid region that use fossil fuel fired warm air furnaces (propane, fuel oil, or natural gas) - albeit the fuel-fired furnace market is more challenging. The combined total of homes in these three secondary markets is 46 million (U.S. EIA, 2011). Khowailed, et al (2011) estimated that total potential annual shipments of CCHPs could reach ~275,000 assuming 1) the technology demonstrates consistent and reliable energy savings vs. the alternatives, and 2) a product rollout at a competitive price by a credible market leader. If CCHPs fully replaced the existing ASHPs and electric furnaces in the primary market they could yield annual primary energy savings of about 0.106 EJ (0.1 Quads), equivalent to about 5.4 million MT (5.9 million tons) of annual CO_2 emissions reduction.

CYCLE CONCEPT EVALUATION SUMMARY

The U.S. Department of Energy's Building Technology Office (DOE/BTO) established space heating capacity targets for CCHPs, listed in Table ES-1.

Table ES-1: U.S. Air-Source CCHP heating capacity targets – 2013

Outdoor Temperature	Heating Capacity
8.3°C (47°F)	9-21 kW (2.5-6 tons), nominal rating
-25°C (-13°F)	≥75% of nominal rating

U.S. CCHP R&D efforts described in the Task 1 and Task 2/3 reports focused on analyses and experimental (lab and field) investigation of several advanced VC cycles for ASHPs. Vapor injection (VI) cycle concepts, two-capacity compressors, variable speed (VS) compressors, parallel compressors, two-stage cycles with economizers, a liquid-flooded compressor cycle concept, and several other advanced cycle approaches have been investigated. Based on early stage analyses, three CCHP cycle concepts were identified as among the most promising for meeting the goals noted in Table ES-1 – two-stage economizer cycle, an oil-flooded compressor cycle concept, and a single-stage cycle concept using parallel compressors.

Two-Stage Economizer System Concept

A field test of an advanced two-stage ASHP designed for cold climate operation has been completed at Camp Atterbury, a U.S. Army base outside Edinburgh in Indiana (Caskey et al., 2013). The heat pump is a two-compressor (two-stage) system with an economizer VI loop, similar to the concept analyzed by Bertsch et al. (2008). It featured a large tandem scroll compressor (two parallel compressors) for capacity boosting during low ambient temperature heating operation and a variable speed scroll compressor for cooling operation and moderate ambient temperature heating. The test was conducted under the DOD's Energy Security Technology Certification Program (ESTCP). Two identical military barracks from available buildings located at Camp Atterbury were selected for the field demonstration. The originally installed HVAC system was a natural gas furnace with a split system A/C. A side-by-side performance comparison between the originally installed HVAC systems and the two pre-commercial heat pump units developed at Purdue University was conducted during the 2012-2013 heating season. Only commercially available components were selected for all parts of the heat pump units with help from three industrial partners, namely Ingersoll Rand - The Trane Company, Emerson Climate Technology, and Danfoss. The heat pump units had a design heating capacity of 18.34 kW (62,580 BTU/h) at an ambient temperature of -20^{o}C (4^{o}F).

The heat pump performance was compared to the existing HVAC system. For the monitored period at the Army site the ASHP system achieved approximately 19% source energy savings vs. the baseline gas furnace system but utility costs were higher due to the low price

the Army pays for natural gas at the site. Using average Indiana residential electricity and gas prices, the utility costs for the ASHP and baseline furnace would have been comparable. This operation cost equivalence despite the energy savings of the ASHP is because the price for natural gas in Indiana is about one-third that of electricity per unit of energy delivered, which is true of most locations in the United States. The ASHP used no electric backup heating during the test period. Using ASHRAE Standard 55 (ASHRAE, 2010) to evaluate the thermal comfort indicated that the heat pump was able to maintain comfort levels throughout the heating season. Furthermore, while the first cost of the two-stage ASHP will be higher than that of a conventional single-stage ASHP, the installation and maintenance costs are estimated to be comparable.

Two-Port Vapor Injected Compression with Regeneration Concept

Additional research at Purdue University's Herrick Labs focused on the experimental investigation conducted with a commercially available 5-ton heat pump that was retrofitted with a two-port vapor injected scroll compressor. The injection ports within the two compression pathways were located in the fixed scroll with different distances from the suction chamber. The vapor at the two injection pressure levels was generated using two flash tank separators in a cascade configuration. This configuration made it necessary to not only control the superheat but also the liquid levels in the separators and subcooling of the refrigerant leaving the condenser.

Baseline performance data of the heat pump without vapor injection was obtained and compared with that of the two-port vapor injection system. For the baseline, the injection lines to the compression pockets were plugged within the fixed scroll to reduce dead volume and re-expansion losses. Also, the vapor-separator section was shut off and bypassed. In the second step, the plugs were removed and a staged expansion process was performed using the separator section. The generated vapor from each separator was injected into the respective compressor port causing an intercooling effect on the compression process.

With identical compressor speed, a 28% improvement in capacity was achieved at the 8.33°C design point, when compared to the baseline without vapor injection. When the baseline and vapor injected system capacity were matched by adjusting compressor speed, the COP increased by up to 6% at -8.33°C. Results of a bin-type analysis of the experimental results predict an improvement in the heating seasonal performance factor (HSPF) of 6% for Minneapolis and nearly 7% for ANSI/AHRI 210/240 cold climate region V.

Oil-flooded Compressor System Concept

Further research at Purdue University's Herrick Labs focused on the experimental investigation conducted with a commercially available 5-ton heat pump that was retrofitted with oil flooded compression and regeneration. The indoor coil face area was kept unchanged while an additional heat exchanger was added as the oil cooler in the air flow path. In addition, a counter-flow plate heat exchanger with low pressure drops was used as the regenerator.

The results show that by injecting oil in the compression process and using internal regeneration, the improvements in COP and heating capacity range from 4% to 15% and from 1% to 19%, respectively, depending on the oil mass fraction and operating temperatures compared with a conventional heat pump (without regenerator and without oil injection).

Single-Stage Cycle with Parallel Compressors

Research at ORNL investigated several different ASHP cycle configurations to identify those with potential to meet the heating capacity degradation target limit listed in Table ES-1. Two-capacity compressor, variable speed compressor, and dual, equal parallel single speed compressor (tandem compressor) systems were investigated. Nine of the system options investigated are listed in Table ES-2 along with the baseline conventional single speed compressor ASHP used for relative performance comparison.

Table ES-2: ASHP design and sizing options

#	Equipment Sizing Scenarios
1	Single speed heat pump having rated HSPF of 9.6: sized such that rated cooling capacity matches building design cooling load [BASELINE].
2	Single heat pump, having a two-stage scroll compressor: sized such that rated high-stage (100%) cooling capacity matches building design cooling load.
3	Single heat pump, having a two-stage scroll compressor: sized such that rated low-stage (67%) cooling capacity matches building design cooling load.
4	Single heat pump, having a variable speed scroll compressor: sized such that rated cooling capacity at 2700 rpm matches building design cooling load.
5	Single heat pump, having a variable speed scroll compressor: sized such that rated cooling capacity at 3600 rpm matches building design cooling load.
6	Single heat pump, having a variable speed scroll compressor: sized such that rated cooling capacity at 4500 rpm matches building design cooling load.
7	Single heat pump, having a two-stage scroll compressor: sized such that 80% of rated cooling capacity matches building design cooling load.
8	Single heat pump, having a tandem scroll compressor pair: sized such that rated cooling capacity with one compressor matches building design cooling load.
9	Single heat pump, having a single speed VI scroll compressor: sized such that rated cooling capacity matches building design cooling load.
10	Two identical single speed heat pumps with rated HSPF of 9.6: sized such that rated cooling capacity of one unit matches building design cooling load; both units used for heating.

Note: All variable speed compressor system options have a speed range of 1800 - 7200 rpm; option 8, tandem compressor pair contains two identical compressors; the two-stage compressor options include one compressor having two capacity levels, i.e. 100%/67%.

Table ES-3 lists the heating capacity ratio and the heating COPs at 8.3°C and -25°C for each of the systems in Table ES-2. Four of the options (4, 5, 8, and 10) have estimated capacity ratios near the target level noted in Table ES-1 (≥75%). COPs at -25°C for these options range around 45-55% of the nominal COPs at 8.3°C. Estimated HSPF ratings are calculated based on the method prescribed in AHRI Standard 210/240 (AHRI, 2008) for U.S. region IV (mildly cold climate). The VS compressor-based designs offered somewhat greater low temperature capacity capability while the tandem compressor designs were somewhat less complex and had almost as much capacity capability.

Table ES-3: Predicted ASHP system performance indices

Options	COP @ 8.3°C (47°F)	Heating Capacity Ratio @ -25°C (-13°F)	COP @ -25°C (-13°F)	Region IV HSPF Rating (per AHRI Standard 210/240)
	[W/W]	[-]	[W/W]	[W/W (Btu/Wh)]
1.	3.58	40%	1.92	2.80 (9.55)
2.	3.79	42%	2.09	2.92 (9.96)
3.	3.78	57%	2.09	2.92 (9.98)
4.	4.30	94%	1.89	3.40 (11.61)
5.	4.14	74%	1.89	3.43 (11.71)
6.	3.80	61%	1.89	3.40 (11.59)
7.	3.79	52%	2.09	2.95 (10.05)
8.	4.38	75%	1.98	3.31 (11.31)
9.	3.75	43%	2.12	2.96 (10.09)
10.	3.58	80%	1.92	N/A

Based primarily on its relatively simple cycle concept (Figure ES-4), the tandem approach appeared to offer a more cost-effective approach compared to VS-compressor-based approaches so this concept was chosen for in-depth laboratory and field evaluation. A laboratory prototype test system was built by modifying a 17.5 kW (~60,000 Btu/h or 5-ton) rated cooling capacity, single-speed, conventional ASHP and replacing its original compressor with a pair of equal size, single-speed compressors providing 10.6 kW (~36,000 Btu/h or 3 tons) of rated cooling capacity. Parallel compressor CCHP systems using three different scroll compressor designs were evaluated in the lab: 1) conventional scroll compressor optimized for space cooling operation; 2) scroll compressors optimized for space heating operation; and 3) VI scroll compressors. The cycle concept in Figure ES-4 was used in the case of the cooling-optimized and heating-optimized compressors and is considered a 'more cost effective' concept. For the VI compressor system the cycle design is more complex (Figure ES-5) and is considered a 'premium design' concept. For all cases, the compressors were insulated and placed outside the outdoor air flow stream to minimize the compressor shell heat losses.

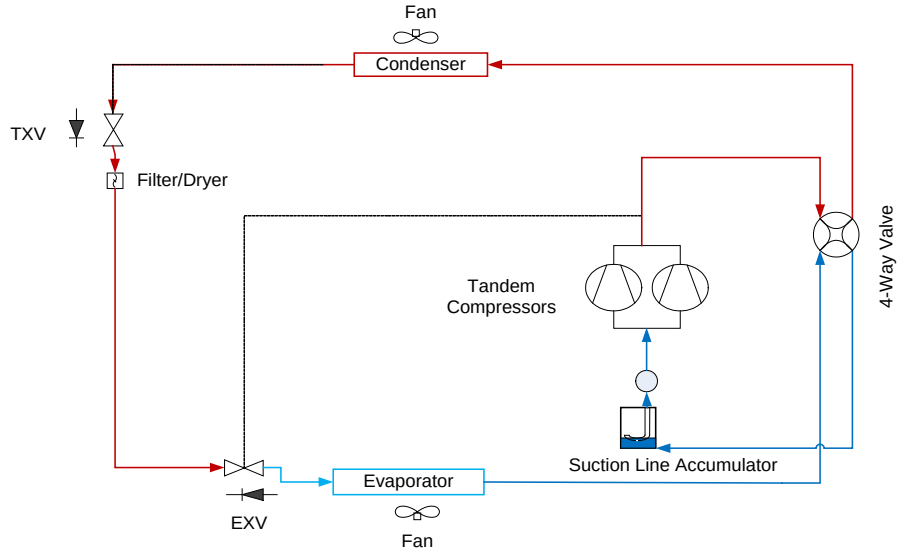

Figure ES-4: Cycle schematic for tandem, single-speed compressor CCHP with electronic expansion valve (EXV) to optimize discharge temperature in heating mode

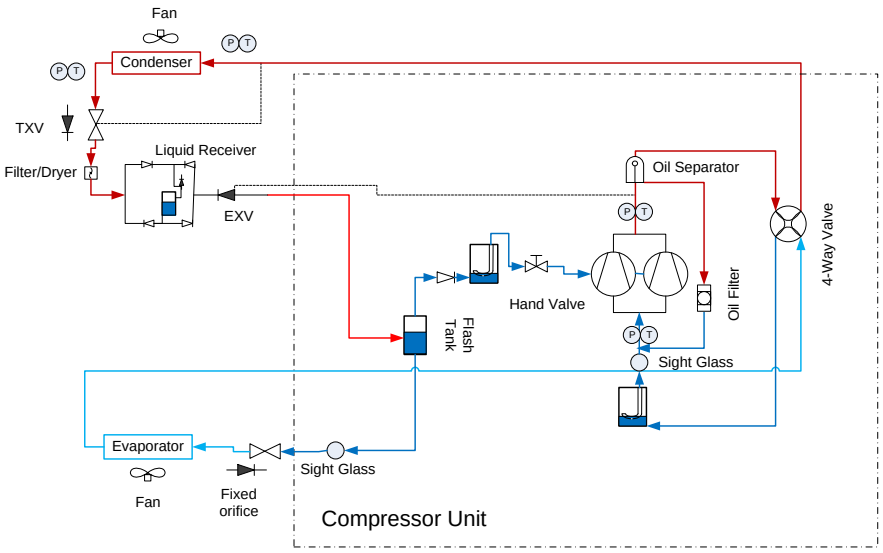

Figure ES-5: Cycle schematic for CCHP using tandem VI compressors and an EXV for heating mode refrigerant flow control

Tables ES-4 and ES-5 summarize the lab tested performance results for the parallel compressor lab breadboard with all three compressor types. Table ES-4 shows the lab-measured performance indices at 8.3°C, -8.3°C, and -25°C (47°F, 17°F and -13°F) outdoor temperature conditions with one or two compressors. Table ES-5 compares relative seasonal heating COP ratings (SCOPhs) [heating seasonal performance factors (HSPFs)] as calculated per AHRI Standard 210/240 in Region IV and V climates for the parallel compressor systems and a high efficiency baseline ASHP. The DHR_{min} building load level is generally representative of a very well insulated house (exceeding the 2015 U.S. code minimum insulation levels: Rice et al, 2015). DHRmax on the other hand is representative of an existing home with insulation levels below 2006 code minimum levels. The dropoff in seasonal efficiencies going from Region IV to the colder Region V climate is about 10.5% and 15.5% for the DHRmin and DHRmax load lines, respectively. Space heating performance was somewhat better at all ambient temperature test conditions for the heating-mode-optimized tandem compressor pair vs. the cooling-mode-optimized pair. It is also notable that the drop in SCOPh for the heating optimized and VI parallel tandem designs between the min and max heating load lines is 1.3% or less in Region IV. This indicates that these designs maintain their seasonal performance well over the full range of house performance levels. By comparison, the single-speed baseline loses 23% in seasonal performance in Region IV between the DHRmin (rated) and DHRmax heating load lines. The SCOPh robustness of the tandem designs is also in contrast to recently tested variable-speed designs which lose 10 to 20% SCOPh in Region IV for representative heating loads approximately halfway between DHRmin and DHRmax levels (Rice et al, 2016). A similar performance robustness advantage is realized in Region V at higher heating load lines for the parallel tandem design, due to the boosted performance at -8.3°C (17°F) and below.

Table ES-4: Lab measured performance indices of parallel compressor CCHPs

	Ambient/Comp(s)	8.3°C, 1 Comp	-8.3°C, 2 Comp	-8.3°C, 1 Comp	-25°C, 2 Comp
Cooling mode optimized compressors	COP [-]	4.09	2.76	2.89	1.85
	Capacity, kW (Btu/h)	11.1 (37,960)	14.8 (50,455)	7.6 (25,860)	8.8 (30,040)
	Capacity Ratio -25°C vs. 8.3°C	100%	133%	68%	79%
	Discharge Temperature, °C [°F]	50.0 (122)	83.4 (183)	55.0 (131)	125.0 (257)
Heating mode optimized compressors	COP [-]	4.24	2.80	2.97	1.94
	Capacity, kW (Btu/h)	11.6 (39,717)	14.9 (50,921)	7.6 (25,917)	8.9 (30,245)
	Capacity Ratio -25°C vs. 8.3°C	100%	128%	65%	76%
	Discharge Temperature, °C [°F]	51.1 (124)	82.8 (181)	51.1 (124)	100.6 (213)
VI compressors	COP [-]	4.44	2.95	3.20	1.98
	Capacity, kW (Btu/h)	11.6 (39,720)	17.4 (59,362)	7.9 (26,918)	10.2 (34,913)
	Capacity Ratio -25°C vs. 8.3°C	100%	149%	68%	88%
	Discharge Temperature, °C [°F]	(52.2 (126)	70 (158)	52.8 (127)	84.4 (184)

Table ES-5: Heating Seasonal Performance Ratings of CCHPs using tandem single-speed compressors (per AHRI Standard 210/240)

Load	SCOPh (HSPF, Btu/Wh) Baseline	SCOPh (HSPF, Btu/Wh) cooling optimized	SCOPh (HSPF, Btu/Wh) heating optimized	SCOPh (HSPF, Btu/Wh) VI compressors
	Heating Season Ratings, Region: IV			
DHRmin	2.80 (9.55)	3.24 (11.04)	3.29 (11.21)	3.47 (11.84)
DHRmax	2.15 (7.35)	3.19 (10.90)	3.21 (10.95)	3.46 (11.80)
	Heating Season Ratings, Region: V			
DHRmin	2.47 (8.42)	2.90 (9.90)	2.94 (10.03)	3.13 (10.68)
DHRmax	1.96 (6.68)	2.69 (9.18)	2.71 (9.26)	2.96 (10.10)

The tandem VI compressor system configuration achieved 2 to 7% better COPs than the tandem, single-speed heating-optimized system configuration. It achieved an 88% heating capacity ratio with ~2.0 COP at -25°C, and ~4.4 COP and 11.7 kW capacity at the 8.3°C nominal rating condition. Figure ES-6 compares the heating capacities of the tandem single-speed compressors (heating optimized) and the tandem VI compressors, at two speed levels, as a function of the ambient temperature. DHRmax and DHRmin house load lines for the DOE Region V climate are overlaid on the VI prototype capacity data. These indicate the potential for the CCHP prototypes to eliminate supplemental electric heat use in tight and well-insulated homes (aka DHRmin heating loads).

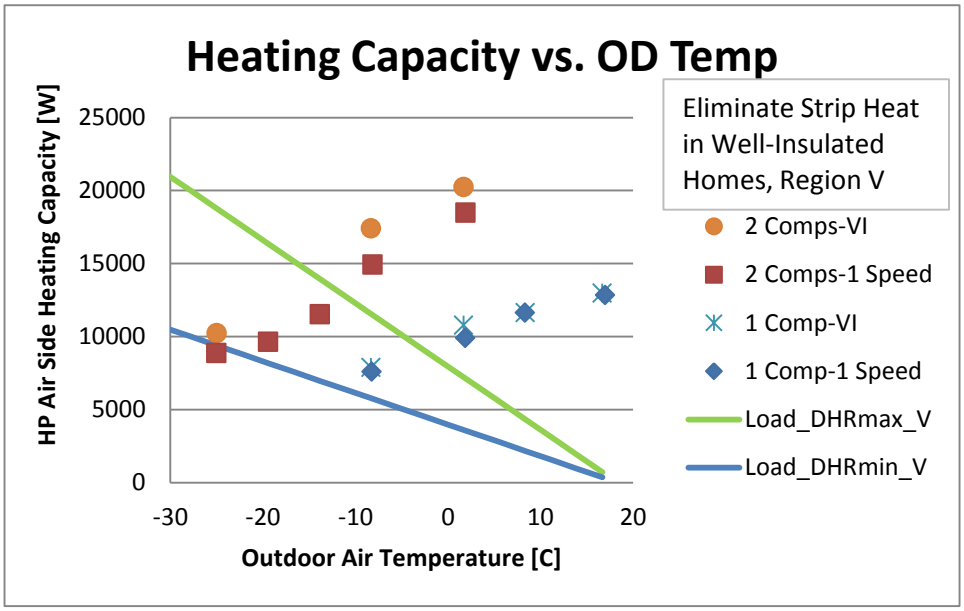

Figure ES-6: Heating capacity vs. ambient temperature, for tandem single-speed compressors and tandem VI compressors

A prototype CCHP using parallel heating-optimized scroll compressors was constructed and installed in an occupied, single-story ranch home in central Ohio in January 2015 for field testing. The prototype replaced the original home HVAC system – a conventional single-speed ASHP with rated cooling capacity of ~10.0 kW (34000 Btu/h) at 35°C (95°F) and heating capacity of ~10.3 kW (35000 Btu/h) at 8.3°C (47°F), equipped with a 19.5 kW supplemental resistance heater for second stage and full backup heating.

The field test prototype was built by modifying a two-capacity ASHP of nominal 17.6 kW (5-ton) cooling capacity - its original 2-capacity compressor was replaced with a heating-optimized tandem scroll compressor pair and controls added to stage the compressors. For the field test, the original 2-capacity ASHP control was retained but re-wired with a relay to enable calling the second compressor for second stage heating. Supplemental resistance heating elements were used for a third heating stage as needed. For defrosting, the CCHP prototype used a demand defrost control and operated both compressors to minimize defrost time.

A slightly different refrigerant schematic (Figure ES-7) was used in the field prototype for two primary reasons. First the lab testing showed that the system low temperature heating with heating-optimized compressors was much less sensitive to compressor discharge temperature than with the cooling-optimized compressors. Secondly, after installing the tandem compressor pair in the outdoor section it became difficult to find room for the EXV components required for the discharge temperature control scheme. So it was decided to simplify the refrigerant flow control to more conventional suction superheat control using a TXV with optimized system charge for heating mode. Figure ES-8 shows the outdoor unit of the prototype as installed at the test home, where one can see the compressors were wrapped by a thermal insulation layer.

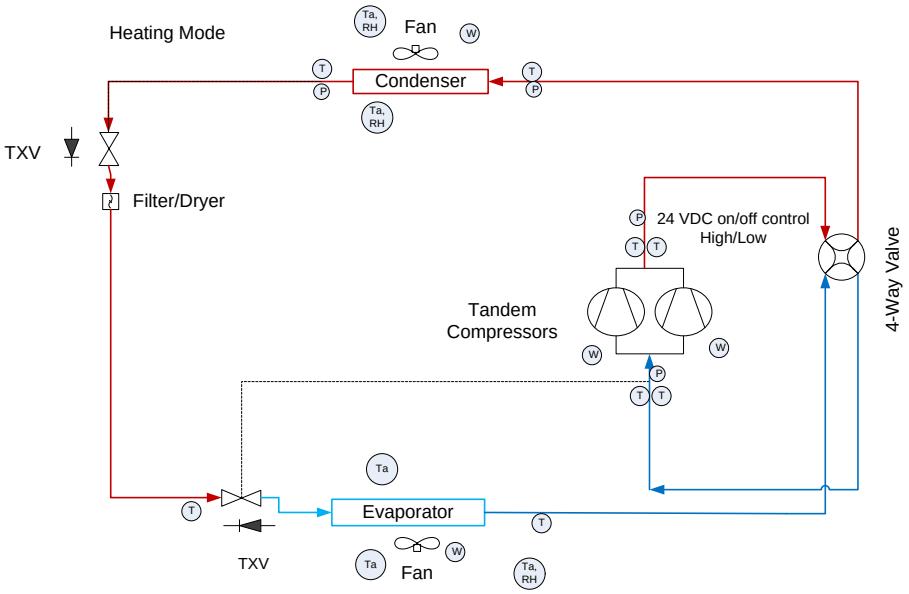

Figure ES-7: Field test prototype CCHP refrigerant schematic

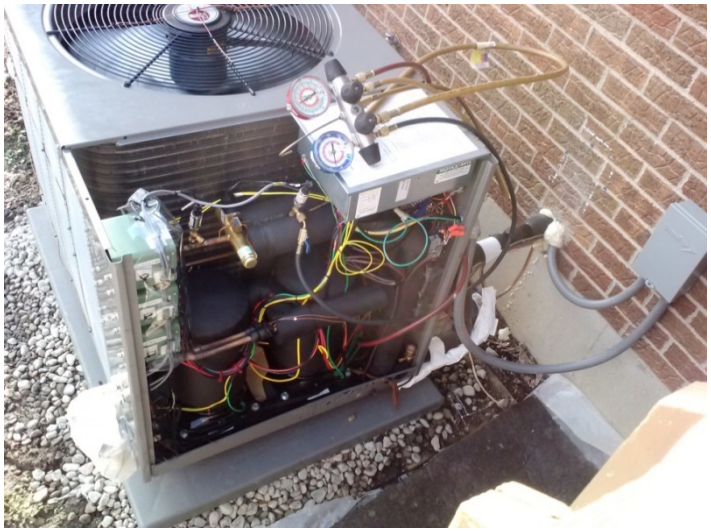

Figure ES-8: Outdoor unit of parallel compressor CCHP field test prototype

Field performance was monitored during three periods: 1) February through April, 2015 heating; 2) June through August, 2015 cooling; and 3) December, 2015 through January, 2016 heating. During the Feb.-Apr. 2015 period the minimum outdoor temperature experienced was 25°C (-13°F).

Figure ES-9 illustrates runtime fractions for two compressor operation and total compressor run time (either one or two compressors operating) versus ambient temperature bins for the first heating test period. At the lowest (rightmost) temperature bin, total compressor run time was 100% but the second compressor still cycled at an 80% rate. This indicates that the CCHP prototype still had some extra heating capacity capability even at this extreme condition.

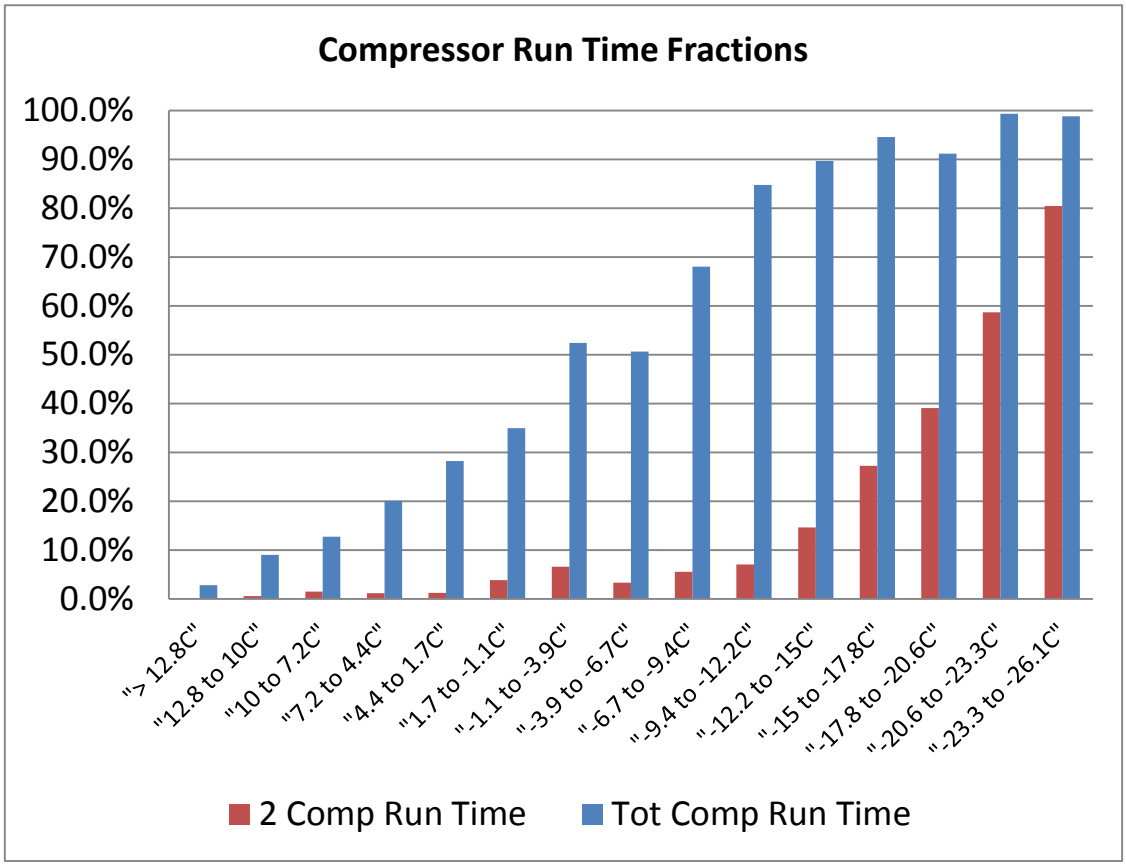

Figure ES-9: Compressor run time fractions, February-April, 2015

Figure ES-10 shows delivered heating capacities for one- and two-compressor operation and the measured delivered building heating load line. It can be seen that the second compressor was needed when the ambient temperature fell below -12.2°C (10°F). At the -25°C (-13°F) condition, the CCHP delivered 8.9 kW of heating, which is 75% of the lab-measured capacity of 11.6 kW at 8.3°C.

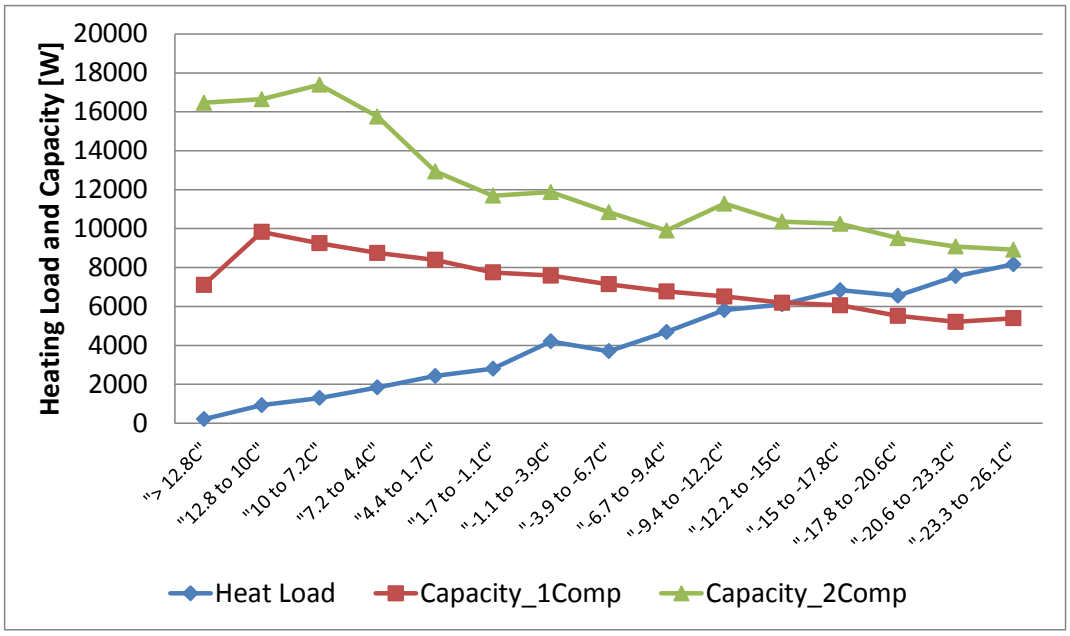

Figure ES-10: Delivered heating by CCHP and building load line, February-April, 2015

Overall, supplemental resistance heating (third stage) operation was minimal in the first heating test period, with most of the usage traceable to either system control issues or occupant behavior. (No defrost tempering resistance heat was used at the engineer homeowner's request.) At -25°C, the resistance energy use was 3.2% of the total even though the second compressor still cycled at 80%. This means that the heat pump responded slower than needed at this condition allowing space temperature to fall below the 1.1 °K dead band limit and activate the supplemental heater. Much of the resistance heat use seen during low outdoor temperatures could have been eliminated by changing the control to require two-compressor operation below a certain ambient temperature. Some 3rd stage operation was seen even at moderate ambient temperatures (between about 7.2°C to -10.0°C) but was mainly due to the thermostat setback operation by the homeowner. When the homeowner left for extended periods the thermostat set point would be lowered and then set back up when the homeowner returned. At times this resulted in the setup being high enough to trigger brief periods of 2nd and 3rd stage operation when they ordinarily would not be needed. Modifying the control to lock out the supplemental heater above a set outdoor temperature could eliminate most of this inadvertent 3rd stage operation.

Figure ES-11 shows field-measured COPs by outdoor temperature bin for single-compressor and two-compressor operation as well as a "total" COP. The total COP was calculated by the total energy delivery divided by the total energy consumed and includes the impacts of cycling losses, supplemental resistance heat use, frosting/defrosting losses, and losses due to switching between one- and two-compressor operation. For the 7.2°C to 10°C bin, the single-compressor COP was 4.05 while the total COP was 3.83 (lower because of cycling losses and occasional two-compressor operation). A control modification to prevent two-compressor operation above a set outdoor temperature would allow the total COP at mild outdoor temperatures (higher than about 2°C or so) to much more closely follow the single compressor COP curve.

It is encouraging to see that, at -25°C, the total COP was 2.2 i.e. 120% more efficient than resistance heating. The field COP at -25°C is higher than that measured in the lab (1.94 given in Table ES-4) mainly because the field return air temperature is 1.1 to 2.2°C lower than the controlled value in the lab.

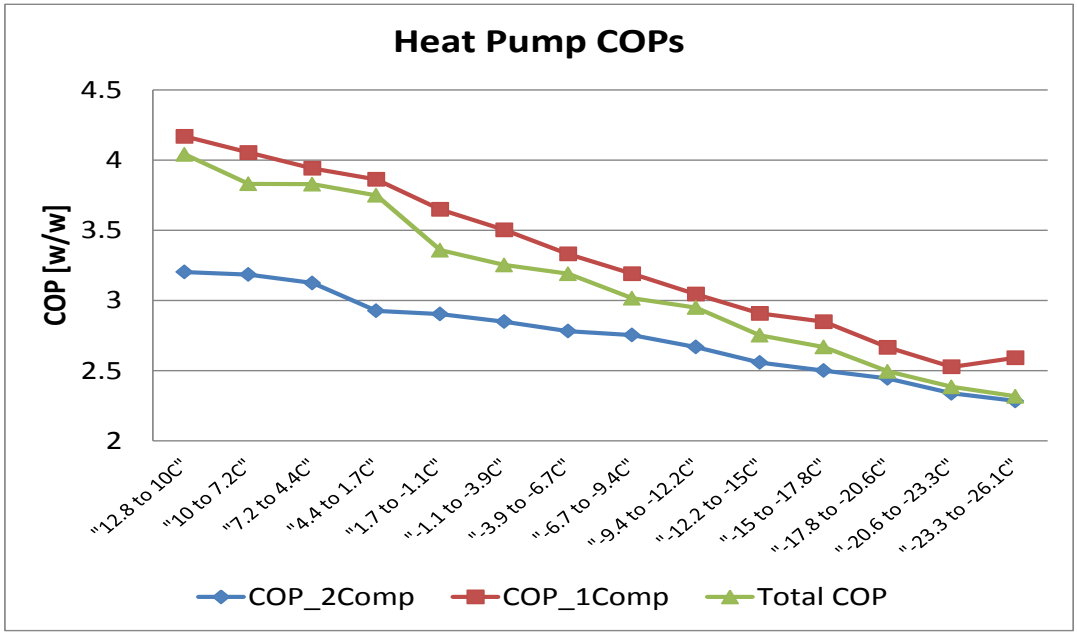

Figure ES-11: Field COPs in heating mode, February-April, 2015

In the first heating operation test period, the overall average field-measured COP was 3.16.

Cooling season data for the CCHP prototype was recorded from June through August of 2015. Prior to the start of the cooling season the control board was adjusted to allow only single compressor operation. In this case, the indoor and outdoor heat exchangers, sized for the base 17.5 kW ASHP, were oversized for single compressor operation, thus leading to superior cooling performance. The averaged field measured COP over the test period was 5.2, with an average ambient temperature of 25.6°C. Figure ES-12 below shows the field measured average COPs per temperature bin. The dropoff in COP at the lowest temperature bin is most likely due to increased cycling losses at the low cooling loads in this temperature bin offsetting the higher steady-state COPs from lower ambient temperatures.

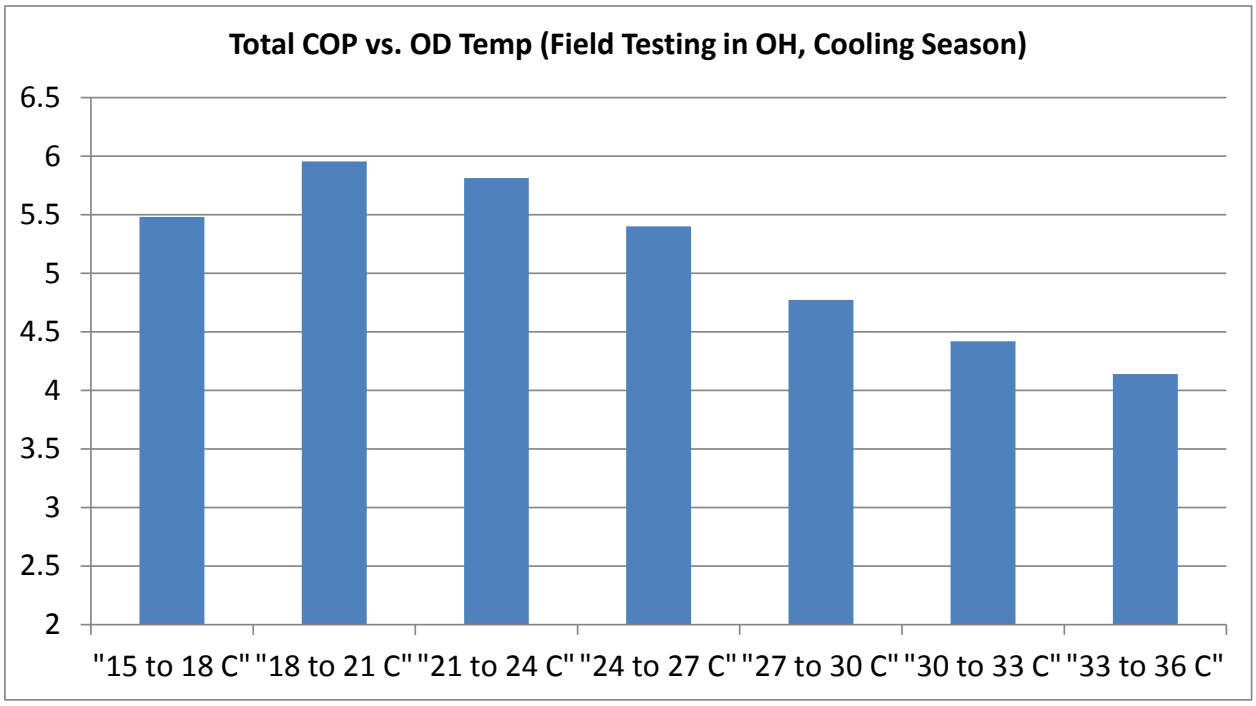

Figure ES-12: Field COPs in cooling mode

Figure ES-13 shows monthly electricity billing data for the field test home from June 2012 to November 2015 (about two years before installation of the prototype CCHP and for a year afterward). Note here that the kWh from the electric bills has had 800 kWh in “base” consumption (due to lights, water heater, appliances, etc.) subtracted so that it represents the heat pump usage only. In comparison to the previous single-speed ASHP in the same house, >40% HVAC energy reduction was achieved by the CCHP during the coldest months with similar monthly average temperatures (around -6 to -7°C). It can be seen that there are no apparent energy savings in the 2015 cooling months. This was due to a change in the family --- the homeowners had a new baby in the 2015 summer. So they set the thermostat to a lower temperature than they had used in previous summers and the heat pump ran more frequently offsetting the better efficiency of the CCHP prototype.

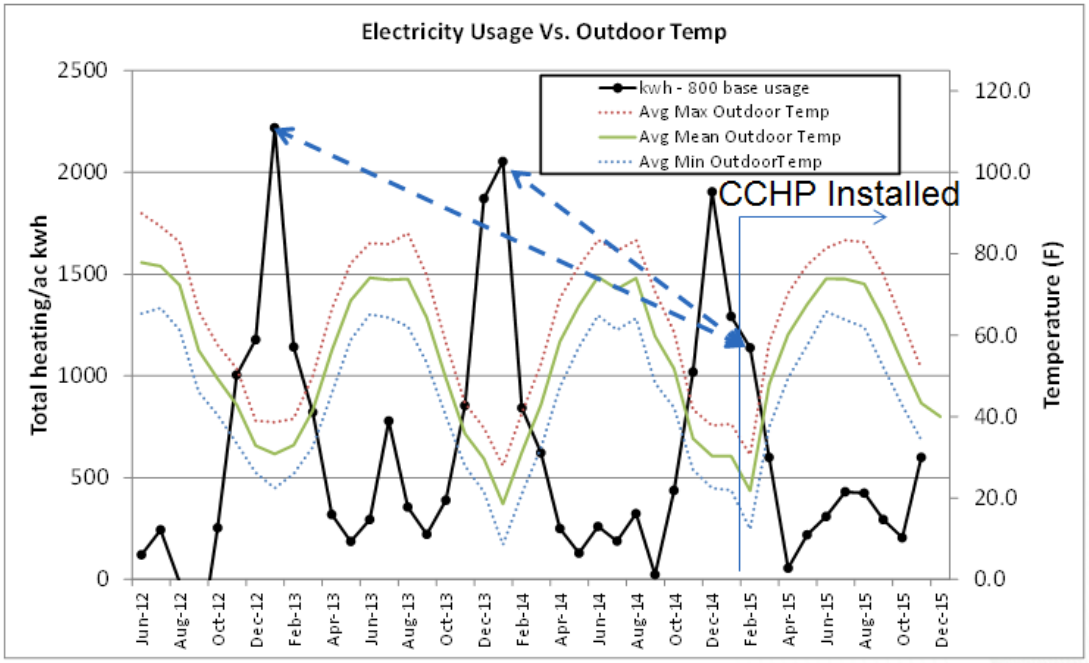

Figure ES-13: Monthly electric bills for field test home before/after installing the prototype CCHP

Before the project ended it was possible to collect another set of heating data from December 2015 through January 2016. Before data collection began, an outdoor temperature controller was added to the CCHP system to prevent the second compressor from running when the ambient temperature is above -12.2°C. However, the homeowner also adopted a higher thermostat setting of 21.7°C, about 1.7°C higher than the previous heating seasons due to the new family member. Due to the higher thermostat setting, the return air temperatures to the CCHP in 2016 were consistently about 2.2°C higher than those in 2015 leading led to a higher heating demand in 2016. Consequently, the second compressor ran more frequently in 2016. Figure ES-14 compares the average heat pump COPs per temperature bin for both heating test periods. Because of the higher temperature setting and the ~2.2°C higher return air temperature to the CCHP, the average heat pump heating COPs per temperature bin during the 2nd test period were 10% to 15% lower than those during the 1st period. The field measured, averaged COP for the 2nd period was 2.84, or about 10% lower than the 1st period average of 3.16.

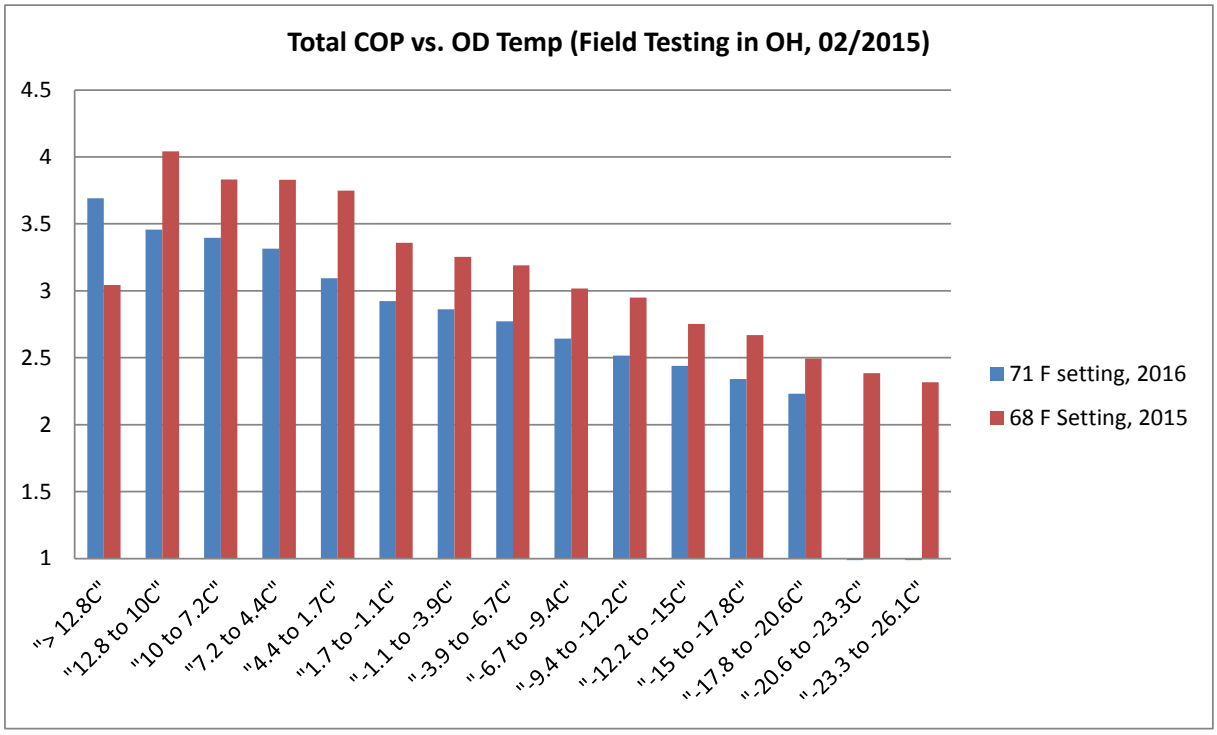

Figure ES-14: Average bin COPs for the two heating test periods

A second CCHP field test prototype system has been constructed based on the tandem VI compressor lab prototype design of Figure ES-5. It was installed at the Cold Climate Housing Research Center in Fairbanks, AK in May 2016 and field testing began in June 2016. Results will be reported after the planned one-year field test is concluded.

U.S. Team Report

IEA HPT TCP Annex 41
"Cold Climate Heat Pumps"

Task 1 – Literature and Technology Review

Submitted by:

Ray Herrick Laboratories, Purdue University
Lead: Eckhard A. Groll (contact: groll@purdue.edu)
Contributors: Christian K. Bach (contact: cbach@okstate.edu)
Stephen L. Caskey (contact: scaskey@purdue.edu)
Alejandro C. Lavernia (contact: alaverni@purdue.edu)
Nicholas Salts (contact: nsalts@purdue.edu)

Oak Ridge National Laboratory
Lead: Van Baxter (contact: vdb@ornl.gov)
Contributors: Bo Shen
Omar Abdelaziz
C. Keith Rice
Gerald Groff, consultant
Gannate Khowailed, CSRA Inc.
Karen Sikes, CSRA Inc.

January 2017

TABLE OF CONTENTS

LIST OF TABLES

LIST OF FIGURES

1 INTRODUCTION

During the mid-1970s, following the first oil embargo, heat pumps became of greater interest to northern U. S. electric power companies, particularly for those experiencing large peak demands during the heating season, as shortages of natural gas and oil led to increased usage of direct electric heating. Air-source heat pumps (ASHP), given their wider market presence relative to other heat pump types, almost universal applicability, but with inherent efficiency and capacity issues at cold outdoor temperatures were of primary interest for improvement as an electrical heating system alternative at that time. ASHPs based on the simple vapor compression cycle suffer both heating capacity (output) and efficiency (coefficient of performance or COP) degradation as the outdoor ambient temperature drops. At the same time, building heat demand is increasing so ASHPs require a supplemental heating source – usually direct electric resistance heating elements - to bridge the gap between the building heat demand and the ASHP heating output. This characteristic results in lower seasonal performance and limits peak electric demand reduction potential leading to limited acceptance of ASHPs in areas that experience large numbers of hours at cold temperatures (loosely defined as ≤-7°C for purposes of Annex 41). A primary criterion for ASHPs to achieve good seasonal performance in cold areas is achieving high heating output at low ambient temperatures so as to minimize reliance on supplemental heat sources and maximize the overall system heating seasonal performance factor (HSPF or SPF_h).

With increasing concern for technology options that can result in reduced CO_2 emissions, it is appropriate to revisit research and development work undertaken in different countries on heat pump systems for cold climates and to examine technology improvements that could lead to expanded usage of electric heat pumps for applications in cold regions. Accordingly, in 2010 the U. S. Department of Energy's Building Technology Office (DOE/BTO) solicited R&D proposals focused on advancing heat pump technology for cold climate applications. The performance targets specified in the solicitation are listed in Table 1 below.

Table 1: U. S. DOE cold climate heat pump performance targets, 2010

Outdoor Temperature	Heating COP	Heating Capacity
8.3°C (47°F)	4.5, nominal rating	14 kW (48,000 Btu/h), nominal rating
-25°C (-13°F)	≤50% reduction from nominal	≤25% reduction from nominal

At the same time, the U. S. proposed to the IEA Heat Pump Programme (IEA HPP) that a new Annex be established to collaborate with other HPP members to improve performance of heat pumps for cold climates. Annex 41 was officially approved in May of 2012. The principal focus of Annex 41 is on electrically driven ASHPs since that system type has the biggest performance challenges given its inherent low ambient temperature performance problems alluded to above. However, the Annex is open to ground source heat pumps and natural gas (engine or sorption) driven ASHPs as well at the Participants' discretion. Availability of heat pump systems with improved low ambient performance would help bring about a much stronger heat pump market presence in cold areas which today rely predominantly on fossil fuel furnace heating systems. A primary technical objective of the Annex is to define pathways to enable ASHPs to achieve an "in field" heating $SPF_h \geq 2.63$ W/W (HSPF ≥9.0 Btu/Wh), the minimum level necessary in order to gain recognition as a renewable technology in the EU.

The U. S. Department of Defense (DOD) has estimated that buildings accounted for 24% of its energy consumption in 2007 (U.S. DOD WSTIAC, 2009). Several mandates, including Executive Order 13514, "Federal Leadership in Environmental, Energy, and Economic Performance" (EO 13514, 2009), calling for the improvement on the efficiency of federal buildings are affecting the current and future stock of DOD buildings. The use of heat pumps designed for cold climates is a promising approach to improve the HVAC efficiencies to aid

compliance with these mandates. The goals are to create a clean energy economy that the Federal Government will lead by example. One significant goal is mandatory energy reductions to reach net-zero-energy buildings by 2030 (EO 13514). The Energy Independence and Security Act of 2007 includes Section 315, “Improved Energy Efficiency for Appliances and Buildings in Cold Climates” specifically addressing advancements for cold climates. One requirement of the act is the reduction of fossil fuels in new or renovated buildings, 55% by 2010 then 100% by 2030 (EISA, 2007).

In May of 2006, the Secretary of Defense commissioned an Energy Security Task Force, ESTF, to develop a roadmap to reduce the fossil fuels requirement for the DOD. A heat pump designed for cold climates has the ability to replace fossil fuel heating methods with an efficient, electricity based system. CO_2 emission reductions can be very substantial compared to fossil fuel heating systems in areas where the electricity is predominantly produced from renewable energy sources.

2 BACKGROUND – ENERGY USE AND INCREASING ENERGY PRICES

World energy consumption is projected to increase by 53% from about 530 EJ (505 quads) in 2008 to 810 EJ (770 quads) in 2035 (Conti et al., 2011). Energy consumption by Organization for Economic Co-operation and Development (OECD) member countries is projected to increase by only 18% while that by non-OECD countries is projected to increase by 85% over this time span. Due to the increase in demand from non-OECD countries, it is expected energy prices will continue to increase from 2008 levels in spite of new developments in extraction methods such as fracking for natural gas or unconventional reserves such as oil tar sands. For the United States, current forecasts project the increase of energy prices (in 2011 dollars); Brent spot oil from $111 per barrel in 2011 to $163 per barrel in 2040, Henry Hub spot natural gas below $4 per million BTU through 2018 to $7.83 per million BTU in 2040, and mine mouth price of coal from $2.04 per million BTU in 2011 to $3.08 per million BTU in 2040 (EIA, 2013). In percentages, the expected increase in the cost of energy is 47% for oil, roughly 90% for natural gas, and 51% for coal. These projected increases in fossil fuel prices could lead to increases in electricity prices of similar magnitude as well. With increases in consumption and costs of this magnitude, the urgency for reductions in U.S. energy consumption becomes evident.

The buildings sector in the United States accounted for about 42 EJ (40 quads) of primary energy consumption (~41% of the U. S. total) in 2010, making it the sector accounting for the largest consumption. The U. S. Energy Information Administration (EIA) projects this will increase by 17% by 2035. Space heating is responsible for ~22.5%, or roughly 9.5 EJ (9 quads) of this consumption (DOE, 2011). Fossil fuels account for about 6.7 EJ (6.3 quads) or 70% of the space heating energy consumption leaving a large potential for alternative heating methods employing electricity.

Offsetting the consumption of fossil fuels on-site with electricity presents an opportunity to utilize renewable sources for power generation. Heat pumps are efficient technologies that employ electricity to achieve space heating where the heat output is a multiplier of the power consumption. Heat pumps specifically designed for cold climates were one of 15 technologies selected for the refined study of the reduction of primary energy consumption of HVAC systems in commercial buildings (Roth et al., 2002). Business case analyses conducted by Oak Ridge National Laboratory predict a cumulative energy savings potential of 0.53 EJ (0.5 quads) from 2015 to 2030 for a cold climate heat pump assuming a 25% penetration rate when compared to conventional electric heat pump and electric resistance units (Khowailed et al., 2011).

3 BRIEF U. S. HEAT PUMP MARKET HISTORY

3.1 National Shipments & Trends

Since heat pump sales first emerged as a significant alternative for space heating and cooling of buildings during the 1950s, market sales have experienced significant volatility originating from:

- Government efficiency regulations and test methods
- Government and utility incentives for heat pumps
- Modifications to international trade barriers
- Technological breakthroughs
- Major swings in the housing market
- Economic recessions
- Availability, cost and rate structures of electricity and natural gas
- Favorable customer and utility experiences with certain models

The section below provides a high level overview of how the heat pump market has evolved in the U.S. since its inception, accompanied by explanations of the underlying market drivers.

3.1.1 1950 – 1969

Early growth of heat pumps was very rapid following the wide-scale acceptance of residential forced-warm air heating systems and central air conditioning, in addition to the potential for abundant, low-cost electricity that nuclear power could supply. However, sales were soon slowed substantially due to poor product reliability resulting from inexperience or inadequate product testing on the part of many manufacturers who attempted to capitalize on the emerging market opportunity (Groff and Ertinger, 1984).

3.1.2 1970 – 1989

Despite the negative experiences mentioned above, heat pump sales grew at modest rates, mostly in mild climate zones with low electric rates, up until 1973 when the first oil embargo occurred. From 1973 to 1978, heat pump sales (or shipments) grew from ~100,000 to over 560,000 annually, as shown in Figure 1, and heat pumps began to gain traction in the colder northern climate areas where natural gas and heating oil dominated. In the same period, the fraction of heat pump sales to northern areas of the U. S. rose from 15% to over 35%. The rise is significant because these areas accounted for 75% of U. S. space-heating energy use at the time (Groff and Ertinger, 1984).

A recession from 1979-1981 together with greater-than-expected availability of natural gas dampened the heat pump sales growth rate considerably. But by 1983, sales had reached ~700,000 per year, and projections indicated that by 1990 they should reach 1,000,000 units annually (Groff and Ertinger, 1984). Continued availability of adequate natural gas supplies and relatively low gas prices vs. electricity generally dampened heat pump sales growth so that the 1,000,000 annual sales level was not reached until the mid-1990's.

3.1.3 1990 – 2009

The United States experienced a relatively small economic downturn in 2001. A surge in heat pump sales is seen in 2005, which analysts believe is directly tied to the government regulation to increase the minimum seasonal energy efficiency ratio (SEER) for heating and cooling equipment from 10 to 13 – a 30% improvement. The change, which went into effect in 2006, caused an increase in equipment costs, and as a result, manufacturers in many

cases chose to ship out as much inventory as possible in 2005 since this stock would not meet the new standard. The lasting impact of this change on the heat pump market continues to be felt since some manufacturers were unable to produce at full capacity in 2006 while still meeting the new standard.

Heat pump shipments, along with most HVAC shipments, were also significantly impacted by the economic recession as well as the associated housing market decline, beginning in 2007 and intensifying over the next couple of years. When new single-family home construction drops (63 percent reduction in four years), the demand for new heat pumps was also depressed. The resulting steep drop in heat pump shipments between 2007 and 2009 is seen in Figure 1 (AHRI, 2010-2017; AHRI, 2012).

Since construction of new houses fell considerably during this time period, only 22% of heat pumps sold were installed in new homes during 2009. This indicates growing heat pump sales for add-on and replacement applications that usually require lower investments (Lapsa and Khowailed, 2011). Furthermore, high energy prices led some consumers and businesses to make upgrades by replacing inefficient equipment, including older heat pumps, which assisted sales.

3.1.4 2010 to date

The heat pump market has shown resilience to the aforementioned housing crisis and economic downturn, with 2014-2015 shipments recovering to somewhat exceed the previous 2005-2006 peak. Furthermore heat pump shipments appear to be recovering faster than gas furnaces, increasing their market share. Figure 2 displays how heat pump shipments compared to those of competing heating technologies for the period 1990 to 2012. Compared to the market peaks in 2005-2006, heat pump shipments dropped by ~17% during the 2009-2012 period while combined gas and oil furnace shipments fell by ~35%. ASHP shipments rebounded starting in 2013 and exceeded the 2005-2006 levels in 2014-2015.

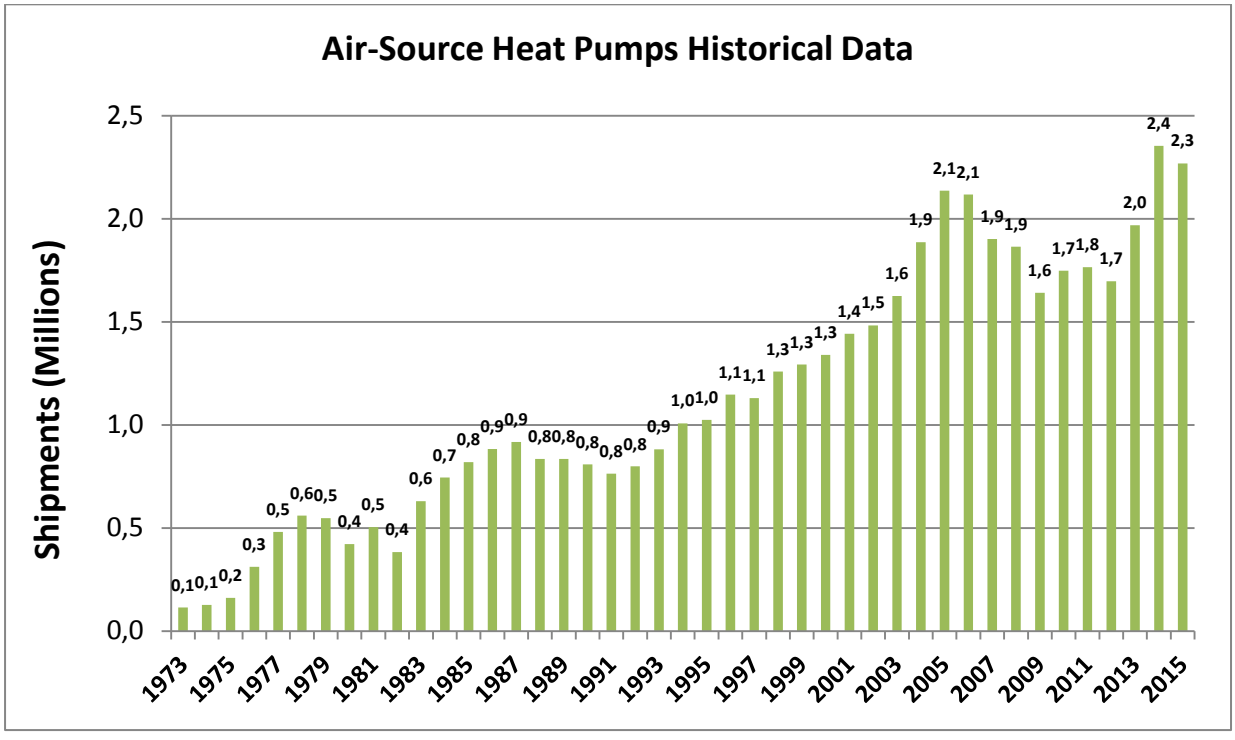

Figure 1: U.S. air source heat pump shipments (AHRI, 2010-2017)

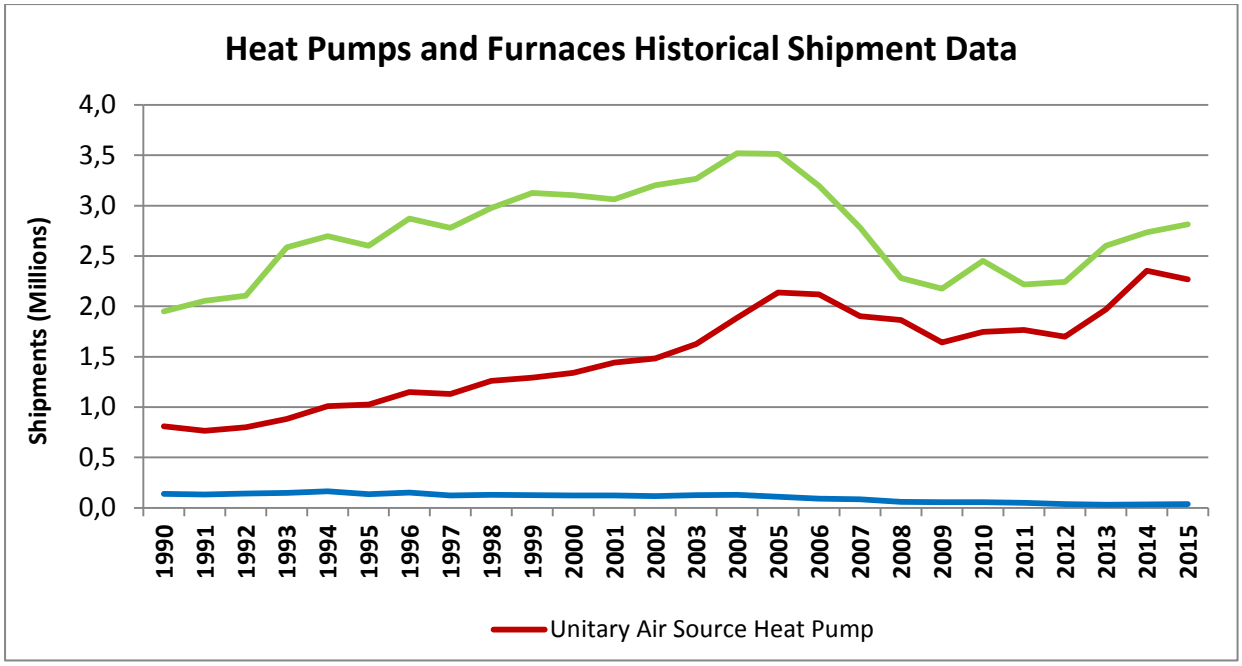

Figure 2: Unit shipments of heating equipment in the United States (AHRI, 2010-2017)

3.2 Regional Shipments & Trends

The South U. S. census region has been best suited for heat pumps due to relatively lower electricity prices and moderate weather presenting a favorable market for ASHPs. The 2009 Residential Energy Consumption Survey (EIA, 2009) data highlights the primary heating equipment used in homes across the country. As of 2009, 9.8 million U.S. homes relied on heat pumps for their primary heating equipment, representing about 8.6% of the 114 million homes in the United States. A majority are in the South region with 7.5 million of the region's homes using heat pumps as their primary heating equipment (about 18% of the total 42 million homes located here).

Figure 3 provides a visual display of heat pump presence across the United States as of 2009. As indicated by the greener shades, the South clearly has the highest overall share of heat pump of all U.S. census regions. Within this region, the South Atlantic division shows the most penetration, with Virginia having the largest share of heat pump technologies among all the states (36% of its 3 million homes use heat pumps as the primary heating technology). Heat pump penetration is not as high in the West South Central division of the South region, with only 4% of homes in Texas, Arkansas, Louisiana, and Oklahoma relying on heat pumps for their heating purposes. Only 2% of homes in the Northeast region use heat pumps, largely driven by 400,000 homes in Pennsylvania. Similarly, only 2% of homes in the Midwest region use heat pumps. The West region shows a somewhat stronger presence of heat pump technologies with about 5% of the homes currently using them as their primary heating system, mainly driven by 600,000 homes in Arizona. The relatively wider availability of natural gas to residential areas in the West South Central division and Northeast, Midwest, and West regions is at least partially responsible for the lower market share of electric heat pumps in those areas. It should be noted that the 18 states shaded grey in Figure 3 had insufficient data, either because no cases were in the reporting sample, data was withheld due to a Relative Standard Error (RSE) of the sample being greater than 50 percent, or fewer than 10 households were sampled. Based on the overall regional data described above however, the heat pump share of homes in these states is estimated at <2%.

The lower market presence of heat pumps in northern areas of the U. S. is not due to any inadequacy of heat pump performance or reliability. One of the authors of this report (Groff) has personal knowledge of individual electric heat pumps operating successfully in locales with winter temperatures reaching extremes as low as -50°C (-58°F). Heat pump life studies sponsored by the Electric Power Research Institute (EPRI) covering heat pump installations in parts of nine U. S. states (Alabama, northern Illinois, Indiana, Kentucky, Michigan, Ohio, Tennessee, Virginia, and West Virginia) showed median heat pump service lifetimes ranging from ~20.5 years in southern locations to ~15-16 years in northern locations (Lovvorn and Hiller, 2002; Lovvorn et al, 2001; Bucher et al, 1989; Pientka, 1987). Median life for the compressor from these studies was estimated at ~13.5 years in the Alabama studies indicating that no more than one compressor replacement was typically required during the service life of the heat pump installations surveyed (Lovvorn et al, 2001). Bucher et al, (1989) noted that for the heat pumps that required compressor replacement in their study, only 4.6% required more than one compressor replacement during their service lifetime.

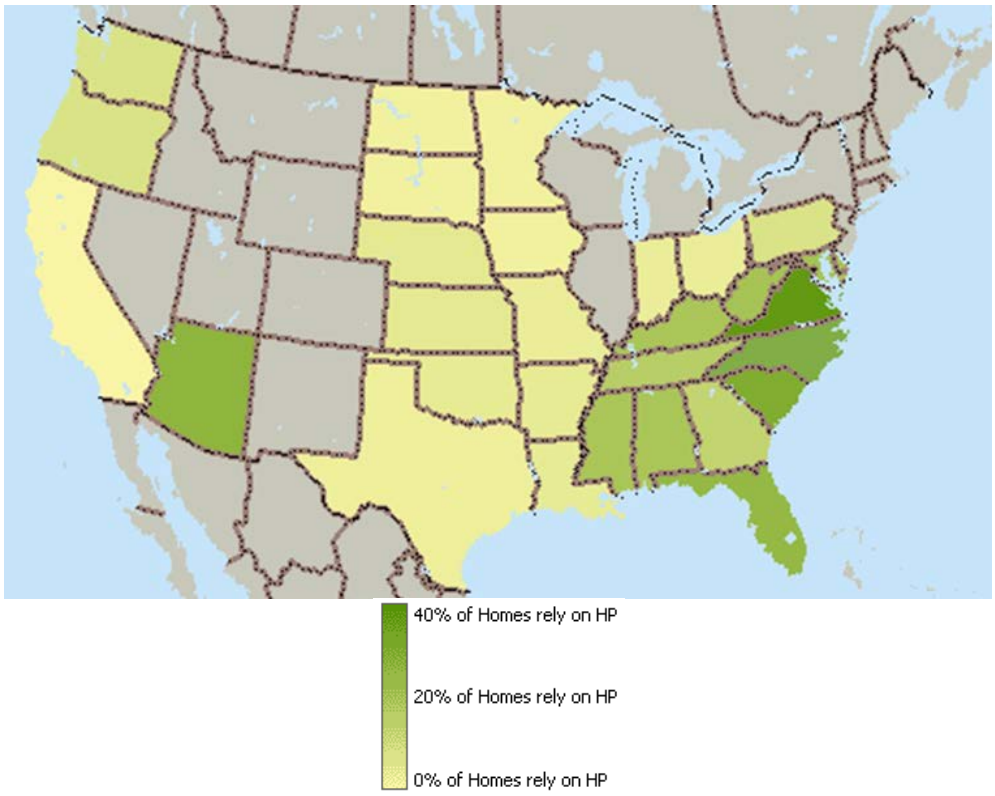

Figure 3: Percentage of homes using heat pump technology as the main heating equipment, as of 2009 (EIA, 2009)

As shown in Figure 4, heat pumps have increased in market share (relative to other heating systems) in the United States for approximately the past 12 years, maintaining close to 40% of the national market over the past couple of years. A closer look at how heat pumps fare in the four individual census regions, however, shows mixed performance. As of 2012, heat pumps accounted for well over half of all heating systems installed in new single-family houses in the South, with significant boosts beginning around 2002 (U.S. Census Bureau, 2013). A U.S. population shift from colder to warmer climates (U.S. EIA, 2013), like the South, is believed to have an overall positive impact on heat pump sales given that region's favorable market for ASHPs as noted above. More houses built in this region likely means more heat pumps installed over time, and this population shift is anticipated to continue through 2030.

The Midwest region experienced a similar boost in shipments starting in 2002, capturing approximately 20% of the market by 2009-2010, but this gain has started to tail off in recent years. The West demonstrated its highest market share back in the early 1980s, but has since lost ground to competing technologies. Finally, the Northeast has experienced rather steady, although minimal, market share at roughly 10% (U.S. Census Bureau, 2016).

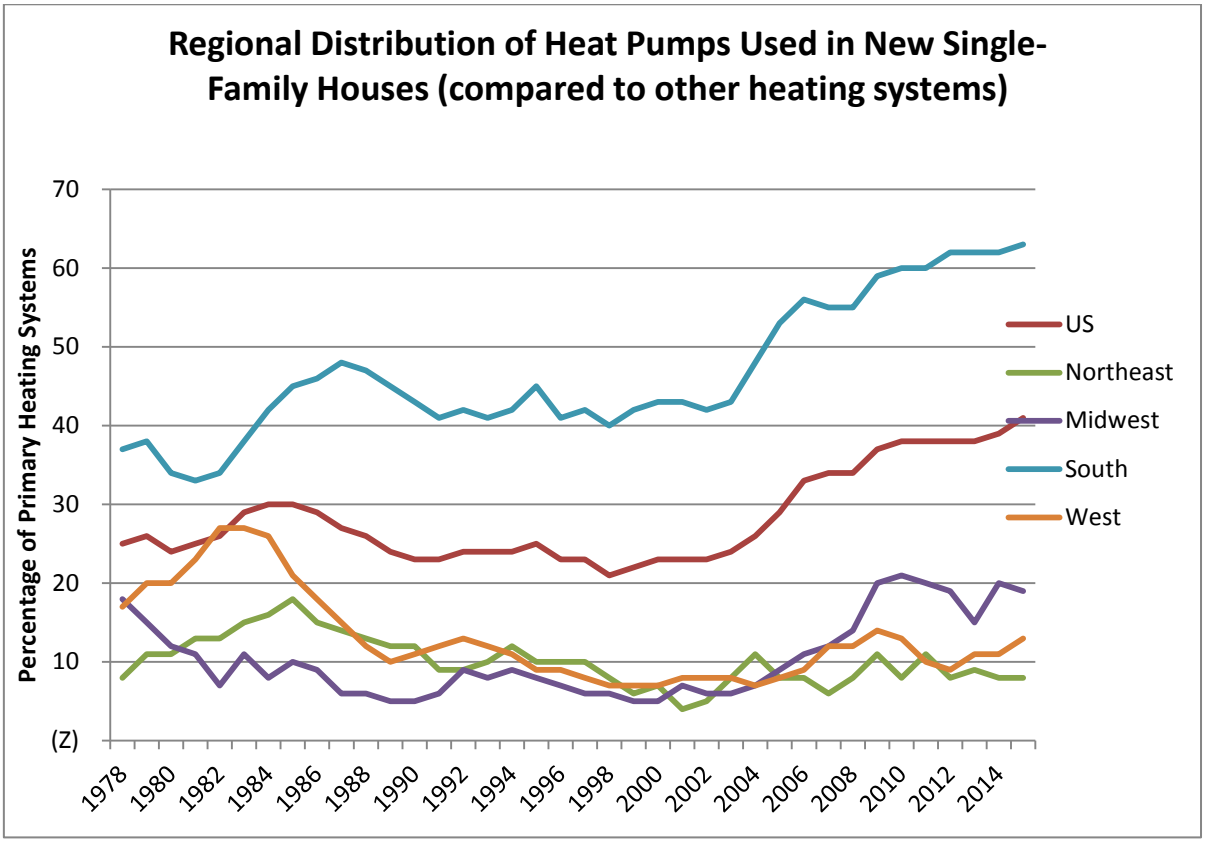

Figure 4: Heat pump market share by region

The introduction of cold climate heat pumps (CCHP) and other improved technologies is expected to aid in the expansion of the heat pump market beyond the Sunbelt areas into the colder regions traditionally dominated by gas furnaces. The Residential Energy Consumption Survey (RECS) heating stock data in 2001, 2005, and 2009 for cold / very cold regions of the country shows that gas furnaces are slowly losing traction within the market and that electric furnaces and HPs are gaining momentum, showing promise for the future penetration of cold climate heat pumps. Furthermore, regional standards for gas furnaces are expected to become stricter in the near future, requiring an increase in the minimum efficiency to an annual fuel utilization efficiency (AFUE) rating of 90% in the cold / very cold (northern) part of the country, which will increase the initial equipment cost, potentially leading to new trends in heating equipment (Khowailed et al., 2011).

3.3 Preliminary CCHP Market Estimate – 2010

As described by Khowailed et al. (2011), cold climate heat pump (HP) technology is relevant to a substantial portion of the U.S. population, especially with more than one-third of U.S. housing stock concentrated in colder regions of the country (blue-shaded areas in Figure 5, below) and another 31% in the mixed-humid climate region (green-shaded area).

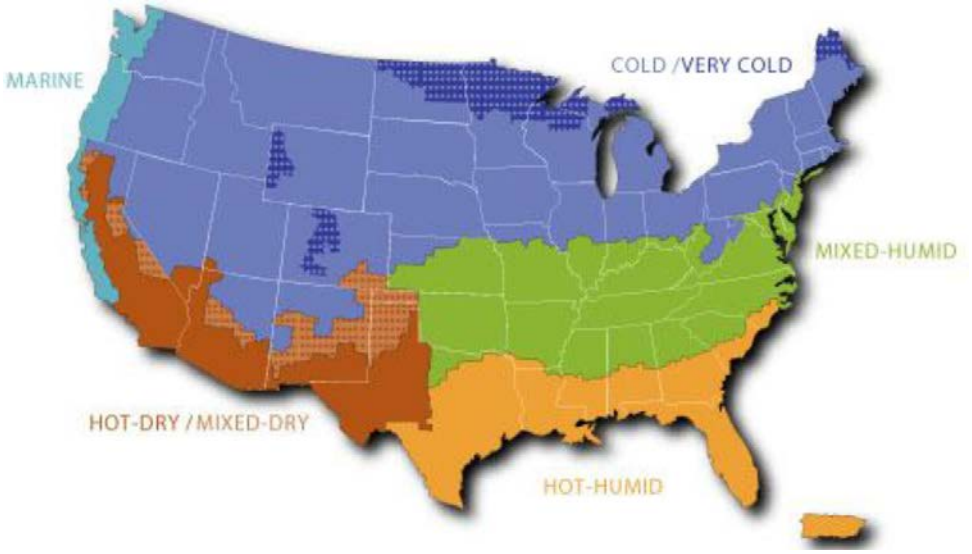

Figure 5: Building America Climate Regions adopted in RECS2009 (U.S. EIA, 2011)

The primary target market for CCHPs is the 2.6 million U.S. homes using electric warm air furnaces and HPs in the cold/very cold regions (U.S. EIA, 2011). Secondary markets for CCHPs are comprised of 1) homes in the mixed-humid region of the country with conventional ASHPs or electric furnaces, and 2) homes in the cold/very cold region and the mixed-humid region that use fossil fuel fired warm air furnaces (propane, fuel oil, or natural gas) - albeit the fuel-fired furnace market is more challenging. The combined total of homes in these three secondary markets is 46 million (U.S. EIA, 2011). Khowailed, et al (2011) estimated that total potential annual shipments of CCHPs could reach ~275,000 assuming the technology demonstrates consistent and reliable energy savings vs. the alternatives, and a product rollout at a competitive price by a credible market leader. If CCHPs fully replaced the existing ASHPs and electric furnaces in the primary market they could yield annual primary energy savings of about 0.106 EJ (0.1 Quads), equivalent to about 5.4 million MT (5.9 million tons) of annual CO_2 emissions reduction.

4 LITERATURE REVIEW

A review of previous and current literature was performed to examine the results of earlier cold climate specific ASHP R&D activities and to identify candidate heat pump technology advances that could achieve sufficient heating capacities and desirable efficiencies while operating at low outdoor temperatures. Ultimately, the goal of the literature review is to highlight the development status of technologies that could lead to greater heating seasonal efficiency for heat pumps (particularly ASHPs) in colder climate locations. Much of the current literature review summarized in this section is taken from a Master's Thesis by Caskey (2013).

4.1 Pre-1990 Cold Climate Heat Pump R&D in the United States

Considerable research and development activity was begun in the U. S. in the late 1970's and early 1980's to improve the performance of ASHPs, resulting in higher efficiency and more reliable products for northern U. S. applications (Groff and Reedy, 1978; Groff et al., 1978, Groff et al., 1979; Bullock et al., 1980). A great deal was learned about the technology needs to enable heat pumps to become more attractive for colder climate applications. In intervening years, advanced heat pump designs have been pursued (and some have been brought to the market) that incorporate design concepts or features for improved cold climate performance (see for instance Hadley et al., 2006). While many of these improved heat

pump designs have been technically successful, market opportunities were limited due to the continuing relatively low cost of fossil fuels vs. electricity and to the higher initial cost of these products and systems.

In the mid-1970s electric utility companies were motivated to sponsor research into alternative electrically operated heating products as an alternative to direct electric heaters and gas or oil furnaces. Notable programs launched during this period were undertaken by EPRI, EESERCO (a consortium of Northeastern U.S. utilities) and Niagara Power Corporation (now National Grid). Westinghouse's research group was awarded a contract by EPRI to identify heat pump design concepts (including in combination with solar energy utilization) that would be effective in the colder climates. EESERCO and Niagara Mohawk sponsored similar projects that were focused on more practical design solutions (i.e. that could be carried to actual product development). These latter studies (as undertaken by the Carrier Corporation Research Division), included field monitoring of ASHPs in residences in four northern U. S. cities with varying climate conditions – Boston, MA; Syracuse, NY; Minneapolis, MN; and Seattle, WA. All of these locations experienced at least 2800 °C-days (5,000 °F-days) of heating. In addition a detailed seasonal performance (SPF) simulation model was developed, calibrated using data from the field monitoring, and used for parametric studies (Groff and Reedy, 1978; Groff et al., 1978). The heat pumps used in the field studies were single-speed ASHPs typical of those available in the 1960s and 1970's, applied to residences and one commercial building – see Figure 6 for two examples.

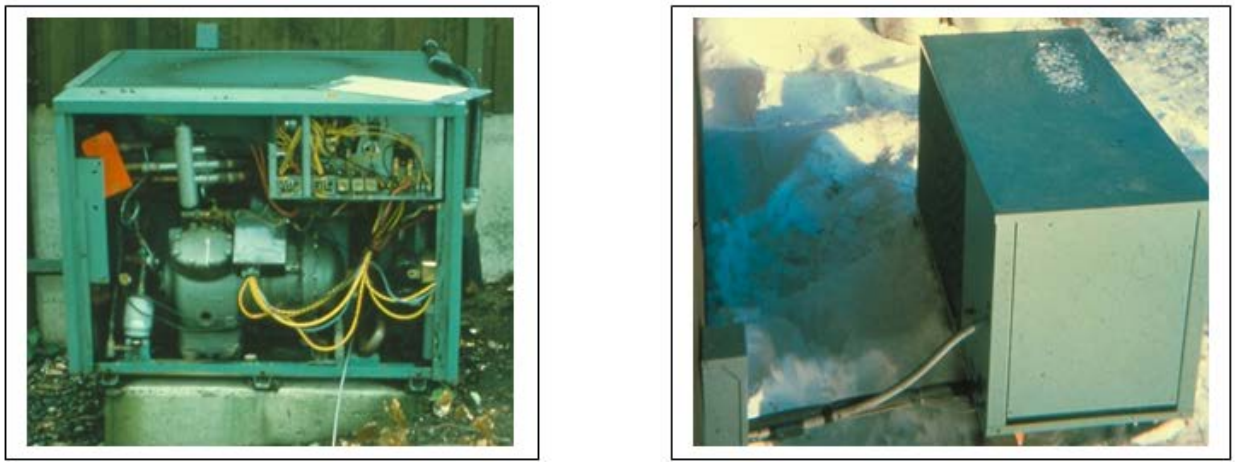

Figure 6: Sample outdoor sections of heat pumps field tested from 1976-1978: left, ca 1960's unit installed in Seattle residence (note semi hermetic compressor); right, ca 1970's unit originally installed in Minneapolis residence (note - unit was undersized)

Field measured SPFs for the tested heat pumps ranged from 1.20 in the coldest location (Minneapolis), to 1.5-1.6 (Boston and Syracuse), to 2.2 in the mild Seattle location. These values were impacted by the fact that the 1976 winter experienced much lower outdoor temperatures than average for the three coldest locations. Using the calibrated SPF model it was projected that for average weather at these locations, the SPFs would have been slightly higher, ranging from about 1.3 to 2.3 (Groff and Reedy, 1978; Groff et al., 1978). The heat pump tested in Minneapolis was undersized for the house and location, so a subsequent year of testing was undertaken using a larger and more efficient ASHP (30% increased capacity and 19% higher COP at the 8°C (or 47°F) rating point). The field measured heating season results showed an increase in SPF of 24% (1.49 vs. 1.2 the previous year) (Groff et al., 1979). This illustrates the inherent advantage of increasing the heat pump size (heating capacity) for improving SPF in colder locations.

Bullock et al. (1980) described a more detailed heat pump sizing study based on ranges of heat pump capacity levels, house load (e. g. thermal envelope) characteristics, climatic conditions (e.g. locations) and economic factors (operating and maintenance costs, fuel costs, and fuel cost escalation rates). A metric called the size ratio (SR) was defined as shown in Figure 7 to characterize the heating capacity of a heat pump relative to its heating load at the standard rating temperature of 8.33°C (47°F). Four local climate levels were considered, denoted as A-D with A the mildest and D the most severe (highest heating degree-days). Three house thermal envelope levels were considered – 3 being the most insulated, least infiltration (with lowest heating requirement) and 1 the lowest (with highest heating requirement). Three different fuel cost escalation rate (I_{ESC}) assumptions were considered as well – 0-10%. Figures 8 and 9 illustrate typical results generated for a mild and severe climate, respectively. It can be seen that for the more severe climate (Figure 8), the SR is much more dependent on the range of house load levels and fuel cost factors. Generally, higher values for I_{ESC} favor larger SR values. More heavily insulated houses (aka house level 3) also tend to favor higher SR values – however the absolute heat pump size for more efficient homes would generally be smaller due to the smaller absolute heating requirement. Figure 10 illustrates the range of optimum SR values vs. heating degree days. For this figure, the "upper" boundary would be typical for better insulated homes with a high I_{ESC} assumption. Conversely, the "lower" boundary would pertain to less insulated dwellings and a low I_{ESC} assumption.

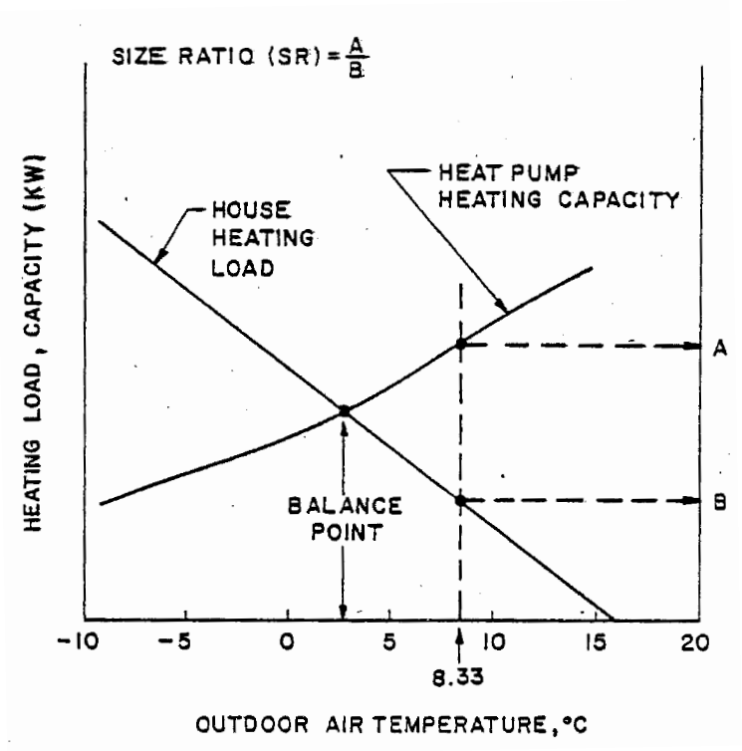

Figure 7: Size Ratio (SR) definition (from Bullock et al., 1980)

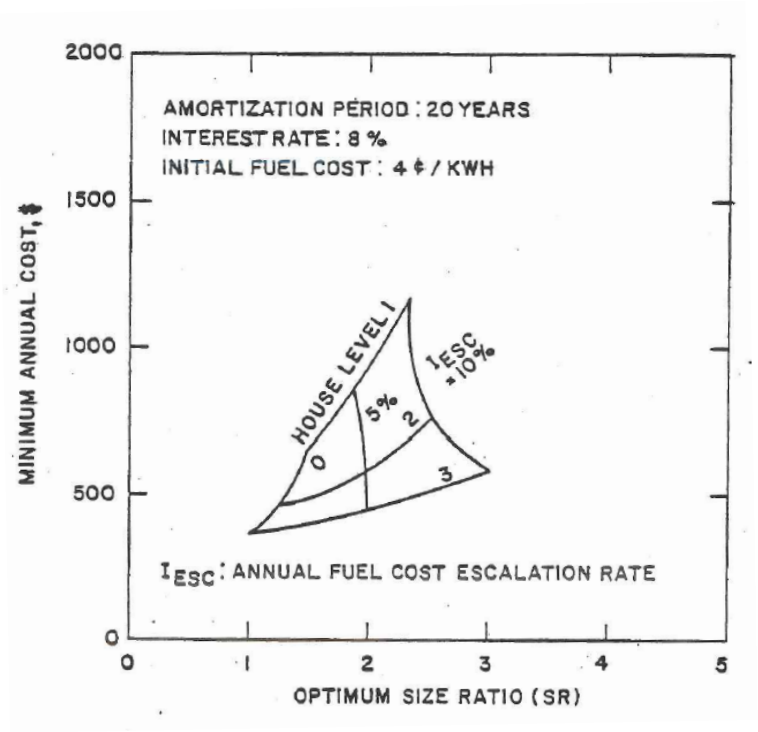

Figure 8: Heat pump minimum annual cost vs. Size Ratio for mild location - climate A (from Bullock et al., 1980)

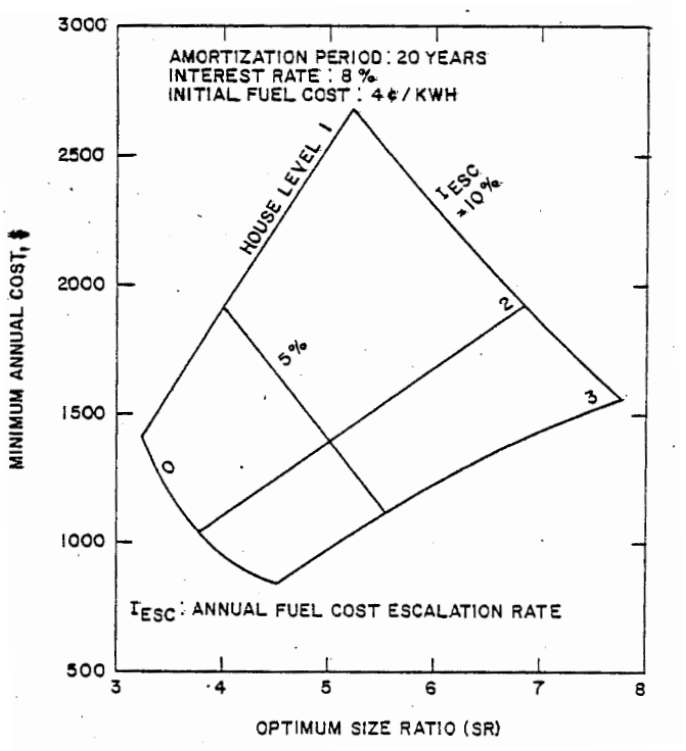

Figure 9: Heat pump minimum annual cost vs. Size Ratio for severe location - climate D (from Bullock et al., 1980)

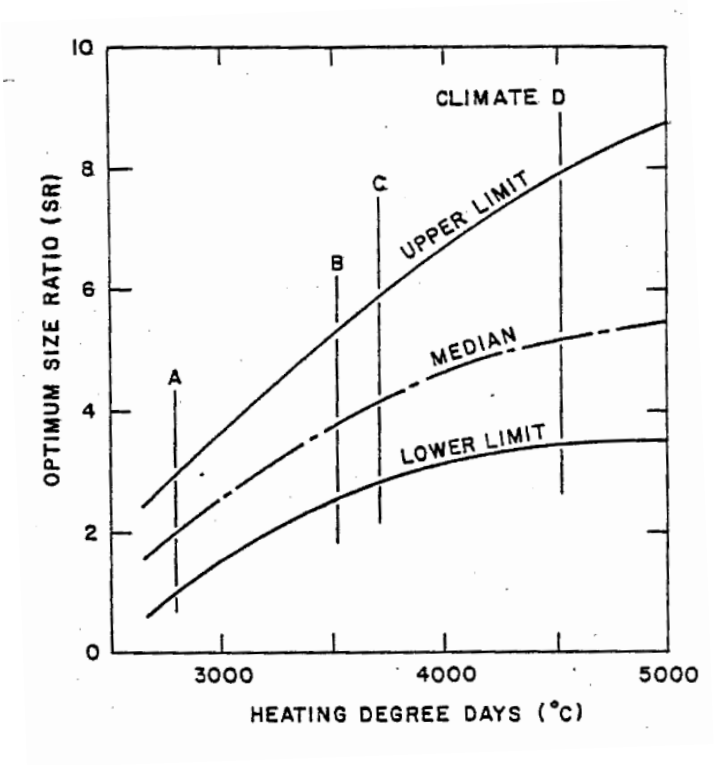

Figure 10: Optimum Size Ratio (SR) vs. heating degree-days (from Bullock et al., 1980)

It is important to note, as pointed out in Bullock et al. (1980), the curves in Figure 9 are not "general" but are tied to the particular set of assumptions about the house and cost parameters used. Also note that the foregoing information was developed for single-speed ASHP equipment of circa 1970 design, far less efficient than current models being marketed in the United States.

From the field testing and computer studies, new product designs were formulated by the Carrier Research group, leading to prototype models that were also tested in the field over the following years. Among the most important features for good cold climate performance included in the prototypes were demand defrost systems, application of properly sized receivers, and minimization of reversing valve thermal losses.

In parallel with the field studies above, the Carrier group also analytically examined the energy savings potential of thermostat night setback control. Results indicated that use of night setback with heat pumps in colder climates could yield modest improvements in heating SPF. But careful system control (especially of the electric supplemental heaters) would be critical. The study concluded that night set back was not recommended for existing heat pump technology at the time (see Bullock, 1978).

The Carrier group was also invited to join Électricité de France (EdF) in a program to investigate electric ASHPs (both air-to-air and air-to-water types) for heating in the French climates. Field tests were conducted on several residences with various existing heating system types and for two large commercial buildings. These studies were reported in papers by Groff et al. (1984) and by Groff and Moreau (1983). From these studies, two prototypes with functions and features for improved cold climate performance were designed and fabricated. These units were installed in U.S. and French homes and were monitored to determine actual performance. A number of the design elements developed for these prototypes were utilized in later Carrier products including a 3 piece heat pump for cold climate applications (pictured in Figure 11) that incorporated an outdoor fan-coil unit, an

indoor fan-coil unit and an indoor compressor box (to enable capture of compressor heat to the indoor environment).

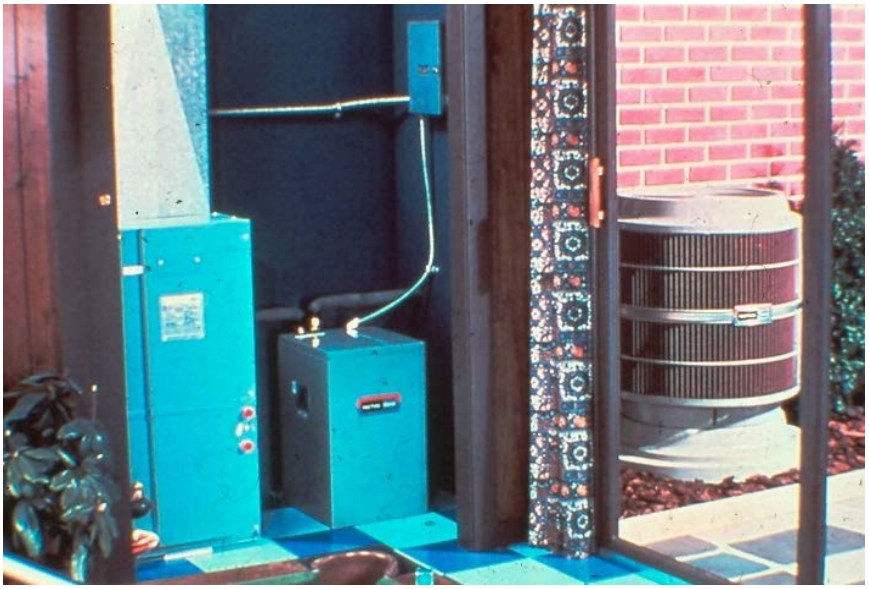

Figure 11: Early 1980's 3-piece ASHP design for northern climate applications

More advanced designs incorporating various approaches for capacity modulation (multiple compressors, multiple speed or displacement compressors, inverter-driven system technology, etc.) can be and have been developed (Lannus, 1993; Hadley et al., 2006) with varying degrees of market success. Variable capacity systems also have an advantage in that they can operate at lower capacity or lower compressor speed in the cooling season, thus avoiding cooling performance penalties that typically accrue from oversizing. Modifications to the vapor compression cycle itself (incorporation of ejectors, multiple stage cycles, etc.) can also be used to boost low temperature capacity and efficiency. The following section discusses some of the more recent developments.

4.2 Recent U. S. R&D Efforts and Developments - Low Outdoor Temperature Air-Source Heat Pumps

4.2.1 Multi-stage compressor system investigation

A conference paper by Bertsch et al. (2006) investigated in detail three heat pump technologies for use in cold climates. The authors first identified the four principle problem areas faced by ASHPs when operating at low outdoor temperatures. The first issue is a lack of heating capacity caused by lower refrigerant flow rates at the low temperatures when the heating load is the largest – which leads to significant need for a backup heating source, usually provided by electric resistance heaters, to supplement the heat pump output. The second issue is that the discharge temperature of the compressor reaches high levels due to the low suction pressures and high compressor pressure ratio experienced at low ambient temperature operation. The third issue is that the heat pump COP decreases quickly under low outdoor temperature operation. The last main problem involves sizing the heat pump capacity. If the heat pump capacity is sized to meet house design heating loads at a very low outdoor temperature, this leads to oversizing for cooling, resulting in frequent cycling and degraded cooling seasonal performance.

Six different heat pump technologies were identified that have the potential to solve some of these issues by varying degrees. Table 2 provides a side-by-side comparison between these

six technologies and a conventional heat pump and shows the number of heating modes, efficiency, output, and discharge temperature of each technology.

Table 2: Comparing different heat pump technologies to a single-stage baseline (Bertsch et al., 2006)

#	Concept	Preferred Compressor*)	Number heat output steps	Relative Efficiency	Relative Heat output	Discharge temperature
1	1-stage cycle	LT	1	100%	100%	High
2	2-stage w. intercooler	2-stage	1	130%	100%	Acceptable
		Sc, Recip, Rot	3	130%	140%	Acceptable
3	2-stage w. economizer	2-stage	1	130%	100%	Low
		Sc, Recip, Rot	3	130%	150%	Low
4	Cascade cycle	Sc, Recip, Rot	1	140%	140%	Low
5	Refrigerant injection	Sc, Screw	2	Comparable	115%	High
6	Oil cooling	Recip, Rot	1	Comparable	Comparable	Acceptable
7	Mechanical subcooling	LT + Sc	2	110%	120%	High

*) Sc…Scroll, Recip…Reciprocating, Rot…Rotary, LT…Low temperature

Three of these technology options were selected for detailed comparison - the two-stage using an intercooler, the two-stage using an economizer and the cascade cycle. It can be seen from Table 2 that these three technologies have the highest relative efficiency and relative heat output with low or acceptable discharge temperatures. The schematic for each of these three technologies is shown in Figure 12.

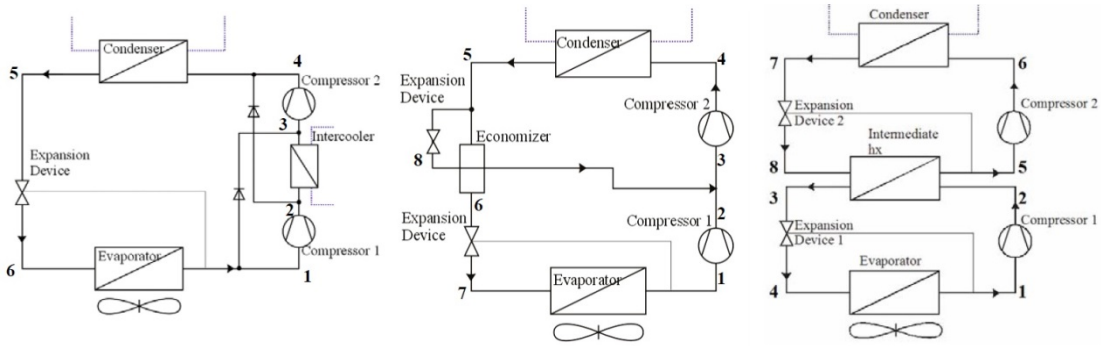

Figure 12: Heat pump schematic - Intercooler (Left) - Economizer (Middle) - Cascade (Right) (Bertsch et al., 2006)

System simulation models were created for each of the three technologies to simulate the heating capacity and performance for comparison. The supply temperature for each was fixed to 50°C (122°F) which is somewhat higher than typical for single-stage heat pumps (≤100°F). A plot of the COP versus outdoor temperature for each heat pump technology is shown in Figure 13 and is compared to a second law efficiency of 50%. The intercooler and economizer cycles show similar performance at temperatures above 0°C (32°F) while the cascade cycle performs relatively better at colder temperatures. All cycles show COPs above 2 at the low outdoor temperatures indicating reasonably good efficiency during these extremes.

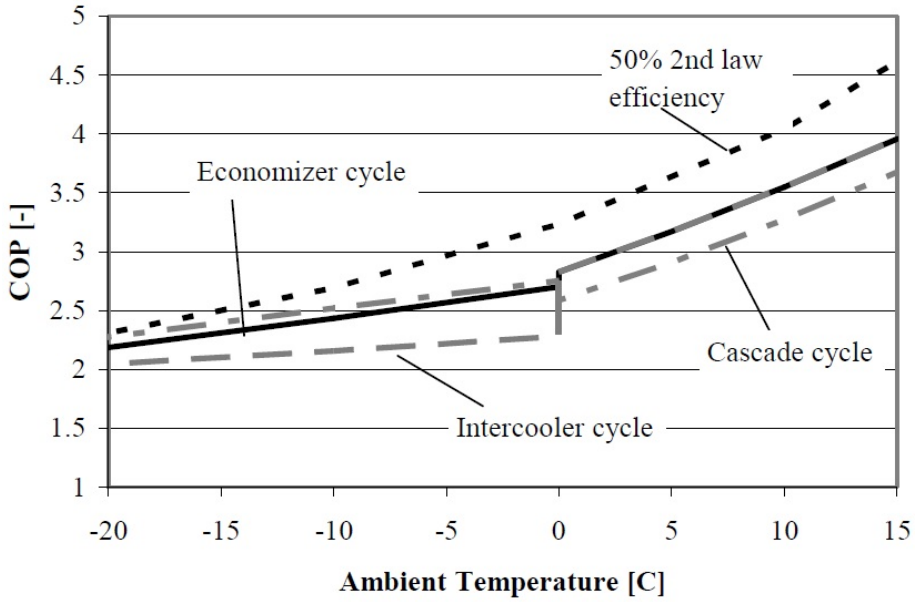

Figure 13: Comparison of the COP for the three technologies compared to a 50% second law efficiency (Bertsch et al., 2006)

The heating capacity compared to a linear heating demand of a building is plotted versus the outdoor temperature for all three technologies in Figure 14. All three cycles have similar capacities at the low ambient temperatures. The only noticeable difference between these technologies is at the warmer ambient temperatures. The cascade cycle COP is considerably lower than that of the economizer and intercooler cycles, and this is most likely due to the sizing selected for the high stage cycle. Bertsch et al. assumed the cascade cycle has an additional outdoor heat exchanger to allow for the high side cycle to operate without the low side cycle. Overall, all three cycles are predicted to be able to satisfy the heating load. The conclusion made from these results and the equipment required is that the two-stage economizer cycle would be the best choice for an ASHP in colder climates.

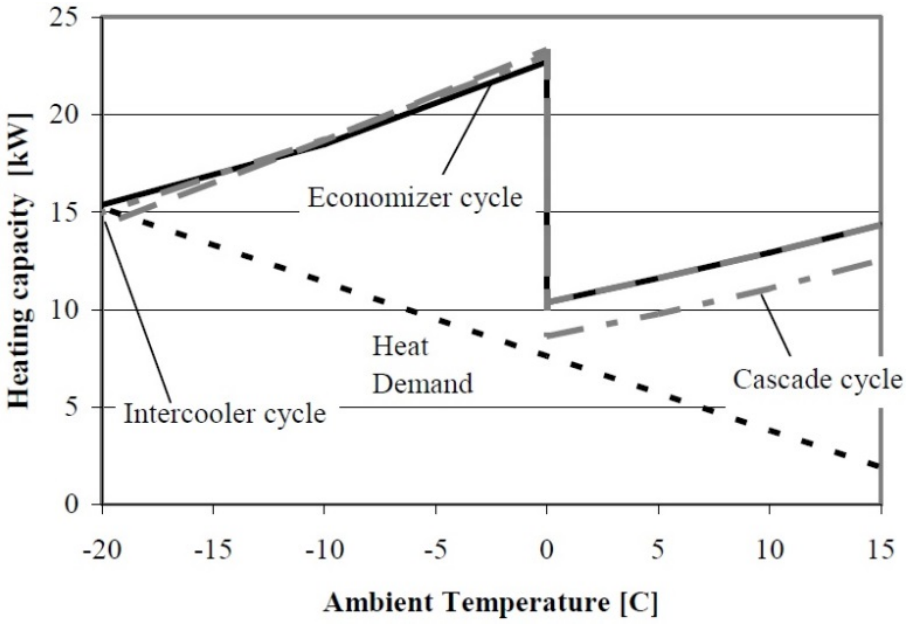

Figure 14: Comparison of the heating capacity for the three technologies (Bertsch et al., 2006)

4.2.2 Vapor injection (VI) heat pump

Heat pumps with compressor vapor injection (VI) can be classified into two fundamental configurations. One utilizes a flash tank also known as an open economizer and the other uses a heat exchanger economizer or closed economizer. Figure 15 shows a schematic of each system. The flash tank cycle uses an expansion valve before a fixed volume tank to separate the liquid and vapor refrigerant at an intermediate pressure. The saturated vapor is drawn from the top of the tank and enters an injection port on the compressor. The saturated liquid is expanded further to the evaporation pressure. For the economizing heat exchanger cycle, the subcooled liquid leaving the condenser is separated into two streams; one is expanded to an intermediate pressure and heated by subcooling the other refrigerant stream through the heat exchanger. The superheated refrigerant enters the injection port on the compressor. If the phase separation process in the flash tank was perfect and the superheat entering the injection port of the compressor from the economizer heat exchanger was zero, the ideal cycles of both systems would be thermodynamically identical (Wang et al., 2009).

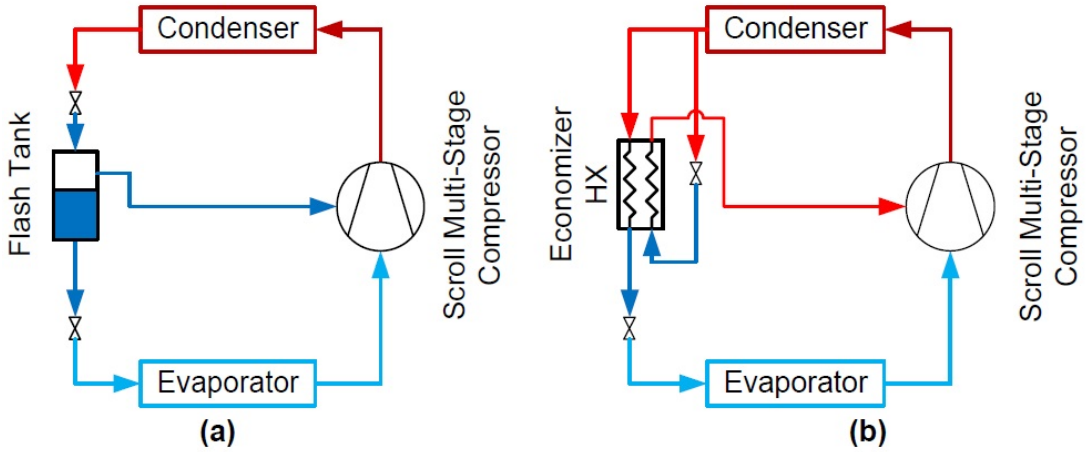

Figure 15: Schematic of two VI cycles with (a) flash tank (b) economizer heat exchanger (Abdelaziz et al., 2011)

These systems create a multi-stage compression process within one compressor by mixing the superheated vapor in the compressor with saturated or a smaller degree of superheated vapor. As the number of injection ports is increased to approach continuous injection, the compression process will follow the refrigerant vapor saturation curve. One model predicts that continuous injection will improve the system COP between 18% and 51% for common air-conditioning and refrigeration applications, where higher temperature lift cycles benefit most significantly (Mathison et al., 2011). Abdelaziz and Shen (2012) conducted an optimization analysis of the two cycles in Figure 15. Optimizations were conducted to 1) minimize heat exchanger (HX) area subject to prescribed capacity and COP at rating conditions (47°F or 8.3°C) followed by 2) analysis to maximize system efficiency subject to a minimum capacity constraint at a low temperature operation condition (-15°F or -26.1°C). Their results suggested that the flash tank cycle of Figure 15(a) offers both lower system HX sizes and better performance at the low ambient condition.

Experimental results on an 11 kW R410a heat pump with flash tank VI showed about 30% heating capacity improvement with 20% COP gain at the ambient temperature of −17.8°C (0°F) when compared to a conventional system having the same compressor displacement volume (Wang et al., 2009). The system capacity for both heating and cooling compared to the conventional system is shown in Figure 16 as a function of the outdoor temperature. The system heating and cooling capacity increases when vapor injection is used compared to the conventional system.

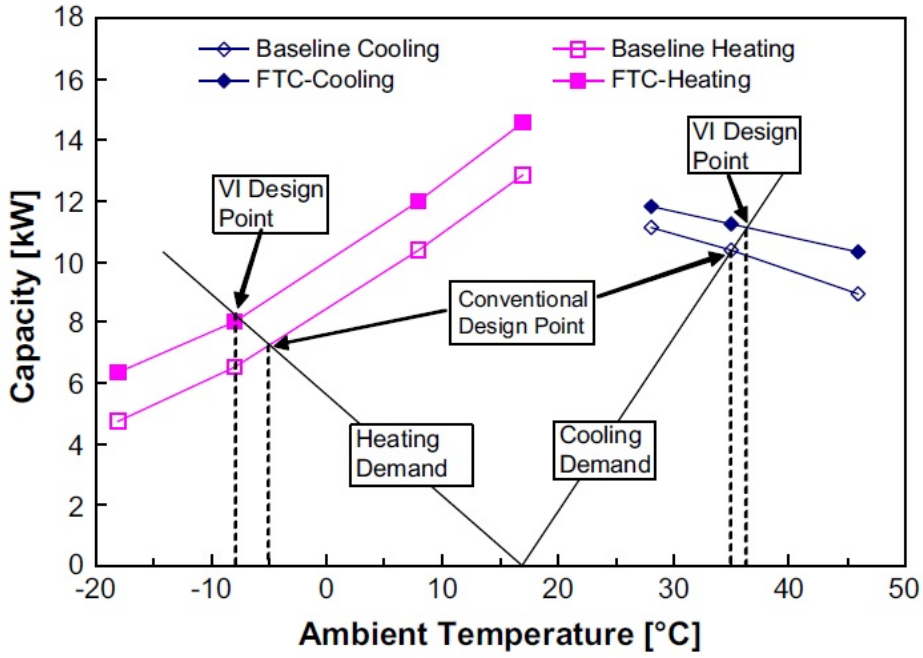

Figure 16: Flash tank VI cycle (FTC) compared to conventional (baseline) heat pump (Wang et al., 2009)

When comparing the two types of VI cycles, experimental results have shown the flash tank cycle to have a heating capacity and COP of 10.5% and 4.3% higher, respectively, than the economizing heat exchanger cycle (Ma and Zhao, 2008). A literature review of VI cycles concluded that the flash tank cycle is more favorable in terms of the performance improvement and cost while the economizing heat exchanger has the advantage of wider VI operating range (Xu et al., 2011). For R-410A, there have been some experimental and theoretical investigations of the air-source, vapor injection heat pump, but additional experimental results are needed to fully understand the various VI cycle options (Rohm et al., 2011).

VI cycle concepts utilizing multi-port compressors (one implementation of multi-stage VI compression) have also been investigated (Song, 2013; Ramaraj, 2012; Mathison et al., 2011). Figure 17 illustrates the cycle concept (a) and an example implementation in a scroll compressor (b). Previous theoretical and experimental work has shown that economizing holds significant potential to improve the performance of vapor compression equipment. Mathison et al. (2011) predicted that the maximum performance improvement with economizing can be achieved by continuously injecting two-phase refrigerant to maintain a saturated vapor state in the compressor. For an R-410A cycle evaporating at 5°C and condensing at 40°C, the cycle model predicts that economizing will improve the COP by approximately 18% in this limiting case. The benefits are even greater for a larger temperature lift application, such as a cold climate heat pumps; the model predicts that economizing can provide up to a 51% improvement in COP for a cycle using R-404A with an evaporation temperature of -30°C and a condensing temperature of 40°C. However, continuously injecting refrigerant is not only beyond the capabilities of current compressors, but also requires the development of equipment to continuously supply refrigerant to the compressor at the desired pressure and quality. In addition, injecting a two-phase mixture introduces the possibility for damage to the compressor if the evaporation process within the compressor is not well-understood.

Mathison (2011) demonstrated that using a finite number of injection ports and saturated vapor in place of a two-phase mixture provides a practical means for approaching the limiting cycle performance. For the R-410A cycle evaporating at 5°C and condensing at 40°C, the model predicted that injecting saturated vapor through three ports will provide a 12% improvement in COP, which is approximately 69% of the maximum benefit provided by economizing with continuous injection of two-phase refrigerant. Therefore, the development of the economized cycle currently focuses on using saturated vapor injection with two or three ports.

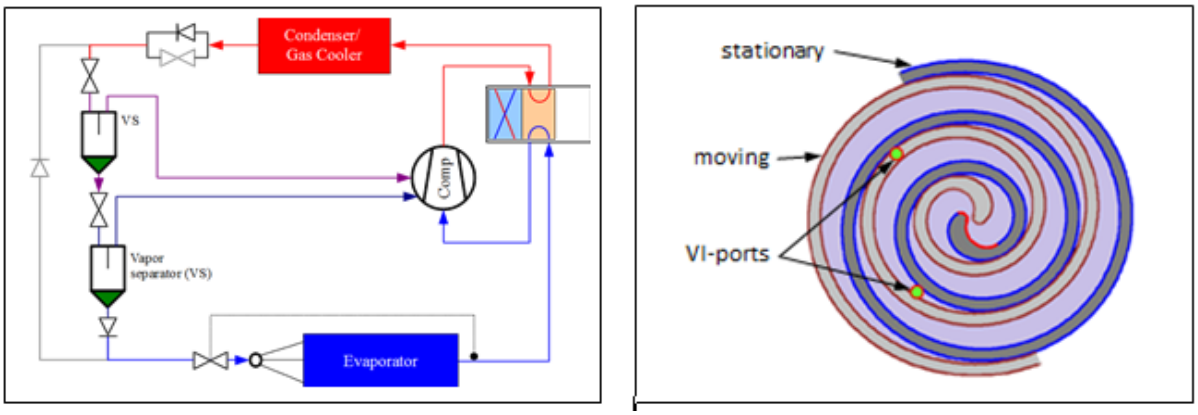

Figure 17: Multi-port VI compressor concept

4.2.3 Two-stage ASHPs with economizing

The only difference between a two-stage economizer (see schematic in Figure 12 (middle)) and VI cycle is two individual compressors are used with a mixing chamber in between instead of directly injecting vapor into a compressor chamber of the compressor. By compressing the refrigerant in stages, a second-law-based thermodynamic analysis shows the increase in irreversible losses at high-temperature differences can be minimized. A two-stage R-134a refrigeration system operating at -30°C evaporating and 60°C condensing has a 24% improvement in performance compared to a single-stage system (Zubair et al., 1996). Analysis on a cascade system highlights the reduction of entropy generation when compressing in stages. Going from 1 to 2 stages reduced the superheat losses significantly from 94 kJ/K-hr to 0.106 kJ/K-hr to reach an overall reduction of desuperheating entropy generation of 78% (Ratts et al., 2000).

An R-134a two-stage heat pump with both an economizing heat exchanger and a flash tank was used for heating water from a waste energy source. In spite of the higher source temperatures used, the experimental results demonstrated that the frequency control of the high-stage compressor to control the intermediate pressure resulted in an ability to improve the performance by as much as 5.2% as compared to the single-stage system without economizing under identical heat source conditions (Kwon et al., 2013). A normalized pressure was calculated using the three system pressures to identify the optimal operating point for fixed heat source temperatures. A plot of three different source temperatures for COP versus the normalized pressure is shown in Figure 18.

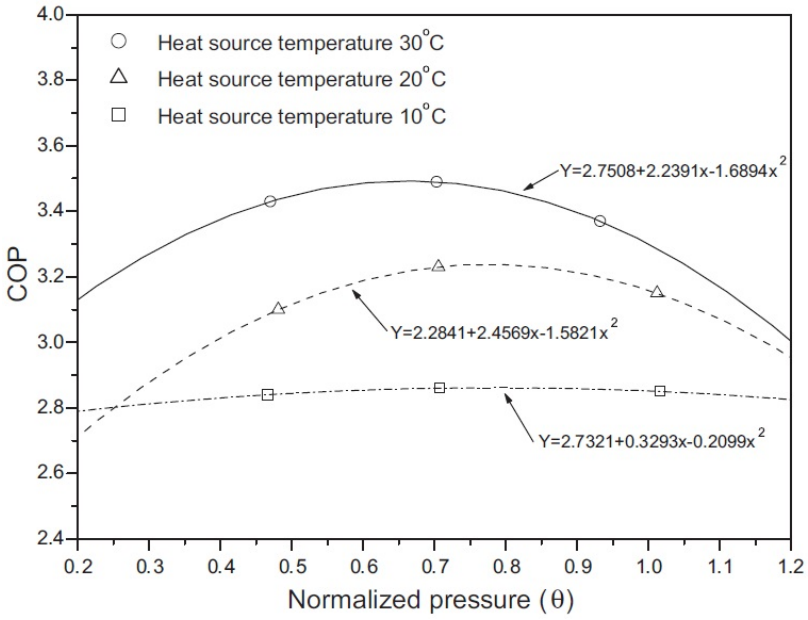

Figure 18: COP vs. normalized pressure of two-stage heat pump (Kwon et al. 2013)

An R-410A two-stage heat pump with an economizing heat exchanger was lab tested down to ambient temperatures of -30°C (-22°F), achieving a heating capacity and COP of roughly 11 kW and 2.1 respectively (Bertsch et al., 2008). The plots of the experimental results compared to the simulation of the system heating capacity and COP are shown in Figure 19. This capacity is about 85% of that measured for single-stage operation at the US rating condition of 8.3°C (47°F) vs. the ≥75% DOE goal listed in Table 1. The two-stage heat pump is shown to have much larger heating capacities than a conventional heat pump at low outdoor temperatures. Note that the system's measured space heating capacity in two-stage operation at ~-27°C (~-17°F) is very close to that at the standard U.S. rating condition of 8.3°C (47°F) when operating in single-stage mode. The system could also be easily built from off-the-shelf components with little modifications which identifies the commercialization potential of a two-stage heat pump with economizing heat exchanger. A field test prototype was built and tested in Indiana – results are discussed later in the Task2/3 part of this report.

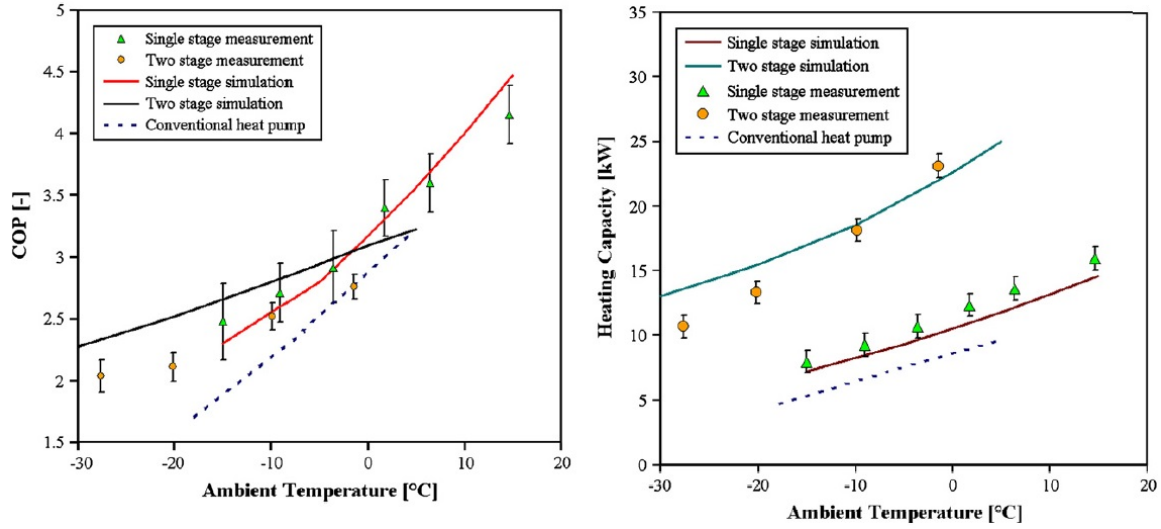

Figure 19: Experimental results of two-stage heat pump compared to simulation results; manufacturer's data was used to indicate performance of conventional HP (Bertsch et al. 2008)

4.2.4 Oil-flooded compressor concept investigation

The oil flooding concept utilizes oil injection into the compressor suction port(s) to absorb the heat of compression (reducing discharge temperature) and approach an isothermal compression process (Bell, 2011). Figure 20 illustrates a cycle schematic and p-h diagram of the concept. The addition of compressor flooding with regeneration in vapor compression systems results in a more isothermal compression process that can have a significant beneficial impact on system efficiency for large temperature lifts. For refrigerants with large pressure differences across the compressor, the use of a hydraulic expander can also help to recapture some of the work of compression of the flooding liquid. The engineering challenges in implementation of this technology are reasonable, which suggests that it could be applied readily in new equipment. Analyses indicate this concept has both capacity and efficiency advantages over VI cycles for low-temperature applications (Bell et al., 2011). In particular, the injection of oil results in an increase in refrigerant mass flow rate and overall isentropic efficiency and a decrease in the compressor discharge temperature. The analyses conducted so far clearly suggest that designing an efficient scroll compressor with oil injection for application to a low-source-temperature ASHP application will be possible with respect to energy performance and manufacturability.

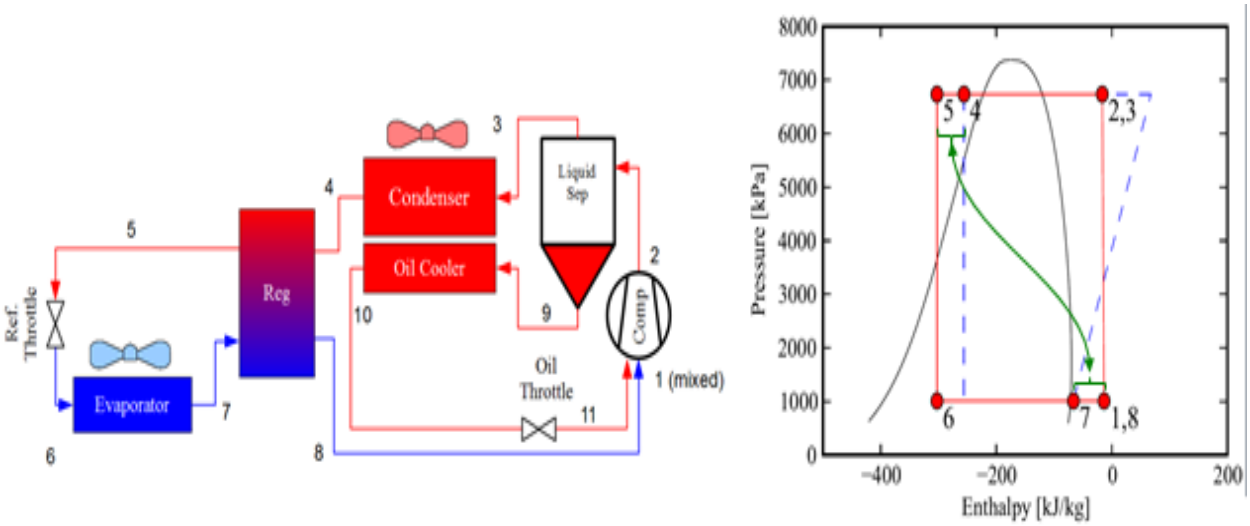

Figure 20: Schematic (left) and p-h cycle diagram (right) of flooded compressor cycle concept – from Bell (2011)

4.2.5 Cold climate field tests

A field test was performed in several northern U. S. locations on a commercially available, multi-capacity ASHP (Hadley et al., 2006) – *Note – product no longer manufactured today*. The manufacturer's data indicate a heating COP of 2.0 at -23.3°C (-10°F) for the heat pump, as shown in Table 3. Additional heating COPs at different ambient temperatures are compared to those of a standard ASHP.

Table 3: Manufacturer's heating COP data for field test ASHP designed for cold climates (CCHP) compared to a conventional air source heat pump (Std. ASHP) (Hadley et al., 2006)

Outdoor Air Temp.	-20°F	-10°F	0°F	10°F	20°F	30°F	40°F	50°F
CCHP	1.9	2.0	2.2	2.2	2.5	2.8	3.1	3.3
Std. ASHP	na	na	2.0	2.3	2.5	2.8	3.1	3.6

Five of the advanced heat pumps were monitored over a winter in Oregon and Idaho. Six months after the installation, one heat pump had a compressor failure that required replacement. The reason for the failure was never determined. Another complication occurred where a booster compressor never engaged at another location. The measured average heating COP for outdoor temperatures between -23.3°C and -20.5°C (-10°F and -5°F) was 1.2, about 40% lower than the manufacturer's data indicated. The results for all five heat pumps at different temperature bins are shown in Table 4. Overall the average field-measured COPs are considerably lower than the manufacturer's published values.

Table 4: Experimental results of the measured heating COP for all 5 locations (Hadley et al., 2006)

Outdoor Temperature Bin	-15°F to -10°F	-10°F to -5°F	-5°F to 0°F	0°F to 5°F	5°F to 10°F	10°F to 15°F	15°F to 20°F	20°F to 25°F	25°F to 30°F	30°F to 35°F	35°F to 40°F	40°F to 45°F	45°F to 50°F	50°F to 55°F
Chiloquin	-	-	-	-	-	1.3	1.5	1.6	1.6	1.7	1.9	1.9	1.8	2.0
Burley	-	-	1.7	1.1	1.2	1.3	1.4	1.5	1.6	1.7	1.6	1.7	1.7	1.6
Paul	1.5	1.5	1.6	1.6	1.6	1.6	1.6	1.7	1.8	1.9	2.0	2.1	2.1	1.9
Rigby	1.3	1.2	1.2	1.3	1.3	1.3	1.4	1.4	1.5	1.6	1.6	1.6	1.5	1.4
Ashton	-	1.0	1.4	1.3	1.2	1.2	1.2	1.3	1.3	1.3	1.4	1.4	2.0	1.7
Average	**1.4**	**1.2**	**1.5**	**1.3**	**1.3**	**1.4**	**1.4**	**1.5**	**1.6**	**1.6**	**1.7**	**1.7**	**1.8**	**1.7**

4.2.6 Summary – Recent R&D studies

The simulation and experimental results of several different heat pump cycles were presented that showed sufficient capacity and performance at low outdoor temperatures compared to conventional single-stage ASHPs for cold climates. The two-stage cycle presents an easier commercialization path due to the use of off-the-shelf components. Additional field testing is required to further validate the technology as market ready due to complications seen in previous field testing.

4.3 Complementary CCHP Market Promotion Activities

The US Northease Energy Efficiency Partnership (NEEP) established a voluntary specification for cold climate ASHPs to help promote wider use of heat pumps in the northern parts of the US and the Northeast area in particular. The specification was initially established in late 2014 with the most recent update effective January 1, 2017, and can be downloaded from the NEEP web site http://www.neep.org/initiatives/high-efficiency-products/emerging-technologies/ashp/cold-climate-air-source-heat-pump. It covers only air-to-air type variable-speed ASHPs (air-to-water ASHP and GSHPs are excluded). In order to be listed as complying with the NEEP specification, manufacturers' products must have a rated SCOPh ≥2.93 (US HSPF ≥10) for US climate region IV (moderate heating requirements) per AHRI Standard 210/240. In addition they must report space heating capacity and COP (from laboratory test data or engineering data) for at least 8.3°C, -8.3°C, and -15°C (47°F, 17°F, and 5°F) and at lower temperatures if available.

As of March 24, 2017, nearly 300 individual variable-speed ducted and ductless heat pump models were listed as complying with the latest NEEP CCHP specification V2.0. The list can be downloaded from the link above. Over 80% of the products listed are ductless types, either single-zone (2.6 to 9.4 kW nominal heating capacity) or multi-zone (2.9 to 14.1 kW nominal capcity). The remainder are centrally ducted (US type central air distribution systems) of about 6.5 to 16.5 kW nominal heating capacity.

The Electric Power Research Institute (EPRI) has also developed a specification for advanced ASHPs or Next Generation Heat Pumps (NextGen) (Domitrovic, 2017). This specification has two different levels or tiers. Under Tier 1 ASHP products must meet the same SCOPh requirement as for the NEEP specification above (≥2.93) but must also have space heating capacity at -8.3°C ≥80% of the rated capacity at 8.3°C. Under Tier 2, products must have a rated SCOPh ≥3.81 (US HSPF ≥13) for US climate region IV and a space heating capacity at -15°C ≥80% of the rated capacity at 8.3°C (rated performance as calculated per AHRI Standard 210/240). Only about 7% of the products listed on the NEEP website currently meet the more stringent Tier 2 requirements.

5 CONCLUDING REMARKS

All of the advanced ASHP system concepts discussed above can result in improved performance under extreme cold outdoor conditions. All address in one way or another the key challenge for electric-driven ASHPs under these conditions – to maintain or boost heating capacity and thereby reduce usage of backup electric resistance heating, thus yielding better heating SPFs. They also have another characteristic in common – all involve increased system complexity which will result in increased cost compared to conventional ASHPs. A number of viable ASHP products designed for cold climate applications now exist with rated performance that approaches the annual space heating efficiencies of GSHPs, gas-driven ASHPs, or other residential HVAC systems in cold climate locations.

6 ACKNOWLEDGEMENTS

The assembly of this report and the ORNL technical activities described herein are supported by the U. S. Department of Energy, Building Technologies Office (DOE/BTO) under Contract No. DE-AC05-00OR22725 with UT-Battelle, LLC. The official report number is ORNL/TM-2013/472.

The Purdue technical activities have been supported by the U. S. Department of Defense, Environmental Security Technology Certification Program (ESTCP), Energy and Water Projects, Cold Climate Heat Pump 201136, and by the U. S. Department of Energy under Award Number DE-EE0003842.

7 REFERENCES

Abdelaziz O. A., B. Shen, Z. Gao, V. D. Baxter, and I. Iu. 2011. “Development of a high performance air source heat pump for the US market.” Proceedings of the 10th IEA Heat Pump Conference, Tokyo, Japan. CD rom format only.

Abdelaziz O. A. and B. Shen. 2012. “Cold Climates Heat Pump Design Optimization,” *ASHRAE Transactions*, Vol. 112, Part 1.

Abdelaziz O. A. 2013. “ORNL Cold Climate – Experimental Investigations,” presentation at Annex 41, 1st Working Meeting, Purdue University, July 1.

AHRI 2008. ANSI/AHRI Standard 210/240-2008, “Performance Rating of Unitary Air-Conditioning and Air Source Heat Pump Equipment,” Air-Conditioning, Heating, and Refrigeration Institute, Arlington, VA, USA.

AHRI 2010-2017. Central Air Conditioners and Air-Source Heat Pumps Historical Data. Retrieved from AHRI website (www.ahrinet.org) in December 2010 and in January 2017).

AHRI 2012. "HVAC&R & Water Heating Industry Statistical Profile," 2012 Edition.

ASHRAE 2010. ANSI/ASHRAE Standard 55-2010, "Thermal Environmental Conditions for Human Occupancy," American Society of Heating, Refrigerating, and Air-Conditioning Engineers, Atlanta, GA, USA.

Bach C. K., J. A. Braun, E. A. Groll, and W. T. Horton. 2013. "Cold Climate Heat Pumps Performance improvement by modification of compression process and cycle," presentation at Annex 41, 1st Working Meeting, Purdue University, July 1.

Bell I. H. 2011. "Theoretical and Experimental Analysis of Liquid Flooded Compression in Scroll Compressors," PhD Thesis, Herrick Laboratories, Purdue University, West Lafayette, IN, USA.

Bell I. H., E. A. Groll, and J. E. Braun. 2011. "Performance of Vapor Compression Systems with Compressor Oil Flooding and Regeneration," *International Journal of Refrigeration*, Vol. 34, No. 1, pp. 225-233.

Bertsch S. S. 2005. "Theoretical and experimental investigation of a two stage heat pump cycle for Nordic climates," (Doctoral dissertation, Master's thesis, Mechanical Engineering, Herrick Labs 2005-13P, Report).

Bertsch S. S. and E. A. Groll. 2006. "Air Source Heat Pump for Northern Climates Part I: Simulation of Different Heat Pump Cycles," Proceedings of the 11th International Refrigeration and Air Conditioning Conference at Purdue.

Bertsch S. S. and E. A. Groll. 2008. "Two-stage air-source heat pump for residential heating and cooling applications in northern US climates," *International Journal of Refrigeration*, Vol. 31(7), pp. 1282-1292.

Bucher M. E., C. M. Grastataro, and W. Coleman. 1989. "Heat Pump Life and Compressor Survival in Diverse Climates," EPRI Report No. CU-6254, February 1989 (AEP).

Bullock C. E. 1978. "Energy Savings through Thermostat Setback with Residential Heat Pumps," *ASHRAE Transactions*, Vol. 84, Part 1.

Bullock C. E., G. C. Groff, and W. R. Reedy. 1980. "Sizing of Air-to-Air Heat Pumps for Northern Climate Residential Heating Applications," Proceedings of the International HVAC Congress, Berlin, Germany, April 17-18.

Caskey S. L., E. A. Groll, and W. J. Hutzel. 2013. "Cold Climate Heat Pump Field Demonstration of Air-Source Heat Pump with Two-Stage Compression and Economizing," presentation at Annex 41, 1st Working Meeting, Purdue University, July 1.

Caskey S. L. 2013. "Cold Climate Field Test Analysis of an Air-Source Heat Pump With Two-Stage Compression and Economizing," Master's Thesis, Purdue University, Ray W. Herrick Laboratories, West Lafayette, IN.

Census Bureau, U.S. 2016. Census Bureau's Characteristics of New Single-Family Homes Reports.

Conti, J., and P. Holtberg. 2011. "International Energy Outlook 2011," Washington: Independent Statistics and Analysis of US Energy Information Administration.

Department of Defense, U.S., Energy Security Task Force, Office of the Under Secretary of Defense. 2009. The WSTIAC Quarterly, Vol. 9, No. 1.

Department of Energy, U.S. 2011. "Buildings Energy Databook," Office of Energy Efficiency & Renewable Energy.

Energy Independence and Security Act of 2007. Public Law, (110-140), 2.

Energy Information Administration, U.S. (EIA) 2009. "Residential Energy Consumption Survey," Tables HC6.8, HC6.9, HC6.10, and HC6.11. Accessed September 2013.

Energy Information Administration, U.S. (EIA) 2013. "Annual Energy Outlook (AEO)." Early Release Overview, Release Date: December 5, 2012, Report Number: DOE/EIA-0383ER.

Energy Information Administration, U.S. (EIA) 2013. "Annual Energy Outlook 2013," DOE/EIA-0383(2013), retrieved September 2013.

Executive Order. 2009. 13514. Federal Leadership in Environmental, Energy, and Economic Performance.

Groff G. C. and W. R. Reedy. 1978. "Investigation of Heat Pump Performance in the Northern Climate through Field Monitoring and Computer Simulation," *ASHRAE Transactions*, Vol. 84, Part 1.

Groff G. C., C. E. Bullock, and W. R. Reedy. 1978. "Heat Pump Performance Improvements for Northern Climate Applications," pp. 838-846 in Proceedings of the 13th International Energy Conversion Engineering Conference, San Diego, CA, USA, September. Society of Automotive Engineers. Paper no. 789455.

Groff G. C., W. R. Reedy, and C. E. Bullock. 1979. "Recent Investigation of Air-Source Heat Pump Performance in Cold Climates," Paper E1-25 in Proceedings of the 15th International Congress of Refrigeration, Venice, Italy, September 23-29. International Institute of Refrigeration.

Groff G. C. and J. P. Moreau. 1983. "An Investigation of Air-to-Water Heat Pump Performance in New and Existing French Homes," *ASHRAE Transactions*, Vol. 89, Part 1.

Groff G. C. and R. E. Ertinger. 1984. "Heat Pumps in the USA – Projections for the Future," Published in the Proceedings of the 1st International Energy Agency Heat Pump Conference, Graz, Austria, May.

Groff G. C., C. E. Bullock, and R. E. Hough. 1984. "An Investigation of Electric Heat Pumps Applied to Commercial Buildings," Published in the Proceedings of the 1st International Energy Agency Heat Pump Conference, Graz, Austria, May.

Hadley A., J. Callahan, and R. Stroh. 2006. "Without strip heat: In-Situ monitoring of a multi-stage air source heat pump in the Pacific Northwest," Bonneville Power Administration.

Khowailed G., K. G. Sikes, and O. A. Abdelaziz. 2011. "Preliminary Market Assessment for Cold Climate Heat Pumps," Oak Ridge National Laboratory report ORNL/TM-2011/422, August.

Kwon O., D. Cha, and C. Park. 2013. "Performance evaluation of a two-stage compression heat pump system for district heating using waste energy," *Energy*.

Lannus A. 1993. "Expanding the Limits: Heat Pump Technology and markets in North America," p. 373-380 in *Heat Pumps for Energy Efficiency and Environmental Progress*. Proceedings of the 4th International Energy Agency Heat Pump Conference, Maastricht, The Netherlands, April 26-29.

Lapsa M. and G. Khowailed. 2011. "The Evolution of the U.S. Heat Pump Market," Proceedings of the 10th International Energy Agency Heat Pump Conference, Tokyo, Japan.

Lovvorn N., C. C. Hiller, and A. Bartolucci. 2001. "Heat Pump Life in Alabama—Revisited: A Follow-Up Survey 13 Years Later," EPRI, Palo Alto, CA, and Alabama Power Company, Birmingham, AL: 2001. 1006265.

Lovvorn N. and C. C. Hiller. 2002. "Heat Pump Life Revisited," *ASHRAE Transactions*, Vol. 108, Part 2.

Mahderekal I., B. Shen, E. A. Vineyard. 2012. "System Modeling of Gas Engine Driven Heat Pump," Proceedings of 14th International Refrigeration and Air Conditioning Conference at Purdue, West Lafayette, IN.

Mathison M. M., J. E. Braun, and E. A. Groll. 2011. "Performance Limit for Economized Cycles with Continuous Refrigerant Injection," *International Journal of Refrigeration*, Vol. 34, pp. 234-242.

Mathison M. M. 2011. "Modeling and Evaluation of Advanced Compression Techniques for Vapor Compression Equipment," PhD Thesis, Purdue University, Ray W. Herrick Laboratories, West Lafayette, IN.

Pientka K. A. 1987. "Heat Pump Service Life and Compressor Longevity in a Northern Climate," *ASHRAE Transactions*, Vol. 93, Part 1.

Ramaraj S. 2012. "Vapor compression enhancements for cold climate heat pumps," Master Thesis, Herrick Laboratories, Purdue University, West Lafayette, IN, USA.

Rice, C. K., B. Shen, and S. S. Shrestha, 2015, *An Analysis of Representative Heating Load Lines for Residential HSPF Ratings*, ORNL TM-2015/281, UT-Battelle LLC, Oak Ridge National Laboratory, July.

Rice, C. K., B. Shen, and S. S. Shrestha, 2016. *Revised Heating Load Line Analysis: Addendum to ORNL/TM-2015/281*, ORNL/TM-2016/293, , UT-Battelle LLC, Oak Ridge National Laboratory, July.

Ratts E. B. and J. S. Brown. 2000. "A generalized analysis for cascading single fluid vapor compression refrigeration cycles using an entropy generation minimization method," *International Journal of Refrigeration*, Vol. 23(5), pp. 353-365.

Rohm C. W. and M. S. Kim. 2011. "Effects of intermediate pressure on the heating performance of a heat pump system using R410A vapor-injection technique," *International Journal of Refrigeration*, Vol. 34(8), pp. 1911-1921.

Roth K. W., D. Westphalen, J. Dieckmann, S. D. Hamilton, & W. Goetzler. 2002. "Energy consumption characteristics of commercial building HVAC systems Volume III: Energy savings potential," Report prepared by TIAX LLC for DOE Building Technologies Program.

Ryan J. D. and G. C. Groff. 2002. North American Market Overview. pp. 26-37 in *Heat Pumps – Better by Nature*. Proceedings of the 7th International Energy Agency Heat Pump Conference, Beijing, China, May 19-22.

Shen B. and C. K. Rice. 2012. "Multiple-Zone Variable Refrigerant Flow System Modeling and Equipment Performance Mapping," Conference CD of ASHRAE 2012 Winter Conference, Chicago, IL.

Shen B., O. Abdelaziz, and C. K. Rice. 2012a. "Auto-Calibration and Control Strategy Determination for a Variable-Speed Heat Pump Water Heater Using Optimization," *HVAC&R Research*, Vol. 18(5), pp. 904–914, 2012.

Shen B., C. K. Rice., and E. A. Vineyard. 2012b. "Development of 20 IEER Rooftop Units – A Simulation Study," Proceedings of 14th International Refrigeration and Air Conditioning Conference at Purdue, West Lafayette, IN.

Shen B. 2013. "Cold Climate Heat Pump – ORNL System Modeling and Analysis," presentation at Annex 41, 1st Working Meeting, Purdue University, July 1.

Shen, B., S. S. Shrestha, and O. A. Abdelaziz. 2013. "Assessment of Main Strategies for Achieving Performance Targets for Cold Climate Heat Pump," draft ORNL Report (under review), February, 2013.

Song. 2013. "Modeling and experimental validation of multi-port vapor injected scroll compressor," Master Thesis, Herrick Laboratories, Purdue University, West Lafayette, IN, USA.

Wang S. and A. Majumdar. 2004. "Digital Scroll Technology," *ISHRAE Journal*, January-March, Issue 2004.

Wang X., Y. Hwang, and R. Radermacher. 2009. "Two-stage heat pump system with vapor-injected scroll compressor using R410A as a refrigerant," *International Journal of Refrigeration*, Vol. 32(6), pp. 1442-1451.

Xu X., Y. Hwang, and R. Radermacher. 2011. "Refrigerant injection for heat pumping/air conditioning systems: literature review and challenges discussions," *International Journal of Refrigeration*, Vol. 34(2), pp. 402-415.

Zubair S. M., M. Yaqub, and S. H. Khan. 1996. "Second-law-based thermodynamic analysis of two-stage and mechanical-subcooling refrigeration cycles," *International Journal of Refrigeration*, Vol. 19(8), pp. 506-516.

U.S. Team Report

IEA HPT TCP Annex 41
Cold Climate Heat Pumps"

Tasks 2 and 3 – Simulation Results and Prototype Lab and Field Experiments

Submitted by:

Ray Herrick Laboratories, Purdue University
Lead: Eckhard A. Groll (contact: groll@purdue.edu)
Contributors: Christian K. Bach (contact: cbach@okstate.edu)
Stephen L. Caskey (contact: scaskey@purdue.edu)
Alejandro C. Lavernia (contact: alaverni@purdue.edu)
Nicholas Salts (contact: nsalts@purdue.edu)

Oak Ridge National Laboratory
Lead: Van Baxter (contact: vdb@ornl.gov)
Contributors: Bo Shen
Omar Abdelaziz
C. Keith Rice
Gerald Groff, consultant
Gannate Khowailed, CSRA International
Karen Sikes, CSRA International

January 2017

TABLE OF CONTENTS

LIST OF TABLES

LIST OF FIGURES

1 INTRODUCTION

In 2010 the U.S. Department of Energy's Building Technology Office (DOE/BTO) solicited R&D proposals focused on advancing heat pump technology for cold climate applications – i.e. CCHPs. DOE's CCHP performance targets provided in that solicitation are listed in Table 1 of the Task 1 report. In 2013, DOE modified those goals somewhat in light of analyses results highlighted in Task 1. The revised targets are in Table 1 below; very similar to the 2010 targets with some modification to the nominal heating capacity target and removal of specific COP targets. ASHPs continued to be the primary technology focus.

Table 1: U.S. CCHP performance targets – 2013

Outdoor Temperature	Heating Capacity
8.3°C (47°F)	9-21 kW (2.5-6 tons), nominal rating
-25°C (-13°F)	≥75% of nominal rating

U.S. CCHP R&D efforts described in the Task 1 report and this Task 2/3 report are focusing on analyses and experimental (lab and field) investigation of several advanced VC cycles for ASHPs. Vapor injection (VI) cycle concepts, two-capacity compressors, variable speed (VS) compressors, parallel compressors, two-stage cycles with economizers, a liquid-flooded compressor cycle concept, and several other advanced cycle approaches have been investigated.

In the sections that follow, current U.S. R&D results under Tasks 2 and 3 of Annex 41 are summarized for three cycle concepts identified in Task 1 as among the most promising for meeting the goals noted in Table 1.

2 TWO-STAGE ECONOMIZER SYSTEM

Research at Purdue University's Herrick Labs identified a number of cycle concepts that could be useful for ASHPs in cold climate applications (Bertsch et al., 2006). Of these, three were seen to have the highest relative efficiency and relative heat output with low or acceptable discharge temperatures and were selected for detailed comparison – the two-stage using an intercooler, the two-stage using an economizer, and the cascade cycle. Figure 1 illustrates the three cycles.

System simulation models were created for each of the three technologies to simulate the heating capacity and performance for comparison. The heating supply temperature for each was fixed to 50°C (122°F). Both the intercooler and economizer cycles showed similar performance at temperatures above 0°C (32°F) while the cascade cycle performed relatively better at colder temperatures. All cycles showed COPs above 2 at the low outdoor temperatures indicating reasonably good efficiency during these extremes. All three cycles had similar capacities at the low ambient temperatures. The only noticeable difference between these technologies is at the warmer ambient temperatures. The cascade cycle COP is considerably lower than that of the economizer and intercooler cycles, and this is most likely due to the sizing selected for the high-stage cycle. Bertsch et al. (2006) assumed the cascade cycle has an additional outdoor HX to allow for the high side cycle to operate without the low side cycle. Overall, all three cycles are predicted to be able to satisfy the heating load. The conclusion made from these results and the equipment required (relative cycle complexity) is that the two-stage economizer cycle would be the best choice for an ASHP in colder climates.

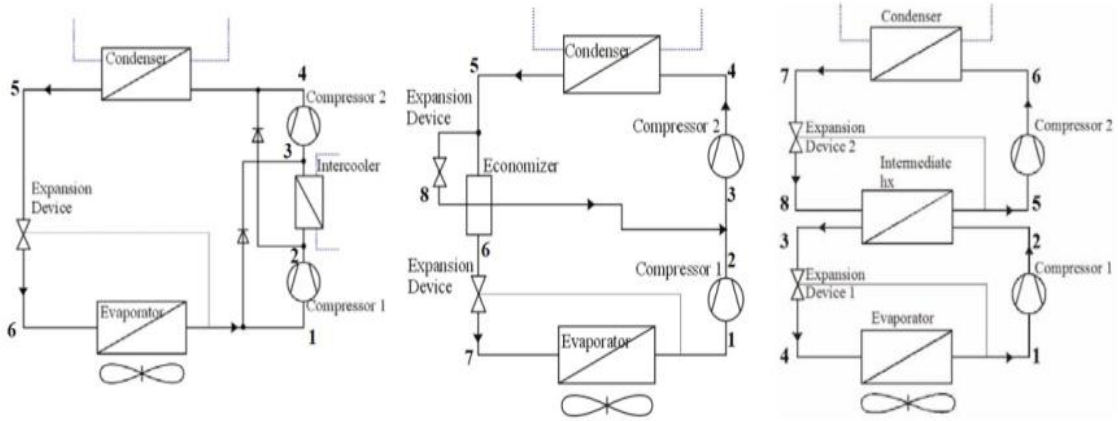

Figure 1: Heat pump cycle schematics - Intercooler (left), Economizer (middle), Cascade (right) (Bertsch et al., 2006)

A two-stage, economizer system using R-410A was experimentally tested down to ambient temperatures of -30°C (-22°F), achieving a heating capacity and COP of roughly 11 kW and 2.1, respectively (Bertsch et al., 2008). The plots of the experimental results compared to the simulation of the system heating capacity and COP are shown in Figure 2. The two-stage heat pump is shown to have much larger heating capacities than a conventional heat pump at low outdoor temperatures. For an outdoor air temperature of about -29°C (~-20°F), the tested capacity was ~11kW or ~85% of the measured capacity at the U.S. nominal heat pump rating condition of ~8.3°C (47°F) compared to the desired target of 75% (Table 1). The lab test system was easily built using off-the-shelf components with little modification, showing promise for being manufacturable with relatively low cost premium compared to conventional ASHPs.

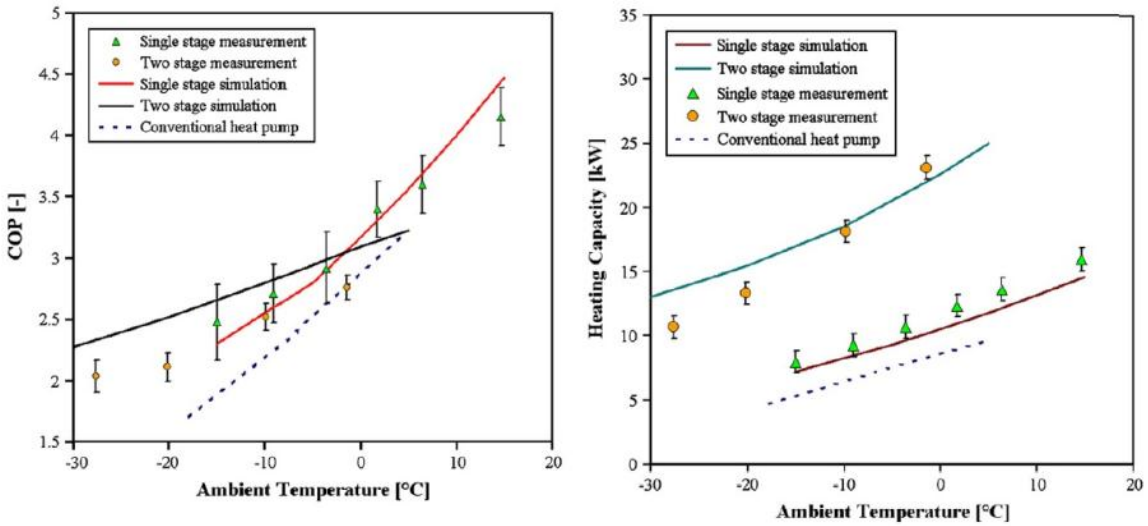

Figure 2: Experimental results of two-stage heat pump compared to simulation results; manufacturer's data was used to indicate performance of the conventional single-stage ASHP (Bertsch et al., 2008)

A field test of an advanced two-stage ASHP designed for cold climate operation has been completed at Camp Atterbury, a U.S. Army base outside Edinburgh in Indiana (Caskey et al., 2013). The heat pump was a two-compressor (two-stage) system with an economizer VI loop, similar to the concept analyzed by Bertsch et al. (2008). It featured a large tandem scroll compressor (two parallel compressors) for capacity boosting during low ambient temperature heating operation and a variable speed scroll compressor for moderate ambient

temperature heating and cooling operation. The test was conducted under the DOD's Energy Security Technology Certification Program (ESTCP). Two identical military barracks from available buildings located at Camp Atterbury were selected for the field demonstration. The originally installed HVAC system was a natural gas furnace with a split system A/C. A side-by-side performance comparison between the originally installed HVAC system and the two pre-commercial heat pump units developed at Purdue University was conducted during the 2012-2013 heating season. Only commercially available components were selected for all parts of the heat pump units with help from three industrial partners, namely Ingersoll Rand - The Trane Company, Emerson Climate Technology, and Danfoss. The heat pump units had a design heating capacity of 18.34 kW (62,580 BTU/h) at an ambient temperature of -20°C (4°F).

The heat pump performance was compared to the existing HVAC system using six performance objectives that are listed in Table 2. The objective of the project was to reach or surpass the success criteria listed for each performance objective.

Table 2: ESTCP project performance objectives of the cold climate heat pump

Performance Objective	Metric	Data Requirements	Success Criteria
Quantitative Performance Objectives			
1. Reduce primary energy for heating (Energy)	Therms or kW-hr	Electric and gas use metered	Reduce primary energy use by 25%
2. Reduce costs (Finances)	$	Base rates for electricity and fuel	10% reduction in heating costs
3. Reduce emissions (Environment)	Metric ton CO_2 equivalent	Conversions for fuels	Reduce CO_2 emissions by 15%
Qualitative Performance Objectives			
4. Ease of installation	Ability of a technician-level individual to install the heat pump	Feedback from the technicians on installation time	A field technician team is able to install the system
5. Maintenance	Ability of a technician-level individual to maintain the heat pump	Feedback from the technicians on maintenance calls	A field technician team is able to operate the system
6. Comfort	Maintain temperature within comfort range of building occupants	Indoor temperature readings and survey of occupants	80% of occupants satisfied with indoor conditions

Caskey et al. (2013) discussed results of the field test from the 2012-2013 heating season in general comparison with the criteria listed in Table 2. For the monitored period at the Army site, the ASHP system achieved approximately 19% source energy savings vs. the baseline gas furnace system but utility costs were higher due to the low price the Army pays for natural gas at the site. [NOTE – the choice of baseline system was dictated by the project sponsor, the U.S. Department of Defense.] Using average Indiana residential electricity and gas prices, the utility costs for the ASHP and baseline furnace would have been comparable. This operation cost equivalence, despite the energy savings of the ASHP, is because the price for natural gas in Indiana is about one-third that of electricity per unit of energy delivered, which is true of most locations in the United States. The ASHP used no electric backup heating during the test period. Using ASHRAE Standard 55 (ASHRAE, 2010) to evaluate the thermal comfort indicated that the heat pump was able to maintain comfort levels throughout the heating season. Furthermore, while the first cost of the two-stage

ASHP will be higher than that of a conventional single-stage ASHP, the installation and maintenance costs are estimated to be comparable.

3 TWO-PORT VAPOR INJECTED COMPRESSION WITH REGENERATION CONCEPT

An experimental investigation was conducted at Purdue University using a commercially available 5-ton heat pump that was retrofitted with a two-port vapor injected scroll compressor. The injection ports within the two compression pathways were located in the fixed scroll with different distance from the suction chamber. The vapor at the two injection pressure levels was generated using two flash tank separators in a cascade configuration. This configuration made it necessary to not only control the superheat but also the liquid levels in the separators and subcooling of the refrigerant leaving the condenser.

Baseline performance data of the heat pump without vapor injection was obtained and compared with that of the two-port vapor injection system. For the baseline, the injection lines to the compression pockets were plugged within the fixed scroll to reduce dead volume and re-expansion losses. Also, the vapor-separator section was shut off and bypassed. In the second step, the plugs were removed and a staged expansion process was performed using the separator section. The generated vapor from each separator was injected into the respective compressor port causing an intercooling effect on the compression process.

The heat pump is a split air-to-air system with an outdoor unit and indoor unit. The indoor unit contains the AC-mode expansion device, the heat exchanger, and the indoor blower. The outdoor unit contains the outdoor heat exchanger and blower motor, the compressor, vapor separators, and control valves necessary to facilitate the different operating modes of the system. Only heating mode operation was considered during the testing. The compressor is operated on a variable speed drive, allowing a closer match between heating requirement of the building and the capacity of the heat pump. For single stage operating mode, Figure 3 (B0), the vapor separators are bypassed by an electronic expansion valve (EXV). The refrigerant is evaporated and superheated in the outdoor heat exchanger, then passes through the 4-way valve and accumulator (acc) to the compressor suction. The refrigerant is compressed by the compressor and passes through discharge muffler (M) and the 4-way valve to the indoor heat exchanger, where it is condensed and subcooled. The subcooled refrigerant travels through the bypass valve in the thermostatic expansion valve (TXV) and the filter drier back to the EXV. In flash gas bypass operating mode (B0 FGB), Figure 4, the flash gas from the expansion process is taken off using the low pressure (LP) separator before the evaporator and bypassed through a control valve directly to the accumulator while the liquid refrigerant is drained to the evaporator.

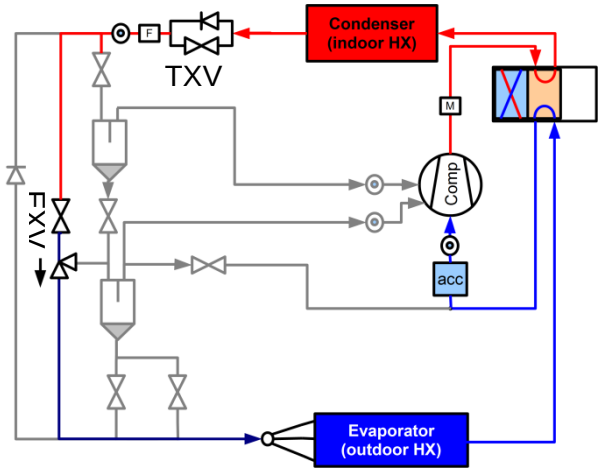

Figure 3: Single stage operating mode (B0)

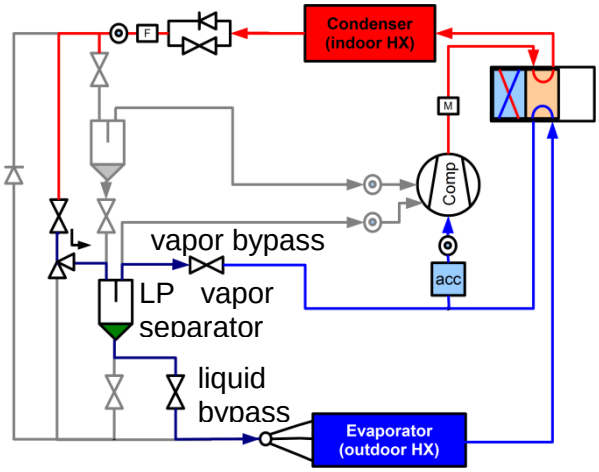

Figure 4: Flash gas bypass operating mode (B0 FGB)

The injection ports of the compressor are internally plugged for both the B0 and B0 FGB configurations. This was done to reduce re-expansion losses. These plugs are removed for the vapor injected configuration (B1), Figure 5. In that configuration, the expansion process is split up into three stages, where the flash gas from the high pressure and intermediate pressure expansion is injected into the injection ports of the compressor. For the vapor injected mode with hybrid control, as indicated in Figure 6, the last expansion process is done using 5 balancing valves, where each valve controls the superheat of a neighboring circuit pair of the outdoor heat exchanger. This approach, named reduced hybrid control, reduces the number of balancing valves when compared to hybrid control as introduced by Kim *et al.* (2008) by 50% for an even number of circuits. The tested heat pump additionally used 2-step balancing valves, which are expected to be cheaper to produce than electronic expansion valves.

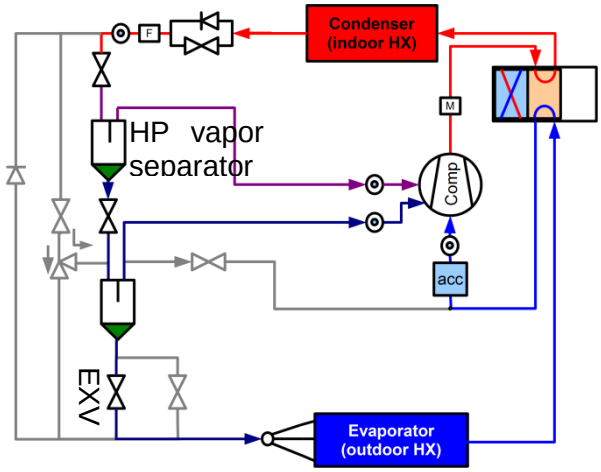

Figure 5: Vapor injection operating mode (B1)

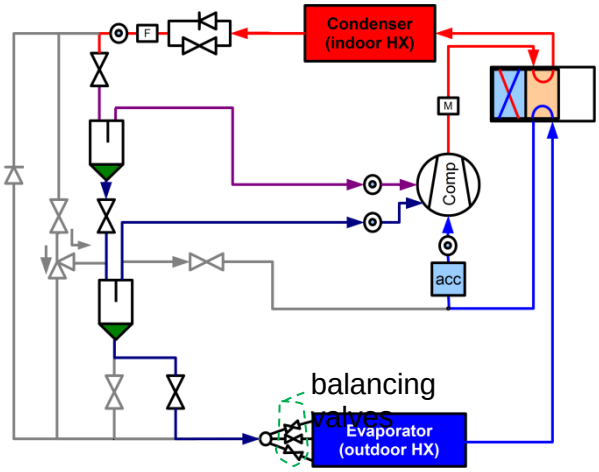

Figure 6: Vapor injection operating mode (B1H)

Refrigerant inlet and outlet temperatures were measured for all major components. Air inlet and outlet temperatures were measured using thermocouple grids for both indoor and outdoor units. Inlet dew point was measured for the indoor and outdoor units with the outlet dew point measured at the outdoor unit. Chilled mirror sensors were used for all dew point temperature measurements. The relative humidities at the air inlet of the indoor and outdoor units were measured as a backup in case of sensor failure. The air-side flow rate of the

indoor unit was measured using an ASHRAE nozzle box that follows ASHRAE 41.2 (ASHRAE, 1987).
The different operating modes lead to different methods for controlling the system. For the B0 configuration, superheat was the only controlled variable; subcooling was between 4 and 5 K for clean coil operating conditions. For the B0 configuration with flash gas bypass, subcooling was additionally controlled. For the vapor injected configurations, liquid levels in the two separators were controlled to allow the charge in the system to balance. Superheat for the vapor injected system was either controlled by a single valve or, in case of the hybrid control scheme, by the balancing valves. The balancing valves were used to equalize the superheats and to move the overall superheat to the target value. The setpoint for both superheat and subcooling was 5 K for all system configurations. It was necessary to increase the superheat setpoint for some operating conditions to maintain stable operation of the system.

Test data was taken under steady state operating conditions, e.g. no or only small trend in discharge temperature and all other temperatures and pressures. The start of the steady state period was judged during system operation, after the start of that period, at least 30 minutes of steady state data was taken. This resulted in 30 minutes or more of steady state data after the final data selection. The average absolute mismatch between useful airside and refrigerant side capacity was 2.2%, with the maximum occurring value being 3.7%. Reported values in this paper are based on the refrigerant side, due to the better accuracy of these measurements.

Figures 7 and 8 show the improvement in COP and capacity relative to the baseline system (B0). Vapor injection leads to significant improvement in capacity, with about 11% at high ambient temperature and 28% at -8.3°C ambient temperature. For the “fix capacity” case, compressor speed was reduced to match the baseline B0 capacity – with exception of the H1 test, where no further reduction of compressor speed was possible. The COP improvements are smaller – with identical compressor speed than for the baseline, up to 3.7% improvement is possible. If capacity is matched, more than 6% COP improvement is possible. COP improvement tends to increase towards lower ambient temperatures. One of the reasons for this is that the performance improvement due to vapor injection becomes more important than the re-expansion losses at the injection ports since the cooling effect of the injected vapor becomes more significant. The flash gas bypass only leads to a COP (3%) and capacity (7%) improvement for the H2 condition, but did not lead to any benefits for the other operating conditions.

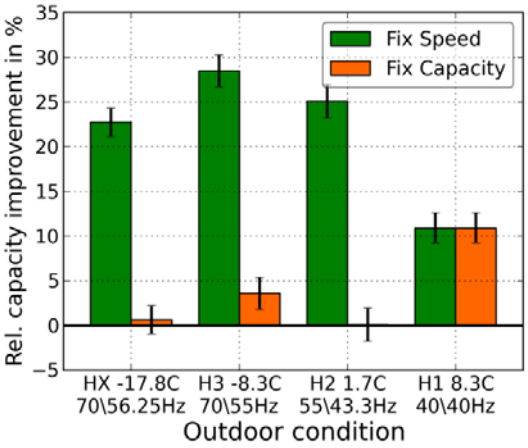

Figure 7: Relative capacity improvement, B1 vs. B0

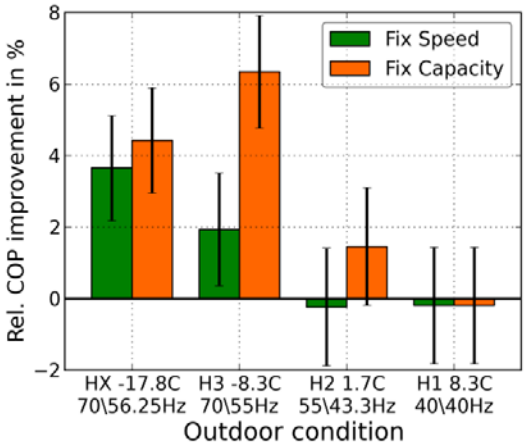

Figure 8: Relative COP improvement B1 vs. B0

One benefit of the vapor injection is that the capacity degrades less towards lower ambient temperature if the same compressor speed is used. Figure 9 shows that the capacity for the vapor injected system increases by nearly 7% as ambient temperature decreases from the H1 to the H3 test while compressor speed is increased from 40 to 70 Hz. For the same conditions, the B0 system capacity decreases by 2%. The differences in COP are less pronounced as shown in Figure 10. The COP for all tested system configurations – even at the lowest ambient temperature – exceeds 2. COP decreases from the highest ambient temperature to the lowest ambient temperature. For the B0 system, the COP for HX conditions (i.e., with additional HX) is 70% of the COP for H1 conditions. For the vapor injected system, a relative COP of 72% of H1 conditions is maintained under HX conditions. Application of the hybrid control leads to additional improvement of COP and capacity over the vapor injected system with a standard distributor.

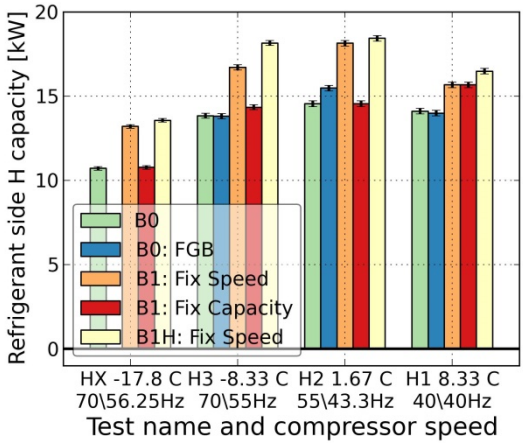

Figure 9: Relative capacity improvement, B1 vs. B0

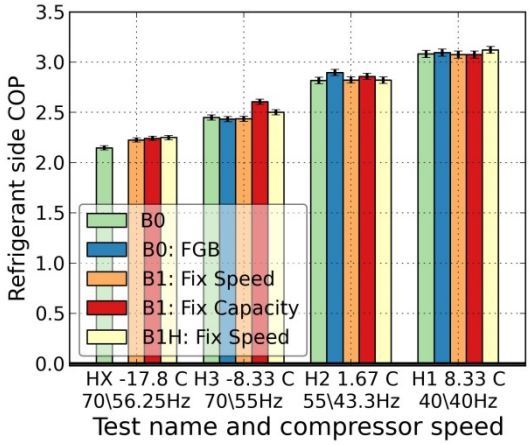

Figure 10: Relative COP improvement B1 vs. B0

4 OIL-FLOODED COMPRESSOR SYSTEM

The oil flooding concept utilizes oil injection into the compressor suction port(s) to absorb the heat of compression (reducing discharge temperature) and approach an isothermal compression process (Bell et al., 2011). Figure 11 illustrates a cycle schematic and p-h diagram of the concept. The addition of compressor flooding with regeneration in VC systems results in a more isothermal compression process that can have a significant beneficial impact on system efficiency for large temperature lifts. For refrigerants with large pressure differences across the compressor, the use of a hydraulic expander can also help to recapture some of the work of compression of the flooding liquid. The engineering challenges in implementation of this technology are reasonable, which suggests that it could be applied readily in new construction. Analyses indicate this concept has both capacity and efficiency advantages over VI cycles for low-temperature applications (Bell et al., 2011). In particular, the injection of oil results in an increase in refrigerant mass flow rate and overall isentropic efficiency and a decrease in the compressor discharge temperature. The analyses conducted so far clearly suggest that designing an efficient scroll compressor with oil injection for application to a low-source-temperature ASHP application will be possible with respect to energy performance and manufacturability.

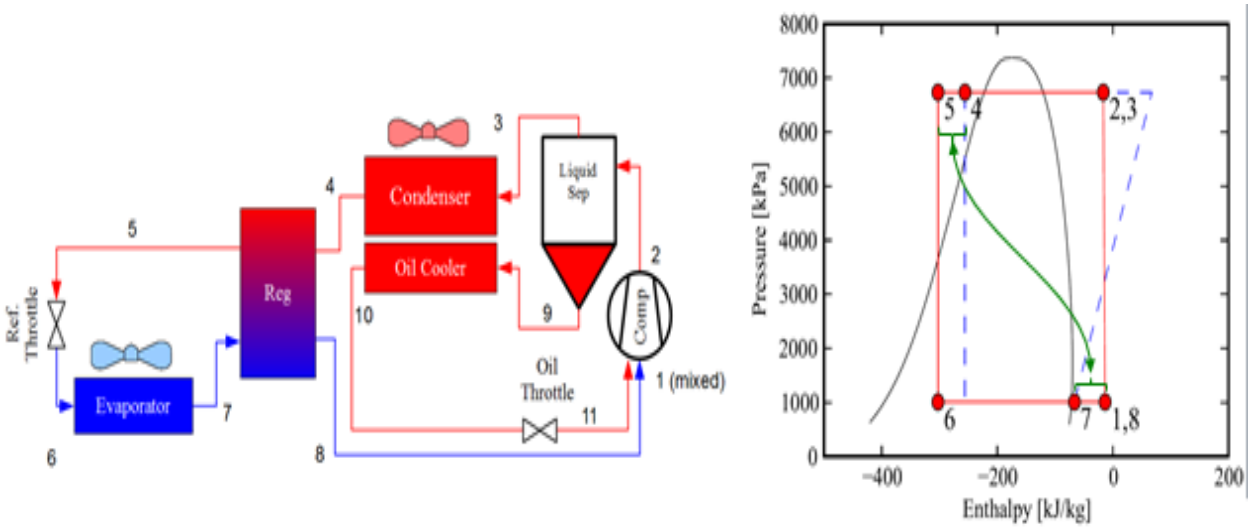

Figure 11: Schematic (left) and p-h cycle diagram (right) of flooded compressor cycle concept - from Bell et al. (2011)

As depicted in Figure 12, a commercial 5-ton (17.6 kW) R410A packaged heat pump system was retrofitted with an oil-flooded scroll compressor, an oil separator, a regenerator (internal heat exchanger), and an oil cooler. Although the reversible packaged heat pump is designed to run in heating mode as well as in cooling mode, it was decided to focus on the heating mode operation only. A schematic of the retrofitted heat pump can be found in Figure 13. The schematic can be divided into two separate loops: oil loop and refrigerant loop.

For the refrigerant loop, the superheated vapor is compressed from the evaporating pressure to the condensing pressure in the compressor. After compression, the two-phase mixture (oil and refrigerant) is separated inside the oil separator. Then, the refrigerant passes through the reversing valve and goes into the indoor unit where it rejects heat to the indoor air flow. At the outlet of the indoor unit, the refrigerant is subcooled and flows through the Thermostatic Expansion Valve (TXV), which works as a straight tube in heating mode. The fluid is then further subcooled in the regenerator before flowing through the mass flow meter and filter-dryer. Afterwards, the refrigerant is expanded to the evaporating pressure through an Electronic Expansion Valve (EXV2) and two parallel piston expansion valves (fixed orifice valves). Compared with the baseline system, this EXV2 has been added to the commercial packaged heat pump in order to control the superheat at the outlet of the evaporator. After the expansion devices, the low-pressure two-phase mixture is evaporated and superheated in the outdoor unit. At the outlet of the evaporator, the fluid passes through the regenerator to be further superheated by heat transfer with the subcooled liquid refrigerant flow. The flow then passes through the reversing valve and accumulator, and goes back to the compressor suction.

In the oil loop, the oil is injected into the scroll set at the inlet of both suction chambers. After compression, the oil is separated from the refrigerant in the oil separator (there is still a small amount of refrigerant in the oil due to the solubility of refrigerant into oil). Then, the oil is cooled down in the oil cooler by heat transfer with the indoor air flow. The liquid oil passes through the oil mass flow meter and is expanded in the Electronic Expansion Device (EXV1) before going back to the compressor.

As can be seen in Figure 13, a solenoid valve has been placed before the EXV1. It is directly connected to the power consumption of the compressor. If the compressor is running, the solenoid valve is open. Otherwise, it is closed. Its aim is to close the oil loop when the

system is not running and to prevent the migration of oil from the top of the system to the bottom of the system by gravity.

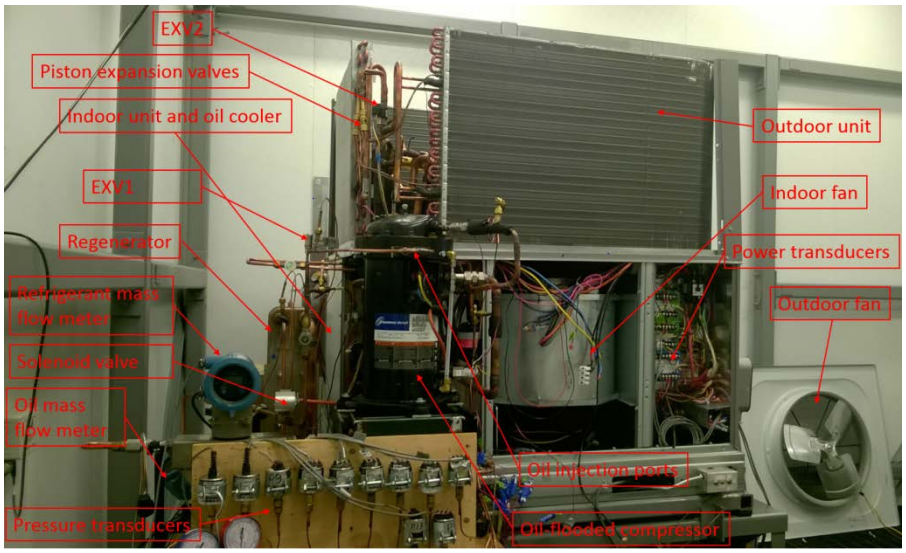

Figure 12: Experimental setup

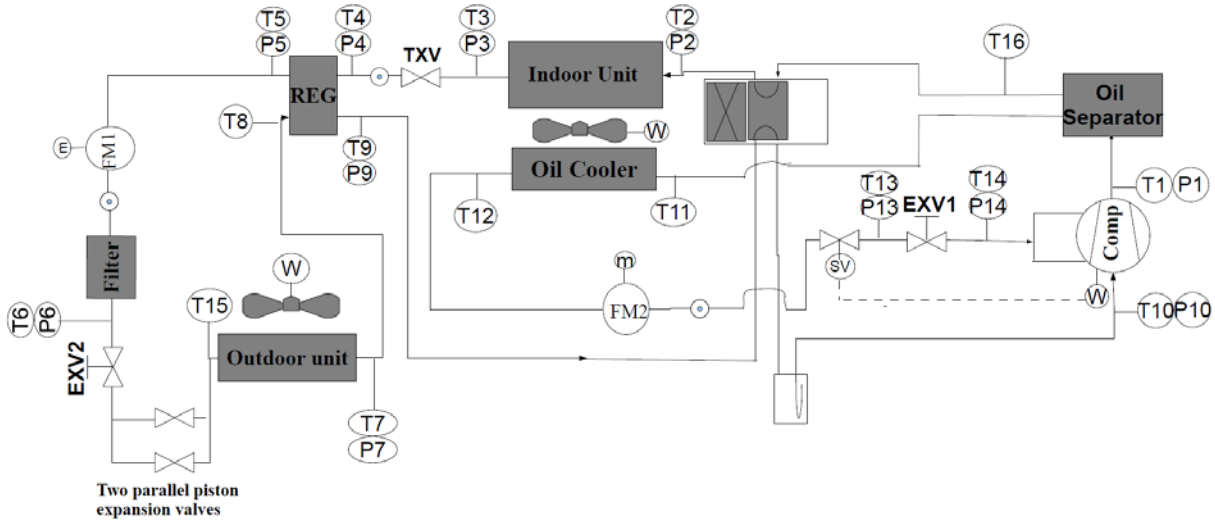

Figure 13: Schematic of a packaged heat pump using oil-flooded compression with regeneration technology

The modified heat pump was tested in psychrometric chambers in order to fully understand the effect of oil-flooded compression with regeneration on system performance in heating mode. The test matrix used for this test stand was inspired by the AHRI Standard 210/240. Since there is no standard for oil-flooded systems, a test matrix with different oil mass fractions was created and is presented in Table 3. In order to investigate the impact of oil mass fraction on the system performance, the oil mass fraction varies for each test from 0.0 to 0.3, in 0.05 intervals. The oil mass fraction is defined by:

$$x_o = \frac{\dot{m}_o}{\dot{m}_o + \dot{m}_r} \quad (1)$$

Table 3*:* Test matrix for oil-flooded heat pump in heating mode

Test *	Air entering the indoor unit			Air entering the outdoor unit			Indoor air flow rate	
	T [°F]	T [°C]	RH [%]	T [°F]	T [°C]	RH [%]	CFM	[m³/s]
H1	70	21.1	≤ 56.03	47	8.33	72.64	1750	0.826
H2	70	21.1	≤ 56.03	35	1.67	81.80	1750	0.826
H3	70	21.1	≤ 56.03	17	-8.33	69.41	1750	0.826
H4	70	21.1	≤ 56.03	0	-17.78	min	1750	0.826
* For every test in heating mode, the oil mass fraction varies from 0.0 to 0.30, in 0.05 intervals.								

The following comments about the test matrix can be made:

- In the AHRI Standard 210/240, the H4 test is missing. As oil-flooding is particularly interesting for low temperature applications, a very low temperature test (H4 test) has been added to the test matrix so as to evaluate the performance at these conditions.
- For the indoor unit, the relative humidity must be below 56.03%. Since the value is not imposed, a fixed set point of 50% has been chosen.
- For the H4 test, the relative humidity in the outdoor room is set to minimum.

To evaluate the performance of the heat pump equipped with the oil-flooded compressor and regenerator, steady-state experimental data were recorded for each test listed in the test matrix[4]. The superheat at the outlet of the evaporator was controlled by EXV2 at a value of 5°C for every test. Steady state was maintained for at least 30 minutes for every test condition. The recorded data were then processed in order to evaluate the performance of the system. A total of 33 experimental points were obtained: 23 for the test matrix, 6 additional points at higher superheat for evaluating the influence of superheat and the last 4 points for determining system performance both without the regenerator and oil injection.

Figures 14 to 19 show the performance of the oil-flooded compressor for different outdoor room temperatures, a fixed indoor room temperature (21.11°C) and a fixed superheat of 5°C at the outlet of the evaporator. The isentropic efficiency of the compressor must account for the effect of oil injection and is defined by:

$$\varepsilon_{is,cp} = \frac{\dot{m}_r \cdot \left(h_{r,ex,cp,is} - h_{r,su,cp}\right) + \dot{m}_o \cdot \left(h_{o,ex,cp,is} - h_{o,su,cp}\right)}{\dot{W}_{cp}} \quad (2)$$

where $\dot{m}_r$ and $\dot{m}_o$ are the mass flow rate of refrigerant and oil, respectively, $\dot{W}_{cp}$ is the compressor power consumption, $h_{r,ex,cp,is}$ and $h_{o,ex,cp,is}$ are respectively the enthalpies at the compressor discharge with an isentropic compression between suction and discharge. Figure 14 shows that the isentropic efficiency has a maximum for an oil mass fraction of approximately 0.1 at a given outdoor room temperature. The increase of the isentropic efficiency at low oil mass fraction is most likely due to reduced internal leakage and friction. The decrease at higher oil mass fraction might be due to different reasons: higher pressure drops through suction and discharge ports due to oil injection, higher pressure drops through the compression process due to the oil viscosity, higher power consumption used to pump the oil from low pressure to high pressure and more irreversibilities in the two-phase flow (such as non-homogeneous equilibrium). The isentropic efficiency is also higher at higher outdoor air (ambient) temperatures mainly because the refrigerant mass flow rate is higher, the electromechanical losses are lower and the built-in volume ratio is more suited to the pressure ratio of the system (lower over-compression at higher outdoor temperatures, i.e. the external pressure is too high at low outdoor room temperature).

[4] For tests H2, H3 and H4, the maximum oil mass fraction was limited to 0.25 by the system, therefore no data are available for an oil mass fraction of 0.3. For test H1, the oil mass fraction was limited to 0.2.

The volumetric efficiency of the compressor is calculated according to the following expression (Ramaraj et al. 2014):

$$\varepsilon_{vol,cp} = \frac{\dot{m}_r + \dot{m}_o}{\rho_{m,su,cp} \cdot \dot{V}_{s,cp}} \quad (3)$$

where the volume flow rate and the inlet mixture density are given by:

$$\dot{V}_{s,cp} = V_{s,cp} \cdot N_{rot,cp} \quad (4)$$

$$\rho_{m,su,cp} = \frac{(1 - x_o) + S \cdot x_o}{(1 - x_o) \cdot v_r + S \cdot x_o \cdot v_o} \quad (5)$$

and where v_r and v_o are the specific volume of refrigerant and oil, respectively, and S is the slip ratio, which was taken to be 1 (i.e., a homogeneous two-phase flow). As can be seen in Figure 15, the volumetric efficiency increases with the oil mass fraction and seems to stabilize at higher oil mass fraction. This increase is probably due to lower internal leakage. For instance, the volumetric efficiency between $x_o = 0$ and $x_o = 0.25$ increases by 6.64% at $T_{out} = -17.78°C$.

As expected, the discharge temperature decreases when oil is injected as shown in Figure 16, the temperature difference between no oil injection and $x_o = 0.25$ is approximately 35-40°C depending on the outdoor room temperature. Moreover, at a given oil mass fraction, the discharge temperature increases slightly when the outdoor room temperature decreases. However, a higher increase could have been expected. This slight increase could be explained by two opposing effects. On one hand, the pressure ratio increases when the outdoor room temperature decreases, which tends to increase the temperature difference between suction and discharge temperature. On the other hand, the compressor suction temperature decreases at lower outdoor room temperature, which limits the discharge temperature. The lower suction temperature is mainly due to lower temperatures at the inlet of the regenerator (high pressure side, T4 in Figure 16) because of lower condensing temperatures at low outdoor temperatures. The lower suction temperature leads to lower superheat at the outlet of the regenerator (low pressure side, T9 in Figure 16). Beside this observation, Figure 17 shows that the compressor temperature ratio (between discharge temperature and suction temperature) is significantly higher at lower outdoor room temperature and a more isothermal compression is achieved when the oil mass fraction increases.

As can be seen in Figure 18, the refrigerant mass flow rate tends to increase with oil injection. It is probably due to lower internal leakage. It can also be due to lower temperatures in the suction chamber (i.e. higher density and therefore higher mass flow rate). The refrigerant mass flow rate also increases with the outdoor air temperature because of higher density at the suction (since the evaporating pressure is higher).

Regarding the compressor power consumption shown in Figure 19, no general trends can be pointed out. Indeed, for $T_{out} = 8.33°C$ and $T_{out} = 1.67°C$, a minimum is reached for an oil mass fraction of approximately 0.1. At low oil mass fraction, the power consumption decreases due to the sealing properties of oil and the higher isentropic and volumetric efficiencies of the compressor. At higher oil mass fraction, the opposite effect occurs since the isentropic efficiency decreases. However, at lower temperature, the same trends cannot be pointed out. For $T_{out} = -8.33°C$, the power consumption decreases until $x_o = 0.25$ and for $T_{out} = -17.78°C$, a maximum is reached around $x_o = 0.05$ and then it decreases.

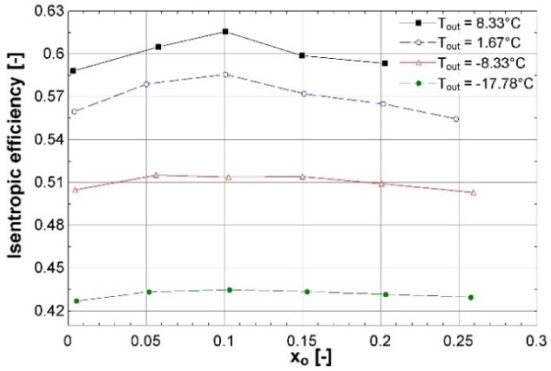

Figure 14: Compressor isentropic efficiency

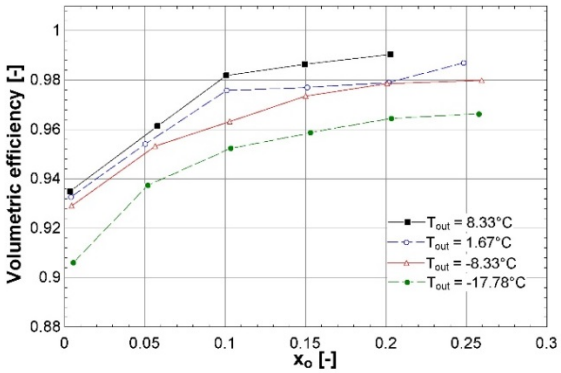

Figure 15: Compressor volumetric efficiency

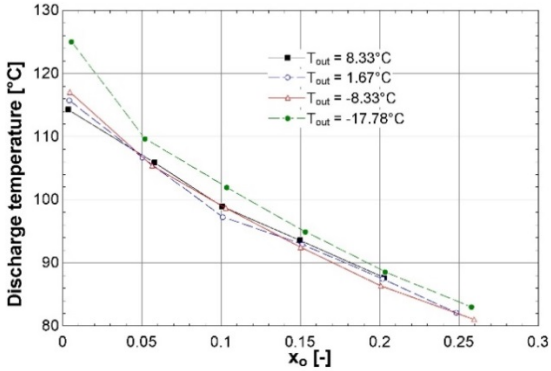

Figure 16: Compressor discharge

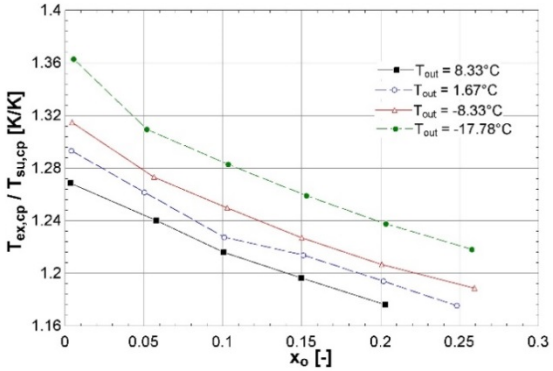

Figure 17: Compressor temperature ratio

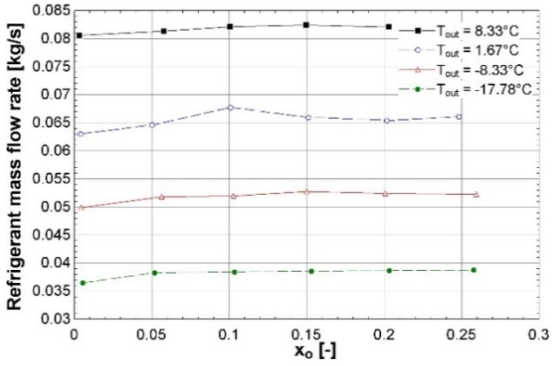

Figure 18: Refrigerant mass flow rate

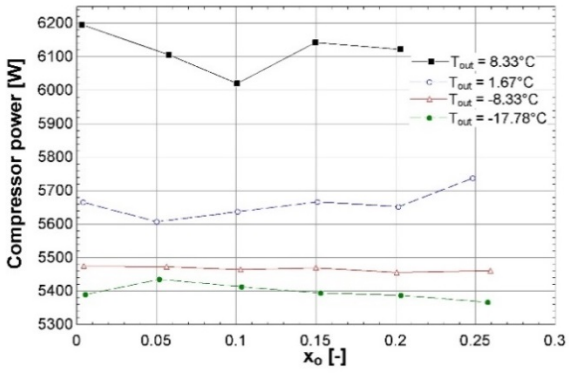

Figure 19: Compressor power

The coefficient of performance of the heat pump in the absence of auxiliary heat is given by:

$$COP = \frac{\dot{Q}_a}{\dot{W}_{cp} + \dot{W}_{in,fan} + \dot{W}_{out,fan}} \quad (6)$$

where $\dot{W}_{in,fan}$ and $\dot{W}_{out,fan}$ are the indoor and outdoor fan power consumption, respectively, and $\dot{Q}_a$ is the heating capacity calculated on the air side. The air-side capacity should also be equal to the sum of the oil cooler capacity, the condenser capacity and the indoor fan power consumption:

$$\dot{Q}_a = \dot{Q}_{o,oc} + \dot{Q}_{r,cd} + \dot{W}_{in,fan} \quad (7)$$

where $\dot{Q}_{o,oc}$ is the heat transfer rate in the oil cooler (oil side) and $\dot{Q}_{r,cd}$ is the heat transfer rate in the condenser (refrigerant side).

Figure 20 shows the effect of oil mass fraction on heating capacity for various outdoor temperatures and a fixed indoor room temperature (21.11°C). It reaches a maximum around $x_o = 0.10 - 0.15$ at high outdoor air temperatures (8.33°C and 1.67°C) and does not reach a maximum even for $x_o = 0.25$ at lower temperatures (-8.33°C and -17.78°C). The increases in maximum capacity due to oil injection compared to $x_o = 0$ are: 1.2% for $T_{out} = 8.33°C$ at $x_o = 0.15$, 5.0% for $T_{out} = 1.67°C$ at $x_o = 0.1$, 4.3% for $T_{out} = -8.33°C$ at $x_o = 0.25$ and 5.7% for $T_{out} = -17.78°C$ at $x_o = 0.25$. At a given outdoor temperature, the condensing temperature does not have a significant dependence on oil mass fraction. When the oil mass fraction is increased, the refrigerant mass flow rate tends to increase (see Figure 7), which increases the capacity. But at the same time, the superheat at the inlet of the condenser decreases (which decreases the capacity) because the discharge temperature of the compressor decreases. However, when the oil mass fraction increases, the cooling of oil increases as well, which increases the capacity since more oil is cooled down by the air flow (i.e. the oil cooler capacity is increased). Overall, these opposing effects result in an increase of heating capacity when oil mass fraction is increased.

For the COP, the same trends can be pointed out as shown in Figure 21. For $T_{out} = 8.33°C$ and $T_{out} = 1.67°C$, the COP increases as the oil mass fraction is increased and reaches a maximum for $x_o = 0.1$ before decreasing. The increases in maximum COP associated with oil injection compared to no oil injection are 3.3% and 5.6% for $T_{out} = 8.33°C$ and $T_{out} = 1.67°C$, respectively. The increase in COP with oil mass fraction at low values is because the capacity increases (see Figure 9) and the compressor power consumption decreases (see Figure 8). At higher oil mass fractions, the opposite effect occurs: compressor power consumption increases whereas capacity decreases. At lower outdoor air temperatures ($T_{out} = -8.33°C$ and $T_{out} = -17.67°C$), the COP also increases with oil injection but a maximum is not reached, even for $x_o = 0.25$. This is consistent with the trends that there is no minimum for the compressor power consumption (see Figure 8) and no maximum for the capacity (see Figure 8) over the range of oil mass fractions tested. The COP improvements for oil flooding over no flooding (i.e., between $x_o = 0$ and $x_o = 0.25$) are 4.5% and 6.1% for $T_{out} = -8.33°C$ and $T_{out} = -17.67°C$, respectively.

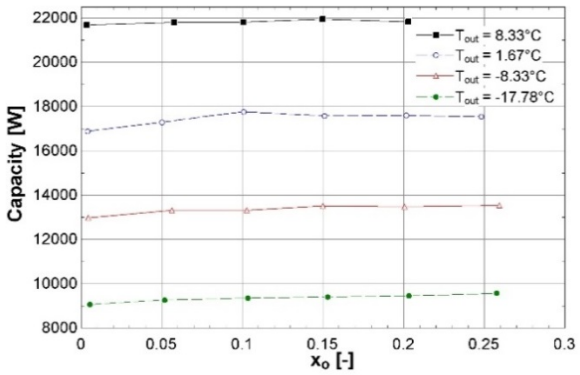

Figure 20: Heating capacity of heat pump

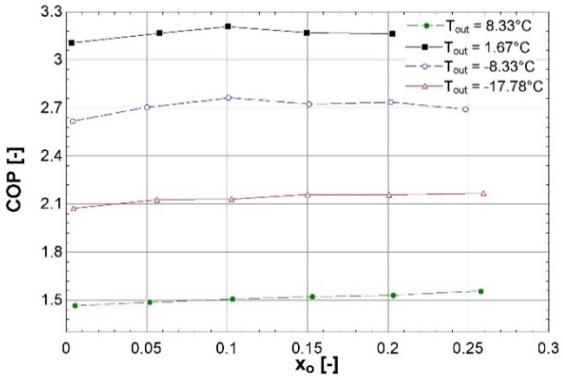

Figure 21: COP of heat pump

Experimental data were recorded at 8.33°C (outdoor temperature) for two different superheats at the outlet of the evaporator: 5°C and 10°C. Figures 22 and 23 show the influence of variations in superheat on COP and heating capacity. It can be seen that the influence is high. Indeed, the COP is decreased by 0.5 (i.e. a decrease of around 15%) between 5°C and 10°C superheat and the heating capacity is decreased by more than 4000 W (i.e. a decrease of around 20%) between 5°C and 10°C superheat. This high influence is

due to a large decrease in evaporating temperature (it decreases from -3°C at 5°C superheat to -11°C at 10°C superheat). Indeed, it seems that this lower evaporating temperature hurts the performance much more than the superheat. It must be pointed out that the capacity is mainly decreased by the refrigerant mass flow rate that decreases from 0.08 kg/s to 0.06 kg/s between -3°C and -11°C evaporating temperature. The opening of the EXV2 (see Figure 2) was approximately 40% open for 5°C superheat and only 25% open for 10°C superheat. The expansion valve opening of 25% lowered the evaporating pressure to balance the flow through its constriction.

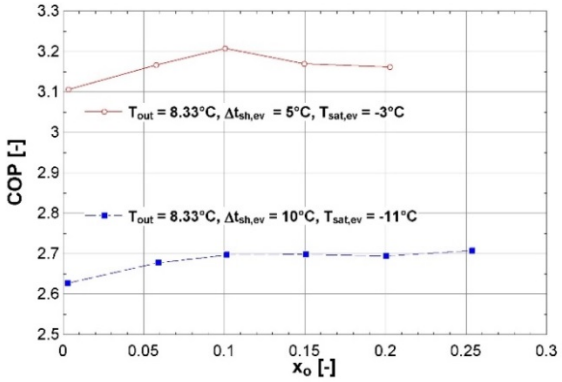

Figure 22: Influence of superheat on COP

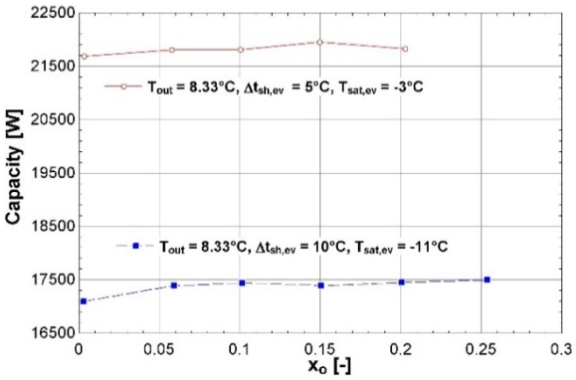

Figure 23: Influence of superheat on heating capacity

In order to compare the performance of the oil-flooded system with regeneration to that of a conventional heat pump system, some tests were run without the regenerator and without oil injection in the oil-flooded compressor. The results obtained with this baseline system were then used to identify the performance improvement by oil-flooding and regeneration. To compare these two systems, the COP improvement is defined as follows:

$$COP_{imp} = \frac{COP_{oil-flooded} - COP_{baseline}}{COP_{baseline}} \quad (8)$$

where $COP_{oil-flooded}$ is the COP of the oil-flooded system with regeneration and $COP_{baseline}$ is the COP of the baseline system (without oil injection and without regeneration). An analogous expression is used for the heating capacity improvements. Using the 4 experimental points available for the conventional heat pump (one point for each outdoor room temperature of the test matrix) and the 23 experimental points available for the heat pump with oil-flooding, the results of Figures 24 and 25 were generated to show the COP and capacity improvements as a function of oil mass fraction. The COP improvements range between 4% and 15% and the capacity improvements are between about 1% and 19%. Most of the experimental points are characterized by a superheat of 5°C at the outlet of the evaporator. However, it must be pointed out that for the baseline system, the test at $T_{out} = 8.33°C$ was carried out with a superheat of 7.5°C (instead of 5°C) at the outlet of the evaporator because without the regenerator, the system could not reach the lower superheat even with the EXV2 fully open (see Figure 13). As explained in previous section, the superheat influences the performance. Therefore, this explains why the capacity and COP improvements are greater for $T_{out} = 8.33°C$. Therefore, the results for the other three operating temperatures are more meaningful and are the focus of additional analysis and discussion.

The three points without oil injection (i.e. $x_o = 0$ in Figure 24 and 25) are analyzed first. It can be seen that even without oil injection, the COP increases (between 4 and 8%) between the conventional heat pump and the heat pump with regeneration, which clearly shows the

benefit of the regenerator. Several factors directly or indirectly influence the higher COP with regeneration:

- The condensing temperature is slightly lower (by approximately 2°C) and the evaporating temperature slightly higher with regeneration. Therefore, the pressure ratio is lower with the regenerator.
- The compressor power consumption is lower (by approximately 200 W) with the regenerator. This is due to both a lower refrigerant mass flow rate and a lower pressure ratio through the compressor.
- The heating capacity is higher with regeneration (see Figure 14). The capacity increases with regeneration because the superheat at the inlet of the condenser is higher due to a higher superheat at the inlet of the compressor. However, two opposite effects decrease the capacity: the refrigerant flow rate and the condensing temperature are lower with the regenerator. But in general, the heating capacity was increased for the cases considered.

When oil is injected into the compressor of the system with regeneration, the maximum COP is reached at $x_o = 0.1$ and the COP improvement is 10.3% for $T_{out} = 1.67°C$. For the two lowest outdoor temperatures, the maximum COP is not reached even for an oil mass fraction of $x_o = 0.25$. At this oil mass fraction, the COP improvements are 13.3% and 14.3% at outdoor temperatures of -8.33°C and -17.78°C, respectively.

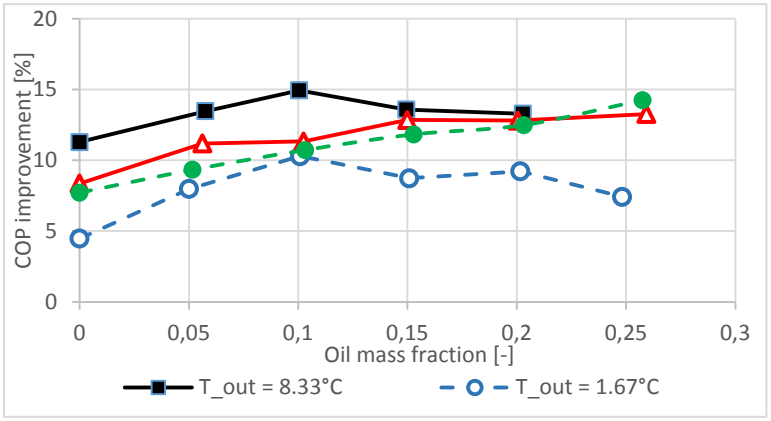

Figure 24: COP improvement between oil-flooded system with regeneration and baseline system

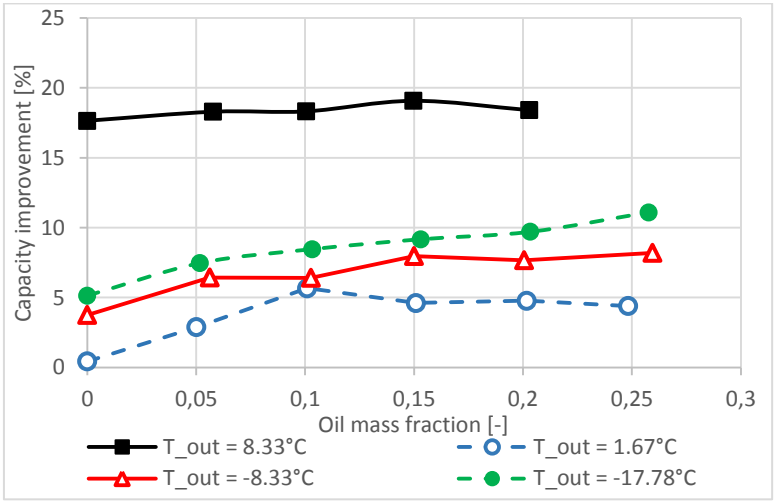

Figure 25: Capacity improvement between oil-flooded system with regeneration and baseline system

5 SINGLE-STAGE ASHP WITH TWO PARALLEL COMPRESSORS

Research at ORNL investigated several different ASHP cycle configurations to identify those with potential to meet the heating capacity degradation target limit listed in Table 1. Two-capacity compressor, variable speed compressor, and dual, parallel single speed compressor (tandem compressor) systems were investigated. Nine of the system options investigated are listed in Table 4 along with a baseline conventional single speed compressor ASHP.

Table 4: ASHP design and sizing options

#	Equipment Sizing Scenarios
1	Single speed heat pump having rated HSPF of 9.6: sized such that rated cooling capacity matches building design cooling load [BASELINE].
2	Single heat pump, having a two-stage scroll compressor: sized such that rated high-stage (100%) cooling capacity matches building design cooling load.
3	Single heat pump, having a two-stage scroll compressor: sized such that rated low-stage (67%) cooling capacity matches building design cooling load.
4	Single heat pump, having a variable speed scroll compressor: sized such that rated cooling capacity at 2700 rpm matches building design cooling load.
5	Single heat pump, having a variable speed scroll compressor: sized such that rated cooling capacity at 3600 rpm matches building design cooling load.
6	Single heat pump, having a variable speed scroll compressor: sized such that rated cooling capacity at 4500 rpm matches building design cooling load.
7	Single heat pump, having a two-stage scroll compressor: sized such that 80% of rated cooling capacity matches building design cooling load.
8	Single heat pump, having a tandem scroll compressor pair: sized such that rated cooling capacity with one compressor matches building design cooling load.
9	Single heat pump, having a single speed VI scroll compressor: sized such that rated cooling capacity matches building design cooling load.
10	Two identical single speed heat pumps, having rated HSPF of 9.6: sized such that rated cooling capacity of one unit matches building design cooling load; both units used for heating.

Note: All variable speed compressor system options have a speed range of 1800 - 7200 rpm; option 8, tandem compressor pair contains two identical compressors; the two-stage compressor options include one compressor having two capacity levels, i.e. 100%/67%.

Table 5 lists the heating capacity ratio and the heating COPs at 8.3°C and -25°C for each of the systems in Table 4. Four of the options (4, 5, 8, and 10) have estimated capacity ratios near the target level noted in Table 1 (≥75%). COPs at -25°C for these options range around 45-55% of the nominal COPs at 8.3°C. Estimated HSPF ratings are calculated based on the method prescribed in AHRI Standard 210/240 (AHRI, 2008) for U.S. region IV (mildly cold climate). The VS compressor-based designs offered somewhat greater low temperature capacity capability while the tandem compressor designs were somewhat less complex and had almost as much capacity capability.

Table 5: Predicted ASHP system performance indices

Options	COP @ 8.3°C (47°F)	Heating Capacity Ratio @ -25°C (-13°F)	COP @ -25°C (-13°F)	Region IV HSPF Rating (per AHRI Standard 210/240-2008)
	[W/W]	[-]	[W/W]	[W/W (Btu/Wh)]
1.	3.58	40%	1.92	2.80 (9.55)
2.	3.79	42%	2.09	2.92 (9.96)
3.	3.78	57%	2.09	2.92 (9.98)
4.	4.30	94%	1.89	3.40 (11.61)

5.	4.14	74%	1.89	3.43 (11.71)
6.	3.80	61%	1.89	3.40 (11.59)
7.	3.79	52%	2.09	2.95 (10.05)
8.	4.38	75%	1.98	3.31 (11.31)
9.	3.75	43%	2.12	2.96 (10.09)
10.	3.58	80%	1.92	N/A

Based primarily on its relatively simple cycle concept (Figure 26), the tandem approach appeared to offer a relatively more cost-effective approach compared to VS compressor based approaches (Shen et al., 2014). So the following experimental investigations were based on the tandem compressor concept for several reasons.

1. The system refrigerant flow cycle is very similar to that of conventional ASHPs (Figure 26); the major difference is replacement of one large compressor with two equal-size, smaller compressors.
2. Equal tandem, single-speed compressors generally have larger operation envelope than a VS compressor of the same maximum capacity, in terms of pressure ratio and discharge temperature.
3. A VS compressor is usually optimized at one speed level. When moving away from the optimum speed level, especially at maximum and minimum speeds, the VS compressor tends to have some efficiency degradation.
4. A two-capacity heat pump using tandem compressors is easily adaptable to a wide range of 2-stage thermostats available on the market.

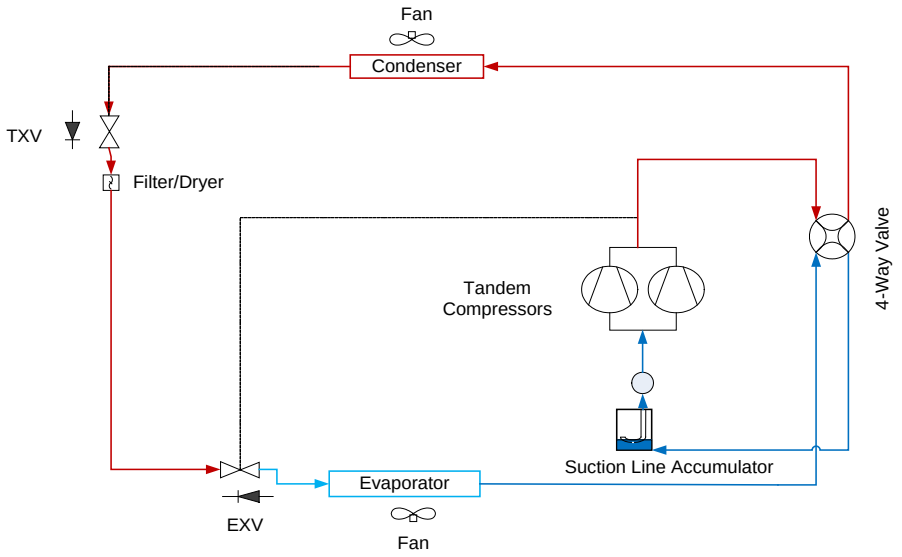

Figure 26: CCHP using tandem, single-speed compressors and an EXV for discharge temperature control in heating mode

The laboratory prototype was built by modifying a 17.5 kW (~60,000 Btu/h or 5-ton) rated cooling capacity, single-speed, conventional ASHP, having a factory rated seasonal heating COP (SCOPh) of about 2.5 (seasonal heating seasonal performance factor, or HSPF of about 8.5 Btu/Wh). A pair of equally sized (10.6 kW or 3-ton nominal cooling capacity), single-speed compressors were used to replace the existing compressor. Parallel compressor CCHP systems using three different scroll compressor designs were evaluated in the lab: 1) conventional scroll compressor optimized for space cooling operation; 2) scroll compressors optimized for space heating operation; and 3) VI scroll compressors. For all cases the compressors were insulated and placed outside the outdoor air flow stream to

minimize the compressor shell heat losses. Testing data confirmed that the insulation layer reduced the compressor heat loss by 50%, and boosted the capacity and COP at -25°C (-13°F) by more than 5%. For the lab test system an electronic expansion valve (EXV) was added for refrigerant flow control in the space heating mode to optimize the compressor discharge temperature based on the outdoor air temperature. Refrigerant flow control for space cooling (air-conditioning) used the existing thermostatic expansion valve (TXV) supplied with the base ASHP. The two heat exchangers, indoor blower (2-speed), and outdoor fan (1-speed) were unchanged. Figure 27 shows the indoor air handler section of the prototype. An air flow monitor (pitot tube array) was used to measure the indoor air flow rate at the exit of the indoor air handler. Averaging thermocouple grids were used to measure the return and supply air temperatures for the indoor section as well as the air temperature entering the outdoor coil section. Watt transducers were used for the electric power of the compressors, blower and outdoor fan individually. Pressure transducers and insertion probe thermocouples were used to measure the refrigerant conditions around the system.

Figure 27: Lab Prototype – Indoor Air Handler

The sections which follow introduce the CCHP lab prototypes investigated using tandem single-speed or VI compressors. All the prototypes used R410A refrigerant.

5.1 'More Cost-Effective' Option - Equal Tandem, Single-Speed Compressors

The lab test system evaluated for this option is shown in Figure 26. The design considerations are summarized as below:

1. Two types of equal size, single-speed compressors: conventional scroll compressor design optimized for space cooling operation and a special heating-optimized pair with design features, allowing them to operate at discharge temperatures up to 138°C [280°F]. This enables the CCHP system to operate down to extremely low ambient temperatures.

2. Current two-capacity heat pumps on the market use a single, two-capacity compressor having a displacement volume split ratio of 100% to 67%. In comparison, the equal-size tandem compressor approach provides a volume split ratio of 100% to 50%, yielding a larger over-capacity potential in heating mode when only the lower capacity was used in cooling mode. This enabled the prototype to reach the >75% heating capacity target at -13°F (-25°C).
3. The CCHP is sized to match an assumed 10.5 kW (36,000 Btu/h or 3-ton) building design space cooling load using only one of the tandem compressors. Since the system retained the heat exchangers of the base 17.5 kW (5-ton) heat pump, the heat exchangers are unloaded when only one compressor is operating (for space cooling or space heating at mild outdoor temperatures). This yields higher system efficiency at these conditions and is the key that enabled the CCHP lab prototypes to reach a nominal rated COP > 4.0 at 8.3°C (47°F).
4. For the prototypes, the compressors were well insulated and placed outside the outdoor air flow stream (shown in Figure 28) to minimize the shell heat losses at very low ambient heating operation. Adding the insulation impairs the cooling performance somewhat by loading the condenser more; however, this effect is mitigated since only one compressor is used for space cooling; e.g. the condenser (outdoor heat exchanger) oversized for cooling.
5. Heating mode discharge temperature control, which uses an EXV, coupled with a suction line accumulator, is intended to optimize the active charge in the system over an extensive operation range. This mitigates the typical charge imbalance problem between cooling and heating modes. A standard thermostatic expansion valve (TXV) is used for cooling mode.

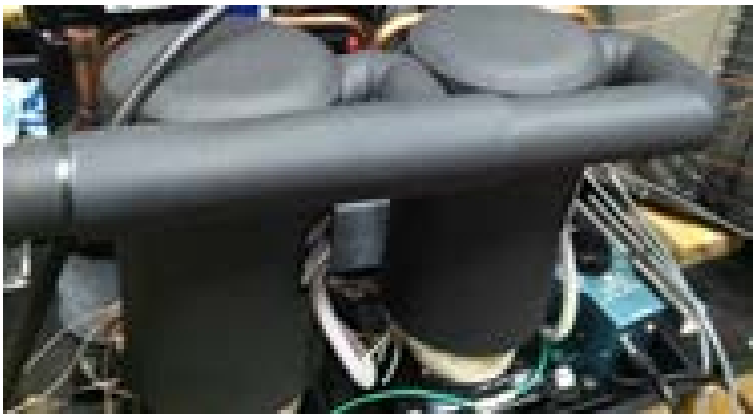

Figure 28: Insulated tandem compressors

As noted earlier, the lab prototype CCHP used the original two-speed indoor blower from the base single-speed ASHP. At high speed the air flow rate was 0.83 m^3/s (1750 CFM) with a power consumption of 460 W; at low speed the air flow and power consumption were 0.67 m^3/s (1420 CFM) and 270 W, respectively. The outdoor fan was fixed-speed, consuming 300 Watts. We evaluated two samples of tandem compressors – one pair optimized for space cooling mode (typical design practice for conventional ASHPs) and a specially-made pair optimized for heating mode.

Figures 29 and 30 show measured capacity and COP vs. ambient temperature, respectively for the CCHP prototype using the cooling-mode optimized compressor pair. These lab test results indicate that this system met the heating capacity target, achieving 77% of the nominal rated capacity at -25°C (-13°F). COP at -25°C was ~1.9, and the rating point COP (at 8.3°C or 47°F) was 4.1.

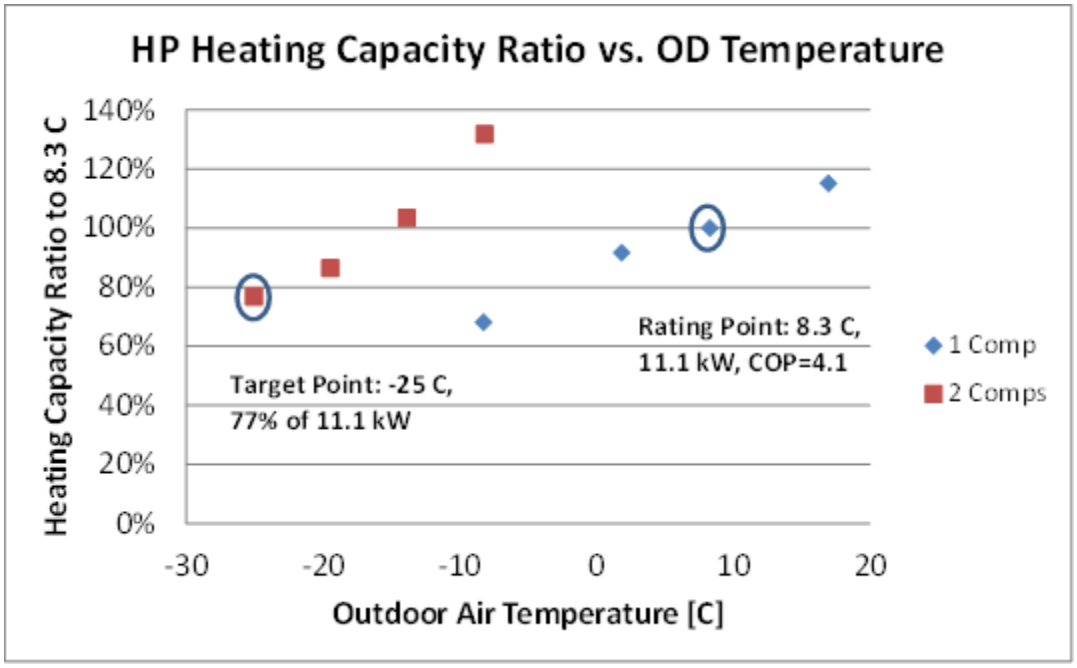

Figure 29: Lab prototype heating capacity ratio with cooling-optimized compressors (relative to capacity at the nominal 8.3°C (47°F) rating point, with one compressor)

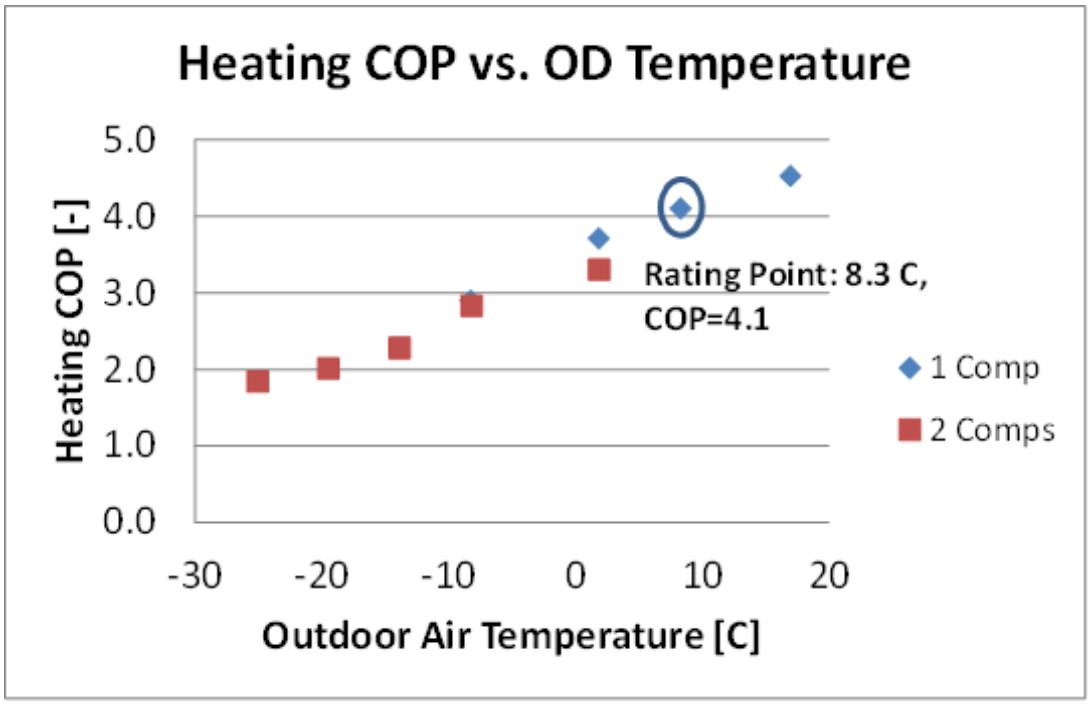

Figure 30: Lab prototype heating COP with cooling-optimized compressors

Space heating performance was somewhat better at all ambient temperature test conditions using the heating-mode-optimized tandem compressor pair. Table 6 shows the lab-measured performance indices at 8.3°C, -8.3°C, and -25°C (47°F, 17°F and -13°F) outdoor temperature conditions with one or two compressors. Table 7 shows SCOPhs (HSPFs) as calculated per AHRI Standard 210/240 in Region IV and V climates. The DHR_{min} and DHR_{max} building load levels are generally representative of a very tight and well insulated house and a rather poorly insulated house, respectively. The dropoff in seasonal efficiencies going from Region IV to the colder Region V climate is about 10.5% and 15.5% for the DHRmin and

DHRmax load lines, respectively. It is also notable that the drop in SCOPh for the heating optimized tandem design between the min and max heating load lines is 1.3% in Region IV. This indicates that this design maintains seasonal performance well over the full range of house performance levels. By comparison, the single-speed baseline loses 23% in seasonal performance in Region IV between the DHRmin (rated) and DHRmax heating load lines. The SCOPh robustness of the tandem design is also in contrast to recently tested variable-speed designs which lose 10 to 20% SCOPh in Region IV for representative heating loads approximately halfway between DHRmin and DHRmax levels (Rice et al, 2016). A similar performance robustness advantage is realized in Region V at higher heating load lines for the parallel tandem design, due to the boosted performance at -8.3°C (17°F) and below.

Table 6: Performance indices of CCHPs using tandem single-speed compressors

	Ambient/Comp(s)	**8.3°C, 1 Comp**	**-8.3°C, 2 Comp**	**-8.3°C, 1 Comp**	**-25°C, 2 Comp**
Optimized for cooling mode	COP [-]	4.09	2.76	2.89	1.85
	Capacity, kW (Btu/h)	11.1 (37,960)	14.8 (50,455)	7.6 (25,860)	8.8 (30,040)
	Capacity Ratio vs. 8.3°C	100%	133%	68%	79%
	Discharge Temperature, °C [°F]	50.0 (122)	83.4 (183)	55.0 (131)	125.0 (257)
Optimized for heating mode	COP [-]	4.24	2.80	2.97	1.94
	Capacity, kW (Btu/h)	11.6 (39,717)	14.9 (50,921)	7.6 (25,917)	8.9 (30,245)
	Capacity Ratio vs. to 8.3°C	100%	128%	65%	76%
	Discharge Temperature, °C [°F]	51.1 (124)	82.8 (181)	51.1 (124)	100.6 (213)
%COP Increment		3.7%	1.4%	2.8%	4.9%

Table 7: Heating Seasonal Performance Factors of CCHPs using tandem single-speed compressors

Load	**SCOPh (HSPF, Btu/Wh) cooling optimized**	**SCOPh (HSPF, Btu/Wh) heating optimized**
	Heating Season Ratings, Region: IV	
DHRmin	3.24 (11.04)	3.29 (11.21)
DHRmax	3.19 (10.90)	3.21 (10.95)
	Heating Season Ratings, Region: V	
DHRmin	2.90 (9.90)	2.94 (10.03)
DHRmax	2.69 (9.18)	2.71 (9.26)

One noticeable advantage of the heating-optimized tandem pair is that they achieved improved performance at -25°C (-13°F) with a much lower discharge temperature than the cooling-optimized pair. This indicates that the heating-optimized compressor design can operate at very low ambient temperatures without approaching the discharge temperature limit of 138°C, and have potential to provide larger heating capacities at extremely low ambient temperatures.

Figures 31 and 32 show the variation in space heating COP and capacity (air-side measurements), respectively, vs. compressor discharge temperature for the -25°C ambient condition. The blue symbols represent performance with the heating-optimized tandem compressors and the red symbols represent that with the cooling-optimized compressors. One can see that the prototype with the heating-optimized compressors achieves its maximum COP at a much lower discharge temperature than the system using the cooling-optimized compressors; about 101°C (213°F) vs. 125°C (257°F). Looking at the heating

capacity data (Figure 31) it can be seen that the heating-optimized compressors experience much less sensitivity to discharge temperature. Increasing the discharge temperature from about 93°C to 127°C (200°F to 260°F) results in only about a 3% capacity increase with the heating-optimized compressors versus about a 9% increase for the cooling-optimized compressors. Therefore, there is less benefit in using the EXV for discharge temperature control (Figure 26) with the heating-optimized compressors. So the refrigerant cycle could potentially be simplified further to use a TXV for refrigerant flow control (based on evaporator exit superheat) in both heating and cooling operation.

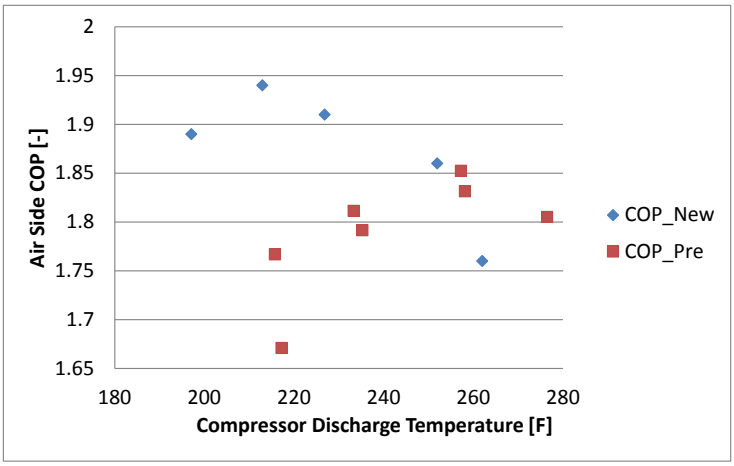

Figure 31: Prototype CCHP air-side heating COP vs. compressor discharge temperature for heating-optimized (new) and cooling-optimized (pre) compressors at -25°C outdoor temperature

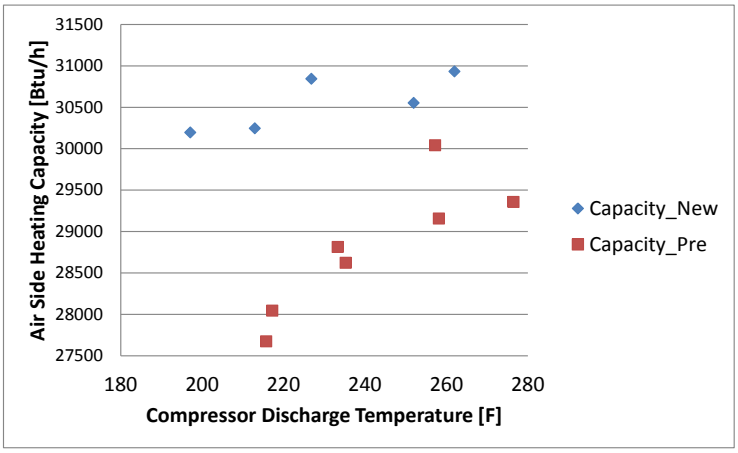

Figure 32: Prototype CCHP air-side heating capacity vs. compressor discharge temperature for heating-optimized (new) and cooling-optimized (pre) compressors at -25°C outdoor temperature

Field Test Site and Equipment Setup

An occupied, single-story ranch home in central Ohio (shown in Figure 33), was selected to host a field test of a tandem, single-speed compressor CCHP prototype. The prototype system replaced the original home HVAC system – an ASHP with rated cooling capacity of ~10.0 kW (34000 Btu/h) at 35°C (95°F) and heating capacity of ~10.3 kW (35000 Btu/h) at 8.3°C (47°F), equipped with a 19.5 kW supplemental resistance heater for second stage heating.

Figure 33: Field testing home

A two-capacity ASHP of nominal 17.6 kW (5-ton) cooling capacity was modified to create the field test prototype CCHP by replacing its original 2-capacity compressor with a heating-optimized tandem scroll compressor pair and adding controls needed to stage the compressors. For the field test, the original 2-capacity ASHP control was retained and re-wired with a relay enable calling the second compressor for second stage heating. A standard commercially available 24 VDC, 2-stage thermostat (wi-fi enabled) was used. Its Y1 signal calls the first stage (one compressor, and low speed indoor blower) and its Y2 signal calls the second stage (two compressors and high speed indoor blower). The outdoor fan ran at a constant speed in both stages. The thermostat can be programmed manually to prevent running the second stage, and this was done for cooling operation. The original 2-capacity unit had a demand defrost control that measures the outdoor air coil surface temperature and refrigerant temperature to initiate the defrosting cycle. During defrosting, the prototype operated both compressors to minimize defrost time. The thermostat was set up as follows to initiate first or second stage heating operation:

- If the zone air temperature is <0.6°C (1.0°F) below the thermostat set point, the first stage (single-compressor) is enabled;
- If the zone air temperature is >0.6°C (1.0°F) below the thermostat set point, the second stage (two compressors) is enabled;
- If the zone air temperature falls to >1.1°C (2.0°F) below the thermostat set point, supplemental resistance heat will be activated.

As illustrated above in Figure 32, the performance of the heating-optimized compressors is relatively insensitive to discharge temperature. In addition, after placing the tandem compressors in the outdoor unit, there was hardly any room left to install any other components, as indicated in Figure 34. Based on these observations, and discussion with Emerson/Copeland engineers (compressor manufacturers and partner in the tandem CCHP system development R&D effort) it was decided to simplify the refrigerant flow control to more conventional suction superheat control using a TXV with optimized system charge for heating mode (Figure 35, below). The recommended charge for the base 2-capacity ASHP, optimized for cooling mode, was 7.6 kg (17 lbs) of R-410A. The charge for the CCHP prototype, optimized for heating mode, was 9% lower, 6.9 kg (15.5 lbs). With this charge, condenser subcooling degree in cooling mode at 27.8°C (82°F) was 1.7K (3R) with one compressor. In heating mode subcooling was around 11.1 K (20 R) at -8.3°C (17°F) with both compressors. Figure 34 shows the outdoor unit of the prototype as installed at the test home, and one can see the compressors were wrapped by a thermal insulation layer. Figure 36 illustrates the indoor air handler and data acquisition system, which were located in the basement.

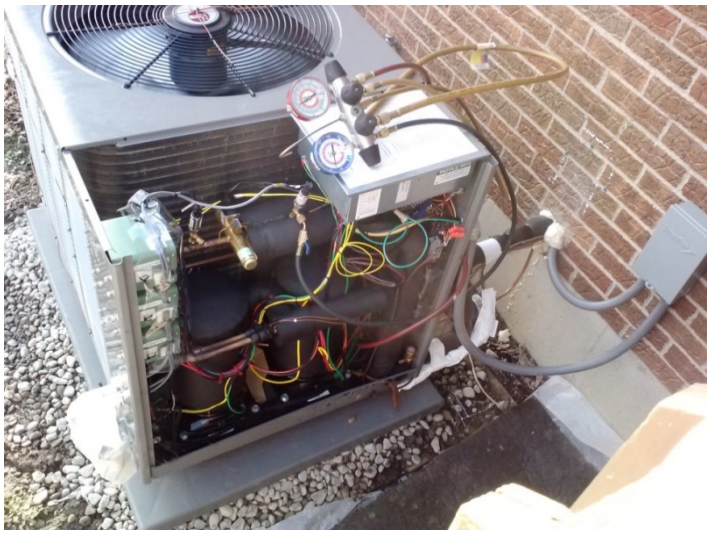

Figure 34: Outdoor unit of field investigation

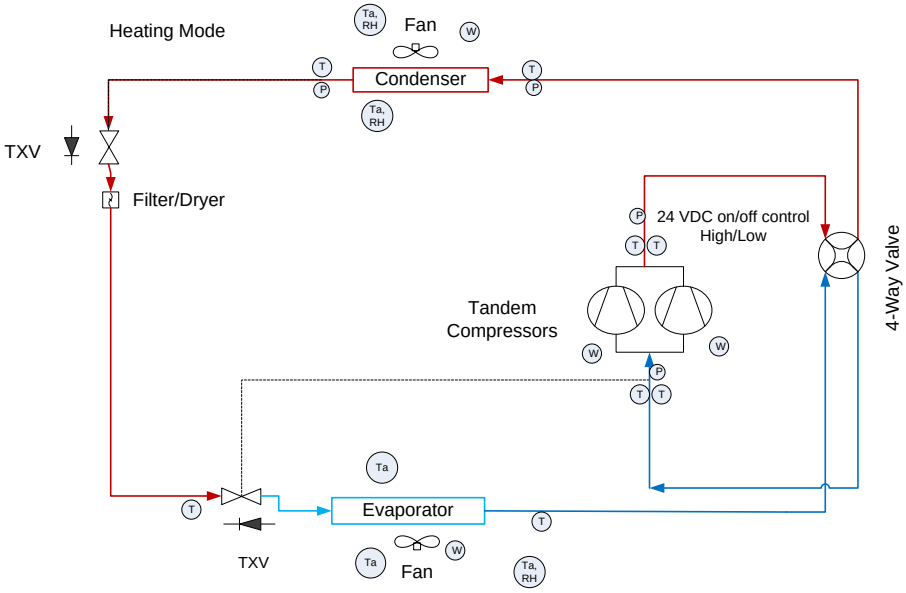

Figure 35: System diagram of field testing HP and instrumentation

Figure 36: Indoor air handler and data acquisition system

Field Data Acquisition and Measurement System

Since the field test was in an occupied home, a wireless data acquisition (DAQ) system was designed to eliminate wire connections between the indoor and outdoor units of the prototype, and minimize interruptions on the home owner. As illustrated in Figure 37, the DAQ controller and measurement devices were used to monitor the outdoor unit with data relayed to the indoor host computer via wireless communication. The host computer and other measurement devices were used to monitor the indoor unit. Data was transmitted through Dropbox via an internet connection back to ORNL for analysis.

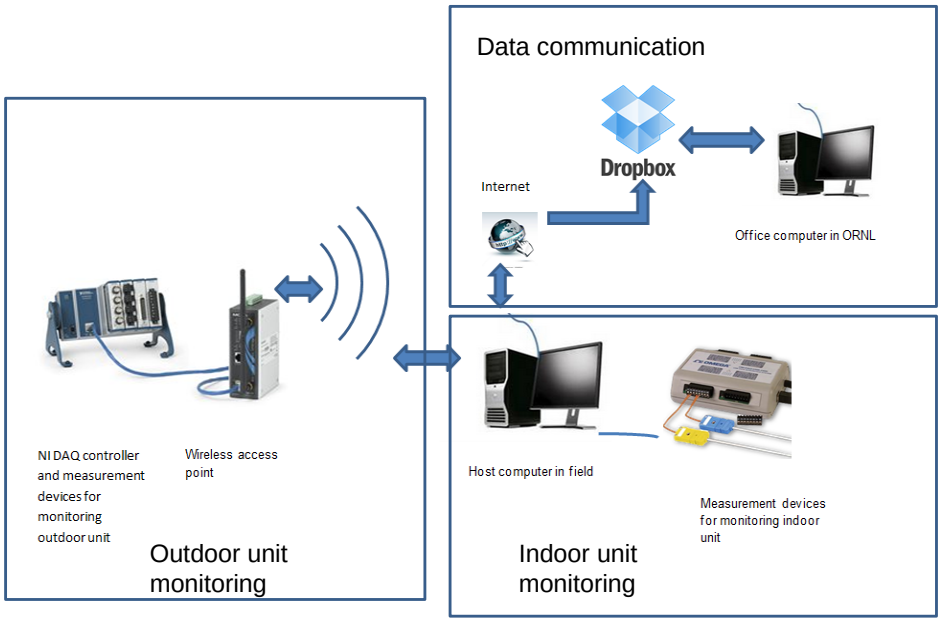

Figure 37: Data acquisition system schematic for CCHP field test

Figure 35 describes the system diagram and instrumentation. Air temperature entering and leaving the outdoor coil were measured using T-type thermocouples. Outdoor humidity was monitored using a Relative Humidity sensor. Three thermocouples were evenly placed at the entrance of the indoor unit to measure the average return air temperature, and a RH sensor was used to measure the return RH. At the exit of the indoor coil, and upstream of the blower, three thermocouples and a RH sensor were used to monitor the supply air state. Thermocouples were soldered on refrigerant tube walls and well insulated to measure the refrigerant temperatures entering and leaving the indoor coil and suction and discharge temperatures of each compressor. Four pressure transducers were used to measure the refrigerant pressures entering and leaving the indoor coil and the compressors. Four Watt transducers were used to measure the outdoor fan, indoor blower and compressor power, individually. Another Watt transducer was used to measure the total power consumption of the outdoor unit. The total outdoor power consumption was determined using the larger of the total power measurement or sum of the individual power measurements. An additional thermocouple was placed in the air duct downstream of the indoor unit to indicate operation of the electric supplemental heater. The DAQ system scanned all the sensors and recorded the data every half minute.

The field testing was conducted using the test home's existing ductwork system. To minimize the interruption on the home owner, no air flow monitor was installed in the duct. Instead, a "true flow grid" was used to perform measurements of the air flow rates once during the heating season and again during the cooling season. As shown in Figure 38, the "true flow grid" is composed of a grid of pitot tubes. It is usually used in the air filter slot of indoor air handlers, to provide one time air flow measurement during field installation and diagnosis.

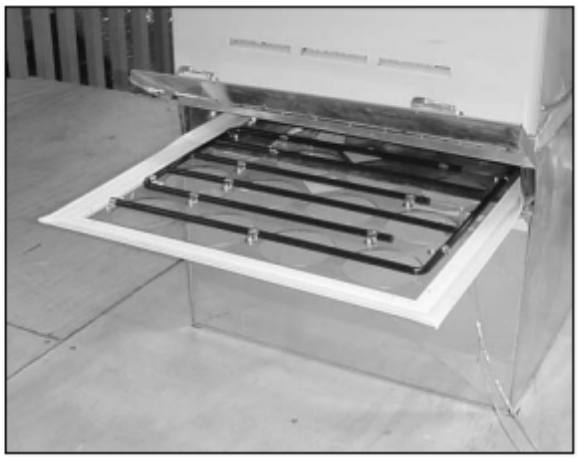

Figure 38: True flow grid air flow monitor

For heating mode, the measured air flow rates are given below:

1. For single-compressor operation heating mode with low fan speed setting - measured reading was 0.53 m^3/s (1120 CFM) with True Flow meter (or about 7% less than indicated by the air handler product literature for cooling operation with the same setting), at a blower power of 230 W.
2. For two-compressor operation in heating mode with high fan speed setting - measured reading was 0.64 m^3/s (1350 CFM) with True Flow meter (or about 10% lower than indicated by the air handler product literature for cooling operation with the same setting), at a blower power of 430 W.

One reason for the lower measured air flow in heating mode compared to the product literature is that the latter correspond to cooling operation. Converting the product literature flows to heating operation and assuming the blower drives the same CFM at its exit, a scale factor for heating flow vs. cooling flow can be computed based on the ratio of supply air density in heating vs. that in cooling mode. The computed scale factor was 0.92, indicating an 8% lower air flow for heating operation. Therefore, the "True flow grid" measured indoor air flow rates were considered credible and were used for the entire heating season. The measured blower power was used to indicate which flow rate was applicable, i.e. for blower power <350 W, the air flow rate was assumed as 0.53 m^3/s; for blower power >350 W, the air flow rate was assumed 0.64 m^3/s.

Measurement of the duct external static pressure indicated that the existing duct system was relatively restrictive at high speed blower operation, resulting in larger blower power consumption than the manufacturer's data indicated. The indoor blower used an ECM motor and was able to maintain a constant volumetric flow rate at the blower exit, regardless of the external static pressure.

Field Heating Performance

2015 heating season operation was monitored from the beginning of February to the end of April 2015 for three full months. During that period the coldest day saw the field temperature drop to -25°C (-13°F).

Figure 39 illustrates runtime fractions for two compressor operation, and total compressor run time (either one or two compressors operating), versus ambient temperature bins (decreasing in temperature from left to right). It can be seen that the second compressor operated more at the lower ambient temperatures as expected. At the lowest temperature of -25°C, total compressor run time was 100% but the second compressor still cycled at an

80% rate. This indicates that the CCHP prototype still had some extra heating capacity capability even at this extreme condition.

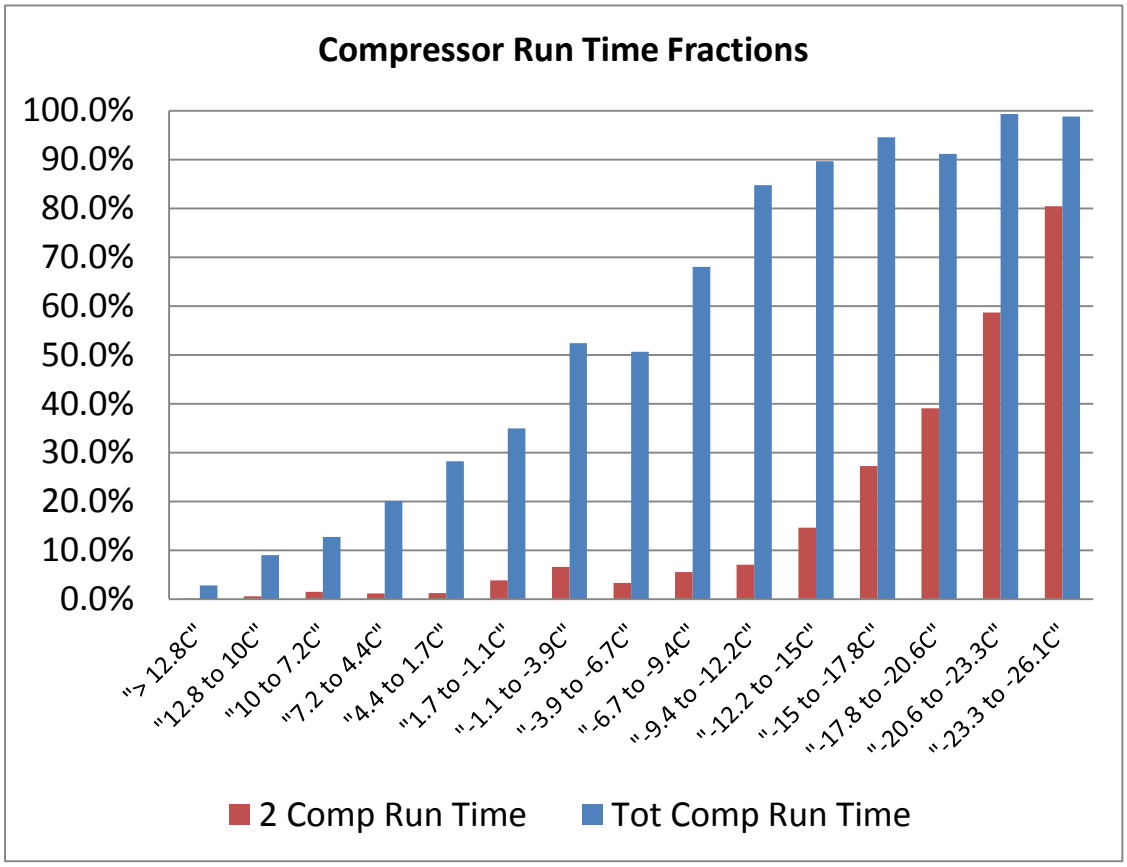

Figure 39: Compressor run time fractions during 2015 winter

Figure 40 shows delivered heating capacities for one- and two-compressor operation, in comparison to the total delivered heating load line. It can be seen that the second compressor was needed when the ambient temperature fell below -12.2°C (-10°C). At the -25°C condition, the CCHP delivered 8.9 kW (30,416 Btu/h) of heating, which is 75% of the rated capacity of 11.6 kW (39,717 Btu/h), as measured in the lab (see Table 6).

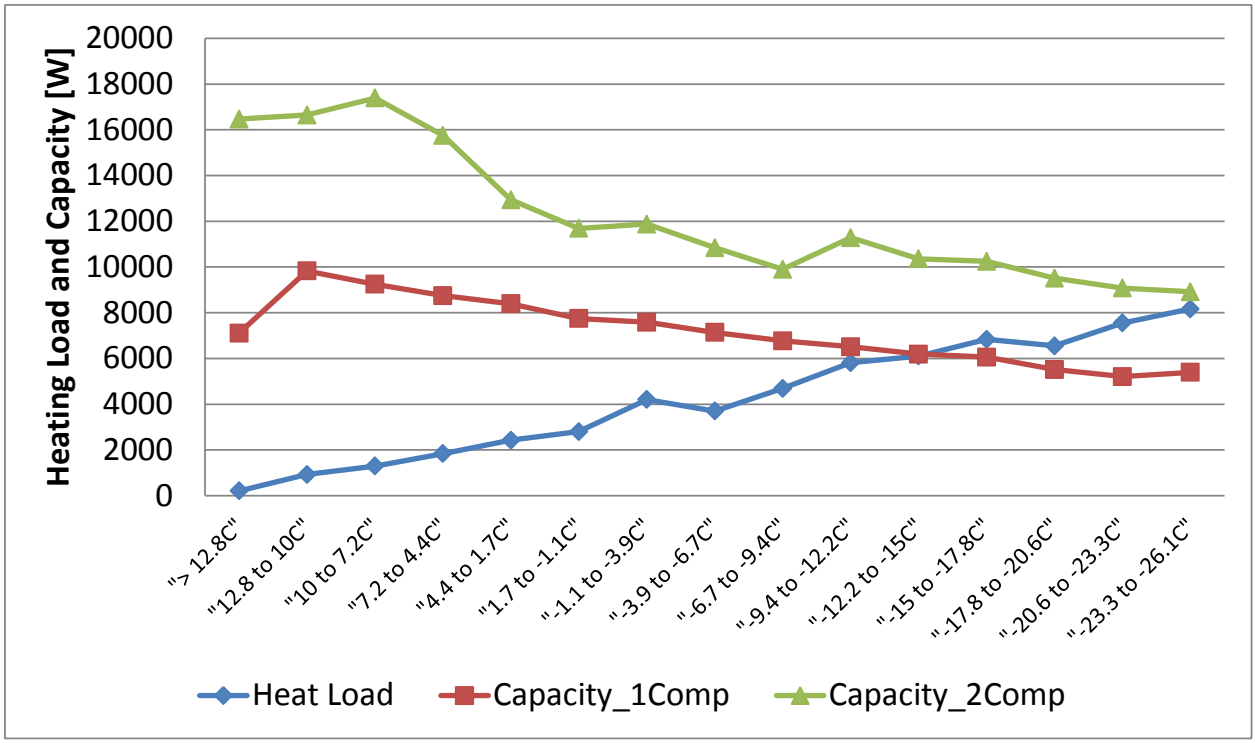

Figure 40: Delivered heat capacities and measured building heating load line

Figure 41 illustrates percentage of supplemental resistance heat use to the total energy use in each temperature bin. Overall resistance heat use was negligible, with most of the usage traceable to either system control issues or occupant behavior. (No defrost tempering resistance heat was used at the engineer homeowner's request.) At -25°C, the resistance energy use was 3.2% of the total even though the second compressor still cycled at 80%. This means that the heat pump responded slower than needed at this condition allowing space temperature to fall below the 1.1 K dead band limit and activate the supplemental heater. Much of the resistance heat use seen during the test period could have been eliminated by changing the control to prevent running only one compressor below a certain ambient temperature. The resistance heat usage at moderate ambient temperatures (between 7.2°C to -6.7°C) was mainly due to the thermostat setback operation by the homeowner. When the homeowner left for extended periods the thermostat set point would be lowered and then raised back up when the homeowner returned. At times this resulted in temperature setting being increased by more than the 1.1K resistance heat trigger point. Modifying the control to lock out the supplemental heater above a set outdoor temperature could eliminate most of this inadvertent usage.

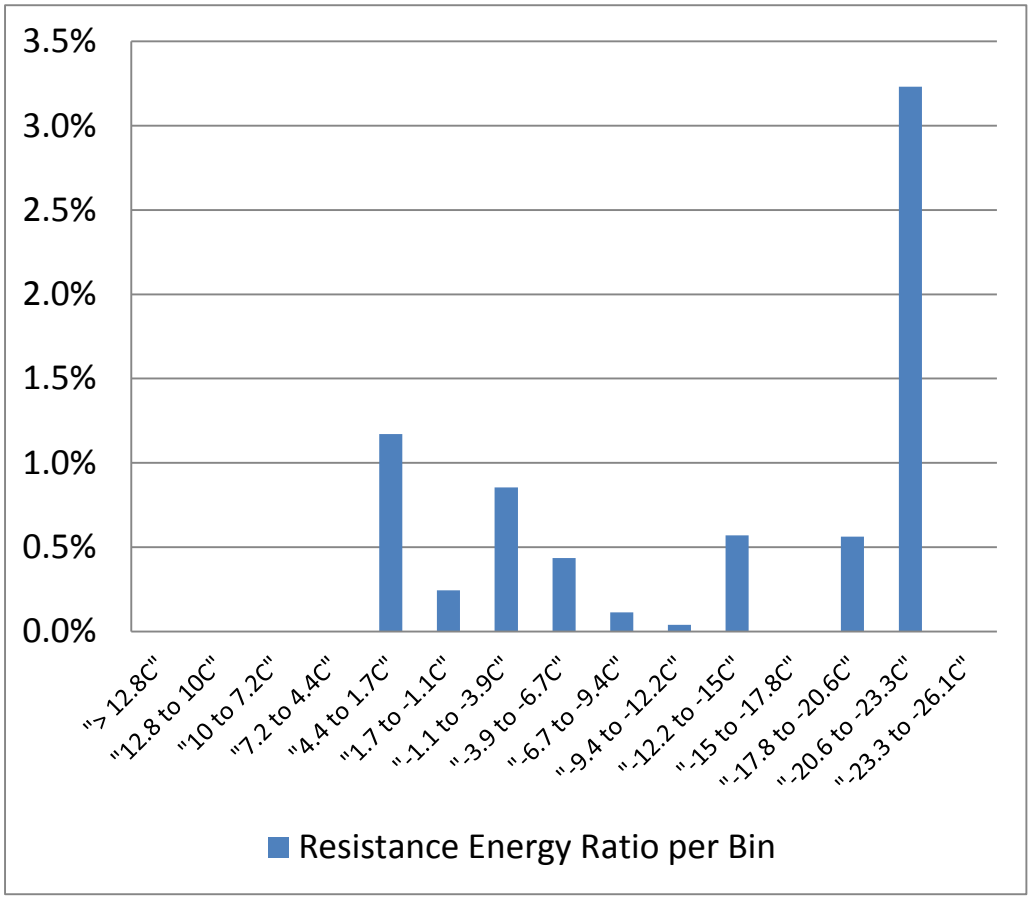

Figure 41: Supplemental resistance heat uses

Figure 42 shows the return and supply air temperatures. The return temperature profile indicates that the homeowner set the thermostat at 20°C during the majority of time when the heat pump was operating. At -25°C, the heat pump was able to deliver supply air at 30°C out of the indoor blower before the resistance heater, with the high air flow rate of 0.64 m^3/s. It should be mentioned that we allowed the indoor air flow rate to change with the compressor staging without consideration of the ambient temperature, due to the desire to simplify the control during the field testing.

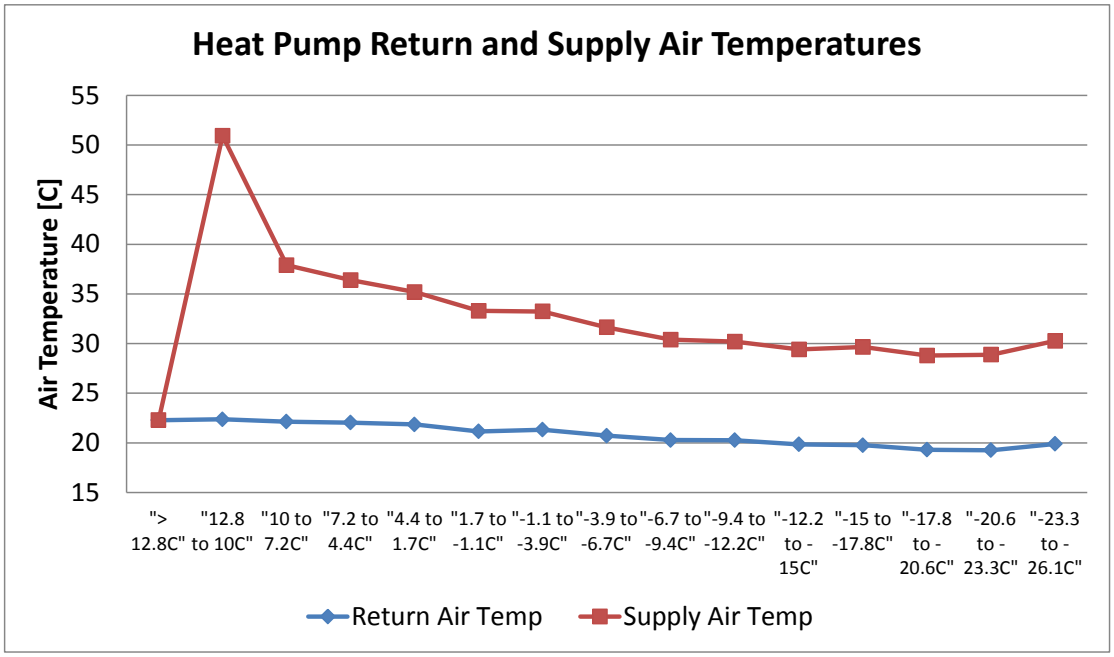

Figure 42: Return and supply air temperatures

Figure 43 presents the defrost runtime fraction (time ratio) and the ratio of the added heating load due to defrost to the total heating energy (load ratio) delivered in each temperature bin. It was concluded that defrost frequency and resultant energy losses were minimal for the CCHP for two reasons. First, when operating in the outdoor temperature range where the outdoor coil is most prone to frost build-up (roughly -5°C to 5°C), generally only one compressor was running leading to slow frost formation because the outdoor HX was relatively oversized and evaporating temperature higher than for typical ASHP systems. Secondly, when two compressors were needed at low ambient temperatures, the outdoor humidity level was generally very low and hardly any moisture condensed on the outdoor coil.

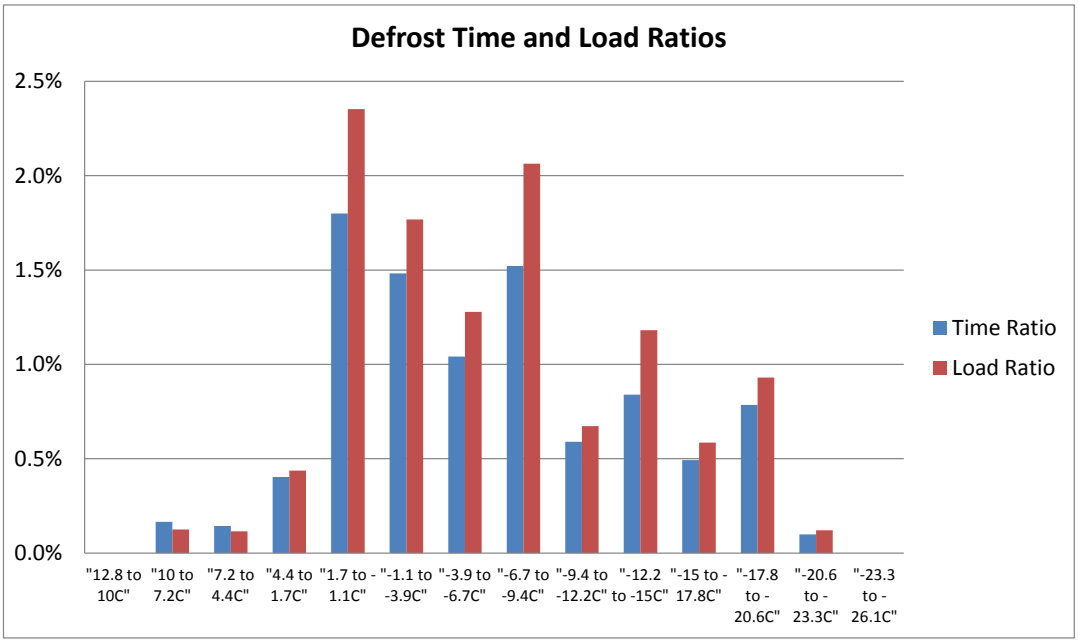

Figure 43: Defrost time ratio and load relative to capacity delivered in each bin

Figure 44 shows field-measured COPs by outdoor temperature bin for single-compressor and two-compressor operation as well as a "total" COP. The total COP was calculated by the total energy delivery divided by the total energy consumed and includes the impacts of cycling losses, supplemental resistance heat use, frosting/defrosting losses, and losses due to switching between one- and two-compressor operation. For the 7.2°C to 10°C bin, the single-compressor COP was 4.05 while the total COP was 3.83 (lower because of cycling losses and occasional two-compressor operation). It should be mentioned that a control modification to prevent two-compressor operation above a set outdoor temperature would allow the total COP at moderate heating conditions to much more closely follow the single compressor COP curve.

It is encouraging to see that, at -25°C, the total COP was 2.2 i.e. 120% more efficient than resistance heating. The field COP at -25°C is higher than that measured in the lab (1.94 given in Table 6) mainly because the field return air temperature is 1.1 to 2.2°C lower than the controlled value in the lab. In addition, the field COP was also boosted a bit due to the small amount of one-compressor operation.

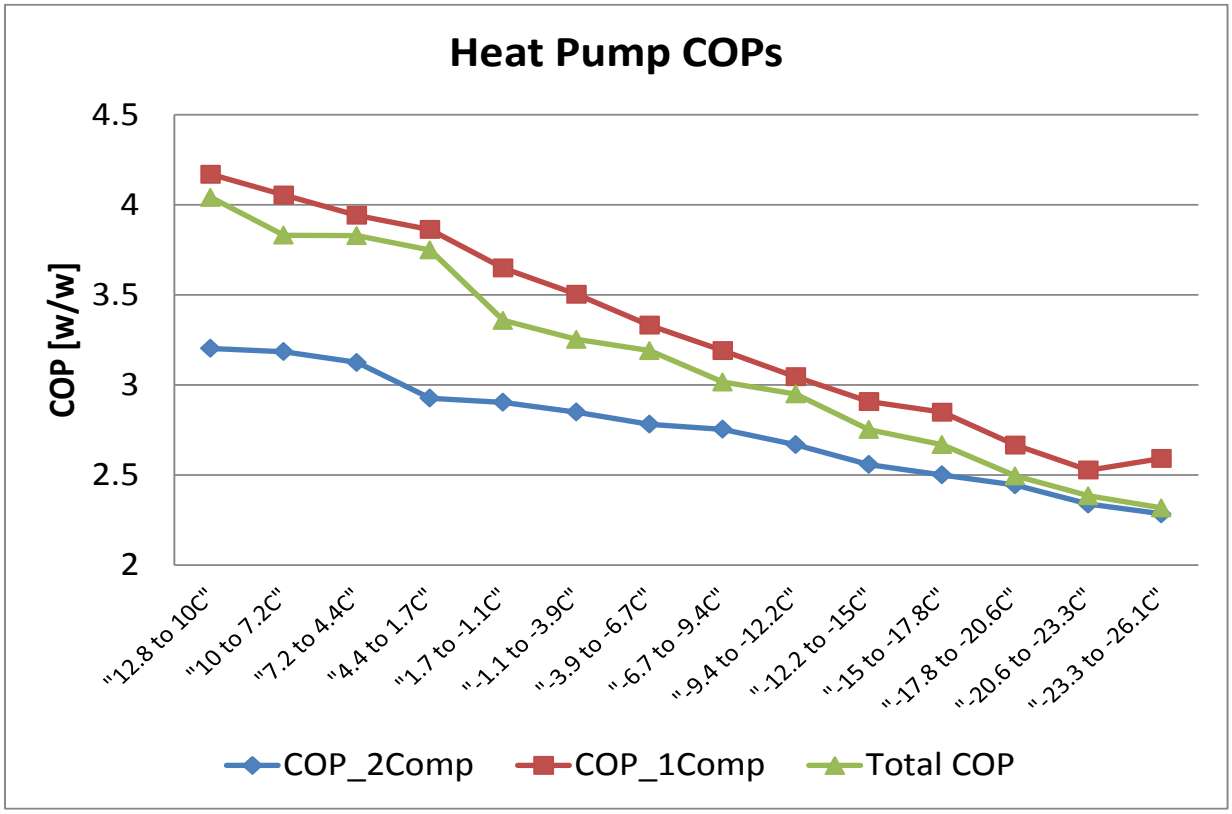

Figure 44: Field COPs in heating mode

In the three months of heating operation in 2015, the overall average field-measured COP was 3.16, compared to the 3.29 to 3.21 predicted ratings value for the AHRI 210/240 DHRmin and DHR-max load lines, respectively. Figure 45 compares heat energy delivered per temperature bin from the 2015 winter field data with that for a house having the AHRI 210/240 load characteristic in region IV. It can be seen that the test home in 2015 had a higher percentage of the total heating energy delivered at lower ambient temperatures because the 2015 winter in Ohio was much colder than usual.

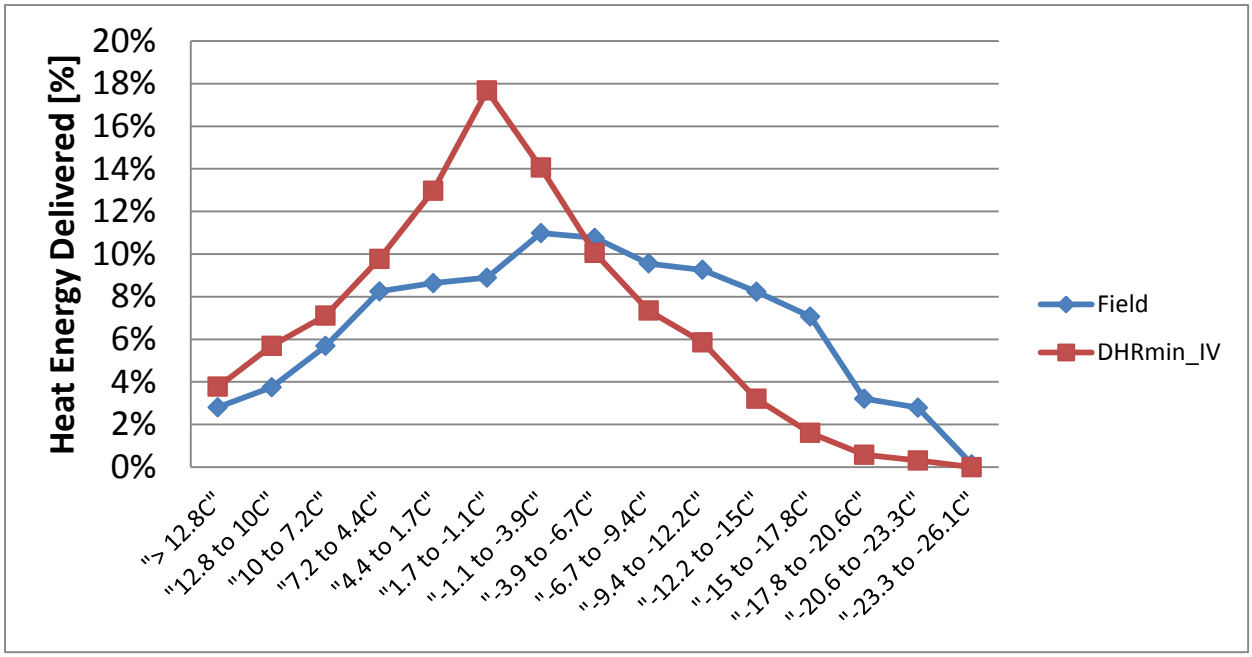

Figure 45: Field-measured heat energy delivered by bin in 2015 vs. AHRI 210/240 house load

Field Cooling Performance

Cooling season data for the CCHP prototype was recorded from June through August of 2015. Prior to the start of the cooling season the control board was adjusted to allow only single compressor operation with low-speed indoor blower operation. One-time measurement of the cooling mode indoor air flow rate using the "True Flow Grid" indicated an air flow quantity of 0.65 m^3/s (1380 CFM). This is in excellent agreement with the rated airflow of 0.65 m^3/s (1375 CFM) given in the air handler product literature.

Figure 46 shows average, delivered cooling capacities per outdoor temperature bin (air-side measurement). As the outdoor temperature increased from 15.6 to 23.9°C the cooling capacity increased due to the reduced cycling losses. As the temperature increased further the cooling capacity decreased due to increasing condensing temperature. For the 32.2°C to 35°C temperature bin, the field average capacity was right at 10.6 kW (3-ton).

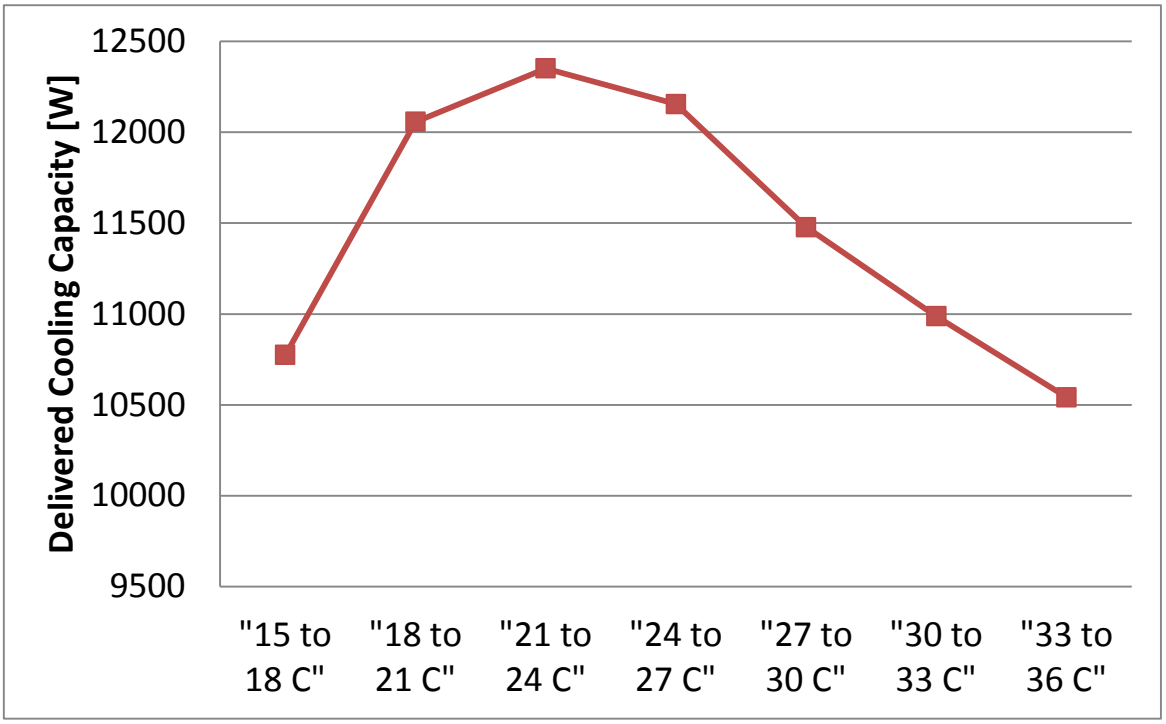

Figure 46: Delivered cooling capacities

As noted earlier, during the cooling season only single-compressor operation was permitted for the CCHP prototype. In this case, the indoor and outdoor heat exchangers, sized for the base 17.5 kW ASHP were oversized for the single compressor, thus leading to superior cooling performance. The averaged field measured COP over the test period was 5.2, with the return air temperature varying from 21.1 to 25.6°C, and an average ambient temperature of 25.6°C (78°F). Figure 47 below shows the field measured average COPs per temperature bin. It can be seen that for the highest temperature bin), the average field COP is 4.1.

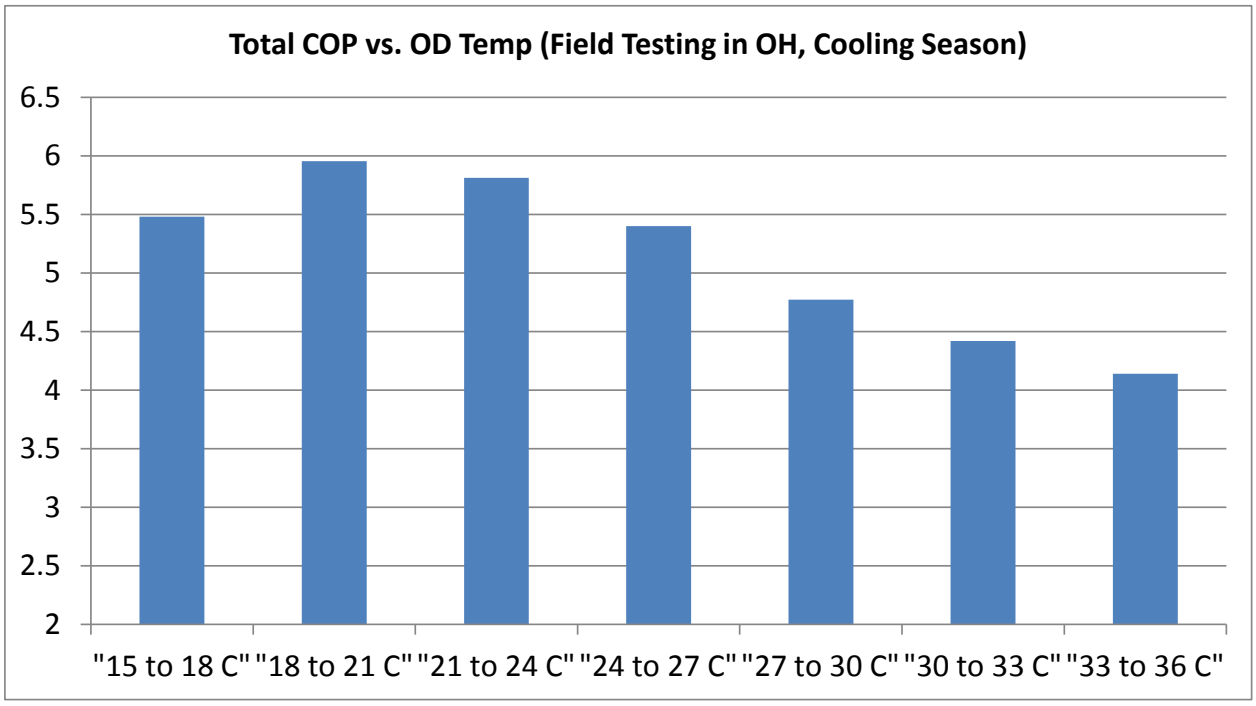

Figure 47: Field COPs in cooling mode

Comparison of Utility Billing Data Before and After Installing the CCHP

Figure 48 compares monthly electricity billing data for about two years before and one year after installation of the prototype CCHP. Note here that the kWh from the electric bills has had 800 kWh in "base" consumption (due to lights, water heater, appliances, etc.) subtracted so that it represents the heat pump usage only. As shown in Figure 48 below, in comparison to the previous single-speed ASHP in the same house, >40% energy reduction was achieved during the coldest months with similar monthly average temperatures (around -6 to -7°C).

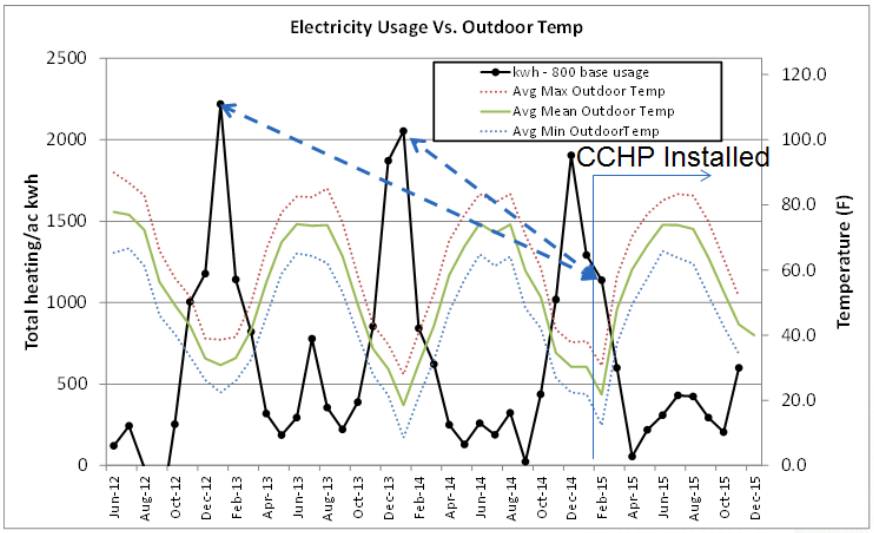

Figure 48: Comparing electric bills of the field testing home before/after installing the CCHP with tandem single-speed compressors

Figure 49 compares the field measured kwh/day vs. outdoor temperature with similar data extracted from the monthly billing statements. It can be seen that the field data is very close to that from the two monthly electricity bills when the CCHP prototype was operating, which indicates good field measurement accuracy. The field data indicate that the CCHP unit has lower average daily energy use at all temperatures with the savings increasing as the temperature drops.

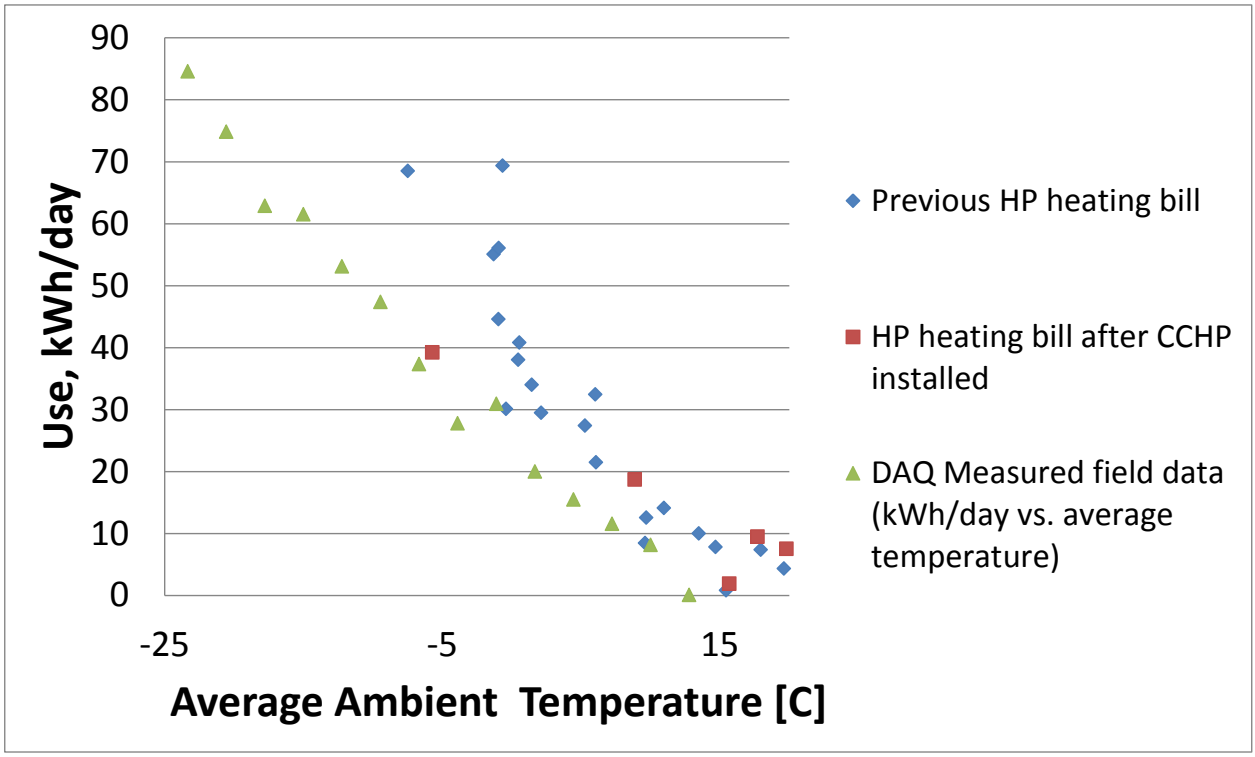

Figure 49: Overlay of the field testing data with the electricity bills

In Figure 48, it can also be seen that there are no apparent energy savings in the cooling months. This was due to a change in the family situation change --- the home owners had a new baby in the 2015 summer. So they set the thermostat to a lower temperature than they had used in previous summers and the heat pump ran more frequently.

Sensitivity Study of Field Heating Performance – Feb. – Apr. 2015 vs. Dec. 2015 – Jan. 2016

Before the project ended another set of heating data from December 2015 through January 2016 was collected. For this period the homeowner adopted a higher thermostat setting of 21.7°C, about 1.7°C higher than the previous heating season due to the new family member. In addition an outdoor new temperature controller was added to the CCHP system to prevent the second compressor from running when the ambient temperature was above -12.2°C.

Due to the higher thermostat setting, the return air temperatures to the CCHP in 2016 were consistently 4°F (2.2°C) higher than those in 2015 (Figure 50) leading to bigger heating loads per temperature bin in 2016, as illustrated in Figure 51. Consequently, the second compressor ran more frequently in 2016. As shown in Figure 52 in the temperature bin from -20°C to -17.8°C, the second compressor run time fraction was 88% in 2016 vs. ~40% in 2015 (Figure 39). On the other hand, the resistance heat did not operate in 2016. Thus, the prototype CCHP was able to fully meet the building heating load with the higher temperature setting.

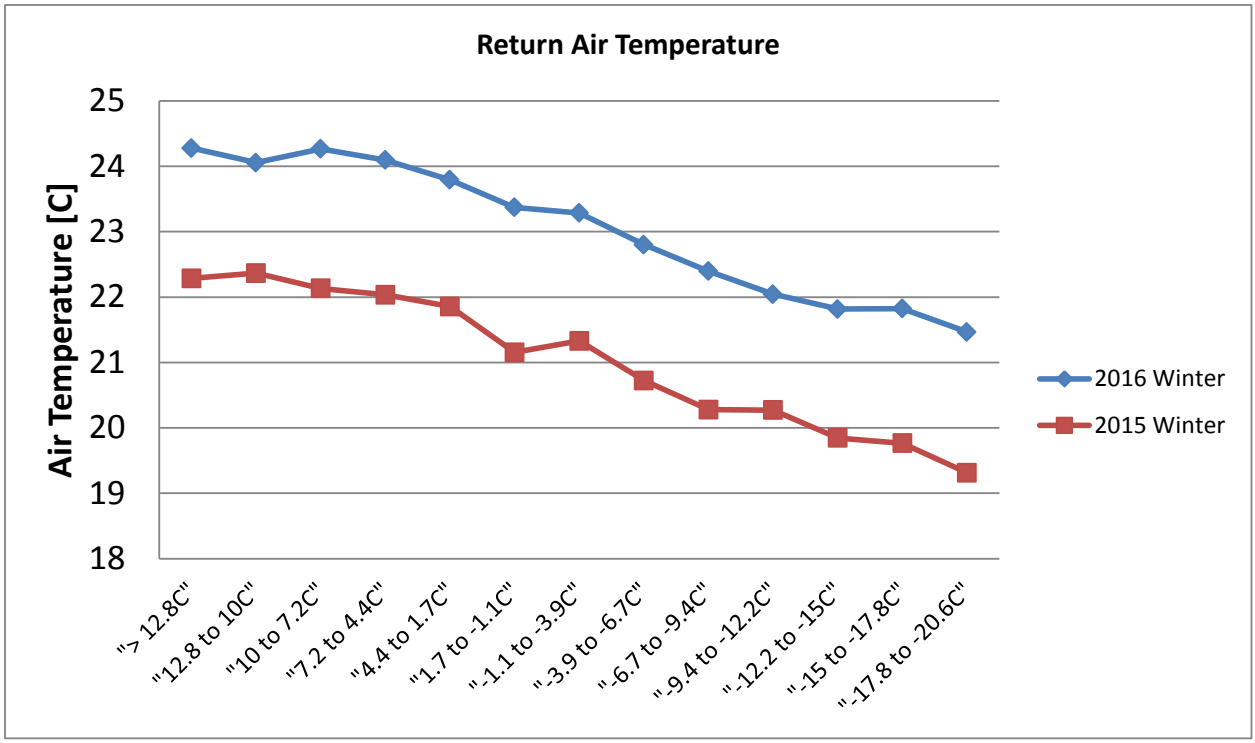

Figure 50: Return air temperatures in 2015 and 2016 heating seasons

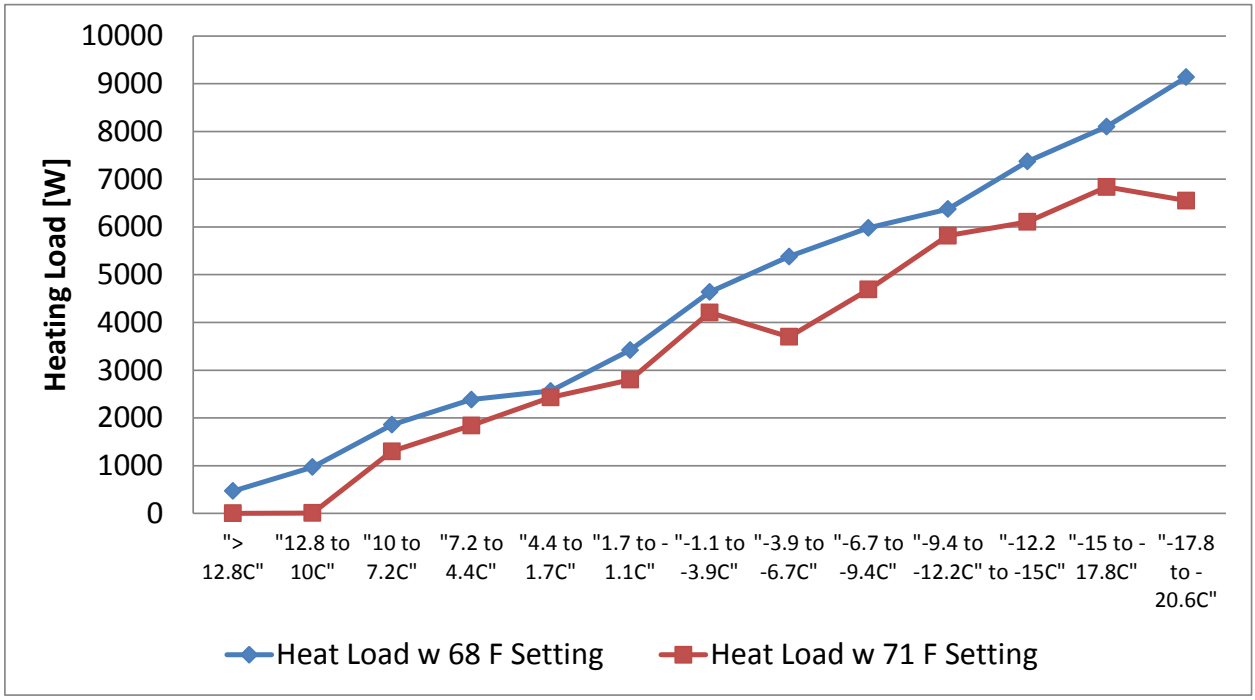

Figure 51: Comparing building heating loads in 2015 and 2016

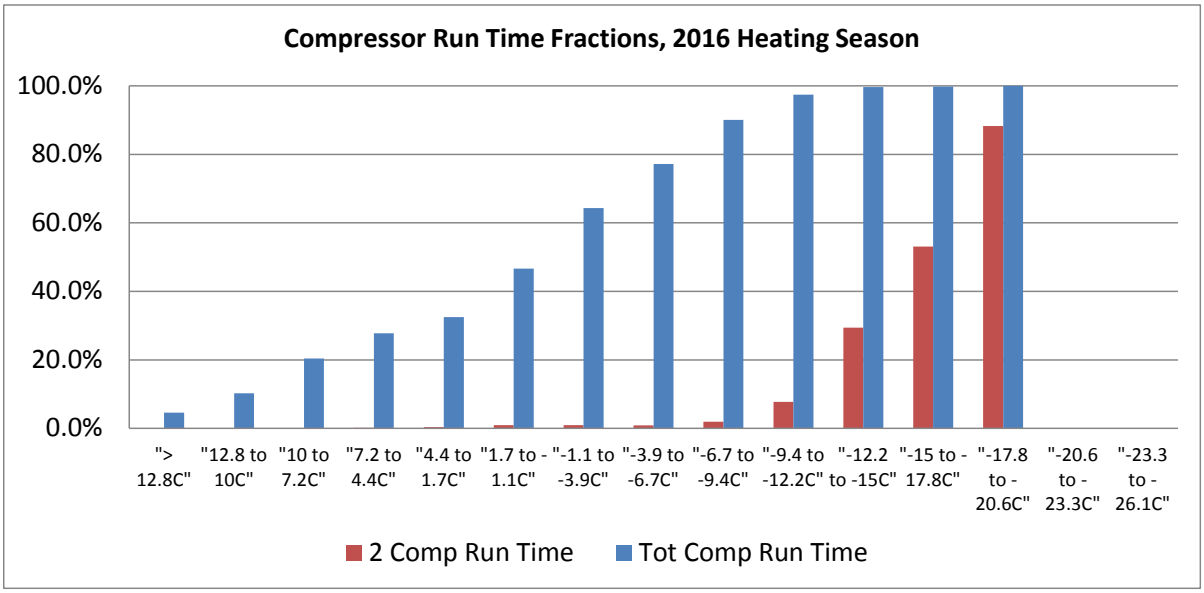

Figure 52: Compressor runtime fractions for the 2016 heating season

Figure 53 compares the average heat pump COPs per temperature bin for the 2015 and 2016 heating test periods. Because of the higher temperature setting and the ~2.2°C higher return air temperature to the CCHP, the heat pump heating COPs of 2016 are 10% to 15% lower than those of 2015. The field measured, averaged COP in 2016 was 2.84, or about 10% lower than the 2015 average of 3.16.

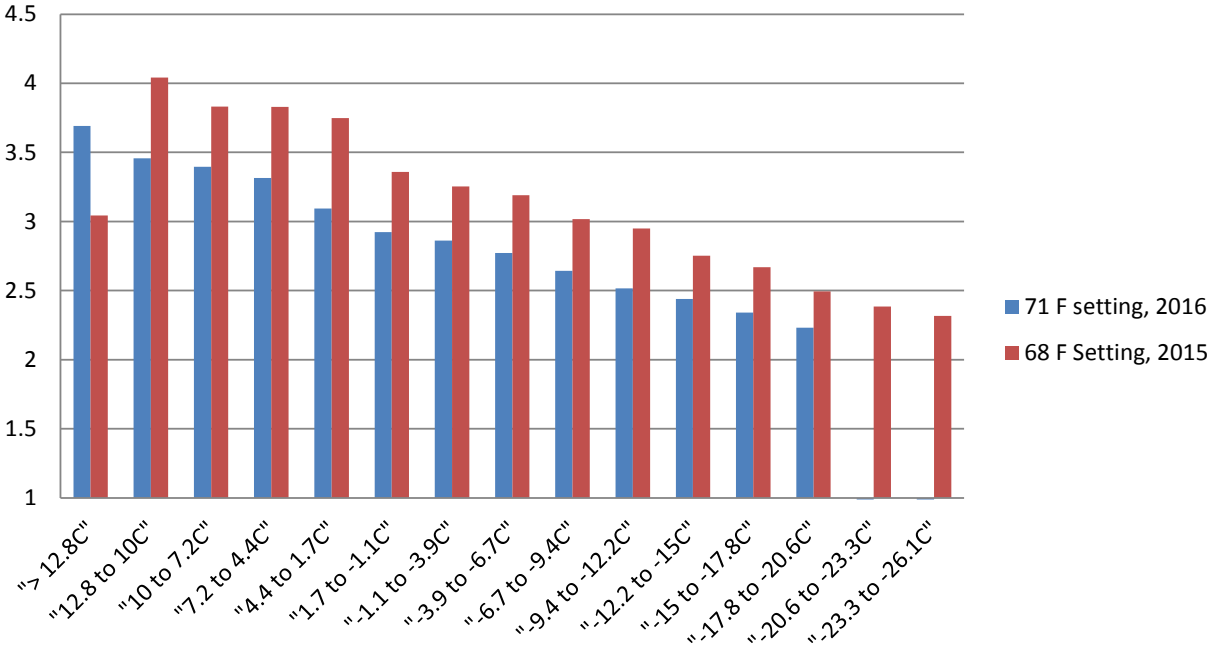

Figure 53: Average total COPs in 2015 and 2016

5.2 'Premium' Option - Equal Tandem, VI Compressors

It has been shown that application of vapor injection (VI) technology to a compressor can yield increased heating capacity and efficiency. A sample pair of tandem VI compressors was obtained from Emerson Climate Technologies and the performance evaluated in the same breadboard unit as used for the 'more cost-effective' configuration. The tandem VI

compressors were investigated in three scenarios. The first used a TXV to control the evaporator exit superheat (similar to the approach used in the field test tandem system discussed previously in Figure 35); the second (Figure 54) used an EXV to control the compressor discharge temperature; the third (Figure 55) coupled the discharge temperature control with a suction line heat exchanger (SLHX).

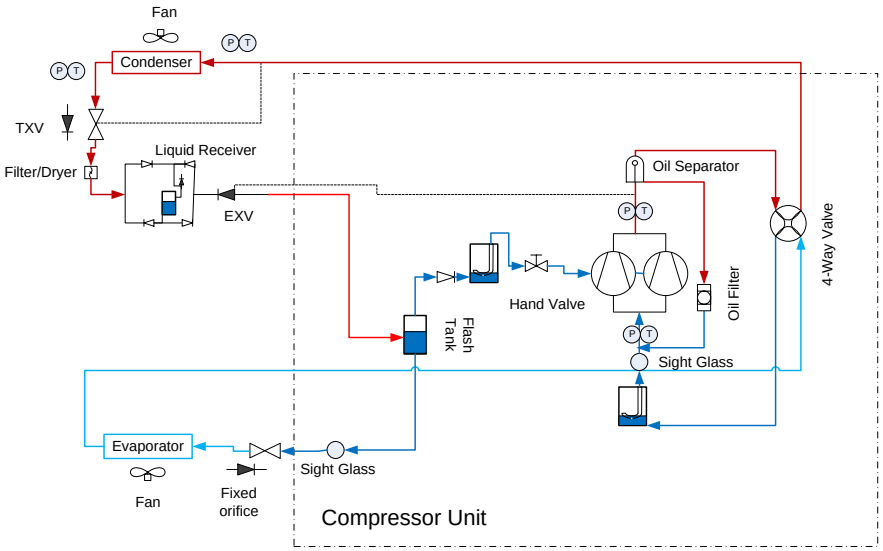

Figure 54: CCHP using tandem VI compressors and an EXV for discharge temperature control in heating mode

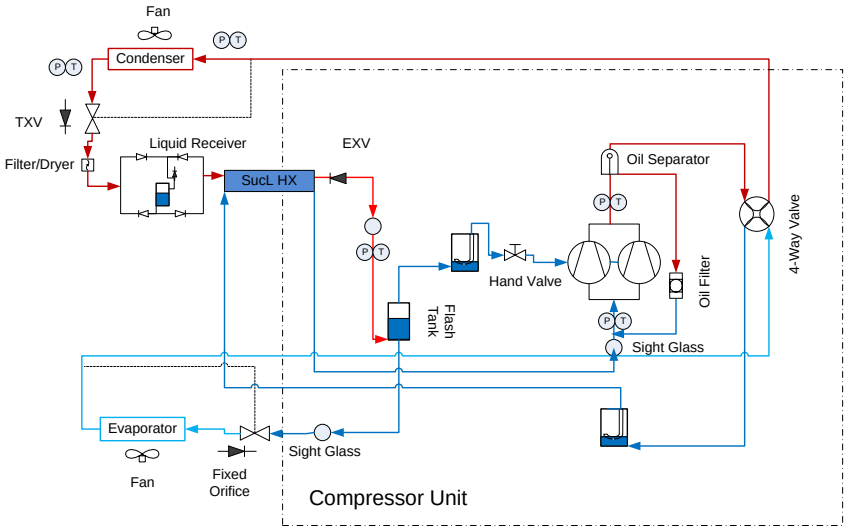

Figure 55: CCHP using tandem VI compressors, discharge temperature control and suction line heat exchanger

It was observed that the discharge temperature control approach led to better performance with the VI tandem pair than compressor suction superheat control. Tests of the lab breadboard prototype with and without the SLHX indicated no net improvements in COP or heating capacity. Use of an SLHX was observed to increase the compressor suction superheat degree and discharge temperature, which increased the heating capacity per unit refrigerant mass flow rate. However, the increased suction superheat also decreased the suction density, and reduced the compressor mass flow rate. In addition, the compressor efficiency appeared to decrease due to elevated suction and discharge temperatures. Consequently, neither capacity nor efficiency gain was observed with the SLHX so it was not considered further for the final design VI tandem prototype design.

The tandem VI compressor system configuration of Figure 54 achieved 5% better COPs than the tandem, single-speed heating-optimized system configuration of Figure 35 at various ambient conditions. It achieved an 88% heating capacity ratio and 2.0 COP at -25°C, and a 4.4 COP and 11.7 kW (40,000 Btu/h) capacity at the 8.3°C nominal rating condition. Figure 56 compares the heating capacities of the tandem single-speed compressors (heating optimized) and the tandem VI compressors, at two speed levels, as a function of the ambient temperature. Figure 57 compares the heating COPs. In Figure 56, DHRmax and DHRmin house load lines for the DOE Region V climate (e.g., U. S. cold region) are overlaid on the VI prototype capacity data. These indicate the potential for the CCHP prototypes to eliminate supplemental electric heat use in tight, well-insulated homes (aka DHRmin) in Region V.

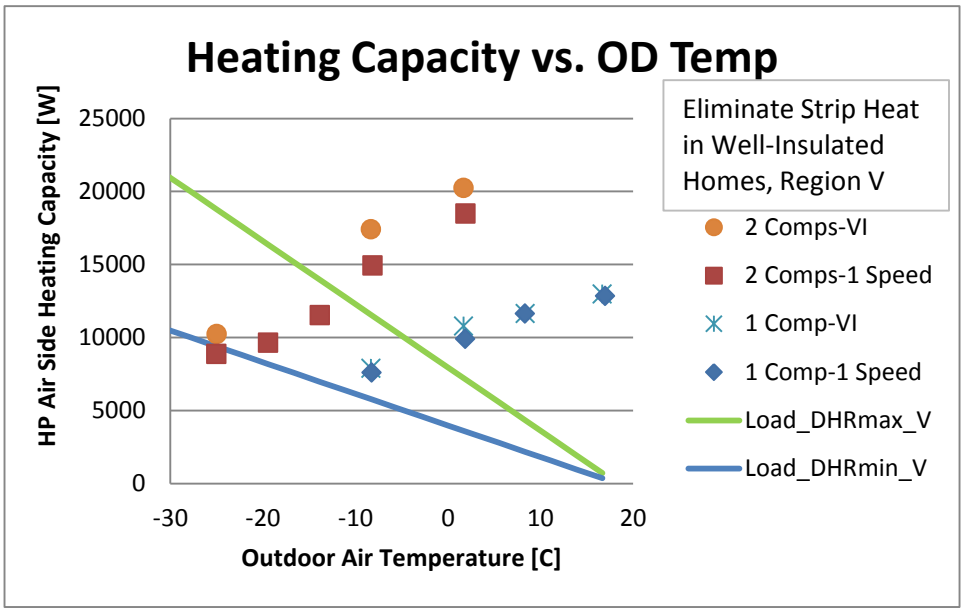

Figure 56: Heating capacity vs. ambient temperature, for tandem single-speed compressors and tandem VI compressors versus Region V house load lines

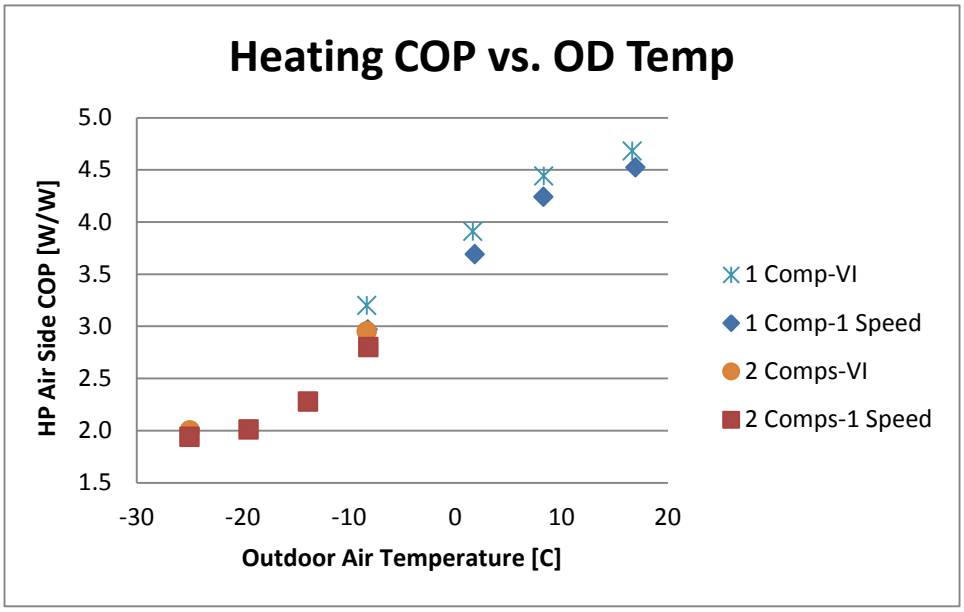

Figure 57: Heating COP vs. ambient temperature, for tandem single-speed compressors and tandem VI compressors

Table 8 reports the calculated SCOPhs (HSPFs) from the lab-measured data for the tandem VI compressor CCHP lab prototype with discharge temperature control for DOE climate regions IV and V. It is especially notable that the drop in SCOPh for the VI tandem design between the min and max heating load lines is less than 1% in Region IV and 5.4% in Region V. This indicates that this design maintains seasonal performance extremely well over the full range of house performance levels. As noted earlier, this performance is in contrast to much larger drops with higher heading loads for current ducted variable-speed units tested at ORNL (Rice et al, 2016). Figure 58 shows supply air temperature as a function of the ambient temperature. For this figure in the case of the tandem single-speed compressor system, the indoor air flow rate was set to Low for one-compressor operation. For two-compressor operation the indoor air flow rate was set to High when the ambient temperature ≥-8.3°C, and it was set to low, with the ambient temperature <-8.3°C, as to maintain a more comfortable supply air temperature. However, for the tandem VI compressor system, since it had higher heating capacity, the indoor air flow was always set at High when running two compressors. It can be seen that down to -25°C, both the tandem single-speed compressors and VI compressors were able to maintain supply air temperature higher than 31.7°C (89°F).

Table 8: Heating Seasonal Performance Factors of CCHPs using tandem VI compressors and discharge temperature control (per AHRI Standard 210/240)

Load	SCOPh (HSPF, Btu/Wh)
	Heating Season Ratings, Region: IV
DHRmin	3.47 (11.84)
DHRmax	3.46 (11.80)
	Heating Season Ratings, Region: V
DHRmin	3.13 (10.68)
DHRmax	2.96 (10.10)

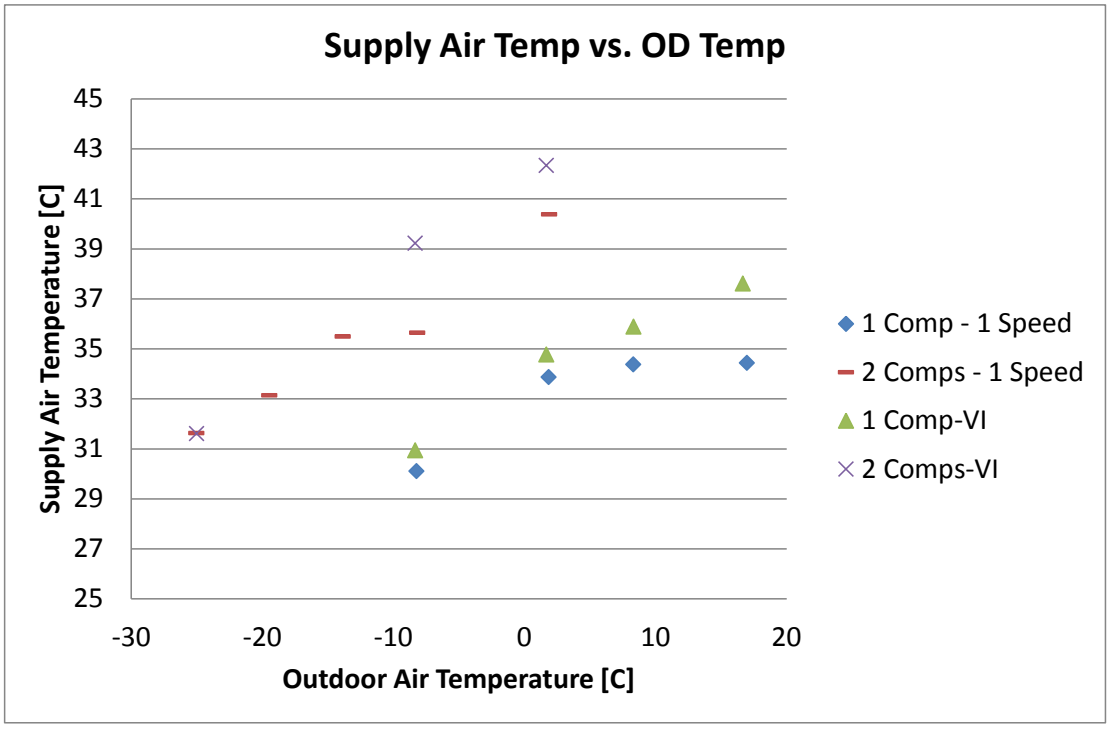

Figure 58: Supply air temperature vs. ambient temperature, for tandem single-speed compressors and tandem VI compressors

A second CCHP field test prototype system has been constructed based on the tandem VI compressor lab prototype design of Figure 54 starting from a baseline 17.5 kW single-speed ASHP. It was installed at the Cold Climate Housing Research Center in Fairbanks, AK in May 2016 and field testing began in June 2016. Shortly after testing began it became apparent that the electric power supply system experienced a number of power outages causing loss of data. After installing an uninterruptible power supply (UPS) system and monitoring, further computer loss of data was minimized.

The 2016/2017 heating season began in the latter part of August. For August through September the unit ran in low stage (one compressor) almost exclusively, matching the building heating load adequately. Outdoor temperatures ranged from 15.6°C down to -9.4°C (60°F to 15°F). It was observed that this CCHP required almost no defrost operation during this period (defrost accounting for <1% of the total heat pump run time). With only one compressor in operation, the outdoor heat exchanger is oversized leading to slow frost accumulation.

In October, however, when ambient temperatures went down to 0°F, two-compressor operation occurred more frequently. A fault occurred in the defrost control algorithm so that defrost operation failed to initiate and frost covered the entire outdoor coil. After applying a fix to the algorithm, the system operated normally in all modes. Figure 59 shows average heating COPs for each temperature bin for September 2016 through March 2017 with minimum outdoor temperatures as low as -34.4°C (-30°F). The CCHP demonstrated average COPs >1.8 with space heating capacity >75% of the rated capacity (10.6 kW @ 8.33°C).

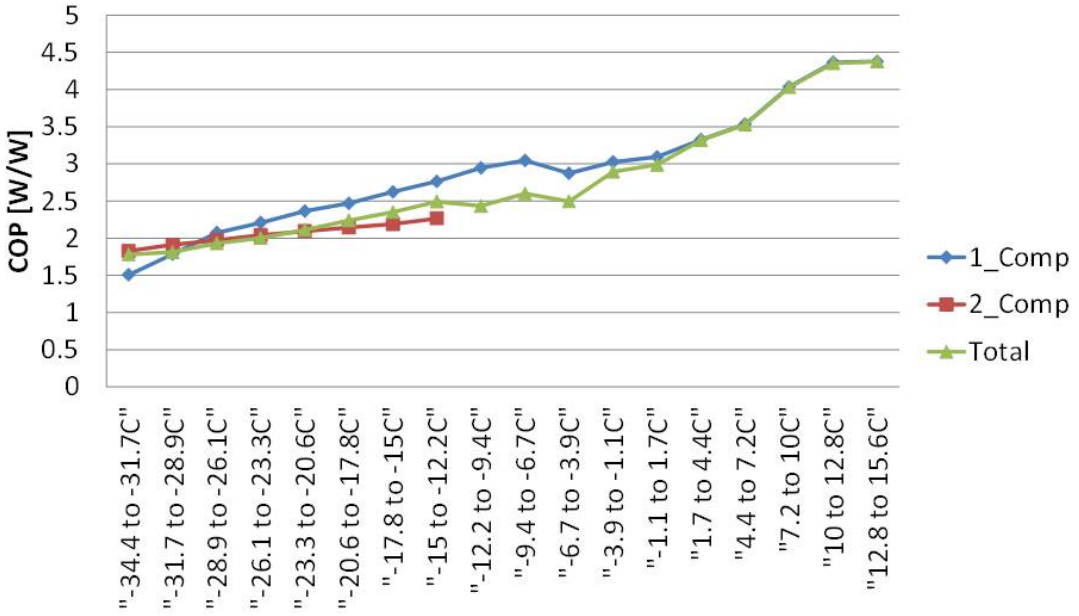

Figure 59: Field-measured average space heating COP vs. ambient temperature bin, for tandem VI compressor CCHP field test unit

Figure 60 shows the field-measured average delivered heating capacities for each outdoor temperature bin for both single and dual-compressor operation. At the lowest temperaturs bin of -34.4°C to -31.7°C (about -30°F to -25°F), with two compressors, the average delivered capacity was 7.9 kW (27000 Btu/h). This is 75% of the nominal rated heating capacity (36000 Btu/h (10.6 kW)) of the “starting point” heat pump unit at 8.3°C (47°F). Note that the average bin heating capacity decreases as the ambient temperature drops to ~15°C (only one compressor operating for majority of the time). As the outdoor temperature

decreased from -15°C to -35°C, two-compressor operation took place for an increasing portion of the time with the average bin operating heating capacity (rate) increasing with temperature as the run time for the second compressor increased as needed to match the increasing building load.

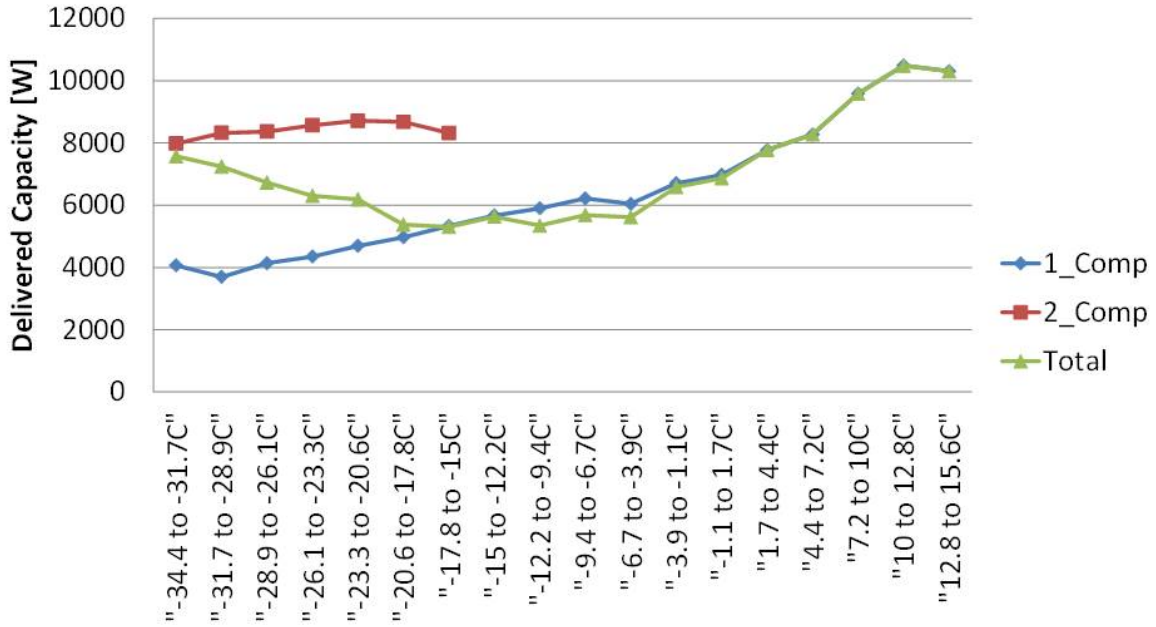

Figure 60: Field-measured average delivered space heating vs. ambient temperature bin, for tandem VI compressor CCHP field test unit

Full monitored field performance results for the VI tandem system will be reported after the planned one-year field test is concluded.

6 REFERENCES

AHRI 2008. ANSI/AHRI Standard 210/240-2008, "Performance Rating of Unitary Air-Conditioning and Air Source Heat Pump Equipment," Air-Conditioning, Heating, and Refrigeration Institute, Arlington, VA, USA.

Baxter, V. D., E. A. Groll, O. A. Abdelaziz, B. Shen, G. C. Groff, K. Sikes, and G. Khowailed. 2013. IEA HPP Annex 41 – Cold Climate Heat Pumps: Task 1 Report – Literature and Technology Review – United States, Oak Ridge National Laboratory, Report Number - ORNL/TM-2013/472, October.

Bell I. H., E. A. Groll, and J. E. Braun. 2011. "Performance of Vapor Compression Systems with Compressor Oil Flooding and Regeneration," *International Journal of Refrigeration*, Vol. 34, No. 1, pp. 225-233.

Bertsch S. S. and E. A. Groll. 2006. "Air Source Heat Pump for Northern Climates Part I: Simulation of Different Heat Pump Cycles," Proceedings of the 11th International Refrigeration and Air Conditioning Conference at Purdue.

Bertsch S. S. and E. A. Groll. 2008. "Two-stage air-source heat pump for residential heating and cooling applications in northern US climates," *International Journal of Refrigeration*, Vol. 31(7), pp. 1282-1292.

Caskey S. L. 2013. “Cold Climate Field Test Analysis of an Air-Source Heat Pump with Two-Stage Compression and Economizing,” Master’s Thesis, Purdue University, Ray W. Herrick Laboratories, West Lafayette, IN.

Liegeois O., Winandy E., 2008: Scroll Compressors for Dedicated Heat Pumps: Development and Performance Comparison, International Compressor Engineering Conference at Purdue University, Paper 1906, July 14 – July 17, 2008

Rice, C. K., B. Shen, and S. S. Shrestha, 2016. *Revised Heating Load Line Analysis: Addendum to ORNL/TM-2015/281*, ORNL/TM-2016/293, UT-Battelle LLC, Oak Ridge National Laboratory, July.

Shen, B., O. A. Abdelaziz, and C. K. Rice. 2014. “Compressor Selection and Equipment Sizing for Cold Climate Heat Pumps,” paper no. P.6.11 in the Proceedings of the 11th IEA Heat Pump Conference 2014, May 12-16 2014, Montréal (Québec) Canada.

Yang, B., Blatchley, T., Bach, C.K., Braun, J.E., Horton, W.T., and Groll, E.A., “Application of Oil Flooded Compression with Regeneration to a Packaged Heat Pump System,” Proc. of the 15th Int’l Refrig. and Air Cond. Conf. at Purdue, Paper 2631, Purdue University, West Lafayette, IN, July 14-17, 2014, 10 pages.

U.S. Team Report

IEA HPT TCP Annex 41
"Cold Climate Heat Pumps"

Task 4 – Concluding Remarks and Potential Future Work

January 2017

TABLE OF CONTENTS

1 CONCLUDING REMARKS

Both the two-stage economizer and single-stage parallel compressor ASHP cycle approaches discussed above have demonstrated the capability in laboratory testing to achieve the heating capacity improvement target given in Table 1 (in both the Task 1 and Task 2/3 reports) – heating capacity at -25°C (-13°F) ≥75% of the nominal rated capacity at 8.3°C (47°F). A field demonstration of the two-stage economizer was conducted at a U.S. army base in Indiana. Compared to the chosen baseline of a gas furnace heating system the CCHP achieved ~19% source energy savings. A field demonstration of the parallel compressor system demonstrated field-measured heating SPFs of 2.84 and 3.16 in two heating seasons. Estimated rated seasonal heating COPs of the parallel compressor concept based on the AHRI Standard 210/240 calculation procedure range from about 2.7 to 3.3 depending on house insulation level and climate conditions. This is 18 to 49% higher than the performance ratings of a high-efficiency conventional single-speed ASHP baseline using the same procedure. Using VI-compressors in the parallel system, seasonal COPs are estimated to range from about 3.0 to 3.5 (24 to 61% better than the single-speed ASHP).

The oil-flooded cycle concept does not show much heating capacity improvement but is significantly more efficient at low ambient temperatures than the single-speed base ASHP. Estimated seasonal performance of the oil-flooded concept based on lab performance measurements ranged from 8-10+% better than the baseline depending on location. Projected seasonal heating COPs for the oil-flooded system ranged from 2.6 to 3.0 for several northern U.S. location.

All of these approaches involve increased system complexity to varying degrees, which implies increased first cost compared to conventional ASHPs. Cost effectiveness compared to conventional ASHPs in cold locations has yet to be proven. The parallel compressor system has a relatively simpler refrigeration cycle so may hold the greatest promise. On the other hand, these designs promise to maintain the rated performance levels well for heating loads higher than those used for the ratings calculation.

2 POSSIBLE FUTURE WORK

The R&D activities carried out relative to this CCHP design option have demonstrated its potential to significantly improve the performance of ASHP systems for cold climate residential building applications. Performance ratings computed using current U.S. standard procedures range from 18-61% better than those of a very efficient conventional single-speed ASHP base unit. A few next-step development activities are given below.

- All of the analyses and testing work done so far for the parallel compressor CCHP concept have been based on refrigerant R-410A. This refrigerant has been preferred by most system manufacturers for the past 10-15 years. However it does have a relatively high global warming impact (GWP) of 1950 (IPCC AR5). Some work to evaluate performance impacts of switching to a lower GWP refrigerant (GWP <~700) seems in order.
- Work with manufacturer partner(s) to take the air-to-air system development the next steps to demonstrate a pre-commercial prototype. Efforts are underway to attract the interest of U.S. manufacturers.
- Evaluate concept potential for other heat pump system types, e.g., air-to-water, water/brine-to-air, etc.
- Future work on the vapor-injected compression with economizing system should include improving the vapor injected compressor: In the tested configuration, the injection ports did not include check valves. This is most likely the cause for the smaller performance improvement than predicted by the simulations.

- On the evaporator side, a larger fin pitch and tube diameter should be used for cold climate heat pumps to reduce the effects of frost-build up and refrigerant side pressure drop.
- Future research on oil-flooded compression with regeneration systems should focus on determining an optimal oil mass fraction as a function of outdoor temperature and superheat. In addition, it would be useful to control the superheat at the inlet of the compressor instead of the outlet of the evaporator to allow the refrigerant to leave the evaporator as two-phase flow and to be superheated in the regenerator.

PART 3: ADDENDUMS

This page intentionally left blank.

ADDENDUM A: PUBLICATIONS AND OTHER OUTREACH IN CONTEXT OF ANNEX 41

Journal articles

Badache, M. P. Eslami-Nejad, M. Ouzzane, Z. Aidoun, L. Lamarche, A new modeling approach for improved ground temperature profile, Renewable Energy 85 (2016) 436-444

Badache, M., Ouzzane, Eslami-Nejad, P., M., Aidoun, Z., Experimental study of a transcritical carbon dioxide direct-expansion ground coupled heat pump. Energy and building, 2016.

Bach, C.K.; Groll, E.A.; Braun, J.E. and Horton, W. T., "Dual port vapor injected compression: In-system testing versus test stand testing, and mapping of results," Renewable Energy, Vol. 87, Part 1, March 2016, Pages 819 – 833.

Eslami-Nejad, P. M. Ouzzane, Z. Aidoun, Modeling of a two-phase CO_2-filled vertical, Applied Energy, Volume114, February 2014

Eslami-Nejad, P., Ouzzane M., Aidoun Z., 2015. A Quasi-transient Model of a Transcritical Carbon Dioxide Direct-Expansion Ground Source Heat Pump for Space and Water Heating. Applied Thermal Engineering journal, 91, 259-269.

Eslami-Nejad, P., Hakkaki-fard A., Aidoun Z., (2016), Ouzzane M., Assessment of ground source, air source and hybrid heat pumps for a single family building in cold climates, ASHRAE Transactions, Vol 122, Part 2, June 2016.

Gschwend, A., Menzi, T., Caskey, S.L., Groll, E.A., and Bertsch, S.S., "Energy consumption of cold climate heat pumps in different climates – comparison of single-stage and two-stage systems," *Int'l J. Refrigeration*, Vol. 62, February 2016, Pages 193-206.

Hakkaki-Fard, A., Aidoun Z., Eslami-Nejad P., (2016). Evaluation of refrigerant mixtures in three different cold climates residential air-source heat pumps, ASHRAE Transactions, Vol 122, Part 2, June 2016.

Hakkaki-Fard, A., Eslami-Nejad P., Aidoun Z., Ouzzane M., 2015. A techno-economic comparison of a direct expansion ground-source and an air-source heat pump system in cold climates. Energy journal, 87, 49-59.

Hakkaki-Fard, A., Aidoun, Z., and Ouzzane M., Applying refrigerant mixtures with thermal glide in cold climate air-source heat pumps, Appl. Therm. Eng., 62, 2014, pp. 714-722.

Hakkaki-Fard, A., Aidoun, Z., and Ouzzane M., Improving cold climate air-source heat pump performance with refrigerant mixtures, Appl. Therm. Eng., 78, 2015, pp. 695–703.

Kagawa, N., Matsuguchi, A., Watanabe, K., 2012, "Measurements of Isobaric Heat Capacity of R32", Int. J. Refrig., Vol. 35, pp. 1014–1020.

Ouzzane, M., P. Eslami-Nejad, M. Badache, Z. Aidoun, New correlations for the prediction of the undisturbed ground temperature, Geothermics 53 (2015) 379-384.

Ouzzane, M., P. Eslami-Nejad, Z. Aidoun, L. Lamarche, Analysis of the convective heat exchange effect on the undisturbed ground temperature, Sol. Energy 108 (2014) 340e347.

Ramaraj, S., Yang, B., Braun, J.E., Groll, E.A, and Horton, W.T., "Experimental Analysis of Oil Flooded R410A Scroll Compressor," Int'l J. Refrigeration, Vol. 46, October 2014, Pages 185-195.

Ramaraj, S., Braun, J.E., Groll, E.A, and Horton, W.T., "Performance analysis of liquid flooded compression with regeneration for cold climate heat pumps," Int'l J. Refrigeration, Vol. 68, August 2016, Pages 50–58.

Japan team --- IJACR 2013 paper

Japan team --- JSRAE 2014 paper

18 total

Conference papers

Badache, M., Ouzzane, M., Aidoun, Z., Experiments on a CO_2 direct-expansion ground coupled heat pump. Proc. GSCE, ROME - ITALY, July 2016.

Badache M., Eslami-Nejad P., Ouzzane, M., Aidoun .Z, Lamarche L., Nouvelle approche pour l'évaluation du profil de température du sol, Proc. CIFQ, Sherbrooke, Juin 2015

Bach, C.K., Groll E.A., Braun, J.E., Horton, W.T., and Vetsch, B., "Application of two hybrid control methods of expansion valves and vapor injected compression to heat pumps," Proc. 11th Int'l Energy Agency Heat Pump Conf., Montreal, Canada, May 12-14, 2014.

Bach, C.K., Vetsch, B., Groll, E.A., Braun, J.E., and Horton, W.T., "Experimental Investigation of Vapor Injected Compression for Cold Climate Heat Pumps," Proc. of the 15th Int'l Refrig. and Air Cond. Conf. at Purdue, Paper 2111, Purdue University, West Lafayette, IN, July 14-17, 2014, 10 pages.

Bach, C.K., Groll, E.A., Braun, J.E., and Horton, W.T., "Effects of Vapor Injected Compression, Hybrid Evaporator Flow Control, and Other Parameters on Seasonal Energy Efficiency," Proc. of the 15th Int'l Refrig. and Air Cond. Conf. at Purdue, Paper 2675, Purdue University, West Lafayette, IN, July 14-17, 2014, 10 pages

Benovsky, P., H. Rusche, M. Ridzon, M. Popovac, C. Reichl, T. Fleckl, Dropwise Condensation Modeling Vortrag: Engineering Mechanics 2014, 20th International Conference, Svratka, Czech Republic (invited); 12.05.2014 - 15.05.2014; in: "im 2014", Brno University of Technology, 1st Edition (2014), ISBN: 978-80-214-4872-8; Paper-Nr. 80 to 83, 4 S.

Caskey, S.L., Kultgen, D., Gschwend, A., Groll, E.A., Hutzel, W.J., and Bertsch, S.S., "Cold Climate Field Test of an Air-Source Heat Pump with Two-Stage Compression and Economizing," Proc. 11th Int'l Energy Agency Heat Pump Conf., Montreal, Canada, May 12-14, 2014.

Eslami-Nejad P., Badache M., Ouzzane M., Aidoun Z., (2017), Direct expansion ground source heat pump using CO_2 as refrigerant: Test facility and theoretical model presentation. Abstract submitted to IGSHPA 2017, Denver, CO, USA.

Eslami-Nejad P., Hakkaki-fard A., Aidoun Z., Ouzzane M, 2015. Direct Expansion Ground-Source vs Air-Source Heat Pumps: Is the "Hybrid" System a Solution to Expensive Ground Loop Installations in Cold Climates? 2015 ASME Power and Energy, San Diego, California, USA, 28 June to 2 July

Hakkaki-Fard, A., Aidoun, Z., and Ouzzane M., 2014. Air-source heat pumps with refrigerant mixtures for cold climates, 11th International Energy Agency Heat Pump Conference, Montreal, May 12-16.

Hakkaki-Fard, A., Aidoun, Z., and Ouzzane M., Assessment of refrigerant mixtures performance with thermal glide for cold climate air-source heat pumps, HEFAT2014, 10th International Conference on Heat Transfer, Fluid Mechanics and Thermodynamics, 14 – 16 July, 2014, Orlando, Florida.

KAGAWA N, MATSUGUCHI A, YAMAYA K, WATANABE K. BEHAVIOR OF ISOBARIC HEAT CAPACITY OF R 32 IN THE GAS PHASE, 2012, Proc. the 6th Asian Conference on Refrigeration and Air Conditioning Paper No.2954 (Xi'an, 8/27/2012).

Kaneko, A., M. Katsuta, and Y. Hamano, Research of Heat Transfer and Pressure Drop Characteristic of Concavo-Convex Plate, Proceedings of the 6th Asian Conference on Refrigeration and Air Conditioning, CRA2012 Xi'an, China (2013).

Katsuta, M., Recent Development in Heat Pump Technology-Including Recent Progress in Basic Research , IEA HPP Workshop, Waseda University, International Conference center (2013-11)

Le Lostec, B. Nouanegue, H.F. (2014) On-site performance of air source heat pumps, 11th International Energy Agency Heat Pump Conference, Montreal, May 12-16, paper n.O.2.4.3

Menzi, T., Caskey, S.L., Kultgen, D., Groll, E.A., Hutzel, W.J., and Bertsch, S.S., "Analysis of Heating and Cooling Options for Military Barracks in the Midwest U.S.," Proc. 11th CLIMA 2013 Congress, Prague, Czech Republic, June 16-19, 2013.

Popovac, M., S. Seichter, C. Reichl, P. Benovsky, Implementation and application of the frost growth and densification model for numerical analysis of heat pump frosting performance Ammonia and CO_2 Refrigeration Technologies, April 16-18, 2015, Ohrid, Republic of Macedonia

Popovac, M., S. Seichter, P. Benovsky, T. Fleckl. Ch. Reichl, Numerical Analysis of the Frosting Performance of the air-side of a heat-pump, 24th IIR international congress of refrigeration, August 16-22, 2015, ICR2015, Yokohama, Japan

Reichl, Ch., J. Emhofer, F. Lörcher, A. Strehlow, M. Popovac, P. Wimberger, C. Köfinger, A. Zottl, T. Fleckl, Transient Acoustic Signatures of the GreenHP with special focus on icing and defrosting, submitted to 12th IEA Heat Pump Conference, May 15-18 Rotterdam, The Netherlands, 2017.

Reichl, Ch., J. Emhofer, F. Lörcher, A. Strehlow, M. Popovac, P. Wimberger, C. Köfinger, A. Zottl, T. Fleckl, GreenHP: Strömungs-Analyse der Verdampfer-Luftseite Jahrestagung des Deutschen kälte- und klimatechnischen Vereins, Kassel, Deutschland, 16.-18. November 2016

Reichl, Ch., J. Emhofer, T. Fleckl, Analyse der Luftströmung und Schallemissionen der Verdampfer-Luftseite der GreenHP mit speziellem Fokus auf Vereisung und Enteisung e-nova 2016, Nachhaltige Technologien, Gebäude – Energie – Umwelt, University of Applied Sciences Pinkafeld, Österreich, 24.-25. November 2016

Reichl, Ch., A. Strehlow, T. Oltersdorf, S. Braungardt, M. Pröhl, P. Benovsky, M. Popovac, T. Fleckl, GreenHP: Next Generation Heat Pump for Retrofitting Buildings – new evaporator

component for large capacity air-to-water heat pumps, Advanced HVAC & Natural Gas Technology Conference, May 6-9, 2015, Radisson BLU Hotel Latvija Conference Center, Riga, Latvia; DOI: 10.7250/rehvaconf.2015.015; page 100-109

Reichl, Ch., J. Emhofer, F. Lörcher, A. Strehlow, M. Popovac, P. Wimberger, C. Köfinger, A. Zottl, T. Fleckl, GreenHP: Strömungs-Analyse der Verdampfer-Luftseite Jahrestagung des Deutschen kälte- und klimatechnischen Vereins, Kassel, Deutschland, 16.-18. November 2016

Reichl, Ch., J. Emhofer, T. Fleckl, Analyse der Luftströmung und Schallemissionen der Verdampfer-Luftseite der GreenHP mit speziellem Fokus auf Vereisung und Enteisung e-nova 2016, Nachhaltige Technologien, Gebäude – Energie – Umwelt, University of Applied Sciences Pinkafeld, Österreich, 24.-25. November 2016

Schyns, D., Yang, B., Braun, J.E., Horton, W.T., and Groll, E.A., "Experimental results on a new prototype packaged heat pump system retrofitted with oil flooded compression and regeneration technology," Proc. of the 16th Int'l Refrig. and Air Cond. Conf. at Purdue, Paper 2694, Purdue University, West Lafayette, IN, July 11-14, 2016, 12 pages

Shen B., O. A. Abdelaziz, C. K. Rice, and V. D. Baxter, 2017, "Field Investigation of an Air-Source Cold Climate Heat Pump", submitted to 12th IEA Heat Pump Conference, Rotterdam, Netherlands, May 15-18, 2017.

Shen B., O. A. Abdelaziz, C. K. Rice, V. D. Baxter, and H. Pham, 2016, "Cold Climate Heat Pumps Using Tandem Compressor", Conference Paper (OR-16-C039) in Proceedings of 2016 ASHRAE Winter Conference, Orlando, FL, Jan 23-27,2016.

Shen B., O. A. Abdelaziz, V. D. Baxter, and C. K. Rice, 2014, "Compressor Selection and Equipment Sizing for Cold Climate Heat Pumps", Conference Paper in 11th International Energy Agency Heat Pump Conference

Strehlow, A., C. Martín-Callizo, T. Oltersdorf, M. Popovac, Ch. Reichl, GreenHP: Heat Exchangers for Next Generation Heat Pump, 4th International Congress and Exhibition on Aluminium Heat Exchanger Technologies for HVAC&R, 10-11 June, 2015, Hotel Radisson Blu Scandinavia, Düsseldorf, Germany

Zottl, A., T. Fleckl, and B. Palm, 2016, "GreenHP: Design and Performance of the Next Generation Heat Pump for Retrofitting Buildings," Conference Paper (ST-16-C034) in Proceedings of 2016 ASHRAE Summer Conference, St. Louis, MO, USA, June 25-29, 2016.

Zottl, A., T. Fleckl, M. Monsberger, B. Palm, GreenHP Design und Effizienz der nächsten Luft-Wärmepumpengeneration für die Sanierung im urbanen Raum, Annual Meeting of the Deutscher Kaelte und Klimatechnischer Verein 2015: Deutsche Kaelte-und Klimatagung 2015 Dresden, 18.-20.11.2015, Deutscher Kaelte- und Klimatechischer Verein (DKV)

Japan team --- Proceedings of Japan Society of Refrigerating and Air-Conditiong Engineers (JSRAE), 5 conference papers (all in JAPANESE)

38 total

Other publications

Annex 41, Report for the Austrian Funding Agency (June 2017)

Baxter, V. D., E. A. Groll and B. Shen, 2014, “Air Source Heat Pumps for Cold Climate Applications: Recent U. S. R&D Results from IEA HPP Annex 41”, Journal Article in Federation of European Heating, Ventilation, and Air Conditioning Associations (REHVA) European HVAC Journal.

Baxter, V. D., E. A. Groll, O. A. Abdelaziz, B. Shen, G. Groff, K. Sikes, and G. Khowailed, 2013, “IEA HPP Annex 41 – Cold Climate Heat Pumps: Task 1 Report – Literature and Technology Review – United States”, ORNL Report, ORNL/TM-2013/472

Baxter, V. D., E. A. Groll, and K. Sikes, 2013, “IEA HPP Annex 41 – Cold Climate Heat Pumps: Summary Interim Report”, ORNL/TM-2015/6.

Le Lostec, B., (2013a) Évaluation de l’impact en puissance et en énergie des thermopompes au Québec, Rapport technique LTE-RT-2013-0131

Le Lostec, B., (2013b) Effet de la température d’arrêt (« cut-off ») sur la performance des thermopompes conventionnelles, Rapport technique LTE-RT-2013-0130

Popovac, M., S. Seichter, P. Benovsky, C. Reichl: Numerical analysis of the air-side heat pump performance, Poster: OpenFOAM User Meeting (PFAU7), Montanuniversität Leoben; 18.11.2013.

Reichl, Ch., S. Seichter, M. Popovac, P. Benovsky, T. Fleckl, Experimentelle und numerische Methoden für die Untersuchung von Vereisung und Abtauverhalten von Verdampfern in Luftwärmepumpen, DKV Tagung 2014, Düsseldorf, Deutschland; 19.11.2014– 21.11.2014, in „Deutsche Kälte-Klimatagung 2014“

Seichter, S., Ch. Reichl, M. Popovac, P. Benovsky, Qualitative & quantitavie investigation of icing and condensation on fins and heat exchanger packages, 19th ERCOFTAC AHS Pilot Centre Meeting, 23. Mai 2014, Udine, Italy

Seichter, S., Ch. Reichl. T. Fleckl, M. Monsberger, Wind tunnel for qualitative and quantitative investigations of icing and condensation
ESAT 2014, 27th European Symposium on Applied Thermodynamics, July 6th-9th, Eindhoven University of Technology, The Netherlands

Zottl, T. Fleckl, M. Monsberger, GreenHP, Konzept der nächsten Luft/Wasser-Wärmepumpengeneration für den Einsatz im Gebäudebestand
Nachhaltige Gebäude, Versorgung - Speicherung – Optimierung, 25.-26.11.2015, Leykam

Zottl, M. Monsberger, T. Fleckl, Green Heat Pump, Luft/Wasser Wärmepumpen der nächsten Generation für den Einsatz im Gebäudestand
Luft-/Wasser-Wärmepumpen: Chancen und Risiken, 11.02.2014, OTTI Regensburg

Japan team --- JSRAE heat pump seminar keynote lecture

13 total

<u>Models, etc.</u>

Austrian team

- A model on the Engineering Equation Solver (EES) platform for different cycle configurations

Canadian CanmetENERGY team

- A model for ground temperature profile determination for ground source heat pump
- New correlations for the prediction of the undisturbed ground temperature for ground source heat pump
- Model of a two-phase CO_2-filled vertical borehole
- Quasi-transient model of a transcritical carbon dioxide direct-expansion ground source heat pump for space and water heating
- Model of a ground source, air source and hybrid heat pumps for a single family building in cold climates
- Model of a cold climate air-source heat pumps using refrigerant mixtures with thermal glide
- Model of a solar assisted heat pump using ice slurry as a latent storage

Japan team

- Model of Frost Growth

Workshops

#1 Workshop at 11th IEA Heat Pump Conference in Montréal (all presentations published in Conference Proceedings)

Estimated participants – 40-50

Workshop name	**Date**	**Presenter**	**Title of presentation**
" IEA HPP Annex 41 – Cold Climate Heat Pumps"	May 2014, Montréal	V. Baxter, ORNL, USA	Introduction to Annex 41
		T. Fleckl, AIT, Austria	Advanced methods for the characterization of icing effects on evaporators in air-to-water heat pumps
		M. Katsuta, Waseda University, Japan	Recent technology for cold climate heat pumps in Japan
		C. Bach, Herrick Labs, Purdue University USA	Cold climate heat pumps: performance improvement by modification of compression process and cycle
		S. Caskey, Herrick Labs, Purdue University	Air-source heat pump with two-stage compression and economizing
		R. Sunyé, NRCan, Quebec, Canada	Cold climate heat pumps R&D at NRCan
		B. Shen, ORNL, USA	Advanced system analyses
		Bo Shen, ORNL, USA	Experimental project update

#2 – Workshop at 24th ICR in Yokohama (all presentations published in ICR Proceedings)
Estimated participants – 75 total

Workshop/conference name	Date	Presenter	Title of presentation
" IEA HPP Annex 41 – Cold Climate Heat Pumps"	August 2015, Yokohama	M. Katsuta, Waseda University, Japan	Welcome from host country
		V. Baxter, ORNL, USA	Introduction to Annex 41
		M. Katsuta, Waseda University, Japan	Frosting phenomena between concavity and convexity plate under forced convection & Development of CO_2 thermo syphon for ground heat source assisted heat pump system
		K. Ohno, Waseda University, Japan	Dynamics of heat pump system with frost formation process
		L. Zhang, Central Research Institute of the Electric Power Industry (CRIEPI)	A new method for preventing air-source heat pump water heaters from frosting
		T. Fleckl, AIT, Austria	Investigation on icing effects of lab scale heat exchangers
		E. Groll, Herrick Labs, Purdue, USA	Update on cold climate heat pump research at the Ray W. Herrick Laboratories at Purdue University
		D. Giguère for B. Le Lostec, Hydro-Quebec, Canada	Field performance of cold climate heat pump
		D. Giguère, Canmet Energy, Canada	Cold climate air-source heat pumps using refrigerant mixtures with thermal glide
		B. Shen, ORNL, USA	Tandem, single-speed compressor air-source heat pump system laboratory and preliminary field test results
		R. Rieberer, TU-Graz, Austria	Liquid Injection – a suitable solution for cold climate heat pumps?
		K. Saito, Waseda University, Japan	Dynamics of heat pump system with frost formation process
		V. Baxter, ORNL, USA	Closing remarks - Annex 41 final report plan and schedule

Kickoff and Experts'/Working meetings

1. Kickoff #1, San Antonio, TX, USA; June 23, 2012
2. Kickoff #2, Nuremberg, Germany; October 10, 2012
3. Working meeting #1, Purdue University, West Lafayette, IN, USA; July 1-2, 2013
4. Working meeting #2, Montréal, Québec, Canada; May 12, 2014 (at close of Workshop 1)
5. Working meeting #3, Austrian Institute of Technology, Vienna, Austria; May 8, 2015
6. Working meeting #4, Orlando, FL, USA; January 22, 2016 (just before ASHRAE meeting)

In addition the Japanese Annex 41 team organized several internal meetings :

- 1 kick-off meeting and 13 working meetings from ~2012-2016
- 1 experts' meeting per year from ~2012-2016; 5 total

The Japan team was also the lead organizer of the Annex 41 workshop at the 2015 ICR in Yokohama

Experts' networks collaborated with or within

US and Austrian teams --- ASHRAE, ASME, DKV, IIR, RHEVA, USNC/IIR

CanmetENERGY team from Canada --- collaboration with 4 universities (Sherbrooke University, Concordia University (Montréal), Ecole Polytechnique (Montréal) and Ecole de technologie Superieur or ETS (Montréal))

Japan team --- collaboration with researchers from 5 manufacturers, 7 universities, 4 electric power companies, NEDO, and HPTCJ

This page intentionally left blank.

ADDENDUM B: LEGAL TEXT FOR ANNEX 41

Cold Climate Heat Pumps
(Improving low ambient temperature performance of Air-Source Heat Pumps)

1 BACKGROUND

During the 1970s, following the first oil embargoes, heat pumps became of great interest to northern electric power companies. This was particularly true of those experiencing large peak demands during the heating season, as shortages of natural gas and oil led to increased usage of direct electric heating. Air-source heat pumps (ASHP), given their greater availability and almost universal applicability, were of primary interest at the time. It is generally recognized, however that ASHPs based on the simple vapour compression cycle suffer both heating capacity (output) and efficiency (coefficient of performance or COP) degradation as the outdoor ambient temperature drops. At the same time building heat demand is increasing so ASHPs require a supplemental heating source – usually direct electric resistance heat elements - to bridge the gap between the building heat demand and the ASHP heating output. This characteristic causes lower seasonal performance (heating SPF) and limits peak electric demand reduction potential leading to limited acceptance of ASHPs in areas that experience large numbers of hours at very cold temperatures (e.g., at or below -7°C). A primary criteria for ASHPs to achieve good seasonal performance in cold areas is achieving high heating output at low ambient temperatures so as to minimize reliance on supplemental heat sources.

Considerable research and development activity was undertaken to improve the performance of ASHPs in the late 1970's and 1980's, resulting in higher efficiency and more reliable products (see references 1-3). During the decade from 1975 to 1985 a great deal was learned about the technology needs to enable heat pumps to become more competitive for northern climate applications. In intervening years heat pump designs have been pursued (and some have been brought to the market) that incorporate design concepts or features for improved cold climate performance (references 4 and 5 describe two US product examples). Most of these have not been successful due to the continuing relatively low cost of fossil fuels and the higher cost of these products and systems.

With increasing concern for technology options that can result in reduced CO_2 emissions, it is appropriate to revisit research and development work undertaken in different countries on heat pump systems for cold climates and to examine technology improvements that could lead to more successful heat pumps for future building applications in cold regions. ASHPs have the biggest challenges given their inherent low ambient temperature performance problems alluded to above. Availability of ASHP systems with improved low ambient performance would help bring about a much stronger heat pump market presence in cold areas which today rely predominantly on fossil fuel furnace h eating systems.

References:

1. Groff, G.C., and Reedy, W.R., Investigation of Heat Pump Performance in the Northern Climate Through Field Monitoring and Computer Simulation, ASHRAE Transactions, Vol. 84, Part I, pp.767-785, 1978.
2. Sizing of Air-to-Air Heat Pumps for Northern Climate Residential Heating

Applications, Bullock, C.E., Groff, G.C. and Reedy, W.R., Proceedings of International HVAC Congress, Berlin, 1980.
3. Heat Pump Performance Improvements for Northern Climate Applications, Groff, G.C., Bullock, C.E., and Reedy, W.R., Proceedings of the 13th Intersociety Energy Conversion Engineering Conference, San Diego, 1978.

4. Acadia™ Heat Pump, 2010. "Product & Technology Review#19", http://tinyurl.com/prodtech, accessed December 30, 2010.
5. Hadley, A., Callahan, J. Strok, R. 2006. "Without strip heat: In-situ monitoring of a multi-stage air source heat pump in the Pacific Northwest," ACEEE Summer Study on Energy Efficiency in Buildings, 2006.

2 DESCRIPTION OF TECHNICAL SECTOR

The primary technical sector is high efficiency (low energy) residential buildings, though commercial buildings can also benefit from the technology. Availabity of viable ASHP system solutions for efficient buildings in cold climate locations would significantly extend the market reach of heat pump technologies.

3 OBJECTIVES AND SCOPE

This project is primarily focused on air-source heat pumps with air or hydronic heating systems (e.g., air-to-air or air-to-water heat pumps) since these products have the greatest challenge in providing sufficient heat output and maintaining high efficiency levels at lower outdoor temperatures. While electrically driven air-source heat pumps will be the main focus, thermally activated air-source heat pumps (engine-driven, absorption, etc.) may also be considered within the scope of the project. Ground-source heat pumps may also be included at the discretion of individual participants. The main technical objective is to identify technical solutions that can lead to improved ASHPs with a heating SPF ≥ 2.63 W/W, the minimum level necessary in order to gain recognition as a renewable technology in the EU.

These objectives have parallel interest under the IEA Framework of Implementing Agreements as the intent is to identify, quantify, and deliver information to key industry stakeholders and policy makers and to provide pertinent resources to building owners and operators. The objectives will be achieved by independent studies and investigations performed by the country-specific participants. The main output of this Annex is information sharing on viable means to improve ASHP heating performance under cold (≤ -7°C) ambient temperature conditions so that better cross-country understanding is achieved to reduce energy consumption (and the related CO_2-mmissions) while satisfying the needs of building owners and operators.

4 MEANS

Each participating Annex partner will focus ***on those ASHP types and applications of primary interest to their residential and commercial building sectors***. As noted in the scope, participants may include GSHPs in the scope of their contributions as well, but ASHPS are the primary overall focus of this Annex. It is anticipated that each country's recognized standards, industry practices, and measurement instrumentation approaches will serve as the basis for the individual Annex partner efforts.

The Annex work is subdivided into the following tasks:

Task 1: Critical literature survey
Undertake literature review and critical analysis of the results from prior related research work with reference to projects and studies in various IEA HPP member countries and particularly in the countries participating in this Annex. The objective for this project stage will be to identify a number of potentially strong ASHP system design possibilities for further evaluation and study. Concepts that feature new technologies or insights, as well as advancements to conventional vapor compression systems will be welcome. It is expected that frosting of outdoor heat exchangers, sizing of the equipment for cold climates, controls

(including improved defrost controls) and system design and integration will represent major focus areas.

During this phase of the project it will also be important to formulate current specifications for heat pump systems, as appropriate to individual high efficiency building needs in the various countries, and to agree on overall performance objectives for improved ASHP systems for building space conditioning, water heating, etc., in cold climate locations.

Task 2: System design and application studies - modeling and/or laboratory-controlled measurements

Building on the literature search, and working with pertinet country experts, develop consensus performance targets for the advanced ASHP technology development to be included in the participant's investigations. As an example, the specific aim of the current U. S. Department of Energy's R&D is to demonstrate laboratory prototypes with heating capacity of up to 18 kW (~60,000 Btu/h) and a COP of 4.5 at the nominal U. S. Air-Conditioning, Heating, and Refrigeration Institute (AHRI) 8.3°C rating condition. The specific cold ambient performance goals are to limit COP and capacity degradation from the nominal rated levels to ≤25% at -25°C (-13°F). These objectives are subject ot review and modification based on input from the research institutions and potential industry partners involved and are focused on the prevailing central air-to-air heat pump type with central air distribution approach used in US systems. Other participants would establish their own performance targets based upon the heat pump and distribution systems of most interest to their industry and end users.

This task may comprise a number of subtasks depending upon individual participants' needs and interests:

1. Model advanced system concepts – e.g. system & component sizing for cold climates, concepts to reduce frosting/defrosting inefficiencies, modifications to vapor compression cycle to enhance heating capacity (multi-stage and/or cascaded vapor compression cycle concepts, etc.), advanced compressor concepts (variable capacity and/or single capacity), improved controls, system design & integration for cold climates, etc.
2. Based on critical review of subtask 1 results develop a design for a laboratory prototype advanced ASHP system based on the best cycle configuration. In this task, detailed design tools will be used to properly size the system components.
3. Fabricate the lab prototype system and conduct laboratory tests.
4. Prepare country report covering Tasks 1 and 2 and submit to Operating Agent (OA).
5. OA collates country reports and prepares Annex Interim report

Task 3: Simulations of energy savings impacts of prototype advanced ASHP design

This task will involve simulated performance projections to an agreed upon format for the preferred ASHP concept (or concepts) to determine energy savings potential over a range of climatic regions and other parameters (e.g. sizing, electric rates, control options, etc.).

Task 4: Report and information dissimenation

Each participant's final report will address the results of the tasks above. The common format simulations from Task 3 is intended to enable characterization of each concept on a common basis. These final country reports will be assembled into a final Annex report by the OA. This report will also suggest further areas for study and equipment development.

5 TARGET AUDIENCE AND BENEFITS

The sectors targeted for this Annex include:

- HVAC practitioners responsible for designing, selecting, and sizing heat pump systems in varied applications with a focus on cold ambient locations.
- Building owner/operators in cold regions interested in achieving improved comfort conditioning and efficiency performance from their HVACR equipment.
- Entities charged with minimizing energy utilization (i.e., utilities, utility commissions, energy agencies, legislative bodies, etc.) in varied heat pump applications and geographic conditions.

6 TIME SCHEDULE

The Annex shall tentatively commence 1 July 2012, and remain in force until 30 September 2015. Within the limits of the terms of the Agreement, this Annex may be extended by two or more of the participating countries (Participants), acting in the Executive Committee and taking into account any recommendation of the IEA's Committee on Energy Research and Technology concerning the terms of this Annex 41. Extensions shall thereafter apply only to those Participants.

The following is a tentative work schedule for the different tasks – exact timing will depend upon the actual start date of the Annex.

Start Date	End Date	Activity
July 2012	March 2013	Task 1 – Critical literature survey
	June 2012	Initial organizing meeting, San Antonio, US
	October 2012	Second organizing meeting, Nuremberg, Germany
December 2012	May 2014	Task 2 – System design and application studies
	July 1-2, 2013	First working meeting, Purdue University, West Lafeyette, IN, US
	March 2014	Draft Country reports on Tasks 1 and 2 due to OA
	May 2014	OA forwards interim report to ExCo and Heat Pump Centre
	May 2014	Open workshop at 11th IEA Heat Pump Conference, Montreal Canada – discuss interim results
	May 2014	Second working meeting, Montreal, Canada
June 2014	February 2015	Task 3 – Simulations of energy savings impacts
	February 2015	Interim web meeting – discuss Task 3 results and plans for final report
March 2015	September 2015	Task 4 – Report and information dissemination
	August 2015	Open workshop – final results Final working meeting – final issues for Annex report Location – 2015 IIR Congress in Japan
	September 2015	OA forwards Annex report to ExCo and Heat Pump Centre

7 DELIVERABLES

The deliverables of the Annex are:

a. An Internet website (linked to the HPC-site), that will serve as the participants' portal for sharing their country efforts and viewing the work done by other countries.
b. Progress reports to the HPC four times annually for publication in the Newsletter, and semi-annually to the HPP Executive Committee (May and November).

c. An annual summary report for inclusion in the HPP Annual report describing the work carried out under the Annex.
d. Final report consolidating the salient findings of the individual country inputs. This report will re-state the objectives of the Annex, its key findings, a description of the results of the Tasks undertaken by the Annex Participants, and recommendations for further study.

8 FUNDING

a. Participant's Financial Obligations: Each Participant (country) will bear the costs of its own participation in the Annex, including any necessary reporting, travel costs to undertake their portion of the effort, and costs to organize and hold working meetings hosted by the country. Approximately one face-to-face working meeting per year is anticipated during the course of the Annex (schedule to be determined by the Participants). It is envisioned that many of the Annex activities can be undertaken via web-conferencing and e-mail communications.
b. Publications: The cost/effort to prepare the draft Final Report and summary assessments described in paragraph 7 above ('Deliverables') shall be equally shared by all the Participants.
c. Each Participant shall make a direct financial contribution to the Operating Agent to cover coordination, report submission/review/consolidation, and other Annex-related costs.

The table below shows the fees per Participant, based upon varying numbers of Participants. Each Participant's fee shall be paid in 3 annual installments.

Number of participants	Participants' fees		
	2012/13	2013/14	2014/15
3	$ 5000	$ 5000	$ 5000
4	$ 4250	$ 4250	$ 4250
>4	$ 3750	$ 3750	$ 3750

Each Participating country's fee shall be paid in US$ as shown in the above Table.

9 SPECIFIC OBLIGATIONS AND RESPONSIBILITIES OF THE PARTICIPANTS

a. Each Participant shall nominate a lead representative to participate in the work under this Annex and act as the point of contact (POC) with the Operating Agent. At his/her discretion the POC may appoint other individuals to lead the Participant's work in each of the Annex Tasks as defined in Section 4.
b. Each Participant shall carry out the equivalent of at least 6-12 person months of task-sharing work during the Annex period unless otherwise agreed by the Participants.
c. Each Participant shall contribute to the working meetings and workshop(s) on the results achieved through the activities conducted under this Annex, including the identification of speakers and participants.
d. Each Participant shall make a direct financial contribution to the Operating Agent to cover co-ordination and report preparation expenses and other Annex related costs.
e. Each Participant shall provide a Country Report as identified in Section 4 (Task 4) and shall contribute to the deliverables identified in Section 7.

10 SPECIFIC OBLIGATIONS AND RESPONSIBILITIES OF THE OPERATING AGENT

The Operating Agent shall:

a. Develop, in co-operation with the Participants, a detailed work schedule, a framework for the Country Reports, and a budget for all the activities carried out under this Annex, including methodology and time schedule
b. Provide the Executive Committee with periodic reports describing the progress of the work being accomplished under the Annex
c. Deliver the results as described in Section 7 ('Deliverables')
d. Provide to the Executive Committee, within six months after completion of all the Annex work, a draft of the Final Report for its approval and transmittal to IEA headquarters.
e. In co-ordination with the Participants, use its best efforts to avoid duplication with activities of other related programs and projects implemented by or under the auspices of the Agency or by other competent bodies
f. Provide the Participants with necessary guidelines for the work they carry out, assuring minimum duplication of effort
g. Co-ordinate the efforts of all Participants and ensure the flow of information within the Annex
h. Provide general administration

The IEA Heat Pump Centre will assist in the establishment of the Annex, in the organisation of any workshop(s) and the publication of the proceedings, and publication of the Final Report.

11 INFORMATION AND INTELLECTUAL PROPERTY

a. *Executive Committee's Powers.* The publication, distribution, handling, protection and ownership of information and intellectual property arising from this Annex shall be determined by the Executive Committee, acting by unanimity, in conformity with this Annex.
b. *Right to Publish.* The Participants shall have the right to publish information provided to or arising from their contribution to the Annex under Section 9b, except for proprietary information, as defined in paragraph (c) below.
c. *Proprietary Information.* For the purposes of this Annex, proprietary information shall mean information of a confidential nature such as trade secrets and know-how (for example, computer programmes, design procedures and techniques, chemical compositions of materials, or manufacturing methods, processes or treatments) which is appropriately marked provided that such information:
    1. Is not generally known or publicly available from other sources
    2. Has not previously been made available by its owner(s) to others without obligation concerning its confidentiality; and
    3. Is not already in the possession of the recipient Participant(s) without obligation concerning its confidentiality.

It shall be the responsibility of each Participant supplying proprietary information, and of the Operating Agent, to identify such information as proprietary and to ensure that it is appropriately marked. The Participants and the Operating Agent shall take all necessary measures in accordance with this paragraph, the laws of their respective countries and international law to protect the proprietary information provided to or arising from this Annex.

d. *Production of Relevant Information by Governments.* The Operating Agent should encourage the governments of all Agency Participating Countries to

make available or identify to the Operating Agent all published or otherwise freely available information known to them that is relevant to the Annex.

e. *Production of Relevant Information by Participants.* Each participant agrees to provide to the Operating Agent all previously existing information, and information developed independently of the Annex, which can assist or is needed by the Operating Agent to carry out its functions in this Annex, which is freely at the disposal of the Participants, and the transmission of which is not subject to any contractual and/or legal limitations, under the following conditions:

1. The Participant will make such information available, at its own costs, provided that such costs are not substantial
2. If substantial costs are necessary for the Participant to make such information available, the Operating Agent and all Participants will determine the charge of the costs for each participant, upon approval of the Executive Committee.

f. *Use of Confidential Information.* If a Participant has access to confidential information which would be useful to the Operating Agent in carrying out the studies, assessments, analysis or evaluations described in this Annex, such information may be communicated to the Operating Agent but shall not become part of any report or other form of documentation issued as part of this Annex, nor shall it be communicated to the other Participants, except as may be agreed between the Operating Agent and the Participant who supplies such information. This information has to be marked clearly as "confidential".

g. *Acquisition of Information for the Annex.* Each Participant shall inform the Operating Agent of the existence of information that can be of value to the Annex, but which is not freely available, and each Participant shall endeavour to make such information available to the Annex under reasonable conditions, in which event the Executive Committee may, acting unanimity, decide to acquire each information.

h. *Reports on Work Performed under the Annex.* The Operating Agent shall, in collaboration with the other Participants, prepare reports on all work performed under the Annex and the result thereof, including studies, assessments, analysis, evaluations and other documentation, but excluding proprietary information, in accordance with paragraph 11(c) above.

i. *Copyright.* The Operating Agent, or each Participant for its own results, may take appropriate measures necessary to protect copyrightable material generated under this Annex. Copyright obtained shall be the property of the Operating Agent, for the benefit of the Participants provided, however, that Participants may reproduce and distribute such material, but shall not publish it with a view to profit, except as otherwise provided by the Executive Committee. The Contracting Parties understand and agree that the name, acronym and emblem of the IEA has been notified to the World Intellectual Property Organisation (WIPO) Secretariat according to Article 6 of the Paris Convention for the Protection of Industrial Property, as amended on 28 September 1979. The Contracting Parties further understand and agree that the OECD/IEA shall retain the copyright to all IEA deliverables, materials or publications published or to be published by the IEA or jointly by the IEA and a third party to this Annex. Should the Contracting Parties use any such deliverables, materials or publications they shall give full acknowledgement to the OECD/IEA as being the source of the material with a copyright notice in the following form: © OECD/IEA, (year of publication).

j. *Authors.* Each Participant shall, without prejudice to any rights of authors under its national laws, take necessary steps to provide the co-operation from its authors required to carry out the provisions in this paragraph. Each

Participant shall assume the responsibility to pay awards or compensation required to be paid to its employees according to the laws of its country.

12 OPERATING AGENT

The Oak Ridge National Laboratory (ORNL) aned Purdue University, U.S.A. are designated as Co-Operating Agents.

Contact information for the Co-Operating Agents:

Name	Van D. Baxter
Affiliation	Oak Ridge National Laboratory
Postal address	Box 2008, Bldg 3147, MS-6070 Oak Ridge, TN 37831-6070
Telephone number	865-574-2104
E-mail address	vdb@ornl.gov

Name	Eckhard A. Groll
Affiliation	Purdue University
Postal address	Ray W. Herrick Laboratories 140 S. Martin Jischke Drive West Lafeyette, IN 47907
Telephone number	765-496-2201
E-mail address	groll@purdue.edu

13 PARTICIPANTS IN THIS ANNEX

The Contracting Parties which are Participants in this Annex are the following:

Organization	**Country**
Austrian Institute of Technology (AIT) Technical University of Graz	Austria
Natural Resources Canada	Canada
New Energy and Industrial Technology Development Organization	Japan
Department of Energy	USA

(Japan, the US, and Canada [pending approval and financing] have agreed to join the Annex. Austria and Italy have expressed interest in joining the Annex as well pending approval and financing. Other countries that have previously indicated potential interest in joining the Annex include: Finland, Germany, the Netherlands, Norway, Sweden, and Switzerland.)

14 RESEARCH ORGANIZATIONS PARTICIPATING IN THIS ANNEX

The contracting parties are the ones signing the contract, but others may carry out the research work, state those parties in the table below.

Organization	Contact person	Country	Email	Website	Annex NT leader (Y/N)
Austrian Institute of Technology (AIT)	Dr. Thomas Fleckl & Dr. Christoph Reichl	Austria	*Thomas.fleckl@ait.ac.at* *christoph.reichl@ait.ac.at*		Y
Institute of Thermal Engineering, Graz University of Technology	Dr. René Rieberer	Austria	***rene.rieberer@tugraz.at***		
CanmetENERGY	Dr. Daniel Giguère	Canada	daniel.giguere@canada.ca		Y
Hydro-Québec - Institut de recherche LTE	Dr. Brice Le Lostec	Canada	lelostec.brice@lte.ireq.ca		
Waseda Univeristy	Prof. Masafumi KATSUTA	Toyko, Japan	katsuta@waseda.jp		Y
Oak Ridge National Laboratory	Omar Abdelaziz	Oak Ridge, TN US	abdelazizoa@ornl.gov		Y
Purdue University	Prof. Eckhard Groll	W. Lafeyette, IN US	groll@purdue.edu		Y

IEA Heat Pump Centre
c/o RISE - Research Institutes of Sweden
PO Box 857
SE-501 15 BORÅS
Sweden
Tel: +46 10 516 5512
E-mail: hpc@heatpumpcentre.org

www.heatpumpingtechnologies.org

Report no. HPT-AN41-1

www.heatpumpingtechnologies.org